A startling portrait of humanity's first migrants *p. 958*

Beware the spreading mosquitoes *p. 971*

Unraveling the origin of mega-earthquakes *p. 1027*

Science

$15
25 NOVEMBER 2016
sciencemag.org

AAAS

SPECIAL ISSUE

STAYING ON TRACK

How circadian rhythms influence physiology and health

CONTENTS

958 An ancient migrant's toolkit

25 NOVEMBER 2016 • VOLUME 354 • ISSUE 6315

SPECIAL SECTION

CIRCADIAN PHYSIOLOGY

ON THE COVER

A night-shift worker on the Victoria line of the London Underground railway is one of many people whose job or lifestyle choices dissociate them from the normal light-dark cycles of the environment. The physiological consequences of such circadian misalignment are described in a special section beginning on page 986. *Photo: Peter Macdiarmid/Getty Images*

SEE ALSO ▸ LETTERS P. 964 ▸ PODCAST ▸ VIDEO

NEWS

IN BRIEF

IN DEPTH

FEATURE

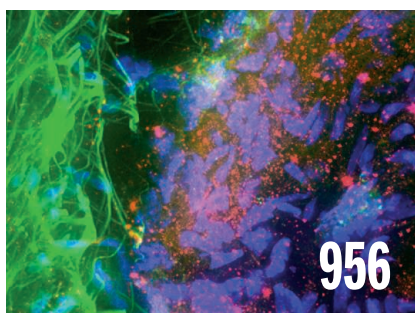

INSIGHTS

LETTERS

PERSPECTIVES

CONTENTS

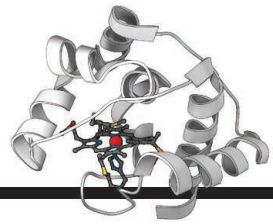

970 & 1048
Organosilicon comes to life

25 NOVEMBER 2016 • VOLUME 354 • ISSUE 6315

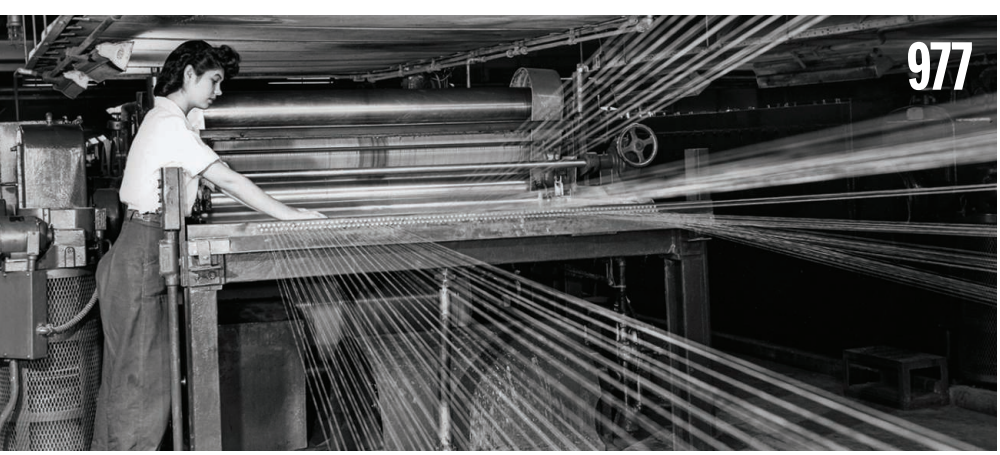

SCIENCE (ISSN 0036-8075) is published weekly on Friday, except the last week in December, by the American Association for the Advancement of Science, 1200 New York Avenue, NW, Washington, DC 20005. Periodicals mail postage (publication No. 484460) paid at Washington, DC, and additional mailing offices. Domestic individual membership and subscription (51 issues): $165 ($74 allocated to subscription). Domestic institutional subscription (51 issues): $1522; Foreign postage extra: Mexico, Caribbean (surface mail) $55; other countries (air assist delivery) $89. First class, airmail, student, and emeritus rates on request. Canadian rates with GST available upon request, GST #1254 88122. Publications Mail Agreement Number 1069624. **Printed in the U.S.A.**
Change of address: Allow 4 weeks, giving old and new addresses and 8-digit account number. **Postmaster:** Send change of address to AAAS, P.O. Box 96178, Washington, DC 20090–6178. **Single-copy sales:** $15.00 current issue, $20.00 back issue prepaid includes surface postage; bulk rates on request. **Authorization to photocopy** material for internal or personal use under circumstances not falling within the fair use provisions of the Copyright Act is granted by AAAS to libraries and other users registered with the Copyright Clearance Center (CCC) Transactional Reporting Service, provided that $35.00 per article is paid directly to CCC, 222 Rosewood Drive, Danvers, MA 01923. The identification code for *Science* is 0036-8075. *Science* is indexed in the *Reader's Guide to Periodical Literature* and in several specialized indexes.

Published by AAAS

Science
AAAS
1200 New York Avenue, NW, Washington, DC 20005
Clarendon House, Clarendon Road, Cambridge, UK CB2 8FH

SUBSCRIPTION SERVICES For change of address, missing issues, new orders and renewals, and payment questions: 866-434-AAAS (2227) or 202-326-6417, FAX 202-842-1065. Mailing addresses: AAAS, P.O. Box 96178, Washington, DC 20090-6178 or AAAS Member Services, 1200 New York Avenue, NW, Washington, DC 20005

INSTITUTIONAL SITE LICENSES 202-326-6730 **REPRINTS:** Author Inquiries 800-635-7181 **COMMERCIAL INQUIRIES** 803-359-4578 **PERMISSIONS** 202-326-6765, permissions@aaas.org **AAAS Member Services** 202-326-6417 or http://membercentral.aaas.org/discounts

Science serves as a forum for discussion of important issues related to the advancement of science by publishing material on which a consensus has been reached as well as including the presentation of minority of conflicting points of view. Accordingly, all articles published in *Science*—including editorials, news and comment, and book reviews—are signed and reflect the individual views of the authors and not official points of view adopted by AAAS or the institutions with which the authors are affiliated.

INFORMATION FOR AUTHORS See pages 624 and 625 of the 5 February 2016 issue or access www.sciencemag.org/authors/science-information-authors

Published by AAAS

EDITORIAL

What now for science ?

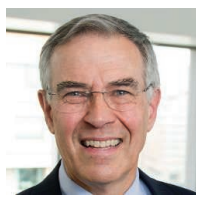

Rush D. Holt is Chief Executive Officer of AAAS and Executive Publisher of the Science *journals*

Faced with the uncertainty of what the 2016 U.S. presidential election means for science, we may find some reassurance in understanding that the health of the nation's scientific enterprise depends on much more than the attitudes of the particular person who is president. We must not forget that members of Congress and other national, state, local, and international officials also make policy and collectively constitute a considerable force that is in many ways more influential than the president alone. There is now important work to do ensuring that all citizenry, including the president, understand the powerful benefits of science and that decisions made with scientific input are more likely to succeed.

"...decisions made with scientific input are more likely to succeed."

As the nation readies for a transition in leadership, an immediate question for most scientists is federal funding for government science agencies in the coming years. Here, there is actually less uncertainty. Congress, for several years, has been on a "sequestration" path that, without a substantial turnover in Congress's majorities (as there was not), will reduce the fraction of the budget for discretionary funding, which includes science funding. The election thus preserves a trend whose reversal might have been hoped for, but was always unlikely.

A truer uncertainty is the role of science advice in the new administration. President-elect Trump's wish to drive economic progress and thereby improve people's lives cannot come about without advancing science, technology, innovation, and an education system that prepares a capable workforce. He would be wise to appoint a science adviser who is a respected scientist or engineer. The adviser should be fully integrated into the most senior decision-making processes not just on topics with an obvious science connection such as infectious-disease response, but on many matters with science and technology embedded, including diplomacy, cybersecurity, agriculture, advanced manufacturing, and resilient infrastructure.

Beyond research funding and science advice, there is much more that determines the health of the scientific enterprise. Will the U.S. join other nations in collaborative research in which there is full access to data and free exchange of researchers? Will scientists be appointed throughout the agencies? Will government scientists be able to speak freely about their research? In regulatory agencies, will accepted scientific findings be given precedence over political influence? Will financial and tax policies reward science-based activities in the private and public sectors?

Most important, will the next administration be evidence-based? Over recent decades, a disturbing trend in the U.S. government has been for ideological assertions to crowd out evidence. This trend accelerated with this year's campaign in which candidate Trump made statements that were unsubstantiated or contradicted by accepted scientific facts. Will there be members in the new administration who are familiar with the practices and findings of scientific investigation?

What are scientists to do? Certainly at the American Association for the Advancement of Science (AAAS), following a tradition nearly 170 years old, we will advocate forcefully that science be fully and positively integrated into public policy making. Science need not be politically partisan. Given that the economic and technological benefits of research are appealing to citizens across the political spectrum, science can bridge differences. The openness and directness of scientists' communication can be unwelcome to politicians, but the scientific community must present its best understanding of relevant evidence clearly, directly, and without condescension. We must make clear that an official cannot wish away what is known about climate change, gun violence, opioid addiction, fisheries depletion, or any other public issue illuminated by research.

This election is said to have been about rejecting the political establishment. We cannot let that mean rejecting established facts. We hope that President Trump will be more grounded in specific facts than was candidate Trump and pay more attention to the process of careful, open vetting of hypotheses and claims.

–Rush Holt

Published online 17 November 2016; 10.1126/science.aal4180

NEWS

> "We oppose taxpayer funding of animal experimentation. That's it. We don't take a position on cosmetics testing any more than we do on vegan nutrition."
>
> **Anthony Bellotti, former Republican strategist and founder of White Coat Waste**, to *The Washington Post*. His group is calling for more government disclosure on animal research.

IN BRIEF

Chernobyl confinement slides into place

The structure will fully encapsulate Chernobyl's Unit 4 reactor, destroyed in 1986.

In April 1986, an explosion and fire destroyed the Chernobyl Nuclear Power Plant's Unit 4 reactor, spreading radioactive contamination from Ukraine across a wide swath of Europe. This week, engineers are putting the finishing touches on the New Safe Confinement (NSC), an arch-shaped structure that will fully encapsulate the reactor and contain any lingering radioactive materials. Immediately after the disaster, Soviet troops hastily threw up a concrete "sarcophagus" over the eviscerated reactor and the scattered nuclear materials that continue to pose a potent threat. The sarcophagus was never meant to be a long-term solution. The $1.6 billion NSC, however, is intended to last a century. Built on rails next to Unit 4 by the Novarka joint venture, the 25,000-ton NSC is now sliding, ever so gently, into place. Tall enough to contain the Statue of Liberty and nearly as long as two American football fields, the NSC is designed to withstand moderate tornadoes and a magnitude-6 earthquake, an event estimated to strike the area once every 10,000 years. The NSC is no sealed-off tomb: It will allow work to begin on the daunting challenge of cleaning up the site and decommissioning the reactor.

PHOTO: FRANCIS VIGOUROUD

AROUND THE WORLD

Argentine scientists face cuts

BUENOS AIRES | Scientists in Argentina are bracing for hard times. Later this month, the country's senate is expected to approve a 2017 budget that would deal a crippling blow to research. Researchers and students have been staging protests since news of the pending cuts broke last month. When Argentine President Mauricio Macri took office in December 2015, he vowed to double the share of spending on science and technology in the government's budget from 0.7% to 1.5%. But, faced with an economic downturn, the government intends to cut the science and technology budget by $198 million, to $2.1 billion in 2017—an 8.5% decrease. Argentina's National Scientific and Technical Research Council (CONICET) will have to devote 96% of its $655 million budget next year to salaries for researchers and scholars, leaving just $26 million for research projects, lab equipment, and scholarships. "It is not clear whether [CONICET] will have the sufficient funds to open new positions," says Jorge Aliaga, a physicist and former dean of the Faculty of Exact and Natural Sciences at the University of Buenos Aires; Aliaga and others worry the cuts will spark an exodus of young scientists. **http://scim.ag/Argentinabudget**

Harm reduction underused

LONDON | Scientifically proven methods to protect people who inject heroin and other illicit drugs from infections have not been adopted by many of the countries that need them most, suggests a new global report by the U.K.-based nonprofit Harm Reduction International. Nearly 12 million people in 158 countries injected illicit drugs in 2014, according to United Nations estimates, and needle or syringe sharing can widely spread three viruses. More than half of these drug users have hepatitis C, 14% are infected with HIV, and 9% live with the hepatitis B virus. Despite the disease risks, 68 countries do not provide users with clean needles and syringes, states the new report, and 70 do not offer oral opiate substitution drugs like methadone. "Despite the growth of support for harm reduction around the world, criminalisation and prison continue to be the

Published by AAAS

Environmental DNA in whale shark feeding grounds near Qatar reveals their genetic diversity.

DNA in seawater reveals shark numbers

Some giants' secrets can be read in a small sample of water. Assessing the wild populations of many species—such as the whale shark, the world's largest fish—can require using invasive methods, such as collecting tissue from many different animals. But this week in *Nature Ecology & Evolution*, scientists report gleaning a wealth of genetic information about a population of whale sharks from fewer than 30 liters of seawater. The seawater was taken from the sharks' feeding grounds in the Arabian Gulf off the coast of Qatar. From the water, the researchers extracted environmental DNA, or eDNA—traces of shed DNA from, for example, feces, urine, or skin. From the sequenced DNA, the team estimated the whale sharks' population size across a swath of water spanning the tropical Indian Ocean and the western and central Pacific Ocean. In a separate study, another team of researchers collected seawater off the coast of southwest Greenland, and analyzed the eDNA to assess local fish populations. Those data compared well to catch data derived from bottom trawling—suggesting that the eDNA is a good proxy for more invasive methods, particularly in remote regions such as at the poles or in deep waters, the team reported last week in *PLOS ONE*.

CREDITS: (PHOTO) STEFFEN SANVIG BACH, MAERSK OIL RESEARCH AND TECHNOLOGY CENTRE, QATAR; (MAP) AIRVISUAL.COM/EARTH

dominant paradigm of drug control, fueling ill-health and human rights abuses around the world," the report states. "People are continuing to die needlessly, because too many governments are addicted to prohibition."

Surgeon General flags addiction

WASHINGTON, D.C. | Funders should accelerate research on alcohol addiction and other drug abuse disorders, U.S. Surgeon General Vivek Murthy said in a major report issued last week. Better understanding of the neurobiology of addiction at the molecular, cellular, and circuit levels will enable new interventions and answer key questions, stated the report, titled *Facing Addiction in America: The Surgeon General's Report on Alcohol, Drugs, and Health*. Those questions include why some people are more likely to misuse substances and what makes certain individuals especially vulnerable to stress-induced relapse. The report also urges scientists to launch prospective, longitudinal studies illuminating how adolescent substance abuse affects brain structure and function. It emphasizes that addictions, like other chronic disorders such as diabetes, can be effectively treated with medications, behavioral treatments, and changes to lifestyle, but notes that only about one in 10 addicts receives specialized treatment. In 2015, 66.7 million Americans reported binge drinking in the previous month, and 27.1 million used illegal drugs or misused prescription drugs.

Air pollution, in real time

BEIJING | Prompted by concerns over how Beijing's notoriously noxic air was affecting his family, in 2015 data scientist Yann Boquillod founded AirVisual Earth (http://airvisual.com/earth), a social enterprise project that draws on measurements from more than 8000 governmental and citizen-scientist monitoring stations worldwide, as well as from satellite data, to visualize global air pollution in real time. The AirVisual Earth 3D interactive globe shows color-coded concentrations of PM2.5—airborne particulate matter less than 2.5 microns in diameter that can penetrate deep into the lungs. It also charts prevailing wind patterns. Users can zoom in, tilt, and spin the globe for better viewing. The air pollution visualization was crafted "so

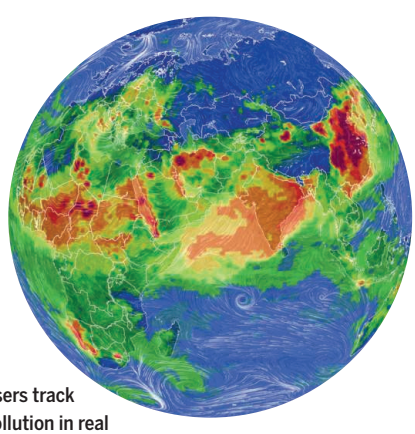

Users track pollution in real time with this interactive visualization tool.

people really understand how bad it is," Boquillod says. He hopes an informed citizenry will pressure governments and communities to clear the air. AirVisual also delivers 3-day air pollution forecasts for 6000 cities to smartphones, and recently began selling low-cost monitors people can use inside their homes or outdoors to track pollution. "People want to share that data," Boquillod says.

Call to protect science in Brexit

LONDON | Since the United Kingdom voted to exit the European Union, the government reassured its own researchers that they will not suffer financially, and told European scientists in the country that they will not be evicted. But last week, a parliamentary committee warned that this reassurance is not enough. The needs of research should be at the center of "Brexit" negotiations, said the House of Commons Science and Technology Committee in its new report. The report stated that the new Department for Exiting the European Union should appoint a chief scientific adviser to keep negotiations focused on issues including funding, personnel, collaboration, regulation, and facilities. Whatever the future immigration policy, the report says, "researcher mobility is a crucial component of the UK's successful research and science sector," and the government must "articulate an ambitious vision for science." That would include using this week's midyear budget statement to raise spending on R&D to 3% of gross domestic product, up from the current 1.7%.
http://scim.ag/Brexitscientists

NEWSMAKERS

Three Qs

The internet isn't the same to all people; some governments restrict or hide certain content, from protest movements to pornography. That has given rise to a new field of research: the science of censorship, which studies this online game of cat and mouse. To learn more, *Science* talked with **Phillipa Gill**, a computer scientist at the University of Massachusetts in Amherst, co-chair of last week's Internet Measurement Conference in Santa Monica, California.

Q: Is some censorship ethical?
A: Most people agree that something like child pornography should be blocked. But there needs to be transparency in censorship. Internet users should know what is being blocked and be able to decide if that's OK or not.

Q: How do you detect the blocking of websites?
A: [My main project is] a platform called ICLab—for Information Controls Lab. We've put it onto the Raspberry Pi [the tiny, cheap computer developed at the University of Cambridge in the United Kingdom]. People around the world—Iran, Turkey, Yemen—plug it into their networks. ICLab does web requests [to see whether sites are blocked or redirected]. … And it also captures data packets and looks at their headers to see if anything is getting injected. Then all that information comes back to us over the internet.

Q: Finding any surprises?
A: Some of the censoring in Iran isn't filtering by the government. It's often servers in the U.S. [that] are restricting access for Iranians, possibly due to sanctions. … A lot of the research [on censorship] so far has focused on the Middle East, for example during the Arab Spring. But U.S. companies are filtering [based on people's geographic location], too.

BY THE NUMBERS

60°

Shift in Pluto's rotation as a result of a large mass of flat, nitrogen ice in a basin on its surface called Sputnik Planitia. The shift, called true polar wander, took place over millions of years (*Nature*).

43%

Fraction of carbon dioxide emissions due to cement production that is ultimately reabsorbed by the cement (*Nature Geoscience*).

1277

Number of coprolites in the world's largest fossilized feces collection, with sources ranging from dinosaurs to insects (*Guinness World Records 2017*).

Recent rules that impose tighter requirements on offshore drilling operations, such as this one in the Gulf of Mexico, could be canceled.

PHOTO: REUTERS/GERALD HERBERT/POOL

U.S. POLICY

Republicans ready a regulatory rollback

Seldom-used law will give Trump, Congress free rein to cancel scores of recent rules

By **David Malakoff**

Get ready for a regulatory reckoning. President-elect Donald Trump and a Republican Congress are poised to erase scores of science-rooted regulations and directives issued by President Barack Obama and his administration. Likely targets include rules and executive orders that aim to reduce greenhouse gas emissions, require agencies to consider climate change as they make policy, protect sensitive environments from energy development, and improve public health.

Many will take time to undo, but a seldom-used law will enable Congress to make quick work of some. The same law could have consequences that far outlast a Trump presidency, because it lets Congress bar agencies from subsequently issuing rules that are "substantially the same" as those it kills.

Environmental advocates and others are bracing for "a concerted effort to replace evidence-based policymaking, grounded in science and technical expertise, with purely political decisions," says Andrew Rosenberg, director of the Center for Science and Democracy at the Union of Concerned Scientists in Boston.

But speaking broadly about plans to trim federal regulation, Representative Paul Ryan (R–WI), the speaker of the House of Representatives, says his party and Trump just want to cut job-killing red tape and "lift the oppressive weight of the regulatory state."

At issue are the 2000 to 3000 regulations that federal agencies issue every year (which typically carry the weight of law), as well as some 200 Obama executive orders and presidential memoranda (which carry less weight because they can be rescinded by another president). Most aren't controversial. But a few dozen orders, memoranda, and so-called major regulations—those estimated to impose costs of more than $100 million per year—have sparked fierce opposition. Automakers and unions have decried major recent regulations that tighten emissions standards on trucks, for example, and energy companies have opposed a suite of rules that limit greenhouse gas emissions from extraction operations and power plants, and put new controls on offshore drilling.

Experts say a Trump administration will not be able to rapidly dismantle many of the rules it dislikes. "Regulations that are already in place are very hard to change … it can take years," says Susan Dudley, director of the Regulatory Studies Center at George Washington University in Washington, D.C. But thanks to an obscure law, the Congressional Review Act (CRA), the next Congress will be able to erase one set of regulations quickly: the roughly 150 major rules the Obama administration has issued since May.

The CRA was crafted by former Representative Newt Gingrich (R–GA)—now a top Trump ally—in the 1990s. It gives lawmakers 60 working days to review new rules. They can vacate a rule with simple majority votes in both the Senate and House. (Last week, the House voted to revise the CRA to allow lawmakers to vacate multiple rules in a single vote, but it is not clear whether the Senate will go along.) If a president agrees, the CRA also bars agencies from writing a similar rule in the future without explicit approval from Congress. "You are not just rolling the regulation back, but almost putting a permanent injunction on it," says policy specialist Amit Narang of Public Citizen in Washington, D.C.

In the 20 years since the CRA was enacted, the threat of a presidential veto has generally made the law irrelevant. But the election of Trump and a Republican Congress opens a rare window for expansive CRA use. Several dozen rules are at high risk, Congress watchers say, including regulations on fracking waste, Arctic drilling, school nutrition standards, and electronic cigarettes. A much-debated rule on who gets paid for working overtime, which applies to postdoctoral students who conduct much of the nation's science, might also be vulnerable, as will any rule the Obama administration issues later this year. The current White House might even decide against issuing some final rules, in order to prevent Congress from using the CRA to prevent future regulation.

In the meantime, Trump advisers have already promised that he will move quickly to rescind Obama executive orders and memoranda on climate change, several of which order agencies and the military to put the issue at the center of their planning efforts. ■

Popocatépetl, a volcano near Mexico City, may warn of its eruptions in its gassy belches.

VOLCANOLOGY

Gas changes signal eruptions

Shifting gas mix warns that magma is on the rise

By **Julia Rosen**

Last month, researchers from the National Autonomous University of Mexico hoped to reach the top of Popocatépetl, a 5400-meter-tall volcano near Mexico City, to install monitoring equipment at its summit crater. But El Popo, as locals call it, rebuffed them with ash and belches of acrid gas—precisely what the scientists wanted to measure. They settled for installing the sensor lower down the mountain, and hope to move it higher next year. The goal is to measure just what—and how much—El Popo has been smoking, because the fumes may hold a promising way to forecast eruptions.

A growing body of monitoring data suggests that a sharp jump in the ratio of carbon to sulfur gases emanating from a volcano can provide days to weeks of warning before an impending outburst. The latest evidence comes from three recent studies, focusing on volcanoes monitored as part of the Volcano Deep Earth Carbon Degassing (DECADE) initiative, managed by the Carnegie Institution for Science in Washington, D.C. They offer hope that geochemical monitoring of gases could someday join the two geophysical mainstays of forecasting: tracking the swelling of Earth's surface and the rise in earthquakes that typically precede eruptions. "It's statistically robust as a forecasting tool," says Tobias Fischer, a volcanologist at the University of New Mexico in Albuquerque, and chair of the DECADE project.

The idea of sniffing out restlessness in volcanic fumes has been around for decades. For instance, a sharp rise in sulfur emissions helped scientists anticipate the 1991 eruption of Mount Pinatubo in the Philippines. Scientists have also keyed in on the carbon-to-sulfur (C-S) ratio in volcanic gases as a particularly helpful metric. In principle, it can signal when a fresh injection of magma is rising from deep in the crust—a prelude to an eruption.

The ratio changes because carbon dioxide (CO_2) dissolved in rising magma bubbles out at depths of 10 kilometers or more, as the pressure drops. Sulfur-rich gases, in contrast, stay in solution up to shallower depths. A spike in the ratio can thus provide warning that a new batch of magma has risen above a deep threshold. A subsequent drop in the C-S ratio could indicate that the magma has climbed further, to depths where sulfur gases are released, but Fischer says this hasn't been observed enough to be reliable.

Despite the simple mechanism, establishing a clear link between the ratios and eruptions requires constant monitoring. Historically, researchers just bottled a few gas samples during a visit to a volcano or used airplanes or remote-sensing tools to watch a volcano for several days or weeks, says Christoph Kern, a physicist with the U.S. Geological Survey in Vancouver, Washington. Either way, Kern says, it was hard to catch an eruption in the act.

But that changed in the early 2000s, when scientists began to develop new devices that could be left on volcanoes to make continuous measurements and transmit the data to researchers. They were solar powered, hardy enough to survive the elements, and cheap enough to risk sacrificing in an eruption. "They're essentially expendable," says Marie Edmonds, a volcanologist at the University of Cambridge in the United Kingdom.

Italian scientists were the first to deploy these instruments at volcanoes like Etna and Stromboli, and they began to notice changes in the C-S ratio in the days and hours prior to eruptions. Since then, U.S. and Japanese geologists have installed instruments at a handful of volcanoes in those countries, and the DECADE project has added them at nine more around the world, including El Popo. Overall, changes in C-S gas ratios seem to be a powerful portent, Fischer says. "Now, we're seeing it at many different volcanoes."

Perhaps the clearest illustration comes from Turrialba in Costa Rica, a volcano that poses a threat to the city of San José, 30 kilometers to the west. Maarten de Moor, a researcher at the Volcanic and Seismic Observatory of Costa Rica, helped install gas sensors on Turrialba in early 2014, just in time for the volcano to start erupting. He led a study, published in the *Journal of Geophysical Research* in August, reporting sharp increases in the C-S ratio of gases a few weeks before each outburst over two eruption cycles (see chart, left). "What we've seen is quite mind-blowing," he says. "These signals are eye-opening."

But for monitoring gas ratios to become a widely used forecasting tool, researchers will need to understand many complicating

A whiff of future eruptions

Spikes in gas ratios occur just days before eruptions at Turrialba, a volcano in Costa Rica.

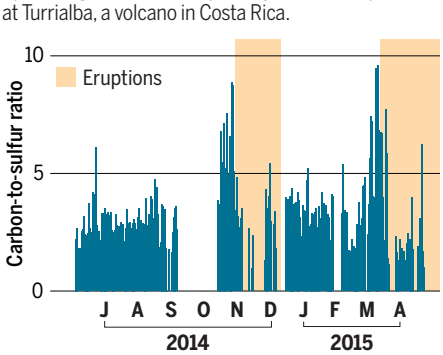

CREDITS: (PHOTO) ATONALTZIN/ISTOCK; (GRAPHIC) J. YOU/*SCIENCE*; (DATA) TURMOIL AT TURRIALBA VOLCANO (COSTA RICA). MAARTEN DE MOOR *ET AL.*, 2016

factors, says Clive Oppenheimer, a volcanologist at the University of Cambridge. "The interpretation of gas chemistry, particularly for the purposes of forecasting, is not an exact science," he says. "Very far from it."

At Turrialba, for instance, there were different sulfur gases in the mix. Sulfur dioxide (SO_2) gas from the magma interacted with underground water to produce hydrogen sulfide during the first eruptive episode, but not the second. De Moor says these observations could indicate that the water eventually boiled off, or that new volcanic conduits formed, bypassing the water reservoirs. At Poás, another Costa Rican volcano, the summit crater contains an acid lake that normally absorbs the SO_2 percolating through it but allows the CO_2 to pass through unimpeded—keeping the C-S ratio relatively high even when an eruption isn't imminent. But DECADE's monitoring efforts have revealed that, in the days before an eruption at Poás, the emissions of sulfur gases spike, exceeding the lake's ability to scrub out the sulfur and causing the C-S ratio to plummet. It's the opposite signal from the one seen at places like Etna and Turrialba, but it's equally reliable, Fischer says.

Satellites could theoretically help researchers monitor many of the world's 550 historically active volcanoes from orbit. Instruments aboard NASA's Terra satellite, for instance, can already measure volcanic sulfur emissions reasonably well. But researchers are still working to measure SO_2 and CO_2 at the same time, and measuring point sources of CO_2 is challenging because of high background levels in the atmosphere. Even a big CO_2 burp from a volcano only increases the concentration measured by satellites by less than a percent, says Florian Schwandner, a geochemist at NASA's Jet Propulsion Lab in Pasadena, California.

For now, the scientists who want to explore the forecasting power of the C-S ratio must wait for ground-based monitors to capture more eruptions. And maintaining these sensors can be a hassle, De Moor says. Even small dustings of ash can cover up solar panels or damage electronics. That's what caused a sensor on Turrialba to stop transmitting data in May, forcing De Moor to visit once a week to download it in person—sometimes in dangerous conditions. But he says he's always careful, and tries to remember a bit of wisdom passed down from Fischer, his Ph.D. supervisor, about taking risks in the name of science. "You are going to make more contributions if you actually survive this." ■

Julia Rosen is a journalist based in Portland, Oregon.

ARCHAEOLOGY

Catching ancient maize domestication in the act

5000-year-old Mexican cobs offer a detailed genetic snapshot of the partly domesticated grain

By **Jessica Boddy**

It wasn't easy to make a meal of teosinte, a grass that was the ancient precursor to maize. Each cob was shorter than your little finger and harbored only about 12 kernels encased in rock-hard sheaths. But in a dramatic example of the power of domestication, beginning some 9000 years ago people in Mexico and the U.S. Southwest transformed teosinte into the many-kerneled maize that today feeds hundreds of millions around the world.

Researchers had already identified a handful of genes involved in this transformation (*Science*, 2 June 2006, p. 1318). Now, studies of ancient DNA by two independent research groups show what was happening to the plant's genes mid-domestication, about 5000 years ago. The snapshot reveals exactly how the genetics changed over time as generations of people selected plants with their preferred traits.

"These results sharpen the focus of what we know at this early period," says Michael Blake, an anthropologist at the University of British Columbia in Vancouver, Canada, who was not involved in the work. "They have implications for understanding later developments in maize domestication and help us to see what people were selecting for at the time."

The first glimpses of maize domestication came in the 1960s, when esteemed U.S. archaeologist Richard MacNeish excavated at caves in Mexico's Tehuacán Valley, a center of early Mesoamerican agriculture. In the dry, dark environment there, he found tiny, well-preserved maize cobs dated to roughly 5300 years ago and harboring only 50 kernels each, compared with the 1000 on modern cobs.

Nearly 60 years later, after the advent of modern sequencing tools, geneticist Jean Philippe Vielle-Calzada at the Center for Research and Advanced Studies of the National Laboratory of Genomics for Biodiversity in Irapuato, Mexico, and his colleagues wanted to find out which genes the ancient domesticators had unwittingly been selecting. But he worried that MacNeish's specimens, now in museums, might have been damaged by handling or improper storage. So he and his team decided to go back to the caves in Tehuacán Valley. Macneish had died, but one of his former students, Angel Garcia Cook, served as guide. "He had all the maps, he knew where to dig," Vielle-Calzada says. "He went back with us at 73 years old. When he went the first time he was 21."

The team discovered several new specimens, dated to about 5000 years ago, from

Genes show that this 5300-year-old maize cob from a museum was half-domesticated: It had modern, sweet-tasting kernels, but they would have dropped easily off the cob before harvest.

PHOTO: BRUCE D. SMITH/SMITHSONIAN

San Marcos cave. They applied shotgun sequencing to three cobs, extracting DNA and breaking it up into short fragments for sequencing. Computer software then reassembled these DNA snippets, eventually reconstructing more than 35% of the ancient maize genome.

Vielle-Calzada's team identified eight genes influencing key traits, as they wrote in the *Proceedings of the National Academy of Sciences* this week. The cobs carried the modern variants of *tb1*, which simplified the plant's branching for easier harvest, and *bt2*, which helped boost the starch content and sweetness of the kernels. But the cobs had the teosinte variant of *tga1*, which encloses the kernels in those hard sheaths—a sign that domestication was only partial.

Meanwhile, archaeologist Nathan Wales of the University of Copenhagen and his colleagues discovered MacNeish's original samples, stored for 60 years in a museum in Andover, Massachusetts. He and his colleagues shotgun sequenced the genome of a 5300-year-old cob called Tehuacan162.

Wales's team was able to sequence 21% of this cob's genome. Their results confirmed and complemented those of Vielle-Calzada's team. The museum cob also had modern variants of *td1* and *bt2*, as reported in *Current Biology* last week. But Tehuacan162 also had a more modern variant of the gene *tga1*, which partly released kernels from their rigid shells, making them easier to eat. Wales's team also found a teosinte gene not seen by the Mexican team: *zagl1*, which makes kernels fall from the cob very easily. That's useful for wild plants spreading their seeds, but frustrating for humans trying to harvest them. These differences may reflect the fact that Tehuacan162 came from a different population of maize, and show that domestication was still in progress in the valley, the researchers say.

Vielle-Calzada was shocked at the teams' similar results. "I'm really amazed to see how convergent the results are," he says. "This is unusual in paleogenomics where it's difficult to get good data from old DNA. This is encouraging."

Robert Hard, an archaeologist at the University of Texas in San Antonio, agrees: "It's remarkable how these studies support each other," he says. That's a good sign that future sequencing can fill in more details, he says. "It's really important that we recognize the significance of transformations in maize," Blake says, adding that knowledge of how certain traits helped maize adapt to drought and disease in the past could help save it from disasters in the future. ■

With reporting by Lizzie Wade.

GEOPHYSICS

Graveyard of cold slabs mapped in Earth's mantle

Resurrected tectonic plates yield visions of a lost planet

By **Paul Voosen**

Earth has a bad habit of erasing its own history.

At intersections of tectonic plates worldwide, slabs of ocean crust dive into the mantle, part of the continuous cycle that not only drives the continents' drift, but also fuels the volcanism that builds up island chains like Japan and mountains like the Andes. The disappearance of these slabs, called subduction, makes it difficult to reconstruct oceans as they existed hundreds of millions of years ago, as well as the mountains flanking them. "Every day, we're losing geologic information from the face of the Earth," says Jonny Wu, a geologist at the University of Houston in Texas. "It's like losing pieces of broken glass as you're trying to put it together again."

But geoscientists have begun to pick up these pieces by peering into the mantle itself, using earthquake waves that pass through Earth's interior to generate images resembling computerized tomography (CT) scans. In the past few years, improvements in these tomographic techniques have revealed many of these cold, thick slabs as they free fall in slow motion to their ultimate graveyard—heaps of rock sitting just above Earth's molten core, 2900 kilometers below.

Now, the complete x-ray of Earth's interior is coming into focus. Next month, at a meeting of the American Geophysical Union in San Francisco, California, a team of Dutch scientists will announce a catalog of 100 subducted plates, with information about their age, size, and related surface rock records, based on their own tomographic model and cross-checks with other published studies. "Step by step we went deeper and deeper, older and older," says Douwe van Hinsbergen, a geologist at Utrecht University in the Netherlands, who led the project along with Utrecht geologists Douwe van der Meer and Wim Spakman.

This "atlas of the underworld," as they call it, holds the ghosts of past geography. By rewinding the clock and bringing these cataloged slabs back to the surface, scientists can figure out the sizes and locations of ancient oceans. Moreover, they can locate

Atlas of the underworld

A catalog of 100 slabs buried in Earth's mantle shows their size, age, and former positions near the surface.

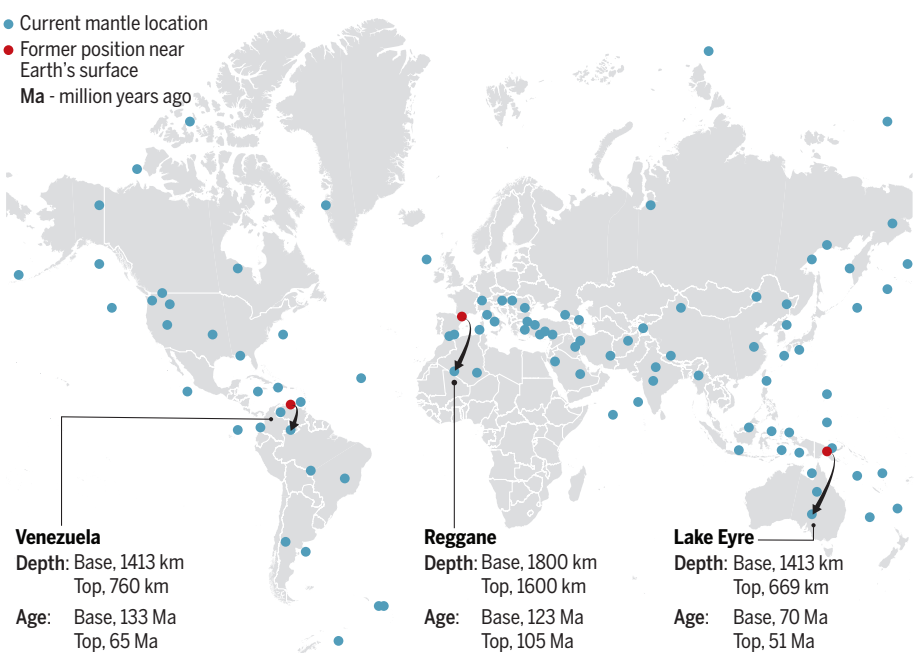

CREDITS: (MAP) J. YOU/*SCIENCE*; (DATA) VAN HINSBERGEN/VAN DER MEER/SPAKMAN/UTRECHT UNIVERSITY

where the sinking slabs would have triggered melting, releasing blobs of magma that rose into the crust and drove volcanism. That has helped earth scientists pinpoint where ancient mountains rose and later eroded away, their traces visible only in unexplained rock records. "It's a pretty exciting time to be able to pull all of these pieces together," says Mathew Domeier, a tectonic modeler at the University of Oslo.

That has only recently become possible, as the underlying technique, mantle tomography, is plagued with uncertainties. It relies on millions of seismic waves received by sensors scattered unevenly around the world. Waves with faster arrival times are assumed to have passed through the colder rock of subducted slabs. But seismometer coverage is patchy; earthquakes—the sources of the seismic waves—don't occur everywhere; and the waves get fuzzier as they pass near the core or travel long distances. "Very often for regions that have the most interesting structures, you have the most uncertainty," says Ved Lekic, a tomographer at the University of Maryland in College Park.

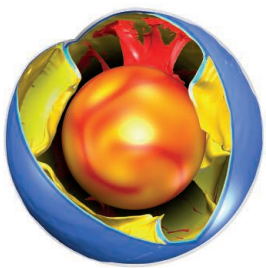

Models show slabs of ocean crust (yellow) falling to Earth's core.

Academic groups around the world use more than 20 models to interpret tomographic data, and their pictures of the mantle and its structures often conflict, says Grace Shephard, a postdoc at the University of Oslo. In the coming months, she will publish a comparison of 14 different models that will assess which slabs seem most likely to be real. Her results could cast doubt on some of the slabs in the Utrecht atlas. But the image of Earth's interior is becoming more believable, thanks to improved computing power and such intercomparison projects.

By now the picture of lost plates is precise enough for scientists to try rewinding the clock, reconstructing vanished worlds. In earlier tomography, the plunging slabs looked like blobs in a lava lamp. But as the models have improved, the slabs in the upper mantle have been revealed to be stiff, straight curtains, says John Suppe, who heads the Center for Tectonics and Tomography at the University of Houston. The images make it clear that as they plunge, the 500-kilometer-thick slabs flex but don't crumple—and that has made it easier for Suppe and others to unwind them. "We're finding these plates unfold fairly easily, and they're not that deformed," Suppe says.

These slab-driven reconstructions are calling into question plate movements inferred from ancient oceanic crust that was scraped off and preserved on the continents, Suppe says. "Almost everywhere we've looked at this," Suppe says, "what we find in the mantle isn't exactly what would be predicted."

The reconstructions are also resurrecting mountains that had been lost to time. For example, in a study published several months ago, Wu and Suppe reconstructed the travels of 28 slabs to recreate the Philippine Sea as it was more than 50 million years ago. Beyond identifying what appears to be a previously unknown piece of ocean crust, they predicted that as one of their paleoplates plunged into the mantle, it threw up a large chain of volcanoes that eventually collided with Asia. That convulsive process could explain mysterious folded rocks in Japan and beneath the East China Sea.

Similarly, slabs beneath North America have helped bring that continent's history of mountain building into clearer focus. By rewinding the clock for some of them, Karin Sigloch, a geophysicist at the University of Oxford in the United Kingdom, showed that North America's western mountain chains, including the Rockies, likely formed between 200 million and 50 million years ago when several small plates were subducted beneath the continent, plastering multiple volcanic archipelagos against the landmass.

Van Hinsbergen and his Utrecht peers hope their comprehensive atlas of slabs will make it possible to reconstruct a fuller picture of ancient geography. In 2012, they used slab tomography to constrain the longitude of volcanic island arcs that 200 million years ago dotted the ocean surrounding the Pangea supercontinent. Two years later they used their global model to estimate the number of subduction zones that would have been active over the past 250 million years, along with the amount of carbon dioxide (CO_2) that subduction-related volcanoes would have emitted. The estimate closely matched geologic proxy records for atmospheric CO_2 over the same period. And earlier this year, Van Hinsbergen published a study in *Science Advances* with Lydian Boschman, a graduate student, that identified several slabs that may have played a role in the birth of the Pacific Ocean. "We have done it," Van Hinsbergen says. "If this was all nonsense, it is really quite a coincidence."

Even with these new techniques, which Suppe together calls "slab tectonics," the mantle's memory of ocean slabs only stretches back 250 million years—the time it takes for one to fall to the bottom of the mantle and be fully recycled. Beyond that, Earth continues to cover its tracks. ■

IMAGE: FABIO CRAMERI

NEUROSCIENCE

Rogue protein's partners offer hope in Parkinson's disease

Two receptor molecules may offer targets for drugs

By **Meredith Wadman**, *in San Diego, California*

Nine years ago, an astonishing observation challenged the then-accepted belief that in Parkinson's disease, brain cells deteriorate on their own, independent of their neighbors. Instead, it suddenly appeared that a misfolded protein spreads from brain cell to brain cell, like an infection. This radical idea, which sparked comparisons to the infectious proteins called prions that cause brain diseases such as kuru, is now largely embraced. It may also point to new approaches to treating the progressive and ultimately fatal movement disorder, which afflicts more than 10 million people.

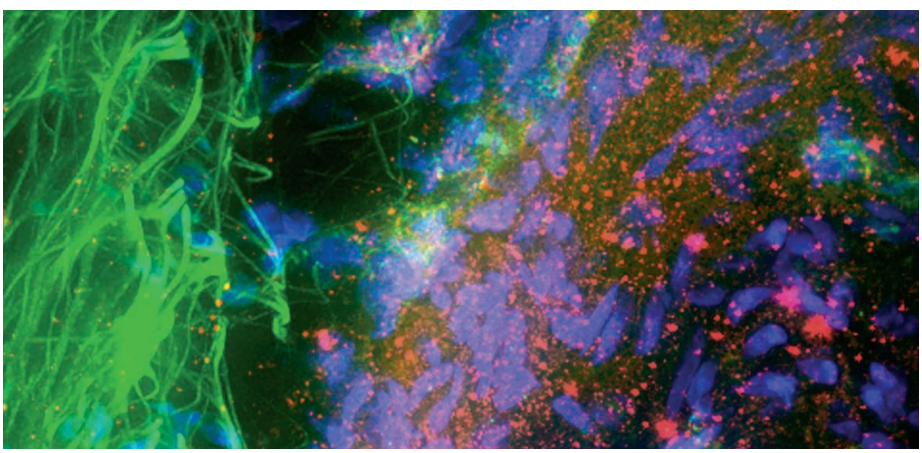

In brain tissue from people with Parkinson's disease, α-synuclein (red) builds up in and around neurons (blue).

Two groups, including one presenting at the Society for Neuroscience conference here last week, now report identifying receptors that bind the aberrant protein on the surface of the cell. The findings could illuminate how a disastrous migration of the rogue protein, α-synuclein, occurs—and offer novel, if still distant, drug targets. "Anything that slows or reduces the uptake of misfolded α-synuclein into neurons could potentially slow disease progression," says Patrik Brundin, a neuroscientist at the Van Andel Institute in Grand Rapids, Michigan.

Parkinson's disease results from the degeneration of dopamine-making neurons, which first causes motor impairments, including tremor and muscle rigidity. Cognitive decline and dementia follow. Deep brain stimulation can relieve the motor symptoms for a time, and the drug levodopa can initially replace the missing dopamine, but neither treatment stops disease progression.

In 2007, a startling new clue came from the brains of elderly people who had Parkison's and died more than a decade after receiving experimental transplants of healthy fetal neurons. Some of those much-younger cells were found to be riddled with the same pathological version of α-synuclein as each host's diseased neurons. The strong implication was that the aberrant protein was spreading from affected cells to healthy ones—seeding more of itself in each—not arising independently in individual cells.

Some researchers question whether the spread of the rogue protein is a cause rather than an effect of Parkinson's disease. But the evidence that it does spread continues to accumulate. At the neuroscience meeting, for example, one group reported that α-synuclein could spread not only among neurons, but also among brain cells called astrocytes. Other findings buttressed a hypothesis that the clumps of the misfolded protein first colonize the gut before traveling along a major nerve to the brain.

Research teams have also begun probing the molecular mechanisms of α-synuclein's ability to spread. At the meeting, Ravindran Kumaran, a neuroscientist in the laboratory of Mark Cookson at the National Institute on Aging in Bethesda, Maryland, described a cell membrane–bound protein that may help explain how toxic aggregates, called fibrils, of α-synuclein are taken into brain cells after being released from neighboring cells. Kumaran and his colleagues, with help from the National Institutes of Health's translational medicine center, systematically knocked out every gene in a human cervical cancer cell line, one by one, and measured the effects on synthetic α-synuclein uptake by the cells. When they turned off a little-known gene called *TM9SF2*, cells took up 75% less of the fibrils. "The effect is huge," says Vincent Seutin, a neurophysiologist at the University of Liège in Belgium who studies dopaminergic neurons. "Statistically it sounds very robust."

Kumaran then discovered that *TM9SF2* is in the top 3% of all genes expressed within the brain. Furthermore, its activity is highest in the substantia nigra and other brain regions that drive many symptoms of Parkinson's disease. The scant data on the protein coded for by *TM9SF2* suggest it is a channel or transporter, importing molecules into cells. Kumaran and his colleagues are now preparing to test whether it affects α-synuclein uptake in cultured neurons from humans and mice.

Another cell surface protein described in the 30 September issue of *Science* may have similar potential. Called LAG-3—it's encoded by lymphocyte activation gene 3—it is widely expressed in immune system cells and, at lower levels, in neurons. Ted Dawson, a neuroscientist at the Johns Hopkins School of Medicine in Baltimore, Maryland, and colleagues screened hundreds of membrane proteins for those that selectively bind to synthetic α-synuclein fibrils in neurons in culture. LAG-3 bound the fibrils tightly, triggering their uptake and subsequent spread from cell to cell. Mice injected with fibrils of the rogue protein developed Parkinson's-like symptoms and brain aggregates of the misfolded protein, but rodents engineered to lack a working *LAG-3* gene had reduced brain lesions and symptoms.

Still, Dawson says, "It's going to be more complicated than one membrane protein." Knocking out *LAG-3* did not fully eliminate symptoms, he notes. "That says that [α-synuclein] is getting into cells in other ways as well." In that respect, the two molecular findings may complement each other—and other players may yet surface as central to α-synuclein's spread. The hope is that several therapeutics will emerge from these multiple drug targets.

"We are just scratching the surface," Cookson says. "But given we had no candidate [membrane receptors for α-synuclein] a couple of months ago and now we've got more than one—that's why there's some interest and some excitement." ■

PHOTO: ROGER J. BICK & MYA C. SCHIESS/UT HOUSTON MEDICAL SCHOOL/SCIENCE SOURCE

THE WANDERERS

Fossils of the first human ancestors to trek out of Africa reveal primitive features and a brutal way of life

By **Ann Gibbons**, *in Dmanisi, Georgia*

PHOTO: © KEN GARRETT

Published by AAAS

The ancient residents of Dmanisi had brains one- third to one-half the size of modern humans'.

PHOTO: MALKHAZ MACHAVARIANI. © THE GEORGIAN NATIONAL MUSEUM

On a promontory high above the sweeping grasslands of the Georgian steppe, a medieval church marks the spot where humans have come and gone along Silk Road trade routes for thousands of years. But 1.77 million years ago, this place was a crossroads for a different set of migrants. Among them were saber-toothed cats, Etruscan wolves, hyenas the size of lions—and early members of the human family.

Here, primitive hominins poked their tiny heads into animal dens to scavenge abandoned kills, fileting meat from the bones of mammoths and wolves with crude stone tools and eating it raw. They stalked deer as the animals drank from an ancient lake and gathered hackberries and nuts from chestnut and walnut trees lining nearby rivers. Sometimes the hominins themselves became the prey, as gnaw marks from big cats or hyenas on their fossilized limb bones now testify.

"Someone rang the dinner bell in gully one," says geologist Reid Ferring of the University of North Texas in Denton, part of an international team analyzing the site. "Humans and carnivores were eating each other."

This is the famous site of Dmanisi, Georgia, which offers an unparalleled glimpse into a harsh early chapter in human evolution, when primitive members of our genus *Homo* struggled to survive in a new land far north of their ancestors' African home, braving winters without clothes or fire and competing with fierce carnivores for meat. The 4-hectare site has yielded closely packed, beautifully preserved fossils that are the oldest hominins known outside of Africa, including five skulls, about 50 skeletal bones, and an as-yet-unpublished pelvis unearthed 2 years ago. "There's no other place like it," says archaeologist Nick Toth of Indiana University in Bloomington. "It's just this mother lode for one moment in time."

Simple stone flakes, like those removed from this core, enabled the Dmanisi hominins to butcher meat.

Until the discovery of the first jawbone at Dmanisi 25 years ago, researchers thought that the first hominins to leave Africa were classic *H. erectus* (also known as *H. ergaster* in Africa). These tall, relatively large-brained ancestors of modern humans arose about 1.9 million years ago and soon afterward invented a sophisticated new tool, the hand ax. They were thought to be the first people to migrate out of Africa, making it all the way to Java, at the far end of Asia, as early as 1.6 million years ago. But as the bones and tools from Dmanisi accumulate, a different picture of the earliest migrants is emerging.

By now, the fossils have made it clear that these pioneers were startlingly primitive, with small bodies about 1.5 meters tall, simple tools, and brains one-third to one-half the size of modern humans'. Some paleontologists believe they provide a better glimpse of the early, primitive forms of *H. erectus* than fragmentary African fossils. "I think for the first time, by virtue of the Dmanisi hominins, we have a solid hypothesis for the origin of *H. erectus*," says Rick Potts, a paleoanthropologist at the Smithsonian Institution's National Museum of Natural History in Washington, D.C.

This fall, paleontologists converged in Georgia for "Dmanisi and beyond," a conference held in Tbilisi and at the site itself from 20–24 September. There researchers celebrated 25 years of discoveries, inspected a half-dozen pits riddled with unexcavated fossils, and debated a geographic puzzle: How did these primitive hominins—or their ancestors—manage to trek at least 6000 kilometers from sub-Saharan Africa to the Caucasus Mountains (see map, p. 960)? "What was it that allowed them to move out of Africa without fire, without very large brains? How did they survive?" asks paleoanthropologist Donald Johanson of Arizona State University in Tempe.

They did not have it easy. To look at the teeth and jaws of the hominins at Dmanisi is to see a mouthful of pain, says Ann Margvelashvili, a postdoc in the lab of paleoanthropologist Marcia Ponce de León at the University of Zurich in Switzerland and the Georgian National Museum in Tbilisi. Margvelashvili found that compared with modern hunter-gatherers from Greenland and Australia, a teenager at Dmanisi had dental problems at a much younger age—a sign of generally poor health. The teen had cavities, dental crowding, and hypoplasia, a line indicating that enamel growth was halted at some point in childhood, probably because of malnutrition or disease. Another individual suffered from a serious dental infection that damaged the jawbone and could have been the cause of death. Chipping and wear in several others suggested that they used their teeth as tools and to crack bones for marrow. And all the hominins' teeth were coated with plaque, the product of bacteria thriving in their mouths because of inflammation of the gums or the pH of their food or water. The dental mayhem put every one of them on "a road to toothlessness," Ponce de León says.

They did, however, have tools to supplement their frail bodies. Crude ones—but lots of them. Researchers have found more than 15,000 stone flakes and cores, as well as more than 900 artifacts, in layers of sediments dating from 1.76 million to 1.85 million years ago. Even though *H. erectus* in East Africa had invented hand axes, part of the so-called Acheulean toolkit, by 1.76 million years ago, none have been found here at Dmanisi. Instead, the tools belong to the "Oldowan" or

The trail of the little people

Short and small-brained, even compared with classic *Homo erectus,* the Dmanisi people or their immediate ancestors emerged from Africa and migrated thousands of kilometers into Asia.

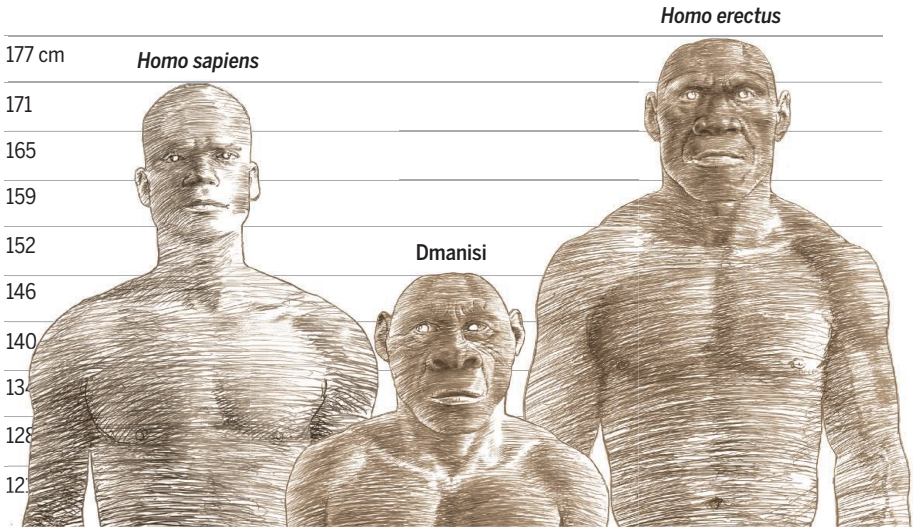

To the ends of earth

By following a trail of stone tools and fossils, researchers have traced possible routes for the spread of early *Homo* out of Africa to the far corners of Asia, starting about 2 million years ago.

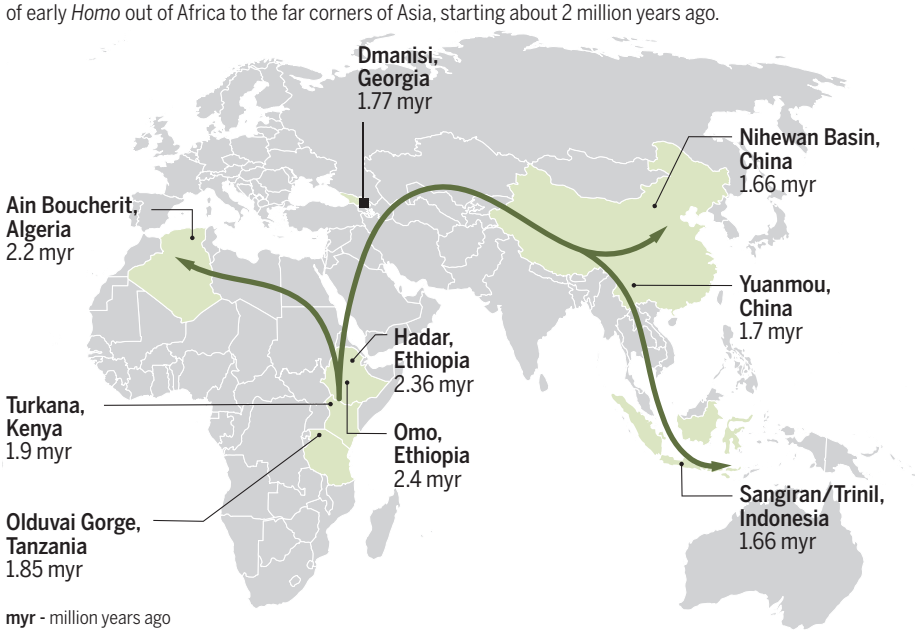

myr - million years ago

"Mode 1" toolkit—the first tools made by hominins, which include simple flakes for scraping and cutting and spherical choppers for pounding. The Oldowan tools at Dmanisi are crafted out of 50 different raw materials, which suggests the toolmakers weren't particularly selective. "They were not choosing their raw material—they were using everything," says archaeologist David Zhvania of the Georgian National Museum.

That simple toolkit somehow enabled them to go global. "They were able to adjust their behavior to a wide variety of ecological situations," Potts says. Perhaps the key was the ability to butcher meat with these simple tools—if hominins could eat meat, they could survive in new habitats where they didn't know which plants were toxic. "Meat eating was a big, significant change," says paleoanthropologist Robert Foley of the University of Cambridge in the United Kingdom.

Even with their puny stone flakes, "these guys were badass," competing for meat directly with large carnivores, Toth says. At the meeting, he pointed to piles of cobblestones near the entrance of an ancient gully, which suggest the hominins tried to fend off (or hunt) predators by stoning them.

They set their own course as they left Africa. Researchers had long thought that *H. erectus* swept out of their native continent in the wake of African mammals they hunted and scavenged. But all of the roughly 17,000 animal bones analyzed so far at Dmanisi belong to Eurasian species, not African ones, according to biological anthropologist Martha Tappen of the University of Minnesota in Minneapolis. The only mammals not of Eurasian origin are the hominins—"striking" evidence the hominins were "behaving differently from other animals," Foley says.

Perhaps venturing into new territory allowed the hominins to hunt prey that would not have known to fear and flee humans, suggests paleoanthropologist Robin Dennell of the University of Exeter in the United Kingdom. Tappen calls that an "intriguing new idea" but thinks it should be tested. Checking the types of animal bones at other early *Homo* fossil sites out of Africa could show whether the mix of prey species changed when hominins colonized a new site, supporting a "naïve prey" effect.

Whatever impelled them, the migrants left behind a trail of tools that have enabled researchers to trace their steps out of Africa. There, the oldest stone tools, likely fashioned by the first members of early *Homo*, such as small-brained *H. habilis,* date reliably to 2.6 million years ago in Ethiopia (and, possibly, 3.3 million years in Kenya). New dates for stone tools and bones with cutmarks at Ain Boucherit, in the high plateau of northeastern Algeria, suggest that hominins had crossed the Sahara by 2.2 million years ago when it was wetter and green, according to archaeologist Mohamed Sahnouni of the National Centre for Research on Human Evolution in Burgos, Spain. His unpublished results, presented at the Dmanisi meeting, are the earliest evidence of a human presence in northern Africa.

The next oldest tools are those from Dmanisi, at 1.85 million years old. The trail of stone tools then hopscotches to Asia, where Mode 1 toolkits show up by nearly 1.7 million years ago in China and 1.6 million in Java, with *H. erectus* fossils. "We pick up little fractions of a current" of ancient hominin movements, Foley says.

The identity of the people who dropped these stone breadcrumbs is a mystery that has only deepened with study of the Dmanisi fossils. The excavation team has classified all the hominins at the Georgia site as *H. erectus*, but they are so primitive and variable that researchers debate whether they belong in *H. erectus*, *H. habilis*, a separate species, *H. georgicus*—or a mix of all three, who may have inhabited the site at slightly different dates.

A new reanalysis of the Dmanisi skulls presented at the meeting added fuel to this debate by underscoring just how primitive

GRAPHICS: GARVIN GRULLÓN/*SCIENCE*

Now the site of a medieval church, the promontory at Dmanisi has been a crossroads for humans and animals for at least 1.8 million years.

most of the skulls were. Using a statistics-based technique to compare their shape and size with the skulls of many other hominins, Harvard University paleoanthropologist Philip Rightmire found that only one of the Dmanisi skulls—at 730 cubic centimeters—fits "comfortably within the confines of *H. erectus*." The others—particularly the smallest at 546 cc—cluster more closely with *H. habilis* in size.

Nor did the Dmanisi hominins walk just like modern humans. A new analysis of cross sections of three toe bones found that the cortical bone—the dense outer layer—wasn't buttressed in the same way as it is in the toes of modern humans. When these hominins "toed off," the forces on their toes must have been distributed differently. They may have walked a bit more like chimps, perhaps pushing off the outside edge of their foot more, says Tea Jashashvili of the University of Southern California in Los Angeles and the Georgian National Museum.

"If there are so many primitive traits, why are they calling it *H. erectus*?" asks Ian Tattersall, a paleoanthropologist at the American Museum of Natural History in New York City. "People are avoiding the question of what *H. erectus* is. Every time new stuff comes up, they're enlarging the taxon to fit new stuff in." Foley ventures: "I haven't the slightest idea of what *H. erectus* means."

Indeed, *H. erectus* now includes the 1-million-year-old type specimen from Trinil on the island of Java as well as fossils from South Africa, East Africa, Georgia, Europe, and China that span roughly 300,000 to 1.9 million years. "They're putting everything into *H. erectus* over huge geographical distances, essentially spread throughout the whole world, and over a vast number of years," Johanson says.

Yet no other species matches the Dmanisi specimens better, Rightmire says. For example, the shapes of their dental palate and skulls match those of *H. erectus*, not *H. habilis*. And the variation in skull size and facial shape is no greater than in other species, including both modern humans or chimps, says Ponce de León—especially when the growth of the jaw and face over a lifetime are considered.

Though the fossils' small stature and brains might fit best with *H. habilis*, their relatively long legs and modern body proportions place them in *H. erectus*, says David Lordkipanidze, general director of the Georgian National Museum and head of the Dmanisi team. "We can't forget that these are not just heads rolling around, dispersing around the globe," Potts adds. Like Rightmire, he thinks the fossils represent an early, primitive form of *H. erectus*, which had evolved from a *H. habilis*–like ancestor and still bore some primitive features shared with *H. habilis*.

Regardless of the Dmanisi people's precise identity, researchers studying them agree that the wealth of fossils and artifacts coming from the site offer rare evidence for a critical moment in the human saga. They show that it didn't take a technological revolution or a particularly big brain to cross continents. And they suggest an origin story for first migrants all across Asia: Perhaps some members of the group of primitive *H. erectus* that gave rise to the Dmanisi people also pushed farther east, where their offspring evolved into later, bigger-brained *H. erectus* on Java (at the same time as *H. erectus* in Africa was independently evolving bigger brains and bodies). "For me, Dmanisi could be the ancestor for *H. erectus* in Java," says paleoanthropologist Yousuke Kaifu of the National Museum of Nature and Science in Tokyo.

In spite of the remaining mysteries about the ancient people who died on this windy promontory, they have already taught researchers lessons that extend far beyond Georgia. And for that, Lordkipanidze is grateful. At the end of a barbecue in the camp house here, he raised a glass of wine and offered a toast: "I want to thank the people who died here," he said. ■

Fossils and scientists mingle at the Georgian National Museum in Tbilisi.

PHOTOS: (TOP TO BOTTOM) © KEN GARRETT; MIRIAN KILADZE, © THE GEORGIAN NATIONAL MUSEUM

INGENUITY: NEXTGEN'S VISION

Research night owls

We asked young scientists from a variety of fields this question: **"Where are you at 2 a.m.? What do you have to do before you can go to sleep?"** In addition to the many scientists who are up late finalizing grant proposals, lesson plans, and conference presentations, we heard from scientists who track nocturnal species, check specimens hourly, and meet with collaborators across the world. Read some of the most interesting responses below. *Edited by* **Jennifer Sills**

It is 2 a.m., and I am...

It is 2 a.m., and I am studying snowshoe hares in the Yukon Territory, Canada. My study site is just outside Kluane National Park, in the beautiful boreal forest surrounded by some of the tallest mountains in North America. It's a cold night in the middle of winter, and it's dead silent. Although our group of researchers works in pairs, we are usually 100 m apart, and somehow in the night, I still feel isolated. All I can hear is the crunching of snow under my snowshoes. I can see every breath in the light of my headlamp as I make my way through the dark forest.

When I come upon a snowshoe hare in a trap, I transfer the animal into my handling bag, take a seat on the snow, and place the hare in my lap. Snowshoe hares are well adapted to these winter conditions and feel like little heaters on my cold hands. I take several body measurements from the hare and check its ear tag (placed earlier by another scientist). If the hare is one of our targets, I put a GPS collar around its neck. I am examining the role of food in the snowshoe hare cycle, and these GPS collars will provide valuable data on movement and habitat selection between control and fed hares. I also collect fecal samples to measure stress and physiological differences.

We do this work at night because the nocturnal hares are difficult to trap during the day. The work brings many challenges, such as navigating in the dark, doing delicate work with cold fingers, hiking while bundled up like a marshmallow, and most of all, getting ready to leave while everyone else is heading to bed. But even though the work is exhausting, I wouldn't trade it for the world. With the cold, dark, and lonely nights come adorable snowshoe hares, close encounters with lynx, and spectacular northern lights!

Yasmine Nicole Majchrzak

Department of Biological Sciences, University of Alberta, Edmonton, AB T6G 2E9, Canada.
Email: majchrza@ualberta.ca

CREDIT: BENEDETTO CRISTOFANI

It is 2 a.m., and I am in the lab collecting mouse organ samples in tubes, which I freeze in liquid nitrogen for future analyses. I study how specific genes oscillate through a 24-hour period in animals with cancer to understand how internal clock and circadian rhythms are involved in tumor formation. The white lab lights shine, keeping me awake and focused after 2 hours of half-sleep on the couch in the meeting room.

Behind double doors, a colleague uses a noctovisor for night vision as she prepares an experimental animal in total darkness to avoid any light disturbance. When she finishes, we meet in the corridor with the gravity of a military operation to transfer the samples. We do not talk unless we have to discuss the experiment. The mood is quite different from the daylight time points, when an air of enthusiasm permeates the lab.

After 2 hours, the work for this time point is finally done. I walk down the dark corridor, marked by the monotone freezer's hum and blinking light. In 2 hours, I must wake up again for the last, and most exhausting, time point. It is a paradox that I have to disturb my own internal clock to figure out how my experimental animals' clocks work at the molecular level, but I know that our efforts might contribute to the most efficiently timed cancer treatments.

Matúš Soták

Department of Epithelial Physiology, Institute of Physiology, Prague, 14220, Czech Republic.
Email: matus@sotak.info

It is 2 a.m., and I am alone, at the Onsala Space Observatory, on a peninsula along the coast of Sweden. The area is fenced, with restricted access to everyone but authorized scientists and the rabbits, boars, deer, and cows that roam the fields around the buildings. I am using a telescope with a 20-m-diameter steerable dish to observe the radio regime of the spectrum of light. Because I am observing at a different wavelength than visible light, I can observe through clouds, and even during the day. I am observing at night because my source is only visible in the sky at night during this part of the year.

I sit in the control room in front of a big desk with several computer monitors showing different vitals of the operations. Behind me is a rack space with spectrum analyzers and other equipment to interpret the signal the telescope is receiving from space. I am using the telescope to look at the carbon monoxide (CO) gas in a cloud of gas and dust that is forming stars in the outer parts of our galaxy. The telescope is set up to be sensitive to the emissions of the CO molecules in the cloud. It focuses the emission to a small instrument, a receiver at the focal point of the telescope dish. There, the photons are converted to a digital signal that we can then store and analyze on a computer. By moving the telescope around, we can see how the emission from the CO varies with position, essentially mapping it.

The observation time is rather hectic in the beginning; I have to plan everything and calibrate the instrument. Once the telescope is set to observe, there is breathing room to do some other work, get more coffee, and eat something. I have never observed with this telescope before so I have to learn how it works, how to control it, and in what order things have to be activated and calibrated. I also have to be flexible and ready to make adjustments throughout the observations to get the most out of my time with the telescope. Observations are exciting because we are collecting light that has traveled tens of thousands of years to reach us, but it is also exhausting. I hope that by doing this work, I will contribute to the understanding of how stars and planetary systems, perhaps much like our own Sun and Solar System, are formed.

Magnus Vilhelm Persson

Department of Earth and Space Sciences, Chalmers University of Technology, Onsala Space Observatory, Onsala, 439 92, Sweden.
Email: magnpe@chalmers.se

It is 2 a.m., and I am alone, dipping Eppendorf tubes of fruit flies into liquid nitrogen and shaking them until the flies' heads pop off. The tubes sizzle as they crust over with ice crystals. A moment ago, the flies were asleep in a pitch-dark incubator; now, they are bobbing around in a swirling mist of freezing liquid. I reach into the liquid with a long pair of tweezers, fish the tubes out and shake them vigorously. The flies' heads ricochet like little pinballs against the walls of the tube, making a flurry of hollow-ringing clinks. Every hour, I have to collect 20 frozen heads from which I extract genes. By measuring the gene products in the flies' heads as the clock ticks by, I am peering into the actions of the same genes that control our nightly rest.

Eugene L. Q. Lee

Department of Brain and Cognitive Sciences and Department of Biology, Massachusetts Institute of Technology, Cambridge, MA 02139, USA.
Email: ellq@mit.edu

It is 2 a.m., and I am on a research vessel at a marine sampling station about 10 km from the coast of Hong Kong. I am surrounded by the sea. I can hear sounds of water lapping the hull and smell the salty wind. It is a typical summer night: warm and a bit humid. Our vessel is equipped with illuminating devices that provide light for us. We are collecting zooplankton samples from different water depths, and at different time points, by pulling a conical plankton net through the water column. It is exhausting work, requiring us to wake up from naps every 2 to 3 hours to collect more samples. After preserving the samples on board, the target zooplanktons will be counted under a dissecting microscope back in the lab. We can then perform statistical tests to examine whether there is any difference in the zooplankton population size at different water depths and between day and night.

Man Kit Cheung

School of Life Sciences, The Chinese University of Hong Kong, New Territories, Hong Kong.
Email: mkcheung@cuhk.edu.hk

It is 2 a.m., and I am walking into the imaging room of the lab. The lights are off and there are no windows. It would be an

excellent place to sleep if it weren't for the humming sound coming from the large black box on the counter or the immense light emitted by the adjacent computer monitor. This black box is an advanced imaging system that can automatically count the number of live cells in a dish by using special light signals to activate a fluorescent dye added to the sample. I am counting my cells for the sixth and final time today. I load a sample in the machine and wait 15 minutes. I have many dishes of cells to count, so I repeat this process multiple times. I have to force myself to stay awake to ensure that the machine is working correctly.

I develop cancer therapeutics and thus I need to know how quickly or slowly a drug works to kill cancer cells. Therefore, I have to count the cells in the dish using this machine every couple of hours—even if it means staying up late into the night. This is a tedious task but vital to knowing whether a drug will be safe to use in patients. I can't go to sleep until I complete my 12-hour experiment to determine whether my latest drug is working or not. If all goes well, I should see fewer live cancer cells!

Cody Lo

Department of Experimental Therapeutics, University of British Columbia, BC Cancer Research Centre, Vancouver, BC V5Z 1L3, Canada.
Email: codylo94@gmail.com

It is 2 a.m., and I am deep in discussions with colleagues in China and Europe about scientific software on Slack, Skype, and email. The laptop hums, router lights blink yellow and green in the darkness, and my family silently sleeps a few rooms away. Scientific business analysis involves collecting feedback, troubleshooting errors, and spinning up new programs to help chemists make molecules at sites across the globe. The wee hours of the morning are a great time to start these conversations, since my coworkers can begin on a problem and hand it off to me before they leave work. Everyone seems to get more done this way, despite the slight loss of sleep.

Michael A. Tarselli

Novartis Institute for BioMedical Research, Cambridge, MA 02139, USA.
Email: mike.tarselli@novartis.com

It is 2 a.m., and I am bobbing around in a dinghy on the Pacific Ocean with two other scientists. I am wearing an orange survival suit and holding a dip net used to capture seabirds. It is dark all around us, but my eyes have adjusted and I can make out the shape of birds floating on the water nearby, as well as the horizon and bright stars mingled with thin pale clouds overhead. The water is calm and quiet except for a few small waves lapping at the side of our boat. It is quite peaceful, and the distant sound of young seabirds calling to their fathers in their characteristic "mwraaaa" serves as an organic soundtrack to our work.

Just as I start to relax, someone spots a group of birds close enough to try and sneak up on and capture. I sit up, breathe in the cold ocean air, grab hold of a boat handle, and prepare for the engine to rev and zoom up to the unsuspecting birds. The three scientists in the dinghy have to work together in perfect coordination: The driver speeds up quickly, the second person holds a bright spotlight focused on the seabird, and the third person leans over the edge of the boat with a net in hand, ready to scoop the bird gently off the water before it dives below the surface. The driver needs to balance speed and precision, slowing down at just the right moment to allow me to quickly scoop the bird into the net without injuring the bird, damaging the net, or knocking someone overboard. Good communication and a calm demeanor are very important for this small team to work together effectively.

CREDIT: BENEDETTO CRISTOFANI

Once we capture a bird, we attach a satellite transmitter to its back, release it, and then track its movements remotely. I am using the information from satellite telemetry to quantify seabird movements in the northern California Current. Specifically, I'm looking at the patterns of seabird associations with the Columbia River plume, a migration corridor for juvenile salmon leaving the Columbia River. We hope to determine whether predators such as seabirds affect smolt survival.

Elizabeth Phillips

School of Aquatic and Fishery Sciences, University of Washington, Seattle, WA 98195-5020, USA.
Email: emp11@uw.edu

It is 2 a.m., and I am near a stream outside Wu Fong Chi Waterfall Park in the foothills of the Snow Mountain Range in Taiwan. During the spring and summer, the air along the bank of the stream is filled with the mating calls of frogs. My laboratory assistants and I are documenting their characteristics, such as call number, duration, and amplitude. We are wearing long-sleeve shirts with lightweight long trousers and waterproof boots. Our battery-powered headlamps are fitted with red filters to avoid disturbing the frogs.

To avoid causing stress to the frogs, we record their sounds in the field instead of catching them and bringing them to the lab. Our parabolic microphone can focus on the sounds emitted by a particular frog. During mating season, each male frog maintains its own territory, so we have to move around to record the calls made by each individual frog. Poisonous snakes are everywhere along the stream. They come out to hunt frogs by localizing the frogs' calls, and we have to be careful not to step on them to avoid being attacked. Meanwhile, mosquitoes swarm us throughout the night.

Nevertheless, the work is exhilarating. It opens our minds to nocturnal biological activities that we would never experience in the lab. We want to document the mating call in the current environment, because soon a hotel will be built near the park's boundaries. We fear that the hotel guests' nighttime activities could alter the mating calls of the frogs and disrupt their breeding activities. We may use these baseline data to create a mitigation plan in the future.

Hong Young Yan

Department of Oceanography, National Sun Yat Sen University, 80424, Kaohsiung, Taiwan and National Museum of Marine Biology and Aquarium, Checheng, Pingtung, 94450, Taiwan.
Email: hong.young.yan@gmail.com

PHOTO: LAUREN BRENT

Like humans, rhesus macaques are highly social, group-living primates that exhibit variation in social status and patterns of social affiliation. Here, female rhesus macaques solidify their social bonds through grooming interactions. These and other social status–linked behaviors have a causal impact on immune function.

GENE EXPRESSION

Proinflammatory primates

Social subordination induces proinflammatory gene expression profiles

By **Robert M. Sapolsky**[1,2]

If you have the choice, don't be a low-ranking, female rhesus monkey. As with many primates, rhesus social groups feature stable, linear dominance hierarchies. Those at the bottom work harder for their calories, have less access to social support (e.g., grooming), and are more subject to displacement aggression from a dominant individual (*1*). Not surprisingly, primate social subordination can produce adverse health outcomes. Depending on the species, gender, and setting, this includes elevated concentrations of glucocorticoids (the adrenal steroids secreted during stressful situations) and increased rates of hypertension, cardiovascular disease, and reproductive dysfunction (*2*). On page 1041 of this issue, Snyder-Mackler *et al.* (*3*) show that primate social subordination promotes a proinflammatory response. Do the trials, tribulations, and inflammatory states of rhesus monkeys apply to us?

To evaluate how status alters immune function in primates, Snyder-Mackler *et al.* examined 45 captive, unrelated female rhesus monkeys. Studying status–health relations in nonhuman primates brings a clarity that is unavailable in human studies. Status differences in other primates are not confounded by differing rates of smoking, drinking, religiosity, gym memberships, or health insurance. Moreover, the use of captive subjects ensures homogeneity in diet, housing, and veterinary care.

Does low status corrode health, and high status promote it? Snyder-Mackler *et al.* addressed the former with an elegant study design. Groups of five females were maintained for a year, which produced stable, linear dominance hierarchies (based on patterns of threats and displacements). Groups were then reorganized; one new group was composed of previously dominant individuals, one of middle-ranking individuals, and so on. Each new group started with a single individual, and new members were added sequentially. Among rhesus monkeys, each new group member reliably winds up with the lowest rank. Thus, with the two phases of social grouping combined, rank reflected extrinsic demographic factors rather than intrinsic individual traits. The authors then examined the immune regulatory consequences of social status. Rank altered gene expression profiles in circulating immune cells, in a cell type–specific manner. Natural killer cells and helper T cells were most sensitive to status with, remarkably, 1676 and 284 genes, respectively, differentially expressed as a function of rank. Subordination produced a proinflammatory profile of increased expression of genes relevant to lymphocyte proliferation, innate immune responses, and cytokine responsiveness.

Snyder-Mackler *et al.* then examined the same gene expression profiles following an immune challenge. Cultured cells from individual rhesus macaques were incubated with or without lipopolysaccharide (LPS), the powerful Gram-negative bacterial stimulant of inflammation. LPS exaggerated the rank differences in gene expression already uncovered—for example, nearly 3500 genes in natural killer cells were expressed differentially. Examining individual genes and coupling that, in a subset of macaques, with an analysis of open chromatin sites (thus, poised for gene expression) revealed a striking rank difference in signal transduction. LPS binds to Toll-like receptor 4 expressed on immune cells, activating either of two very different cell signaling pathways. One involves the adapter protein myeloid differentiation primary response gene 88

[1]Department of Biological Sciences, Stanford University, Stanford, CA 94305, USA. [2]Institute of Primate Research, National Museums of Kenya, Kenya. Email: sapolsky@stanford.edu

(MyD88), whose activation starts a signaling cascade that ultimately activates the canonical proinflammatory transcription factor nuclear factor κB (NF-κB). The second pathway, mediated by the adapter protein Toll/interleukin-1 receptor domain–containing adapter-inducing interferon (TRIF) culminates in activation of interferon regulatory factors (IRFs), promoting an antiviral gene expression profile. After incubation with LPS, natural killer cells from subordinate females had markedly increased expression of constituents of the MyD88–NF-κB proinflammatory pathway; cells from dominant females showed the opposite.

Snyder-Mackler *et al.* analyzed the behavioral correlates of the immune profile. As expected, subordinate females were harassed the most and groomed the least. Across numerous primate species, both factors roughly equally mediate the relationship between rank and glucocorticoid concentrations (*4*). Among subordinate females, grooming frequency was the much stronger predictor of the rank–immune expression profile. In effect, although the misery of harassment can be enflaming, lacking a shoulder to cry on afterwards is worse.

> ***"Do the trials, tribulations, and inflammatory states of rhesus monkeys apply to us?"***

Thus, social subordination biased individuals toward inflammation, both basally and after an inflammatory challenge (see the photo). Importantly, chronic inflammation carries health risks, from fetal life [exposure to maternal inflammation increases vulnerability to metabolic disease in adulthood (*5*)] to old age [chronic low-grade inflammation accelerates many biomarkers of senescence (*6, 7*)].

Proinflammatory responses to social subordination raise a seeming paradox regarding stress and health. Chronic stress can predispose toward inflammation. Yet, high concentrations of glucocorticoids, key mediators of the stress response, have powerful anti-inflammatory effects (prompting the use of synthetic glucocorticoids such as anti-inflammatory steroids). The resolution of this paradox will require considerable revision in the field, with the recognition that, in various circumstances, glucocorticoids are actually proinflammatory, on levels ranging from enhancing migration of inflammatory cells to injury sites, to increasing NF-κB activation (*8*).

The study of Snyder-Mackler *et al.* raises many questions. In some ways, some socially subordinate monkeys resemble humans with anxiety disorders, displaying hypervigilance and constantly scanning the environment for threats. For example, if you have a desirable food, eating is repeatedly disrupted as you look to see who may be coming to appropriate it from you. Other subordinate animals more closely resemble humans with major depression, displaying the learned helplessness of not even bothering to eat, because you expect that losing your food is inevitable. These differing states produce different neuroendocrine profiles (*9, 10*). Will they produce differing immunologic and inflammatory profiles of subordination as well?

Nonhuman primates display stable differences in temperament and personality (e.g., in response to novelty, or extent of social engagement). There are marked neuroendocrine differences among nonhuman primates of the same rank but with differing personalities (*11, 12*). It will be interesting to see if personality modulates the link between social rank and inflammatory state.

Humans belong to many hierarchies that can shift in importance in a context-dependent manner (think of a mail-room clerk acquiring prestige as captain of the company softball team). In addition, humans have invented the primate world's most corrosive form of subordination—socioeconomic status. Low socioeconomic status adversely affects nearly every realm of health, from increased risk of psychiatric disorders to accelerated telomere aging. Surprisingly little of the socioeconomic status–health link arises from differential access to health care, or exposure to risk factors. Instead, much of it is mediated by the psychological stress of low socioeconomic status (*13*). In considering how such stress translates into pathophysiology, experts discuss how low socioeconomic status gets "under the skin." The present study suggests one important potential route. ■

REFERENCES

1. D. G. Lindburg, Ed., *The Macaques: Studies in Ecology, Behavior and Evolution* (Van Nostrand Reinhold, 1980).
2. R. Sapolsky, *Science* **308**, 648 (2005).
3. N. Snyder-Mackler *et al.*, *Science* **354**, 1041 (2016).
4. D. Abbott *et al.*, *Horm. Behav.* **43**, 67 (2003).
5. C. Ingvorsen *et al.*, *Acta Physiol. (Oxf.)* **214**, 440 (2015).
6. C. Franceschi, J. Campisi, *J. Gerontol. A Biol. Sci. Med. Sci.* **69**, S4 (2014).
7. D. Calcada *et al.*, *Mech. Ageing Dev.* **136**, 138 (2014).
8. S. Sorrells, R. Sapolsky, *Brain Behav. Immun.* **21**, 259 (2007).
9. I. Neumann *et al.*, *Prog. Neuropsychopharmacol. Biol. Psychiatry* **35**, 1357 (2011).
10. P. Gold, *Mol. Psychiatry* **20**, 32 (2015).
11. R. Sapolsky, J. Ray, *Am. J. Primatol.* **18**, 1 (1989).
12. A. Clarke, S. Boinski, *Am. J. Primatol.* **37**, 103 (1995).
13. M. Marmot, *The Status Syndrome: How Social Standing Affects Our Health and Longevity* (Owl Books, 2005).

10.1126/science.aal3170

CELL BIOLOGY

Closing the loop

The ATG conjugation system is not essential for autophagosome formation in mammals

By **Beth Levine**

In 1963, the term autophagy was coined by Christian de Duve (Nobel Laureate, 1974) to denote the degradation of cellular self-constituents by the lysosome (*1*). In 2016, the Nobel Prize in Physiology or Medicine was awarded to Yoshinori Ohsumi for "his discoveries of mechanisms for autophagy" (*2*). Such discoveries led to the unveiling of autophagy as an evolutionarily conserved pathway that functions in differentiation and development, physiology, and protection against aging and many diseases (*3*). On page 1036 of this issue, Tsuboyama *et al.* (*4*) uncover a surprising twist to the mechanism in mammalian cells for forming the autophagosomal membrane, the structure that engulfs unwanted cellular cargo for delivery to the lysosome. These findings have implications for understanding the various roles of autophagy-related genes (ATGs) in membrane-trafficking and mammalian health and disease.

One of the key mechanisms of autophagy originally described by Mizushima, Ichimura, Ohsumi, and other colleagues was the action of two ubiquitin-like protein conjugation systems, the ATG12 and the ATG8 (yeast)/light chain 3 (LC3) (mammals) systems, which function in the formation of autophagosome membranes (*5, 6*). The ubiquitin-like ATG12 protein is covalently conjugated to ATG5, whereas ATG8/LC3 is covalently conjugated to the membrane phospholipid phosphatidylethanolamine. These reactions are catalyzed by the common E1-like protein ATG7 and specific E2-like proteins ATG10 and ATG3.

The prevailing paradigm has assumed that the ATG conjugation system proteins are essential for both autophagosomal membrane expansion and completion (see the image). This paradigm has framed our understanding of the molecular mechanisms of autoph-

Center for Autophagy Research, Department of Internal Medicine, Department of Microbiology, and Howard Hughes Medical Institute, University of Texas Southwestern Medical Center, 5323 Harry Hines Boulevard, Dallas, TX 75390-9113, USA. Email: beth.levine@utsouthwestern.edu

agy and how literature in the autophagy field is interpreted. When lipidated ATG8/LC3 is detected, it is commonly presumed that autophagosomes are formed; conversely, when ATG8/LC3 lipidation is not detected, it is presumed that autophagosomes are not formed. Moreover, phenotypes in mice lacking ATG conjugation system proteins are generally attributed to the absence of autophagy. Similarly, the absence of a given phenotype in mice lacking these proteins is presumed to signify the absence of an essential role for autophagy in the biological process under investigation.

Eighteen years after his first description of the ubiquitin-like protein conjugation system in autophagy (*5*), new findings by Mizushima's team challenge these widely held assumptions. There were already underappreciated clues in the literature that some of the presumably "solved" parts of the puzzle might need to be revisited. For example, in embryonic stem cells or mouse embryonic fibroblasts (MEFs) lacking ATG5 or ATG3, precursors of autophagosomes (known as isolation membranes or phagophores) or autophagosome-like structures were detected with electron microscopy. This suggested that unlike in yeast, the ATG conjugation systems were not essential for autophagosome membrane formation in mammalian cells. However, the reliance in mammalian autophagy research on detecting ATG conjugation system proteins (especially lipidated ATG8/LC3) as mainstay markers of autophagosomes (*7*) has hampered delineation of the true function of the ATG protein conjugation system in autophagosomal biogenesis.

An electron microscopy image of a mouse embryonic fibroblast shows a closed autophagosome (the white ring is the surrounding double membrane). This closure is impaired in cells lacking ATG conjugation system proteins.

Tsuboyama *et al.* (*4*) overcome this obstacle by using a different marker of autophagosomes—an autophagosomal soluble *N*-ethylmaleimide–sensitive factor attachment protein receptor (SNARE) protein called syntaxin 17 (STX17)—that localizes to completely formed autophagosomes, but not to autophagosomes not yet fully formed (*8*). The authors show that STX17 is recruited to ringlike structures (presumably autophagosomes) in MEFs that lack components of the ATG conjugation system (ATG3, ATG5, and ATG7) but not in MEFs that lack upstream essential autophagy genes [ATG9A, ATG14, and focal adhesion kinase family interacting protein of 200 kD (FIP200)]. This observation seemingly undermines the dogma that the ATG protein conjugation system, at least in mammalian cells, is essential for autophagosomal membrane biogenesis. However, the transition from isolation membranes (as defined with ATG5 staining) to closed autophagosomes (as defined with STX17 staining) is markedly impaired in MEFs lacking ATG3, suggesting that the ATG conjugation system is indeed important to efficiently "close the loop" in autophagosome formation. Once closed, autophagosomes in cells engineered to lack ATG3 fuse almost normally with lysosomes but have delayed degradation of the inner autophagosomal membrane. This delay is hypothesized to result from impaired fission of the membrane edges, as inferred from a more elliptical versus spherical shape. Consequently, during starvation, long-lived autophagic protein degradation is defective (but not completely absent) in cells deficient in ATG3 and other ATG conjugation system proteins.

Thus, the ATG protein conjugation system may act to promote the efficient closure or fission of the autophagosomal membrane, efficient degradation of the inner autophagosomal membrane, and efficient cargo degradation by the autolysosomal system. It is not yet known how the ATG conjugation system functions in closure or fission of the autophagosomal membrane or precisely how such fission leads to efficient degradation of the inner membrane. Nonetheless, Tsuboyama *et al.* put forth the provocative hypothesis that inward fission may represent a general mechanism by which vacuolar/lysosomal enzymes can degrade membranes.

The lack of an absolute requirement for the ATG protein conjugation system in the formation of completed autophagosomes raises many questions. What are the mechanisms underlying the essential roles of non–protein conjugation system ATG proteins FIP200, ATG9A, and ATG14? Who are the other key players in this process, and how do they orchestrate autophagosome membrane formation? It is also unclear whether the residual autophagic activity in ATG protein conjugation system–deficient cells is physiologically important. Another question is whether such residual autophagic activity explains the embryonic viability of mice that lack ATG protein conjugation system genes (compared with the embryonic lethality of mice that lack ATG genes essential for STX17 recruitment/autophagosome closure). Are there cell type– and stimulus-specific differences in ATG protein conjugation system-dependent effects on autophagosome biogenesis? How might the findings of the current study influence how we measure autophagic activity in future research?

Of note, the study by Tsuboyama *et al.* focuses on what is called "general autophagy"; experiments are performed during starvation or basal conditions in which cargo specificity is presumably lacking. Yet during selective autophagy, the presence of lipidated LC3 on the isolation membrane is crucial for binding receptors on the cargo targeted for degradation such as damaged organelles, protein aggregates, or intracellular pathogens (*9*). Thus, the ATG protein conjugation system might still be essential for selective, if not for general, autophagy.

The findings of Tsuboyama *et al.* reveal surprising missing pieces in our understanding of the mechanisms of autophagosomal membrane biogenesis. Yet like most intriguing new biological observations, they also make us realize how much more complex the puzzle is than we ever envisioned. ■

REFERENCES

1. C. de Duve, *Eur. J. Biochem.* **137**, 391 (1983).
2. https://www.nobelprize.org/nobel_prizes/medicine/laureates/2016/press.html.
3. B. Levine, G. Kroemer, *Cell* **132**, 27 (2008).
4. K. Tsuboyama *et al.*, *Science* **354**, 1036 (2016).
5. N. Mizushima *et al.*, *Nature* **395**, 395 (1998).
6. Y. Ichimura *et al.*, *Nature* **408**, 488 (2000).
7. N. Mizushima, T. Yoshimori, B. Levine, *Cell* **140**, 313 (2010).
8. E. Itakura *et al.*, *Cell* **151**, 1256 (2012).
9. A. Khaminets *et al.*, *Trends Cell Biol.* **26**, 6 (2016).

10.1126/science.aal3145

PHOTO: YURIKO SAKAMAKI

BIOCHEMISTRY

Teaching nature the unnatural

A reengineered enzyme catalyzes C–Si bond formation

By **Hendrik F. T. Klare** *and* **Martin Oestreich**

Silicon is found in nature in many inorganic forms, some of which are constructed by living organisms. Yet, no known biological molecule contains a carbon–silicon (C–Si) bond, and no biological processes to form C–Si bonds have been identified. On page 1048 of this issue, Kan *et al.* (*1*) show that natural as well as reengineered enzymes can promote C–Si bond formation. The resulting chiral compounds mostly consist of one of the two possible stereoisomers (enantiomers).

Methods for C–Si bond formation by chemical means have matured over the past decades. A typical reaction for creating asymmetric (chiral) C–Si compounds is the transition-metal–catalyzed insertion of diazo compounds **1**, which are bench-stable carbenoid precursors, into the silicon–hydrogen bond of triorganosilanes **2** (see the figure). State-of-the-art catalysts are based on copper (*2*), iridium (*3*), and rhodium (*4*) coordinated by elaborate chiral ligands or small peptides (*5*). Enantioselection is generally high—that is, the reaction products are almost pure enantiomers.

Bearing this model reaction in mind, Kan *et al.* investigated the enzyme cytochrome c from *Rhodothermus marinus* (*Rma* cyt c) as a catalyst for this synthetically useful transformation. This small protein contains a heme c moiety, which is an iron(II) porphyrin complex that is covalently attached via sulfide linkages to two cysteine residues. The central iron(II) atom is axially coordinated by the nitrogen atom of a histidine residue and a sulfur atom of methionine side chain M100, resulting in octahedral complexation (see the figure).

This structural motif plays a key role in electron-transfer processes, but no catalytic functions in living systems have been found to date. In contrast, other heme-containing proteins such as cytochrome P450 and myoglobin variants have been shown to form metallocarbenoids with selected diazo-based carbene precursors, thereby functioning as biocatalysts for several unnatural reactions (*6*–*10*). Building on this precedent, Kan *et al.* evaluated these enzymes as promoters for formation of the non-native C–Si bond. The desired bond did indeed form, but control of the stereochemical course of the reaction was marginal.

The authors next investigated *Rma* cyt c. This choice was beneficial in two respects. First, the wild-type protein *Rma* cyt c catalyzed the silicon–hydrogen insertion reaction with high enantioselection [>97% enantiomeric excess (ee)]. Second, an existing x-ray structure of the enzyme (*11*) provided direct insight into its active site, serving as an excellent starting point for further improvement by directed evolution. Following this approach, Kan *et al.* selected methionine residue M100, which needs to dissociate to make room for iron–carbenoid formation, as well as valine V75 and methionine M103, which are in close proximity to the active iron heme center (see the figure). They prepared mutants of the wild-type protein with sequential site-saturation mutagenesis.

Enzyme catalysis of C–Si bonds

Kan *et al.* show that the enzyme *Rma* cyt c can catalyze the formation of C–Si bonds. Altering just a few amino acids in the enzyme improves its activity beyond that of transition-metal catalysts.

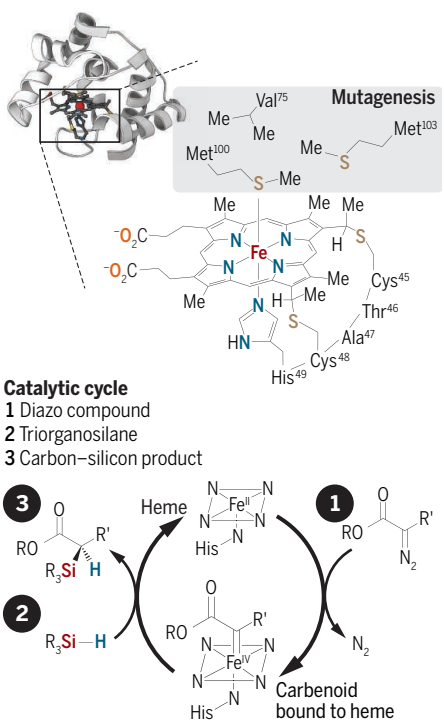

The enzyme *Rma* cyt c V75T M100D M103E (T, threonine; D, aspartic acid; E, glutamic acid) emerged as the superior mutant, catalyzing the C–Si bond formation with unprecedented efficiency (>1500 turnovers and >99% ee), even higher than that of traditional transition-metal catalysts. In view of the fact that natural enzymes have evolved to perform with well-defined functions on specific substrates, it is impressive to see that only a few mutations are needed to reengineer a natural enzyme to catalyze a reaction that was previously reserved for synthetic chemists. Moreover, the novel enzyme accepts a broad range of differently substituted hydrosilanes **2** and tolerates various functional groups, including free alcohols and amines. In all cases, Kan *et al.* observed preferential C–Si bond formation, producing almost all new tetraorganosilanes **3** as single enantiomers.

Kan *et al.* performed their experiments in vitro with non-natural, tailor-made substrates that are not likely to survive in a real biological system. Triorganosilanes **2** are nonpolar, hydrocarbon-like compounds that are likely to be prone to hydrolysis or oxidation before they can pass through the cell membrane. Yet, the authors show that the same reaction also proceeds in vivo—that is, in whole cells of *Escherichia coli* expressing the heme protein *Rma* cyt c V75T M100D M103E.

The beauty and value of Kan *et al.*'s accomplishment lie in the enzyme-promoted formation of an unnatural bond. This closes a crucial gap between biological and chemical catalysis. The impact is unforeseeable, but it seems that we are a big step closer to potentially facilitating industrially relevant reactions such as alkene hydrosilylation with biomolecules. ■

Institut für Chemie, Technische Universität Berlin, 10623 Berlin, Germany. Email: martin.oestreich@tu-berlin.de

REFERENCES

1. S. B. J. Kan, R. D. Lewis, K. Chen, F. H. Arnold, *Science* **354**, 1048 (2016).
2. Y.-Z. Zhang, S.-F. Zhu, L.-X. Wang, Q.-L. Zhou, *Angew. Chem. Int. Ed.* **47**, 8496 (2008).
3. Y. Yasutomi, H. Suematsu, T. Katsuki, *J. Am. Chem. Soc.* **132**, 4510 (2010).
4. D. Chen, D.-X. Zhu, M.-H. Xu, *J. Am. Chem. Soc.* **138**, 1498 (2016).
5. R. Sambasivan, Z. T. Ball, *J. Am. Chem. Soc.* **132**, 9289 (2010).
6. H. Renata, Z. J. Wang, F. H. Arnold, *Angew. Chem. Int. Ed.* **54**, 3351 (2015).
7. T. K. Hyster, T. R. Ward, *Angew. Chem. Int. Ed.* **55**, 7344 (2016).
8. P. S. Coelho, E. M. Brustad, A. Kannan, F. H. Arnold, *Science* **339**, 307 (2013).
9. Z. J. Wang, N. E. Peck, H. Renata, F. H. Arnold, *Chem. Sci.* **5**, 598 (2014).
10. V. Tyagi, R. B. Bonn, R. Fasan, *Chem. Sci.* **6**, 2488 (2015).
11. M. Stelter *et al.*, *Biochemistry* **47**, 11953 (2008).

10.1126/science.aal1951

EPIDEMIOLOGY

Mosquitoes on the move

Spread and hybridization of *Aedes aegypti* mosquitoes raise the risk of Zika, dengue, and other viral epidemics

By **Jeffrey R. Powell**

The mosquito *Aedes aegypti* rose to global attention around 1900 when it was shown to be the vector of yellow fever, a viral disease that was ravaging the New World. After World War II, a partly successful program was mounted to eliminate this invader from the New World through the use of DDT. By the late 1960s, however, the urgency for eliminating *Ae. aegypti* receded after the widespread use of an effective yellow fever vaccine. Eradication efforts were suspended, and the mosquito reestablished itself in its previous, or even a greater, range. The mosquito continues to be a substantial public health threat that requires urgent attention, particularly given recent evidence for hybridization of previously distinct subtypes.

We cannot say that we were not warned. In 1970, Fred Lowe Soper wrote that *Ae. aegypti* "should be studied as a long-term national, regional, and world problem rather than as a temporary local threat to the communities suffering at any given moment from yellow fever, dengue or other *aegypti*-borne disease. No one can foresee the extent of the future threat of *Aedes aegypti* to mankind as a vector of known virus diseases, and none can foretell what other virus diseases may yet affect regions where *Ae. aegypti* is permitted to remain" (*1*).

These words turned out to be prescient. In the 1980s, the dengue fever virus, also transmitted by *Ae. aegypti*, began to cause increasingly severe epidemics wherever the mosquito bred. A third *Ae. aegypti*–borne virus was also rising in importance, especially in Asia and Indian Ocean islands: the virus causing chikungunya fever. Chikungunya virus has caused disease outbreaks in Europe and was first reported in the New World in 2013 (*2*). More recently, the Zika virus, also transmitted by *Ae. aegypti*, has risen to considerable notoriety worldwide. In the past 9 months, yellow fever has reemerged in Africa (*3*). The geographic range of human populations at risk for these diseases coincides with the geographic distribution of the mosquito. With the exception of yellow fever, no *aegypti*-borne diseases have a proven effective vaccine, nor are there medications that specifically treat human infections. Control efforts to limit these diseases thus focus on the mosquito.

Ae. aegypti is a native of Africa, where its ancestral form can still be found. This ancestor, called *Ae. aegypti formosus* (Aaf), is a black mosquito (see the photo, left) found in forests and ecotones in sub-Saharan Africa. It breeds in tree holes and prefers nonhuman animals for blood meals. A "domesticated" form evolved from this sylvan ancestor, possibly as a response to the expansion of the Sahara desert between 4000 and 6000 years ago. This form, closely associated with and spread by humans, is called *Ae. aegypti aegypti* (Aaa). It is a brownish mosquito (see the photo, right) with white scaling on its abdomen, found throughout the tropics and subtropics outside Africa, that breeds in human-generated containers and prefers humans for blood meals.

Aedes aegypti females of the African subspecies *formosus* (left) and the cosmopolitan subspecies *aegypti* (right).

Because of their very distinctive habitats and behaviors, the two forms or subspecies have historically presented different health risks. Aaf was relatively benign, being found in forests with low human densities and preferring nonhumans for blood meals. Human-loving Aaa has been responsible for most of the human disease transmitted by this species. The distribution of the two types is thus of considerable importance.

Several recent observations have upset the simple picture of Aaf residing in sub-Saharan Africa and Aaa residing outside of Africa (see the figure). In sub-Saharan Africa, mosquitoes that would be considered Aaf based on morphology and genetics are now breeding in human habitats, including cities like Dakar, Yaounde, Luanda, and Libreville (*4*–*6*). This is likely a response to expanding urban centers in Africa that encroach on Aaf's native forests. The larval breeding habitat has shifted from tree holes to discarded items like tires, indicating that females have changed their egg-laying behavior. Outbreaks of dengue in African cit-

Yale University, New Haven, CT 06520, USA.
Email: jeffrey.powell@yale.edu

PHOTO: LINDY MCBRIDE/PRINCETON UNIVERSITY

ies (*6*) indicate that these urban Aaf may now preferentially choose humans for their blood meals. The great increase in yellow fever in sub-Saharan Africa in the past year may in part be due to this shift: The most efficient vector of yellow fever virus now resides in densely populated cities in Africa.

Furthermore, Aaa from outside Africa has found its way back to both West Africa (Senegal) and East Africa (Kenya), where it freely interbreeds with Aaf (*5*, *7*). In turn, Aaf has recently been introduced into Argentina, where it is hybridizing with Aaa and where populations now breed in tree holes (*8*), the classic African larval habitat. The consequences of increasing hybridization between the two subspecies remain unclear. Studies of other invasive species have shown that hybridization leads to an increase in genetic variation, which may cause further spread (*9*).

Clearly, the simple dichotomy of two distinct subtypes of *Ae. aegypti* has broken down. Their geographic distributions are beginning to overlap, and they are hybridizing. Ecologically, they can no longer be clearly separated, with Aaf increasingly breeding in urban areas in Africa. Egg-laying behaviors and host preferences are blurring.

Ae. aegypti is also increasing its distribution outside Africa and now breeds year-round in places heretofore free of the species, such as Madeira (*10*), the Black Sea (*11*), California (*12*), and Washington, D.C. (*13*). These expansions are putting at risk large human populations that never experienced *aegypti*-borne viruses and therefore have no immune defenses against them. This greatly increases the likelihood of severe epidemics.

Ae. aegypti's distribution is in a state of flux and likely to continue to grow as trade and human movement increase and climate change increasingly alters ecosystems. Monitoring populations and localities will help to anticipate the spread of the diseases that this mosquito is so efficient at transmitting. Fortunately, tools are available to genetically characterize populations (*5*, *14*). Such genetic characterization is especially important because populations vary considerably in their ability to transmit viruses (*15*). Knowing the genetic makeup of newly introduced mosquitoes and where they came from can give indications of their relative threat and can also guide control efforts, for example, through knowledge of which insecticides have proven effective or ineffective in the source region. ■

REFERENCES

1. J. A. Kerr, Ed., *Building the Health Bridge: Selections from the Writings of Fred L. Soper* (Elsevier, 1970).
2. I. Leparc-Goffart, A. Nougairede, S. Cassadou, C. Prat, X. de Lamballerie, *Lancet* **383**, 514 (2014).
3. D. Lucey, L. O. Gostin, *JAMA* **2016**, 6606 (2016).
4. B. Kamgang *et al.*, *PLOS Negl. Trop. Dis.* **7**, e2590 (2013).
5. A. Gloria-Soria *et al.*, *Mol. Ecol.* **25**, 5377 (2016).
6. T. M. Sharp *et al.*, *Emerg. Infect. Dis.* **21**, 1311 (2015).
7. M. Sylla *et al.*, *PLOS Negl. Trop. Dis.* **3**, e408 (2009).
8. C. Mangudo, J. P. Aparicio, R. M. Gleiser, *Bull. Entomol. Res.* **105**, 679 (2015).
9. D. G. Bock *et al.*, *Mol. Ecol.* **24**, 2277 (2015).
10. A. P. Almeida *et al.*, *Euro. Surveill.* **12**, 3311 (2007).
11. M. Akiner *et al.*, *PLOS Negl. Trop. Dis.* **10**, e0004664 (2016).
12. A. Gloria-Soria *et al.*, *PLOS Neg. Trop. Dis.* **8**, e3029 (2014).
13. A. Lima *et al.*, *Am. J. Trop. Med. Hyg.* **94**, 231 (2016).
14. B. R. Evans *et al.*, *G3* **5**, 711 (2015).
15. S. Sim *et al.*, *PLOS Negl. Trop. Dis.* **7**, e2295 (2013).

10.1126/science.aal1717

Changing dynamics

Year of introduction is given for locations newly infested with *Aedes aegypti* since about 2006.

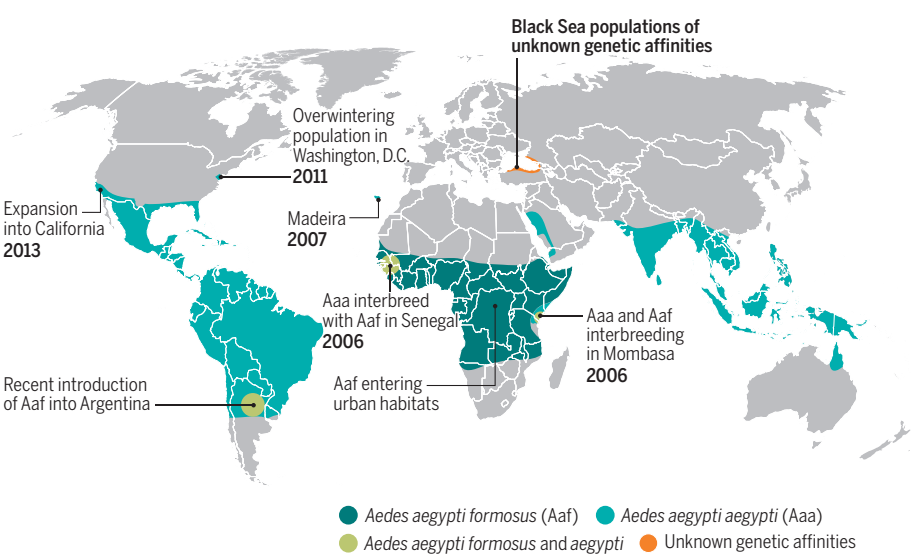

MAP: G. GRULLÓN/SCIENCE

PHYSICS

Bringing order to neutral atom arrays

Cold atom manipulation may enable small quantum systems to be built to order

By **Cindy Regal**

In quantum science, the control of individual particles that was once unimaginable is now routine and expanding rapidly to a variety of platforms harnessing atoms, photons, solid-state circuits, molecules, and more. Yet, implementation on a large scale that retains individual particle control remains a frontier challenge. Large-scale quantum control is predicted to have revolutionary consequences for studying synthetic quantum matter and for information processing that harnesses quantum mechanics—that is, quantum computing. On pages 1021 and 1024 of this issue, Barredo *et al.* (*1*) and Endres *et al.* (*2*) report on an experimental approach in which controlling the spatial distribution of neutral atoms is taken to a new scale.

Neutral atoms have long been considered to have a special knack for scalability with regards to many-body quantum states. In their electronic ground state, they often do not know of each other's presence until they are right on top of each other. Hence, many can be packed into a small volume; they are naturally identical, and laser-cooled reservoirs can consist of billions of atoms. Thus far, large arrays of neutral atoms have been demonstrated in approaches where a quantum-degenerate gas created by special refrigeration is converted to a Mott insulator. But often these techniques are less amenable to individual manipulation and to implementing fast interactions required for realistic computing.

Another approach is to build neutral atom quantum states with a portable "single atom source" in which single atoms are isolated in micrometer-scale traps (*3*). Isolating single atoms can be accomplished surprisingly simply by forcing atoms to leave the trap pairwise by inducing highly

Department of Physics, University of Colorado, Boulder, CO 80309, USA. Email: regal@colorado.edu

Establishing order

Atoms are optically manipulated one at a time and can be controllably placed at the desired point in the checkerboard array, based on Barredo *et al.*

• Trap ● Atom □ Target trap

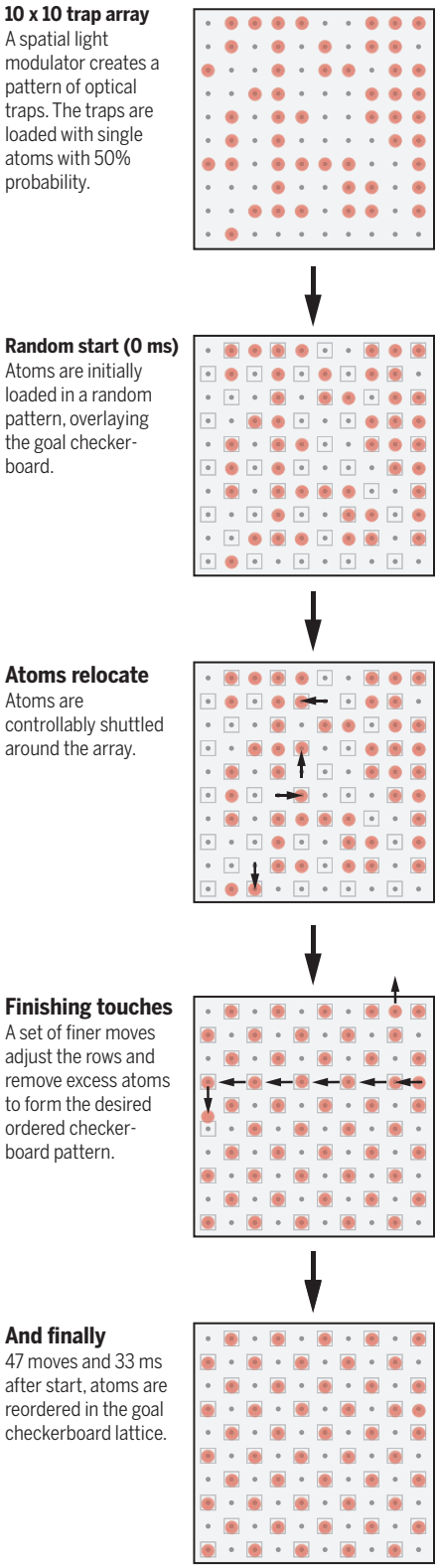

GRAPHIC: C. BICKEL/*SCIENCE*

energetic collisions. However, this technique has a flaw—part of the time there will be no atom left in the trap. This means that there is some disorder associated with the spatial configuration of an array of traps (see the figure, top panel).

The entropy associated with a shifting set of occupied traps can be a serious impediment. Entropy in classical statistical mechanics is defined as the number of microscopic configurations that correspond to a thermodynamic system. The many possible microscopic spatial configurations of atoms lead to an unacceptable entropy. However, there is a relatively simple solution to this problem when one can individually image all the atoms—information. As soon as one knows the configuration of atoms at each iteration before starting an experiment of interest, the entropy is gone, even though the image looks disordered. This technique has been used in a variety of experiments with a handful of atoms (*4*–*6*).

VIDEO

Watch atoms being shuttled around at scim.ag/aaj2145

However, when a specific order in a large array of atoms is required for making a particular computation or state of matter, finding this configuration can be like looking for a needle in a haystack. To address this problem, the first atom-sorting machine used atoms shuttled between two standing wave traps to order seven atoms (*7*). Barredo *et al.* and Endres *et al.* skillfully orchestrate a large number of atoms to map the initial configuration onto compacted and ordered arrays of their choosing. The videos of the atoms being shuttled around (available at scim.ag/aaj2145) is reminiscent of filling a set of holes as in Chinese checkers, but with a big difference—these atoms have the potential to be applied to a quantum experiment.

In the work of Barredo *et al.* and Endres *et al.*, the array assembly relies upon movement of tightly focused optical tweezer traps. Optical tweezers attract dielectric objects to their focus and are often associated with manipulating DNA or sorting cells. The optical tweezer focus can be moved in real time by changing the angle of the beam with an acousto-optic deflector crystal. Endres *et al.* use multiple traps that can all move arbitrarily in one dimension by controlling many individual radiofrequency tones. Barredo *et al.* use a "shuttle" optical tweezer trap to move atoms around on a two-dimensional grid of static traps.

The experimenters and their imaging device are akin to a Maxwell's demon acting on the spatial configuration of the particles (*8*). Maxwell's demon is a thought experiment in which a particle-sorting demon challenges our understanding of the second law of thermodynamics, and it has led to a greater understanding of the relation between entropy and information. Barredo *et al.* and Endres *et al.* first gather information about all the particle positions in parallel by imaging them with a microscope. This information is stored in a desktop computer's memory and is then used to arrange the atoms. To realize the new arrangement is nontrivial, and requires real-time feedback well beyond that of typical cold atom experiments. The atoms need to be guided through a maze of other atoms, where the maze shifts in each iteration of the experiment. The authors developed several algorithms to guide the atoms (see the figure), but finding the most efficient method is a mathematical puzzle that will certainly be honed in future work.

The work of Barredo *et al.* and Endres *et al.* closely follows a key component in a visionary proposal for how to approach zero entropy for a finite system of atoms (*9*). Realizing this vision will require further control to remove entropy arising in all atomic spin and motional degrees of freedom. The atoms in the work of Barredo *et al.* and Endres *et al.* are actually still "hot" in the sense that they are rolling around their individual traps at fairly high temperatures for ultracold atoms, but this can be solved by combining array creation with the ability to cool individual atoms in movable traps (*5*) and bring them in close proximity. Further exciting routes to cold interacting matter do not require full control of temperature if interactions can be made sufficiently dominant; indeed, experiments planned for the near future will combine these ordered arrays with long-range interactions, by exciting the atoms to high-lying Rydberg states (*4, 6*) or via photon-mediated interactions in a photonic crystal.

Barredo *et al.* and Endres *et al.* demonstrate a 50-atom rearrangement in this work, but predict extending it to the alluring prospect of greater than 500 atoms. The rearrangement technique that they introduce will likely be widely adopted as it applies to anything that can be trapped in an optical tweezer, from molecules to a variety of other atomic species. ■

REFERENCES

1. D. Barredo *et al.*, *Science* **354**, 1021 (2016).
2. M. Endres *et al.*, *Science* **354**, 1024 (2016).
3. N. Schlosser *et al.*, *Nature* **411**, 1024 (2001).
4. M. Saffman *et al.*, *Rev. Mod. Phys.* **82**, 2313 (2010).
5. A. M. Kaufman *et al.*, *Science* **345**, 306 (2014).
6. H. Labuhn *et al.*, *Nature* **534**, 667 (2016).
7. Y. Miroshnychenko *et al.*, *Nature* **442**, 151 (2006).
8. J. C. Maxwell, *Theory of Heat* (Longmans, Green, London, 1875).
9. D. S. Weiss *et al.*, *Phys. Rev. A* **70**, 040302(R) (2004).

10.1126/science.aaj2145

RETROSPECTIVE

Susan Lindquist (1949–2016)

An unflappable biologist was an indomitable advocate for brave and meaningful inquiry

By **Luke Whitesell**[1] *and* **Sandro Santagata**[2]

On 27 October, Susan Lee Lindquist, professor at the Massachusetts Institute of Technology (MIT), died of cancer at the age of 67. She was a formidable academic leader, dedicated mentor, beloved friend, and devoted wife and mother who will be deeply missed.

Susan was born in Chicago, Illinois, in 1949 to parents of Swedish and Italian ancestry. This rich blend of genes and cultures was reflected in her ability to balance the dramatic against the carefully reasoned. She earned a bachelor's degree in microbiology at the University of Illinois in 1971, followed by a doctorate in biology from Harvard University in 1976. After a postdoctoral fellowship at the University of Chicago, she joined its molecular biology department and set about deciphering how cells regulate protein synthesis and folding. She recounted an environment far from supportive for women, yet she persisted and thrived. She ignored warnings that her career would flounder when she switched organisms or undertook difficult areas of study. Rather, she demonstrated an ability to choose the right questions at the right time and helped found the field of heat-shock biology.

Susan accepted a joint appointment as professor of biology at MIT and director of the Whitehead Institute for Biomedical Research in 2001. She shepherded an unprecedented partnership between MIT, Harvard University, and the Whitehead Institute in launching the Broad Institute for biomedical research. In 2004, she returned to full-time research at the Whitehead Institute but also had appointments at the Broad Institute and at the David H. Koch Institute for Integrative Cancer Research at MIT. During this chapter of her career, Susan concentrated on the biomedical implications of her work and transformed budding yeast into a model organism for studying evolution, biomaterials, and the cellular pathology of neurodegenerative disorders such as Parkinson's, Huntington's, and Alzheimer's diseases. She also strove to apply basic scientific insights to the mission of improving human health. To do so, she co-founded FoldRx Pharmaceuticals and Yumanity Therapeutics to tackle neurodegenerative diseases caused by the pathogenetic misfolding of proteins.

Susan received many prestigious awards, including the U.S. National Medal of Science and the Albany Medical Center Prize in Medicine and Biomedical Research. She was a Howard Hughes Investigator and an elected member of the U.S. National Academy of Sciences, the U.S. National Academy of Medicine, the American Philosophical Society, the American Academy of Arts and Sciences, and the British Royal Society.

More important to Susan than the accolades were the people whom she helped train.

Susan Lindquist was awarded the U.S. National Medal of Science by President Obama in 2009.

During her 15-year career at the Whitehead Institute alone, she guided over 100 postdoctoral fellows, graduate students, and undergraduates to productive careers in research. Her trainees benefited from Susan's love of language, especially poetry, in a very direct way. Every manuscript was carefully crafted during many hours of writing sessions with her, finding just the right words and rendering complicated scientific concepts accessible to both specialists and a wider audience. For Susan, the process of doing the right experiments and doing them well provided essential raw material, but crisp, lucid communication was equally important. Several of her manuscripts on protein-based mechanisms of inheritance and their role in the evolution of organisms are already classics.

Susan valued the creative power of diversity: ethnicity, gender, age, training, and life experience. Basic and applied scientists, physicians, mathematicians, biologists, and chemists all had important contributions. She brought us together, guided us in asking the right questions, and picked us up when we fell down. She was invested in fostering the careers of women in science. She was a role model in balancing the demands of a productive career with a rewarding life outside the lab. Whether at the theater with her husband, Edward, or on a vacation getaway with him and their two daughters, nothing gave Susan greater joy than the love of her family.

Working with Susan was like setting out on a great expedition, finding surprising, serendipitous, and useful treasures along the way. For one of us (L.W.), the journey began on a bus ride from Cold Spring Harbor Laboratory after a meeting. Her approachability and willingness to go beyond the boundaries of her scientific kingdom to a land where "there be dragons" led to a long partnership investigating molecular chaperones and the heat-shock response in human cancers. She was fascinated by the idea that the protein-based mechanisms of evolution in model organisms might fuel the malignant progression and drug resistance of cancers. For many of us, the journey was in the company of cherished colleagues—a generous, hard-driving, supportive, and creative community that mirrored the best qualities of our beloved mentor. And the journey was fun and joyful, perhaps never more so than when Susan tore up the dance floor each year at our Whitehead retreats.

Susan approached the ovarian cancer that killed her not as a reason to quit what she loved doing but rather as a scientific problem that needed to be investigated with every resource she could muster. It was a testament to the respect she had earned over the years to see both academic and corporate leaders rally to her cause with the invariable words "How can I help?" To these generous offers, Susan responded that she wanted insights gleaned from her tumor to help future women overcome this dreadful disease. Susan lived every day with the unshakable conviction that the misery caused by human diseases will ultimately yield to creative and determined scientific investigation. Despite all of her achievements, she felt that her work was still just taking off and beginning to deliver on its promise. ■

10.1126/science.aal3609

[1]Whitehead Institute, Cambridge, MA, USA. [2]Brigham and Women's Hospital, Boston, MA, USA. Email: whitesell@wi.mit.edu; ssantagata@bics.bwh.harvard.edu

PHOTO: OWEN/BLACK STAR/NEWSCOM

POLICY FORUM

BIODIVERSITY

Ten policies for pollinators

What governments can do to safeguard pollination services

By **Lynn V. Dicks,[1] Blandina Viana,[2] Riccardo Bommarco,[3] Berry Brosi,[4] María del Coro Arizmendi,[5] Saul A. Cunningham,[6] Leonardo Galetto,[7] Rosemary Hill,[8] Ariadna V. Lopes,[9] Carmen Pires,[10] Hisatomo Taki,[11] Simon G. Potts[12]**

Earlier this year, the first global thematic assessment from the Intergovernmental Science-Policy Platform on Biodiversity and Ecosystem Services (IPBES) evaluated the state of knowledge about pollinators and pollination (*1*, *2*). It confirmed evidence of large-scale wild pollinator declines in northwest Europe and North America and identified data shortfalls and an urgent need for monitoring elsewhere in the world. With high-level political commitments to support pollinators in the United States (*3*), the United Kingdom (*4*), and France (*5*); encouragement from the Convention on Biological Diversity's (CBD's) scientific advice body (*6*); and the issue on the agenda for next month's Conference of the Parties to the CBD, we see a chance for global-scale policy change. We extend beyond the IPBES report, which we helped to write, and suggest 10 policies that governments should seriously consider to protect pollinators and secure pollination services. Our suggestions are not the only available responses but are those we consider most likely to succeed, because of synergy with international policy objectives and strategies or formulation of international policy creating opportunities for change. We make these suggestions as independent scientists and not on behalf of IPBES.

[1]*University of East Anglia, Norwich NR4 7TL, UK.* [2]*Universidade Federal da Bahia, 40170-210 Salvador, Bahia, Brazil.* [3]*Swedish University of Agricultural Sciences, 75007 Uppsala, Sweden.* [4]*Emory University, Atlanta, GA 30322, USA.* [5]*Universidad Nacional Autónoma de México, Tlalnepantla, México 54090, Mexico.* [6]*The Australian National University, Canberra, Australia Capital Territory 2601, Australia.* [7]*Universidad Nacional de Córdoba, National Scientific and Technical Research Council (CONICET), Córdoba, Argentina.* [8]*Commonwealth Scientific and Industrial Research Organisation (CSIRO) Land and Water, James Cook University, Cairns, Queensland 4878, Australia.* [9]*Universidade Federal de Pernambuco, 50670-901 Recife, Pernambuco, Brazil.* [10]*Embrapa Recursos Genéticos e Biotecnologia, CEP 70770-917 Brasília, DF, Brazil.* [11]*Forestry and Forest Products Research Institute, Tsukuba, Ibaraki 305-8687, Japan.* [12]*University of Reading, Reading RG6 6AR, UK. Email: lynn.dicks@uea.ac.uk*

PHOTO: SALLY MUNDY/ALAMY STOCK PHOTO

A bumblebee (*Bombus terrestris*) collecting pollen from a blueberry flower. Unregulated trade in bumblebees puts them outside their native range.

RISK REDUCTION

Pesticides are the most heavily regulated of the interacting drivers of pollinator declines (*7*). Risk assessment and use regulation can reduce pesticide hazards at national scales (*2*), yet such regulation is uneven globally. Many countries do not have national pesticide regulation and control systems or adhere to the International Code of Conduct on Pesticide Management (ICCPM), recently updated by the United Nations (*8*, *9*). International pressure to raise pesticide regulatory standards across the world should be a priority. This includes consideration of sublethal and indirect effects in risk assessment and evaluating risks to a range of pollinator species, not just the honey bee, *Apis mellifera*.

Another priority is to capitalize on the profile of integrated pest management (IPM) in international policies, such as the ICCPM (*9*) and the European Union's (EU's) Sustainable Use of Pesticides Directive (*10*). IPM combines pest monitoring with a range of pest control methods, such as crop rotation, field margin management, and biological control; pesticides are used as a last resort, only when other strategies are insufficient (*11*). IPM can decrease pesticide use and reduces risks to nontarget organisms, so it should be linked to pollinator health and pollination.

Genetically modified (GM) crops pose potential risks to pollinators through poorly understood sublethal and indirect effects (*1*). For example, GM herbicide-tolerant crops lead to increased herbicide use, reducing the availability of flowers in the landscape, but consequences for pollinators are unknown. GM crop risk assessments in most countries do not capture these effects. They evaluate only direct effects of acute exposure to proteins expressed in the GM plants, usually in terms of the dose that kills 50% of adults (LD_{50}), and only for honey bees, not other pollinators. International guidance to improve GM organism risk assessment is being developed under the CBD's Cartagena Protocol on Biosafety (*12*); this presents an opportunity to encourage inclusion of indirect and sublethal effects on a range of pollinator species.

There are substantial risks from movement of managed pollinators around the world (*1*). Managed pollinators, including newly domesticated species, offer opportunities to grow businesses and improve pollination services. Commercial bumble bee trade has grown dramatically, leading to invasions of *Bombus terrestris* beyond its native range and increasing the risk of disease transfer to native wild bee populations, potentially including other bee species (*13*). The issue of invasive species has been highlighted in the UN Sustainable Development Goals and the CBD's Strategic Plan for Biodiversity, which parties to the CBD are implementing in national strategies and action plans. This creates momentum and opportunity for regulators to consider limiting and better managing pollinator movement within and between countries.

SUSTAINABLE FARMING

Agriculture is a major driver of pollinator declines, through land-use change; intensive practices, such as tillage and agrochemical use; and declines in traditional farming practices. Agriculture also provides opportunities to support wild pollinators (*1*). We propose two complementary policy objectives: (i) promote ecological intensification of agriculture (*14*) and (ii)

support diversified farming systems (*15*).

Ecological intensification involves managing ecological functions, such as pollination and natural pest regulation, as part of highly productive agriculture. It can be as profitable and productive as conventional approaches at a farm level, even with up to 8% of land out of production to provide habitats that support beneficial organisms (*16*).

A major barrier to uptake of ecological intensification is uncertainty about ecological and agronomic outcomes. To tackle uncertainty, a promising option is to adjust crop insurance schemes to provide incentives, such as lower premiums or smaller loss thresholds, for farmers who take action to promote pollinators. Insurance is a key element in "climate-smart agriculture" (*17*) but has yet to be tested or adopted for more general agricultural sustainability.

Another barrier, lack of knowledge among farmers and agronomists, can be addressed by extension services. For example, national Farm Advisory Systems are obligatory for member states under the EU's Common Agricultural Policy. The extent to which these provide information relevant to ecological management could be improved.

Ten pollinator policies

1. Raise pesticide regulatory standards.
2. Promote integrated pest management (IPM).
3. Include indirect and sublethal effects in GM crop risk assessments.
4. Regulate movement of managed pollinators.
5. Develop incentives, such as insurance schemes, to help farmers benefit from ecosystem services instead of agrochemicals.
6. Recognize pollination as an agricultural input in extension services.
7. Support diversified farming systems.
8. Conserve and restore "green infrastructure" (a network of habitats that pollinators can move between) in agricultural and urban landscapes.
9. Develop long-term monitoring of pollinators and pollination.
10. Fund participatory research on improving yields in organic, diversified, and ecologically intensified farming.

Diversified farming systems (including some organic farms, home gardens, agroforestry, mixed cropping, and livestock systems) incorporate many pollinator-friendly practices, such as flowering hedgerows, habitat patchiness, and intercropping (*1*). Support for these systems can be achieved through financial incentives, such as European agri-environment schemes (*18*), or market-based instruments, such as certification schemes with a price premium—both used to support organic farming. In at least 60 countries, these practices and farming systems depend on indigenous and local knowledge (*2*). To secure people's ability to pursue pollinator-friendly practices, their tenures and rights to determine their agriculture policies (food sovereignty) must be recognized and strengthened (*19*).

BIODIVERSITY AND ECOSYSTEM SERVICES

Policy interest in pollinators stems largely from their role in food production (*2*). Historically, the most widely adopted policy approaches for biodiversity conservation have been to identify and protect threatened species and to create protected areas. These remain critical but are not sufficient to maintain the substantial global value of pollination services in agriculture, for two reasons. First, the spatial separations between protected areas, as well as between protected areas and croplands, are usually large relative to daily movements of most pollinators. Second, although pollinator diversity is important, the bulk of crop pollination is from relatively few common, widespread species rather than rare or threatened species (*20*). For crop pollination, the policy goal should be to secure a minimum level of appropriate habitat, with flower and nesting resources, distributed throughout productive landscapes at scales that individual pollinators can move between. This fits the definition of "green infrastructure" identified by the EU in 2013 (*21*). It involves a diverse range of land managers, with overview and coordination at regional scales. As examples, small patches of habitat on public lands might be conserved through regulation, whereas protection or restoration of habitat on private land might be achieved through incentive payments (*18*) or by encouraging voluntary action (*22*). To conserve wider pollinator diversity and functions not relevant to agriculture, this approach must be integrated within strategically planned habitat and species protection policies (*20*, *23*).

INCREASING KNOWLEDGE

There are substantial knowledge gaps about the status of pollinators worldwide and the effectiveness of measures to protect them (*1*). Evidence is largely limited to local-scale, short-term effects and is biased toward Europe and North America. There is a need for long-term, widespread monitoring of pollinators and pollination services. Recent research funded by the U.K. government as part of the National Pollinator Strategy for England (*4*) compared ways to achieve this monitoring, with varying levels of professional and volunteer involvement (*24*).

Finally, we suggest funding research on how to improve agricultural yields in farming systems known to support pollinators. This underpins several policies in our list. It also resonates with a global focus on improving food production and food security, especially on small farms (<2 ha), which represent more than 80% of farms and farmers, and 8 to 16% of farmed land (*2*, *25*). To ensure that findings are considered credible, salient, and legitimate by agricultural communities, the research should prioritize knowledge coproduction and exchange between scientists, farmers, stakeholders, and policy-makers. Such approaches can be supported through national and international research funding or institutional infrastructure. ■

REFERENCES AND NOTES

1. IPBES, "Summary for policymakers of the assessment report of the Intergovernmental Science-Policy Platform on Biodiversity and Ecosystem Services on pollinators, pollination, and food production" (Secretariat of IPBES, Bonn, Germany, 2016).
2. IPBES, "The assessment report of the Intergovernmental Science-Policy Platform on Biodiversity and Ecosystem Services on pollinators, pollination and food production" (IPBES, Bonn, Germany, 2016).
3. Pollinator Health Task Force, "National strategy to promote the health of honey bees and other pollinators" (White House, Washington, DC, 2015).
4. Department for Environment, Food, and Rural Affairs, "The National Pollinator Strategy: For bees and other pollinators in England" (Defra, Bristol, 2014).
5. Ministère de l'Écologie du Développement Durable et de l'Énergie, "Plan national d'actions « France Terre de pollinisateurs » pour la préservation des abeilles et des insectes pollinisateurs sauvages" (Ministère de l'Écologie du Développement Durable et de l'Énergie, Puteaux, France, 2016).
6. Subsidiary Body on Scientific, Technical, and Technological Advice of the CBD, "Implications of the IPBES assessment on pollinators, pollination and food production for the work of the Convention," Twentieth meeting of SBSTTA, Montreal, Canada, 25 to 30 April 2016.
7. D. Goulson, E. Nicholls, C. Botías, E. L. Rotheray, *Science* **347**, 1255957 (2015).
8. G. Ekström, B. Ekbom, *Outlook Pest Manag.* **21**, 125 (2010).
9. Food and Agriculture Organization of the United Nations (FAO), World Health Organization, "The international code of conduct on pesticide management" (FAO, Rome, 2014).
10. European Commission, "Directive 2009/128/EC of the European Parliament and of the Council of 21 October 2009 establishing a framework for Community action to achieve the sustainable use of pesticides" (Official Journal of the European Union, Brussels, 2009).
11. G. Ekström, B. Ekbom, *Criti. Rev. Plant Sci.* **30**, 74 (2011).
12. CBD, "Report of the ad hoc technical expert group on risk assessment and risk management" (UNEP/CBD/BS/RARM/AHTEG/2015/1/4, CBD, 2015).
13. P. Graystock *et al.*, *J. Appl. Ecol.* **50**, 1207 (2013).
14. R. Bommarco, D. Kleijn, S. G. Potts, *Trends Ecol. Evol.* **28**, 230 (2013).
15. C. Kremen, A. Iles, C. Bacon, *Ecol. Soc.* **17**, 44 (2012).
16. R. F. Pywell *et al.*, *Proc. R. Soc. London Ser. B* **282**, 20151740 (2015).
17. FAO, *Climate-Smart Agriculture Sourcebook* (FAO, Rome, 2013).
18. P. Batáry, L. V. Dicks, D. Kleijn, W. J. Sutherland, *Conserv. Biol.* **29**, 1006 (2015).
19. C. Laroche Dupraz, A. Postolle, *Food Policy* **38**, 115 (2013).
20. D. Kleijn *et al.*, *Nat. Commun.* **6**, 7414 (2015).
21. European Commission, "Green infrastructure (GI)—Enhancing Europe's natural capital" (COM/2013/0249 final, EC, Brussels, 2013).
22. A. Santangeli *et al.*, *Biol. Conserv.* **197**, 209 (2016).
23. D. Senapathi *et al.*, *Curr. Opin. Insect Sci.* **12**, 93 (2015).
24. C. Carvell *et al.*, "Design and testing of a National Pollinator and Pollination Monitoring Framework. Final summary report to the Department for Environment, Food and Rural Affairs (Defra), Scottish Government, and Welsh Government: Project WC1101" (Defra, Bristol, 2016).
25. International Food Policy Research Institute, in *2016 Global Food Policy Report* (IFPRI, Washington, DC, 2016), chap. 1.

10.1126/science.aai9226

A worker adjusts rayon threads at a factory in Richmond, Virginia, in the 1950s.

PHOTO: HAGLEY ARCHIVE/SCIENCE SOURCE

OCCUPATIONAL HEALTH

Toxic textiles

A physician uncovers the disturbing history of an "ecofriendly" fiber

By **Emily Monosson**

Fake Silk
The Lethal History of Viscose Rayon
Paul David Blanc
Yale University Press, 2016. 325 pp.

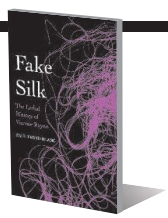

In this slim, action-packed book, Paul David Blanc takes the reader on a historical tour that touches on chemistry, occupational health, and the maneuverings of multinational corporations. Our guide is a small, "elegant" molecule called carbon disulfide—a compound that is a key ingredient in the making of viscose (better known as rayon) and is also insidiously toxic, having devastated the minds and bodies of factory workers for more than a century.

Fake Silk: The Lethal History of Viscose Rayon unveils a story that, in Blanc's words, "deserves to be every bit as familiar as the cautionary tales of asbestos insulation, leaded paint, or the mercury-tainted seafood in Minimata Bay." Who knew that the fabric that has had its turn on the high-fashion runway, as a pop-culture joke (remember leisure suits?), and more recently as a "green" textile had such a dark side?

Rayon is a cellulose-based textile in which fibers from tree trunks and plant stalks are spun together into a soft and absorbent fabric. First patented in England in 1892, viscose-rayon production was firmly established by the American Viscose Company in the United States in 1911. Ten years later, the factory was buzzing with thousands of workers. "[E]very man, woman, and child who had to be clothed" were once considered potential consumers by ambitious manufacturers.

However, once the silken fibers are formed, carbon disulfide—a highly volatile chemical—is released, filling factory workrooms with fumes that can drive workers insane. Combining accounts from factory records, occupational physicians' reports, journal articles, and interviews with retired workers, Blanc reveals the misery behind the making of this material: depression, weeks in the insane asylum, and, in some cases, suicide. Those who were not stricken with neurological symptoms might still succumb to blindness, impotency, and malfunctions of the vascular system and other organs. For each reported case, I could not help but wonder how many others retreated quietly into their disabilities or graves.

Yet, "[a]s their nerves and vessels weakened, the industry they worked in became stronger," writes Blanc. In *Fake Silk*, he exposes an industry that played hardball: implementing duopolies and price-fixing and influencing federal health standards. Viscose manufacturers, he writes, served as a "prototype of a multinational business enterprise, an early model of what would become the dominant modus operandi for large business entities after World War II."

The business of transforming plants into products is once again on the rise as consumers increasingly shun petroleum-based synthetic materials. China now accounts for 60% of rayon production, with India, Thailand, and several other countries accounting for the rest. (According to Blanc, U.S. production of viscose rayon has "gone offline.") Yet, despite modernization of the manufacturing process—including improved ventilation—worker safety, writes Blanc, is not a given. The few available reports on contemporary production suggest that recommended exposure limits are often exceeded. ("Not to worry," Blanc derisively notes when writing about the risk to consumers. "Any carbon disulfide that might have been in the fiber would have long since vaporized into the ... factory well before it ever got to the savvy shopper.")

The fabric's recent rebirth as an ecofriendly product [marketed by one manufacturer with the tagline "Nature returns to Nature" (*1*)], notes Blanc, is a "real tour de force of corporate chutzpah." But Blanc does not let the consumer off the hook either, noting our persistent blind spot when it comes to fast fashion and worker safety.

Reading *Fake Silk,* I could not help but wonder about the manufacturing process behind my T-shirt or the new dress hanging in my closet. Was someone harmed in the making of the kitchen sponge I just unwrapped? (The sponge and the cellophane it came in are also products of the cellulose carbon disulfide process.)

Years ago, I taught a class focused on toxic textiles. Had Blanc's book *Fake Silk* been available at the time, it certainly would have been on the reading list—with a caveat. Although his passion for the topic shines through, the book's sometimes excruciating detail (there are nearly 60 pages of notes) almost derailed me, particularly in the early chapters. But what at first seemed like a weakness eventually turned into a strength. In the end, I could almost see the parade of scientists, politicians, and industrialists who pushed and pulled this industrial fiber while factory workers and their families suffered.

"I am motivated by a desire to memorialize the terrible suffering that has occurred," writes Blanc. With *Fake Silk*, he has surely succeeded. ■

The reviewer is the author of Evolution in a Toxic World *(Island Press, Washington, DC, 2012). Email: emonosson@gmail.com*

REFERENCE

1. "Nature returns to Nature"; www.lenzing-fibers.com/en.

10.1126/science.aak9834

HEALTH POLICY

Embodied inequality

A diverse group of scholars tackles the relationships between health care and social justice

By **Daniel Goldberg**

Understanding Health Inequalities and Justice
New Conversations Across the Disciplines
Mara Buchbinder, Michele Rivkin-Fish, and Rebecca L. Walker, Eds.
UNC Press, 2016. 348 pp.

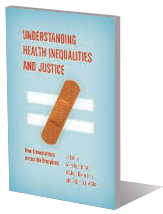

Inequality is core to virtually any Western conception of health justice. There is robust debate over which inequalities, if any, are unethical and over priority-setting among inequalities. *Understanding Health Inequalities and Justice*, edited by three scholars (two anthropologists and a philosopher) represents one of the latest contributions to this conversation.

The book is ambitious, aiming to "change the conversation about health inequalities and justice." The method for doing so is to "move beyond disciplinary divides." Based on issues explored at a 2013 conference at the University of North Carolina Institute for Arts and Humanities, the text is divided into three sections: "Interrogating Normative Perspectives on Health Inequality and Justice," "Disrupting Assumptions and Expanding Perspectives through Cases," and "Rethinking Evidence and the Making of Policy." To promote the interdisciplinary perspectives the editors deem essential to the book's aim, many of the chapters engage one or more of the other chapters in the book.

Anthologies arising from conferences typically struggle with coherence. This is unsurprising because the papers presented at a meeting typically were not conceptualized or written in dialogue with the other presented papers. The editors and authors are therefore to be commended for producing a readable, well-organized book that builds logically and sequentially from start to finish.

However, truly interdisciplinary scholarship is akin to a tiger—much spoken of but rarely seen in the wild. Collaborations between scholars hailing from different disciplines are not in and of themselves interdisciplinary. The criterion that distinguishes interdisciplinary scholarship from multi- or crossdisciplinary work is integration. To qualify, scholarship must successfully integrate the disciplinary perspectives into a cohesive whole that is not reducible to the sum of its disciplinary parts.

Most of the chapters in *Understanding Inequalities* do not achieve this kind of synthesis. Although the majority of them feature some attempt to engage work in at least one other chapter, most of these attempts feel forced and rushed, with much of the dialogue appearing only at the very end of the chapter. That said, several of the book's strongest chapters do succeed in demonstrating interdisciplinarity.

Insurance policies that promote early extraction may explain why Latino children tend to exhibit poorer oral health than their peers.

In chapter 5, anthropologists Sarah Horton and Judith Barker set out to determine the causes and effects of the high rate of oral disease in Latino children. The authors successfully integrate ethnographic analysis with population-level data. The analysis of individual and community narratives reveals a crucial point that population-level surveillance alone would miss: "Children's premature extractions may, over time, permanently affect their oral cavities; they may in fact produce the malocclusions, or 'crooked teeth,' that some parents lamented."

Horton and Baker elegantly demonstrate how state-level dental insurance programs in the United States promote such extractions as public policy precisely because alternative therapies are costly and time-consuming. "Parents' complaints of 'cracked' baby teeth yielding 'crooked' permanent teeth are not whimsical 'folk beliefs' but are supported by the expert literature," they conclude.

Carla Keirns's chapter on health care reform in the United States reflects her unique training in medicine, health services research, history, and bioethics and demonstrates the moral tension between policies that improve absolute population health but at the same time intensify the disadvantages of the least well-off. Health care reform in Massachusetts decreased the number of uninsured, she notes, but at the same time it "nearly bankrupted safety-net hospitals that had long served the most vulnerable because it failed to account for the clustering of the remaining uninsured at a few facilities." Keirns argues that the utilitarian assumptions driving economic modeling for health insurance reform produce comparatively less focus on inequitable distribution of benefits in favor of attention to aggregate benefits.

Nevertheless, much of the book is more fairly characterized as cross- or multidisciplinary conversations than as integrative, interdisciplinary work. This is not an evaluative statement; there is pressing need for cross-, multi-, and interdisciplinary work addressing health inequalities and justice. And, in fact, the book does succeed in pushing "new conversations across the disciplines" on these subjects.

Ultimately, regardless of the extent to which it merits the label "interdisciplinary," *Understanding Inequalities* is successful in its principal aims. Almost every chapter is interesting and provocative, and the book merits a place on the bookshelf of anyone interested in the myriad questions that attend health inequalities and justice. ■

The reviewer is at the Center for Bioethics and Humanities, University of Colorado Anschutz Medical Campus, Aurora, CO 80045, USA. Email: daniel.goldberg@ucdenver.edu

10.1126/science.aaj2241

PHOTO: CATHY YEULET/ISTOCK IMAGES

Rush Holt met with CAST Executive Secretary Shu Wei previous to signing an agreement on research integrity, science education, and engaging the public in science.

PHOTO: CHINA ASSOCIATION FOR SCIENCE AND TECHNOLOGY

Northeast Asia trip bolsters ongoing scientific cooperation

Chief Executive Officer Rush Holt offers strategy for building trust in science

By **Michaela Jarvis**

AAAS Chief Executive Officer Rush Holt urged a strong commitment to bringing the public and the science community closer together during a visit to Northeast Asia earlier this month. Over the course of a week-long trip to major science organizations in Tokyo, Beijing, and Seoul, Holt explained that only by encouraging ordinary citizens to demand evidence as they make decisions governing such important matters as their health, safety, and the environment, will the best outcomes be achieved.

"If societies and economies are to progress in the best possible ways, it will be because the public understands that science belongs to them, and not just to the scientists," said Holt, in a keynote speech at the opening of Science Agora, Japan's largest scientific forum, which is organized by the Japan Science & Technology Agency (JST). "The public can ask at every turn, what is the evidence? They can demand that others show a respect for evidence and demand that others not push evidence aside in favor of opinion and ideology."

"Science is a public undertaking for the benefit of the people," said Holt, who is also the executive publisher of the *Science* family of journals.

The 2 to 9 November trip to Asia—Holt was accompanied by AAAS Chief International Officer and Director of the Center for Science Diplomacy Tom Wang—continued a long history of AAAS engagement in the region. Over several decades, AAAS has built relationships with like-minded organizations there, comparing methods of dealing with local as well as global science-related challenges, bolstering advantageous scientific collaboration, and even helping to improve diplomatic relations, which Holt noted in a keynote speech at the opening of the Korea Foundation for the Advancement of Science & Creativity (KOFAC) Annual Conference, pointing out that "Science requires cooperation—and also engenders cooperation."

Earlier this year, AAAS signed a memorandum of understanding with the Korea Institute of S&T Evaluation and Planning (KISTEP) and expanded a liaison group of associations for the advancement of science to include JST and KOFAC. Representing one of AAAS's longest international collaborations, the China Associa-

There will be no increase in AAAS membership rates in 2017. For information on current rates, please visit **https://www.aaas.org/news/aaas-membership-rates-2017.**

Workers moved bags of contaminated debris after the 2011 earthquake, tsunami, and nuclear accident at Fukushima Daiichi power plant.

tion for Science and Technology (CAST) has shared a partnership with AAAS since 1978, before the normalization of diplomatic ties between the United States and the People's Republic of China.

Continuing that relationship, Holt and Wang met with officials at CAST and renewed a memorandum of understanding to continue collaboration in upholding research integrity and to support education through the advancement of science. This latest version of the agreement between AAAS and CAST will also strengthen ongoing efforts aimed at engaging the public in science and technology, Wang said in a media interview in Beijing.

The trip also included meetings with directors of the Chinese Academy of Sciences; China's Ministry of Science and Technology; the Japanese Ministry of Education, Culture, Sports, Science and Technology; South Korea's Ministry of Science; and KISTEP.

Students Yoko Oura, Ryo Endo, and Misato Nakatake and Holt at the JST-AAAS press conference.

Also this fall, Brian Lin, director of editorial strategy for the AAAS science news service EurekAlert!; Joy Ma, editorial content manager for EurekAlert! Chinese; and *Science Advances* Managing Editor Philippa Benson traveled to the region with a set of complementary goals—to help promote worldwide communication of scientific advances to and from the region, which is in general seeing a dramatic increase in scientific research.

This month's AAAS trips occurred amid an increasing need for science input on global challenges such as climate change and, even more broadly, for achieving the United Nations Sustainable Development Goals, which were internationally agreed upon last year to provide a path for all of society to an environmentally sustainable future. Holt referred to the goals as "an opportunity to communicate the lesson that science exists to benefit humankind and is relevant to people's lives and welfare."

The trip also coincided with an acute lack of public trust in science felt in many countries. In Japan, that lack is connected mainly to the 2011 earthquake, tsunami, and resultant nuclear disaster at the Fukushima Daiichi power plant, which left 18,000 dead and dislocated thousands more. According to online surveys by the National Institute of Science and Technology Policy in Japan, the disaster dramatically reduced the percentage of Japanese citizens confident in science and technology from about 84% to about 40%, although that figure has rebounded to about 66%.

A press conference held at Science Agora and jointly sponsored by JST and AAAS brought high school students who lived in the disaster area at the time of the nuclear accident to speak about their experiences and about their own trust in science with Holt and JST President Michinari Hamaguchi.

PHOTOS: (TOP TO BOTTOM) ISSEI KATO/REUTERS; SCIENCE AGORA 2016

The students said people in their communities are reluctant to believe what scientists say in local presentations about, for example, the relative safety of small doses of radiation.

"Rather than trusting those presentations, people are worried, because they cannot really trust science and technology," said Yoko Oura, a third-year high-school student at the Fukushima Prefectural Fukushima High School who plans to study medicine.

The students said that before the disaster, they were taught only about the advantages of nuclear power, not about its associated risks, reporting that their schools brought them to the nuclear facility on field trips.

Holt commented that omitting the dangers presented a misleading depiction of science, wherein everything is known and every risk eliminated. Holt told the students that, even apart from their tragic experience and disillusionment, science education should in general present "what we don't know."

"That would be much more interesting, it would be much more exciting, and it would be more realistic," Holt said. What scientists still do not understand is where "the adventure, the challenge, and the importance" of science lie, he added.

Holt expanded on this theme in his keynote speech at Science Agora, emphasizing that keeping ordinary citizens unaware of how science works sets up the potential for loss of trust.

"If scientists insist on presenting ourselves as the sole keepers of truth and let the general public think of us as set apart, we should not be surprised that people will accuse us of not telling the truth when bad things happen," Holt said.

Hamaguchi agreed, expressing a commitment to minimize the insularity of the Japanese scientific community.

"I have to say that in Japan, scientists attempt to stay in the ivory tower," Hamaguchi said. "At JST, we are trying to nurture scientists to build a bridge between society and science."

Wang, referring to all the events and meetings he and Holt participated in involving the three countries, said such dialogue helps to foster scientific progress in order to benefit society worldwide.

"The countries we visited are among the world's most advanced in science and technology, and the visit allowed AAAS to strengthen ties to the key scientific institutions there," Wang said. "These international partnerships are critical to building strong scientific communities that are well connected with our broader societies to confront the global challenges facing all of us."

Holt met with KOFAC Acting President WonKi Choi.

PHOTO: KOREA FOUNDATION FOR THE ADVANCEMENT OF SCIENCE & CREATIVITY

2016 AAAS Fellows approved by the AAAS Council

In October 2016, the Council of the American Association for the Advancement of Science (AAAS) elected 391 members as Fellows of AAAS. These individuals will be recognized for their contributions to science and technology at the Fellows Forum to be held on 18 February 2017 during the AAAS Annual Meeting in Boston, MA. Presented by section affiliation, they are:

Section on Agriculture, Food, and Renewable Resources

Michael F. Antonlin, *Colorado State University*
David R. Benson, *University of Connecticut*
Kelly A. Brayton, *Washington State University*
Steven D. Clouse, *National Science Foundation*
Katrien M. Devos, *University of Georgia*
Markus Flury, *Washington State University*
Walter Gassmann, *University of Missouri*
Maria Lucia Ghirardi, *National Renewable Energy Laboratory*
Alice C. Harmon, *University of Florida*
Stephen H. Howell, *Iowa State University*
Howard S. Judelson, *University of California, Riverside*
Pal Maliga, *Rutgers, The State University of New Jersey*
B. Gail McLean, *U.S. Department of Energy*
P.V. Vara Prasad, *Kansas State University*
Karen-Beth Goldberg Scholthof, *Texas A&M University*
Bir Bahadur Singh, *Texas A&M University*
Wallace E. Tyner, *Purdue University*
Rajeev K. Varshney, *International Crops Research Institute for the Semi-Arid Tropics (India)*
Guo-Liang Wang, *Ohio State University*
Rongling Wu, *Pennsylvania State University*

Section on Anthropology

Tom Boellstorff, *University of California, Irvine*
Anthony Di Fiore, *University of Texas at Austin*
Nathaniel J. Dominy, *Dartmouth College*
Owen K. Mason, *Geoarch Alaska/University of Colorado Boulder*
William M. Maurer, *University of California, Irvine*
Karen R. Rosenberg, *University of Delaware*
Gary T. Schwartz, *Arizona State University*
Mary S. Willis, *University of Nebraska-Lincoln*

Section on Astronomy

William J. Borucki, *NASA Ames Research Center*
Edward J. Groth, *Princeton University*
Nancy A. Levenson, *Space Telescope Science Institute*
Barbara Sue Ryden, *Ohio State University*
David R. Soderblom, *Space Telescope Science Institute*
Snežana Stanimirović, *University of Wisconsin-Madison*
Curtis John Struck, *Iowa State University*
Rosemary F.G. Wyse, *Johns Hopkins University*

Section on Atmospheric and Hydrospheric Sciences

Robert W. Corell, *Global Science Associates/ University of Tromsø (Norway)*
Konstantine P. Georgakakos, *Hydrologic Research Center/Scripps Institution of Oceanography, University of California, San Diego*
Steven M. Gorelick, *Stanford University*
W. Andrew Jackson, *Texas Tech University*
Cindy Lee, *Stony Brook University*
Venkatachalam Ramaswamy, *National Oceanic and Atmospheric Administration*
Jiří Šimůnek, *University of California, Riverside*
Lynne D. Talley, *Scripps Institution of Oceanography/ University of California, San Diego*
Hanqin Tian, *Auburn University*
Eric F. Wood, *Princeton University*
Renyi Zhang, *Texas A&M University*

Section on Biological Sciences

John Howard Adams, *University of South Florida*
Charles D. Amsler, *University of Alabama at Birmingham*
José M. Argüello, *Worcester Polytechnic Institute*
Ralph B. Arlinghaus, *University of Texas MD Anderson Cancer Center*
Steven N. Austad, *University of Alabama at Birmingham*
Paul Babitzke, *Pennsylvania State University*
Ian Thomas Baldwin, *Max Planck Institute for Chemical Ecology (Germany)*
Jill S. Baron, *U.S. Geological Survey*
Welcome W. Bender, *Harvard Medical School*
Patricia E. Berg, *George Washington University*
Eleanor A. Blakely, *Lawrence Berkeley National Laboratory*
George S. Bloom, *University of Virginia*
David L. Brautigan, *University of Virginia School of Medicine*
Volker P. Brendel, *Indiana University*
David Alan Brow, *University of Wisconsin-Madison*
John E. Burris, *Burroughs Wellcome Fund*
Hannah V. Carey, *University of Wisconsin-Madison*
Junjie Chen, *University of Texas MD Anderson Cancer Center*
Suzie Chen, *Rutgers, The State University of New Jersey*
Xiaodong Cheng, *University of Texas Health Science Center*
Janice E. Clements, *Johns Hopkins University School of Medicine*
Robert A. Copeland, *Epizyme, Inc.*
William A. Cramer, *Purdue University*
William A. Cresko, *University of Oregon*
Thomas E. Dever, *National Institute of Child Health and Human Development/NIH.*
James Andrew DeWoody, *Purdue University*
Michael B. Elowitz, *California Institute of Technology/Howard Hughes Medical Institute*
John J. Ewel, *University of Florida*
Stephen P. A. Fodor, *Cellular Research, Inc.*
Kathleen R. Foltz, *University of California, Santa Barbara*
David A. Fruman, *University of California, Irvine*
Phillip "Andy" Futreal, *University of Texas MD Anderson Cancer Center*
George Fu Gao, *Chinese Academy of Sciences/ Chinese Center for Disease Control and Prevention*
David Moore Glover, *University of Cambridge (UK)*
Barbara Lynn Golden, *Purdue University*
Joel Mitchell Goodman, *University of Texas Southwestern Medical School*
Steven R. Goodman, *University of Tennessee Health Science Center*
Max E. Gottesman, *Columbia University*
Geoffrey L. Greene, *University of Chicago*
Wei Gu, *Columbia University*
Xun Gu, *Iowa State University*
Phyllis Ida Hanson, *Washington University School of Medicine in St. Louis*
Jeffrey Field Harper, *University of Nevada, Reno*
Jack Jacek Hawiger, *Vanderbilt University School of Medicine*
Wolf-Dietrich Heyer, *University of California, Davis*
Timothy T. Hla, *Boston Children's Hospital/ Harvard Medical School*
Robert Dan Holt, *University of Florida*
Karen W. Hughes, *University of Tennessee, Knoxville*
Neil Hunter, *University of California, Davis/ Howard Hughes Medical Institute*
Jerard Hurwitz, *Memorial Sloan Kettering Cancer Center*
Sue L. Jaspersen, *Stowers Institute for Medical Research*
Henry B. John-Alder, *Rutgers, The State University of New Jersey*
Monica J. Justice, *The Hospital for Sick Children/ University of Toronto (Canada)*
Yibin Kang, *Princeton University*
Michael Kaspari, *University of Oklahoma*
Terri Goss Kinzy, *Rutgers, The State University of New Jersey*
Mark Kirkpatrick, *University of Texas at Austin*
Yuan-Chuan Lee, *Johns Hopkins University*
Jane Barbara Lian, *University of Vermont College of Medicine*
Jon Martin Lindstrom, *University of Pennsylvania Perelman School of Medicine*
Michael C. Lorenz, *University of Texas McGovern Medical School at Houston*
Michael S. Marks, *Children's Hospital of Philadelphia Research Institute/University of Pennsylvania Perelman School of Medicine*
Sarah Mathews, *Australian National Herbarium, CSIRO*
Glenn Merlino, *National Cancer Institute/NIH*
Peter B. Moyle, *University of California, Davis*
Gregory M. Mueller, *Chicago Botanic Garden*
Mary C. Mullins, *University of Pennsylvania Perelman School of Medicine*
Mona Nemer, *University of Ottawa (Canada)*
Kathleen J. Newton, *University of Missouri*
Krishna K. Niyogi, *Howard Hughes Medical Institute/ University of California, Berkeley/Lawrence Berkeley National Laboratory*
Ann Carol Palmenberg, *University of Wisconsin-Madison*
David Patterson, *University of Denver*
James C. Paulson, *The Scripps Research Institute*
Debra P. C. Peters, *U.S. Department of Agriculture*
Anne L. Plant, *National Institute of Standards and Technology*
Clifton A. Poodry, *Howard Hughes Medical Institute*
Kathleen Postle, *Pennsylvania State University*
A. Gururaj Rao, *Iowa State University*
John Franklin Rawls, *Duke University*
Monica Roth, *Rutgers, The State University of New Jersey*
Karla J. F. Satchell, *Northwestern University*
Martin A. Schwartz, *Yale University*
Phillip Andrew Scott, *University of Pennsylvania School of Veterinary Medicine*
Zu-Hang Sheng, *National Institute of Neurological Disorders and Stroke/NIH*
Ali Shilatifard, *Northwestern University Feinberg School of Medicine*
James J. Smith, *Michigan State University*
Patricia A. Sobecky, *University of Alabama*
John R. Speakman, *Chinese Academy of Sciences (China)/University of Aberdeen (UK)*
Jonathan P. Staley, *University of Chicago*
Janet L. Stein, *University of Vermont College of Medicine*
Carol A. Stepien, *University of Toledo/NOAA Pacific Marine Environmental Laboratory*
Gary D. Stormo, *Washington University School of Medicine in St. Louis*
Surachai Supattapone, *Dartmouth College*
Dean G. Tang, *Roswell Park Cancer Institute/ University at Buffalo, SUNY*
Ross A. Virginia, *Dartmouth College*
Sharlene C. Weatherwax, *U.S. Department of Energy*
Alissa M. Weaver, *Vanderbilt University School of Medicine*
Steven A. Whitham, *Iowa State University*
Michael Robert Willig, *University of Connecticut*
Donald R. Zak, *University of Michigan*

Section on Chemistry

James B. Ames, *University of California, Davis*
Paul A. Aristoff, *Aristoff Consulting*
Raymond Dean Astumian, *University of Maine*
Lisa M. Berreau, *Utah State University*
R. Morris Bullock, *Pacific Northwest National Laboratory*
Mark R. Chance, *Case Western Reserve University*
Jorge L. Colón, *University of Puerto Rico, Río Piedras*
Catherine E. Costello, *Boston University School of Medicine*
Gerard Charles Dismukes, *Rutgers, The State University of New Jersey*
Jean-Pol Dodelet, *Institut national de la recherche scientifique (INRS) (Canada)*
Patrick H. Dussault, *University of Nebraska-Lincoln*
David Fielder Eaton, *Light Insights, LLC*
Irving Robert Epstein, *Brandeis University*
William H. Green, *Massachusetts Institute of Technology*
István T. Horváth, *City University of Hong Kong*
Hilkka Inkeri Kenttämaa, *Purdue University*
Craig W. Lindsley, *Vanderbilt University*
Fred Edward Lytle, *Indigo BioAutomation*
Julie T. Millard, *Colby College*
Stephen L. Morgan, *University of South Carolina*

Published by AAAS

James Henderson Naismith, *University of St. Andrews (UK)/Sichuan University (China)*
Thomas J. Pinnavaia, *Michigan State University*
Martyn Poliakoff, *University of Nottingham (UK)*
Robert Powers, *University of Nebraska-Lincoln*
Chad M. Rienstra, *University of Illinois at Urbana-Champaign*
William L. Schinski, *Chevron (Retired)*
Diane Grob Schmidt, *University of Cincinnati*
David K. Shuh, *Lawrence Berkeley National Laboratory*
Brock Spencer, *Beloit College*
Hans-Peter Steinrück, *Universität Erlangen-Nürnberg (Germany)*
Tjerk P. Straatsma, *Oak Ridge National Laboratory*
Dean J. Tantillo, *University of California, Davis*
Donald A. Tomalia, *NanoSynthons LLC/University of Pennsylvania/Virginia Commonwealth University*
Shiou-Chuan (Sheryl) Tsai, *University of California, Irvine*
David H. Waldeck, *University of Pittsburgh*
Daniel John Weix, *University of Rochester*
Hong-Cai "Joe" Zhou, *Texas A&M University*

Section on Dentistry and Oral Health Sciences

Luisa A. DiPietro, *University of Illinois at Chicago*
Christopher H. Fox, *International and American Associations for Dental Research*
Arthur R. Hand, *University of Connecticut*
Michael Lansdell Paine, *University of Southern California*

Section on Education

Amy L. Chang, *American Society for Microbiology*
Florence Dowdell Fasanelli, *AAAS (Retired)*
Mary Anne Holmes, *University of Nebraska-Lincoln*
Judith Marie Iriarte-Gross, *Middle Tennessee State University*
William F. McComas, *University of Arkansas*
Linda L. Slakey, *University of Massachusetts Amherst*
Eric Paul Wiertelak, *Macalester College*

Section on Engineering

Chandra Mauli Agrawal, *University of Texas at San Antonio*
Kaustav Banerjee, *University of California, Santa Barbara*
Michael Bass, *University of Central Florida*
Kamran Behdinan, *University of Toronto (Canada)*
Gerald M. Borsuk, *Naval Research Laboratory*
Susmita Bose, *Washington State University*
Alexander N. Cartwright, *State University of New York*
Shu-Ching Chen, *Florida International University*
Jianjun Cheng, *University of Illinois at Urbana-Champaign*
Simon R. Cherry, *University of California, Davis*
Brian T. Cunningham, *University of Illinois at Urbana-Champaign*
David Darwin, *University of Kansas*
Peter Francis Davies, *University of Pennsylvania*
Z. Hugh Fan, *University of Florida*
Philippe M. Fauchet, *Vanderbilt University*
James H. Garrett Jr., *Carnegie Mellon University*
Roger Ghanem, *University of Southern California*
David Arthur Gough, *University of California, San Diego*
Ashwani K. Gupta, *University of Maryland, College Park*
Chih-Ming Ho, *University of California, Los Angeles*
Hongxing Jiang, *Texas Tech University*
Ali Khounsary, *Illinois Institute of Technology*
Ilona Kretzschmar, *City College of City University of New York*
Sidney Leibovich, *Cornell University*
Frank L. Lewis, *University of Texas at Arlington*
Xuelong Li, *Chinese Academy of Sciences*
Zheng-Hong Lu, *University of Toronto (Canada)*
Carmen S. Menoni, *Colorado State University*
Matthew W. Ohland, *Purdue University*
Jeffrey Alan Packer, *University of Toronto (Canada)*
Joan M. Redwing, *Pennsylvania State University*
Paul Sajda, *Columbia University*
Kamal Sarabandi, *University of Michigan*
Mohammad Shahidehpour, *Illinois Institute of Technology*
Michael J. Solomon, *University of Michigan*
Yu Sun, *University of Toronto (Canada)*
Mason B. Tomson, *Rice University*
Judson W. Virden Jr., *Pacific Northwest National Laboratory*
Xin Zhang, *Boston University*
Wei Hong (Katie) Zhong, *Washington State University*
Yimei Zhu, *Brookhaven National Laboratory*

Section on General Interest in Science and Engineering

Paul G. Heltne, *Chicago Academy of Sciences*
Igor Linkov, *U.S. Army Engineer Research and Development Center*

Section on Geology and Geography

Bryan Charles Chakoumakos, *Oak Ridge National Laboratory*
Peter U. Clark, *Oregon State University*
Henry J. B. Dick, *Woods Hole Oceanographic Institution*
Michelle Anne Kominz, *Western Michigan University*
Zhe-Xi Luo, *University of Chicago*
Stephen J. Mackwell, *Universities Space Research Association*
Alan C. Mix, *Oregon State University*
Bruce L. Rhoads, *University of Illinois at Urbana-Champaign*
John W. Valley, *University of Wisconsin-Madison*
Herman B. Zimmerman, *National Science Foundation (retired)*

Section on History and Philosophy of Science

Heather E. Douglas, *University of Waterloo (Canada)*
Michael A. Osborne, *Oregon State University*
Susan G. Sterrett, *Wichita State University*

Section on Industrial Science and Technology

Baohua Gu, *Oak Ridge National Laboratory/ University of Tennessee, Knoxville*
Harald Hess, *Janelia Farm Research Campus, HHMI*

Section on Information, Computing, and Communication

Divyakant Agrawal, *University of California, Santa Barbara*.
Rajeev Alur, *University of Pennsylvania*
Philip A. Bernstein, *Microsoft Research*
Elisa Bertino, *Purdue University*
Vijayakumar Bhagavatula, *Carnegie Mellon University*
Ronald F. Boisvert, *National Institute of Standards and Technology*
Lynn Conway, *University of Michigan*
Inderjit S. Dhillon, *University of Texas at Austin*
Dmitry B. Goldgof, *University of South Florida*
Ramesh C. Jain, *University of California, Irvine*
Frederick E. Petry, *Naval Research Laboratory*
Eugene Santos Jr., *Dartmouth College*
Howard E. Shrobe, *Massachusetts Institute of Technology*
Larry Lee Smarr, *University of California, San Diego*
Diane L. Souvaine, *Tufts University*
Josep Torrellas, *University of Illinois at Urbana-Champaign*
Gene Tsudik, *University of California, Irvine*
Zhi-Hua Zhou, *Nanjing University (China)*
Wenwu Zhu, *Tsinghua University (China)*

Section on Linguistics and Language Sciences

Jonathan David Bobaljik, *University of Connecticut*
Shari R. Speer, *Ohio State University*
Dieter Wunderlich, *Center for General Linguistics (Germany)*

Section on Mathematics

James W. Cogdell, *Ohio State University*
Robert M. Guralnick, *University of Southern California*
David Kinderlehrer, *Carnegie Mellon University*
Santiago Schnell, *University of Michigan*

AAAS NEWS & NOTES

Section on Medical Sciences

Stephen J. Brandt, *Vanderbilt University Medical Center*

David E. Briles, *University of Alabama at Birmingham*

Powel H. Brown, *University of Texas MD Anderson Cancer Center*

Wendy Cozen, *University of Southern California*

Wael El-Rifai, *Vanderbilt University Medical Center*

Andrew R. Hoffman, *Stanford University Medical Center*

Eugenie S. Kleinerman, *University of Texas MD Anderson Cancer Center*

Edison Tak-Bun Liu, *The Jackson Laboratory*

Peter Lobel, *Rutgers Robert Wood Johnson Medical School*

Charles J. Lockwood, *University of South Florida*

Robert L. MacDonald, *Vanderbilt University Medical Center*

Joseph Bernard Margolick, *Johns Hopkins University*

Christopher J. Molloy, *Rutgers, The State University of New Jersey*

Jeffrey N. Myers, *University of Texas MD Anderson Cancer Center*

Martin G. Myers Jr., *University of Michigan*

Liise-anne Pirofski, *Albert Einstein College of Medicine*

David Brent Polk, *University of Southern California/ Children's Hospital Los Angeles*

David T. Scadden, *Harvard University/Massachusetts General Hospital*

Michael D. Schneider, *Imperial College London (UK)*

Dong Moon Shin, *Emory University*

Lawrence Steinman, *Stanford University School of Medicine*

Terrence L. Stull, *Phoenix Children's Research Institute*

David J. Tweardy, *University of Texas MD Anderson Cancer Center*

Thomas J. Walsh, *Weill Cornell Medicine*

Joe Brice Weinberg, *Duke University Medical Center*

Edward T. H. Yeh, *University of Texas MD Anderson Cancer Center*

Jia Long Zhuo, *University of Mississippi Medical Center*

Section on Neuroscience

Jesús Avila, *CSIC-Universidad Autónoma de Madrid (Spain)*

Azad Bonni, *Washington University in St. Louis*

Roger James Colbran, *Vanderbilt University*

Charles August Greer, *Yale University School of Medicine*

Kristen M. Harris, *University of Texas at Austin*

Daniel Johnston, *University of Texas at Austin*

Yueming Li, *Memorial Sloan Kettering Cancer Center*

Kenneth Paul Mackie, *Indiana University*

Elly Nedivi, *Massachusetts Institute of Technology*

Ardem Patapoutian, *The Scripps Research Institute*

Henry L. Paulson, *University of Michigan*

Gary Edward Pickard, *University of Nebraska-Lincoln*

Martin C. Raff, *University College London (UK)*

Clifton W. Ragsdale, *University of Chicago*

Laura P. W. Ranum, *University of Florida*

Nina Felice Schor, *University of Rochester Medical Center*

Amita Sehgal, *University of Pennsylvania Perelman School of Medicine*

Leslie P. Tolbert, *University of Arizona*

Benjamin L. Wolozin, *Boston University School of Medicine*

Section on Pharmaceutical Sciences

Per Artursson, *Uppsala University (Sweden)*

Ah-Ng Tony Kong, *Rutgers, The State University of New Jersey*

Shyam S. Mohapatra, *University of South Florida*

James M. O'Donnell, *University at Buffalo, SUNY*

Craig K. Svensson, *Purdue University*

Section on Physics

John R. Arrington, *Argonne National Laboratory*

Luis Balicas, *Florida State University*

Alice Bean, *University of Kansas*

John Michael Blondin, *North Carolina State University*

Andrea Cavalleri, *Max Planck Institute for the Structure and Dynamics of Matter (Germany)*

Bradley B. Cox, *University of Virginia*

Scott A. Crooker, *Los Alamos National Laboratory*

Steven T. Cundiff, *University of Michigan*

David J. Dean, *Oak Ridge National Laboratory*

Jerry P. Draayer, *Louisiana State University*

Henry O. Everitt III, *U.S. Army*

Jonathan L. Feng, *University of California, Irvine*

Mary K. Gaillard, *University of California, Berkeley/Lawrence Berkeley National Laboratory*

Berend T. Jonker, *Naval Research Laboratory*

Wolfgang Ketterle, *Massachusetts Institute of Technology*

Dennis K. Killinger, *University of South Florida*

Albert John Lazzarini, *California Institute of Technology*

Don Lincoln, *Fermilab*

William C. Louis III, *Los Alamos National Laboratory*

Jay N. Marx, *LIGO Laboratory, California Institute of Technology*

Howard S. Matis, *Lawrence Berkeley National Laboratory*

A. Alan Middleton, *Syracuse University*

Louis M. Pecora, *Naval Research Laboratory*

Hrvoje Petek, *University of Pittsburgh*

Kevin T. Pitts, *University of Illinois at Urbana-Champaign*

L. Ramdas Ram-Mohan, *Worcester Polytechnic Institute*

Markus B. Raschke, *University of Colorado*

Brian C. Sales, *Oak Ridge National Laboratory*

Jorge O. Sofo, *Pennsylvania State University*

Din Ping Tsai, *Academia Sinica (Taiwan)*

Brian D. Wirth, *University of Tennessee, Knoxville*

Kun Yang, *Florida State University*

Arjun G. Yodh, *University of Pennsylvania*

Section on Psychology

Norma Graham, *Columbia University*

Ruben C. Gur, *University of Pennsylvania*

James Henry Howard Jr., *Catholic University of America*

Elizabeth F. Loftus, *University of California, Irvine*

Ricardo Felipe Muñoz, *Palo Alto University/ University of California, San Francisco*

Abigail J. Stewart, *University of Michigan*

Jyotsna Vaid, *Texas A&M University*

Bencie Woll, *University College London (UK)*

Section on Social, Economic, and Political Sciences

Douglas L. Anderton, *University of South Carolina*

Christopher B. Barrett, *Cornell University*

Richard T. Carson, *University of California, San Diego*

Holly Doremus, *University of California, Berkeley School of Law*

Stanley Presser, *University of Maryland, College Park*

Section on Societal Impacts of Science and Engineering

Clinton J. Andrews, *Rutgers, The State University of New Jersey*

Brenda Ekwurzel, *Union of Concerned Scientists*

John S. Gardenier, *National Center for Health Statistics (Retired)*

Kaye Husbands Fealing, *Georgia Institute of Technology*

Section on Statistics

Alicia L. Carriquiry, *Iowa State University*

Michael R. Kosorok, *University of North Carolina at Chapel Hill*

George Ostrouchov, *Oak Ridge National Laboratory*

Jane F. Pendergast, *Duke University Medical Center*

Dale L. Preston, *HiroSoft International Corporation*

Francisco J. Samaniego, *University of California, Davis*

Yu Shyr, *Vanderbilt University Medical Center*

Hal S. Stern, *University of California, Irvine*

Anastasios A. Tsiatis, *North Carolina State University*

Xiao-Hua (Andrew) Zhou, *University of Washington/ Peking University (China)*

Lixing Zhu, *Beijing Normal University/ Hong Kong Baptist University*

Published by AAAS

ON THE CLOCK

Our bodies' internal timepieces drive daily rhythms and influence health

PHOTO: JOE BELCOVSON/SALK INSTITUTE

By **L. Bryan Ray** *and* **John Travis**

Benjamin Franklin, the sage of colonial America, advised that "Early to bed and early to rise, makes a man healthy, wealthy, and wise." Recent studies in circadian biology bear him out. Staying in synchrony with the 24-hour light-dark cycle of Earth does indeed provide benefits, if not to the pocketbook, at least to health and brain function.

Circadian biology is the study of the biochemical clocks that keep time in our brains and most cells in our bodies. Evidence is accumulating that misalignment of these clocks with the daily light-dark cycle of our environment can have profound effects on physiology, raising the risk of disease. At the same time, modern society generates pressures that tend to push activity and sleep out of sync with circadian biology. From extended work hours and shift work, to frequent air travel across time zones, to consumption of digital information late at night on electronic screens emitting "daylight" cues, many of us are subject to some amount of circadian disruption—including scientists whose research demands work at night. Learning how to have a healthy life despite these circadian disruptions will require a new understanding of how biological clocks influence physiological processes, which could ultimately lead to new applications in circadian medicine.

INSIDE

RELATED ITEMS

- LETTERS P. 964
- PODCAST
- VIDEO

It matters not only what, but when you eat. These mice ate the same amounts of a high-fat diet, but the thinner one was restricted to eating during the active phase of its circadian cycle.

THE SCIENTIFIC NIGHT SHIFT

Sometimes the pursuit of data clashes with a researcher's own circadian rhythms

By **Sam Kean**

All Rodrigo Medellín wanted was a nap. A biologist at the National Autonomous University of Mexico in Mexico City, he had been trapping bats for several nights in a row in the Lacandon rainforest near Guatemala, and was exhausted. "So I lay on the ground," he says, and blithely fell asleep. Forty winks later, he awoke uneasily. One of the deadliest snakes in Mexico, a tawny fer-de-lance, was slithering by his head, 30 centimeters away. "I did not move and let her pass," he recalls.

Even after the coast cleared and he set about his bat hunt again, fear wouldn't loosen its grip on his sleep-deprived mind. That entire night, "I kept hallucinating more snakes," he says. Every twitching shadow concealed another serpent, every rustling leaf had fangs. Although a veteran of the night shift, Medellín greeted that dawn frazzled.

Working nights is unavoidable, or at least commonplace, in certain scientific fields. If you want to study bat behavior or stellar nebulae or sleep physiology, you may have to become half-nocturnal yourself, and scientists who sign up for the night shift encounter problems that just don't arise during the day. They tumble down embankments in the pitch black, nod off midexperiment, and grow paranoid in the witching hours. It's a tough gig, and for these and other reasons psychologists and sleep experts take a dim view of night work, which can disrupt sleep, throw hormones out of whack, and make you measurably dumber. "Human beings are meant to be regulated by light," says Candice Alfano, a psychologist at the University of Houston in Texas who's leading a study for NASA that includes a focus on circadian rhythm disruptions. "We still have that biology, even though our social culture has changed dramatically."

And yet, few of the nocturnal researchers *Science* talked to would give up their work. Amid the misery and exhaustion, science after hours can still produce moments of serenity, even euphoria. "Either you're getting to know more about the natural world, or you're getting to know more about yourself," Medellín says. "It's always a source of happiness to me."

THE CHALLENGES faced by researchers on the night shift vary significantly by discipline. Biologists, for instance, sometimes upend their whole lives to match the nondiurnal schedules of certain plants and animals.

Nicky Creux, a postdoc at the University of California (UC), Davis, studies sunflowers, whose buds open up just before dawn. That means getting up at 3:30 a.m. for weeklong stretches to set up cameras and dissecting equipment, in order to track the minute-by-minute emergence and growth of anthers and styles, plant reproductive organs. Although she's naturally a morning lark, "Cycling out to the fields in the dark is pretty miserable," she laughs. At the end of one recent 6-day stretch, her fine motor skills basically broke down from exhaustion: She kept dropping the tiny flower parts and losing them in the grass. She's hoping the lost data won't submarine the whole week.

Creux's social life suffered as well, because she essentially lived those weeks in a different time zone from everyone around her. "Friends want to go to dinner and I can't," she says. "I have to be in bed by 8 p.m." She also found it hard to abandon the lab to rest while others nearby were still hard at work. "As a scientist, you're used to working 12-hour shifts, and staying until 7 p.m. I had to get my head around the fact that it's okay to go home at 3." Alfano says that like traditional night workers, such as hospital staff, janitors, and truckers, scientists can feel tempted to "cheat" and attend daytime events with friends and family. That can compromise an

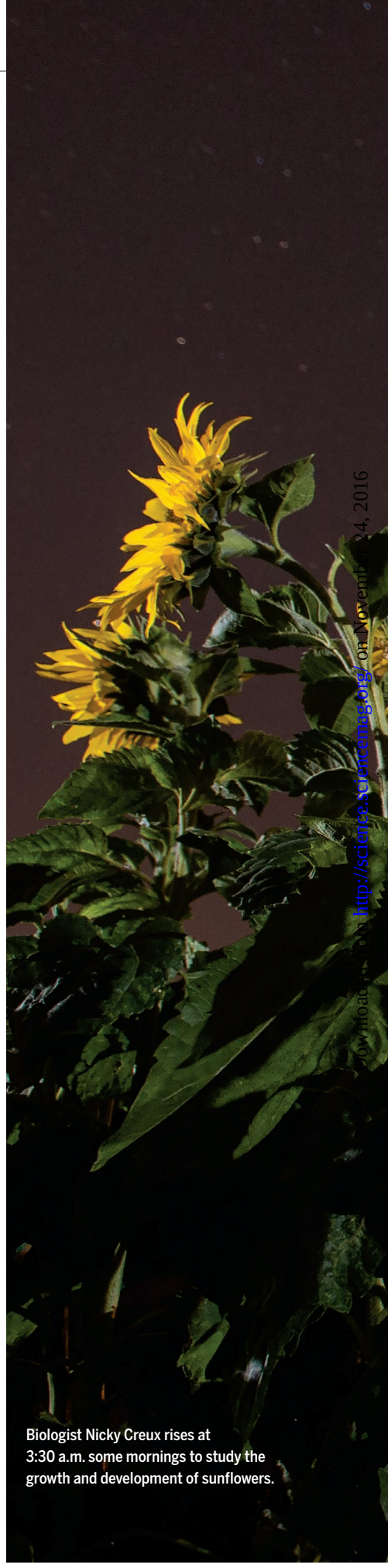

PHOTO: NOAH BERGER

Biologist Nicky Creux rises at 3:30 a.m. some mornings to study the growth and development of sunflowers.

Published by AAAS

The IceCube Neutrino Observatory at the South Pole attracts a special breed of scientists who can withstand the months-long days or nights.

already spotty sleep schedule. "At some point, you're really pushing the limit of what your sleep-wake system can do," she says.

Beyond the strange hours, nocturnal biologists often work in environments that can prove dangerous to human beings, who lack the dim light vision and sharp senses of smell or hearing that most night-adapted species rely on. Hong Young Yan, a fish and frog biologist at the Taiwan National Academy of Science in Taipei, was tramping along a dark trail at night once when a colleague went tumbling down a 30-meter embankment. "Suddenly, he just disappeared," Yan says. The colleague lived, but sprained an ankle and cried with pain as he limped back to camp. Another time, Yan walked smack into a beehive in the dark, and the colony erupted. "We had to run and jump into a stream" to dodge the swarm, he says.

To help his students overcome their fear of the dark, Medellín performs a little hazing ritual, which involves creeping up behind them in a jaguar mask. He gets a lot of screams. "Some might call it a bit of abuse," Medellín says, but he argues that maintaining a calm demeanor is essential when you dwell among the bats or other nocturnal animals: "The dark is much more comfortable, if you accept it."

UNLIKE BIOLOGISTS, astronomers usually moonlight indoors, in relative comfort. But being sedentary has its own downside: drowsiness.

Brent Miszalski, an astronomer in Cape Town who observes at the South African Astronomical Observatory in Sutherland, recalled one night during a multiweek telescope run when he helped clean up after a pipe burst. "I didn't do anything particularly strenuous," he says, "but the physical work, combined with the exhaustion, meant that when I had to start observing again, I fell asleep in the chair." He's far from alone.

Drowsiness hits regulars on the night shift for two reasons. First, night work violates our body's expectations about when to sleep and when to remain alert. Second, compensatory daytime sleep usually stinks. Exposure to sunlight prevents the brain from producing melatonin and other natural soporifics. As a result, people sleep fewer hours, and less deeply, during the day. Alfano likens the overall feeling to chronic jet lag.

The poor sleep experienced by night workers also has knock-on effects. It can raise blood pressure and alter levels of hormones, such as ghrelin and leptin, that affect appetite and satiety. As a result, "People tend to snack through night shifts instead of sitting down to eat meals, and those snacks are often quite unhealthy," says Philip Tucker, a psychologist at Swansea University in the United Kingdom who studies shift workers. Not surprisingly, longtime night shift workers suffer from obesity and other conditions such as cardiovascular disease at rates up to double that of daytime workers.

No studies specifically examine whether scientists on the night shift suffer those problems. And most researchers don't work at night for months or years at a stretch. Indeed, there's a trend nowadays toward less night work. Computer technology has automated many tasks, and many observatories and particle accelerators have dedicated technicians to run the complex instruments. Astronomers, for example, can observe the sky remotely by requesting a series of observations and simply waiting for the results, without having to travel and turn their daily routine upside down.

Still, night shifts remain a tradition and even a badge of honor in many fields, and the on/off schedules at such facilities—at Miszalski's observatory, most astronomers work a "night week" each month—can be physically grueling. "It's the worst of both worlds," Tucker says. "A week [at night] definitely disrupts the body clock. But by the time you get to the end, and are approaching adjustment, you go back" to daytime hours, wiping you out all over again. In order to minimize such disruptions, Miszalski prefers working 2-week-long observation shifts every few months.

The toll on the body can impair the mind as well. Night work may slow down mental processing, shorten attention span, and leave people feeling unmotivated. NASA scientist-astronaut Tracy Caldwell Dyson, who studied gas chemistry in orbit, had to endure several "slam-shifts" during her two tours on the

PHOTO: STEPHAN RICHTER, ICECUBE/NSF

International Space Station. These consisted of a full day's work, a "silly 2-hour nap," she says, and another immediate shift, usually to coordinate with ground crews in Russia. During such shifts, Dyson and other astronauts occasionally took computer tests to measure mental sharpness—matching patterns, or adding up strings of small numbers. The results were clear, she says: "We're kidding ourselves to think we're at our best when sleep is compromised."

Astronomer Vivian U, a postdoc at UC Riverside, once tried writing a paper overnight at the United Kingdom Infrared Telescope on Mauna Kea in Hawaii, where the 4267-meter elevation can exacerbate the mental loopiness caused by an extended stint of night work. Feeling inspired, she crafted a brilliant analogy about the similarities between the formation of galaxies and apples falling from trees. The next morning she realized it was gibberish.

All joking aside, night shift–induced mental fogginess does increase the odds of mishaps. Overnight workers contributed in small but significant ways to the accidents at Three Mile Island in Pennsylvania and Chernobyl in Ukraine as well as the Challenger space shuttle explosion. Several studies have found that medical staff working daylong, or longer, shifts make more errors (e.g., misreading electrocardiogram outputs, giving the wrong medication) when chronically deprived of sleep. Nor does the danger stop at work. Studies of doctors and nurses on night shifts found them twice as likely to get in wrecks or nod off behind the wheel on the drive home.

Some facilities have informal rules to save scientists from somnolent stupidity. "I was told to never send an email from the control room at night," says Lizette Guzman-Ramirez, an astronomer at Leiden Observatory in the Netherlands. "You get up and read it the next morning, and it doesn't make any sense." Similarly, some nocturnal scientists have developed tricks to stay alert at 3 a.m. Miszalski and his co-workers have "nonsense conversations" or even "make animal noises" to perk up. When Guzman-Ramirez worked a few 14-hour nights by herself at a telescope in South Africa, she belted out pop songs at the top of her lungs. "I remember singing a lot of 'Torn,' by Natalie Imbruglia," she says. "It was my go-to karaoke song, and I perfected it."

If 14-hour overnight shifts sound bad, then pity poor polar scientists. During the polar winter they often endure several months without sunlight—the ultimate night shift. Not surprisingly, polar stations attract night owls. "I've always had this loathing for sunrise, because I knew I should be in bed already," says Mack van Rossem, a physicist at the IceCube Neutrino Observatory at the South Pole. But without a sunrise to cap his all-nighters during the winter, Van Rossem found himself drifting through 32-hour "days," where he'd sleep for 10 hours at once and work for 22. Now that the sun has risen for the year—it poked its head over the horizon in mid-September and won't set again for months—he's had trouble sleeping, logging 6 hours a night at most. "It definitely takes me a few hours to get going now," he says.

Polar scientists also struggle with another facet of winter life. Many outdoor polar experiments require absolute darkness, and residents at the bases must cover their windows to prevent light from leaking out. "So you're in a box all the time," Van Rossem says. "I really missed being able to look out the window."

John Parker, a medical doctor at the Australian Antarctic base at Davis, agrees. "When you're not looking out the window, your perspective of life changes," he says. "Small things become much larger." He called it mental "myopia," and in a detail worthy of Edgar Allan Poe, even found himself growing paranoid in the endless nighttime: "I'd lose something and think, 'Someone's taken it!' A bit of suspicion comes in." Other scientists who worked overnight shifts elsewhere reported similar, if subtler, mood swings, growing more irritable and snappy with colleagues.

Despite these rough patches, Parker appreciated his months-long night shift in Antarctica, calling it an adventure. Activities like dart nights and costume parties helped defuse tension, and the 16-person team held a barbecue in September to welcome the sun back. "It was cloudy, so we didn't see anything," he laughs, "but it was a special event." He'd definitely overwinter there again—following a suitable break. "Maybe after having some fresh fruit."

MANY SCIENTISTS who work at night share Parker's sentiments: It was miserable, and I loved it. Some savored the profound quiet, or a perfect sunrise, or shimmering green aurorae on white snow. Some learned to appreciate different tenors of darkness—the relatively bright desert sky at night versus caves and undercanopies so black that opening or closing your eyes makes no difference. If nothing else, some enjoyed binge-watching movies or catching up on neglected work. This past winter in Antarctica, Parker completed a memoir about several humanitarian medical missions he's served on. "And I can say I wrote my book in 1 night," he adds.

As they age, many nocturnal scientists find that their capacity for night work has diminished. Yet they still relish the chance to connect more deeply with some beloved species or natural wonder, and somehow the sacrifice and discomfort of night work makes it all the more special.

Sergio Speziale, a mineral physicist at the German Research Centre for Geosciences in Potsdam, has pulled many a long night at synchrotrons and other particle accelerators around the world, and his time served has left him feeling philosophical. "Repeated night shifts tend to amplify the effect of whatever happens," he says. "If things are really cool and interesting, there's a more euphoric approach to discovery. When things fall apart, the sadness is amplified, too. Working nights will always remain in my mind. It's sometimes good to experience that in life." ■

Bat biologist Rodrigo Medellín says, "The dark is much more comfortable if you accept it."

PHOTO: AMY COOPER

PERSPECTIVE

Circadian clocks: Not your grandfather's clock

Fred W. Turek[1,2,3]*

The last 20 years have seen the rapid evolution of our understanding of the molecular genes and networks that enable almost all forms of life to generate 24-hour—or circadian—rhythms. One finding has been particularly exciting: that the molecular circadian clock resides in almost all of the cells of the body and that the clock regulates the timing of many cellular and signaling pathways associated with multiple disease states. Such advances represent a new frontier for medicine: circadian medicine.

The first time a biomedical researcher sees the locomotor activity record of a rodent (e.g., mouse or hamster) that is "free running" without time cues such as a light-dark cycle, they are awestruck at the precise timing of the animal's daily activity: an almost invariant period close to 24 hours [i.e., circadian, from the Latin words circa (about) and dies (day)], day after day, week after week, month after month. What is the internal timing mechanism that enables a living organism to keep such precise track of the geophysical day imposed by the rotation of the earth even when external entraining factors (primarily the 24-hour light-dark cycle) have been removed? Indeed, the precision of the rhythmic expression of a physiological or behavioral rhythm that varies as little as 1 to 2 min over 24 hours for months is so remarkable it led to a school of thought in the 1950s and '60s that concluded that an organism could not keep such accurate time, so the timing must in fact be coming from some unknown physical timing cue impinging on life from the cosmos.

By the 1970s, the overriding consensus in the field was that the "clocks" regulating circadian rhythms in essentially all forms of life were located within the organism. In mammals, an apparent master circadian clock was found to be located in an area of the anterior hypothalamus, the suprachiasmatic nucleus (SCN), because lesioning the SCN abolished circadian rhythms (*1*, *2*). Because even unicellular organisms generate circadian rhythms and because studying mutations in the DNA of flies, fungi, or plants revealed that single genes somehow regulate the period of the clock, it was clear that circadian rhythms were generated by intracellular events. However, the fundamental mechanisms by which genes, proteins, and cellular processes could produce precise circadian oscillations was unknown, and no circadian clock genes had been identified in higher organisms. Investigators from that early era who now find themselves old enough to be grandfathers or grandmothers could not have predicted how rapidly the field would advance to uncover the fundamental molecular mechanisms and networks of the clock system that we now know regulates thousands of circadian rhythms at the cellular, metabolic, physiological, and behavioral levels. Nor did we ever imagine that this molecular clock would be embedded in a vast array of cellular processes that underlie health and disease. The circadian clock we know today is indeed not your "grandfather's clock."

As discussed in detail in the four review articles in this special section of *Science*, dozens of circadian clock genes are now known to regulate the cycling of mRNAs and proteins through transcriptional and translational feedback loops. The rapid pace of the discovery of the molecular clock was aided by the finding that the core clock genes are remarkably conserved across species as diverse as flies, mice, and humans, allowing for the integration of genetic and molecular discoveries across model species and humans. The use of a chemical mutagen coupled with phenotypic screening led to the discovery of the *Clock* mutant mouse, which expressed an abnormally long circadian period of 27 to 28 hours (*3*). When this first mammalian clock gene was cloned in 1997, it was a pleasant surprise to find that a homologous gene, when mutated in the fly, also altered the circadian period (*4*). Later in 1997, mammalian homologs of the first circadian clock gene cloned in the fly in 1984 (*per*) were found in mice and humans (*5*). Binding partners of the CLOCK and PER proteins (BMAL1 and CRY, respectively) were soon discovered, and the scaffold of the driver (CLOCK-BMAL1) and repressor (PER-CRY) limbs of the transcriptional-translational feedback oscillator was now in place to allow an in-depth understanding of the core molecular clock. The pace of discovery surrounding circadian clocks was featured by *Science* in their year-end Breakthrough of the Year: The Runners-Up selections in back-to-back years (1997 and 1998) when it was noted that "a volley of rapid-fire discoveries revealed the stunning universality of the clock's working" (*6*).

Although the discovery of the core clock genes and proteins was of great importance in the field, a corollary discovery had an equal impact and was not expected: The clock genes are expressed in almost all of the cells of the body not just the SCN. Furthermore, expression of the core circadian clock genes is cyclical, and the molecular clock regulated the timing of the

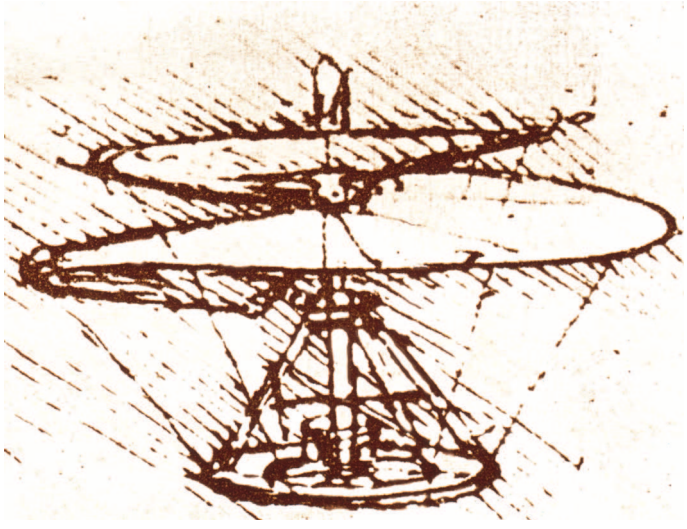

SHEILA TERRY/SCIENCE SOURCE

Fig. 1. Leonardo da Vinci's helical air screw. A blueprint, albeit an imperfect and incomplete one, of how circadian disorganization at the cellular level can be linked to pathophysiological states is available and awaits explanation that could lead to a new era for medicine: circadian medicine. Leonardo da Vinci drew the blueprint of the helicopter about 450 years before a helicopter was even built and could fly. The ongoing and expected rapid advances in circadian medicine should allow the present circadian blueprint to go from the bench to the bedside to standard clinical care and a healthy lifestyle in a period of time that is an order of magnitude less than that needed to go from da Vinci's blueprint to flight.

[1]Director, Center for Sleep and Circadian Biology, Northwestern University, Cook Hall, 2220 Campus Drive, Evanston, IL 60208, USA. [2]Charles E. and Emma H. Morrison Professor of Biology, Department of Neurobiology, Weinberg College of Arts and Sciences, Northwestern University, Evanston, IL 60201, USA. [3]Professor, Departments of Neurology and Psychiatry and Behavioral Sciences, Feinberg School of Medicine, Northwestern University, Chicago, IL 60611, USA.
*Corresponding author. Email: fturek@northwestern.edu

expression of hundreds—if not thousands—of "clock-controlled genes" (CCGs). It is estimated that almost half of the genes in the mouse genome oscillate with a circadian period in one or more organs of the body and that the cycling RNAs and proteins vary in different organs (*7*). Many of the CCGs are part of key cellular and signaling pathways that regulate metabolism and immune, hormonal, and neural functions. Thus, circadian synchronization within the cell and between organ systems of the whole organism is critical to health and well-being, and the breakdown of this 24-hour temporal order could lead to pathological conditions at many levels of organization.

"Thus, circadian synchronization within the cell and between organ systems of the whole organism is critical to health and well-being, and the breakdown of this 24-hour temporal order could lead to pathological conditions at many levels of organization."

This rapid evolution of circadian biology has led to unanticipated new avenues for understanding health and disease etiology. Although disrupted circadian rhythms, including disturbed sleep-wake cycles, were thought to be symptomatic of diseases, there is a growing awareness that this disruption may contribute to the development, progression, and severity of disease states, including depression, neurological disorders, obesity, diabetes, cardiovascular disease, and gastrointestinal disorders.

Circadian disorder can also occur when humans "voluntarily" disrupt the normal phase relation between their internal circadian clock(s) and the solar day. For many years it has been known that shift workers live in a chronic state of circadian misalignment and that they have an increased prevalence of many adverse health outcomes (*8*). Similarly, individuals flying across multiple time zones experience the malaise of jet lag, as it may take up to a week for the internal clock to synchronize with the local time. More recently, investigators have focused on a form of chronic circadian misalignment, referred to as "social jet lag," whereby circadian disruption that is equivalent to traveling across 2 to 4 time zones twice a week occurs in individuals who change the timing of their sleep-wake cycle during the week to conform to work or school compared with weekends when there are fewer restrictions on sleep or wake time. An increase in body mass index correlated with the magnitude of social jet lag has been found in large epidemiological studies (*9*).

The implication of the misalignment of the timing of food intake has received considerable attention since it was discovered that mice eating at the "wrong" time of day (during the light period for nocturnal mice) gain more weight than mice eating at the "right" time of day (during the dark period for mice), despite taking in similar amounts of calories and showing the same amount of activity (*10*). In addition, the normal rhythm of food intake in *Clock* mutant mice, as well as in mice fed a high-fat diet, is disrupted, such that mice eat about the same amount during the day as they do during the night and gain more weight than control animals (*11*, *12*). It is particularly noteworthy that the temporal patterns of sleep and feeding behaviors, although they have little effect on the SCN pacemaker, can entrain circadian oscillations in peripheral organs; this leads to desynchronization between central and peripheral oscillators, the health implications of which could well be involved in the etiology of multiple disease states.

A major issue that the circadian biomedical community faces today is how to bring to clinical practice the enormous advances in linking the molecular clock mechanisms to the numerous cellular and signaling pathways associated with many disease states. Although some progress has been made in influencing clinical care practitioners to take into account circadian changes in pharmacokinetics when determining optimal time of day and dose for drug treatment (*13*), there has been little progress in considering circadian disorganization as a clinically relevant risk factor and/or a contributor to the etiology of the disease state. There is a consensus in the circadian community about the need for biomarkers to assess circadian function, including molecular, cellular, and physiological signals, in health and disease (*14*); however, this is unlikely to occur until we can easily and routinely measure, in some depth, the overall internal circadian organization of an individual over the 24-hour day. For now, no single time point of biomarkers at even the "omics" level (e.g., transcriptomics, metabolomics, or proteomics) (*15*) is sufficient to differentiate and quantify the exact nature of disease-relevant circadian reprograming or disruptions that may have occurred (e.g., loss of rhythmicity of certain pathways and internal desynchrony among organs).

It is anticipated that rapid advances in systems biology, information technologies, and the development of a new generation of wearable or implantable biosensors will make it possible in the future to monitor hundreds—if not thousands—of circadian oscillating biomarkers in body fluids on a routine basis. Data could then be made available via remote-monitoring medical servers to physicians and other health care providers with the tools to continuously track in real time the entire "circadianome" of the individual. These data could be integrated with precision medicine initiatives, which will not be "precise" without the consideration of the circadian profile over time in healthy individuals or of changes that occur with the progression of a particular disease or disorder. Just as Leonardo da Vinci sketched the blueprint of a helicopter more than 400 years before one was actually built that could fly (Fig. 1), we have the blueprint of the molecular circadian clock, albeit an incomplete and imperfect one, to bring the advances in our understanding of the circadian clock system and its relation to multiple physiological and pathophysiological cellular pathways to application in standard clinical care. Given that advances in the circadian field and their implications for medicine are anticipated to continue to evolve at a rapid pace, it should not take 400 years to fully integrate the complex circadian organization that exists within health and disease states into a new frontier for medicine: circadian medicine.

REFERENCES AND NOTES

1. F. K. Stephan, I. Zucker, *Proc. Natl. Acad. Sci. U.S.A.* **69**, 1583–1586 (1972).
2. R. Y. Moore, V. B. Eichler, *Brain Res.* **42**, 201–206 (1972).
3. M. H. Vitaterna *et al.*, *Science* **264**, 719–725 (1994).
4. R. Allada, N. E. White, W. V. So, J. C. Hall, M. Rosbash, *Cell* **93**, 791–804 (1998).
5. H. Tei *et al.*, *Nature* **389**, 512–516 (1997).
6. *Science* News and Editorial Staff, *Science* **282**, 2157–2161 (1998).
7. R. Zhang, N. F. Lahens, H. I. Ballance, M. E. Hughes, J. B. Hogenesch, *Proc. Natl. Acad. Sci. U.S.A.* **111**, 16219–16224 (2014).
8. C. L. Drake, K. P. Wright, in *Principles and Practices of Sleep Medicine*, M. Kryger, T. Roth, W. Dement, Eds. (Elsevier, Philadelphia, ed. 6, 2016), pp. 715–725.
9. T. Roenneberg, K. V. Allebrandt, M. Merrow, C. Vetter, *Curr. Biol.* **22**, 939–943 (2012).
10. D. M. Arble, J. Bass, A. D. Laposky, M. H. Vitaterna, F. W. Turek, *Obesity (Silver Spring)* **17**, 2100–2102 (2009).
11. C. B. Green, J. S. Takahashi, J. Bass, *Cell* **134**, 728–742 (2008).
12. F. W. Turek *et al.*, *Science* **308**, 1043–1045 (2005).
13. K. Griffett, T. P. Burris, *Bioorg. Med. Chem. Lett.* **23**, 1929–1934 (2013).
14. P. C. Zee *et al.*, *Sleep* **37**, 219–227 (2014).
15. K. L. Eckel-Mahan *et al.*, *Proc. Natl. Acad. Sci. U.S.A.* **109**, 5541–5546 (2012).

ACKNOWLEDGMENTS

Thanks to M. Vitaterna, P. Jiang, K. Summa, and K. Lind for their helpful editorial comments.

21 October 2016; accepted 25 October 2016
10.1126/science.aal2613

REVIEW

Circadian time signatures of fitness and disease

Joseph Bass[1]* and Mitchell A. Lazar[2,3]*

Biological clocks are autonomous anticipatory oscillators that play a critical role in the organization and information processing from genome to whole organisms. Transformative advances into the clock system have opened insight into fundamental mechanisms through which clocks program energy transfer from sunlight into organic matter and potential energy, in addition to cell development and genotoxic stress response. The identification of clocks in nearly every single cell of the body raises questions as to how this gives rise to rhythmic physiology in multicellular organisms and how environmental signals entrain clocks to geophysical time. Here, we consider advances in understanding how regulatory networks emergent in clocks give rise to cell type–specific functions within tissues to affect homeostasis.

Developments in genetics and biochemistry have revealed pervasive regulation of cell and organismal function on a 24-hour circadian time scale across all photosensitive forms of life. The observation that photosensitive forms of life exhibit intrinsic timekeeping mechanisms was first established in the 18th century by de Mairan's observation of the autonomous leaf movement of the *Mimosa* plant. Internal circadian clocks emerged in cyanobacteria, the first organism capable of oxygenic photosynthesis, more than 2.5 billion years ago and enabled the anticipation of daily changes in the light-dark environment tied to the rotation of Earth. Insight into the selective advantage of temporal organization in lower organisms has focused on the integral role of clocks in DNA damage repair, the timing of oxygenic photosynthesis, and how temporal organization provides a means of averting futile energetic cycles.

The subsequent discovery of the molecular clock in animals established that genes control behavior. The circadian system is fundamentally a genetically encoded anticipatory mechanism that underlies both gene-environment and brain-behavioral interactions. As such, the study of molecular clocks provides insight into the dynamic control of genome biology and its link to systems physiology (Fig. 1). Here, we review progress in establishing the temporal principles of circadian regulation at the level of genome dynamics, and the role of both proper timing and mistiming in fitness and pathologic conditions. Our focus is mainly on findings applicable to mammalian cell and organismal physiology, although where appropriate, we provide reference to advances from prokaryotic, plant, and *Drosphila melanogaster* experimentation.

[1]Department of Medicine, Division of Endocrinology, Metabolism and Molecular Medicine, Feinberg School of Medicine, Northwestern University, Chicago, IL 60611, USA. [2]Division of Endocrinology, Diabetes, and Metabolism, Department of Medicine, Department of Genetics, Perelman School of Medicine, University of Pennsylvania, Philadelphia, PA 19104, USA. [3]The Institute for Diabetes, Obesity, and Metabolism, Perelman School of Medicine, University of Pennsylvania, Philadelphia, PA 19104, USA.
*Corresponding author. Email: j-bass@northwestern.edu (J.B.); lazar@mail.med.upenn.edu (M.A.L.)

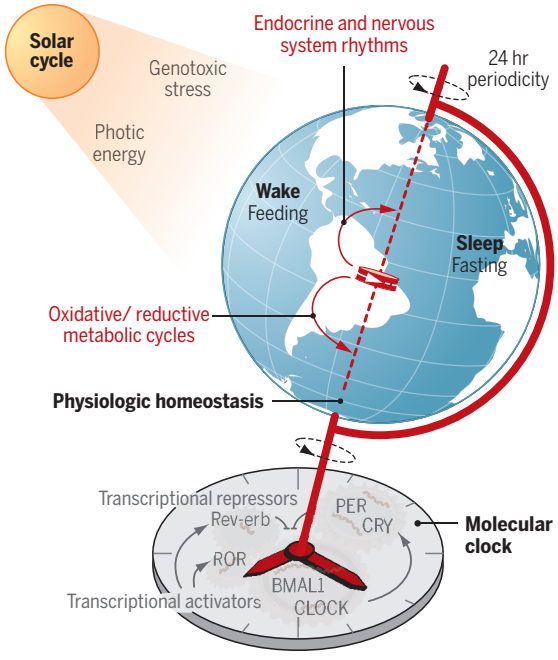

Fig. 1. Geophysical time drives circadian maintenance of homeostasis. The molecular clock is composed of an autoregulatory negative transcription feedback loop that synchronizes physiology and behavior in anticipation of the light-dark cycle. The illustration depicts variation in physiology for diurnal species (active in light); however, circadian cycles also govern sleep/wake and physiologic processes in nocturnal species (active in the dark), with an inverted phase. Exposure to sunlight induces DNA damage each day while also providing energy for oxygenic photosynthesis, processes that may explain the evolution of circadian clocks across four kingdoms of life. Clocks partition oxygenic and reductive metabolic cycles each day and separate these in coordination with the sleep/wake cycle. Although many physiologic processes maintain constancy of the internal milieu, including glucose metabolism, response to perturbation is tuned to circadian time.

Properties of the core clock and its output mechanisms

Nearly two centuries after de Mairan, Konopka and Benzer demonstrated in *D. melanogaster* that a single locus controls these rhythms in animals, although the molecular and cellular basis for this observation was not known (*1*). Formulation of the properties of these oscillators was transformed more than 14 years later with positional cloning of core clock genes and recognition that these encode transcription factors (TFs) that underlie daily rhythms of locomotor activity.

The discovery that PER (for "Period"), the first identified clock TF, itself undergoes 24 hours cycling (*2*) led to the idea that oscillation of the molecular clock relies on negative feedback, a central tenet in the field. PER is itself a repressor of the expression of transcriptional activators (a CLOCK/BMAL1 or CLOCK/NPAS2 heterodimer in mammals) that function in the forward limb as the transcriptional feedback loop. In mammals, the repressive TFs of the clock include the PER heterodimer partner called CRY (for "Cryptochrome"), in addition to a second level of repression mediated by another TF called Rev-erb (Fig. 2). Each day, entrainment of the clock to light occurs through activation of *Per* gene transcription in the negative limb, followed by its nuclear translocation and then repression of the activator limb (*3*).

All of these factors have been validated by using loss-of-function genetic models in mice. Intriguingly, several clock TFs—including PER, CLOCK, BMAL1, and NPAS2—contain a motif called the PAS domain that is found in other TFs that respond to environmental metabolites, xenobiotics, and oxygen fluctuation. Moreover, Rev-erb is a member of the nuclear receptor (NR) superfamily composed of TFs that respond to hormones, metabolites, and xenobiotics. Indeed, both Rev-erbα and Rev-erbβ have been shown to bind and respond to molecular heme (*4*, *5*), and the activating NR that opposes Rev-erb function, called ROR, is also regulated by metabolites, including cholesterol and other sterols (*6*). Thus, whereas the clock transcriptional process exhibits fixed 24-hour periodicity, the core clock components may also sense fluctuations in the cellular environment (*7*).

In addition to regulation of gene transcription through feedback repression, posttranslational signaling steps plays a central role in setting the correct pace of the clock cycle (Fig. 2). Best characterized in animal clocks has been the action of the casein kinase proteins, which phosphorylate and thereby modulate stability of the PER proteins and temperature invariance of the

clock cycle (*8*). In addition, members of the F-box cullin-like family of ubiquitin ligases Fbxl3 and Fbxl21 mediate CRY stability and proteasomal degradation (*3*). Phenotype-driven genetic screens and proteomic analysis of clock repressor complexes have highlighted the importance of phosphorylation and the interplay between activator and repressor complexes as a determinant of the circadian periodicity (*9*). Despite these advances, fundamental biochemical properties of the circadian clock remain unexplained, especially how the time constant remains invariant even when temperature shifts up to 10°C. Studies in syndromic sleep disorders in which families with heritable very early [familial advanced sleep-phase syndrome (FASPS)] or very late [delayed sleep-phase syndrome (DSPS)] bedtime tendency have identified mutations in the orthologous human clock genes, demonstrating conservation of the central pacemaker molecules across humans (*10*).

Cell type–specific regulation of the core clock and its outputs

The discovery that the transcriptional clock mechanism exists in essentially every cell of the body was a major breakthrough that also raised questions of hierarchy and specificity (*11*). The clock mechanism is composed of TFs that work in the genome by binding to specific DNA sequences; as such, the basic mechanism of transcriptional stimulation and negative feedback is universal. TFs regulate each other's expression via action at enhancer and repressor sites, for which access requires open chromatin. In this context, there is evidence that the core TFs can act as pioneer factors to open chromatin that might otherwise be inaccessible (*12*, *13*).

Yet an early hallmark of the tissue-specific clock transcriptome was the finding that despite the large number of oscillating RNAs in most organs (by some estimates more than 10%) (*14*), the identity of oscillating RNAs is divergent across tissues (*15*). Thus, the distinct clock output of each cell type not only contributes to tissue specificity but to organ-specific manifestations of circadian misalignment (Fig. 3). In addition to controlling each other's expression, core clock TFs bind and directly regulate clock output genes. Many of these clock-controlled genes are expressed in a tissue-specific manner and must therefore be regulated differently than the ubiquitous clock mechanism. An emerging theme in understanding clock-dependent, cell type–specific gene regulation is that core clock TFs act at tissue-specific enhancers established at clock output genes early in development (*16*–*19*).

Critical to this are lineage-specific TFs, which either function as pioneer factors early in ontogeny or bind to the genome at particular regions of chromatin that are already open in specific tissues. Cell type–specific TFs, such as FOXa in liver (*20*) and the pancreatic and duodenal homeobox 1 factor in pancreas (*17*), then contribute to further opening of chromatin through epigenomic mechanisms involving recruitment of transcriptional coregulators, including enzymes that modify histones or

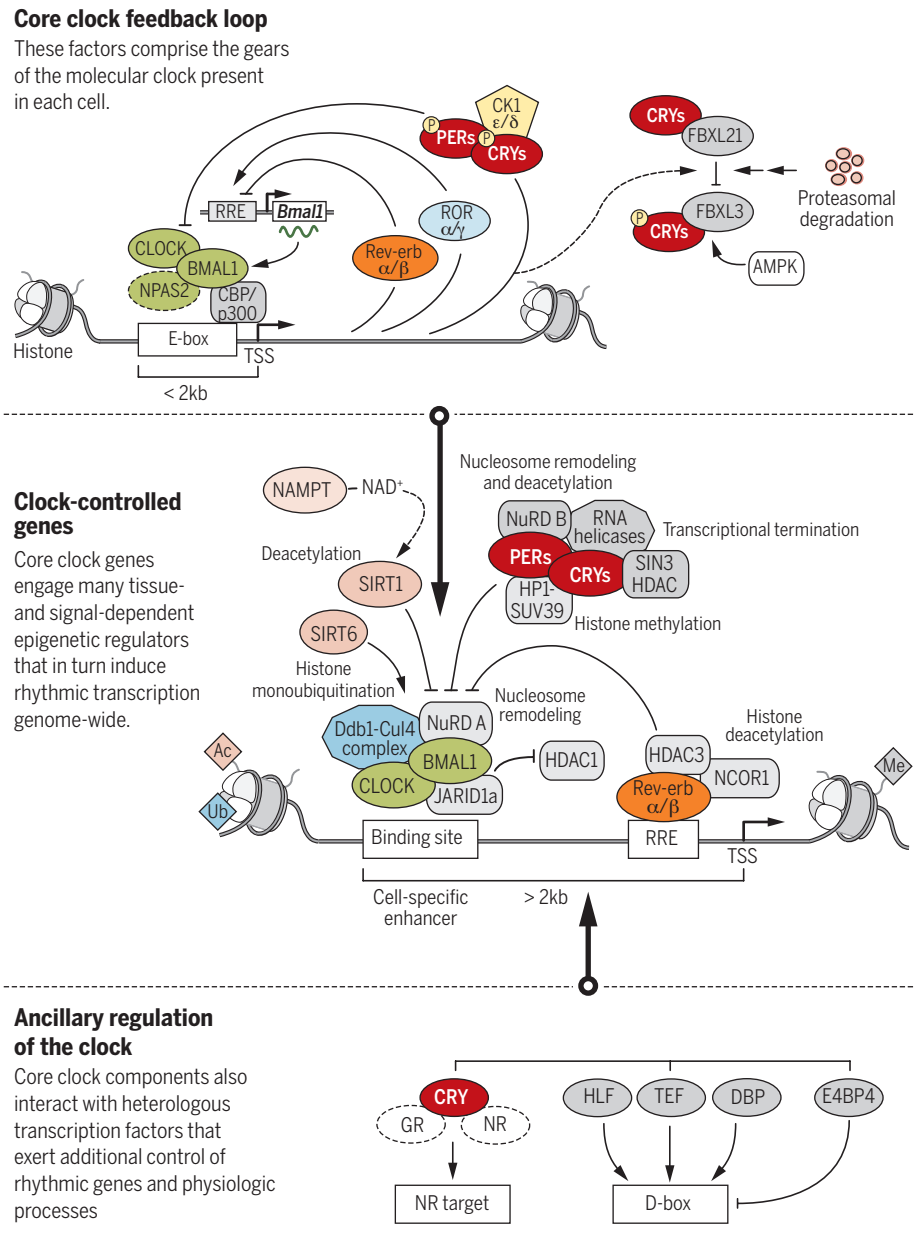

Fig. 2. Molecular regulation of cellular circadian processes. A unifying model of the circadian system involves a defined set of core clock genes that are essential for generation of ~24-hour oscillation in genome-wide transcription. The heterodimeric basic helix-loop-helix TFs CLOCK/BMAL1 and the CLOCK paralog NPAS2 compose the forward limb of the mammalian clock and bind to genomic enhancer elements to positively control circadian clock output genes as well as two distinct repressive pathways required for the negative feedback inherent in clock function. The repressive pathways involve the heterodimeric basic helix-loop-helix TFs PER/CRY and NRs Rev-erbα/β, which function both competitively and noncompetitively with activating ROR NRs at Rev-erb/ROR-response element (RRE)–containing enhancers that control *Bmal1* transcription as well as circadian clock output genes. The clock cycle is regulated through turnover of the repressors after phosophorylation mediated by CK1e/d and executed through ubiquitin-mediated proteasomal degradation involving FBXL3. Posttranscriptional regulation also plays a role in physiologic rhythms, including rhythmic regulation of RNA polyadenylation. Clock factors act through both direct and indirect mechanisms through binding to cell type–specific enhancers far from the transcription start site to regulate a wide array of clock-controlled genes. Both generation of the core clock transcription cycle and its output rhythms engage numerous epigenetic modifiers such as HDACs, methyltransferases, and nucleosome remodeling factors. Clock cycles are also sensitive to environmental signals, including metabolites, DNA damage activation, and signal transduction pathways, all of which feedback to modulate rhythmic transcription but do so differently in distinct tissues in both physiologic and pathologic states. HLF, hepatic leukemia factor; TEF, thyrotroph embryonic factor; DBP, albumin D-box binding protein.

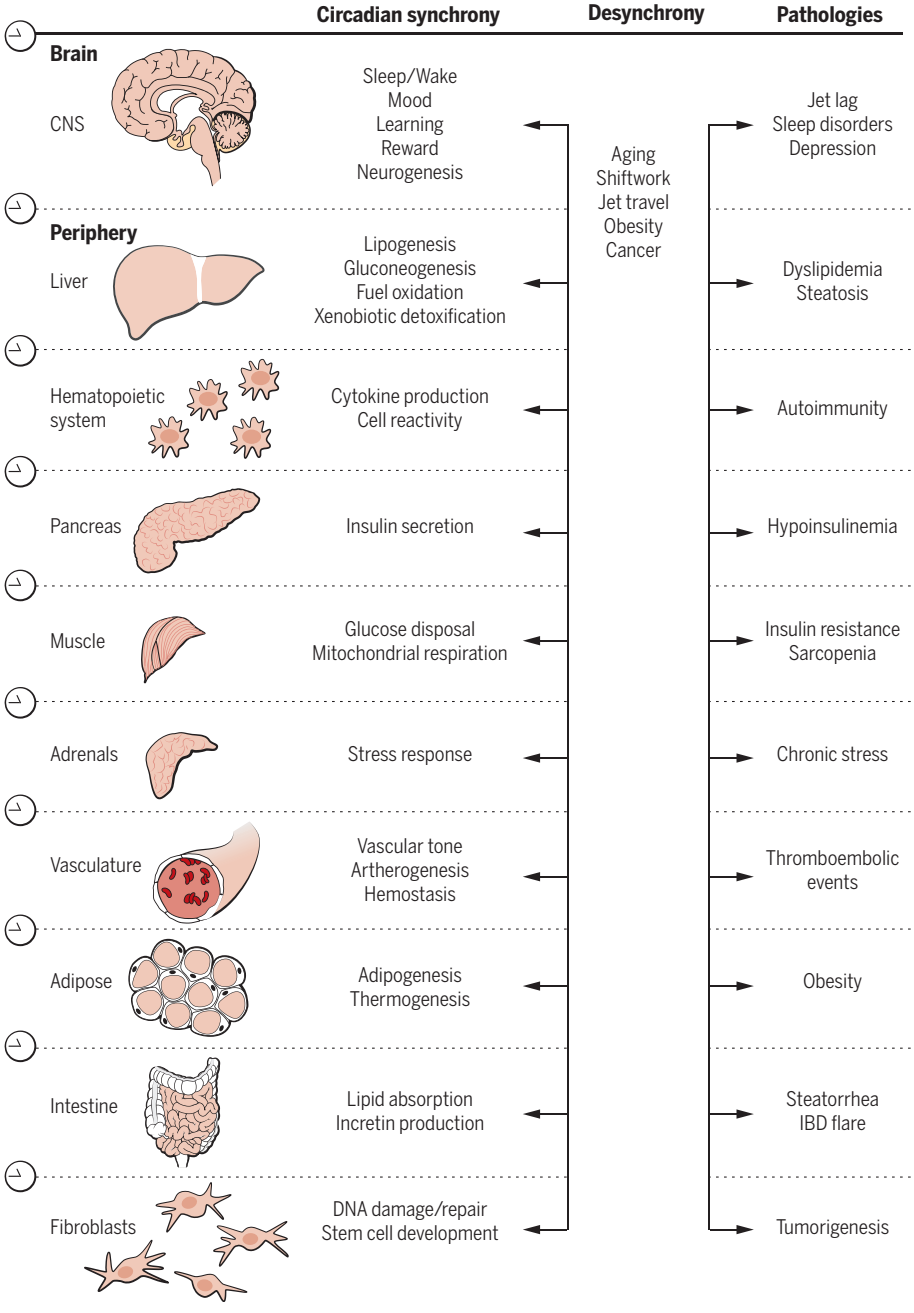

Fig. 3. Circadian systems in physiological cross-talk and disease. The circadian system is organized hierarchically with master pacemaker neurons in the central nervous system entrained to light each day, in turn conducting a distributed network of local clocks expressed in most peripheral cells and tissues. Within the brain, the clock plays a role not only in maintaining the timing of sleep/wake cycle relative to light but also in many behaviors, including learning, reward, and neurogenesis. Peripheral tissue clocks are entrained to the brain clock, although feeding and temperature are dominant in some physiological settings. Peripheral clocks may also become uncoupled and desynchronized from the central pacemaker during aging, shiftwork, jet travel, overnutrition, obesity, or cancer. Circadian disruption and associated impairment in sleep contributes to the molecular pathogenesis of disorders such as metabolic syndrome, obesity, diabetes, autoimmunity, and cancer.

remodel nucleosomes. This opens up binding sites that core clock TFs directly recognize via their DNA-binding specificity, and their binding further alters the epigenome via recruitment of coregulatory complexes. For example, histone acetylation controlled by histone acetyltransferases (HATs) and histone deacetylases (HDACs) is highly circadian across the genome at tissue-specific enhancers dictated by core TFs within the liver (*18*, *19*). Further, regulation of histone methylation status also contributes to circadian transcription timing (*21*, *22*). Complementing these direct mechanisms, the core TFs can also act indirectly by tethering to the cell type–specific factor even in the absence of a nearby canonical binding site. For Rev-erbα, this provides a means of regulating circadian output genes independently of RORs, which compete for control of core clock genes (*23*). In this context, there is evidence that the core TFs can act as pioneer factors to open chromatin that might otherwise be inaccessible.

Adding another layer of complexity to genomic activity of circadian TFs has been the identification of interactions between the core clock repressor CRY and the glucocorticoid receptor (GR). CRY binding modulates the balance between activating and repressive functions of the GR (*24*), and this coupling is perhaps consistent with the large number of sites that CRY occupies genome-wide. Moreover, whereas original predictions of clock-controlled genes focused on promoter proximal elements, genomic approaches revealed a broader portrait of clock regulation encompassing a far wider range of cell type–specific locations residing many thousands of nucleotides distant from classical regulatory regions (*16*, *25*).

Regulation of transcription by core clock TFs is also controlled by metabolites such as acetyl coenzyme A (CoA), S-adenosyl methionine, and nicotinamide adenine dinucleotide (oxidized form) (NAD^+). For example, the activating TFs, including BMAL1, recruit HATs, including p300 and CBP [cyclic adenosine monophosphate (cAMP) response element–binding protein (CREB)–binding protein], whose activity requires acetyl CoA, which may be rate-limiting. Furthermore, the activity of the clock proteins can be modulated by their own acetylation, as well as their deacetylation controlled by the sirtuin SIRT1, whose activity is regulated by NAD^+ (*26*, *27*). NAD^+ synthesis is in turn regulated in a circadian manner by the core clock through both direct (*28*, *29*) and indirect control of the rate-limiting salvage pathway enzyme nicotinamide phosphoribosyltransferase (NAMPT), a robustly cycling transcript. NAD^+ levels are further modified by reduction to NADH, as determined by energy transfer, which is cell type–specific and additionally regulated by metabolic demands. The circadian production of NAD^+ also controls the activity of mitochondrial SIRT3, which modulates cellular respiration (*30*). Mounting evidence further suggests that both NAD^+ levels and circadian function decline with age, perhaps in part because of the consumption of NAD^+ with poly(ADP-ribose) polymerase (PARP) activity in response to cumulative genotoxic stress. In this context, reduced organismal "fitness" during aging may be attributable in part to age-related decline in activity of NAD-SIRT1, in turn reducing clock function (*31*). The transcriptional activities of the core clock components of the NR family, Rev-erbα/β and RORα/γ, are additionally regulated by heme and cholesterol, respectively, which are also products of cellular oxidative metabolism (the bidirectional signals affecting the molecular clock cycle are illustrated in Fig. 2).

There are many unanswered questions about the role of the cell-autonomous circadian clock and its tissue-specific function and outputs. In this context, it is important to note that RNA rhythms alone do not capture the full spectrum of clock-controlled networks; for instance, both poly-adenylation and oscillation of the proteome have been shown to exhibit rhythmic regulation (*32*, *33*). Further, rhythmic oscillation of the redox state of the antioxidant peroxiredoxin proteins has been demonstrated in organisms ranging from eubacteria to human red blood cells, indicating that metabolic oscillations may maintain an additional level of timekeeping (*34*, *35*). It has been speculated that the other rhythmic processes, such as the cell cycle, may be coupled to the clock mechanism, and indeed, in isolated cells both the circadian clock and the cell cycles may be synchronized through sequential nutrient restriction and stimulation. Nonetheless, whereas the periodicity of cell cycle varies across tissues in response to nutrient conditions and growth factors, a key feature of the circadian clock is its invariant 24-hour rhythmicity, leaving open the question as to how local factors may align these distinct processes.

Systems-level circadian organization

Although the clock mechanism appears to be quite similar across cell types, it is critical to understand the extent and mechanism of coordination with the central clock. The expression of core clock genes in animals is highly synchronized under free-running conditions via the control of the central clock in the suprachiasmatic nucleus (SCN), which exerts its influence through the rhythmic integration of the sleep-wake cycle, neuroendocrine circuits, and autonomic nervous system. Light, the dominant Zeitgeber of behavioral rhythms, activates specialized photoreceptor cells expressing the pigment melanopsin (*36*, *37*) that in turn tracks via retinal hypothalamic projections to the SCN. SCN neurons exhibit photic resetting through the induction of immediate early genes downstream of the salt-inducible kinase 1 and CREB-regulated transcription coactivator 1 (*38*). Redox flux within the SCN has also been shown to modulate excitability of these neurons (*39*). SCN projections in turn entrain hypothalamic areas central to sleep and arousal through projections to the ventrolateral preoptic area (VLPO), lateral hypothalamic area (LHA), and midbrain [addressed in depth in (*40*)].

Although the molecular underpinnings of sleep remain largely mysterious, analyses of narcolepsy, a syndrome characterized by abrupt episodes of somnolence and cataplexy, have uncovered a role of the hypocretin/orexin as a neuropeptide connecting circadian and metabolic systems. Indeed, mutations in the ORX2 receptor lead to a Mendelian form of canine narcolepsy (*41*), whereas in mice, ablation of the ORX receptor alters energetics and susceptibility to diet-induced obesity (*42*). Further support for a functional convergence between circadian systems and energy balance comes from the finding that genetic disruption of the molecular clock in mice leads to a combination of sleep disturbance (FT), obesity, and metabolic syndrome (*43*). Indeed, the observation of sleep alteration across most genetic models of circadian TF disruption underscores the interconnection between circadian and sleep processes (*44*). Further, mutations of mouse and human Dec2, which represses clock activator proteins, also leads to short sleep (*45*). Intriguingly, human subjects with narcolepsy display a tendency for increased body weight, emphasizing the close molecular, genetic, and anatomic interplay between centers controlling sleep-wake cycles, appetitive circuits, and energy balance (*46*).

A distinct aspect of SCN neurons is that the rhythmic output from these cells arises from neuronal coupling, which is thought to render the pacemaker highly stable to signals that shift peripheral tissue clocks (*47*), most notably the liver, which can be entrained by restricting food availability to the light period when animals are not typically eating and at rest (*48*, *49*). In addition to feeding schedule, the nutritional state of an organism can have major effects on circadian rhythms of extra-SCN neurons and peripheral tissues (*50*, *51*), although the detailed mechanisms through which individual tissues respond to such changes remains incompletely known.

The circadian clocks of cultured cells can also be synchronized by glucocorticoids and temperature shifts (*52*–*54*). In addition, circadian control of temperature rhythms in turn generates rhythmic induction of cold-inducible RNA-binding protein, generating rhythmic variation in RNA splicing (*55*). Moreover, there is evidence that the peripheral clocks of intact organisms can be synchronized by an as yet unknown blood-borne factor that activates transcription mediated by the serum responsive factor (*56*). Furthermore, systemic changes in the metabolic state of the organism emanating from pathology in one tissue (for example, hypoxia due to lung disease) could lead to changes in metabolites, such as NAD^+ affecting other tissues and cell types in the manner described above. Also, the systemic burden of cancer can alter circadian rhythms in peripheral tissues, and circadian disruption may exacerbate tumor growth (*57*). A major unanswered question concerns the interplay of these multiple systemic factors in controlling the phase and synchrony of circadian rhythms in the living organism. This is a very complex issue, but progress will be critical to better understand normal physiology as well as the mechanisms by which circadian desynchrony predisposes to disease. Another unresolved point is whether clock TFs might participate in early stages of tissue ontogeny, as suggested by studies of clock function in stem cell differentiation and malignancy (*58*, *59*).

Physiology and pathophysiology: What's right in fitness and goes wrong in disease?

An anchoring concept in considering how and why timing has evolved derives from Bernard and Cannon's concept of homeostasis as the self-organizing ability of multicellular organisms to maintain a constant internal milieu. Whereas homeostasis in a biochemical pathway adjusts to the steady state with environmental perturbation, the circadian oscillatory process enables anticipation of recurrent variation arising from the light-dark cycle. Clocks represent a paradigm of how genes interact with environment and, in animals, how the central nervous system coordinates behavior with peripheral tissue physiology. Organ-specific disease states ensue when these mechanisms are challenged beyond the limits of homeostasis (Fig. 3).

The observation that clocks with near-24-hour periods are found across all kingdoms of life suggests that intrinsic timekeeping provides a selective advantage. Resonance studies have shown that variants with short or long period lengths survive best when the external light cycle matches the internal period length in prokaryotes (*60*). Although proof of selective advantage is harder to come by in mammals, there do appear to be health benefits related to circadian alignment. For example, clinical studies in which circadian misalignment has been introduced in a controlled laboratory setting in human subjects result in severe dysregulation of glucose homeostasis, insulin action, and appetitive control (*61*, *62*). Whereas misalignment of feeding time with endogenous clock time contributes to diet-induced obesity in mouse models (*50*, *63*), alignment of feeding and activity through restriction of food access to the nighttime in rodents protects from fatty liver (*64*), and similar strategies to control eating time may likewise improve human metabolic health (*65*).

In human subjects, a metric of period length can be estimated based on bedtime and waking propensity because the phase of sleep/wake cycle with respect to day/night hours corresponds with individual chronotype. Such stratification indicates that individuals with mismatched internal circadian cycles with the 24-hour day also exhibit increased risk of disorders such as obesity (*66*). Population analyses such as the Nurse's Health Study further indicate that individuals subjected to shiftwork, a condition characterized by chronic and repeated misalignment between internal clock time and the external light/dark cycle, associated with greater incidence of breast cancer (*67*) and metabolic disease (*68*). Exposure to blue light at night with electronic readers and staying up late on weekends (referred to as social jetlag) may induce circadian disturbance similar to effects of shiftwork (*66*, *69*), suggesting that the risk of shiftwork disorder may be more widespread than anticipated from work schedules alone. Sleep loss itself has been implicated in metabolic and proliferative disorders, and the effects may be difficult to separate from circadian disruption per se because the two processes are intimately interrelated. Although beyond the scope of the present Review, both sleep and circadian disruption have also been tied to neurodegenerative and mood disorders. A unifying concept may be that temporal disruption common in modern society establishes a chronic challenge with respect to circadian

cycles. Our 24-hour clock was fixed in time before the advent of electric light, jet travel, blue light–emitting computer screens, and 24/7 food availability; circadian disruption may be thought of as a sustained environmental stressor leading to ongoing conflict between endogenous biologic cycles and the environment.

Whereas disruption of the circadian system arises under imposed shiftwork conditions, clock function also declines with aging in mammals (*70*), raising the possibility that dysregulation of circadian processes may be a factor contributing to diseases of aging. Indeed, life span extension associated with caloric restriction can be abrogated through disruption of the clock in insects (*71*), whereas disruption of core clock genes has also been associated with hallmarks of early aging in mice (*72*). Insofar as accumulation of DNA damage and cancer risk also increase with aging, emerging epidemiologic and experimental evidence has implicated clock disruption as a factor in tumorigenesis. Studies in Per2 mutant mice have revealed increased radiation-induced lymphoma associated with dysregulation of cell cycle (*73*), whereas abrogation of both activator and repressor arms of the clock was shown to sensitize to lung tumorigenesis (*57*). In contrast, disruption of the *Cry* gene in mice has been implicated in tumor protection because of increased susceptibility to cell death (*74*). Conversely, DNA damage has been shown to shift circadian oscillations because of sequestration of Cry1 by the deubiquitinase Herpes virus–associated ubiquitin-specific protease (*75*). Bidirectional interplay between clock TFs and the oncogene Myc also facilitates tumor cell glycolysis (*76*).

The rhythmic coupling of circadian transcription and DNA repair, involving enzymes such as photolyases, may align the zenith of repair with the peak of ultraviolet genotoxic effects of Sun exposure each day (*77*). Alternatively, circadian cycles involving antioxidant enzymes such as the peroxiredoxins may provide rhythmic protection against the toxic effects of superoxide radicals produced during the oxygenic phase of the photosynthetic reaction cycle. In either case, circadian variation in cell functions has implications for chronopharmacology in cancer and other diseases, in which optimizing treatments may benefit from delivery of agents at specific times in the day/night cycle (*78*).

A key question arising from the connections between circadian function, aging, and organismal health relates to the observation that clocks are present not only in the brain but also throughout the body, where they exert broad effects at every level of organization, from genome regulation to control of protein biosynthesis and cell signaling. In this regard, impaired glucose metabolism is another hallmark of aging that has escalated coincident with the secular trend of circadian disruption due to light at night, shiftwork, and jet travel. In the past decade, experimental and human genetic studies have provided mechanistic insight into cell-specific pathways through which circadian disruption affects disease and metabolic physiology. Intrinsic rhythms of glucose metabolism have been well-characterized in human studies (*79*). Indeed, human genome-wide association studies using blood glucose as a phenotype have identified polymorphisms in both CRY2 (*80*) and the melatonin receptor 1b (MTR1B) (*81*) with glucose levels, which is concordant with experimental genetic analyses showing that circadian gene ablation in pancreas leads to β-cell failure and diabetes mellitus (*82*). Genetic studies have also shown that ablation of the liver clock results in fasting-induced hypoglycemia due to impaired oxidative metabolism, indicating opposing actions of the clock in liver and pancreas. Indeed, the circadian system is crucial for pancreatic β-cell health throughout life because ablation limited to adulthood severely impairs insulin secretion (*17*).

With regard to studies in the mouse, analyses across multiple time points and studies in organotypic explants provide complementary strategies to address whether particular pathologies arise beause of circadian disruption, or instead arise because of actions of clock factors independent of their function in timekeeping. In addition to studies of glucose regulation, clinical and experimental genetic studies have also elucidated the mechanism underlying the clustering of hypertensive crises and myocardial infarction in early morning. Indeed, SCN control of both the autonomic nervous system and neuroendocrine system directly controls daily variation in vascular tone, whereas cell-intrinsic clocks have been shown to contribute to atherogenesis and possibly to thromboembolic disease (*83*, *84*). Uncovering new facets of pathophysiology in individuals with shiftwork disorder such as diabetes mellitus and cardiovascular disease may pave the way to specifically treat the molecular clock in attempts to reverse diseases of misalignment. Although still in an early phase, small-molecule agonists of the clock have been shown to exert beneficial effects on metabolism (*85*).

Conclusions

The mechanism of circadian timing can now be understood as involving negative transcriptional feedback driving self-sustained rhythms within cells and organisms in anticipation of the light-dark cycle. The molecular circadian clock exerts broad effects at each level of organization, from gene transcription to inter-organ communication that is essential for physiologic homeostasis. Although remarkable strides have been made in identifying core components of the clock, major questions remain regarding the biophysical mechanisms underlying transcriptional oscillations, including an elucidation of the kinetic determinants of the 24-hour harmonic, the origin of temperature invariance, and the basis of entrainment. Increasing evidence has revealed an important influence of the clock cycle on genome-wide transcription, although how core clock factors affect the assembly and interplay of coactivator and corepressor complexes to modulate transcription, particularly within cell type–specific enhancers, and how posttranslational modifications, nutrient environment, and cell signaling might influence transcriptional cycles remains incompletely understood. Still unresolved is the question of whether biochemical reactions, such as redox oscillators, might produce autonomous circadian rhythms in anucleated cells or in tissues devoid of transcription.

The societal custom of moving the clock backward each fall provides a reminder of the potential for conflict between artificial light and our inner timepiece, which is entrained by the Sun and set to the 24-hour day. Understanding how regulatory networks emergent in the clock maintain temporal homeostasis has implications for the design of both human and experimental animal studies, in which time of day has been largely ignored. Including time as a variable may open new insight into pathophysiology in basic studies of behavior, metabolism, cardiovascular disease, cancer, and even aging. This concept extends from the organism to its component tissues, whose specialized functions depend on circadian rhythms much as varied genres of music all rely on time signatures. Indeed, the full reach of time was eloquently captured by jazz great Duke Ellington with his declaration that "It don't mean a thing if it ain't got that swing."

REFERENCES AND NOTES

1. R. J. Konopka, S. Benzer, *Proc. Natl. Acad. Sci. U.S.A.* **68**, 2112–2116 (1971).
2. P. E. Hardin, J. C. Hall, M. Rosbash, *Nature* **343**, 536–540 (1990).
3. C. L. Partch, C. B. Green, J. S. Takahashi, *Trends Cell Biol.* **24**, 90–99 (2014).
4. L. Yin *et al.*, *Science* **318**, 1786–1789 (2007).
5. S. Raghuram *et al.*, *Nat. Struct. Mol. Biol.* **14**, 1207–1213 (2007).
6. J. A. Kallen *et al.*, *Structure* **10**, 1697–1707 (2002).
7. B. E. McIntosh, J. B. Hogenesch, C. A. Bradfield, *Annu. Rev. Physiol.* **72**, 625–645 (2010).
8. A. Mehra *et al.*, *Cell* **137**, 749–760 (2009).
9. J. M. Hurley, J. J. Loros, J. C. Dunlap, *Trends Biochem. Sci.* **41**, 834–846 (2016).
10. C. R. Jones, A. L. Huang, L. J. Ptáček, Y.-H. Fu, *Exp. Neurol.* **243**, 28–33 (2013).
11. A. Balsalobre, F. Damiola, U. Schibler, *Cell* **93**, 929–937 (1998).
12. J. S. Menet, J. Rodriguez, K. C. Abruzzi, M. Rosbash, *eLife* **1**, e00011 (2012).
13. K. S. Zaret, J. Lerner, M. Iwafuchi-Doi, *Mol. Cell* **62**, 665–667 (2016).
14. S. Panda *et al.*, *Cell* **109**, 307–320 (2002).
15. K.-F. Storch *et al.*, *Nature* **417**, 78–83 (2002).
16. B. Fang *et al.*, *Cell* **159**, 1140–1152 (2014).
17. M. Perelis *et al.*, *Science* **350**, aac4250 (2015).
18. D. Feng *et al.*, *Science* **331**, 1315–1319 (2011).
19. N. Koike *et al.*, *Science* **338**, 349–354 (2012).
20. C. S. Lee, J. R. Friedman, J. T. Fulmer, K. H. Kaestner, *Nature* **435**, 944–947 (2005).
21. L. DiTacchio *et al.*, *Science* **333**, 1881–1885 (2011).
22. H. A. Duong, C. J. Weitz, *Nat. Struct. Mol. Biol.* **21**, 126–132 (2014).
23. Y. Zhang *et al.*, *Science* **348**, 1488–1492 (2015).
24. K. A. Lamia *et al.*, *Nature* **480**, 552–556 (2011).
25. G. Rey *et al.*, *PLOS Biol.* **9**, e1000595 (2011).
26. G. Asher *et al.*, *Cell* **134**, 317–328 (2008).
27. Y. Nakahata *et al.*, *Cell* **134**, 329–340 (2008).
28. Y. Nakahata, S. Sahar, G. Astarita, M. Kaluzova, P. Sassone-Corsi, *Science* **324**, 654–657 (2009).
29. K. M. Ramsey *et al.*, *Science* **324**, 651–654 (2009).
30. C. B. Peek *et al.*, *Science* **342**, 1243417 (2013).
31. H.-C. Chang, L. Guarente, *Cell* **153**, 1448–1460 (2013).
32. S. Kojima, E. L. Sher-Chen, C. B. Green, *Genes Dev.* **26**, 2724–2736 (2012).
33. A. B. Reddy *et al.*, *Curr. Biol.* **16**, 1107–1115 (2006).
34. R. S. Edgar *et al.*, *Nature* **485**, 459–464 (2012).
35. I. S. Kil *et al.*, *Mol. Cell* **59**, 651–663 (2015).
36. I. Provencio, G. Jiang, W. J. De Grip, W. P. Hayes, M. D. Rollag, *Proc. Natl. Acad. Sci. U.S.A.* **95**, 340–345 (1998).

37. S. Hattar *et al.*, *Nature* **424**, 75–81 (2003).
38. A. Jagannath *et al.*, *Cell* **154**, 1100–1111 (2013).
39. T. A. Wang *et al.*, *Science* **337**, 839–842 (2012).
40. C. B. Saper, T. E. Scammell, J. Lu, *Nature* **437**, 1257–1263 (2005).
41. L. Lin *et al.*, *Cell* **98**, 365–376 (1999).
42. H. Funato *et al.*, *Cell Metab.* **9**, 64–76 (2009).
43. F. W. Turek *et al.*, *Science* **308**, 1043–1045 (2005).
44. A. D. Laposky, J. Bass, A. Kohsaka, F. W. Turek, *FEBS Lett.* **582**, 142–151 (2008).
45. Y. He *et al.*, *Science* **325**, 866–870 (2009).
46. A. Aran *et al.*, *Sleep* **33**, 1457–1464 (2010).
47. A. C. Liu *et al.*, *Cell* **129**, 605–616 (2007).
48. F. Damiola *et al.*, *Genes Dev.* **14**, 2950–2961 (2000).
49. K. A. Stokkan, S. Yamazaki, H. Tei, Y. Sakaki, M. Menaker, *Science* **291**, 490–493 (2001).
50. A. Kohsaka *et al.*, *Cell Metab.* **6**, 414–421 (2007).
51. K. L. Eckel-Mahan *et al.*, *Cell* **155**, 1464–1478 (2013).
52. A. Balsalobre *et al.*, *Science* **289**, 2344–2347 (2000).
53. C. Saini, J. Morf, M. Stratmann, P. Gos, U. Schibler, *Genes Dev.* **26**, 567–580 (2012).
54. E. D. Buhr, S.-H. Yoo, J. S. Takahashi, *Science* **330**, 379–385 (2010).
55. I. Gotic *et al.*, *Genes Dev.* **30**, 2005–2017 (2016).
56. A. Gerber *et al.*, *Cell* **152**, 492–503 (2013).
57. T. Papagiannakopoulos *et al.*, *Cell Metab.* **24**, 324–331 (2016).
58. P. Janich *et al.*, *Nature* **480**, 209–214 (2011).
59. R. V. Puram *et al.*, *Cell* **165**, 303–316 (2016).
60. Y. Ouyang, C. R. Andersson, T. Kondo, S. S. Golden, C. H. Johnson, *Proc. Natl. Acad. Sci. U.S.A.* **95**, 8660–8664 (1998).
61. O. M. Buxton *et al.*, *Sci. Transl. Med.* **4**, 129ra43 (2012).
62. A. W. McHill *et al.*, *Proc. Natl. Acad. Sci. U.S.A.* **111**, 17302–17307 (2014).
63. D. M. Arble, J. Bass, A. D. Laposky, M. H. Vitaterna, F. W. Turek, *Obesity (Silver Spring)* **17**, 2100–2102 (2009).
64. M. Hatori *et al.*, *Cell Metab.* **15**, 848–860 (2012).
65. D. Jakubowicz, O. Froy, J. Wainstein, M. Boaz, *Steroids* **77**, 323–331 (2012).
66. T. Roenneberg, K. V. Allebrandt, M. Merrow, C. Vetter, *Curr. Biol.* **22**, 939–943 (2012).
67. E. S. Schernhammer *et al.*, *J. Natl. Cancer Inst.* **93**, 1563–1568 (2001).
68. A. Pan, E. S. Schernhammer, Q. Sun, F. B. Hu, *PLOS Med.* **8**, e1001141 (2011).
69. A.-M. Chang, D. Aeschbach, J. F. Duffy, C. A. Czeisler, *Proc. Natl. Acad. Sci. U.S.A.* **112**, 1232–1237 (2015).
70. T. J. Nakamura *et al.*, *J. Neurosci.* **31**, 10201–10205 (2011).
71. S. D. Katewa *et al.*, *Cell Metab.* **23**, 143–154 (2016).
72. R. V. Kondratov, A. A. Kondratova, V. Y. Gorbacheva, O. V. Vykhovanets, M. P. Antoch, *Genes Dev.* **20**, 1868–1873 (2006).
73. L. Fu, H. Pelicano, J. Liu, P. Huang, C. Lee, *Cell* **111**, 41–50 (2002).
74. N. Ozturk, J. H. Lee, S. Gaddameedhi, A. Sancar, *Proc. Natl. Acad. Sci. U.S.A.* **106**, 2841–2846 (2009).
75. S. J. Papp *et al.*, *eLife* **4**, e04883 (2015).
76. B. J. Altman *et al.*, *Cell Metab.* **22**, 1009–1019 (2015).
77. S. Gaddameedhi, C. P. Selby, W. K. Kaufmann, R. C. Smart, A. Sancar, *Proc. Natl. Acad. Sci. U.S.A.* **108**, 18790–18795 (2011).
78. S. Dulong, A. Ballesta, A. Okyar, F. Lévi, *Mol. Cancer Ther.* **14**, 2154–2164 (2015).
79. E. Van Cauter, K. S. Polonsky, A. J. Scheen, *Endocr. Rev.* **18**, 716–738 (1997).
80. J. Dupuis *et al.*, *Nat. Genet.* **42**, 105–116 (2010).
81. N. Bouatia-Naji *et al.*, *Nat. Genet.* **41**, 89–94 (2009).
82. B. Marcheva *et al.*, *Nature* **466**, 627–631 (2010).
83. A. M. Curtis *et al.*, *Proc. Natl. Acad. Sci. U.S.A.* **104**, 3450–3455 (2007).
84. B. Cheng *et al.*, *Proc. Natl. Acad. Sci. U.S.A.* **108**, 17147–17152 (2011).
85. Z. Chen, S.-H. Yoo, J. S. Takahashi, *Cell. Mol. Life Sci.* **70**, 2985–2998 (2013).

ACKNOWLEDGMENTS

Work on circadian rhythms is supported in the J.B. laboratory by National Institute of Diabetes and Digestive and Kidney Diseases (NIDDK) grants R01DK100814 and 2R01DK090625 and in the M.A.L. laboratory by NIDDK grant R01DK45586 and the JPB Foundation. M.A.L. serves on advisory boards for Pfizer and Eli Lilly and Company. J.B. has a financial interest in Reset Therapeutics, a biotechnology company developing therapeutics related to sleep and metabolism. We thank B. Marcheva for the figures. We apologize that space limitations prevented citation of all relevant literature.

10.1126/science.aah4965

REVIEW

Immunity around the clock

Kevin Man,[1] Andrew Loudon,[2]* Ajay Chawla[1,3]*

Immunity is a high-cost, high-benefit trait that defends against pathogens and noxious stimuli but whose overactivation can result in immunopathologies and sometimes even death. Because many immune parameters oscillate rhythmically with the time of day, the circadian clock has emerged as an important gatekeeper for reducing immunity-associated costs, which, in turn, enhances organismal fitness. This is mediated by interactions between extrinsic environmental cues and the intrinsic oscillators of immune cells, which together optimize immune responses throughout the circadian cycle. The elucidation of these clock-controlled immunomodulatory mechanisms might uncover new approaches for treating infections and chronic inflammatory diseases.

Virtually all life on Earth is exposed to regular 24-hour environmental cycles generated by the planet's rotation. This in turn has led to the evolution of daily (circadian) rhythms, driven by cell-autonomous biological clocks, which enable organisms to anticipate and adapt to the temporal changes in their environment (*1*). The sleep-wake cycle is perhaps the most obvious output of the circadian system, but numerous other physiological systems are under circadian control, including behavior and locomotor activity; body temperature; the cardiovascular, digestive, and endocrine systems; and metabolic and immune functions (*2*–*7*).

In mammals, the central circadian pacemaker is located in the suprachiasmatic nucleus (SCN), which entrains peripheral clocks found in nearly every cell of the body (*2*, *3*). The SCN oscillator has two distinct properties. First, it is the only part of the circadian system that has retinal innervation, allowing it to be entrained by the solar cycle. Second, unlike the peripheral clocks, which dampen over time, the interneuronal signaling pathways that establish communication between the SCN neurons endow it with an unlimited capacity to generate circadian outputs. At the organism level, circadian coherence in peripheral tissues is maintained by rhythmic generation of entrainment cues by the SCN, including circadian oscillations in body temperature, activity of the sympathetic nervous system (SNS), and circulating concentrations of glucocorticoids. The coherence between central and peripheral circadian clocks confers an adaptive advantage, and its disruption has been suggested to decrease organismal fitness. In support of this, lifestyles that disrupt inherent timing systems, such as exposure to abnormal lighting schedules in chronic shift work, are associated with an increased risk of cancer, metabolic disorders, and cardiovascular and cerebrovascular disease (*4*). Also, many human diseases exhibit circadian rhythmicity in their pathology, including myocardial infarction, asthma, and rheumatoid arthritis (*4*, *5*).

Although diurnal variation in host immune responses to lethal infection was demonstrated over 50 years ago (*8*, *9*), only recently have studies started to uncover the multiple aspects

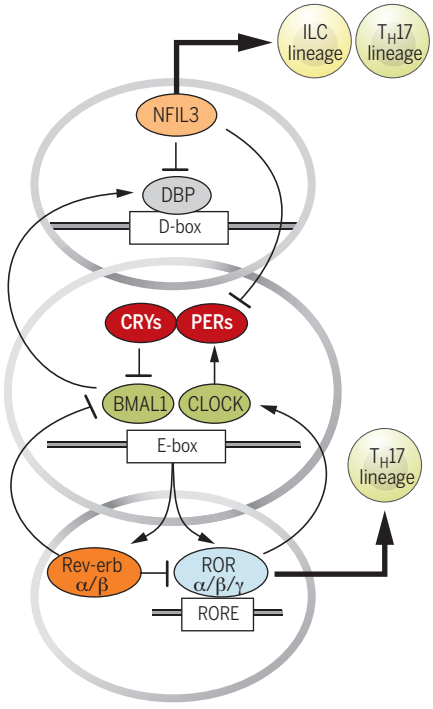

Fig. 1. Interlocking loops of the molecular clock drive immune responses. The circadian pacemaker is controlled by three interlocked transcription-translation feedback loops, involving rhythmic transcriptional repressors that act on D-box, E-box, and RORE sites. Genes driving the core clockwork also regulate multiple noncircadian pathways. Two of the circadian oscillators, NFIL3 and RORα, also regulate development of ILCs and T_H17 cells. Lines terminating in perpendicular bars denote inhibition. DBP, albumin D-box binding protein; CRYs, cryptochromes; PERs, Periods.

[1]Cardiovascular Research Institute, University of California, San Francisco, CA 94143, USA. [2]Faculty of Biology, Medicine and Health, University of Manchester, Manchester, UK. [3]Departments of Physiology and Medicine, University of California, San Francisco, CA 94143, USA.
***Corresponding author. Email: andrew.loudon@manchester.ac.uk (A.L.); ajay.chawla@ucsf.edu (A.C.)**

of immune function that are under circadian control, such as host-pathogen interactions, trafficking of leukocytes, and the activation of innate and adaptive immunity (*5*–*7*). These observations together suggest that the circadian oscillators gate immune responses to anticipate environmental threats, such as those that might be encountered when foraging for food or looking for shelter, and to limit the costs of immune activation. Here we highlight these recent advances in our understanding of how circadian oscillators limit immune and inflammatory responses to enhance organismal fitness. In particular, we discuss the circadian gating of immune responses, how oscillatory immune responses are generated and maintained, and the emerging knowledge of cell-autonomous functions of circadian oscillators in immune cells. A better understanding of how the cellular clock controls immune responses might lead to the development of chronotherapeutics to treat disorders of chronic inflammation and dysregulated immunity.

The clock of immune cells

In mammals, circadian timekeeping arises from conserved transcription-translation feedback oscillator loops driven by a set of dedicated clock proteins (*1*–*3*). CLOCK and BMAL1 (also known as ARNTL) transcription factor heterodimers drive the expression of the genes encoding Period (PER) proteins, cryptochromes (CRY), and REV-ERB nuclear receptors by binding to the E-box regulatory sequences in the promoters of these genes (Fig. 1). After a delay, the encoded proteins enter the nucleus and inhibit their own expression by modulating the transcriptional activity of CLOCK-BMAL1 heterodimers. Two additional circuits cooperate with the core clock to establish robust 24-hour rhythms (Fig. 1). First, the nuclear receptor RORα, which shares DNA binding sites with REV-ERBs, induces expression of *Bmal1* in a feedforward loop, whereas REV-ERBs represses the transcription of *Bmal1* by competing for the same site in a negative feedback loop. Second, albumin D-box binding protein and the repressor nuclear factor interleukin 3 (NFIL3, also known as E4BP4) form an additional loop that regulates transcription of genes containing D-box sequences, including those for PER. These rhythmic feedback mechanisms generate oscillations in gene expression that convey circadian timing cues to cellular processes. The formation, trafficking, and degradation of different clock protein complexes throughout this transcriptional cycle establish the intrinsic 24-hour period of the cellular clock.

"Nearly every arm of the immune response (innate and adaptive) has been reported to oscillate in a circadian manner."

In addition to their functions in the cellular clock, circadian oscillators also participate in the development and specification of immune cell lineages. For example, NFIL3 is required for the development of a common precursor that gives rise to all innate lymphoid cell (ILC) lineages, including ILC1s, natural killer (NK) cells, ILC2s, and ILC3s (*10*–*13*). At least for ILC3s, NFIL3 is only required for their development through the common ILC precursor, but not for their maintenance in the intestines or lymphoid tissues (*12*). This specific requirement of NFIL3 in the development of ILCs and NK cells might be independent of its functions in the cellular clock. If so, it would suggest that the transcriptional regulators that make up the clock might cooperate with other factors to control nonrhythmic expression of target genes, as was recently demonstrated for BMAL1 and REV-ERBα (*14*, *15*). For example, REV-ERBα regulates nonrhythmic functions in the liver by recruiting the transcriptional repressor complex containing nuclear co-repressor (NCoR) and histone deacetylase 3 (HDAC3) to lipid metabolism genes (*14*). This mechanism might also be relevant to the development of interleukin-17–producing $CD4^+$ T helper (T_H17) cells because their numbers are increased in *Nfil3*-null mice and decreased in *Rorα*-null mice (*16*, *17*), whereas deletion of *Bmal1* in mouse T cells does not affect T_H17 development in lymphoid organs and epithelial barriers (*18*). Also, rhythmic changes in the microbiota provide another mechanism by which alterations in T_H17 cells and ILCs are maintained at barrier sites (*19*, *20*). This is, in part, regulated by rhythmic, cellular clock–based expression of Toll-like receptors in the intestinal epithelial cells (*21*), which sense commensal derived molecular patterns to maintain intestinal homeostasis.

Circadian gating and host fitness

The immune system, which consists of innate and adaptive immunity, defends against noxious stimuli, such as infections and tissue injury (*22*). Although a controlled immune response is beneficial to the host (e.g., it confers protection

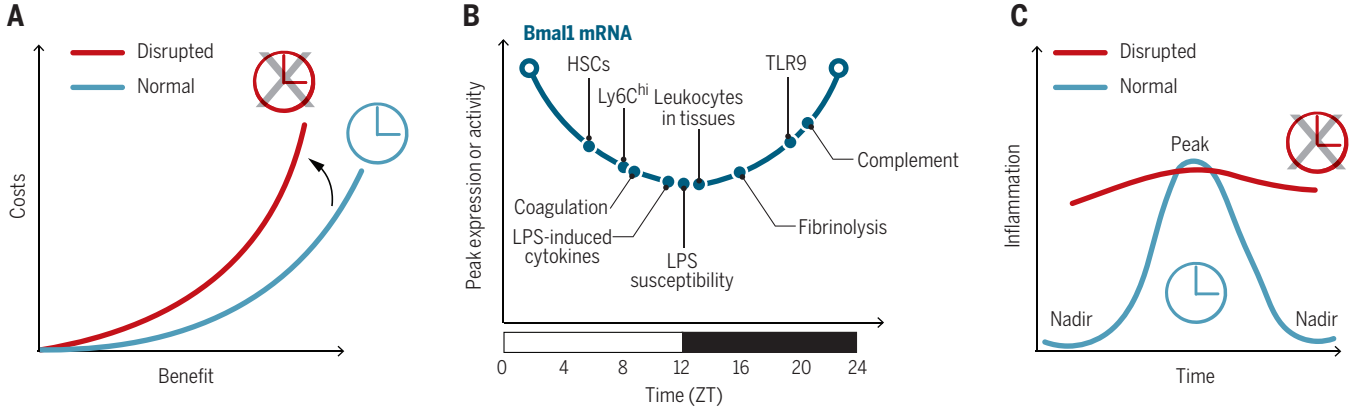

Fig. 2. Gating of immune responses by the circadian clock. (**A**) Cost-benefit trade-offs of immunity. The circadian clock functions to minimize the costs (including both direct costs and vulnerabilities) and maximize the benefits of immunity. Disruption of the circadian clock increases the costs of immunity for a given level of benefit. (**B**) The circadian clock temporally gates various arms of the innate immune response. Peaks of innate immune parameters are plotted on a curve depicting the oscillation of *Bmal1* mRNA during a circadian cycle. ZT, Zeitgeber time. ZT0 is the start of the light phase and ZT12 is the beginning of the dark phase during a 24-hour light-dark cycle. HSCs, hematopoietic stem cells; LPS, lipopolysaccharide; TLR, Toll-like receptor. (**C**) Temporal gating of inflammatory responses by the circadian clock. The curve depicts the rhythmic changes in an inflammatory parameter, such as production of cytokines or chemokines or trafficking of immune cells. The cellular clock generates the nadirs in this inflammatory parameter, and its disruption is associated with derepression of the nadirs without a substantive change in the peak, increasing the duration of inflammation.

against pathogens and promotes tissue repair), a dysregulated immune response can be harmful (e.g., it can cause septic shock). This double-edged sword of the immune or inflammatory response highlights the general principle that activation of immunity provides protection but also incurs costs. There are two types of costs that are incurred when immunity is activated: direct costs and vulnerabilities (*23*). Direct costs are unavoidable and incurred every time that the immune response is activated, such as the metabolic costs of immune activation or the collateral damage to tissues. In contrast, costs from vulnerabilities are rare but, when incurred, are catastrophic, such as with septic shock. Whereas direct costs can be reduced by decreasing the amplitude or duration of the immune response, reducing the frequency or probability of immune activation minimizes costs associated with vulnerabilities. Studies from the past decade suggest that the circadian oscillators function to minimize both direct costs and vulnerabilities associated with innate immune activation (Fig. 2A). Because natural selection optimizes the cost-benefit tradeoffs of traits in a given environment (*24*), we suggest that the observed anticipatory immune responses are a consequence of this Darwinian selection process, in which the circadian clock minimizes costs and maximizes benefits of immunity to enhance organismal fitness.

There are three mechanisms by which the circadian oscillators might reduce direct costs and vulnerabilities associated with inflammatory response. First, the circadian oscillators might temporally limit various aspects of innate immunity to distinct phases of the day-night cycle, thereby preventing their synchronous activation. For example, innate immunity—which comprises barrier defenses, antimicrobial peptides, complement and coagulation factors, cytokines and chemokines, and phagocytes (neutrophils, monocytes, macrophages, and dendritic cells)—provides a multilayered defense against pathogens. Although nearly all aspects of the innate immune system exhibit rhythmic oscillations, their peaks and nadirs occur at different phases of the circadian cycle (*5*, *25*–*32*) (Fig. 2B). This temporal gating of innate responses to distinct circadian phases decreases vulnerability to septic pathology, because their synergistic activation contributes to the clinical manifestations of septic shock (*33*). Second, the circadian oscillator might control the duration of inflammatory response by limiting the expression of inflammatory genes to a particular phase of the circadian cycle. In support of this, deletion of BMAL1 or REV-ERBα does not significantly alter the peak of lipopolysaccharide (LPS)–induced inflammatory response in macrophages, but it diminishes its nadir (*34*). This loss of circadian gating has the net effect of prolonging the duration of the innate inflammatory response (Fig. 2C), which decreases fitness by increasing immunopathology and susceptibility to septic shock (*35*). A third mechanism for reducing the costs of innate immunity is to temporally gate the trafficking of innate immune cells to sites of inflammation. Although the gating of neutrophils and monocytes is regulated by distinct processes, the loss of these processes results in increased susceptibility to endotoxin- or infection-induced tissue injury and sepsis, respectively (*27*, *28*). These examples illustrate that temporal gating by the circadian oscillators reduces the costs of immunity (Fig. 2A). A corollary of this concept is that severe infection might suppress this gating mechanism to maximize the inflammatory response. Indeed, during endotoxemia, the normal rhythmic outputs of the circadian clock are disrupted, resulting in the emergence of new gene expressions and metabolic rhythms that might function to support host immunity but also increase tissue damage and the probability of experiencing a catastrophic vulnerability (*36*).

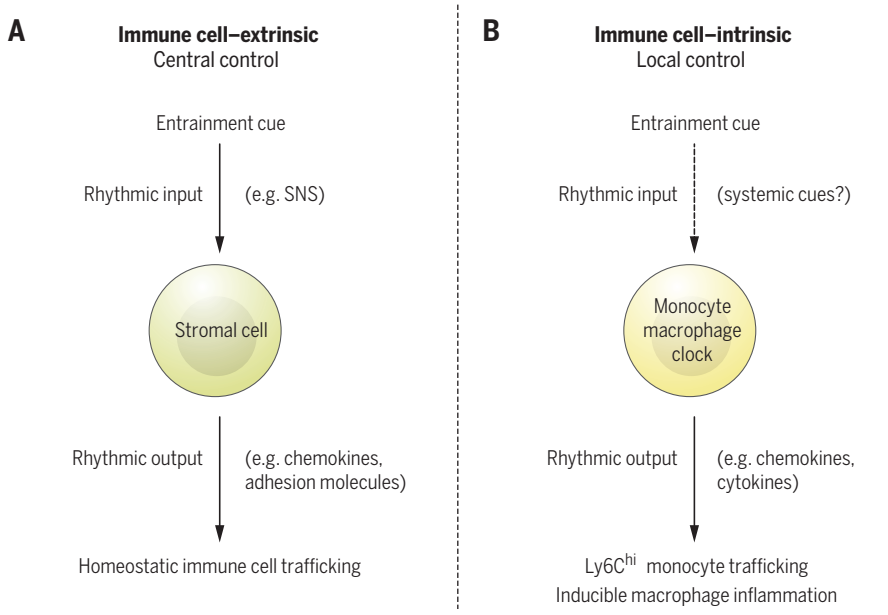

Fig. 3. Cell-extrinsic and -intrinsic generation of oscillatory immune responses. (**A**) Rhythmic oscillations in entrainment cues regulate homeostatic trafficking of hematopoietic stem cells and leukocytes. The SNS (sympathetic nervous system) provides the central entrainment cue that controls expression of chemokines and adhesion molecules in stromal cells, such as bone marrow stromal cells and endothelial cells, which imparts rhythmicity to trafficking of hematopoietic stem cells and leukocytes. (**B**) Cell-intrinsic clocks regulate basal and inducible programs in myeloid cells for maintenance of local homeostasis.

Generation of oscillatory immune responses

Nearly every arm of the immune response (innate and adaptive) has been reported to oscillate in a circadian manner. For example, rhythmic oscillations occur in the trafficking of innate and adaptive immune cells, susceptibility to bacterial infections and endotoxin-mediated septic shock, expression of pattern recognition receptors and their downstream signaling pathways, phagocytosis, secretion of complement and coagulation factors, and production of cytokines and chemokines (*5*, *25*–*32*). In principle, these rhythmic oscillations in the immune system can be generated by two mechanisms—cell-extrinsic (immune cell–nonautonomous) or cell-intrinsic (immune cell–autonomous)—which provide a framework for understanding hierarchical oscillatory behaviors and their entrainment by environmental cues (Fig. 3).

The rhythmic trafficking and recruitment of immune cells under homeostasis is largely controlled by oscillators working in a cell-extrinsic manner. For example, the rhythmic release of hematopoietic stem cells under homeostasis is orchestrated by the central clock acting through the SNS. In this case, the oscillatory release of norepinephrine from the adrenergic nerves regulates the rhythmic expression and secretion of the chemokine CXCL12 (C-X-C motif chemokine ligand 12) by bone marrow stromal cells (*37*). Because CXCL12 is required for retention of hematopoietic stem cells in their bone marrow niche, its diminished circadian secretion results in their rhythmic egress from the bone marrow into the circulation. This example illustrates the general process by which extrinsic signals regulate the rhythmic trafficking of immune cells into tissues. In this case, extrinsic entrainment cues act upon tissue-specific stromal cells to generate oscillatory outputs, including the rhythmic expression of chemokines and adhesion molecules, which supports rhythmic

trafficking of immune cells into tissues (*27*, *37*) (Fig. 3A).

Although the rhythmic discharge by the SNS is the dominant entrainment cue for recruitment of innate immune and hematopoietic stem cells (*6*), homeostatic oscillations of the adaptive immune cells in circulation might be entrained by glucocorticoids. For example, numbers of circulating T and B cells display an antiphasic relationship with serum corticosterone concentrations, implicating glucocorticoids as a potential entrainment cue for establishing the peak and nadir of T and B cells in circulation (*7*, *38*). The involvement of external cues in the generation of oscillatory behaviors in T cells is also suggested by immunization experiments, which demonstrate that antigen-specific responses show a strong dependence on time of day (*7*, *39*). This temporal gating of T cell activation and proliferation might be dependent on oscillatory input from the antigen-presenting cells, because disruption of the master circadian oscillator *Bmal1* in T and B cells did not significantly alter their development or responses to infectious or autoimmune challenges (*18*). These findings together indicate that cell-autonomous clocks might be less important in driving oscillatory behaviors in adaptive immune cells, which operate on longer time scales and might rely on external cues from circulating hormones or antigen-presenting cells to generate rhythmic outputs.

Cell-autonomous circadian clocks provide a second mechanism for generating rhythmic oscillations in immune cells. Thus far, most studies have focused on cells of the myeloid lineage, including monocytes and macrophages. Independent of entrainment cues, rhythmic oscillations in the trafficking of inflammatory monocytes (designated Ly6C^{hi} monocytes for high expression of Ly6C differentiation antigen) and the circadian gating of inflammatory responses in macrophages are primarily under the control of the cell-autonomous clock (Fig. 3B). For example, diurnal oscillations in the abundance of Ly6C^{hi} monocytes, which enhance organismal fitness during infection, are generated in a cell-autonomous manner by BMAL1 (*28*). In this case, BMAL1 is required for the suppression of Ly6C^{hi} monocytes in circulation, which reduces the host's vulnerability to septic shock. In support of this, myeloid cell disruption of *Bmal1* abolishes the troughs of the Ly6C^{hi} monocyte rhythm, rendering mice susceptible to death by sepsis. In an analogous manner, the oscillatory transcriptional outputs generated by BMAL1 regulate rhythmic expression of ~8% of the macrophage genome and establish the circadian phase during which signaling by endotoxin is most effective (*29*).

The cellular clock establishes the basal oscillations in gene expression and immune responses, but environmental stimuli can modulate these oscillatory immune functions in two important ways. First, external stimuli, such as LPS, can disrupt the phase, period, and amplitude of the cellular circadian clock, resulting in the loss of basal oscillatory rhythms and a shift from anticipatory to pathogen-associated responses (*28*, *36*). Second, core components of the cellular clock can interact with signal-dependent transcription factors to exert rhythmic anti-inflammatory effects. This is perhaps best illustrated by the anti-inflammatory effects of glucocorticoids in the setting of endotoxin-induced lung inflammation. In this case, the rhythmic recruitment of neutrophils to the inflamed lung requires BMAL1-dependent oscillations in the expression of the chemokine gene *Cxcl5* in lung epithelial cells (*40*). Loss of *Bmal1* in lung epithelia, but not in myeloid cells, disrupts both rhythmic neutrophil recruitment and the anti-inflammatory effects of glucocorticoids in mice; this is likely caused by impaired recruitment of the glucocorticoid

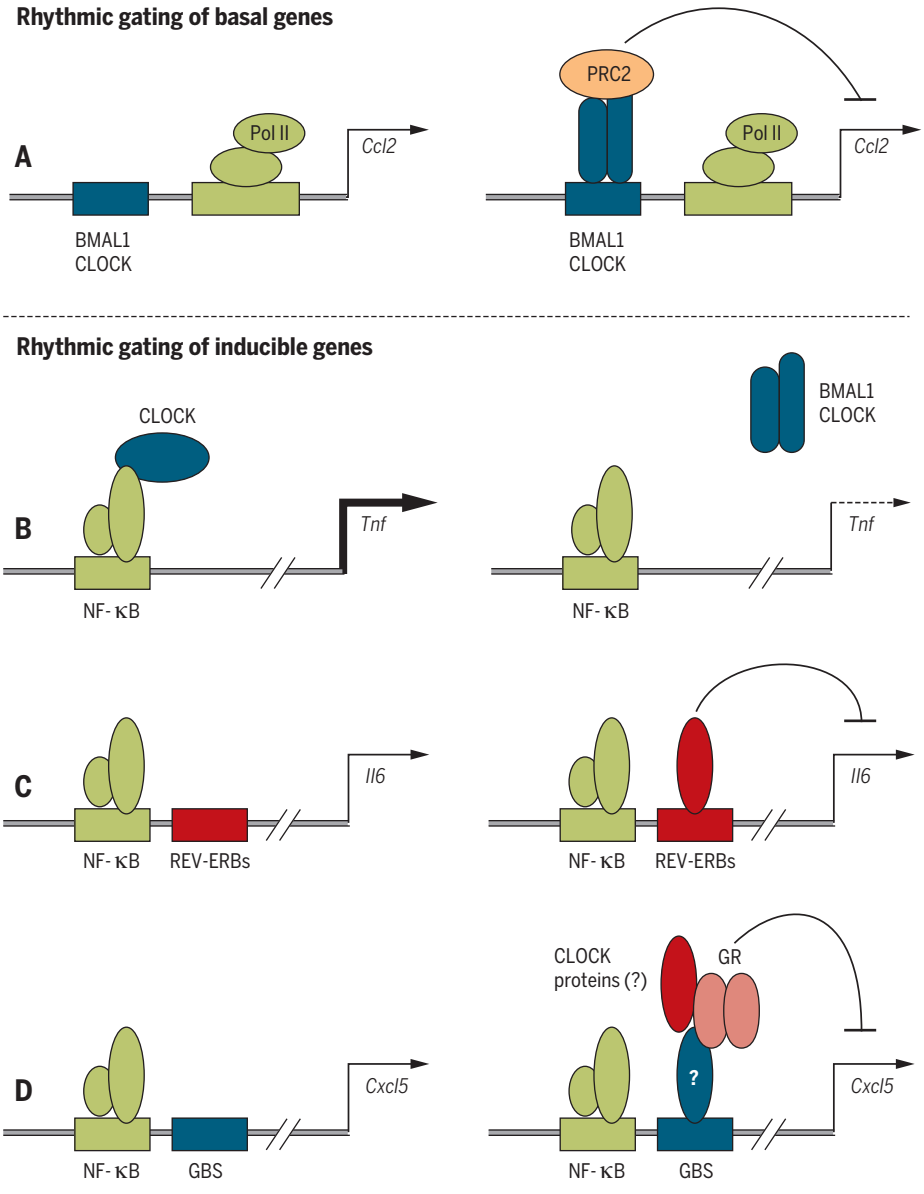

Fig. 4. Models for anti-inflammatory actions of the clock in myeloid cells. (**A**) Rhythmic gating of basal genes. Interactions between CLOCK-BMAL1 heterodimers and PRC2 (polycomb repressor complex 2) results in rhythmic repression of chemokine genes (such as *Ccl2*). Pol, RNA polymerase. (**B** to **D**) Rhythmic gating of inducible genes. Several modes of action are proposed for rhythmic gating of LPS-induced inflammatory genes. The CLOCK protein can acetylate the p65 subunit of NF-κB to induce expression of TNF (tumor necrosis factor), and its rhythmic sequestration by BMAL1 can drive oscillations in TNF expression (B). Recruitment of REV-ERB repressor complexes to inflammatory genes, such as *Il6*, can rhythmically repress their expression (C). Glucocorticoid receptor (GR)–mediated repressive effects on inflammatory chemokines require a functional cellular clock, which may be essential for recruitment of glucocorticoid receptor complexes to the glucocorticoid binding site (GBS) on the *Cxcl5* gene (D). Hash marks on arrows denote discontinuity in the DNA sequence.

receptor to the *Cxcl5* enhancer. This example thus illustrates that loss of BMAL1 not only disrupts cellular rhythmic outputs but also alters the amplitude of inflammatory response by preventing their gating by anti-inflammatory factors, such as the glucocorticoid receptor.

Anti-inflammatory actions of cellular clocks

A defining feature of the cellular clock in innate immune cells is its ability to gate and repress inflammatory responses. Two mechanisms have been proposed by which the circadian oscillators rhythmically modulate basal inflammatory responses in cells. First, basal oscillations in chemokine gene expression is mediated by interactions between BMAL1 and the Polycomb repressor complex 2 (PRC2) (*28*). The rhythmic binding of BMAL1-CLOCK to E-boxes in promoters of chemokine genes, such *Ccl2*, *Ccl8*, and *S100a8*, provides a direct mechanism for temporal gating of these genes by PRC2 during the circadian cycle (Fig. 4A). Second, loss of CRY proteins, which are potent transcriptional repressors and function in the negative feedback loop of the cellular clock, augments both basal and inducible inflammatory responses. This derepression of inflammation is a consequence of increased adenylyl cyclase activity in cells, resulting in protein kinase A–mediated phosphorylation of the p65 subunit of nuclear factor **κB** (NF-κB) and its constitutive activation (*41*). However, it is not known whether these inhibitory functions of CRY proteins are rhythmic or constitutive.

In contrast, rhythmic modulation of inducible gene expression relies on interference with the transcription factor NF-κB, the major transcriptional activator of inflammation. On the basis of LPS-induced inflammatory responses, three different mechanisms have been proposed to rhythmically limit NF-κB activity on promoters and enhancers of inflammatory genes. First, CLOCK can directly interact with the p65 subunit of NF-κB to enhance its transcriptional activity on promoters of inflammatory genes. In this model, the sequestration of CLOCK by BMAL1 results in rhythmic repression of inflammatory genes (Fig. 4B), whereas loss of BMAL1 causes their derepression through constitutive recruitment of CLOCK to NF-κB–regulated promoters (*42*). However, it is unclear how specificity is achieved, because only a subset of NF-κB–induced genes are rhythmically expressed in LPS-stimulated cells. Second, REV-ERBs, which form the negative feedback loop of the cellular clock, can mediate repression through recruitment of NCoR complexes of HDAC3 (*43*). Although REV-ERBα and -β have thousands of binding sites in macrophage-specific enhancer-like regions (*44*), they repress a subset of inflammatory genes in a signal-dependent manner by inhibiting enhancer-specific transcription (*45*). Thus, the circadian oscillations in REV-ERBs would dictate their ability to temporally gate inflammatory gene expression (Fig. 4C). In support of this, genetic deletion of *Rev-erbα* derepresses a subset of inflammatory genes in macrophages without affecting the cellular rhythm, whereas its pharmacological agonism inhibits LPS-stimulated inflammation (*34*). The third mechanism for circadian gating of inflammation involves the glucocorticoid receptor, which participates in establishing synchrony between the peripheral clocks. Although serum concentrations of glucocorticoids oscillate in a circadian manner, they do not modulate the rhythmic inflammatory responses of macrophages, which are preserved in adrenalectomized mice (*29*). The rhythmic recruitment of the glucocorticoid receptor by BMAL1 to promoters of inflammatory genes, such as *Cxcl5*, might be necessary for their periodic repression (Fig. 4D), suggesting that the circadian clock gates the anti-inflammatory effects of glucocorticoids locally rather than systemically (*40*).

Conclusions and perspectives

Much progress has been made on understanding how immune functions are regulated by biological clocks, but a number of questions remain. How is specificity achieved in gating of immune responses? Is this primarily controlled by the master clock protein BMAL1 or by its downstream target proteins, the REV-ERBs and CRYs? Furthermore, what is the molecular code by which BMAL1, REV-ERBs, and CRYs modulate expression of inflammatory genes? Because the circadian clock is a critical regulator of metabolism (*4*, *46*), it will be important to determine whether oscillations in immunity are driven by clock-controlled changes in cellular metabolism. If so, it might indicate that metabolic priming by the cellular clock contributes to the time-of-day dependence of immune responses. Although the immune system senses and responds to the external world, it is not known whether environmental signals can entrain adaptive and innate immunity. If so, the nature of the entrainment cues and the molecular basis by which they modulate immune functions in different environments should be investigated. A primordial function of the circadian oscillator is to temporally compartmentalize biochemically incompatible programs to distinct phases of the circadian cycle, such as photosynthesis during the day and nitrogen fixation at night in cyanobacteria (*1*). However, it is not known whether this feature of the oscillator is used to separate mutually incompatible programs in immune cells, such as those controlling cell fate specification or polarization. Last, does the cellular oscillator contribute to observed heterogeneity in resident and recruited populations of immune cells or to cellular desynchrony during an immune response? Addressing these questions will enhance our basic understanding of how the circadian clock optimizes immune functions to anticipate changes in the environment and will provide mechanistic insights to facilitate the development of chronotherapies for treating inflammatory disorders.

REFERENCES AND NOTES

1. D. Bell-Pedersen *et al.*, *Nat. Rev. Genet.* **6**, 544–556 (2005).
2. M. Stratmann, U. Schibler, *J. Biol. Rhythms* **21**, 494–506 (2006).
3. J. A. Mohawk, C. B. Green, J. S. Takahashi, *Annu. Rev. Neurosci.* **35**, 445–462 (2012).
4. J. Bass, J. S. Takahashi, *Science* **330**, 1349–1354 (2010).
5. A. M. Curtis, M. M. Bellet, P. Sassone-Corsi, L. A. O'Neill, *Immunity* **40**, 178–186 (2014).
6. C. Scheiermann, Y. Kunisaki, P. S. Frenette, *Nat. Rev. Immunol.* **13**, 190–198 (2013).
7. N. Labrecque, N. Cermakian, *J. Biol. Rhythms* **30**, 277–290 (2015).
8. F. Halberg, E. A. Johnson, B. W. Brown, J. J. Bittner, *Proc. Soc. Exp. Biol. Med.* **103**, 142–144 (1960).
9. P. G. Shackelford, R. D. Feigin, *Science* **182**, 285–287 (1973).
10. X. Yu *et al.*, *eLife* **3**, e04406 (2014).
11. W. Xu *et al.*, *Cell Rep.* **10**, 2043–2054 (2015).
12. T. L. Geiger *et al.*, *J. Exp. Med.* **211**, 1723–1731 (2014).
13. C. Seillet *et al.*, *J. Exp. Med.* **211**, 1733–1740 (2014).
14. Y. Zhang *et al.*, *Science* **348**, 1488–1492 (2015).
15. G. Yang *et al.*, *Sci. Transl. Med.* **8**, 324ra16 (2016).
16. X. Yu *et al.*, *Science* **342**, 727–730 (2013).
17. X. O. Yang *et al.*, *Immunity* **28**, 29–39 (2008).
18. S. Hemmers, A. Y. Rudensky, *Cell Rep.* **11**, 1339–1349 (2015).
19. M. Gury-BenAri *et al.*, *Cell* **166**, 1231–1246.e13 (2016).
20. C. A. Thaiss *et al.*, *Cell* **159**, 514–529 (2014).
21. A. Mukherji, A. Kobiita, T. Ye, P. Chambon, *Cell* **153**, 812–827 (2013).
22. R. Medzhitov, *Nature* **454**, 428–435 (2008).
23. D. Okin, R. Medzhitov, *Curr. Biol.* **22**, R733–R740 (2012).
24. S. C. Stearns, R. Medzhitov, *Evolutionary Medicine* (Sinauer Associates, 2016).
25. A. C. Silver, A. Arjona, W. E. Walker, E. Fikrig, *Immunity* **36**, 251–261 (2012).
26. D. Mauvoisin *et al.*, *Proc. Natl. Acad. Sci. U.S.A.* **111**, 167–172 (2014).
27. C. Scheiermann *et al.*, *Immunity* **37**, 290–301 (2012).
28. K. D. Nguyen *et al.*, *Science* **341**, 1483–1488 (2013).
29. M. Keller *et al.*, *Proc. Natl. Acad. Sci. U.S.A.* **106**, 21407–21412 (2009).
30. M. M. Bellet *et al.*, *Proc. Natl. Acad. Sci. U.S.A.* **110**, 9897–9902 (2013).
31. M. Hayashi, S. Shimba, M. Tezuka, *Biol. Pharm. Bull.* **30**, 621–626 (2007).
32. M. Casanova-Acebes *et al.*, *Cell* **153**, 1025–1035 (2013).
33. D. Rittirsch, M. A. Flierl, P. A. Ward, *Nat. Rev. Immunol.* **8**, 776–787 (2008).
34. J. E. Gibbs *et al.*, *Proc. Natl. Acad. Sci. U.S.A.* **109**, 582–587 (2012).
35. A. M. Curtis *et al.*, *Proc. Natl. Acad. Sci. U.S.A.* **112**, 7231–7236 (2015).
36. J. A. Haspel *et al.*, *Nat. Commun.* **5**, 4753 (2014).
37. S. Méndez-Ferrer, D. Lucas, M. Battista, P. S. Frenette, *Nature* **452**, 442–447 (2008).
38. T. Kawate, T. Abo, S. Hinuma, K. Kumagai, *J. Immunol.* **126**, 1364–1367 (1981).
39. E. E. Fortier *et al.*, *J. Immunol.* **187**, 6291–6300 (2011).
40. J. Gibbs *et al.*, *Nat. Med.* **20**, 919–926 (2014).
41. R. Narasimamurthy *et al.*, *Proc. Natl. Acad. Sci. U.S.A.* **109**, 12662–12667 (2012).
42. M. L. Spengler *et al.*, *Proc. Natl. Acad. Sci. U.S.A.* **109**, E2457–E2465 (2012).
43. B. Fang, M. A. Lazar, *Cold Spring Harb. Symp. Quant. Biol.* **80**, 233–238 (2015).
44. M. T. Lam *et al.*, *Nature* **498**, 511–515 (2013).
45. D. Z. Eichenfield *et al.*, *eLife* **5**, e13024 (2016).
46. D. Jacobi *et al.*, *Cell Metab.* **22**, 709–720 (2015).

ACKNOWLEDGMENTS

We thank members of the Chawla laboratory for discussions, A. Loh and R. D. Dockrell for comments on the manuscript, and B. Saer for assistance with artwork. Work in authors' laboratories was supported by U.S. NIH grants DK094641, DK101064, DP1AR064158, and P30DK098722 (A.C.); U.K. Biotechnology and Biological Sciences Research Council grants BB/K003097/1, BB/L00954/1, and BB/N015584/1 (A.L.); and Wellcome Trust grant 107851/Z/5/Z (A.L.). The authors apologize that, in the interests of brevity, papers by colleagues may not have been cited. The authors declare that they have no competing financial interests.

10.1126/science.aah4966

REVIEW

Mechanisms linking circadian clocks, sleep, and neurodegeneration

Erik S. Musiek* and David M. Holtzman

Disruptions of normal circadian rhythms and sleep cycles are consequences of aging and can profoundly affect health. Accumulating evidence indicates that circadian and sleep disturbances, which have long been considered symptoms of many neurodegenerative conditions, may actually drive pathogenesis early in the course of these diseases. In this Review, we explore potential cellular and molecular mechanisms linking circadian dysfunction and sleep loss to neurodegenerative diseases, with a focus on Alzheimer's disease. We examine the interplay between central and peripheral circadian rhythms, circadian clock gene function, and sleep in maintaining brain homeostasis, and discuss therapeutic implications. The circadian clock and sleep can influence a number of key processes involved in neurodegeneration, suggesting that these systems might be manipulated to promote healthy brain aging.

Although Benjamin Franklin's aphorism "early to bed, early to rise, makes a man healthy, wealthy, and wise" may not be universally true, he implies that less reliable bedtime hours will earn us poor health, financial poverty, and cognitive impairment. This old adage is particularly relevant today as it pertains to the relationship between circadian rhythms, sleep, and neurodegenerative diseases. Circadian and sleep dysfunction have long been symptomatic hallmarks of various devastating neurodegenerative conditions, including Alzheimer's disease (AD), Parkinson's disease (PD), and Huntington disease (HD) (*1*, *2*). Accumulating evidence indicates that disorders of sleep and of circadian rhythms may occur very early in the course of several neurodegenerative diseases and not only serve as manifestations of disease but also may potentially contribute directly to pathogenesis (*3*–*5*). Herein, we discuss the existing data linking circadian and sleep disruption to neurodegeneration, explore several potential molecular mechanisms linking the circadian clock to neurodegeneration, and address potential therapeutic implications.

The circadian clock in the brain

The circadian system in humans and mice is hierarchical, existing at both the molecular and circuit-based levels (Fig. 1). At the cellular level, the core circadian clock consists of a set of conserved clock proteins which form a transcriptional-translational feedback loop that mediates daily oscillations in gene expression. In humans and mice, the positive transcriptional limb of the circadian clock consists of the basic helix-loop-helix PER-ARNT Sim transcription factor BMAL1 (also called ARNTL), which heterodimerizes with CLOCK (or NPAS2), binds to Ebox motifs throughout the genome, and drives transcription of a host of genes (*6*, *7*). Among the transcriptional targets of BMAL1-CLOCK complexes are several negative-feedback regulators, including the *PERIOD* (*PER1-3*), *CRYPTOCHROME* (*CRY1,2*), and *REVERB* (*NR1D1* and *NR1D2*) genes, which then suppress the positive limb. The core circadian clock oscillates in a cell-autonomous manner and is tuned to a 24-hour period by multiple layers of posttranslational regulation. The positive limb of the clock regulates transcription of hundreds or thousands of transcripts in a tissue- and cell type–specific manner (*8*). In mice and humans, cellular oscillators are synchronized across organs by the suprachiasmatic nucleus (SCN) of the hypothalamus. The SCN receives light:dark input from the retina, synchronizing core clock oscillations in neurons, which are then translated into oscillatory synaptic output to multiple nuclei in the hypothalamus and elsewhere. Ablation of the SCN leads to a loss of these patterns in neuronal activity, as well as a loss of coherent circadian rhythms in clock gene oscillations in most tissues, and ultimately behavioral and physiological arrhythmicity. The SCN clock is also entrained by changes in the light:dark cycle and mediates shifts in peripheral circadian rhythms in this setting.

Dissection of the circadian system can be complicated. Ablation of the SCN abrogates circadian rhythms in nearly all outputs, including sleep (*9*). However, rodents without a functioning SCN continue to have intact peripheral clock gene expression, though the levels may not oscillate (*10*). Arrhythmic mice also still sleep, only with no day-night predilection. Mice can also be rendered arrhythmic through deletion of specific circadian clock genes, in particular *Bmal1* (*11*). Global *Bmal1* deletion not only renders the SCN arrhythmic, but also disrupts cellular clock function. Local, tissue-specific deletion of key clock genes, such as *Bmal1*, in non-SCN regions of the brain can also render that tissue transcriptionally arrhythmic without altering the animal's sleep-wake cycle or behavioral rhythms (*12*). One caveat is that *Bmal1* can exert developmental effects, and regulates many genes that are

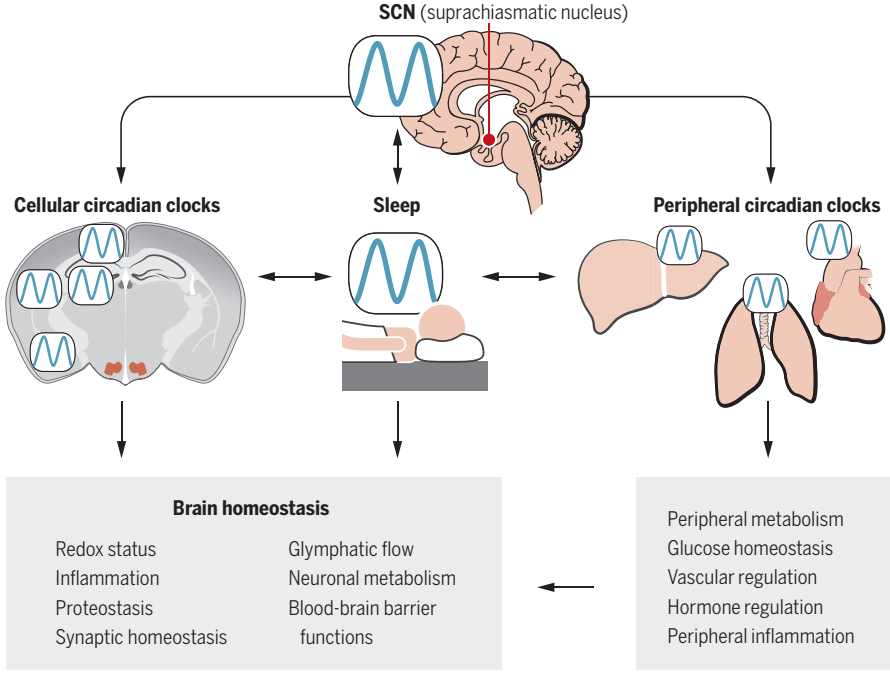

Fig. 1. Impact of sleep and central and peripheral circadian rhythms on brain homeostasis. The SCN synchronizes circadian rhythms in the cellular clocks of cells in the brain, the sleep-wake cycle, and peripheral organs. Cellular clocks within neurons and glia in turn regulate transcription of genes involved in critical processes such as redox homeostasis, inflammation, proteostasis, and metabolism. Sleep influences many of the same pathways, perhaps in some cases through interaction with the cellular clock. Circadian regulation of peripheral metabolism, inflammation, and hormone secretion also affects the brain.

Department of Neurology, Hope Center for Neurological Disorders, and Knight Alzheimer Disease Research Center, Washington University School of Medicine, St. Louis, MO 63110, USA.
*Corresponding author. Email: musieke@neuro.wustl.edu

nonrhythmic, suggesting that some effects of BMAL1 deletion may be noncircadian (*13*).

More complexity comes when considering the interplay between the circadian clock and sleep. Mutations in circadian clock genes, both in mice and in humans, manifest behaviorally as sleep disturbances (*14*, *15*). Conversely, sleep deprivation can alter the expression (*16*, *17*) and DNA binding activity of core clock genes (*18*), demonstrating a bidirectional relationship between sleep and the circadian clock.

Sleep and neurodegeneration

A wide variety of alterations in sleep have been described in human neurodegenerative diseases, including AD, PD, and HD, and are reviewed elsewhere (*19*, *20*). In each of these diseases, sleep disturbances may precede the onset of more typical symptoms, in some cases by decades (*3*–*5*). The most striking example is rapid eye movement (REM) behavior disorder (RBD), a condition in which normal muscle paralysis is lost during REM sleep. More than 80% of all RBD patients will eventually develop PD or another synucleinopathy, often decades later (*5*). Mouse models of AD, PD, and HD pathology also exhibit sleep abnormalities (*21*–*24*). Sleep deprivation increases cerebrospinal fluid (CSF)markers of neuronal injury and alters plasma markers of inflammation in humans (*25*, *26*), and also induces the unfolded protein response in the brain of mice, indicating endoplasmic reticulum stress and potential neuronal injury (*27*). Thus, inadequate sleep could prime the brain for neurodegeneration by promoting processes such as inflammation and synaptic damage, which exert pathogenic effects across diseases.

The relationships between sleep and disease-specific pathways have most clearly been demonstrated in the case of β-amyloid (Aβ), a pathogenic protein instrumental in AD (Fig. 2). Amyloid plaques, which form as a result of aggregation of Aβ species, accumulate in the brains of AD patients years before the onset of cognitive impairment and serve as an early biomarker of AD (*28*). Neurons release Aβ in an activity-dependent manner, and Aβ concentrations in the extracellular space in the brain exhibit clear circadian oscillations, rising during the active period and falling during rest (*29*). These diurnal fluctuations in Aβ persist in constant darkness and are closely correlated to changes in neuronal metabolic activity tied to sleep and wakefulness. Similar Aβ oscillations can be observed in the CSF of humans (*30*). In transgenic mouse models of Aβ deposition like that seen in AD, sleep deprivation greatly accelerates amyloid plaque deposition, whereas promoting sleep with orexin antagonist drugs significantly inhibits plaque formation (*29*). Genetic deletion of orexin, a peptide expressed in the lateral hypothalamus that promotes wakefulness and regulates feeding and metabolism, modestly increases sleep time but strongly suppresses the formation of amyloid plaques in AD model mice (*31*). These basic and translational studies are concordant with epidemiological studies showing that deficient or fragmented

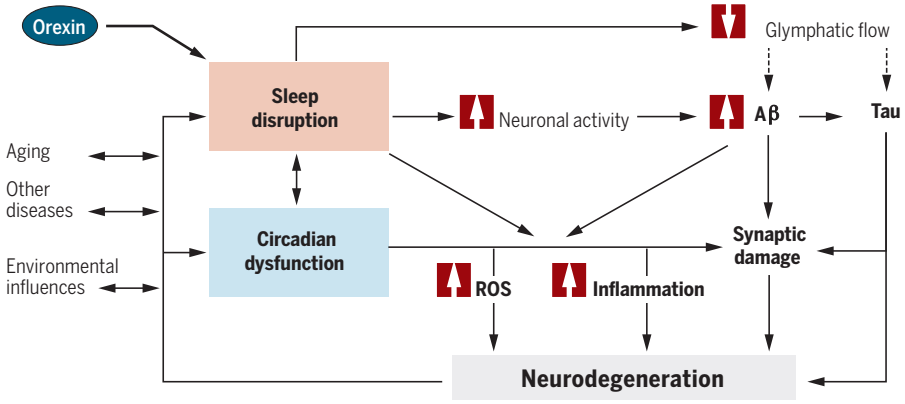

Fig. 2. Proposed mechanisms linking sleep loss, Aβ, and neurodegeneration in AD. Sleep deprivation or fragmentation can result from aging, other diseases, environmental influences, circadian clock (SCN) dysfunction, or neurodegeneration. Increased wakefulness, which is promoted by orexin, causes increased neuronal activity, leading to elevated Aβ production and aggregation. Wakefulness also increases sympathetic output, suppressing glymphatic system function. This could result in decreased clearance of pathogenic proteins (such as Aβ, tau, or synuclein). Sleep loss and clock disruption also promotes oxidative stress, inflammation, and a loss of synaptic homeostasis. These insults combine to promote neurodegeneration, which in turn causes more circadian and sleep dysfunction.

sleep in cognitively normal individuals is a risk factor for the future development of symptomatic AD (*3*, *4*, *32*), and that people with amyloid plaque pathology develop detectable declines in sleep efficiency before the onset of cognitive symptoms (*33*). Human studies have also shown a correlation between concentrations of orexin in the CSF and that of tau protein, another pathologic hallmark of AD and the primary constituent of neurofibrillary tangles. High concentrations of CSF orexin-A, which promote increased wakefulness, were associated with increased amounts of phophorylated tau, a well-described biomarker of neurodegeneration in AD (*34*), though not with CSF Aβ concentration (*35*). Sleep deprivation also exacerbated tau pathology and synapse loss in a mouse model of AD that develops both Aβ and tau pathology (*36*, *37*), although the effects of sleep on tau are not yet fully understood.

A rich literature has demonstrated the critical tie between sleep, synaptic function, and cognition, which is reviewed elsewhere (*38*). Sleep disturbances in aging and neurodegenerative diseases, including AD, can directly influence synaptic homeostasis and cognitive function. As an example, Aβ plaque pathology in the medial prefrontal cortex in humans is associated with disrupted non-REM sleep, which appears to cause impaired learning and memory (*39*).

Sleep also appears to regulate the bulk removal of proteins and other molecules from the brain through regulation of "glymphatic" flow, a recently described phenomenon whereby astrocytes facilitate extracellular fluid transit though the brain (*40*). In mice, slow-wave sleep was associated with increased glymphatic flow, causing a ~60% increase in brain interstitial fluid volume and facilitating accelerated clearance of exogenously added Aβ from the brain (*41*). Blockade of noradrenergic receptors increased glymphatic flow, suggesting that increased noradrenergic output from the autonomic nervous system, as is seen during waking, suppresses glymphatic clearance. As sleep deprivation in mice can cause degeneration of neurons in the locus coeruleus, the primary noradrenergic nucleus in the brainstem (*42*), the effect of chronic sleep disturbances on glymphatic function remains uncertain.

In HD, sleep fragmentation is detectable in carriers of the pathogenic CAG-expanded *huntingtin* gene before the onset of cognitive symptoms (*43*). Mouse models of HD exhibit severe degeneration of sleep rhythms (*23*, *44*), and pharmacologic restoration of sleep by treatment of mice with the sedative clonazepam at the onset of the light phase normalizes clock gene oscillation in these mice and significantly improves cognitive performance (*45*). In this case, the primary dysfunction appears to be in the circadian system, although normalizing the sleep pattern also corrects the circadian deficit, emphasizing the complex interaction between sleep and circadian clocks.

Circadian function and neurodegeneration

Aging is a primary risk factor for many neurodegenerative conditions, and circadian function clearly wanes with age at the level of the SCN output and brain clock gene expression (*46*, *47*). Alterations in behavioral circadian rhythms are evident in patients with several neurodegenerative conditions and in mouse models of these diseases, and are reviewed in detail elsewhere (*1*). AD patients have loss of critical neurons in the SCN, a finding that correlates with impaired behavioral circadian function (*48*, *49*). One postmortem study demonstrated asynchronous clock gene expression between different brain regions in AD patients (*50*). Aβ can facilitate BMAL1 degradation in neuronal cells (*51*), suggesting that AD-related processes could directly influence cellular clock function. PD patients have blunted rhythms of clock gene expression in peripheral blood cells (*52*, *53*), and transgenic mice overexpressing human α-synuclein, a neurodegenerative protein

implicated in PD, develop behavioral and transcriptional circadian deficits (*22*). Mouse models of HD also exhibit severely disrupted SCN output and loss of peripheral clock gene oscillation early in the disease course (*44*, *54*). In aged mice, as well as some HD and PD models, there is intact clock gene oscillation in the SCN but disrupted electrical output, suggesting neuronal network dysfunction in the SCN as the primary lesion (*22*, *44*, *46*). Thus, circadian dysfunction can result from lesions at multiple levels of the circadian system.

Although it is well established that neurodegeneration affects the circadian clock, few studies have addressed the causality of this dysfunction in neurodegeneration. In humans, less robust circadian rhythms or more fragmented activity patterns appear to be risk factors for future dementia, suggesting a possible causative influence of circadian dysfunction on the neurodegenerative process (*55*). Several small studies have associated single-nucleotide polymorphisms in *Clock* and *Bmal1* with increased risk of AD or PD (*56*–*58*). To address this question, we have examined the evidence linking SCN disruption and whole-organism rhythms separately from studies examining clock gene deletion.

Disrupted SCN-mediated circadian rhythms and neurodegeneration

Alterations in coordinated whole-organism circadian function caused by SCN disruption or altered light:dark cycles could have a profound impact on the brain, either by disrupting normal oscillation of cellular clocks in various brain regions, or by disrupting other rhythms, such as the sleep-wake cycle, or rhythms in peripheral organs (Fig. 1). Notably, the circadian clock regulates hippocampal-dependent learning and has potent effects on cognition in the absence of neurodegeneration (*59*-*61*). As an example, simply misaligning the sleep and feeding rhythms in mice causes desynchrony of clock gene oscillation between the SCN and hippocampus, resulting in substantial impairments in learning and memory (*62*). Loss of rhythms in melatonin, a hormone involved in circadian timing, has been observed in several neurodegenerative diseases (*63*, *64*), and melatonin supplementation has been explored as a therapeutic for AD, with modest effect (*65*). Loss of circadian regulation of peripheral processes such as glucose and lipid metabolism (*7*), immune system function (*66*–*68*), hormone secretion, or even gut microbiome oscillations (*69*) could potentially indirectly predispose the brain to degeneration. Many nongenetic models of circadian disruption, such as "jetlag" phase advance protocols, which simulate eastward travel by shifting the time of "lights on" to an earlier time by several hours every few days, induce effects on both the periphery and the brain. Mice exposed to "jetlag," which induces circadian desynchrony, exhibit increased amounts of inflammatory markers in the blood (*70*), diminished hippocampal neurogenesis, and impaired learning and memory (*71*). Altered light:dark schedules, such as a 10 hour:10 hour light:dark paradigm, can also disrupt SCN-mediated rhythms and cause peripheral metabolic alterations, leading to decreased dendritic arborization of cortical neurons and behavioral impairments (*72*). As a human corollary, intercontinental flight attendants subjected to frequent jetlag exhibited hippocampal atrophy, a common feature of AD, when compared to non-jetlagged colleagues (*73*). Thus, the mechanisms linking SCN-mediated circadian rhythms to neurodegeneration are likely multiple and interrelated, and require more detailed analysis in mouse disease models and in humans.

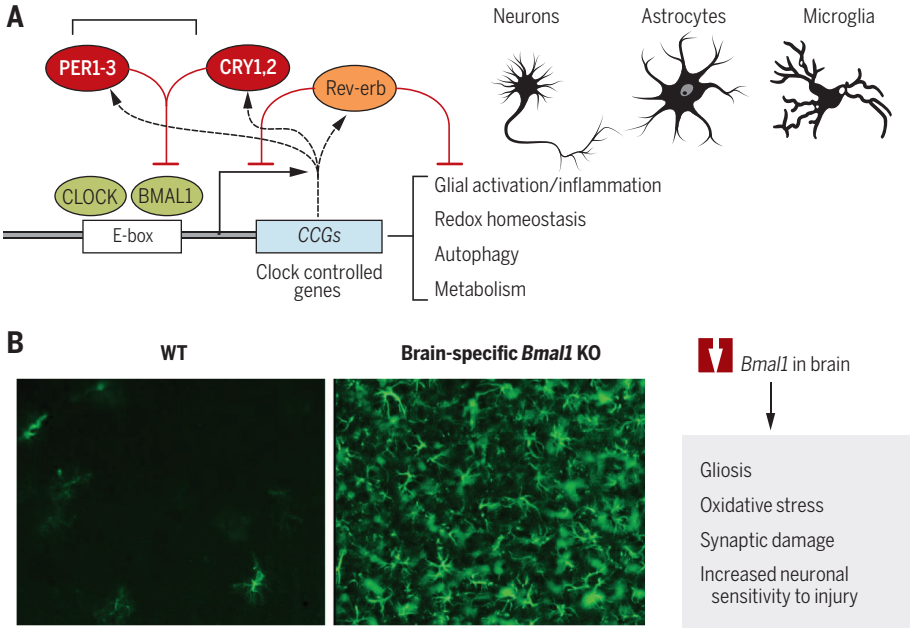

Fig. 3. Core clock genes in the brain regulate neurodegeneration. (**A**) Schematic depicting the core circadian clock. BMAL1 drives transcription of a wide array of clock-controlled genes, which regulate key processes involved in neurodegeneration. The circadian transcriptome could vary between neurons, astrocytes, and microglia. (**B**) Disruption of the cellular clock in the brain with sparing of SCN function, achieved in *Nestin-Cre;Bmal1flox/flox* mice, causes severe reactive astrogliosis in cerebral cortex [as assessed by glial fibrillary acidic protein (GFAP) staining], and promotes oxidative stress and neuronal injury.

Disrupted cellular clocks and neurodegeneration

Circadian clock genes are universally expressed in most cells of the brain, including neurons, astrocytes, and microglia, each of which exhibits circadian clock gene oscillations in culture (*74*, *75*). Transcriptomic studies of cerebellar and brainstem samples from mice demonstrate that several hundred genes exhibit circadian oscillations (*8*). But what do these brain clocks do? And are they important to brain health?

Some insight into these questions can be derived from recent studies of mice harboring deletion of *Bmal1*, which lack detectable circadian rhythms in behavior, sleep-wake cycle, and gene transcription (*11*). *Bmal1*-deficient mice develop striking neurological phenotypes, including profound spontaneous astrogliosis, increased oxidative damage, synaptic degeneration, impaired brain functional connectivity (*12*), impaired learning and memory (*60*), altered hippocampal neurogenesis (*76*–*78*), and lowered seizure threshold (*79*). In some of these cases, it remains unclear if the phenotype is due to loss of *Bmal1* in the cells of the brain itself, or is secondary to whole-animal changes in metabolism. However, mice with brain-specific *Bmal1* deletion that spares the SCN (leaving sleep and peripheral rhythms intact) still develop severe astrogliosis and neuronal loss (*12*) (Fig. 3B). Thus, the positive limb of the circadian clock in the brain appears to be critical for maintaining normal brain function and health independent of sleep or peripheral rhythms. Although the mechanisms linking the cellular circadian clock to neurodegeneration are not fully known, we propose below several candidate molecular processes that exhibit regulation by the clock that are likely contributors to neurodegeneration across diseases (Fig. 3).

Oxidative stress

Neurons are highly sensitive to free radical–mediated injury, and oxidative stress is a conserved pathogenic mechanism in nearly every neurodegenerative condition. Redox homeostasis has been closely linked to the circadian clock across multiple cell and tissue types, and across organisms. Circadian oscillations in peroxiredoxin 6 oxidation occur in organisms ranging from fungi to fruit flies to mice (*80*). Cellular concentrations of reactive oxygen species (ROS), and of the intracellular antioxidant glutathione, exhibit circadian oscillations in *Drosophila* brain (*81*) and in cultured fibroblasts (*82*). Redox oscillations are detectable in the SCN, and alteration of SCN redox state influences neuronal activity and circadian output (*83*). Oxidative stress in flies causes circadian disruption and sleep fragmentation like that seen in aging (*84*). Conversely, disruption of the circadian system by deletion of *Bmal1* causes

increased oxidative stress in multiple organs in mice (*85*), including the brain (*12*). Bmal1 drives transcription of redox-related genes in the brain, including *Nqo1* and *Aldh2* (*12*). As ROS are produced as by-products of increased neuronal activity in the brain, the circadian clock may serve to temporally coordinate the expression of redox defense genes with diurnal variations in brain metabolic activity. Thus, disruption of normal circadian function in the setting of neurologic disease might render the brain more vulnerable to oxidative injury and thereby promote neurodegeneration. Accordingly, diminished *Bmal1* expression exacerbates neuronal death caused by oxidative stress both in vitro and in vivo (*12*).

Inflammation

Neuroinflammation, often propagated by activation of astrocytes and microglia, is a major contributor to neurodegeneration. Astrocytes exhibit robust circadian clock function (*74*), and clock gene deletion leads to pronounced astrocyte activation in vivo (*12*). Microglia also have functional circadian clocks, and the inflammatory response of microglia shows clear circadian variation (*75*, *86*). In the periphery, the circadian clock regulates the responsiveness of macrophages to inflammatory stimuli (*66*), as well as monocyte trafficking to areas of inflammation (*87*). REV-ERBα, a direct BMAL1 transcriptional target, regulates proinflammatory cytokine production in macrophages (*67*). Inflammation also affects the clock, as both BMAL1 and REV-ERBα levels are strongly suppressed in macrophages in response to the inflammogen lipopolysaccharide owing to transcriptional repression by the microRNA miR-155 (*68*). Thus, local inflammation in the hippocampus or cortex could conceivably directly suppress BMAL1 expression in surrounding neurons and glia, leading to impaired Bmal1-mediated expression of oxidative stress response genes and rendering these cells susceptible to neurodegeneration.

Proteostasis

Neurodegenerative diseases are defined pathologically by the aggregation of certain hallmark proteins, including Aβ and tau in AD, α-synuclein in PD, Huntingtin in HD, and TDP-43 in some forms of amyotrophic lateral sclerosis or frontotemporal dementia. Degradation of misfolded proteins is a critical process in the brain, and one that goes awry in a number of disease states. DNA binding of heat shock factor 1 (HSF1), the transcription factor that controls heat shock protein expression, exhibits robust circadian regulation, and HSF1 deletion alters circadian clock oscillation (*88*). Proteasomal degradation of proteins also displays circadian oscillation (*89*), and proteasome function is required for normal circadian clock timing (*90*). The clearance of pathogenic protein aggregates by autophagy has emerged as a crucial mechanism by which the brain forestalls neurodegeneration. Circadian oscillation of autophagy markers has been described in the mouse liver (*91*) and may be regulated by REV-ERBα (*92*). It is unknown whether or how the circadian clock controls rhythmic protein degradation in the brain, but the implications for protein aggregation and deposition in neurodegenerative disease are clear.

The core clock regulates many other potentially neurodegenerative processes in the periphery, including production of the oxidized form of nicotinamide adenine dinucleotide (NAD^+) and activation of the neuroprotective deacetylase Sirt1, both of which also feed back on clock function (*93*–*95*). It will be critical to explore these and other mechanisms in the brain and in models of neurodegeneration, with the hope of unveiling new therapeutic targets.

Therapeutic considerations

The complex interplay between the SCN, sleep-wake nuclei, and cellular circadian clocks makes dissecting the effects of this system on neurodegeneration a daunting task, but it also creates many opportunities for therapeutic intervention. Holistic methods to establish normalized day-night patterns in AD patients through combinations of morning light exposure, enforced daytime activity, consistent bed times, and evening melatonin supplementation have produced some encouraging results, and warrant further study (*65*, *96*). However, an expanding molecular understanding of circadian and sleep systems provides new potential therapeutic targets. Pharmacologic enhancement of SCN oscillations might provide improved circadian rhythms throughout the body and brain, and at the same time normalize sleep-wake timing. Targeting orexin receptors could increase restorative sleep, decrease Aβ deposition, and may indirectly influence circadian clock function, although a negative effect of increased daytime sleepiness would have to be considered in elderly patients. Drugs that directly alter clock gene expression, activity, or oscillation at the tissue level might also be used to enhance clock-mediated transcription of protective genes. Moreover, considering that neurotransmitters, including acetylcholine, can influence the circadian system (*97*), the effect of currently used treatments for neurodegenerative diseases (such cholinesterase inhibitors) on circadian function should be considered.

Conclusion and future directions

The circadian clock and the sleep-wake cycle are multilayered, interconnected systems that affect brain function and neurodegeneration by multiple mechanisms. Despite great progress in understanding the basic mechanisms governing the circadian clock, as well as the neural circuitry of sleep, our knowledge of how these systems are affected in the brain in aging and neurodegenerative disease is still rather superficial. A more detailed understanding of the mechanism by which specific neurodegenerative diseases and pathogenic proteins influence the circadian and sleep systems, as well as the interplay between sleep and circadian systems in aging and neurodegeneration, is needed. Although helpful, current transgenic rodent models of neurodegeneration may not fully capture the mechanistic complexity involved, and more translational methods are needed. The exact function of the core circadian clock in different brain regions and cell types is also lacking, as is knowledge of specific clock-controlled transcriptional pathways in the brain that might influence disease. The glymphatic system and its role in neurodegeneration is another area of research priority. Integrated study of clocks, sleep, and neurodegeneration is still in its infancy, but great potential exists to harness these powerful systems that govern so many critical aspects of brain function for therapeutic benefit in the prevention of neurodegeneration.

REFERENCES AND NOTES

1. A. Videnovic, A. S. Lazar, R. A. Barker, S. Overeem, *Nat. Rev. Neurol.* **10**, 683–693 (2014).
2. C. F. Hatfield, J. Herbert, E. J. van Someren, J. R. Hodges, M. H. Hastings, *Brain* **127**, 1061–1074 (2004).
3. R. Sterniczuk, O. Theou, B. Rusak, K. Rockwood, *Curr. Alzheimer Res.* **10**, 767–775 (2013).
4. A. S. Lim, M. Kowgier, L. Yu, A. S. Buchman, D. A. Bennett, *Sleep* **36**, 1027–1032 (2013).
5. C. H. Schenck, B. F. Boeve, M. W. Mahowald, *Sleep Med.* **14**, 744–748 (2013).
6. J. A. Mohawk, C. B. Green, J. S. Takahashi, *Annu. Rev. Neurosci.* **35**, 445–462 (2012).
7. J. Bass, J. S. Takahashi, *Science* **330**, 1349–1354 (2010).
8. R. Zhang, N. F. Lahens, H. I. Ballance, M. E. Hughes, J. B. Hogenesch, *Proc. Natl. Acad. Sci. U.S.A.* **111**, 16219–16224 (2014).
9. N. Ibuka, H. Kawamura, *Brain Res.* **96**, 76–81 (1975).
10. M. F. Rath, K. Rohde, M. Møller, *Chronobiol. Int.* **29**, 1289–1299 (2012).
11. M. K. Bunger *et al.*, *Cell* **103**, 1009–1017 (2000).
12. E. S. Musiek *et al.*, *J. Clin. Invest.* **123**, 5389–5400 (2013).
13. G. Yang *et al.*, *Sci. Transl. Med.* **8**, 324ra316 (2016).
14. A. Laposky *et al.*, *Sleep* **28**, 395–409 (2005).
15. K. L. Toh *et al.*, *Science* **291**, 1040–1043 (2001).
16. T. Curie, S. Maret, Y. Emmenegger, P. Franken, *Sleep* **38**, 1381–1394 (2015).
17. J. Cedernaes *et al.*, *J. Clin. Endocrinol. Metab.* **100**, E1255–E1261 (2015).
18. V. Mongrain, F. La Spada, T. Curie, P. Franken, *PLOS ONE* **6**, e26622 (2011).
19. A. Iranzo, *Sleep Med. Clin.* **11**, 1–18 (2016).
20. J. K. Holth, T. K. Patel, D. M. Holtzman, Sleep in Alzheimer's disease—Beyond amyloid. *Neurobiology of Sleep and Circadian Rhythyms* (2016), http://dx.doi.org.
21. R. Sterniczuk, R. H. Dyck, F. M. Laferla, M. C. Antle, *Brain Res.* **1348**, 139–148 (2010).
22. T. Kudo, D. H. Loh, D. Truong, Y. Wu, C. S. Colwell, *Exp. Neurol.* **232**, 66–75 (2011).
23. A. J. Morton *et al.*, *J. Neurosci.* **25**, 157–163 (2005).
24. J. H. Roh *et al.*, *Sci. Transl. Med.* **4**, 150ra122 (2012).
25. C. Benedict *et al.*, *Sleep* **37**, 195–198 (2014).
26. D. J. Frey, M. Fleshner, K. P. Wright Jr., *Brain Behav. Immun.* **21**, 1050–1057 (2007).
27. N. Naidoo, M. Ferber, M. Master, Y. Zhu, A. I. Pack, *J. Neurosci.* **28**, 6539–6548 (2008).
28. E. S. Musiek, D. M. Holtzman, *Nat. Neurosci.* **18**, 800–806 (2015).
29. J. E. Kang *et al.*, *Science* **326**, 1005–1007 (2009).
30. Y. Huang *et al.*, *Arch. Neurol.* **69**, 51–58 (2012).
31. J. H. Roh *et al.*, *J. Exp. Med.* **211**, 2487–2496 (2014).
32. C. Benedict *et al.*, *Alzheimers Dement.* **11**, 1090–1097 (2015).
33. Y. E. Ju *et al.*, *JAMA Neurol.* **70**, 587–593 (2013).
34. R. S. Osorio *et al.*, *Sleep* **39**, 1253–1260 (2016).
35. M. Wennström, E. Londos, L. Minthon, H. M. Nielsen, *J. Alzheimers Dis.* **29**, 125–132 (2012).
36. A. Di Meco, Y. B. Joshi, D. Praticò, *Neurobiol. Aging* **35**, 1813–1820 (2014).
37. S. M. Rothman, N. Herdener, K. A. Frankola, M. R. Mughal, M. P. Mattson, *Brain Res.* **1529**, 200–208 (2013).
38. G. Tononi, C. Cirelli, *Neuron* **81**, 12–34 (2014).
39. B. A. Mander *et al.*, *Nat. Neurosci.* **18**, 1051–1057 (2015).
40. J. J. Iliff *et al.*, *Sci. Transl. Med.* **4**, 147ra111 (2012).
41. L. Xie *et al.*, *Science* **342**, 373–377 (2013).
42. J. Zhang *et al.*, *J. Neurosci.* **34**, 4418–4431 (2014).
43. A. S. Lazar *et al.*, *Ann. Neurol.* **78**, 630–648 (2015).
44. T. Kudo *et al.*, *Exp. Neurol.* **228**, 80–90 (2011).
45. P. N. Pallier *et al.*, *J. Neurosci.* **27**, 7869–7878 (2007).
46. T. J. Nakamura *et al.*, *J. Neurosci.* **31**, 10201–10205 (2011).
47. C. A. Wyse, A. N. Coogan, *Brain Res.* **1337**, 21–31 (2010).
48. D. F. Swaab, E. Fliers, T. S. Partiman, *Brain Res.* **342**, 37–44 (1985).

49. J. L. Wang *et al.*, *Ann. Neurol.* **78**, 317–322 (2015).
50. N. Cermakian, E. W. Lamont, P. Boudreau, D. B. Boivin, *J. Biol. Rhythms* **26**, 160–170 (2011).
51. H. Song *et al.*, *Mol. Neurodegener.* **10**, 13 (2015).
52. D. P. Breen *et al.*, *JAMA Neurol.* **71**, 589–595 (2014).
53. Y. Cai, S. Liu, R. B. Sothern, S. Xu, P. Chan, *Eur. J. Neurol.* **17**, 550–554 (2010).
54. E. S. Maywood *et al.*, *J. Neurosci.* **30**, 10199–10204 (2010).
55. G. J. Tranah *et al.*, *Ann. Neurol.* **70**, 722–732 (2011).
56. H. F. Chen, C. Q. Huang, C. You, Z. R. Wang, H. Si-qing, *Arch. Med. Res.* **44**, 203–207 (2013).
57. Q. Chen, X. D. Peng, C. Q. Huang, X. Y. Hu, X. M. Zhang, *Genet. Mol. Res.* **14**, 18515–18522 (2015).
58. Z. Gu *et al.*, *Sci. Rep.* **5**, 15891 (2015).
59. D. Chaudhury, L. M. Wang, C. S. Colwell, *J. Biol. Rhythms* **20**, 225–236 (2005).
60. S. M. Wardlaw, T. X. Phan, A. Saraf, X. Chen, D. R. Storm, *Learn. Mem.* **21**, 417–423 (2014).
61. B. L. Smarr, K. J. Jennings, J. R. Driscoll, L. J. Kriegsfeld, *Behav. Neurosci.* **128**, 283–303 (2014).
62. D. H. Loh *et al.*, *eLife* **4**, e09460 (2015).
63. K. Uchida, N. Okamoto, K. Ohara, Y. Morita, *Brain Res.* **717**, 154–159 (1996).
64. A. Videnovic *et al.*, *JAMA Neurol.* **71**, 463–469 (2014).
65. R. F. Riemersma-van der Lek *et al.*, *JAMA* **299**, 2642–2655 (2008).
66. M. Keller *et al.*, *Proc. Natl. Acad. Sci. U.S.A.* **106**, 21407–21412 (2009).
67. J. E. Gibbs *et al.*, *Proc. Natl. Acad. Sci. U.S.A.* **109**, 582–587 (2012).
68. A. M. Curtis *et al.*, *Proc. Natl. Acad. Sci. U.S.A.* **112**, 7231–7236 (2015).
69. A. Mukherji, A. Kobiita, T. Ye, P. Chambon, *Cell* **153**, 812–827 (2013).
70. O. Castanon-Cervantes *et al.*, *J. Immunol.* **185**, 5796–5805 (2010).
71. E. M. Gibson, C. Wang, S. Tjho, N. Khattar, L. J. Kriegsfeld, *PLOS ONE* **5**, e15267 (2010).
72. I. N. Karatsoreos, S. Bhagat, E. B. Bloss, J. H. Morrison, B. S. McEwen, *Proc. Natl. Acad. Sci. U.S.A.* **108**, 1657–1662 (2011).
73. K. Cho, *Nat. Neurosci.* **4**, 567–568 (2001).
74. L. M. Prolo, J. S. Takahashi, E. D. Herzog, *J. Neurosci.* **25**, 404–408 (2005).
75. L. K. Fonken *et al.*, *Brain Behav. Immun.* **45**, 171–179 (2015).
76. A. A. Ali *et al.*, *Aging* **7**, 435–449 (2015).
77. B. D. Rakai, M. J. Chrusch, S. C. Spanswick, R. H. Dyck, M. C. Antle, *PLOS ONE* **9**, e99527 (2014).
78. P. Bouchard-Cannon, L. Mendoza-Viveros, A. Yuen, M. Kærn, H. Y. Cheng, *Cell Reports* **5**, 961–973 (2013).
79. J. R. Gerstner *et al.*, *Front. Syst. Neurosci.* **8**, 121 (2014).
80. R. S. Edgar *et al.*, *Nature* **485**, 459–464 (2012).
81. L. M. Beaver *et al.*, *PLOS ONE* **7**, e50454 (2012).
82. R. V. Khapre, A. A. Kondratova, O. Susova, R. V. Kondratov, *Cell Cycle* **10**, 4162–4169 (2011).
83. T. A. Wang *et al.*, *Science* **337**, 839–842 (2012).
84. K. Koh, J. M. Evans, J. C. Hendricks, A. Sehgal, *Proc. Natl. Acad. Sci. U.S.A.* **103**, 13843–13847 (2006).
85. R. V. Kondratov, A. A. Kondratova, V. Y. Gorbacheva, O. V. Vykhovanets, M. P. Antoch, *Genes Dev.* **20**, 1868–1873 (2006).
86. Y. Hayashi *et al.*, *Sci. Rep.* **3**, 2744 (2013).
87. K. D. Nguyen *et al.*, *Science* **341**, 1483–1488 (2013).
88. H. Reinke *et al.*, *Genes Dev.* **22**, 331–345 (2008).
89. A. Desvergne, N. Ugarte, I. Petropoulos, B. Friguet, *Free Radic. Biol. Med.* **75** (suppl. 1), S18 (2014).
90. M. Stratmann, D. M. Suter, N. Molina, F. Naef, U. Schibler, *Mol. Cell* **48**, 277–287 (2012).
91. D. Ma, S. Panda, J. D. Lin, *EMBO J.* **30**, 4642–4651 (2011).
92. G. Huang, F. Zhang, Q. Ye, H. Wang, *Autophagy* **12**, 1292–1309 (2016).
93. H. C. Chang, L. Guarente, *Cell* **153**, 1448–1460 (2013).
94. Y. Nakahata, S. Sahar, G. Astarita, M. Kaluzova, P. Sassone-Corsi, *Science* **324**, 654–657 (2009).
95. K. M. Ramsey *et al.*, *Science* **324**, 651–654 (2009).
96. D. Forbes, C. M. Blake, E. J. Thiessen, S. Peacock, P. Hawranik, *Cochrane Database Syst. Rev.*, CD003946 (2014).
97. D. J. Earnest, F. W. Turek, *Proc. Natl. Acad. Sci. U.S.A.* **82**, 4277–4281 (1985).

ACKOWLEDGMENTS

Funding was provided by NIH grants P01NS074969 (D.M.H.) and 5K08NS079405 (E.S.M.), and a New Investigator Research Grant from the Alzheimer's Association (E.S.M.). E.S.M. has received consulting fees from Eisai, Inc. D.M.H. cofounded and is on the scientific advisory board of C2N Diagnostics and consults for Genentech, AbbVie, Eli Lilly, Neurophage, and Denali.

10.1126/science.aah4968

REVIEW

Circadian physiology of metabolism

Satchidananda Panda

A majority of mammalian genes exhibit daily fluctuations in expression levels, making circadian expression rhythms the largest known regulatory network in normal physiology. Cell-autonomous circadian clocks interact with daily light-dark and feeding-fasting cycles to generate approximately 24-hour oscillations in the function of thousands of genes. Circadian expression of secreted molecules and signaling components transmits timing information between cells and tissues. Such intra- and intercellular daily rhythms optimize physiology both by managing energy use and by temporally segregating incompatible processes. Experimental animal models and epidemiological data indicate that chronic circadian rhythm disruption increases the risk of metabolic diseases. Conversely, time-restricted feeding, which imposes daily cycles of feeding and fasting without caloric reduction, sustains robust diurnal rhythms and can alleviate metabolic diseases. These findings highlight an integrative role of circadian rhythms in physiology and offer a new perspective for treating chronic diseases in which metabolic disruption is a hallmark.

A transient rise in blood sugar after a meal indicates metabolic health. A larger meal produces a larger spike, whereas a fat- or protein-rich meal produces a muted spike (compared with a normal meal of equivalent caloric content). Physiological responses to what and how much we eat represent the foundation for basic and translational science aimed at preventing and treating obesity, diabetes, and metabolic diseases, which together afflict close to a billion people worldwide. However, the timing of food consumption independent of total caloric intake and macronutrient quality has emerged as a critical factor in maintaining metabolic health. For instance, when healthy adults eat identical meals at breakfast, lunch, or dinner, the postprandial glucose rise is lowest after breakfast and highest after dinner (*1*), as if the dinner were twice the size of the breakfast. In addition, when healthy adults are given a constant glucose infusion over 24 hours, glycemia rises at night and falls around dawn (*1*), indicating that in addition to what and how much we eat, when we eat helps determine the physiological response to nutrient availability.

Daily rhythms in nutrient use were first documented almost 40 years ago in cells of the master circadian pacemaker located in the hypothalamic suprachiasmatic nucleus (SCN). Experiments in rats fed ^{14}C-labeled deoxyglucose during their habitual (nighttime) feeding period showed that entry of glucose into the SCN was almost negligible, whereas during the day, radiolabeled glucose was readily detected (*2*). Such glucose uptake rhythms were sustained even in the absence of light cues. In all, this elegant experiment proved the existence of a circadian rhythm in nutrient demand and/or uptake in tissues. Over the next decades, research into circadian rhythms has shown that daily rhythms in the function of numerous genes prime the organism to assimilate nutrients, to mobilize these nutrients for various functions, and to discard metabolic waste at specific times of the 24-hour day (*3*, *4*). Whereas circadian rhythms generally refer to ~24-hour oscillations that occur in the absence of external timing cues, daily or diurnal rhythms apparent during normal living conditions emerge from interactions between the internal circadian clock and timing cues, which include light and food. Accordingly, a consistent daily pattern of eating and fasting maintains normal circadian physiology, whereas frequent disruptions in daily activity-rest and eating-fasting rhythms (as occurs in shiftwork) (*5*) or genetic disruption of circadian clock in rodents predisposes to metabolic diseases (*6*). Certain diet regimens (e.g., the frequent eating of energy-dense food) and aging can dampen these daily oscillations and predispose one to metabolic diseases. Therefore, understanding the diurnal physiology of metabolism at a mechanistic level could potentially reveal lifestyle and therapeutic interventions for preventing and treating metabolic diseases.

Cell-autonomous circadian oscillator

In animals, the core mechanism that gives rise to circadian oscillations is a cell-autonomous transcriptional-translational feedback loop (TTFL) present in most cells. The transcription factors CLOCK (or NPAS2) and BMAL1 bind as heterodimers to cis-acting E boxes in the promoters of their own repressors—Cryptochrome (*Cry1* and *Cry2*) and Period (*Per-1*, *-2*, and *-3*)—and of the nuclear hormone receptors *Rev-erb* (-α and -β), and *Ror* (-α, -β, and -γ). ROR and REV-ERB drive rhythmic Bmal1 gene expression by respectively acting so as to activate and repress its expression through RRE elements present in its promoter (Fig. 1) (*7*). REV and ROR proteins also affect the expression of *Cry1*, delaying its expression several hours relative to

Salk Institute of Biological Studies, 10010 North Torrey Pines Road, La Jolla, CA 92037, USA.
Email: satchin@salk.edu

Cry2. Regulated transcriptional and posttranscriptional events involving a growing list of nuclear and cytoplasmic proteins generate endogenous ~24-hour rhythms in the mRNA and protein levels of most of these 13 transcriptional regulators (*7*). In addition to controlling each other's expression, these regulators also drive rhythmic expression of thousands of target genes by binding cis-regulatory sites or through downstream transcriptional regulators. The transcriptional basis of circadian rhythms enables a set of transcriptional regulators to temporally couple their activity with the synchronous rhythmic expression of hundreds or even thousands of genes, with peak expression at distinct times of the day (phase). Such extensive and coordinated gene expression and function would be difficult to achieve with a timing mechanisms based entirely on protein-protein interactions.

Circadian transcription factors also interact with a number of coactivators, corepressors, and chromatin-associated factors that read, write, or erase chromatin histone modification marks to activate or repress transcription (Fig. 1). CLOCK/BMAL1 complexes are often associated with the histone acetyl transferase p300 and CREB-binding protein (CBP) (*8*). CRY/PER repressors are found in complexes with histone deacetylase (HDAC) (*9*). Additionally, MLL1, MLL*3*, WDR5, and EZH2 form complexes with circadian transcriptional factors (*10*). Interactions between REV-ERB and the N-CoR/HDAC3 corepressor are essential for repressive function of REV-ERB (*11*). A histone lysine demethylase, JARID1a (*12*), and a bHLH-PAS protein, USF1 (*13*), help transition between daily cycles of activation and repression by interacting with CLOCK/BMAL1 and PER/CRY complexes. In addition to rhythms in histone modifications, some circadian clock proteins also undergo acetylation and deacetylation. Additional cis-acting promoter elements (e.g., CRE and HSE) mediate rapid adjustment of circadian clock components in response to sudden changes in cellular state. Altogether, circadian clock–mediated transcriptional regulation involves a large number of proteins and functional interactions.

Plasticity of the circadian system

The elaborate circadian transcriptional mechanism has many advantages, given that each component of the circadian system can serve as a node for integrating cellular physiology with the circadian function or to transmit circadian timing information to nonclock proteins. Cellular concentration of certain metabolites–including but not limited to heme, nicotinamide adenine dinucleotide/reduced form of nicotinamide adenine dinucleotide (NAD/NADH), nicotinamide adenine dinucleotide phosphate/reduced form of NADP (NADP/NADPH), adenosine monophosphate/adenosine triphosphate (AMP/ATP), acetyl coenzyme A (AcCoA), alpha keto glutarate (α-KG), *S*-adenosyl methionine (SAM), CO, and polyamine–can affect the function of several circadian transcriptional regulators by modulating histone modifications, protein modifications, protein-protein interactions, protein-DNA interactions, or protein turnover (*14*). Extracellular factors such as temperature, hormones, and metabolites can also affect the clock and thereby constitute mechanisms for local synchrony of cellular clocks or for adjusting the phase of an organ's clock in response to systemic signals. Hence, the circadian physiology of any given cell emerges from integrating the cell-autonomous TTFL, cellular metabolism, and extracellular systemic signals (Fig. 1). Thus, clock proteins can sense daily changes in cellular metabolism and systemic signals and make predictive changes to the circadian transcriptome.

Many circadian clock proteins interact with and modify the function of proteins that are not part of the core clock TTFL. Coupled with their own cycling levels, these clock proteins can "impose" rhythmic functions to nonclock proteins. For example, CRY and REV-ERB proteins interact with the glucocorticoid receptor (GR) to inhibit its transcriptional activity (*15*, *16*). CRY proteins also inhibit signaling downstream of the glucagon receptor, thereby imposing a time-of-day-specific effect of glucagon on gluconeogenesis (*17*). Similarly, REV-ERB and HNF6 interact to regulate lipid metabolism in adult mouse liver (*18*). Additionally, several homologous proteins within the core TTFL (or their interacting partners) are not fully redundant but rather have specific functions. For example, the CLOCK/BMAL complex interacts with SIRT1 or SIRT6 in a locus-specific manner to target different subsets of the circadian transcriptome in the liver (*19*). In many cases, these homologs are not expressed in all tissues. Ror-α is expressed in neural tissue, whereas Ror-γ expression dominates in peripheral tissues (*20*). In summary, the molecular constituents of the clock, partial redundancy among clock components, interactions between clock and nonclock components, and the cyclic expression of downstream tissue-specific components all contribute to tissue-specific molecular circadian physiology, which functions to integrate cell type–specific intra- and extracellular signals to regulate tissue function.

Tissue organization of circadian clocks

The SCN plays a central, high-order role in the circadian regulation of metabolism by sustaining ~24-hour rhythms in activity-rest and feeding-fasting, even under constant darkness. This is achieved through both synaptic and diffusible factors that couple the SCN oscillator with cell type–specific circadian clocks in different brain regions and endocrine cells (*7*). Through a polysynaptic connection, the SCN ensures that the pineal gland produces melatonin in a rhythmic fashion (peak levels at night) to promote sleep in diurnal animals. Similarly, through the paraventricular nucleus (PVN) and the pituitary gland, the SCN drives a circadian rhythm in adrenocorticotropic hormone (ACTH) release, which in turn drives a morning rise in corticosterone release from the adrenal gland. Under natural light-dark (LD) conditions, bright light strongly suppresses the production of melatonin (*21*) and promotes corticosterone production in the adrenal gland through an ACTH-independent sympathetic pathway (*22*). Corticosteroids promote arousal and

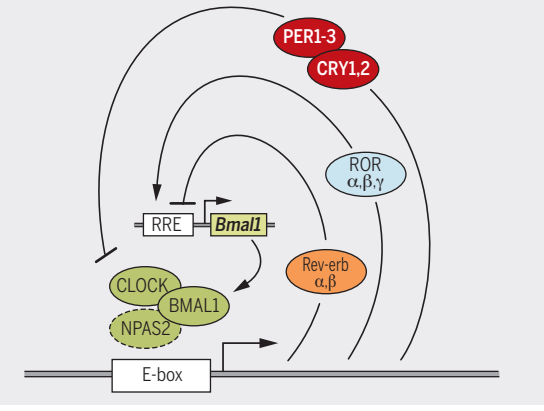

Metabolites directly or indirectly affecting circadian oscillator

NAD(P)/NAD(P)H ratio	NAD^+
Heme	FAD
Sterols	CO
Glucocorticoids	O_2
Polyamine	Glucose

Interacting proteins

p300	NCoR	MTA2	βTRCP
CBP	WDR5	SETX	FBXL3
HDAC	MLL	AMPK	FBXW7
SIRT	NONO	GSK3	PPARγ
JMJD5	NuRD	CK1	GR
JARID1	CHD4	PP1	USF1

Transcription factors that exhibit daily rhythms in metabolic organs

DBP	NFIL3	P-CREB	GR	VDR
TEF	DEC1	ERR	NURR1	
HLF	DEC2	FXR	NOR1	
E4BP4	KLF15	PPARs	TRs	

Systemic factors with diurnal rhythms

Insulin	Growth hormone
Melatonin	Glucocorticoid
Glucagon	Thyrotropin
Body temperature	

Fig. 1. Schematics of cell-autonomous transcription-translation feedback loop (TTFL), constituting the core mechanism of mammalian circadian oscillator. Some of the cellular metabolites and proteins that interact with the clock components are listed. Examples of circadian-regulated transcription factors or systemic factors with daily oscillations further propagate circadian timing to distant genomic and cellular targets.

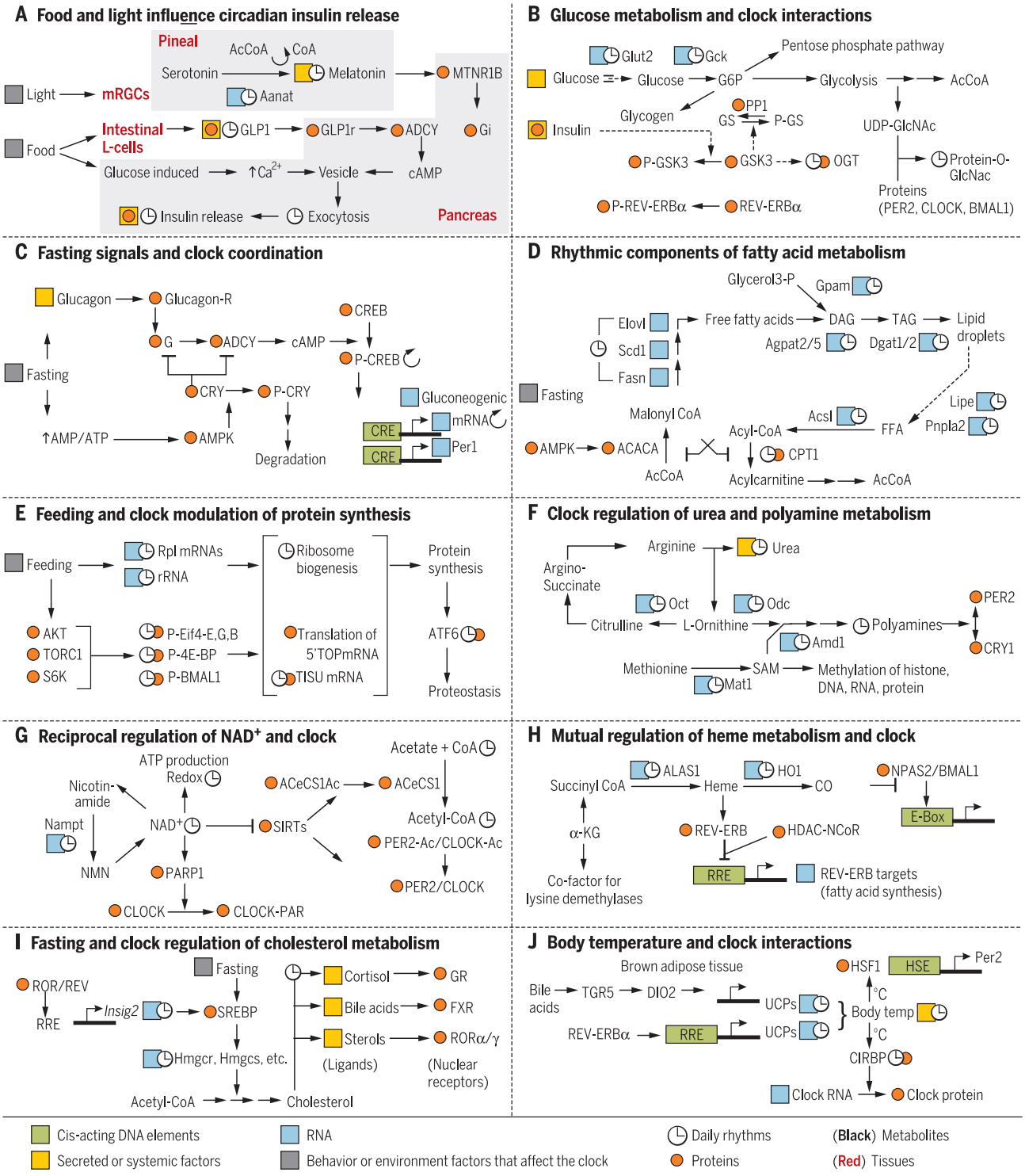

Fig. 2. Examples of circadian regulation of metabolic pathways and metabolic pathways affecting clock components. Cis-acting DNA elements are in green, RNA in blue, proteins in orange; metabolites are shown in black letters, and tissues are underlined. Any RNA, protein, or metabolite (other than clock components) known to show daily rhythms are marked with ↻. Secreted or systemic factors are highlighted in yellow, and behavior or environment factors that can affect the clock are highlighted in gray. (**A**) Light and food intake can interact through multiple tissues to modulate insulin release from pancreatic islet cells. (**B**) Feeding-induced glucose metabolism in the liver affects clock components. (**C**) During fasting, activation of glucagon receptor and AMPK impinge on clock components. (**D**) Fatty acid synthesis and degradation are under feeding-fasting and circadian regulation. (**E**) Circadian clock and feeding signals act together to produce a daily rhythm in protein synthesis. (**F**) Circadian regulation of urea cycle, SAM synthesis, and polyamine production. Polyamines affect interaction between PER2 and CRY1. (**G**) Reciprocal regulation between circadian clock and NAD production. (**H**) Circadian production of meme and CO affect the function of core circadian clock components. (**I**) Fasting and circadian clock regulate cholesterol metabolism and production of several ligands for nuclear hormone receptors. (**J**) Reciprocal regulation between circadian clock and body-temperature rhythm.

alertness and drive catabolic metabolism in adipose tissue and muscle. Both melatonin and cortisol rhythms are detectable in the blood, and both hormones have pleiotropic effects on multiple tissues.

Local SCN outputs are intimately integrated with centers in the hypothalamus involved in hunger-satiety, sleep-arousal, thermoregulation, and osmolarity, as well as a forebrain oscillator that mediates an anticipatory drive for food (*23*). Mechanisms underlying these synaptic interactions are unclear, and both cellular and genetic phenotypes paint a complicated picture. *Npas2*$^{-/-}$ mice show normal overall diurnal rhythms in activity and rest under a LD cycle, yet they lack a siesta-type rest period in the middle of the active period and cannot adjust normally when meal timing is abruptly changed (*24*). On the other hand, hypomorphic *Clock* mutant mice show normal circadian behavior under a LD cycle, yet, owing to low amplitude of the SCN clock, rapidly adjust activity-rest rhythms in response to abrupt changes in the LD cycle, which mimic jet lag or rotating shift work (*25*). Similarly, mutation of a casein kinase 1 (CK1) phosphorylation site in *Per2* advances the sleep onset time (*26*) but does not affect feeding time. A paralogous mutation in *Per1* advances the daily onset of feeding without affecting the timing of activity-rest (*27*). It is unclear whether the different phenotypes seen in these paralogous mutants arise from shared neural mechanisms.

The SCN also communicates with peripheral tissues, including the gut and pancreas, which have their own autonomous circadian clocks. These local clocks mediate responses to nutrient intake and control the release of systemic factors. For example, a circadian clock in secretory cells of the gut drives rhythmic expression of SGLT1, accounting for increased glucose uptake at times of anticipated food intake (*28*). Glucose influx triggers the release of GLP1 incretin that, along with the direct effect of glucose on pancreatic islets, promotes insulin release. In pancreatic islet cells, like in many other cell types, exocytosis is modulated in a circadian manner (*29*). Accordingly, insulin release has a circadian component (Fig. 2A). Overall, the central circadian clock, through direct or indirect effects, generates systemic rhythms in several signaling molecules, including melatonin, glucocorticoids, growth hormones, insulin, glucagon, and GLP1, whose rhythms are further accentuated by LD or feeding-fasting cycles.

Global circadian regulation in the liver

Because the liver plays a central role in nutrient metabolism, is composed of relatively homogeneous cell types, and is easy to access, a number of ≥24-hour time-course "-omics" studies have been conducted using mouse liver tissue. These have included chromatin immunoprecipitation sequencing (ChIP-seq), RNA-seq (and comparable microarray hybridization), ribo-seq, nascent-seq, proteomics, and metabolomics. The majority of these studies used young male mice (<20 weeks old) entrained to a 12-hour light/12-hour dark cycle for several days and fed a standard diet (calories from fat <18%, protein ~25%, carb ~60%) ad libitum. Tissue samples have usually been collected under circadian conditions (constant darkness). Such an approach allows the removal of confounding effects derived from light cues. Normally, the majority of a mouse's daily food intake occurs during the subjective night, but ≥15% of food intake occurs during the subjective day in the form of frequent small snacks. Thus, under the ad libitum–fed condition, mice rarely fast a few contiguous hours. Under such conditions, at least 20% of expressed protein coding genes in the liver show circadian rhythms in transcription, mature mRNA, active translation, or protein levels. Rhythmic gene expression has several advantages. First, bioenergetic modeling of gene expression in yeast demonstrates that rhythmic gene expression is more energy efficient than maintaining constant levels of expression. This form of energy conservation is observed in a range of mammalian and insect tissues (*30*). Conversely, when a mouse is subjected to continuous 24-hour fasting, the number of rhythmic transcripts is reduced by almost 80%. This largely results from reduced peak levels of expression, rather than elevated trough level of rhythmic expression (*30*). Second, rhythmic expression helps to temporally separate incompatible biochemical processes, thereby preventing futile cycles (e.g., the simultaneous biosynthesis and degradation of a given molecule). Because almost 20% of liver transcripts show daily rhythms, it is logical that at least some of the enzymes and regulators in every metabolic pathway are likely to display circadian rhythmicity. More important, these rhythmically regulated pathway components often mediate rate-limiting steps, with peak levels of expression coinciding with substrate availability or metabolic need. Several key rhythmic metabolites exert effects on circadian clock components, thereby integrating the metabolic state with the regulatory mechanism. Sometimes, posttranslational modifiers (e.g., kinases and phosphatases) that regulate key enzymes of metabolic pathways also act on clock components, thus coupling metabolic and circadian regulatory processes. Some of these examples will be highlighted in the following section.

"...rhythmic expression helps to temporally separate incompatible biochemical processes, thereby preventing futile cycles (e.g., the simultaneous biosynthesis and degradation of a given molecule)."

Metabolic pathways, metabolites, and their integration with the circadian clock

Functional annotation of the liver circadian cistrome, transcriptome, and proteome show that these are enriched with metabolic regulators. To maintain energy homeostasis, the liver stores nutrients during feeding periods and taps into this stored energy reserve during fasting periods. Intermediates from these cycles of anabolism and catabolism are used for cellular components and signaling. As feeding and fasting naturally alternate between day and night, interactions among feeding-fasting–driven regulation, metabolism, and circadian clocks have evolved to maintain normal physiology.

Glucose metabolism

Glucose enters hepatocytes where it is phosphorylated. Phosphoglucose is then (i) used for energy production via glycolysis, (ii) stored as glycogen for further use (glucogenesis), or (iii) used in the pentose phosphate pathway (PPP) (Fig. 2B). Expression of the hepatic glucose transporter GLUT2 and glucokinase (GCK) show daily rhythms with peak levels coinciding with periods of feeding (*31*). In the fed state, insulin activates glycogenesis through a signaling cascade that leads to the inhibition of glycogen synthase kinase (GSK3), thereby releasing the activity of glycogen synthase (GS). GSK3 has daily rhythms of phosphorylation and activity and acts on some circadian clock components (e.g., affecting the stability of REV-ERB) (*32*). β-linked *N*-acetylglucosamine (i.e., O-β-GlcNAc or O-GlcNAc), the attachment of UDP-GlcNAc to Ser/Thr residues of proteins, is yet another link between the circadian clock and glucose metabolism. The activity of the enzyme O-GlcNac transferase (OGT) is regulated by GSK3 (*33*) and, accordingly, a number of hepatic proteins show circadian rhythms in O-GlcNAcylation (*34*), including PER2, CLOCK, and BMAL1. The balance between O-GlcNacylation, glycosylation, CK1 phosphorylation, and protein phosphatase 1 (PP1)–mediated dephosphorylation of PER2 determines its stability (*33*). In parallel, O-GlcNacylation of CLOCK and BMAL1 interferes with their ubiquitination and degradation (*35*). Glucose use through the PPP is also connected to the circadian clock. The PPP is essential for nucleotide and amino acid biosynthesis, as well for replenishing the pool of cytoplasmic NADPH. Low NADPH levels activate the transcription factor NRF2, which can drive transcription of *Rev-erb*, thereby affecting the molecular clock (*36*).

In the fasted state, the circadian clock also influences glucose metabolism by interacting with glucagon signaling (Fig. 2C). Glucagon signals through its G-protein–coupled receptor and adenylate cyclase to activate protein kinase A (PKA), which in turn promotes glycogenolysis and gluconeogenesis to supply glucose (*37*). PKA phosphorylates and thereby activates the bZIP transcription factor cyclic AMP response element–binding protein (CREB) so that it binds to cis-acting CRE sites

at the *Per1* and several gluconeogenic promoters, thereby stimulating their transcription (*38*). Additionally, CRY1 inhibits the activation of PKA by negatively regulating the G protein or adenylate cyclase (*17*, *39*). On the other hand, prolonged fasting also increases the ratio of AMP/ATP (adenosine triphosphate) and activates AMP-activated kinase (AMPK), which phosphorylates CRYs and targets them for degradation (*40*). Together, this suggests a mechanism by which CRY1 acts as a balance point between the short- and long-term responses to nutrient deficit.

Lipid metabolism

Fatty acid synthesis and β oxidation are tightly controlled in the liver (Fig. 2D). Mitochondrial acetyl CoA is exported to the cytoplasm via a citrate/palmitate shuttle, where ATP citrate lyase (ACLY) is a rate-limiting enzyme. The circadian peak of ACLY expression coincides with feeding (*31*). The first committed step of fatty acid synthesis is the carboxylation of acetyl CoA by ACACA (acetyl CoA carboxylase) to produce malonyl CoA. ACACA is inactivated via phosphorylation by fasting-induced AMPK. The rate of mitochondrial β oxidation is limited by the entry of fatty acyl groups into the mitochondria by carnitine palmitoyl transferase 1 (CPT1) and CPT2. The levels of L-carnitine, CPT1, and CPT2 show daily rhythms (*41*). Furthermore, high levels of malonyl CoA, which are produced during fatty acid synthesis and peak during feeding, inhibit CPT activity. Such circadian- and product-mediated regulation generates a daily rhythm in fatty acid synthesis and oxidation, which peak during feeding and fasting, respectively. This also gives rise to daily rhythms in several liver lipids (*42*). Rhythmic repression by REV-ERB α generates daily rhythms in many transcripts involved in the fatty acid synthesis pathway. Accordingly, *Rev-erb* $\alpha^{-/-}$ mice exhibit fatty liver disease (*43*, *44*).

Protein

Ingested proteins are degraded to amino acids in the small intestine and transported to the liver. Amino acids rarely remain free in cells, because they can be (i) used for protein synthesis during the fed state; (ii) used for gluconeogenesis during fasting; (iii) metabolized to bioactive molecules (e.g., methionine is adenylated to produce SAM); or (iv) degraded to liberate ammonia, which is fed into the urea cycle. During the fed state, insulin receptor substrate (IRS) downstream kinase AKT activates the mTOR-S6kinase pathway to promote protein translation. AKT or S6K1 also phosphorylates BMAL1 and recruits it to translation complexes, where it promotes complex activity (Fig. 2E) (*45*, *46*). In combination with circadian rhythms in ribosome biogenesis (*47*) and preferential translation of specific subsets of mRNAs (*48*), this general rhythm in protein synthesis is specifically important for liver function, because it is a major source of critical secreted proteins, including albumin, retinol-binding protein, transthyretin, and proteins of the complement pathway.

During overnight fasting, circadian regulation of the transcription factor KLF15 in muscle and liver cells mediates circadian expression of downstream enzymes implicated in amino acid mobilization from muscle and their reuse in the liver for gluconeogenesis and the production of ammonia for the urea cycle (*49*). Accordingly, plasma levels of total amino acids, branched chain amino acids, and urea show circadian rhythms in humans, with peak levels at night (*49*). In the urea cycle, use of mitochondrial L-ornithine (derived from glutatmate) by ornithine carbamoyl transferase (OCT) serves as a critical step in the clearance of CO_2 (Fig. 2F). Circadian regulation of *Oct* is imposed by KLF15. The importance of amino acid metabolism by *Klf15* is demonstrated by the acute metabolic disruption seen in *Klf15*$^{-/-}$ mice when they are fed a protein-rich diet. These mice exhibit hypoglycemia, hyperammonemia, and impaired ureagenesis, which together lead to severe morbidity (*49*). In addition, circadian rhythms in several metabolites, Ca^{2+} [at least in the SCN (*50*)], and Mg^{2+} can affect the activity of Ca^{2+}-activated protein kinases, as well as Mg^{2+} ATP- or Mg^{2+} uridine triphosphate–(glycogen synthesis) using enzymes (*51*).

"Intermediate products of nutrient metabolism give rise to several small molecules that can affect clock function in the cytoplasm or nucleus."

Intermediate metabolites and the circadian clock

Intermediate products of nutrient metabolism give rise to several small molecules that can affect clock function in the cytoplasm or nucleus. Cytoplasmic ornithine is decarboxylated by ornithine decarboxylase (ODC) as the initial step in polyamine biosynthesis. Several genes involved in polyamine production are transcriptionally regulated by the circadian clock components, giving rise to a daily rhythm in polyamine (Fig. 2F) (*52*, *53*). Circadian expression of the *Odc* gene is directly driven by CLOCK/BMAL (*53*). A derivative of methionine plays an important role in this pathway. mRNAs encoding regulatory proteins in methionine production and its adenylation to SAM (Bhmt, Mtrr, Mat1, and Mat2) show daily rhythms (*31*). SAM is a reactive methyl carrier that is used in methyl-group transfer reactions, including histone methylation, as well as the biosynthesis of polyamine, phosphatidylcholine, and the energy-rich phosphocreatine. SAM also inhibits the activity of methyl tetrahydrofolate reductase (MTHFR) and thereby is tightly linked to tetrahydrofolate or one-carbon metabolism, which is required for purine metabolism and RNA synthesis in non-dividing cells (*54*). Several genes involved in tetrahydrofolate metabolism exhibit a circadian rhythm (*31*, *55*). Both reactive methyl-group metabolism and one-carbon metabolism likely signal to the circadian clock through polyamines. Polyamines modulate many protein-protein and protein-DNA interactions, regulating the circadian clock by promoting the interaction between PER2 and CRY1. Age-related dampening of the circadian clock may lead to reductions in polyamine, because supplementing mouse food with polyamine improves circadian rhythms in older mice (*53*).

NAD^+

NAD^+ (oxidized form of NAD) is emerging as a key regulator of metabolism because it (i) functions as an electron carrier, (ii) modulates protein function, and (iii) serves as a substrate for ADP ribosylation. In animal tissues, NAD^+ is either synthesized de novo, or the nicotinic moiety is salvaged from nicotinamide for the synthesis of NAD^+ in a reaction catalyzed by nicotinamide phosphoribosyltransferase (NAMPT). Owing to the short half-life of NAD^+, this salvage pathway is essential for sustained availability of NAD^+. The circadian clock drives daily rhythms in NAMPT, as well as the resulting rhythm in cellular NAD^+ levels (*56*, *57*). Direct binding of NAD^+ to SIRT proteins inhibits their ability to deacetylate target proteins, including clock components (*58*, *59*) and several metabolic enzymes. NAD^+ is also used by PARP1 to add poly(ADP) ribose moieties to CLOCK, which increases CLOCK/BMAL1 affinity to DNA and delays repression by CRY/PER complex (Fig. 2G). This makes the hepatic clock less susceptible to abrupt changes in eating time (*60*).

Acetyl CoA

Acetyl CoA is a major energy metabolite that is generated by glycolysis, β-oxidation, and amino acid metabolism in the mitochondria, which is then transported out of the mitochondria by ACLY. In addition, acetyl CoA is also produced in the cytoplasm or nucleus by de novo synthesis from acetate and CoA by acetyl CoA synthase (AceCS1). The circadian oscillator exerts a dominant effect on the cytoplasm in several ways. First, key rate-limiting steps of the metabolic pathways that generate acetyl CoA are under circadian control. Second, the expression of ACLY is rhythmic. Third, the activity of AceCS1 is regulated by the NAD-dependent deacetylase SIRT1 (*61*, *62*), and as seen above, NAD levels are under strong circadian control (Fig. 2G). Cytoplasmic acetyl CoA can diffuse into the nucleus through nuclear pores, where it can modulate the activity of lysine acetyl transferases with relatively high K_D (low affinity) for acetyl CoA (*63*). Similarly, the concentration of acetyl CoA or the relative ratio of CoA/acetyl CoA can change the specificity of some proteins, such as p300 and CBP

(*63*), both of which are associated with CLOCK/BMAL1 and activate histone acetylation (*55*).

Acetyl CoA is a crucial precursor for the synthesis of several molecule classes, including fatty acids, cholesterol, bile acids, steroid hormones, and ketone bodies (*63*). Many enzymes in these pathways are regulated in a circadian fashion, both at the mRNA and protein levels. In mitochondria, acetyl CoA molecules from pyruvate and fatty acid oxidation are primarily fed into the tricarboxylic acid (TCA) cycle. Two intermediates of the TCA cycle, α-KG and succinyl CoA, can have broader effects on transcription. Alpha-KG is the cofactor for several histone demethylases, and the ratio of succinyl CoA to α-KG has recently been shown to affect histone methylation state (Fig. 2H) (*64*).

Succinyl CoA-Aminolevulinate metabolic network

Succinyl CoA is the starting material for the synthesis of aminolevulinic acid, a reaction catalyzed by ALAS1, whose expression is circadian (*65*). Aminolevulinate is subsequently used for the synthesis of tetrapyrroles, including heme and cytochromes. Heme, among its many functions, is a ligand for REV-ERB. In addition, the degradation of heme is catalyzed by heme oxygenase (HO), which also shows circadian expression (*66*, *67*). Such rhythms in these production and degradation pathways likely produce rhythms in Heme, as well as CO (a product of heme degradation). CO can presumably diffuse into the nucleus, where it can affect the DNA binding function of NPAS2 (Fig. 2H) (*68*). Cytochromes are also tetrapyrroles and function as cofactors for components of the mitochondrial electron transport chain and for cytochrome p450 (Cyp), which is a class of proteins that mediates xenobiotic metabolism. Interestingly, the PAR bZIP transcription factors DBP, TEF, and HLF are clock-controlled, rhythmic genes that drive the expression of a large number of Cyp genes and thereby generate rhythms in xenobiotic metabolism. (*69*).

Interorgan communications

Both fasting and circadian clock regulate the biosynthesis of cholesterol from acetyl CoA (Fig. 2I). Metabolism of cholesterol to produce several ligands for nuclear hormone receptors also shows daily rhythms. The Cyp7 proteins (Cyp7a and Cyp7b) mediate the first step in the metabolism of cholesterol to bile acids. Hepatic expression of Cyp7 is strongly circadian, and peak levels of Cyp7 expression correlate with a reduction in cholesterol and an increase in bile acids (Fig. 2I) (*70*, *71*). Excess bile acids produced in liver can enter the circulation and subsequently activate UCP gene expression within brown adipose tissue (BAT), thereby contributing to thermoregulation (*72*). In BAT, REV-ERB α also imposes a circadian rhythm in UCP expression and contributes to daily rhythm in thermogenesis (Fig. 2J) (*73*). Accordingly, BAT-specific *Rev-erb* $\alpha^{-/-}$ loses the rhythmic repression of UCP proteins and rhythmic fluctuation in body temperature (*73*). Both increases and decreases in temperature are thought to affect the clock throughout the body (*74*). Increases in body temperature can activate HSF1, which in turn activates Per2 gene expression from a cis-acting HSE site within its promoter (*75*). During temperature declines, expression of a cold-inducible RNA binding protein (CIRBP) can bind to CLOCK pre-mRNA and affect its processing (*76*).

In the pineal gland, acetyl CoA is used to produce melatonin by the enzymatic action of AANAT (*77*). Circadian expression of AANAT contributes to the circadian rhythm in melatonin, with peak levels during the night. Illumination in the cyan-blue spectrum can effectively suppress AANAT gene expression and melatonin production (Fig. 2A) (*78*).

Central integration of peripheral metabolic status

The mechanisms described above illustrate the extensive, reciprocal regulation between the circadian clock and cellular metabolism. Notably, these connections extend to the systemic level. For example, metabolic signals from the periphery also affect brain-specific circadian clocks. Although peripheral signals provide feedback to the SCN, these signals are often insufficient to override the robust influence of light. Forcing nocturnal rodents to eat during the day changes the peak phase of expression for nearly all rhythmically expressed genes in the liver without affecting phases of gene expression in the SCN, which remains tied to the LD cycle (*31*, *79*, *80*). However, the phase of circadian gene expression in the pituitary, dorsomedial hypothalamus (DMH), and PVN are affected by daytime feeding (*81*). Daytime access to a limited amount of food also elicits a survival strategy in nocturnal rodents by suppressing the natural circadian drive for daytime sleep and increasing food-seeking activity before the arrival of the daytime meal (*82*). This food anticipatory activity (FAA) seems to be mediated by ketone bodies produced by the liver that act on the dorsal striatum in a Per2-dependent manner (*83*). Such FAA is independent of the circadian clock in the SCN, as normal FAA can be triggered in mice lacking the SCN.

The effect of eating patterns on central nervous system clocks (e.g., the emergence of FAA, which seems to override SCN control of the activity-rest cycle) raises a larger question about the origin

	Circadian rhythm disruption or DIO	Time-restricted feeding	Potential mechanism
	Obesity	↓Fat, ↑lean mass	↓Plasma- and ↓liver-triglycerides
	Glucose intolerance/ insulin resistance	Improved glucose homeostasis	↓Gluconeogenesis ↑PPP and ↑TCA cycle
	Gut dysbiosis	Diverse and dynamic	Altered digestion, absorption, and excretion of nutrients and bile acids
	Cardiovascular diseases	Arrhythmia and improved ↓cardiac function*	ATP-dependent chaperone and improved mitochondria function
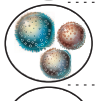	Chronic inflammation	↓Tissue inflammation	↓Macrophage infiltration of WAT ↓IL6 TNFα
	Liver diseases	↓Fibrosis and ↓hepatic fat deposit	Fatty acid synthesis, ↑β oxidation mitochondrian volume
	Increased cancer risk	↓Risk for breast cancer# and ↑breast cancer prognosis	Improved metabolic homeostasis, reduced inflammation
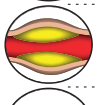	Hypercholesterolemia	↓Cholesterol	Cholesterol metabolism to bile acids
	Sleep disorders	↑Sleep quality# and ↑quantity*	Consolidation of activity and rest
	Compromised muscle function	↑Endurance and ↑flight index*	Ketone bodies, creatine metabolism

Fig. 3. Chronic circadian rhythm disruption by erratic lifestyle or high-fat-diet–induced obesity compromises physiology, whereas time-restricted feeding can restore daily rhythms and improve health. The potential mechanisms are largely based on rodent studies. Few observations have been made in insects (*) and in humans (#). IL, interleukin; TNF, tumor necrosis factor.

of nocturnal or diurnal (N-D) behavior in different species. The phase of the SCN circadian clock in both nocturnal and diurnal species is similar (*84*), implying that the N-D switch may not involve the SCN. The effect of food access time on extra-SCN brain clocks raises the provocative hypothesis that the N-D switch may be driven by complex interactions between the light-dark cycle, the feeding-fasting cycle, and overall energy balance. In mice, reducing the ambient temperature and restricting nutrition quantity can trigger daytime activity, suggesting that diurnality is a strategy for conserving energy (*85*). Understanding the mechanisms by which food, light, and ambient temperature affect the daily sleep-wake cycle and metabolism has increasing importance for humans who are living under diverse work schedules, lifestyles, and food preferences.

Health implication of metabolic and circadian integration of physiology in model organisms

Reciprocal interactions between metabolism and the circadian clock imply that nutrition quality, quantity, and daily eating pattern can affect diurnal rhythms, which in turn determines whole-body physiology. When mice are fed a standard diet ad libitum, they typically consume a majority of their daily food intake during the night. The vast majority of circadian -omics studies have been performed using mice fed a standard diet ad libitum. However, relative to these ad libitum–fed animals, the number and amplitude of rhythmic transcripts is substantially reduced in animals deprived of food or in circadian mutant mice, whereas it is increased in mice fed the same calories within an 8- to 12-hour interval [time-restricted feeding (TRF)]. TRF alone cannot sustain rhythmic expression of a vast majority of hepatic rhythmic transcripts, proteins, or metabolites in mice lacking a functional circadian clock (*31*, *41*, *42*, *48*). When mice are fed a high-fat diet ad libitum, which is a widely used for diet-induced obesity (DIO), mice spread their caloric intake evenly throughout the 24-hour day (*86*). This eating pattern reprograms the hepatic diurnal transcriptome by dampening the oscillation of numerous circadian clock targets (compared to the diurnal transcriptome of mice fed a standard diet) (*87*). However, as seen in mice fed a standard diet, TRF of a high-fat diet improves molecular oscillations (*70*, *71*, *88*).

Subjecting genetically identical animals to caloric restriction or a high-fat diet (beneficial and adverse effects, respectively) has served as a powerful experimental system for understanding the roles of nutrition quantity and quality on health. Similarly, feeding isogenic animals identical, isocaloric diets ad libitum or via TRF has offered a foundation for understanding how the daily eating pattern affects diurnal rhythms and health (*89*). TRF can attenuate the adverse metabolic consequences (i.e., diet-induced pathologies) of high-fat, high-sucrose, or high-fructose diets in rodents and insects (Fig. 3) (*70*, *71*, *88*, *90*). Comparing mice fed a normal or high-fat diet—either ad libitum or via TRF—is yielding new insights into how circadian regulation of metabolism is an integral part of physiology. DIO disrupts the temporal regulation of metabolism by tonic activation, by tonic suppression, or by mistiming the activation of several liver metabolic pathways (e.g., gluconeogenesis, fatty acid synthesis, cholesterol synthesis, bile acid production, and the pentose phosphate pathways). TRF reverses the adverse effects of a high-fat diet in the liver and other metabolic organs. Although the benefit of TRF on body weight is comparable for 8-, 9-, or 12-hour feeding intervals, several metabolic and physiological health indicators are differentially affected by these regimens, suggesting that the duration of fasting is also important (*91*). Similarly, TRF does not reduce body weight in mice fed a standard diet but increases lean mass at the expense of fat mass. TRF benefits are also seen in insects, where it has been shown to (i) support body-weight homeostasis, (ii) reduce age-dependent or high-fat diet-dependent deterioration of cardiac function, (iii) maintain sleep patterns, and (iv) promote flight-muscle function (*90*). Because subjecting model organisms to caloric restriction or DIO has revealed molecular mechanisms of metabolic health, the TRF model will likely yield new insights into how metabolism is temporally regulated. Preliminary studies in flies have shown that TRF and caloric restriction elicit different gene expression signatures and that TRF benefits on cardiac function depend on a functional circadian clock (*90*). However, it is still possible that fasting-induced molecular changes could contribute to TRF benefits. Similarly, it is not known whether TRF has beneficial effects in the absence of a functional clock in rodents. It is also worth mentioning that for many caloric-restriction experiments (both in rodents and in higher animals), the restricted group is often given food at a fixed time of the day and the animals consume the daily ration within a few hours, similar to TRF. In contrast, the control animals are given ad libitum access to food. Because of this experimental design, some of the health benefits seen with caloric restriction may have resulted from TRF. Altogether, these experiments stress the importance of eating patterns in metabolic regulation and have begun to inspire researchers to examine the contribution of daily eating patterns on metabolic outcomes in experimental animals and humans. For example, efforts to improve metabolic homeostasis in mice (or hepatocytes) have revealed two promising strategies: (i) behavioral intervention to improve circadian rhythm and (ii) pharmacological agents that target CRY, REV-ERB, or CLOCK (*92*–*94*). Targeting the interface between circadian rhythms and metabolism may therefore prove effective in alleviating the effect of metabolic disorders.

"Understanding the mechanisms by which food, light, and ambient temperature affect the daily sleep-wake cycle and metabolism has increasing importance for humans who are living under diverse work schedules, lifestyles, and food preferences."

Perspective and conclusion

Although TRF results in health benefits irrespective of nutrition quality and quantity, numerous questions remain. How is "energy balance" explained in TRF? How do different macronutrients, micronutrients, supplements, and medications affect the clock? If timing of food intake can determine metabolic outcomes, can timing of medication be optimized for efficacy? Does TRF during the day versus night have different effects? How can we translate these findings to clinical practice or standard of care?

Close examination of TRF reveals that diurnal rhythms may affect components of energy balance (energy intake = absorption + storage + expenditure). In addition to circadian rhythms in the gut epithelium that affect nutrient absorption (*95*, *96*), the composition of the gut microbiome, with respect to nutrient metabolism, also shows diurnal rhythms (*97*). Compared with ad libitum feeding, TRF does not affect the composition of the predominant cecal microbiome, but TRF mice excrete more simple sugars, which are microbially derived from complex carbohydrates in food (*98*). This implies that complex sugars are digested in the lower intestine (where absorption is relatively low) or that TRF somehow reduces overall sugar absorption. TRF also changes energy storage by increasing metabolically active lean mass and preventing the accumulation of fat mass. Even fat mass in TRF mice has a higher mitochondrial content (*70*, *71*). TRF increases the peak level of Cyp7a/b expression, an effect that correlates with reduced cholesterol and increases in bile acids. Bile acids can act through TGR5 and DIO2 to increase BAT thermogenesis (*72*) and contribute to higher energy expenditure and increased O_2 consumption in TRF mice. However, it is unclear why a considerable amount of bile acids are excreted in the feces of TRF mice. Nevertheless, inhibition of bile acid reabsorption in the gut protects against fatty liver disease (*99*).

Beyond the simple effects of nutrition on energy balance, some food components may affect the circadian clock even when consumed in moderation (i.e., at small caloric levels typically ignored for energy balance). For example, caffeine itself can change the phase of the circadian clock (*100*). As the mere presence of the gut microbiome is necessary for a robust liver

circadian rhythm (*101*), noncaloric artificial sweeteners (*102*), as well as antibiotics known to change the gut microbiome composition, are likely to affect gut or hepatic circadian rhythms. Similarly, the absorption, target function, and clearance of many drugs are likely circadian (*103*). Therefore, systematic analyses of the timing of drug activities (specifically for those with a short half-life or those provided in small doses), as well the resulting prognosis, are warranted.

How might we translate these results into the standard of care? Epidemiological studies have repeatedly shown that sleep deprivation and shift work correlate with higher incidence of metabolic diseases in humans (*104*, *105*). Conversely, overnight fasting (≥13 hours after controlling for sleep and activity) both prevents breast cancer and improves the prognosis of breast cancer patients (*106*, *107*). These observations suggest that daily patterns of activity, sleep, and food intake may dramatically affect human heath and that these patterns should be systematically dissected to determine their roles in health. Preliminary studies using a smartphone app have shown that nearly 50% of nonshift workers distribute their food intake over greater than 15 hours and, therefore, implementing a 10-hour TRF may promote weight loss and improve sleep (*108*). Retrospective analyses of a weight-loss study showed that eating earlier may lead to increased weight loss (*109*), suggesting that the relationship between the eating interval and the day-night cycle may affect metabolism. As stated above, hyperglycemia is sustained for a longer period of time after the evening meal than after the morning meal. This is likely because melatonin inhibits insulin release from pancreatic islets through the melatonin receptor 1B (Fig. 2A). Therefore, the evening rise in melatonin likely causes hyperglycemia (*110*). Because light in the blue spectrum strongly suppresses plasma melatonin level, it raises the interesting possibility that adjusting spectral quality and quantity in the indoor environment may affect metabolism. [However, melatonin action on metabolism extends beyond the pancreas (*111*), and its rise during nighttime feeding in nocturnal rodents adds further complexity to generalization of melatonin effects in both diurnal and nocturnal animals.] The rise of consumer markets for wearable sensors, ubiquity of smartphones, and their increasing use in research offer an unprecedented opportunity to longitudinally measure human feeding behavior, sleep patterns, activity levels, ambient light, body temperature, heart rate, and blood glucose to understand how these factors interact in free-living conditions. These data may reveal how the environment and diet may be manipulated to optimize the circadian physiology of metabolism.

REFERENCES AND NOTES

1. E. Van Cauter, K. S. Polonsky, A. J. Scheen, *Endocr. Rev.* **18**, 716–738 (1997).
2. W. J. Schwartz, H. Gainer, *Science* **197**, 1089–1091 (1977).
3. G. Asher, U. Schibler, *Cell Metab.* **13**, 125–137 (2011).
4. G. Asher, P. Sassone-Corsi, *Cell* **161**, 84–92 (2015).
5. B. Karlsson, A. Knutsson, B. Lindahl, *Occup. Environ. Med.* **58**, 747–752 (2001).
6. R. D. Rudic *et al*., *PLOS Biol.* **2**, e377 (2004).
7. J. A. Mohawk, C. B. Green, J. S. Takahashi, *Annu. Rev. Neurosci.* **35**, 445–462 (2012).
8. J. P. Etchegaray, C. Lee, P. A. Wade, S. M. Reppert, *Nature* **421**, 177–182 (2003).
9. H. A. Duong, M. S. Robles, D. Knutti, C. J. Weitz, *Science* **332**, 1436–1439 (2011).
10. S. Masri, P. Sassone-Corsi, *Nat. Rev. Neurosci.* **14**, 69–75 (2013).
11. L. Yin, M. A. Lazar, *Mol. Endocrinol.* **19**, 1452–1459 (2005).
12. L. DiTacchio *et al*., *Science* **333**, 1881–1885 (2011).
13. K. Shimomura *et al*., *eLife* **2**, e00426 (2013).
14. L. Aguilar-Arnal, P. Sassone-Corsi, *Curr. Opin. Cell Biol.* **25**, 170–176 (2013).
15. K. A. Lamia *et al*., *Nature* **480**, 552–556 (2011).
16. T. Okabe *et al*., *J. Cell Sci.* jcs.190959 (2016).
17. E. E. Zhang *et al*., *Nat. Med.* **16**, 1152–1156 (2010).
18. Y. Zhang *et al*., *Genes Dev.* **30**, 1636–1644 (2016).
19. S. Masri *et al*., *Cell* **158**, 659–672 (2014).
20. T. K. Sato *et al*., *Neuron* **43**, 527–537 (2004).
21. S. Panda *et al*., *Science* **301**, 525–527 (2003).
22. A. Ishida *et al*., *Cell Metab.* **2**, 297–307 (2005).
23. D. K. Welsh, J. S. Takahashi, S. A. Kay, *Annu. Rev. Physiol.* **72**, 551–577 (2010).
24. C. A. Dudley *et al*., *Science* **301**, 379–383 (2003).
25. M. H. Vitaterna *et al*., *Proc. Natl. Acad. Sci. U.S.A.* **103**, 9327–9332 (2006).
26. K. L. Toh *et al*., *Science* **291**, 1040–1043 (2001).
27. Z. Liu *et al*., *Cell Reports* **7**, 1509–1520 (2014).
28. D. B. Rhoads, D. H. Rosenbaum, H. Unsal, K. J. Isselbacher, L. L. Levitsky, *J. Biol. Chem.* **273**, 9510–9516 (1998).
29. M. Perelis *et al*., *Science* **350**, aac4250 (2015).
30. G. Z. Wang *et al*., *Cell Reports* **13**, 1868–1880 (2015).
31. C. Vollmers *et al*., *Proc. Natl. Acad. Sci. U.S.A.* **106**, 21453–21458 (2009).
32. L. Yin, J. Wang, P. S. Klein, M. A. Lazar, *Science* **311**, 1002–1005 (2006).
33. K. Kaasik *et al*., *Cell Metab.* **17**, 291–302 (2013).
34. M. S. Robles, J. Cox, M. Mann, *PLOS Genet.* **10**, e1004047 (2014).
35. M. D. Li *et al*., *Cell Metab.* **17**, 303–310 (2013).
36. G. Rey *et al*., *Cell Metab.* **24**, 462–473 (2016).
37. B. Mayr, M. Montminy, *Nat. Rev. Mol. Cell Biol.* **2**, 599–609 (2001).
38. Z. Travnickova-Bendova, N. Cermakian, S. M. Reppert, P. Sassone-Corsi, *Proc. Natl. Acad. Sci. U.S.A.* **99**, 7728–7733 (2002).
39. R. Narasimamurthy *et al*., *Proc. Natl. Acad. Sci. U.S.A.* **109**, 12662–12667 (2012).
40. K. A. Lamia *et al*., *Science* **326**, 437–440 (2009).
41. A. Neufeld-Cohen *et al*., *Proc. Natl. Acad. Sci. U.S.A.* **113**, E1673–E1682 (2016).
42. Y. Adamovich *et al*., *Cell Metab.* **19**, 319–330 (2014).
43. D. Feng *et al*., *Science* **331**, 1315–1319 (2011).
44. H. Cho *et al*., *Nature* **485**, 123–127 (2012).
45. F. Dang *et al*., *Nat. Commun.* **7**, 12696 (2016).
46. J. O. Lipton *et al*., *Cell* **161**, 1138–1151 (2015).
47. C. Jouffe *et al*., *PLOS Biol.* **11**, e1001455 (2013).
48. F. Atger *et al*., *Proc. Natl. Acad. Sci. U.S.A.* **112**, E6579–E6588 (2015).
49. D. Jeyaraj *et al*., *Cell Metab.* **15**, 311–323 (2012).
50. M. Ikeda *et al*., *Neuron* **38**, 253–263 (2003).
51. K. A. Feeney *et al*., *Nature* **532**, 375–379 (2016).
52. S. Panda *et al*., *Cell* **109**, 307–320 (2002).
53. Z. Zwighaft *et al*., *Cell Metab.* **22**, 874–885 (2015).
54. G. S. Ducker, J. D. Rabinowitz, *Cell Metab.*, 10.1016/j.cmet.2016.08.009 (2016).
55. N. Koike *et al*., *Science* **338**, 349–354 (2012).
56. Y. Nakahata, S. Sahar, G. Astarita, M. Kaluzova, P. Sassone-Corsi, *Science* **324**, 654–657 (2009).
57. K. M. Ramsey *et al*., *Science* **324**, 651–654 (2009).
58. G. Asher *et al*., *Cell* **134**, 317–328 (2008).
59. Y. Nakahata *et al*., *Cell* **134**, 329–340 (2008).
60. G. Asher *et al*., *Cell* **142**, 943–953 (2010).
61. B. Schwer, J. Bunkenborg, R. O. Verdin, J. S. Andersen, E. Verdin, *Proc. Natl. Acad. Sci. U.S.A.* **103**, 10224–10229 (2006).
62. W. C. Hallows, S. Lee, J. M. Denu, *Proc. Natl. Acad. Sci. U.S.A.* **103**, 10230–10235 (2006).
63. F. Pietrocola, L. Galluzzi, J. M. Bravo-San Pedro, F. Madeo, G. Kroemer, *Cell Metab.* **21**, 805–821 (2015).
64. T. TeSlaa *et al*., *Cell Metab.* **24**, 485–493 (2016).
65. K. Kaasik, C. C. Lee, *Nature* **430**, 467–471 (2004).
66. M. F. Rubio, P. V. Agostino, G. A. Ferreyra, D. A. Golombek, *Neurosci. Lett.* **353**, 9–12 (2003).
67. Y. Q. Xu *et al*., *PLOS ONE* **7**, e44237 (2012).
68. E. M. Dioum *et al*., *Science* **298**, 2385–2387 (2002).
69. F. Gachon, F. F. Olela, O. Schaad, P. Descombes, U. Schibler, *Cell Metab.* **4**, 25–36 (2006).
70. M. Hatori *et al*., *Cell Metab.* **15**, 848–860 (2012).
71. A. Chaix, A. Zarrinpar, P. Miu, S. Panda, *Cell Metab.* **20**, 991–1005 (2014).
72. M. Watanabe *et al*., *Nature* **439**, 484–489 (2006).
73. Z. Gerhart-Hines *et al*., *Nature* **503**, 410–413 (2013).
74. E. D. Buhr, S. H. Yoo, J. S. Takahashi, *Science* **330**, 379–385 (2010).
75. H. Reinke *et al*., *Genes Dev.* **22**, 331–345 (2008).
76. J. Morf *et al*., *Science* **338**, 379–383 (2012).
77. D. C. Klein, J. L. Weller, *Science* **169**, 1093–1095 (1970).
78. M. Hatori, S. Panda, *Trends Mol. Med.* **16**, 435–446 (2010).
79. S. Yamazaki *et al*., *Science* **288**, 682–685 (2000).
80. F. Damiola *et al*., *Genes Dev.* **14**, 2950–2961 (2000).
81. A. Mukherji *et al*., *Proc. Natl. Acad. Sci. U.S.A.* **112**, E6691–E6698 (2015).
82. Z. Boulos, A. M. Rosenwasser, M. Terman, *Behav. Brain Res.* **1**, 39–65 (1980).
83. R. Chavan *et al*., *Nat. Commun.* **7**, 10580 (2016).
84. A. A. Nunez, A. Bult, T. L. McElhinny, L. Smale, *J. Biol. Rhythms* **14**, 300–306 (1999).
85. V. van der Vinne, J. A. Gorter, S. J. Riede, R. A. Hut, *J. Exp. Biol.* **218**, 2585–2593 (2015).
86. A. Kohsaka *et al*., *Cell Metab.* **6**, 414–421 (2007).
87. K. L. Eckel-Mahan *et al*., *Cell* **155**, 1464–1478 (2013).
88. H. Sherman *et al*., *FASEB J.* **26**, 3493–3502 (2012).
89. M. P. Mattson *et al*., *Proc. Natl. Acad. Sci. U.S.A.* **111**, 16647–16653 (2014).
90. S. Gill, H. D. Le, G. C. Melkani, S. Panda, *Science* **347**, 1265–1269 (2015).
91. V. D. Longo, S. Panda, *Cell Metab.* **23**, 1048–1059 (2016).
92. T. Hirota *et al*., *Science* **337**, 1094–1097 (2012).
93. L. A. Solt *et al*., *Nature* **485**, 62–68 (2012).
94. B. He *et al*., *Cell Metab.* **23**, 610–621 (2016).
95. M. M. Hussain, X. Pan, *Curr. Opin. Clin. Nutr. Metab. Care* **15**, 336–341 (2012).
96. J. J. Stubblefield, J. Terrien, C. B. Green, *Trends Endocrinol. Metab.* **23**, 326–333 (2012).
97. C. A. Thaiss *et al*., *Cell* **159**, 514–529 (2014).
98. A. Zarrinpar, A. Chaix, S. Yooseph, S. Panda, *Cell Metab.* **20**, 1006–1017 (2014).
99. A. Rao *et al*., *Sci. Transl. Med.* **8**, 357ra122 (2016).
100. T. M. Burke *et al*., *Sci. Transl. Med.* **7**, 305ra146 (2015).
101. V. Leone *et al*., *Cell Host Microbe* **17**, 681–689 (2015).
102. J. Suez *et al*., *Nature* **514**, 181–186 (2014).
103. R. Dallmann, A. Okyar, F. Lévi, *Trends Mol. Med.* **22**, 430–445 (2016).
104. K. Spiegel, R. Leproult, E. Van Cauter, *Lancet* **354**, 1435–1439 (1999).
105. D. M. Arble *et al*., *Sleep* **38**, 1849–1860 (2015).
106. C. R. Marinac *et al*., *JAMA Oncol.* **2**, 1049–1055 (2016).
107. C. R. Marinac *et al*., *Cancer Epidemiol. Biomarkers Prev.* **24**, 783–789 (2015).
108. S. Gill, S. Panda, *Cell Metab.* **22**, 789–798 (2015).
109. M. Garaulet *et al*., *Int. J. Obes.* **37**, 604–611 (2013).
110. T. Tuomi *et al*., *Cell Metab.* **23**, 1067–1077 (2016).
111. S. J. Persaud, P. M. Jones, *N. Engl. J. Med.* **375**, 1090–1092 (2016).

ACKNOWLEDGMENTS

The author thanks A. Chaix, E. Manoogian, L. DiTacchio, and G. Benegiamo for their scientific input, and D. O'Keefe for copyediting the manuscript. Research in the author's laboratory is partially supported by NIH grants EY016807, CA014195, EY019005, American Federation of Aging Research grant M14322, Leona M. and Harry B. Helmsley Charitable Trust's grant 2012-PG-MED002, and Glenn Center for Aging Research.

10.1126/science.aah4967

RESEARCH

An interactive 3D atlas of early human development

de Bakker et al., *p. 1019*

IN *SCIENCE* JOURNALS

Edited by **Stella Hurtley**

A flexible electronic microfluidic biosensor

BIOSENSORS

Better health? Prepare to sweat

Tracking heart rate, calories, and steps with wearable technology is a popular way to monitor general health and fitness. Koh *et al*. take wearable technology one step further by developing a flexible microfluidic device that collects and analyzes sweat. Colorimetric readouts and integrated smartphone image capture detected pH, lactate, glucose, and chloride ion concentrations in sweat while the device was stuck to the skin during a controlled cycling test. Results were comparable to conventional analyses, and the devices remained functional during an outdoor endurance bicycle race. Such microfluidic devices could be used during athletic or military training and could be adapted to test tears, saliva, or other bodily fluids. —CC

Sci. Transl. Med. **8**, 366ra165 (2016).

GEOPHYSICS

Mega-earthquakes go the flat way

Megathrust faults in subduction zones cause large and damaging earthquakes. Bletery *et al*. argue that certain geometric features of the subduction zones relate to earthquake size. The key parameter is the curvature of the megathrust. Larger earthquakes occur where the subducting slab is flatter, providing a rough metric for estimating where mega-earthquakes may occur in the future. —BG

Science, this issue p. 1027

CATALYSIS

Tuning nanoparticle strain

The catalytic activity of metals in heterogeneous catalysts can be altered by applying strain, which changes the crystalline lattice spacing and modifies the metal's electronic properties. Wang *et al*. show how particles of cobalt oxide, a positive electrode for lithium batteries, can expand or contract with charging and transfer strain to adsorbed platinum nanoparticles. For the oxygen reduction reaction used in fuel cells, compressive strain boosted activity by 90%, and tensile strain decreased it by 40%. —PDS

Science, this issue p. 1031

BIOCATALYSIS

Bringing carbon-silicon bonds to life

Organic compounds containing silicon are important for a number of applications, from polymers to semiconductors. The catalysts used for creating carbon-silicon bonds, however, often require expensive trace metals or have limited lifetimes. Borrowing from the ability of some metalloenzymes to catalyze other rare carbene insertion reactions, Kan *et al*. used heme proteins to form carbon-silicon bonds across a range of conditions and substrates (see the Perspective by Klare and Oestreich). Directed evolution experiments using cytochrome c from *Rhodothermus marinus* improved the reaction to be 15 times more efficient than industrial catalysts. —NW

Science, this issue p. 1048; see also p. 970

MEMORY RESEARCH

Protecting memories from stress

It is widely accepted that stress has a negative impact on memory retrieval. But specific approaches to learning can counteract this effect. Smith *et al*. found that when memory was tested immediately after the onset of stress, stress effects were reduced. Furthermore, when subjects learned novel material by using a highly effective learning technique involving practice tests, their memory was also protected against the negative effects of stress. —PRS

Science, this issue p. 1046

PHARMACOLOGY

Targeting the ligand in hypophosphatemia

Patients with chronic kidney disease can have too much circulating FGF-23 (fibroblast growth factor 23). This results in too little circulating phosphate (hypophosphatemia) and the bone-softening disorder rickets. Because available FGF-23 receptor–targeting molecules are not

CREDITS (FROM TOP): DE BAKKER *ET AL.*; KOH *ET AL.*

clinically useful, Xiao *et al*. sought to identify ligand-binding compounds. Their lead compound reduced FGF-23 serum levels and partially reversed hypophosphatemia in a mouse model. Thus, targeting the ligand, rather than the receptor, may be a therapeutic option for hypophosphatemia. —LKF

Sci. Signal. **9**, ra113 (2016).

BEHAVIORAL IMMUNOLOGY

Status alters immune function in macaques

Rhesus macaques experience variable levels of stress on the basis of their position in the social hierarchy. To examine how stress affects immune function, Snyder-Mackler *et al*. manipulated the social status of individual macaques (see the Perspective by Sapolsky). Social status influenced the immune system at multiple levels, from immune cell numbers to gene expression, and altered signaling pathways in a model of response to infection. Macaques possess a plastic and adaptive immune response wherein social subordination promotes antibacterial responses, whereas high social status promotes antiviral responses. —LMZ

Science, this issue p. 1041; see also p. 967

COLD ATOMS

Making perfect atomic arrays

Arrays of atoms can be a useful resource for quantum information. However, loading atoms into arrays is typically a stochastic process, which leads to imperfections. Two groups have now performed defect-free assembly of atoms into arrays (see the Perspective by Regal). The researchers first loaded the atoms stochastically and imaged the system. They then shuttled the atoms around to form perfect arrays. Barredo *et al.* worked with two-dimensional arrays, creating a variety of spatial configurations. Endres *et al.* manipulated atoms along a line. By further cooling down the atoms and generating interactions among them, the techniques may also find use in quantum simulation. —JS

Science, this issue p. 972, p. 1021; see also p. 1024

AUTOPHAGY

Open sesame!

The autophagosome is a double-membraned intracellular structure involved in the disposal of damaged or defunct organelles. Autophagosome formation requires a number of autophagy-related (ATG) proteins. Among them, the key conjugation systems ATG8 and ATG12 are widely exploited in the detection of autophagy in many organisms. However, their precise function in autophagy remains unknown. Tsuboyama *et al.* identified an unexpected role of ATG3, an important enzyme in the ATG conjugation systems, in efficient degradation and opening of the inner autophagosomal membrane after fusion with lysosomes (see the Perspective by Levine). Their live-imaging system revealed the entire life of an autophagosome in mammalian cells. —SMH

Science, this issue p. 1036; see also p. 968

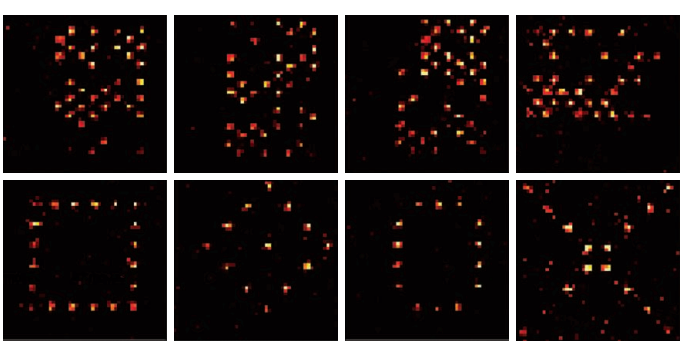

From random to ordered arrays

PHOTOS (FROM LEFT): BARREDO *ET AL.*; SANTIAGO URQUIJO/GETTY IMAGES

IN OTHER JOURNALS

Edited by **Sacha Vignieri** *and* **Jesse Smith**

Classic studies of pouting are helping psychologists explore replication.

PSYCHOLOGY

Continuing the dialog via experiment

Recent discussions about reproducibility within the psychology community have been heated and, at times, acrimonious. The registered replication report by Wagenmakers *et al*. and the comment by Strack map out one way forward, in terms of experimental design, analysis, interpretation, and rebuttal. The original study, a classic from 1988, reported the effect of facial expressions (a smile or a pout) on a subsequent affective judgment. The replication involved 17 laboratories following a vetted experimental design and blinded analysis plan. The overall result is nonreplication, although Strack offers reasons why the original effect was not observed. —GJC

Persp. Psychol. Sci. **11**, 10/1177/1745691616674458, 10.1177/1745691616674460 (2016).

CANCER IMMUNOTHERAPY

Cardiac side effect

Antibodies that block CTLA-4 (cytotoxic T lymphocyte–associated antigen 4) and PD-1 (programmed death 1) allow T cells to launch antitumor immune responses. Although these checkpoint inhibitors improve survival in melanoma patients, inflammation of other tissues is a common side effect. Johnson *et al.* report that two melanoma patients treated with a combination of the checkpoint inhibitors developed fatal cardiac damage. Biopsies revealed that T cells and macrophages that infiltrated the heart were the same as those found in skeletal muscle and the tumor. Neither patient had cardiac risk factors other than hypertension. Review of a safety database suggests that severe

ALSO IN *SCIENCE* JOURNALS

Edited by **Stella Hurtley**

HUMAN DEVELOPMENT

Digital reconstruction of human development

The detailed morphology of human development has intrigued scientists and the medical field alike. However, the scarcity of specimens hampers detailed mapping of tissue architecture. Furthermore, inaccuracies in the description of human development have crept into textbooks from observations of animal models that are extrapolated to humans. By mapping normal developmental processes and patterns, such as the growth and relative placement of organs, congenital anomalies can be better understood. de Bakker *et al*. generated interactive three-dimensional digital reconstructions based on the Carnegie collection of histologically sectioned human embryos spanning the first 2 months of gestation. These interactive models will serve as educational and scientific resources for normal and abnormal human development. —BAP

Science, this issue p. 1019

CELL REPROGRAMMING

For cell reprogramming, context matters

Differentiated cells in a culture dish can assume a new identity when manipulated to express four transcription factors. This "reprogramming" process has sparked interest because conceivably it could be harnessed as a therapeutic strategy for tissue regeneration. Mosteiro *et al*. used a mouse model to study the signals that promote cell reprogramming in vivo. They found that the factors that trigger reprogramming in vitro do the same in vivo; however, they also inflict cell damage. The damaged cells enter a state of senescence and begin secreting certain factors that promote reprogramming, including an inflammatory cytokine called interleukin-6. Thus, in the physiological setting, cell senescence may create a tissue context that favors reprogramming of neighboring cells. —PAK

Science, this issue p. 1020

EPIDEMIOLOGY

Increasing viral threats from mosquitoes

Viral diseases such as dengue, Zika, and yellow fever are transmitted by the mosquito *Aedes aegypti*. In a Perspective, Powell highlights recent changes in the global distribution and genetic characteristics of this insect. The two main genetic subtypes of the mosquito have historically differed in their breeding and host preferences and were found in different geographic regions. However, they are now interbreeding in several locations and spreading into new areas. These changes are putting large human populations at risk of diseases against which they will have no immune defenses. —JFU

Science, this issue p. 971

ICE SHEETS

Fast action with little effect

Pine Island Glacier (PIG) is responsible for a major part of Antarctica's ice loss, with an ice stream whose rate of flow to the sea accelerated by around 75% between 1974 and 2010. Like many similar glaciers, its decay is thought to be linked to warming of the ocean with which it makes contact. Christianson *et al.* report subannual observations of PIG for the period 2009 to 2014, which show that glacier retreat and accelerated ice flow likely were initiated decades ago by such ocean-induced melting, and that transient ocean cooling has only a relatively minor effect on ice flow once marine ice sheet instability is under way. The long-term effects of ocean temperature variability on ice flow still are not known, however. —HJS

Geophys. Res. Lett. 10.1002/2016GL070500 (2016).

The ice–ocean interface helps determine how ice sheets decay.

myocarditis from such combination therapy affects less than 1% of patients. The mechanism for this rare toxic effect is not known. —LDC

New Engl. J. Med. **375**, 1749 (2016); *Proc. Natl. Acad. Sci. U.S.A.* 10.1073/pnas.1603325113 (2016).

CANCER THERAPY

A new direction for breast cancer therapy

Triple-negative breast cancer has the worst prognosis of the breast cancer subtypes. Aggressive forms of this cancer show elevated signaling through the transcription factor MYC, but blocking MYC activity remains challenging because of its role in normal cell function. Horiuchi *et al.* screened the protein kinases expressed by triple-negative breast tumors in hopes of finding a way to thwart MYC indirectly. They identified PIM1, a nonessential protein kinase that was highly active in MYC-positive tumors. Genetic depletion of PIM1 promoted cancer cell death, and preclinical drugs targeting PIM1 impaired the growth of MYC-positive patient tumors in mice. These findings pave the way for the development of PIM1 inhibitors in early-phase clinical trials. —PNK

Nat. Med. 10.1038/nm.4213 (2016).

PLANT-ANIMAL INTERACTIONS

Ants farming plants

Mutualistic interactions between ants and plants are relatively common, most often occurring in plants that produce specific structures for ant occupation. A relationship that more closely approximates farming occurs between ants and fungi, in which ants actively create growing conditions for and propagate the fungal partner. Chomicki and Renner now describe a system in Fiji in which ants in the genus *Philidris* conduct such gardening activities in six different species of epiphytic plants, often simultaneously. Specifically, they not only manage growing conditions but also disperse and plant seeds and pollinate flowers. This more intensive management helps to ensure reestablishment of plants that provide fruits and resources to the ants and that might otherwise be harder to come by. —SNV

Nat. Plants 10.1038/nplants.2016.181 (2016).

MAGNETISM

THz-driven magnetism goes nonlinear

Manipulation of magnetism in solids by terahertz (THz) radiation may enable applications in information storage and processing. Experiments so far have explored a regime in which the magneto-optical response is linear, but entering the nonlinear regime is important for applications. Baierl *et al.* achieved this goal in the antiferromagnetic compound NiO. The magnetic field of the THz radiation that they shone on the sample coupled to the spins in the material, causing them to precess. In addition to a dominant and expected frequency of 1THz, a peak appeared at double that frequency, signifying a nonlinear response. The advance may enable progress toward magnetic THz spin-switching. —JS

Phys. Rev. Lett. **117**, 197201 (2016).

CHEMISTRY

A clean combination of CO and amines

It is rare for synthetically useful chemical reactions to proceed as though two parts are simply cut and pasted together. Wang *et al.* present just such a route to formamides, which are widely used as organic solvents and chemical reagents. The reaction, catalyzed by ruthenium supported on ceria, formally inserts carbon monoxide into a N–H bond of primary or secondary amines. Neither extraneous reagents nor by-products are involved. The authors further demonstrate a continuous flow protocol for dimethylformamide preparation that proceeds for 12 days with less than 5% activity loss. —JSY

Green Chem. 10.1039/c6gc02603f (2016).

PHOTO: NATIONAL GEOGRAPHIC CREATIVE/ALAMY STOCK PHOTO

RESEARCH ARTICLE SUMMARY

HUMAN DEVELOPMENT

An interactive three-dimensional digital atlas and quantitative database of human development

Bernadette S. de Bakker,* Kees H. de Jong, Jaco Hagoort, Karel de Bree, Clara T. Besselink, Froukje E. C. de Kanter, Tyas Veldhuis, Babette Bais, Reggie Schildmeijer, Jan M. Ruijter, Roelof-Jan Oostra, Vincent M. Christoffels, Antoon F. M. Moorman*

INTRODUCTION: The basic human body plan, the arrangement of organs in the body, is laid down during embryonic development. Insight into the formation of this plan informs researchers and clinicians about normal development versus the development of congenital malformations, the latter of which have an incidence of 3% in the human population and cause up to one-quarter of all neonatal deaths. Despite modern technologies such as three-dimensional imaging, the intricate morphogenesis of the developing human body is difficult to understand. Textbooks on human development are often based on the works of early embryologists, some published more than 100 years ago. Because of the limited availability of human embryonic specimens, it is difficult or impossible to independently verify the information carried in these textbooks, or even to assess whether this information is derived from studies on human or animal models.

RATIONALE: Current imaging and computer technology make it possible to reconstruct human development with sufficient resolution to visualize organ development. Stained histological sections (mainly from the Carnegie Collection of human embryos) were digitized, tissues and organs were identified, and knowledge-driven modeling was applied to correct imperfections in the three-dimensional reconstructions.

RESULTS: We created a digital atlas with 14 interactive three-dimensional models of human embryology and a database encompassing 34 embryos spanning the first 2 months of human development. Approximately 15,000 histological sections from the Carnegie Collection were analyzed by trained biomedical students under expert supervision, and up to 150 organs and structures were identified and digitally labeled in each section. The labeled structures were then spatially reconstructed in such a way that the relation between the reconstruction and the original images was preserved. We tested the reproducibility of the manual tracing of the different organs and found that the variability in volumes of segmented structures ranged from 0.3% to 2% between students for simple and complex structures, respectively. The 3D models, supplemented by an object tree with structures named in accordance with the international standard of embryonic terminology, the *Terminologia Embryologica*, are presented as interactive 3D-PDFs, which facilitates exploration of the complex relations between the different organs and allows researchers to develop an independent view of their spatial relations. The 3D reconstructions enable the measurement of the growth of the individual organs and structures, the assessment of the changing position of organs relative to vertebral segments during development, and the verification of remaining ambiguities in the descriptions of the development of organs.

ON OUR WEBSITE

Read the full article at http://dx.doi.org/10.1126/science.aag0053

CONCLUSION: The morphology presented in this atlas is directly connected to the original sections of the embryos in the Carnegie Collection—a connection that was in danger of being lost, with present-day textbook morphology becoming increasingly schematic and deviating from the original substrate. A number of detailed analyses of the development of the kidney, pharyngeal arch cartilages, and notochord show that the current descriptions of the development of these organs are based on comparative animal models rather than on factual observations in human specimens. These examples demonstrate the scientific value of the atlas. This atlas will therefore serve as an educational and reference resource for students, clinicians, and scientists interested in human development and development-related congenital diseases. The 3D-PDFs of the reconstructions, as well as original and labeled images, are freely available (http://3datlasofhumanembryology.com). ■

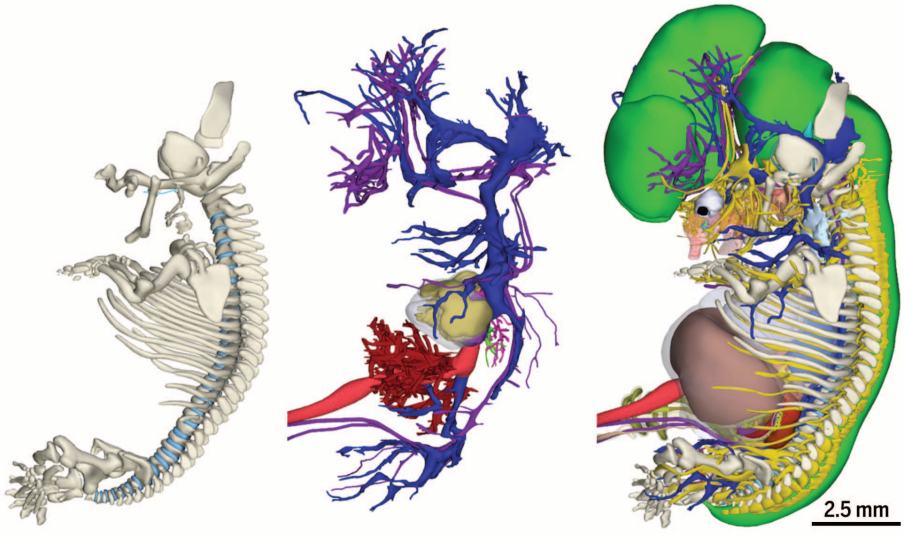

Lateral views of a model of a 7.5-week-old human embryo (16 mm). Left: Skeletal system. Center: Cardiovascular system with transparent heart muscle. Venous system is shown in blue, arterial system in purple, liver vessels in red, and umbilical vein in pink. Right: Reconstructed organs, except skin. Note, for example, the neural tube in green and the nerves in yellow.

The list of author affiliations is available in the full article online.
*Corresponding author. Email: b.s.debakker@amc.uva.nl (B.S.d.B.); a.f.moorman@amc.uva.nl (A.F.M.M.)
Cite this article as B. S. de Bakker *et al.*, *Science* **354**, aag0053 (2016). DOI: 10.1126/science.aag0053

RESEARCH ARTICLE

HUMAN DEVELOPMENT

An interactive three-dimensional digital atlas and quantitative database of human development

Bernadette S. de Bakker,* Kees H. de Jong, Jaco Hagoort, Karel de Bree, Clara T. Besselink, Froukje E. C. de Kanter, Tyas Veldhuis, Babette Bais, Reggie Schildmeijer, Jan M. Ruijter, Roelof-Jan Oostra, Vincent M. Christoffels, Antoon F. M. Moorman*

Current knowledge about human development is based on the description of a limited number of embryonic specimens published in original articles and textbooks, often more than 100 years ago. It is exceedingly difficult to verify this knowledge, given the restricted availability of human embryos. We created a three-dimensional digital atlas and database spanning the first 2 months of human development, based on analysis of nearly 15,000 histological sections of the renowned Carnegie Collection of human embryonic specimens. We identified and labeled up to 150 organs and structures per specimen and made three-dimensional models to quantify growth, establish changes in the position of organs, and clarify current ambiguities. The atlas provides an educational and reference resource for studies on early human development, growth, and congenital malformations.

The basic human body plan is laid down during embryonic development. Insight into the formation of this plan has been shown to provide rational explanations for the relative positions of organs in the adult, as well as for the origin of congenital malformations. Congenital defects have an incidence of 3% in the human population (*1*) and cause up to one-quarter of all neonatal deaths (*2*). Knowledge of normal human development is therefore of great clinical interest, particularly for pediatricians and clinical geneticists. Despite modern approaches such as three-dimensional (3D) reconstruction, it remains difficult to map the intricate morphogenesis of the developing human body. Current textbooks (*3*–*6*) on human development are usually based on the articles and textbooks of various stellar embryologists (*7*–*24*), often published more than 100 years ago. However, it is almost impossible to independently verify the information presented in these textbooks, or even to assess whether this information is derived from studies on human or animal material.

By visualizing development, normal embryogenesis and even malformations can be better understood. In this study, we provide an atlas and database spanning the entire embryonic period of human development, covering early organogenesis based on human embryonic specimens from the Carnegie Collection (table S1). The Carnegie Collection consists principally of serially sectioned normal human embryos in the first 8 weeks of development. It was started by the Carnegie Institution of Washington's Department of Embryology in 1914.

Our interactive atlas allows the user to directly link the annotated organs in the 3D reconstructions with the underlying histological sections of the Carnegie Collection, thereby enabling independent verification and further analyses. The atlas identifies differential growth and the changing relative positions of organs and structures during the first 8 weeks of human development in a quantitative fashion. Initial analyses provide new insights into these relationships.

Data generation and reconstruction pipeline

The degree of detail required for 3D reconstructions of distinct organ systems in early development is currently impossible to obtain with noninvasive techniques such as magnetic resonance imaging (*25*, *26*). Moreover, with a few exceptions, the scarcity of human embryos does not permit tissue identification based on specific immunostaining of the individual organs. Because of these limitations, we chose to analyze histological sections from the Carnegie Collection, with manual identification and labeling of every organ and structure, followed by knowledge-driven modeling to prevent loss of essential detail.

A flowchart of the methods used to generate the 3D reconstructions and morphometric contents of the database is presented in Fig. 1. We imaged and analyzed 17 embryonic stages, with two embryos per stage, spanning the first 2 months of development, which corresponds to Carnegie stages (CS) 7 to 23 (15 to 60 days of development; table S1). We analyzed stages CS7 (15 to 17 days of development), CS8 (17 to 19 days), CS9 (19 to 21 days), CS10 (21 to 23 days), CS11 (23 to 26 days), CS12 (26 to 30 days), CS13 (28 to 32 days), CS14 (31 to 35 days), CS15 (35 to 38 days), CS16 (37 to 42 days), CS17 (42 to 44 days), CS18 (44 to 48 days), CS19 (48 to 51 days), CS20 (51 to 53 days), CS21 (53 to 54 days), CS22 (54 to 58 days), and CS23 (56 to 60 days). Although analysis of two specimens per stage is insufficient to estimate variance in development, the extensive series of embryonic stages allows generalization of continuous patterns of growth. Images were acquired from about 15,000 histologically stained sections, and up to 150 organs and structures per specimen were manually segmented and spatially reconstructed. Structures were identified on the basis of anatomical and histological characteristics and named in accordance with the international standard of embryonic terminology, the *Terminologia Embryologica* (*27*). The morphological reconstructions were prepared with Amira and Blender software (see supplementary materials). The 3D reconstructions were made in such a way that the original sections can be placed within the reconstruction, permitting independent verification of the identification of organs.

The variability of the organ volumes measured by different observers ranged from 0.3% to 2% for simple and complex structures (fig. S1). A smooth and easily recognizable organ, such as the otic vesicle, is considered a simple structure, whereas a small and tangled structure, such as the mesonephros and mesonephric duct, consisting of different types of tissue, is termed a complex structure. This small interobserver variation underscores the reproducibility of the segmentation and reconstruction process.

Because organ morphology gradually and consistently changed both qualitatively and quantitatively in the embryonic series studied, we conclude that no grossly abnormal embryos were included in the study and that the staging of the embryos was accurate.

The applied reconstruction protocol has dual outputs: (i) a series of 14 3D reconstructions that covers the entire embryonic period in an interactive format that can be viewed on different computer types and smartphones (3D-PDF format), and (ii) a set of tables and figures that provides quantitative information about the growth of the distinct structures, as well as demonstrates the changing position of structures relative to the vertebral column. The reconstructions provide spatial information, including observations about the complex and changing relationships between different structures in the developing embryo (supplementary 3D-PDFs). The information in the tables and figures allows interpretation of organ growth relative to the growth of the embryo (data S1) and enables the choice of reference points for analysis of specific organs (data S2).

Department of Anatomy, Embryology and Physiology, Academic Medical Center, Amsterdam, Netherlands.
*Corresponding author. Email: b.s.debakker@amc.uva.nl (B.S.d.B.); a.f.moorman@amc.uva.nl (A.F.M.M.)

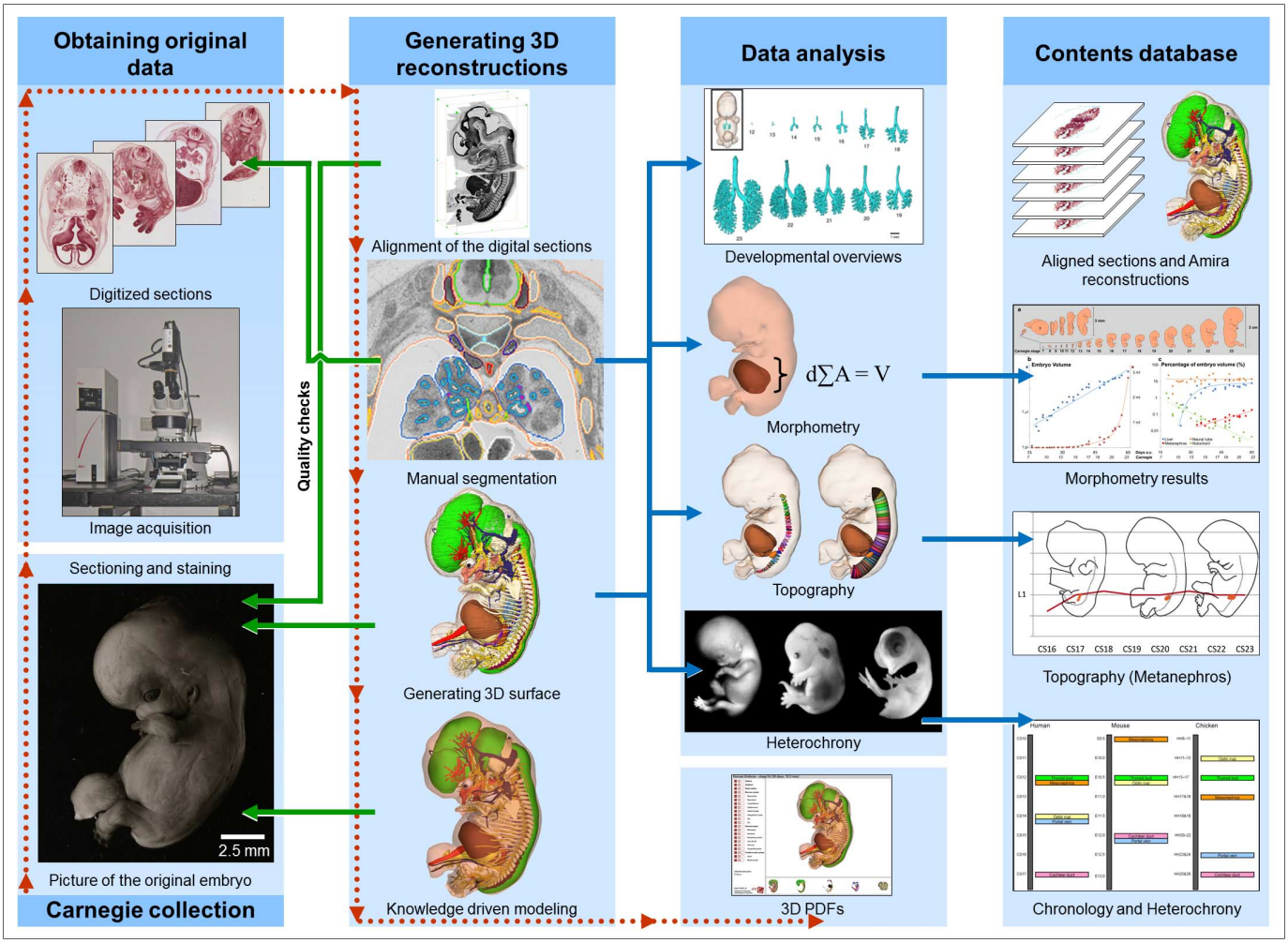

Fig. 1. Flowchart of three-dimensional reconstruction, model generation, and data analysis. Histologically stained sections of the embryos from the Carnegie Collection were imaged, aligned, and segmented. Three-dimensional models were created in the 3D reconstruction package Amira; surfaces were smoothed, without loss of essential details, by knowledge-driven modeling in Blender. The resulting 3D models were then incorporated into interactive 3D-PDF files. Data analysis was performed on the segmented sections and the 3D models. The resource database contains the aligned images, the segmented Amira models, the interactive 3D-PDFs, and tables and graphs of the quantitative, topographic, and developmental data of all structures in every specimen. Green arrows indicate quality checks; red and blue arrows indicate the flow of data toward the contents of the resource database. Stage 20 specimen 462 was used to illustrate this flowchart.

Interactive three-dimensional models of early human development

The supplementary 3D-PDFs comprise 14 interactive 3D-PDF files, covering the first 2 months of human development, and illustrate the complex morphological changes that occur during development. With the interactive version, it is possible to focus on a specific organ, or on the system related to the organ of interest. An example of a 3D model of a CS20 embryo (51 to 53 days) is shown in Fig. 2. This view shows the nervous system in relation to the developing skeleton. Note that the vertebral arches are not yet closed and that the vertebral column and the spinal cord are still of equal length; the relative ascent of the latter has yet to occur.

To illustrate the scientific potential of these models, we analyzed the development of the vasculature in detail, summarized the results in schematics (Fig. 3, table S2, and fig. S2, A to O), and tabulated notable differences from the literature (*3*–*6*, *9*, *28*–*30*) (table S3). Some conspicuous differences from the literature are in the connections of the umbilical arteries with the aorta, the origin of the intestinal arteries, the sprouting of the pulmonary arteries, the origin of the external carotid artery, and the absence of the fifth pharyngeal arch artery in all embryos (table S3). It is difficult to trace when and why the descriptions in textbooks started to deviate from reality in the human embryo, because it is impossible to recover the original sources of these texts.

The organization of embryonic growth

The growth rate of the embryo, as derived from interpolation of the volumes of the series of embryos, is remarkably constant in the first 2 months of development. During this period the embryo grows exponentially; its volume increases 25% per day and reaches a volume of 2790 mm^3 at 60 days of development, or CS23 (Fig. 4, A and B). Nonetheless, there are substantial differences among the growth rates of different organs, which lead to differential relative growth between organs and between developmental phases (Fig. 4C and data S1). The liver initially grows substantially faster than does the entire embryo, but at stage 15/16 its growth rate tapers off to match the overall growth rate (Fig. 4C, blue line). The notochord shows an exponential decline in relative volume, whereas the metanephros grows faster than the total embryo (Fig. 4C, green and red line, respectively). The neural tube (minus neural canal) and its derivatives, in contrast, grow at a rate similar to that of the entire embryo throughout the period analyzed and thus show a constant relative volume of 10% (Fig. 4C, yellow line).

We tabulated the first appearance, and sometimes disappearance, of the different organs and

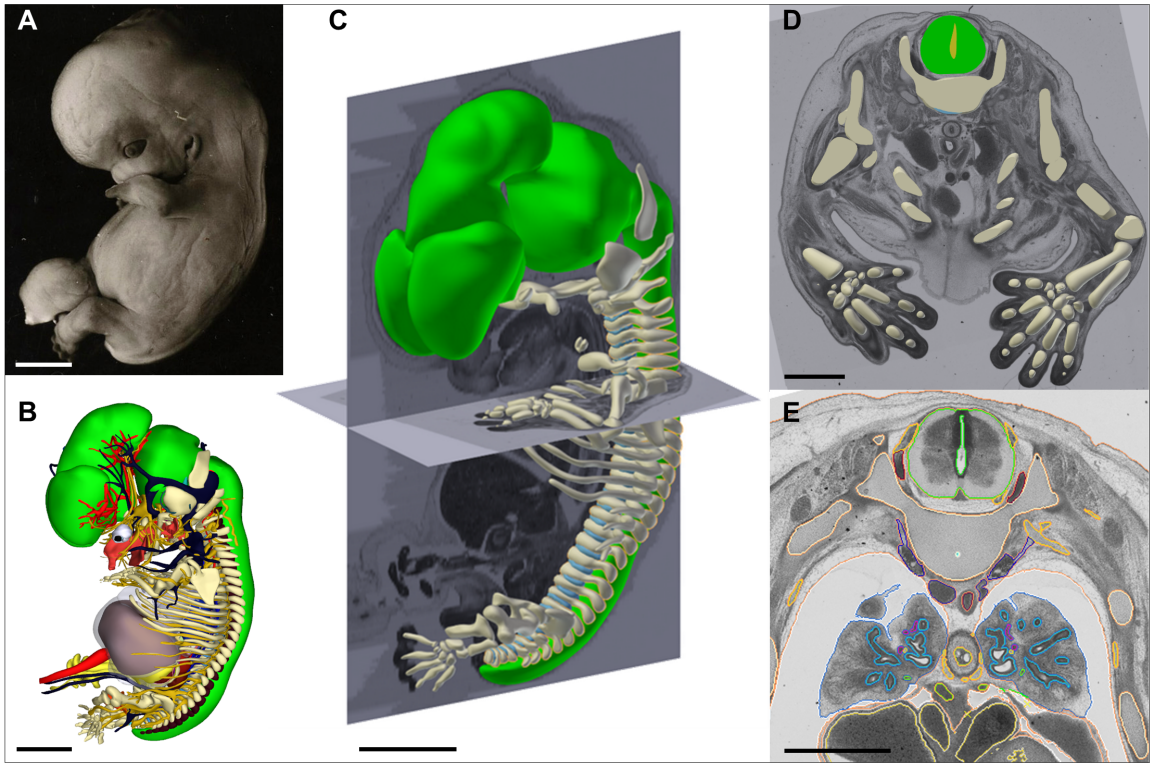

Fig. 2. Three-dimensional model of a stage 20 human embryo (specimen 462 of the Carnegie Collection, 7.5 weeks of development). (**A**) Lateral view of the original embryo before sectioning. (**B**) Lateral view of all reconstructed organs and structures, except for the skin. (**C**) Three-dimensional view of the reconstructed embryo highlighting the skeleton and neural tube. The sagittal plane cuts through the digitized image stack. (**D**) Cranial view on the transverse section from (C) through the shoulder region. (**E**) A detail of a transverse section through the lungs, as presented in Amira. Note the colored outline of each annotated structure. The neural tube is represented in green, the skeleton in off-white; the transparent body cavities enable inspection of the liver (brown). Scale bars, 2.5 mm [(A) to (C)], 1 mm [(D) and (E)].

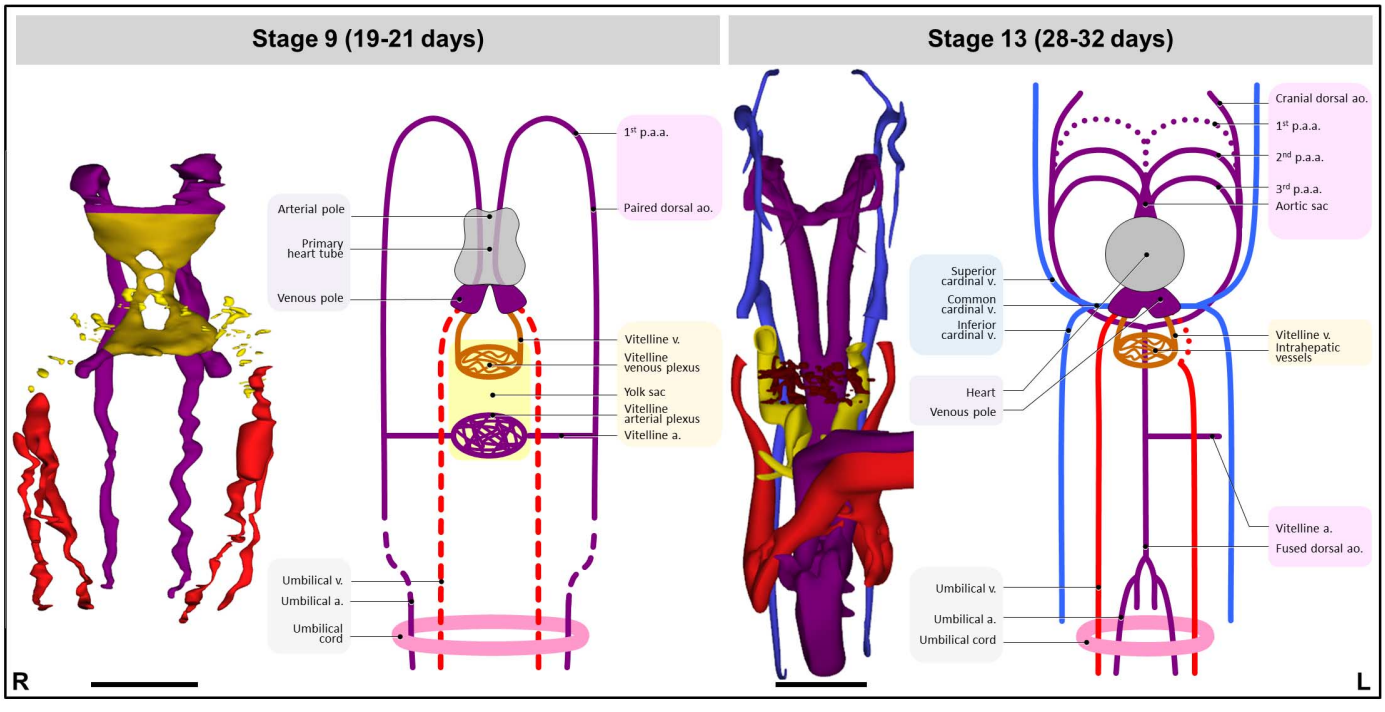

Fig. 3. Development of the vascular system. The developing vascular system is presented in a Carnegie stage 9 embryo (19 to 21 days; left) and a stage 13 embryo (28 to 32 days; right). Dashed lines represent developing vessels; dotted lines represent regressing vessels. See fig. S2, A to O, for a complete schematic overview of the developing vascular system between stage 9 (19 to 21 days) and stage 23 (56 to 60 days). Changes in the vascular system are summarized per stage in tables S2 and S3. Abbreviations: a., artery; ao., aorta; p.a.a., pharyngeal arch arteries; v., vein. Scale bars, 250 μm (stage 9), 500 μm (stage 13).

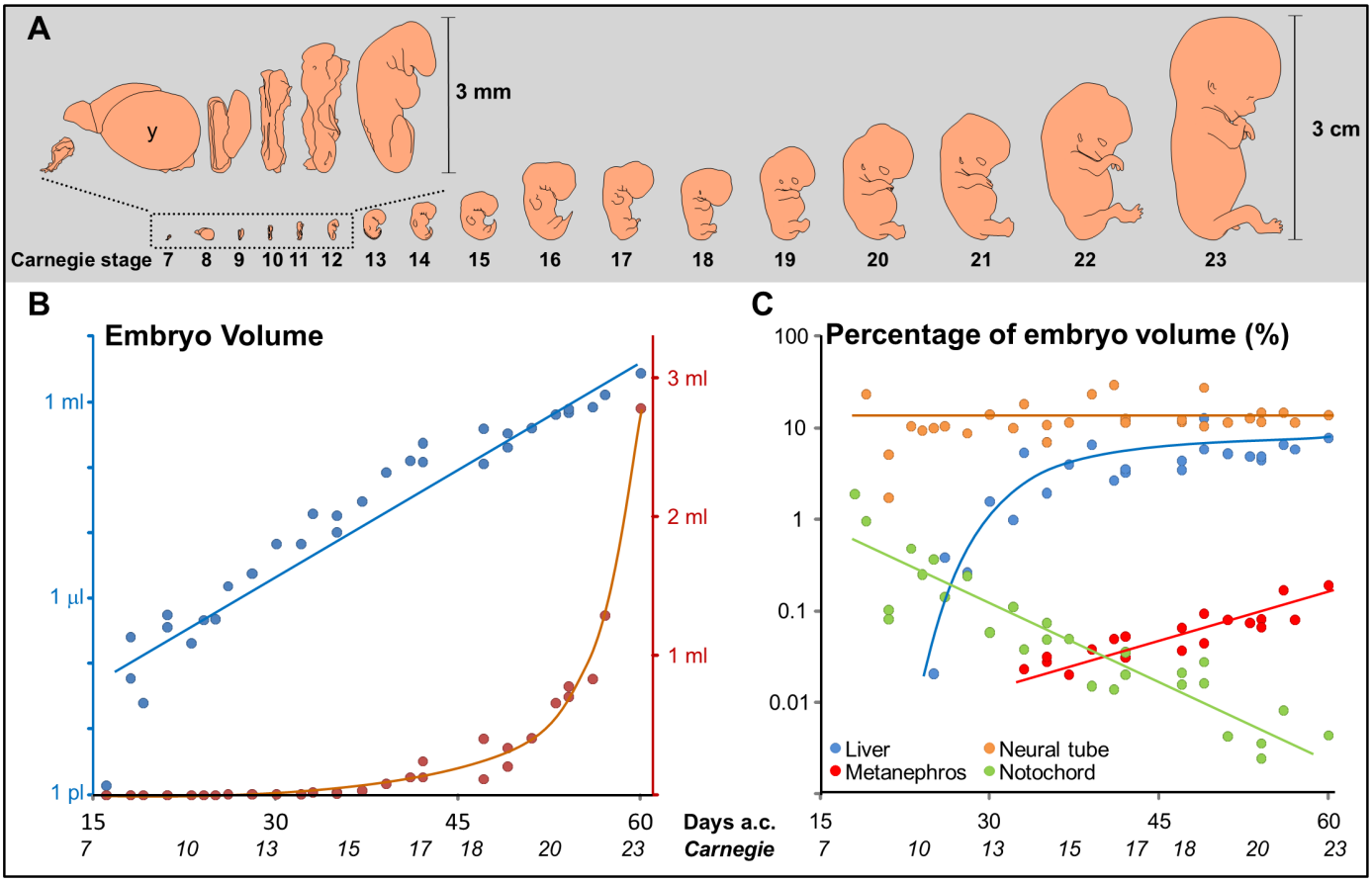

Fig. 4. Growth of the human embryo during the first 2 months of development. (**A**) Length of the embryo between Carnegie stages 7 and 23. Stages 7 to 12 are enlarged. Note the large round yolk sac (y) in stage 8. Drawings (left to right) are of specimens 8752, 8671, H712, 6330, 6784, 8505A, 0836, 8314, 3512, 6517, 8521, 8524, 2114, 462, 7258, 895, and 9226. (**B**) Increase in body volume with respect to days after conception (days a.c.) and Carnegie stages (*x* axis). Embryo volumes are plotted on a logarithmic scale (left *y* axis; blue dots) and on a linear scale (right *y* axis; red dots). The linear relation between log(volume) and days of development indicates a constant growth rate of the embryos in this development period. (**C**) Relative volume of organs as percentage of embryonic volume (*y* axis) with respect to days after conception and Carnegie stages (*x* axis). Neural tube (not including the neural canal), liver, metanephros, and notochord are shown as examples (see data S1 for other organs). The neural tube accounts for a constant relative volume of ~10% of the total volume, whereas the relative volume of the liver first increases, after which it also reaches a steady relative volume of 8%. The relative volume of the notochord decreases exponentially, whereas the relative volume of the metanephros increases exponentially after its first appearance.

structures within the human embryo for each stage, and compared the findings with the corresponding data for mouse and chicken embryos (fig. S3 and data S3). This analysis is of particular importance in teratological studies that apply data from experimental animals to the human situation. The order of appearance of the distinct organs in these species agrees largely with the order reported by Butler and Juurlink (*31*), who based their staging exclusively on the exterior characteristics of the complete embryo. However, we found a consistent difference of one to two stage equivalents when comparing matched mouse and human or chicken developmental stages (fig. S3 and data S3). Thus, our data show that mouse embryonic day 9.5 (E9.5) corresponds to CS12 rather than CS10, and so on. However, we also found different timing of the appearance of some internal organs, such as the choroid plexus, which is first recognizable in mouse stage E11.0 but only five equivalent stages later in human (CS18) and chicken (HH27 to 28) (data S3). Similarly, the regression of the stalk of the pharyngeal hypophysis is completed six stages earlier in mouse (E12.0) than in human (CS21) and chicken (HH33 to 34) (data S3). The adrenal gland, in contrast, starts to develop in the same stage in human (CS18) and mouse (E13.5) embryos, but four equivalent stages later in chicken embryos (HH35) (data S3). In the current literature, the data for the timing of development of structures within the human embryo are anecdotal (*32*, *33*), and textbooks are inconsistent and lack references (*3*–*6*, *18*, *29*, *30*, *34*). Overall, our tabulated human data are consistent with those presented in the atlas of human development by O'Rahilly and Müller (*18*).

Changing organ topography

Regional differences in growth and migration of the organs are usually suggested to explain the changes of the position of organs during development (*3*–*6*, *18*, *35*, *36*). Perhaps the most cited example is the ascent of the primordial kidneys (*3*–*6*, *34*). This ascent, in turn, has led to the notion that fusion of the kidney primordia, prior to their ascent, would account for the horseshoe lesion, the fused middle part allegedly being prevented from ascent by the presence of the midline inferior mesenteric artery, whereas the lateral parts have no impediment to their ascent (*3*–*6*). The greatest weakness of these suppositions is the almost total lack of quantitative data about the relative positions of the different structures during development. Our 3D reconstructions permit us to show the position of each individual organ relative to the developing vertebrae (Fig. 5 and data S2). The primordium of the definitive kidney, or metanephros, can be identified already at CS14, but we could first reliably relate its position to the developing vertebrae at CS16 (Fig. 5). The kidney is then positioned within the lumbar region extending from the fourth lumbar vertebra to the first sacral vertebra. Within a few days, it elongates up to the level of the first lumbar vertebra (CS17). Its cranial margin

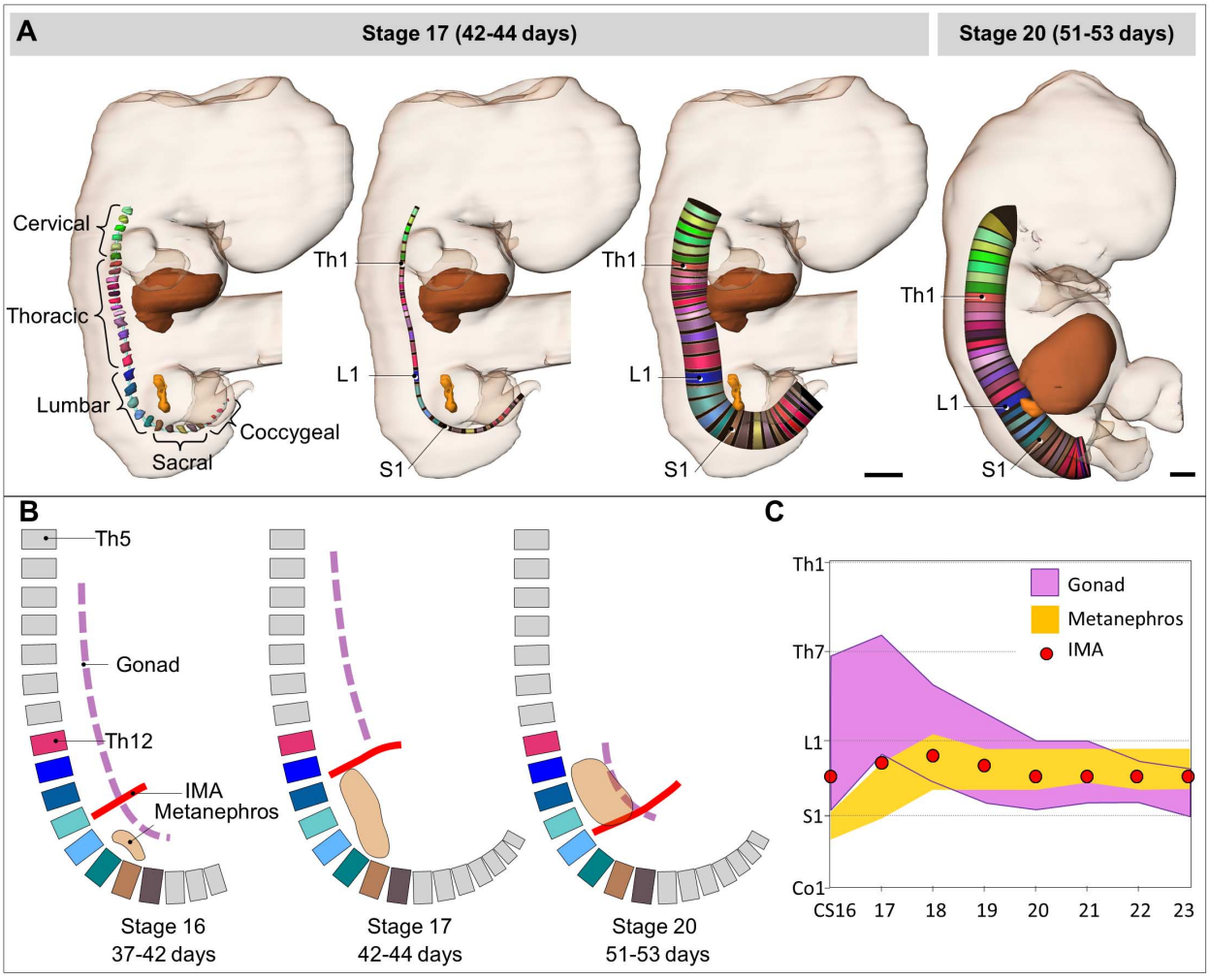

Fig. 5. Assessment of organ position during development. (**A**) To enable determination of the position of organs, planes perpendicular to the notochord were generated from the intersection of the developing vertebrae with the notochord. Left: Reconstruction of the individually labeled vertebrae and notochord. Center: The notochord was skeletonized to a line and masked with the colors of the vertebrae. Right and far right: The skeletonized notochord was expanded to form a cylinder. Each colored disc corresponds to a vertebra, and the planes of these discs, perpendicular to the notochord, now serve as rulers. The user can increase the diameter of the discs to determine which discs intersect with the organ of interest. The most cranial and caudal intersections of an organ with the planes of the discs then give the position of an organ relative to the vertebrae. Stage 17 (specimen 6521) and stage 20 (specimen 462), with annotated liver (brown) and kidneys (orange), are illustrated. Note the caudal shift of the liver from stage 17 (C7-Th10) to stage 20 (Th2-S5), whereas the kidneys remain at the same cranial position (L1), in contrast to descriptions in textbooks. (**B**) Cartoons based on 3D reconstructions. The relation of the metanephros (orange), the gonad (purple), and the inferior mesenteric artery (IMA; red) is indicated in stages 16, 17, and 20. See the text for their positional changes. (**C**) Margins of the position of the metanephros (orange band), the inferior mesenteric artery (red dots), and the gonads (purple band) during development (*x* axis) relative to the vertebrae (*y* axis) (see data S2 for other organs). Th, thoracic; L, lumbar; S, sacral; Co, coccygeal; CS, Carnegie stage. Scale bars in (A), 1 mm.

remains at this "adult" level, whereas during further development its caudal margin "ascends" from the first sacral to the fourth lumbar vertebra, owing to a relatively faster growth of the developing vertebral column. This raises the question of whether such a pattern of growth implies a real ascent of the kidneys during development.

A confounding factor that may have led to the notion of ascent of the kidneys is the hitherto unrecognized substantial difference in growth along the entire length of the aorta, which determines the relative position of the arterial branches (Fig. 5, fig. S2, H to O, and data S2). During development, the branching point of the seventh intersegmental artery remains positioned at the level of the seventh cervical vertebra and that of the umbilical arteries at the level of the third to fourth lumbar vertebrae, whereas the relative positions of the three major intestinal arteries change considerably. From CS16 to CS23, the branching point of the celiac trunk and the superior mesenteric artery "descends" from the sixth and seventh thoracic vertebrae, respectively, to the first lumbar vertebra; the inferior mesenteric artery "descends" only slightly from the first to the third lumbar vertebra. As a consequence, the position of this latter artery changes from the cranial border of the kidney at CS17 to its caudal border from stage 20 onward. Therefore, taking this artery as the point of reference gives the erroneous impression that the kidneys ascend.

Another example is the developing gonads, which are generally assumed to descend during development (*4*–*6*, *29*). Our data show that this is not the case. During the embryonic period, the caudal margin of the developing gonads remains approximately at the level of the fifth lumbar or first sacral vertebra. The cranial margin, however, does not grow proportional with the vertebral column, and thus it "descends" from the level of the fifth thoracic vertebra in CS16 to the

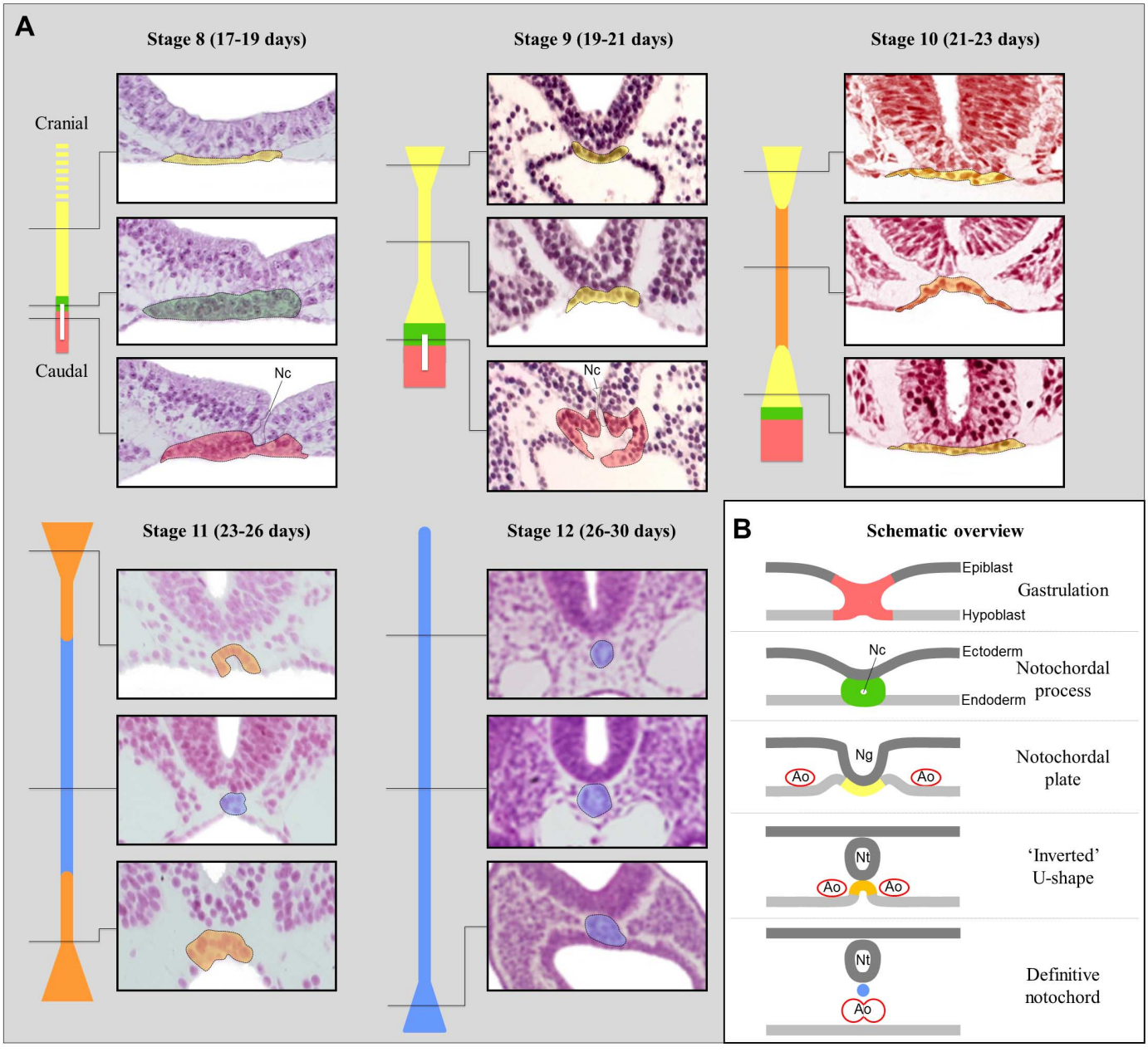

Fig. 6. Schematic overview of the development of the notochord. (**A**) The notochord develops from stages 8 to 12. Three representative transverse sections per stage are shown along with a schematic representation of the developing notochord, showing the position of the sections and the partitions of the developing notochord. The notochordal process and plate develop in craniocaudal direction, whereas formation of the definitive notochord starts in the middle of the embryo, expanding in both directions. The caudal extreme of the developing notochord widens in stage 12 (26 to 30 days) as a result of secondary development in the caudal eminence. (**B**) Schematic overview of the five stages of notochordal development in a transverse view. Red, gastrulation zone; green, notochordal process with notochordal canal; yellow, notochordal plate; orange, "inverted U"–shaped notochord; blue, definitive notochord; Ao, aorta; Nc, neurenteric canal; Ng, neural groove; Nt, neural tube. Presented specimens are 10175, 3709, 6330, 6344, and 8505A.

second lumbar vertebra in CS23 (Fig. 5). Obviously, this does not imply that the gonad, as an organ, truly descends in this period, but merely that it shortens relative to the growing vertebrae. Analysis of 34 specimens of the first 2 months of human development thus enabled us to elicit the information required to describe the changes in the position of internal organs relative to one another (data S2).

Comparative morphological analyses

In the absence of human experimental studies, medical embryologists necessarily rely heavily on data obtained from experimental animals such as chicken and mouse. A proper understanding of the development of birth defects thus requires insight into the similarities and differences between human development and that of these experimental animals. However, it is not clear whether cartoons of certain developmental processes in medical textbooks truly reflect the human situation. The data collected for the current atlas remedy this situation because they allow verification of experimental findings in the developing human. We cite two examples.

The first example is the development of the notochord, represented in textbooks as a mixture of human and animal data (*4*, *5*, *37*). Figure 6

shows the human sections of the relevant developmental stages in our atlas, along with cartoons indicating our observations. These data show that in humans, a group of primitive cells briefly persists after gastrulation. This transient group of cells, through which the neurenteric canal traverses, is dubbed the notochordal process. The ventral side of this cell cluster is incorporated into the endodermal roof of the foregut, and its dorsal side is closely attached to the developing neural tube. This intimate association is often ignored, even though animal studies have shown that the developing notochord induces the formation of the floor plate of the neural tube (*38*) and is attached to the developing neural system (*39*, *40*). Then the notochordal process incorporates entirely into the endoderm, forming the epithelial notochordal plate, which adopts an "inverted U" shape and remains intimately associated with the neural tube. Subsequently, the notochordal cells detach from the endoderm to form the definitive notochord, allowing the two dorsal aortas to fuse between the notochord and the roof of the foregut (Fig. 6B). Similar to gastrulation, the formation of the notochordal process and plate proceeds in the craniocaudal direction. However, in contrast to the mechanism described in several textbooks (*3*–*6*), the formation of the definitive notochord in humans starts in the middle of the embryo and then proceeds in both cranial and caudal directions, similar to what is generally assumed for the closure of the neural tube.

The second example relates to the origin of the derivatives of the pharyngeal arches. According to current theories, the hyoid body develops by fusion of parts of the second and third pharyngeal arch cartilages, and the thyroid cartilage by fusion of parts of the fourth and sixth pharyngeal arch cartilages, as described for lower vertebrates (*41*). In contrast, we observed that in human development, the body of the hyoid bone develops from a single growth center, without overt contributions from the second and third pharyngeal arch cartilages. The thyroid and cricoid cartilages develop separately from mesenchymal thickenings (fig. S4). Anatomical variations of the hyoid-larynx complex occur in up to 25% of the general population (*42*). Most variants are not important in the clinical setting, but they may be important in a forensic context if a fracture of the hyoid bone is suspected. In that case, it is of utmost importance to distinguish between true fractures of the hyoid bone or the thyroid horns, and failure of these parts to fuse during development.

Discussion

The recent expansion of molecular genetic technology has brought with it an improved understanding of the regulatory mechanisms that control the development of the vertebrate building plan. Although the findings in model organisms are being extrapolated to human development, insight into the divergence and conservation of human morphogenesis, as compared to experimental animals, remains crucial to assess whether such extrapolations are justified. A global analysis of the changing position of just a few structures such as the gonads, kidneys, and arteries shows discrepancies with current textbooks and thus demonstrates the value of a 3D atlas based on human embryonic specimens. The generated 3D models are presented in interactive 3D-PDF files (*43*), which facilitates the understanding of complex 3D structures and permits the reader to develop an independent judgment about human embryology. Although new editions of biomedical textbooks update recent molecular insights, the morphogenesis is not updated and has become increasingly schematic as well as alienated from the original human substrate. This 3D atlas reinstates this link because the morphological reconstructions are connected directly to the original sections of the human embryos in the Carnegie Collection.

Our atlas can serve as an educational and reference resource for (bio)medical students, clinicians, and scientists interested in human development and development-related disease. The original images and reconstructions are available for educational use and further scientific analysis. This, in turn, will permit updates and extension of the atlas with time, in cooperation with other research groups.

REFERENCES AND NOTES

1. "Congenital anomalies," WHO Fact sheet No370 (2014).
2. "Birth Defects," WHO Executive board 125th session EB125/7 (2009).
3. B. M. Carlson, *Human Embryology and Developmental Biology* (Elsevier Saunders, ed. 5, 2014).
4. K. L. Moore, T. V. N. Persaud, M. G. Torchia, *The Developing Human: Clinically Oriented Embryology* (Elsevier, ed. 10, 2016).
5. T. W. Sadler, *Langman's Medical Embryology* (Wolters Kluwer Health, ed. 13, 2015).
6. G. C. Schoenwolf, S. B. Bleyl, P. R. Brauer, P. H. Francis-West, *Larsen's Human Embryology* (Elsevier Saunders, ed. 5, 2015).
7. I. Broman, *Die Entwicklung des Menschen vor der Geburt* (J. F. Bergmann, München, 1927).
8. M. Foster, F. M. Balfour, *The Elements of Embryology* (Macmillan, 1874).
9. R. F. Gasser, *Atlas of Human Embryos* (Harper & Row, 1975).
10. C. H. Heuser, A presomite human embryo with a definite chorda canal. *Contrib. Embryol.* **23**, 251–267 (1932).
11. C. H. Heuser, J. Rock, A. T. Hertig, Two human embryos showing early stages of the definitive yolk sac. *Contrib. Embryol.* **31**, 85–99 (1945).
12. W. His, *Anatomie Menschlicher Embryonen vol. I* (Vogel, Leipzig, 1880).
13. W. His, *Anatomie Menschlicher Embryonen vol. II* (Vogel, Leipzig, 1882).
14. W. His, *Anatomie Menschlicher Embryonen vol. III* (Vogel, Leipzig, 1885).
15. F. Keibel, F. P. Mall, *Manual of Human Embryology, Volume I* (Lippincott, 1910).
16. F. Keibel, F. P. Mall, *Manual of Human Embryology, Volume II* (Lippincott, 1912).
17. A. Keith, *Human Embryology and Morphology* (William Wood, Baltimore, 1933).
18. R. O'Rahilly, F. Müller, *Developmental Stages in Human Embryos* (Carnegie Institution, 1987).
19. C. W. Prentiss, L. B. Arey, *A Laboratory Manual and Text-Book of Embryology* (Saunders, 1917).
20. G. L. Streeter, Developmental horizons in human embryos. Description of age group XI, 13 to 20 somites, and age group XII, 21 to 29 somites. *Contrib. Embryol. Carnegie Inst.* **30**, 211–245 (1942).
21. G. L. Streeter, Developmental horizons in human embryos. Description of age group XIII, embryos about 4 or 5 millimeters long, and age group XIV, period of indentation of the lens vesicle. *Contrib. Embryol. Carnegie Inst.* **31**, 27–63 (1945).
22. G. L. Streeter, Developmental horizons in human embryos. Description of age groups XV, XVI, XVII, and XVIII, being the third issue of a survey of the Carnegie collection. *Contrib. Embryol. Carnegie Inst.* **32**, 133–203 (1948).
23. G. L. Streeter, Developmental horizons in human embryos; a review of the histogenesis of cartilage and bone. *Contrib. Embryol. Carnegie Inst.* **33**, 149–168 (1949). pmid: 18144445
24. G. L. Streeter, Developmental horizons in human embryos. Description of age groups XIX, XX, XXI, XXII, and XXIII, being the fifth issue of a survey of the Carnegie Collection. *Contrib. Embryol. Carnegie Inst.* **34**, 165–196 (1951).
25. Y. Matsuda *et al*., Super-parallel MR microscope. *Magn. Reson. Med.* **50**, 183–189 (2003). doi: 10.1002/mrm.10515; pmid: 12815693
26. S. Yamada, T. Nakashima, A. Hirose, A. Yoneyama, T. Takeda, T. Takakuwa, in *The Human Embryo*, S. Yamada, T. Takakuwa, Eds. (InTech, Rijeka, 2012), chapter 7.
27. Federative International Programme on Anatomical Terminologies (FIPAT), *Terminologia Embryologica, International Embryological Terminology* (Georg Thieme Verlag, 2013).
28. S. F. Gilbert, *Developmental Biology* (Sinauer Associates, ed. 9, 2010).
29. W. J. Hamilton, J. D. Boyd, H. W. Mossman, *Human Embryology, Prenatal Development of Form and Function* (Heffers, Cambridge, 1972).
30. H. Tuchmann-Duplessis, P. Haegel, *Illustrated Human Embryology, Vol.2 Organogenesis* (Springer-Verlag, 1974).
31. H. Butler, B. H. Juurlink, *An Atlas for Staging Mammalian and Chick Embryos* (CRC Press, 1987).
32. R. O'Rahilly, D. B. Meyer, The timing and sequence of events in the development of the human vertebral column during the embryonic period proper. *Anat. Embryol.* **157**, 167–176 (1979). doi: 10.1007/BF00305157; pmid: 517765
33. N. J. Sissman, Developmental landmarks in cardiac morphogenesis: Comparative chronology. *Am. J. Cardiol.* **25**, 141–148 (1970). doi: 10.1016/0002-9149(70)90575-8; pmid: 5413193
34. W. J. Larsen, *Human Embryology* (Churchill Livingstone, New York, 1993).
35. W. S. Costa, F. J. Sampaio, L. A. Favorito, L. E. Cardoso, Testicular migration: Remodeling of connective tissue and muscle cells in human gubernaculum testis. *J. Urol.* **167**, 2171–2176 (2002). doi: 10.1016/S0022-5347(05)65122-1; pmid: 11956474
36. F. Müller, R. O'Rahilly, The initial appearance of the cranial nerves and related neuronal migration in staged human embryos. *Cells Tissues Organs* **193**, 215–238 (2011). doi: 10.1159/000320026; pmid: 20980719
37. H. Tuchmann-Duplessis, G. David, P. Haegel, *Illustrated Human Embryology, Vol. 1: Embryogenesis* (Springer-Verlag, 1982).
38. H. W. M. Straaten, J. W. M. Hekking, E. J. L. M. Wiertz-Hoessels, F. Thors, J. Drukker, Effect of the notochord on the differentiation of a floor plate area in the neural tube of the chick embryo. *Anat. Embryol.* **177**, 317–324 (1988). doi: 10.1007/BF00315839; pmid: 3354847
39. A. Jurand, The development of the notochord in chick embryos. *J. Embryol. Exp. Morphol.* **10**, 602–621 (1962). pmid: 13958100
40. A. Jurand, Some aspects of the development of the notochord in mouse embryos. *J. Embryol. Exp. Morphol.* **32**, 1–33 (1974). pmid: 4141719
41. A. S. Romer, *The Vertebrate Body* (Saunders, 1962).
42. P. J. de Santana Júnior *et al*., Which is your diagnosis? *Radiol. Bras.* **42**(4), 11–12 (2009); www.rb.org.br/detalhe_artigo.asp?id=987. doi: 10.1590/0100-3984.2014.47.5qd; pmid: 25741099
43. J. Murienne, A. Ziegler, B. Ruthensteiner, A 3D revolution in communicating science. *Nature* **453**, 450 (2008). doi: 10.1038/453450d; pmid: 18497796

ACKNOWLEDGMENTS

We thank R. J. Cork and R. F. Gasser of the Virtual Human Embryo project (http://virtualhumanembryo.lsuhsc.edu) for kindly providing the photographs of the first series of sections of human embryos of the Carnegie Collection; E. Lockett and E. Wilson of the National Museum of Health and Medicine (Silver Spring, Maryland) for providing access to the Carnegie Collection; G. Burton for generously providing the digital images of a stage

9 embryo of the Boyd Collection, scanned by A. Shelley; O. J. G. B. de Bakker and B. Meijer for their assistance in photographing the sections; K. Aben, Z. Al-Shaibani, C. Berends, H. Boon, F. Bounif, C. Buijs, M. Buijtendijk, D. M. de Bakker, K. de Cuba, B. de Jong, J. de Jong, S. Dekker, I. de Vries, M. de Witte, I. El-Bouyahyaoui, M. Ghariq, E. Groot, C. Hafkamp, N. Hagemeijer, I. Harmsen, L. Hassing, D. Henssen, E. Hodde, D. Hoornstra, B. Hulstein, J. Kruidenier, L. Kuil, T. Lachkar, S. Levy, R. Linschoten, J. Maarleveld, R. Michael, F. Noyola, M. Oppelaar, R. Post, G. Roelandt, M. Seinen, M. Slooter, D. Smidt, F. Stubenrouch, D. Torenstra, O. Turgman, S. van Wieringen, H. van Willigen, M. van der Poel, J. van Genderen, B. Verhoef, M. Warmbrunn, and S. Zomer for annotation of the sections; A. Linnenbank, B. Bakker, P. de Weert, J. Gieskens, G. Lens, J. Kalle, Y. Kim, R. Moolenaar, R. Pesch, J. Pouw, R. Rana, P. Stroombergen, D. van Etten, and P. van der Linden for modeling the structures; and R. H. Anderson and B. A. de Boer for scientific support and critical reading of the manuscript. The atlas content (3D-PDFs, source images, and labeled images in TIFF and AMIRA format) can be downloaded from http://3datlasofhumanembryology.com. Chicken and mouse sections are available from the corresponding authors.

SUPPLEMENTARY MATERIALS

www.sciencemag.org/content/354/6315/aag0053/suppl/DC1
Materials and Methods
Supplementary Text
Figs. S1 to S4
Tables S1 to S3
Data S1 to S3
Supplementary 3D-PDFs (14 Files, Stages 7 to 23)
References (*44*–*51*)

29 April 2016; accepted 11 October 2016
10.1126/science.aag0053

RESEARCH ARTICLE SUMMARY

CELL REPROGRAMMING

Tissue damage and senescence provide critical signals for cellular reprogramming in vivo

Lluc Mosteiro, Cristina Pantoja,* Noelia Alcazar,* Rosa M. Marión, Dafni Chondronasiou, Miguel Rovira, Pablo J. Fernandez-Marcos, Maribel Muñoz-Martin, Carmen Blanco-Aparicio, Joaquin Pastor, Gonzalo Gómez-López, Alba De Martino, Maria A. Blasco, María Abad, Manuel Serrano†

INTRODUCTION: The ectopic expression of transcription factors OCT4, SOX2, KLF4, and cMYC (OSKM) enables reprogramming of adult differentiated cells into pluripotent cells, known as induced pluripotent stem cells (iPSCs), that are functionally equivalent to embryonic stem cells. Expression of OSKM in vivo leads to widespread cell dedifferentiation and reprogramming within tissues and eventually to the formation of teratomas (tumors arising from iPSCs). The molecular mechanisms operating during in vitro OSKM-driven reprogramming have been extensively characterized; however, little is known about in vivo reprogramming.

RATIONALE: The process of OSKM reprogramming is inefficient both in vitro and in vivo. A number of cell-intrinsic barriers have been identified in vitro, most of which are activated by cellular damage and are particularly prominent in aged cells. Mechanistically, these cell-intrinsic barriers for reprogramming are primarily mediated by the tumor suppressors p53, $p16^{INK4a}$, and ARF (the latter two are encoded by the *Ink4a/Arf* gene locus). In this work, we have investigated the effect of these tumor suppressors, cellular damage, and aging on in vivo reprogramming.

RESULTS: We found that the expression of OSKM in vivo not only triggers reprogramming of some cells but also inflicts extensive damage on many other cells, driving them into a state known as cellular senescence. Senescent cells are characterized by their inability to proliferate and by their secretion of inflammatory cytokines. We have observed a positive correlation between senescence and OSKM-driven reprogramming. For example, tissues lacking $p16^{INK4a}$/ARF do not undergo senescence, and their ability to reprogram is severely compromised. By contrast, in tissues lacking p53, damage is rampant; this leads to maximal levels of senescence, exacerbated cytokine production, and increased in vivo reprogramming.

To explore the connection between senescence and reprogramming, we manipulated these processes in vivo through pharmacological interventions. In particular, an increase in senescence produced by palbociclib (a drug that functionally mimics $p16^{INK4a}$) results in higher levels of reprogramming. Conversely, a reduction in senescence achieved by navitoclax (a proapoptotic drug with selectivity against senescent cells) leads to decreased in vivo reprogramming. We found that the cross-talk between senescence and reprogramming is mediated by the cytokine-rich microenvironment associated with senescent cells. This is based, among other evidence, on the observation that pharmacological inhibition of NFκB, a major driver of cytokine production, reduces in vivo reprogramming. Analysis of the inflammatory cytokines produced by senescent cells, both in vivo and in vitro, led us to identify interleukin-6 (IL-6) as a critical secreted factor responsible for the ability of senescent cells to promote reprogramming. In support of this, blockade of IL-6 or its downstream kinase effector PIM potently reduced in vivo reprogramming. These observations can be recapitulated in vitro, where reprogramming efficiency is strongly enhanced by the presence of damaged cells or by the conditioned medium derived from damaged cells. Moreover, immunodepletion of IL-6 from the conditioned medium abolished reprogramming.

ON OUR WEBSITE

Read the full article at http://dx.doi.org/10.1126/science.aaf4445

Having established that senescence promotes reprogramming, we studied whether tissue injury leading to senescence has a positive effect on OSKM-driven reprogramming. In particular, we show that bleomycin-induced tissue damage strongly promotes reprogramming in the lung. Finally, aging, which is associated with higher levels of cellular senescence, also favors OSKM-driven reprogramming both in progeric and in physiologically aged mice.

CONCLUSION: The expression of OSKM in vivo triggers two different cellular outcomes: reprogramming in a small fraction of cells, and damage and senescence in many other cells. There is a strong positive association between these two processes, due to the fact that cellular senescence creates a tissue context that favors OSKM-driven reprogramming in neighboring cells. The positive effect of senescence on reprogramming is mediated by secreted factors, of which IL-6 is a key player. This also applies to tissue injury and aging, where there is an accumulation of senescent cells that send signals to surrounding cells to promote OSKM-driven dedifferentiation and reprogramming. A similar conceptual interplay may occur in physiological conditions, where damage-triggered senescence could induce cell dedifferentiation to promote tissue repair. ■

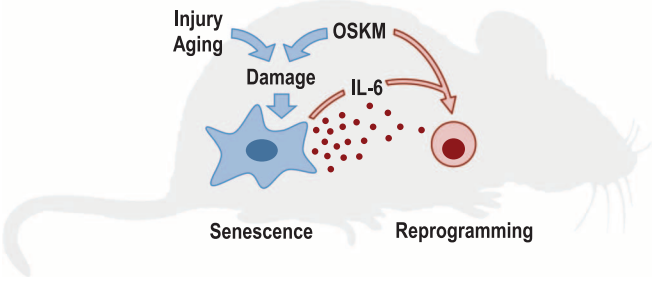

Interplay between cellular senescence and OSKM-driven reprogramming. Expression of OSKM in vivo, apart from inducing the reprogramming of a small population of cells, also induces damage and senescence in many other cells. Senescent cells release factors that promote the reprogramming of neighboring cells, with IL-6 being a critical mediator. Tissue injury and aging, through the accumulation of senescent cells, favor in vivo reprogramming.

The list of author affiliations is available in the full article online.
*These authors contributed equally to this work.
†Corresponding author. Email: mserrano@cnio.es
Cite this article as L. Mosteiro *et al.*, *Science* **354**, aaf4445 (2016). DOI: 10.1126/science.aaf4445

RESEARCH ARTICLE

CELL REPROGRAMMING

Tissue damage and senescence provide critical signals for cellular reprogramming in vivo

Lluc Mosteiro,[1] Cristina Pantoja,[1]* Noelia Alcazar,[1]* Rosa M. Marión,[2] Dafni Chondronasiou,[1] Miguel Rovira,[1] Pablo J. Fernandez-Marcos,[1,3] Maribel Muñoz-Martin,[1] Carmen Blanco-Aparicio,[4] Joaquin Pastor,[4] Gonzalo Gómez-López,[5] Alba De Martino,[6] Maria A. Blasco,[2] María Abad,[1,7] Manuel Serrano[1]†

Reprogramming of differentiated cells into pluripotent cells can occur in vivo, but the mechanisms involved remain to be elucidated. Senescence is a cellular response to damage, characterized by abundant production of cytokines and other secreted factors that, together with the recruitment of inflammatory cells, result in tissue remodeling. Here, we show that in vivo expression of the reprogramming factors OCT4, SOX2, KLF4, and cMYC (OSKM) in mice leads to senescence and reprogramming, both coexisting in close proximity. Genetic and pharmacological analyses indicate that OSKM-induced senescence requires the *Ink4a/Arf* locus and, through the production of the cytokine interleukin-6, creates a permissive tissue environment for in vivo reprogramming. Biological conditions linked to senescence, such as tissue injury or aging, favor in vivo reprogramming by OSKM. These observations may be relevant for tissue repair.

Cell identity can be manipulated in vitro, and this has opened new therapeutic possibilities (*1*). A major achievement in this field was the discovery that four transcription factors—OCT4, SOX2, KLF4, and cMYC (OSKM)—can transform differentiated cells into pluripotent cells, known as induced pluripotent stem cells (iPSCs) (*2*). These cells have the capacity to differentiate into all the cell types of the adult organism. Recent studies have shown that OSKM overexpression in mice results in cell dedifferentiation in multiple tissue types and reprogramming into iPSCs in vivo (*3*, *4*). However, little is known about the molecular mechanisms or cellular contexts that regulate in vivo reprogramming.

Ink4a/Arf promotes in vivo reprogramming

To explore the mechanisms involved in reprogramming in vivo, we focused on the tumor suppressors p53 (encoded by *Tp53*), $p16^{INK4a}$, and ARF (the latter two proteins are encoded by the genetic locus known as *Cdkn2a* or *Ink4a/Arf*). These proteins inhibit in vitro reprogramming, and their deletion or down-regulation increases the efficiency of the process (*5*–*11*). To investigate their role in reprogramming in vivo, we generated reprogrammable mice (carrying a ubiquitous doxycycline-inducible *OSKM* transgene, abbreviated as *i4F* for "inducible four factors") combined with null alleles for *p53* or *Ink4a/Arf*, and we confirmed that the *OSKM* transgene was efficiently induced in mice of the three genotypes (fig. S1A). We evaluated *p53* or *Ink4a/Arf*-heterozygous mice, all in the same inbred pure C57BL6 genetic background, for the development of OSKM-driven teratomas (an assay for pluripotency) after treatment with doxycycline (0.2 mg/ml in the drinking water for 8 days). We used heterozygous mice because the life span of homozygous mice was too short to measure teratoma formation. Unexpectedly, *i4F;Ink4a/Arf*-heterozygous mice were highly resistant to teratoma formation compared to *i4F* control mice (Fig. 1A). This was in contrast to *i4F;p53*-heterozygous mice, which had a higher rate of teratoma formation compared to controls. The organ distribution of teratomas was similar in all three *i4F* mouse strains (fig. S1B). Notably, the kinetics of spontaneous (nonteratoma) tumor development characteristic of *p53* and *Ink4a/Arf*-heterozygous mice was not affected by the induction of OSKM (fig. S1C).

We next investigated which step of teratoma formation—reprogramming, expansion, or differentiation—was affected by the absence of *p53* or *Ink4a/Arf*. We first assessed whether iPSC expansion and differentiation were different between the three genotypes. Subcutaneous injection of *i4F*, *i4F;p53*-null, and *i4F;Ink4a/Arf*-null iPSCs into nude mice produced teratomas with similar efficiency (fig. S1D), suggesting that the differences were not due to a differential ability of the iPSCs from the three genotypes to form teratomas. We next examined the process of reprogramming. Previously, we reported the presence of iPSCs in the blood of *i4F* mice after treatment with doxycycline (*3*). Using this assay, we observed the same trend in reprogramming efficiency as observed for the generation of teratomas—that is, *i4F;p53*-null > *i4F* > *i4F;Ink4a/Arf*-null (fig. S1E). We then focused on in situ reprogramming by studying mice 7 days after treatment with doxycycline and by looking for the expression of the pluripotency marker NANOG in tissues. We found that the pancreatic tissue of *i4F;p53*-null mice contained more $NANOG^+$ cells than that of *i4F* mice, whereas the pancreases of *i4F;Ink4a/Arf*-null mice were essentially devoid of $NANOG^+$ cells (Fig. 1, B and C). In line with these findings, tissue architecture was globally dysplastic in the *i4F;p53*-null pancreas, whereas the pancreas of *i4F* mice showed focal areas of dysplasia. In contrast, tissue architecture was largely unaffected in *i4F;Ink4a/Arf*-null pancreas (Fig. 1B). Similar differences among the three genotypes were also observed in the stomach and the kidney (Fig. 1C and fig. S1, F and G). Together, these results suggest that the absence of *p53* favors reprogramming in vivo, whereas the absence of *Ink4a/Arf* limits reprogramming.

The lower efficiency of in vivo reprogramming of *i4F;Ink4a/Arf*-null mice is in contrast to the higher efficiency of in vitro reprogramming of cells deficient in *Ink4a/Arf* (*6*–*10*). To further investigate this, we obtained mouse embryonic fibroblasts (MEFs) from the three i4F strains and compared their reprogramming efficiency in vitro and in vivo. As expected, both *i4F;p53*-null and *i4F;Ink4a/Arf*-null MEFs had a higher efficiency of in vitro reprogramming compared to controls (fig. S1H). However, when the same set of reprogrammable MEFs was injected into the kidney of wild-type (WT) mice, the efficiency of teratoma formation after doxycycline treatment was *i4F;p53*-null > *i4F* > *i4F;Ink4a/Arf*-null (Fig. 1D and fig. S1, I and J), which is the same pattern observed in whole-body reprogrammable mice (Fig. 1, A to C). When the reprogrammable MEFs were injected into immunocompromised hosts, such as athymic nude mice (lacking T lymphocytes) and NSG mice (lacking T, B, and natural killer lymphocytes), the kinetics of teratoma development maintained the same trend as in immunocompetent C57BL6 mice (fig. S1I). Therefore, the adaptive immune system is not a critical determinant of the differences in reprogramming among genotypes. These results, using the same set of reprogrammable MEFs, indicate that the *Ink4a/Arf* locus plays a dual role during reprogramming, acting as a barrier in vitro but as a promoter in vivo.

To gain insight into the role of *Ink4a/Arf* during in vivo reprogramming, we profiled the transcriptome of the pancreas after treatment with doxycycline (0.2 mg/ml for 7 days) in mice of

[1]Tumor Suppression Group, Spanish National Cancer Research Centre (CNIO), Madrid E28029, Spain. [2]Telomeres and Telomerase Group, CNIO, Madrid E28029, Spain. [3]Laboratory of Bioactive Products and Metabolic Syndrome, Madrid Institute for Advanced Studies (IMDEA) in Food, CEI UAM+CSIC, Madrid E28049, Spain. [4]Experimental Therapeutics Programme, CNIO, Madrid E28029, Spain. [5]Bioinformatics Unit, CNIO, Madrid E28029, Spain. [6]Histopathology Unit, CNIO, Madrid E28029, Spain. [7]Cell Plasticity and Cancer Group, Vall d'Hebron Institute of Oncology (VHIO), Barcelona E08035, Spain.
*These authors contributed equally to this work. †Corresponding author. Email: mserrano@cnio.es

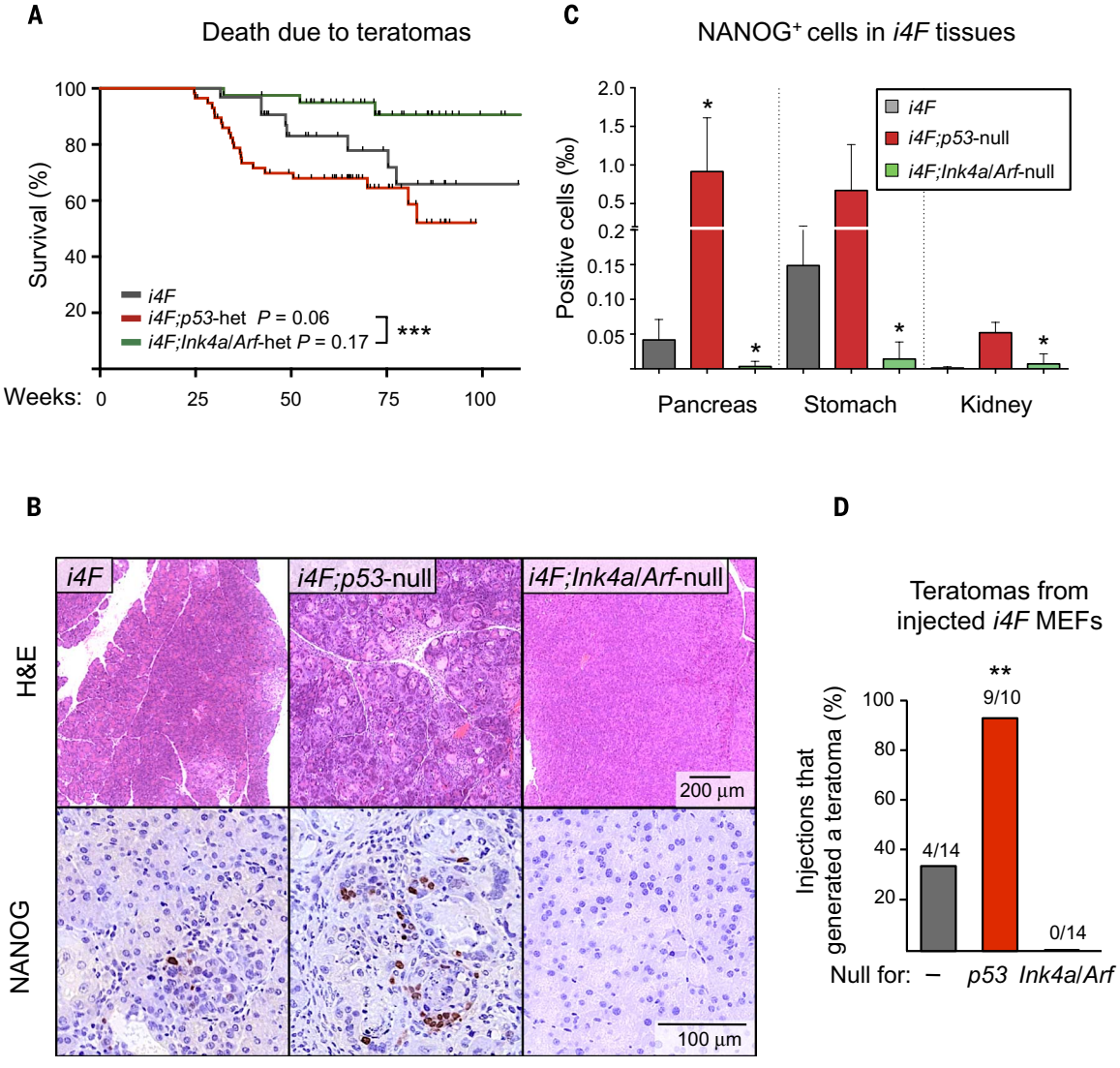

Fig. 1. *p53* limits and *Ink4a/Arf* promotes in vivo reprogramming. (**A**) Incidence of teratomas in mice of the indicated genotypes. Mice were treated with doxycycline (0.2 mg/ml in the drinking water) for 8 days, at 20 to 28 weeks of age. Time (weeks) refers to age. Only mice that died with teratomas were considered; mice that died without teratomas or that were alive appear censored and indicated with ticks. Cohorts were as follows: *i4F*, $n = 33$; *i4F;p53*-het, $n = 58$; *i4F;Ink4a/Arf*-het, $n = 40$. Statistical significance was evaluated using the log-rank test: $^{***}P < 0.001$. (**B**) NANOG immunohistochemistry and hematoxylin and eosin (H&E) staining of pancreas of the indicated genotypes. Mice were treated with doxycycline (0.2 mg/ml) for 7 days and analyzed at the end of the treatment. Images are representative of at least five mice ($n \geq 5$). (**C**) Percentage of NANOG$^+$ cells in the tissues of *i4F* mice of the indicated genotypes treated with doxycycline as in (B). Quantifications were done in a completely automated manner. Graph represents average ± SD ($n = 5$ for pancreas; $n = 4$ for stomach; $n = 3$ for kidney); statistical significance relative to control (*i4F*) was assessed by the unpaired two-tailed Student's *t* test with Welch's correction: $^{*}P < 0.05$. (**D**) Teratoma formation in the kidney of WT syngeneic C57BL6 mice injected with *i4F* MEFs of the indicated genotypes and induced in vivo with doxycycline (2 mg/ml) for 14 days. Teratomas appeared within 6 to 8 weeks after treatment. Statistical significance relative to control (*i4F*) was evaluated using two-tailed Fisher's exact test: $^{**}P < 0.01$.

the three genotypes [Gene Expression Omnibus (GEO) database accession number GSE77722]. Notably, most of the pathways that followed the pattern *i4F;p53*-null > *i4F* > *i4F;Ink4a/Arf*-null (fig. S1K) were related to the immune system and extracellular matrix remodeling, both characteristically associated with cellular senescence (*12*–*16*). Given the well-established involvement of the *Ink4a/Arf* locus in cellular senescence (*17*), we hypothesized that the *Ink4a/Arf* locus may contribute to in vivo reprogramming in a cell-extrinsic manner through the generation of a senescent tissue environment.

Reprogramming in vivo coexists with senescence

To explore the possible association between in vivo reprogramming and senescence, we examined whether both processes coexist within the same tissue context. We performed double stainings for NANOG together with indicators of senescence, such as senescence-associated β-galactosidase (SAβG) or the cell cycle inhibitor p21 (*18*). We found that, upon induction of reprogramming, NANOG$^+$ cells in the stomach (Fig. 2A) and the pancreas (fig. S2A) generally appeared in close proximity to clusters of SAβG$^+$ or p21$^+$ cells. Moreover, there was a positive correlation between the extent of senescence and the number of reprogrammed cells. Specifically, *i4F;p53*-null pancreas showed widespread SAβG$^+$ staining, whereas *i4F* pancreas had focal SAβG$^+$ clusters, and *i4F;Ink4a/Arf*-null pancreas had few SAβG$^+$ cells (Fig. 2B). This trend (*i4F;p53*-null > *i4F* > *i4F;Ink4a/Arf*-null) was also observed for p21, infiltration of macrophages (F4/80), proliferation [bromodeoxyuridine (BrdU) incorporation], DNA damage (γH2AX), and apoptosis (active caspase-3) (Fig. 2B). Stomach and kidney also presented the same pattern (fig. S2, B and C).

Moreover, transcription factors responsible for cytokine production upon tissue damage, such as NFκB (p65RelA), STAT3 (phospho-STAT3), and SMAD2 (phospho-SMAD2), also followed the same pattern as reprogramming, damage, and senescence (*i4F;p53*-null > *i4F* > *i4F;Ink4a/Arf*-null) (Fig. 2C). In line with this, the expression levels of mRNAs corresponding to *Ink4a* and *Arf* and a panel of cytokines, chemokines, growth factors, and tissue remodeling proteins were consistent with a strong senescence and inflammatory response upon induction of reprogramming in *i4F;p53*-null pancreas, a moderate response in *i4F* pancreas, and a minimal response in *i4F;Ink4a/*

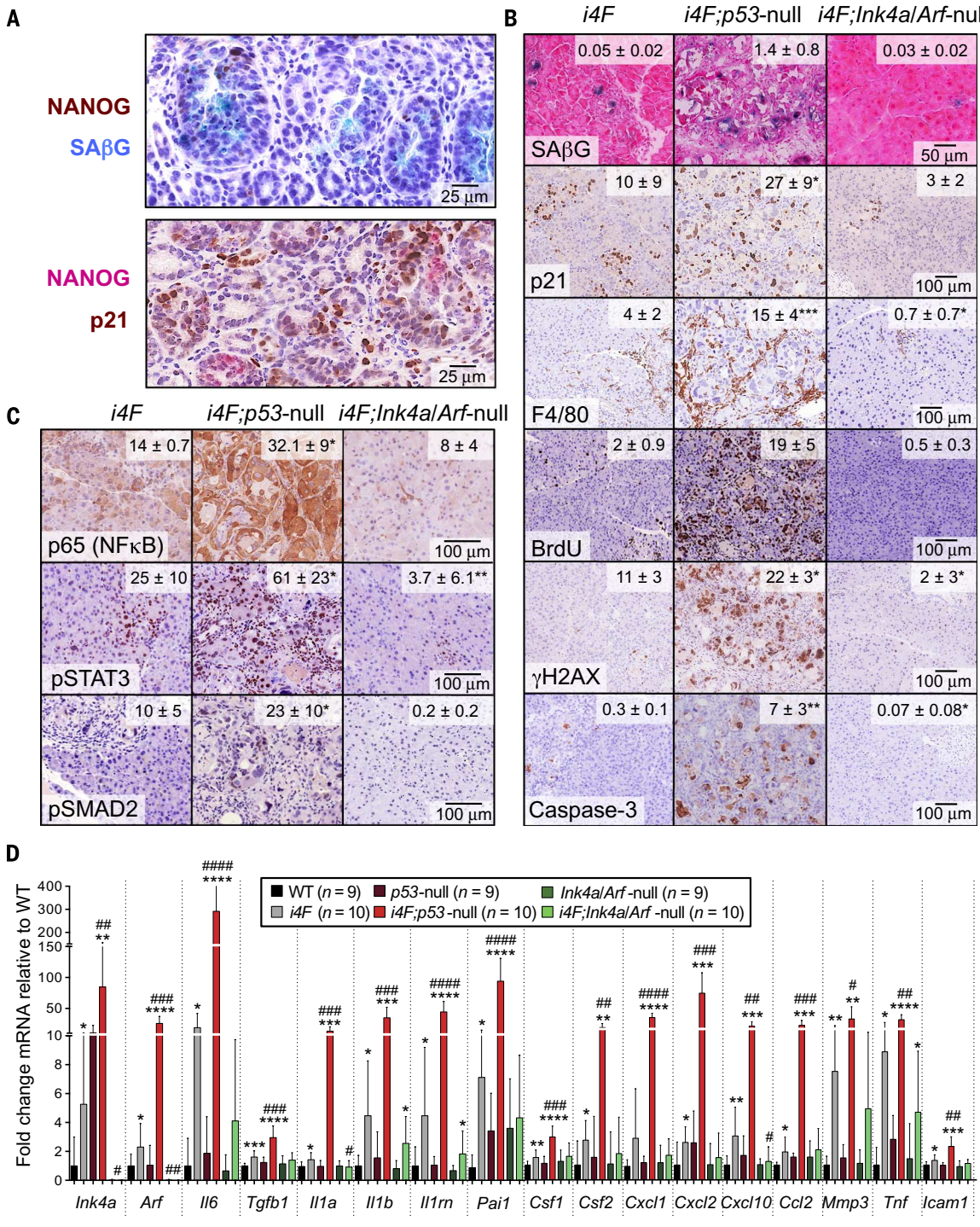

Fig. 2. Senescence and reprogramming coexist. (**A**) (Top) Double staining of NANOG (dark brown) and SAβG (light blue) in the stomach of *i4F* mice. (Bottom) Double staining of NANOG (magenta) and p21 (dark brown) in the stomach of *i4F* mice. Mice were treated with doxycycline (1 mg/ml in the drinking water) for 7 days and analyzed at the end of the treatment. (**B**) Staining of the pancreas. Mice were treated with doxycycline (0.2 mg/ml) for 7 days and analyzed at the end of the treatment. All quantifications were done in a completely automated manner and correspond to either the relative percentage of stained surface (SAβG, F4/80, γH2AX, and caspase-3) or the relative percentage of positive cells (p21 and BrdU). Values correspond to average ± SD ($n = 3$ to 5 mice per group). Statistical significance relative to *i4F* control was evaluated using the unpaired two-tailed Student's *t* test with Welch's correction: $^{*}P < 0.05$; $^{**}P < 0.01$; $^{***}P < 0.001$. (**C**) Staining of the pancreas, as in (B). The staining of p65 (NFκB) is quantified as relative percentage of positive surface, and the staining of pSTAT3 and pSMAD2 is quantified as relative percentage of positive cells. (**D**) mRNA levels of the indicated cytokines in the pancreas. Mice were treated with doxycycline as in (B). Values are relative to WT. Bars correspond to average ± SD; statistical significance was evaluated using the unpaired two-tailed Student's *t* test with Welch's correction. Comparison of each *i4F* genotype with its own non-*i4F* control is indicated as follows: $^{*}P < 0.05$; $^{**}P < 0.01$; $^{***}P < 0.001$; $^{****}P < 0.0001$. Comparisons of *i4F;p53*-null or *i4F;Ink4a/Arf*-null with *i4F* are indicated in the same manner but using the symbol "#."

Arf-null pancreas (Fig. 2D). In addition, serum levels of cytokines interleukin-6 (IL-6) and tumor necrosis factor–α (TNFα) increased upon OSKM activation, and this increase was most prominent in *i4F;p53*-null mice (fig. S2D).

We speculate that, in the absence of *p53*, cells cannot protect themselves from the effects of OSKM overexpression, leading to unrestrained cell proliferation, DNA damage, senescence, inflammation, and high levels of secreted factors. Moreover, it has been reported that the secretory activity of senescent cells [known as senescence-associated secretory phenotype (SASP)] is exacerbated in the absence of p53 (*14*). In contrast, in the absence of *Ink4a/Arf*, OSKM does not induce cellular senescence, which translates into lower levels of secreted factors and inflammation. Thus, OSKM triggers two divergent cellular outcomes, damage-induced cellular senescence and cellular reprogramming, that coexist in close proximity within tissues.

Senescence promotes in vivo reprogramming

To explore the link between senescence and in vivo reprogramming, we used small molecules to decrease or increase the number of senescent cells. To eliminate senescent cells, we took advantage of the hypersensitivity of senescent cells to the inhibition of Bcl-family proteins (*19*–*21*). Simultaneous treatment of *i4F* mice with doxycyline and the potent Bcl-2/Bcl-xL/Bcl-w–inhibitor navitoclax (also known as ABT263) reduced the amount of senescent cells and their associated secreted factors in pancreatic tissue undergoing reprogramming (Fig. 3, A and B). The reduction in the number of senescent cells was accompanied by a decrease in reprogramming, as measured by the number of NANOG$^+$ cells (Fig. 3A). Conversely, to increase senescence, we used the (CDK4/CDK6)-inhibitor palbociclib (also known as PD0332991), which can be considered as a p16^{INK4a} functional mimetic (*22*). Treatment with palbociclib increased the number of senescent cells, the production of their associated cytokines, and reprogramming in the pancreas (fig. S3, A and B). These observations suggest that senescence positively regulates in vivo reprogramming.

The master transcription factor NFκB plays a critical role in promoting the secretory activity of senescent cells (*16*, *23*, *24*). To evaluate the possible role of NFκB as a link between senescence and reprogramming, *i4F* mice were simultaneously treated with doxycycline and with an inhibitor of the NFκB-activating kinases IKKs (BAY 11-7082) (*25*). BAY 11-7082 diminished the expression of SASP factors, which led to decreased in vivo reprogramming (Fig. 3, A and B). BAY 11-7082 also reduced the extent of senescence (Fig. 3A), likely reflecting the loss of SASP-mediated paracrine senescence (*26*).

We next investigated which of the SASP factors play a dominant role during in vivo reprogramming. It was recently reported that IL-6 enhances in vitro reprogramming and can replace leukemia inhibitory factor (LIF), a related cytokine often used for reprogramming in vitro (*27*). We found that among the SASP factors tested, IL-6 showed the most marked up-regulation upon OSKM induction and a good correlation with the degree of reprogramming (~300-fold in *i4F;p53*-null mice, ~20-fold in *i4F* mice, and ~4-fold in *i4F;Ink4a/Arf*-null mice) (see Fig. 2D). We therefore tested the role of IL-6 by treating reprogrammable mice simultaneously with doxycycline and anti–IL-6 antibodies. We found that the anti–IL-6 antibodies abolished the increase in IL-6 serum levels characteristic of OSKM activation (fig. S3C). Blockade of IL-6 in vivo reduced not only reprogramming, as measured by the abundance of NANOG$^+$ cells, but also senescence and the expression of SASP factors (Fig. 3, C and D). The reduction of senescence upon anti–IL-6 is consistent with the known paracrine role of IL-6 in senescence (*15*). Reciprocally, injection of recombinant IL-6 (rIL-6) in *i4F* mice increased the extent of reprogramming (fig. S3, C and D). Furthermore, treatment of *i4F;p53*-null mice with anti–IL-6 antibodies also reduced reprogramming, senescence, and SASP (fig. S3, E to G). These results indicate that IL-6 is one of the critical cytokines linking senescence and reprogramming.

To reinforce the role of IL-6, we tested the involvement of the PIM kinases, which are activated by IL-6 through the JAK/STAT pathway (*28*), and reinforce NFκB activity through phosphorylation of p65RELA (*29*, *30*). Moreover, PIM1 is known to mediate the effects of IL-6 during in vitro reprogramming (*27*). Simultaneous treatment of *i4F* mice with doxycycline and with a PIM inhibitor (ETP-995, abbreviated as PIMi) (fig. S3, H to J, and supplementary text) resulted in a profound reduction of senescence, SASP factors, and reprogramming (Fig. 3, C and D). We conclude that senescence promotes in vivo reprogramming through the SASP, with IL-6 being a critical mediator.

Ink4a/Arf promotes cytokine production

To investigate the mechanism linking senescence to reprogramming, we examined the impact of senescent cells and their secretome on in vitro reprogramming. We used γ-irradiation (20 Gy) to induce a robust senescence response in primary fibroblasts (*14*). Coculture of reprogrammable *i4F* MEFs with γ-irradiated WT or *p53*-null MEFs increased in vitro reprogramming, whereas coculture with γ-irradiated *Ink4a/Arf*-null MEFs had no effect (Fig. 4A). To determine whether the positive effect of irradiated MEFs on reprogramming was mediated by secreted factors, we added conditioned medium (CM) from γ-irradiated MEFs to reprogrammable *i4F* MEFs. We found that CM from γ-irradiated WT MEFs enhanced reprogramming and that CM from γ-irradiated *p53*-null cells was even more potent in promoting reprogramming. In contrast, CM from γ-irradiated *Ink4a/Arf*-null MEFs had little effect (Fig. 4B).

To identify candidate mediators, we analyzed the CMs from the previous experiment in an array with immobilized antibodies for 40 cytokines. Two cytokines present in the CM from γ-irradiated WT or *p53*-null cells were noticeably absent in the CM from γ-irradiated *Ink4a/Arf*-null MEFs, namely, IL-6 and TNFα (Fig. 4C). Analysis of mRNA levels confirmed that a functional *Ink4a/Arf* locus is necessary for the expression of *Il6* and *Tnf* mRNAs upon γ-irradiation (Fig. 4D). We next added anti–IL-6 antibodies to the CM from γ-irradiated WT cells and found that they abolished the effect of CM and almost completely prevented reprogramming (Fig. 4E). This result supports the idea that IL-6 has a pivotal role in reprogramming. Finally, we explored whether the requirement of *Ink4a/Arf* for IL-6 production upon γ-irradiation is due to *Ink4a* or *Arf*. We infected WT MEFs with retroviruses encoding short hairpin RNAs (shRNAs) against *Ink4a* or *Arf*. We found that sh*Arf*-MEFs retained normal induction of *Il6* mRNA, whereas sh*Ink4a*-MEFs failed to up-regulate *Il6* upon γ-irradiation (fig. S4). These observations recapitulate in vitro the concept that senescent cells promote reprogramming through the *Ink4a/Arf* locus and the production of IL-6.

Tissue injury and aging promote reprogramming

Given the link between senescence and reprogramming, we wondered whether biological conditions characterized by higher levels of senescence, such as tissue injury, would also promote in vivo reprogramming. To address this, we focused on the lung because, despite expression of the *OSKM* transgene (*3*), we have never observed in vivo reprogramming in the lung under our experimental conditions. To induce cellular senescence in the lung, we chose the DNA-damaging agent bleomycin, which is a well-known model of lung injury and fibrosis (*31*, *32*). Two weeks after treatment with bleomycin, the lungs of WT mice showed signs of fibrosis and senescence (Fig. 5A and fig. S5A). Notably, the lungs of *i4F* mice treated with bleomycin and subsequently induced with doxycycline showed an abundant number of senescent cells, enhanced expression of p21, clusters of NANOG$^+$ cells, and dysplastic foci (Fig. 5A and fig. S5B). They also showed an increase in the mRNA levels of SASP factors, including *Il6* (Fig. 5B). Consistent with our previous observations, doxycycline-treated *i4F* mice that had not been treated with bleomycin did not show evidence of reprogramming or senescence in the lungs (Fig. 5A) and showed only modest up-regulation of SASP (Fig. 5B). This experiment indicates that the infliction of tissue damage by an exogenous factor renders the lung permissive to OSKM-induced in vivo reprogramming.

Following on the concept that tissue injury facilitates OSKM-induced reprogramming, we examined whether aging—a condition characterized by systemic accumulation of cellular damage and senescence (*17*)—also promotes OSKM-driven reprogramming. We first analyzed in vivo reprogramming in a mouse model of progeria (*Terc*-null mice of the second generation or *G2Terc*-null). The premature aging phenotype in these mice is due to the absence of telomerase

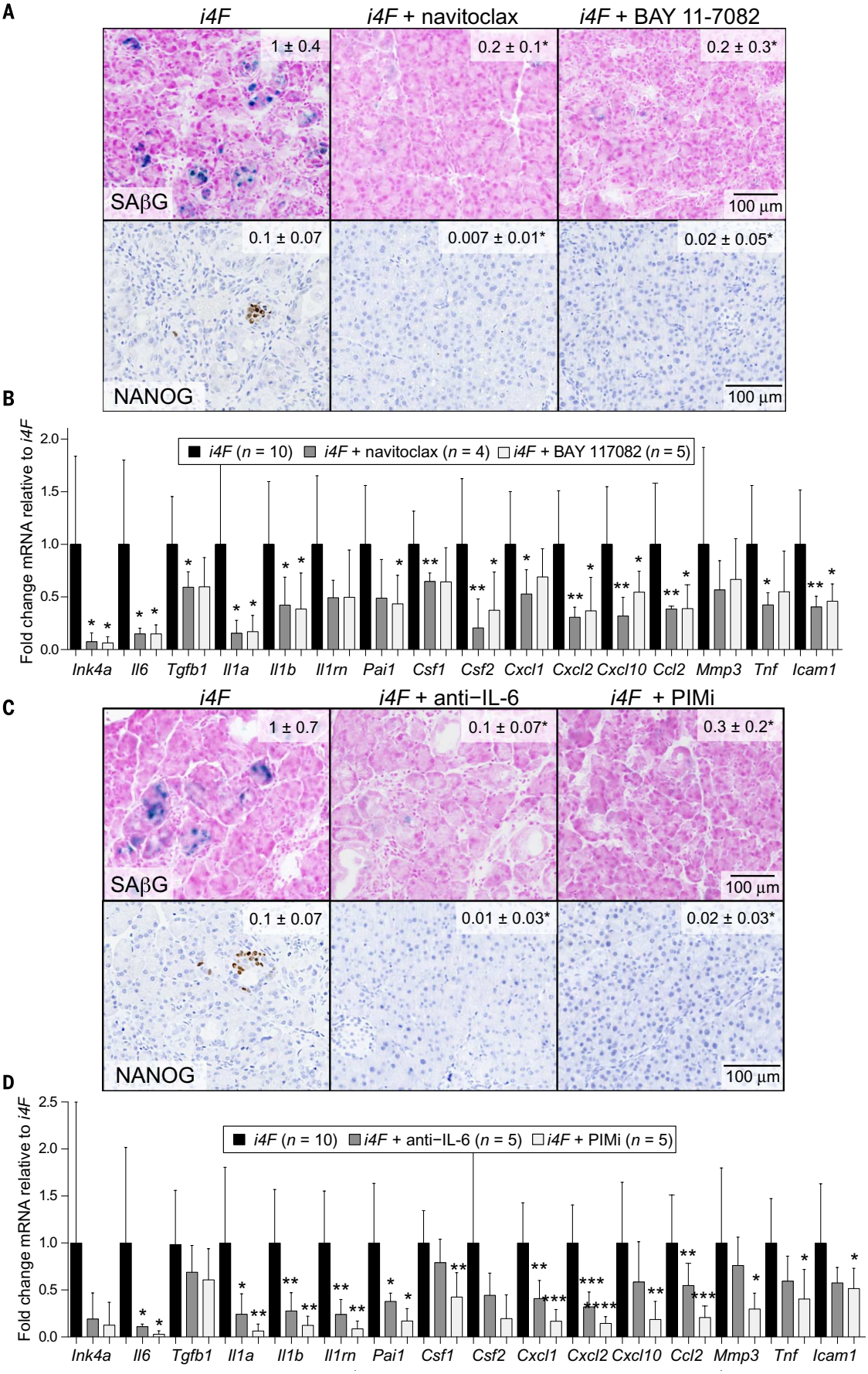

Fig. 3. Senescence enhances in vivo reprogramming. (**A**) Staining of the pancreas of *i4F* mice treated with doxycycline (1 mg/ml in the drinking water) and, where indicated, with navitoclax (25 mg/kg daily by oral gavage) or BAY 11-7082 (20 mg/kg daily by intraperitoneal injection). Mice were analyzed at the end of the treatment (7 days). Quantifications were done as explained in Fig. 2B. Values for SAβG indicate relative percentage of stained surface, and those for NANOG indicate relative ‰ of positive cells (NANOG is measured by the number of positive cells per thousand). Images are representative of at least three mice ($n \geq 3$). (**B**) mRNA levels of the indicated genes in the pancreas of the same mice as in (A). (**C**) Staining of the pancreas of *i4F* mice treated with doxycycline (1 mg/ml in the drinking water) and, where indicated, with anti–IL-6 (1 mg, three times per week, intraperitoneally) or PIM inhibitor (PIMi) (50 mg/kg daily by oral gavage). Mice were analyzed at the end of the treatment (7 days). Quantifications were done as explained in Fig. 2B. Values for SAβG indicate relative percentage of stained surface, and those for NANOG indicate relative ‰ of positive cells. Images are representative of at least five mice ($n \geq 5$). (**D**) mRNA levels of the indicated genes in the pancreas of the same mice as in (C). Values in all panels correspond to average ± SD. Statistical significance relative to control was assessed by the unpaired two-tailed Student's *t* test with Welch's correction: $^{*}P < 0.05$; $^{**}P < 0.01$; $^{***}P < 0.001$; $^{****}P < 0.0001$.

activity that leads to critically short telomere length (*33*, *34*). Upon activation of OSKM, the pancreas of *i4F;G2Terc*-null mice displayed substantially higher levels of senescence, SASP factors, and reprogramming, as compared with control *i4F* mice derived from the same parental strains (Fig. 6, A and B). These results are consistent with the hypothesis that tissue damage, in this case due to short telomeres in a mouse model of premature aging, promotes OSKM-induced in vivo reprogramming.

Finally, we examined the effect of physiological aging on reprogramming. We compared side by side the impact of OSKM expression in old (>65 weeks of age) and young (7 to 9 weeks of age) *i4F* mice. Consistent with our observations in *Terc*-null progeric mice, activation of OSKM in old mice resulted in higher levels of senescent cells in the pancreas and increased levels of $NANOG^+$ cells and teratoma formation, as compared with young mice treated in parallel (Fig. 6C and fig. S6A). As expected (*35*), the mRNA levels of *Ink4a* were higher in old WT mice than in young WT mice (Fig. 6D). Moreover, upon induction of OSKM, the mRNA levels of *Ink4a* and SASP-related factors were higher in old *i4F* mice than in the corresponding young controls (Fig. 6D). To further strengthen the effect of aging in reprogramming, we injected *i4F* MEFs into the kidneys of old (>95 weeks of age) WT mice, and this resulted in a higher and faster teratoma formation after treatment with doxycycline, as compared with *i4F* MEFs injected into young (10 weeks of age) WT mice (fig. S6B). Together, these results indicate that senescent tissue environments, such as those associated with exogenously induced tissue damage or with aging, favor in vivo reprogramming.

Discussion

Here, we provide insight into the mechanism of in vivo reprogramming. We show that, apart from inducing cellular reprogramming, OSKM produces damage and senescence in many other cells. Damaged cells secrete signals that strongly promote in vivo reprogramming in neighboring cells. This process is mediated by the induction of cellular senescence and the ensuing production of cytokines, with IL-6 being of particular relevance. It is well established that *Ink4a/Arf*, DNA damage, and short telomeres are intrinsic barriers for in vitro reprogramming and, accordingly, in vitro reprogramming efficiency decreases in aged cells (*7*, *8*, *36*). In vivo, however, *Ink4a/Arf*, DNA damage, and short telomeres play an additional positive and dominant extrinsic role in reprogramming by creating a senescent tissue context that strongly promotes reprogramming through the production of factors, such as IL-6. In the absence of p53, OSKM-induced damage is unrestrained and the secretory activity of damaged cells is markedly exacerbated. Therefore, p53 is a strong barrier for reprogramming through both intrinsic and extrinsic mechanisms. We have also uncovered a number of pharmacologically actionable targets that can modulate in vivo reprogramming. Finally, there is growing support for the hypothesis that tissue damage can provoke cellular plasticity conducive to tissue repair (*37*). In this context, our results suggest that senescence may contribute to reprogramming-like cellular plasticity upon tissue damage.

Materials and methods

Reprogrammable mice

To generate reprogrammable mice combined with null alleles for *p53*, *Ink4a/Arf*, or *Terc*, we used the reprogrammable mouse line known as *i4F*-B, which carries a ubiquitous doxycycline-inducible *OSKM* transgene, abbreviated as *i4F*, and inserted into the *Pparg* gene (*3*). Reprogrammable *i4F*-B mice were crossed with mice deficient in *p53* (*38*), *Ink4a/Arf* (*39*), or *Terc* (*33*). The *i4F;p53*-null and *i4F;Ink4a/Arf*-null mice are in a pure C57BL/6J.Ola.Hsd genetic background and were compared to *i4F* mice of the same genetic background; the *i4F;Terc*-null mice are in a mixed genetic background enriched for C57BL/6J.Ola.Hsd and were compared to *i4F* mice of the same mixed genetic background derived from the same parental mice.

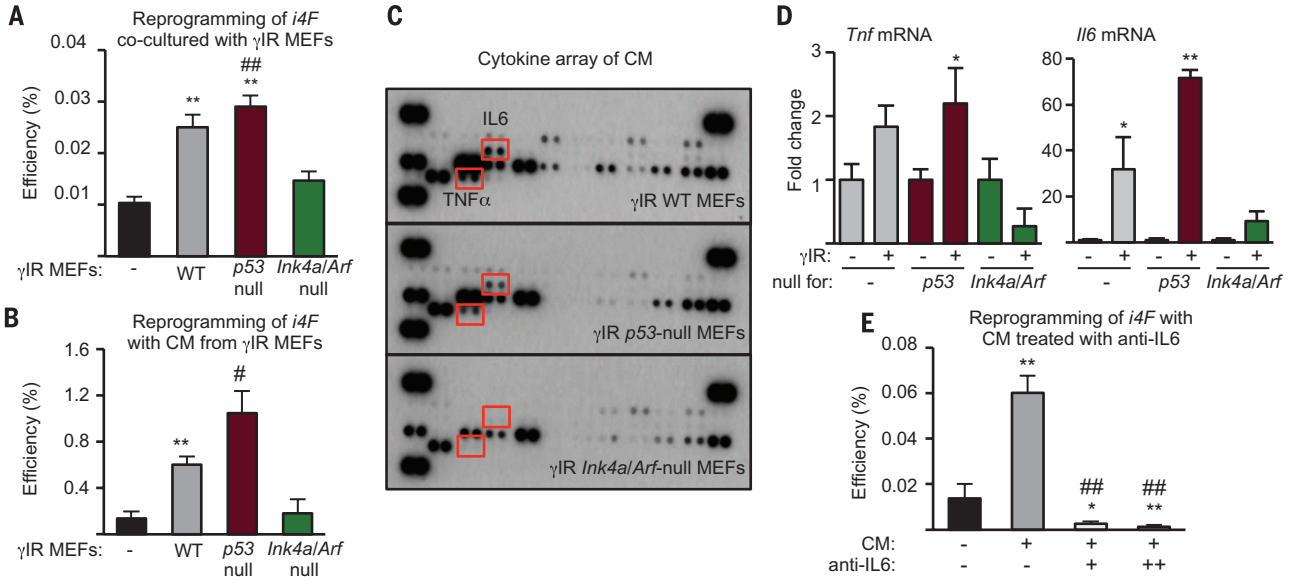

Fig. 4. Senescence enhances in vitro reprogramming. (**A**) Reprogramming efficiency of *i4F* MEFs cocultured with γ-irradiated (γIR) MEFs (ratio, 1:3) from the indicated genotypes. (**B**) Reprogramming efficiency of *i4F* MEFs treated with CM from γ-irradiated MEFs from the indicated genotypes. CM was collected every day for 3 days after γ-irradiation. (**C**) Cytokine profile of the CM from γ-irradiated MEFs of the indicated genotypes. All cytokines are detected in duplicate. IL-6 and TNFα are marked with red rectangles. (**D**) *Tnf* and *Il6* mRNA levels in nonirradiated and γ-irradiated MEFs of the indicated genotypes at day 3 after γ-irradiation. (**E**) Reprogramming efficiency of *i4F* MEFs treated with CM from γ-irradiated WT MEFs in the absence or presence of increasing amounts of anti–IL-6 (+, 0.03 mg of antibodies per milliliter of CM; ++, 0.1 mg of antibodies per milliliter of CM). In (A) to (E), graphs represent average ± SD; statistical significance relative to control was assessed by the two-tailed Student's *t* test with Welch's correction. A total of three biological replicates were performed, each with independent MEF isolates ($n = 3$). In (A) and (B), comparisons of each genotype of γ-irradiated MEFs to the non–γ-irradiated control are indicated as follows: $^*P < 0.05$; $^{**}P < 0.01$. Comparisons of γ-irradiated *p53*-null or γ-irradiated *Ink4a/Arf*-null with γ-irradiated WT MEFs are indicated in the same manner but using the symbol "#." In (D), comparisons of each genotype with its own non–γ-irradiated control are indicated as follows: $^*P < 0.05$; $^{**}P < 0.01$. In (E), comparisons of each condition to the control without CM are indicated as follows: $^*P < 0.05$; $^{**}P < 0.01$. Comparisons of each condition to the control without anti–IL-6 are indicated in the same manner but using the symbol "#."

Animal procedures

Animal experimentation at the CNIO, Madrid, was performed according to protocols approved by the CNIO-ISCIII Ethics Committee for Research and Animal Welfare (CEIyBA). To check the proper induction of the *OSKM* transgene, mice of the three genotypes, *i4F*, *i4F;p53*-null, and *i4F;Ink4a/Arf*-null, were intraperitoneally injected with 500 µl of doxycycline (4 mg/ml; Sigma) dissolved in physiological serum (0.9% w/v NaCl). After 9 hours, mice were sacrificed and samples were taken for analysis. In general, mice of 10–13 weeks of age of both sexes were treated with 0.2 mg/ml doxycycline in the drinking water (supplemented with 7.5% sucrose) for 7 days. For the simultaneous treatment with chemicals (except in the case of palbociclib), mice were treated with the corresponding inhibitor (see *Chemical treatments*) and with 1 mg/ml of doxycycline in the drinking water for 7 days. In the case of palbociclib, doxycycline was administered by intraperitoneal injection (500 µl of doxycycline 2 mg/ml dissolved in physiological serum every second day for 5 days) to avoid severe dysplasia in the colon. In the case of the *i4F;G2Terc*-null mice and bleomycin-treated mice, together with their corresponding controls, treatment with 0.2 mg/ml of doxycycline was performed for 2 weeks. For the reprogramming experiment in aged mice, we used old *i4F* mice that were >65 weeks old and young *i4F* mice that were 7–9 weeks old. For proliferation analysis, bromodeoxyuridine (5-bromo-2′-deoxyuridine), purchased from Sigma #B5002, was daily injected intraperitoneally at 50 µg/g during the first 5 days of treatment. For survival analyses (death due to teratomas and death due to tumors), *i4F*, *i4F;p53*-het, and *i4F;Ink4a/Arf*-het mice, together with their respective non-reprogrammable controls, were treated with 0.2 mg/ml of doxycycline for 8 days, at the age of 20–28 weeks. Mice were monitored and sacrificed and the cause of death was determined by histological analysis.

Teratoma formation by exogenous MEFs

The kidney was the only location where injected reprogrammable MEFs produced teratomas upon doxycycline treatment, which could be related to the reported permissivity of the kidney to the transplantation of differentiated iPSCs (*40*) (the other locations that we tested and did not produce teratomas were liver, spleen, muscle, dermis, and intraperitoneal). For teratoma formation in the kidney, MEFs of the three genotypes (*i4F*, *i4F;p53*-null, and *i4F;Ink4a/Arf*-null) were trypsinized and 5×10^5 cells, resuspended in iPSC medium (see below), were injected into the kidney of wild-type C57BL/6J, nude (Hsd: athymic Nude/Nude from Harlan Ibérica) and NSG (NOD.Cg-*Prkdc*^{scid} *Il2rg*^{tm1Wjl}/SzJ from Charles River) mice of 10 weeks of age, previously treated for 10 days with 2 mg/ml of doxycycline. We used C57BL/6J mice of > 95 weeks of age for the teratoma formation in old hosts. After injection, mice were treated for 14 days with the same dose of doxycycline. Mice were sacrificed when teratomas were palpable and teratomas were processed for histological analysis.

Teratoma formation by exogenous iPSCs

For subcutaneous teratomas, iPSCs were trypsinized and 1×10^6 cells were subcutaneously injected into the flanks of athymic nude mice (Hsd: athymic Nude/Nude; Harlan Ibérica). Teratomas were isolated when the diameter reached >1.5 cm and processed for histological analysis.

Isolation of iPSCs from the blood

Whole peripheral blood was collected directly from the heart of doxycycline-induced *i4F*, *i4F;p53*-null and *i4F;Ink4a/Arf*-null mice at the time of necropsy, and was subjected to two rounds of erythrocyte lysis in ammonium chloride solution (Stem Cells). First round of lysis with 10 ml, for 15 min r.t., followed by centrifugation, and a second round of lysis with 3 ml, for 15 min at r.t., followed by neutralization with 12 ml of iPSC medium. Cells were resuspended, plated on feeders and cultured in iPSC medium in the absence of doxycycline.

Chemical treatments of the mice

Treatment of *i4F* mice with the Bcl-2/Bcl-xL/Bcl-w–inhibitor navitoclax, also known as ABT263 (Active Biochem, #A-100) (*19*, *20*), was performed by daily oral gavage for 7 days at 25 mg/kg, dissolved in 15% DMSO/PEG400. Treatment with the CDK4/CDK6 inhibitor palbociclib, also known as PD033299 (Selleckchem #S1579) (*22*), was performed by oral gavage for 5 days at 100 mg/kg, dissolved in 50 mM sodium lactate. Treatment with the inhibitor of NFκB-activating kinases IKKs, also known as BAY 11–7082 (Selleck Chemicals, S2913) (*25*), was performed by daily intraperitoneal injection during one week at 20 µg/g, dissolved in 10% DMSO/PBS. For inhibition of IL-6, we intraperitoneally injected 1 mg of an anti–IL-6 antibody (BioXCell, BE0046) formulated in PBS, three times per week to the *i4F* mice and daily

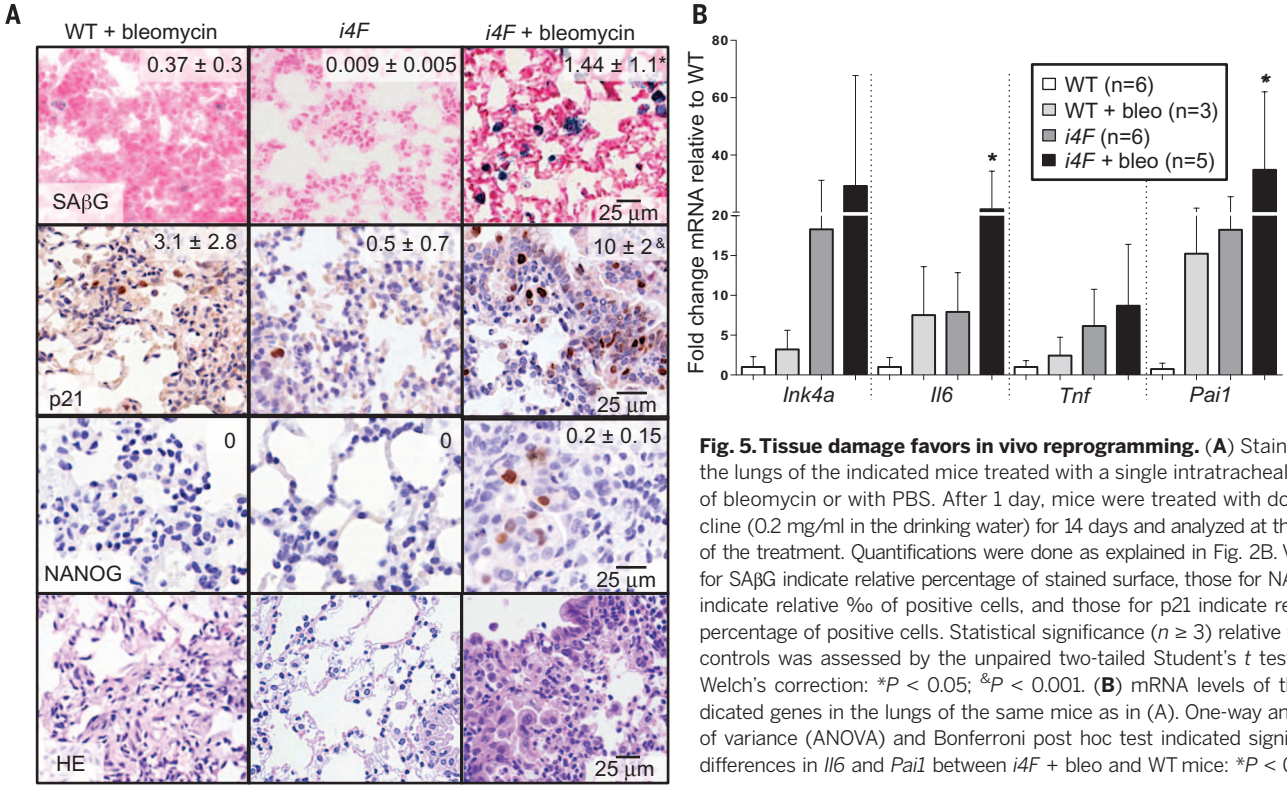

Fig. 5. Tissue damage favors in vivo reprogramming. (**A**) Staining of the lungs of the indicated mice treated with a single intratracheal dose of bleomycin or with PBS. After 1 day, mice were treated with doxycycline (0.2 mg/ml in the drinking water) for 14 days and analyzed at the end of the treatment. Quantifications were done as explained in Fig. 2B. Values for SAβG indicate relative percentage of stained surface, those for NANOG indicate relative ‰ of positive cells, and those for p21 indicate relative percentage of positive cells. Statistical significance ($n \geq 3$) relative to *i4F* controls was assessed by the unpaired two-tailed Student's *t* test with Welch's correction: $^{*}P < 0.05$; $^{\&}P < 0.001$. (**B**) mRNA levels of the indicated genes in the lungs of the same mice as in (A). One-way analysis of variance (ANOVA) and Bonferroni post hoc test indicated significant differences in *Il6* and *Pai1* between *i4F* + bleo and WT mice: $^{*}P < 0.05$.

to the *i4F;p53-null* mice, during one week. For treatment with recombinant IL-6 (ABYNTEK BIOPHARMA, S.L, #AI081) mice were intraperitoneally injected with 5 μg of rIL-6 every other day, over the course of 6 days. Treatment with the PIM inhibitor was performed by daily oral gavage for 7 days at 50 mg/kg, dissolved in 10% NMP (N-methylpyrrolidone)/90% PEG300. PIMi was developed at CNIO; for a detailed description, see the supplementary text. Control mice were treated with the corresponding vehicle. All mice were simultaneously treated with 1 mg/ml of doxycycline in the drinking water during the indicated time of treatment with the drugs, except in the case of palbociclib, in which mice were intraperitoneally injected with 500 μl of doxycycline (2 mg/ml) dissolved in physiological serum every second day for 5 days. To induce pulmonary damage, bleomycin (Sigma #15361) was inoculated intratracheally in *i4F* mice at 2U/kg in males and 1.5U/kg in females and the following day mice were treated with doxycycline (0.2 mg/ml) for 14 days.

Cell culture

Primary MEFs were obtained from embryos at E13.5 and cultured in DMEM supplemented with 10% of FBS and penicillin-streptomycin. IPSCs were cultured over mitomycin-C inactivated feeder cells on gelatin-coated plates and in "iPSC medium": high-glucose DMEM supplemented with KSR (15%, Invitrogen), LIF (1000 U ml^{-1}), non-essential amino acids, penicillin-streptomycin, Glutamax and β-mercaptoethanol. Cultures were routinely tested for mycoplasma and were always negative. For retroviral transduction, we transfected HEK293T (5×10^6) cells with retroviral vectors expressing mouse shRNA against *Ink4a*, *Arf* and *Ink4a/Arf*, and the corresponding empty vector LMP, all kindly provided by Scott Lowe (*41*), and packaging vectors using Fugene HD (Roche). Viral supernatants were collected twice

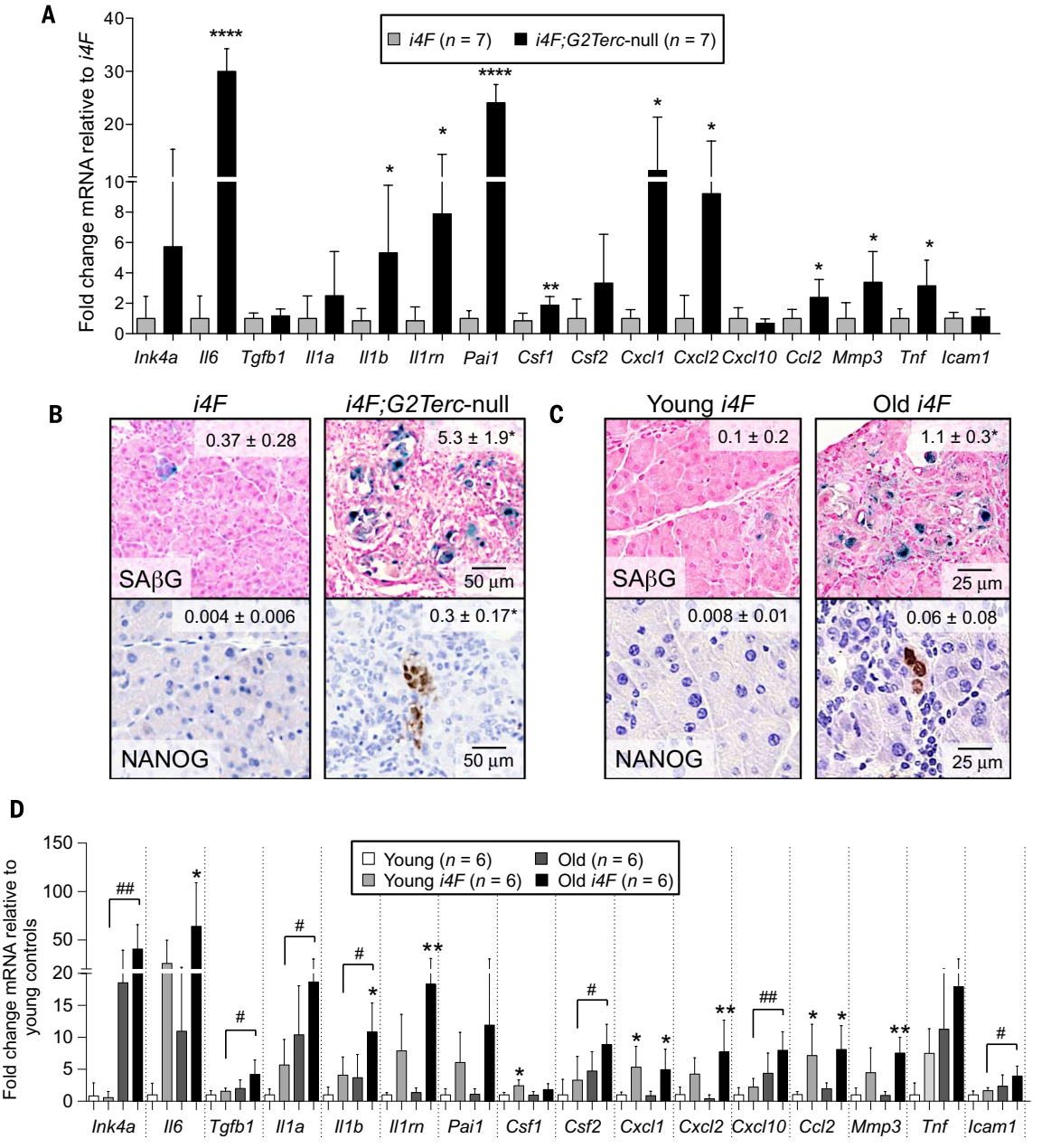

Fig. 6. Aging promotes in vivo reprogramming. (**A**) mRNA levels of the indicated genes in the pancreas of *i4F* and *i4F;G2Terc*-null mice treated with doxycycline (0.2 mg/ml in the drinking water) for 14 days and analyzed at the end of the treatment. Statistical significance relative to control was assessed by the unpaired two-tailed Student's *t* test with Welch's correction: $*P < 0.05$; $**P < 0.01$; $****P < 0.0001$. (**B**) Stainings of the pancreas of the same mice shown in (A). Quantifications were done as explained in Fig. 2B. Images are representative of at least four mice ($n \geq 4$). (**C**) Stainings of the pancreas of young (7 to 9 weeks) and old (>65 weeks) *i4F* mice treated with doxycycline (0.2 mg/ml in the drinking water) for 7 days and analyzed at the end of the treatment. Images are representative of at least three mice ($n \geq 3$). (**D**) mRNA levels of the indicated genes in the pancreas of the same mice shown in (C). Statistical significance was evaluated using one-way ANOVA and Bonferroni post-hoc test. Comparisons of each *i4F* genotype with its own control are indicated as $*P < 0.05$ and $**P < 0.01$. Comparisons of old *i4F* to young *i4F* are indicated in the same manner but with the symbol "#". Values in (A) to (D) correspond to average ± SD. In (B) and (C), values for SAβG indicate relative percentage of stained surface, and those for NANOG indicate relative ‰ of positive cells.

a day on two consecutive days starting 36 h after transfection and were used to infect WT MEFs, previously plated at a density of 8×10^5 cells per 10 cm plates. Previous to infection, polybrene was added to the viral supernatants at a concentration of 8 μg/ml. For in vitro reprogramming, *i4F*, *i4F;p53*-null and *i4F;Ink4a/Arf*-null MEFs were plated at a density of 3×10^5 cells per well in 6-well gelatin-coated plates and were cultured in iPSC medium with doxycycline (1 μg/ml). Medium was changed every 48 h. Reprogramming plates were stained for alkaline phosphatase activity (AP detection kit, Sigma Aldrich) and AP^+ colonies were scored. For co-culture reprogramming experiments, 3×10^5 γ-irradiated MEFs (20 Gy) were plated in 35-cm-diameter plates and, on top of them, 1×10^5 *i4F* MEFs of the three studied genotypes were plated. For in vitro reprogramming with conditioned medium (CM) from γ-irradiated MEFs, *i4F* MEFs were cultured in iPSC medium or CM with doxycycline (1 μg/ml) for 14 days. To produce the CM, 1.5×10^6 of γ-irradiated MEFs (20 Gy) were plated in 10-cm-diameter gelatin-coated plates, and cultured in 10 ml of iPSC medium. The medium was collected and filtered (0.22 μm) everyday for 3 days. CM preparations were used freshly or stored frozen at −20°C. To block IL-6 during in vitro reprogramming, anti–IL-6 antibody (BioXCell, BE0046) or control IgG (Santa Cruz Biotechnology sc-2027) were added to the CM at 0.1 mg/ml or 0.03 mg/ml.

Cytokine array

Cytokine levels in conditioned medium (CM) were analyzed using the Mouse Cytokine Array (ProteomeProfiler mouse Cytokine Array Panel A from R&D Systems), following the manufacturer's instructions. Pixel density was determined using the Image J Software.

Determination of cytokine levels in serum

Cytokine levels in serum were analyzed using the BD Cytometric Bead Array (CBA) Mouse Soluble Protein Master Buffer Kit from BD (#558266), following the manufacturer's instructions. For IL-6 and TNF detection, specific Mouse Flex Sets from BD were used (#558301 and #558299, respectively). Fluorescence beads detection was determined by Flow Cytometry using the FACS-Canto II Cytometer.

RNA-seq methods

Total RNA from pancreas was extracted from *i4F*, *i4F;p53*-null and *i4F;Ink4a/Arf*-null mice (n = 5 per genotype). Samples of total RNA (1 μg/ml) with RNA Integrity Numbers in the range 7.4 to 9.4 (Agilent 2100 Bioanalyzer) were used. PolyA+ fraction was purified and randomly fragmented, converted to double stranded cDNA and processed through subsequent enzymatic treatments of end-repair, dA-tailing, and ligation to adapters, following Illumina's "TruSeq Stranded mRNA Sample Preparation Part # 15031047 Rev. D" protocol. Adapter-ligated library was completed by PCR with Illumina PE primers (8 cycles). The resulting purified cDNA library was applied to an Illumina flow cell for cluster generation and sequenced on an Illumina HiSeq2000, following manufacturer's protocols. The complete set of reads has been deposited in the GEO repository (accession number GSE77722). Reads were aligned to the mouse genome (GRCm38/mm10) with TopHat-2.0.4 (*42*) using Bowtie 0.12.7 (*43*) and Samtools 0.1.16 (*44*), allowing two mismatches and five multihits. Estimation of transcript abundances and differential expression were calculated with Cufflinks 1.3.0 (*42*) using the mouse genome annotation data set GRCm38/mm10 from the UCSC Genome Browser. GSEA (*45*) was used to perform a gene set enrichment analysis of Reactome, NCI and KEGG pathways. RNA-seq gene list preranked by statistic was used, setting 'gene set' as the permutation method and we run it with 1000 permutations. Only those gene sets with significant enrichment levels (FDR q-value<0.05) were considered.

Analysis of mRNA levels

Total RNA was extracted from MEFs with Trizol (Invitrogen), following the provider's recommendations. For pancreas samples, total RNA was isolated by acid guanidinium thiocyanate-phenol-chloroform extraction. Up to 5 μg of total RNA was reverse transcribed into cDNA using iScript™ Advanced cDNA Synthesis Kit for RT-qPCR (BioRad #172-5038). Quantitative real time-PCR was performed using GoTaq® qPCR Master Mix (Promega #A6002) in a QuantStudio 6 Flex thermocycler (Applied Biosystem). Primers used are listed in Table 1. For input normalization, we used the housekeeping gene *Actin*.

Immunohistochemistry

Tissue samples were fixed in 10% neutral buffered formalin (4% formaldehyde in solution), paraffin-embedded and cut in 3 μm sections, which were mounted in superfrost®plus slides and dried. For different staining methods slides were deparaffinized in xylene and re-hydrated through a series of graded ethanol until water. Serial sections were stained with hematoxylin and eosin (HE) and Masson's trichrome staining was used to assess the presence of fibrotic areas in the lungs. For immunohistochemistry, an automated immunostaining platform was used (Ventana discovery XT, Roche). Antigen retrieval was first performed with high pH buffer (CC1m, Roche), endogenous peroxidase was blocked and slides were then incubated with the appropriate primary antibodies as detailed: NANOG (Cell Signalling Technology, 8822); p65 (NFκB) (Santa Cruz Biotechnology, sc-372); phosphorylated STAT3 (Tyr705) (Cell Signalling Technology, 9145); phosphorylated SMAD2 (phospho-Ser465 and phospho-Ser467) (Cell Signaling Technology, 3101); p21 (HUGO-291 CNIO); F4/80 (D10, CNIO); phosphorylated histone 2A.X (Ser139) (Millipore, 05–636); activated caspase-3 (Cell Signalling Technology, 9661); MYC (Abcam, ab32072) and bromodeoxyuridine (GE Healthcare, RPN202). After the primary antibody, slides were incubated with the corresponding secondary antibodies and visualization systems (OmniRabbit, Ventana, Roche) conjugated with horseradish peroxidase (Chromomap, Ventana, Roche). Immunohistochemical reaction was developed using 3,30-diaminobenzidine tetrahydrochloride (DAB) as a chromogen and nuclei were counterstained with hematoxylin. Finally, the slides were dehydrated, cleared and mounted with a permanent mounting medium for microscopic evaluation. Whole digital slides were acquired with a slide scanner (Mirax Scan, Zeiss), and images captured with the Pannoramic Viewer Software (3DHISTECH). Image analysis

Table 1. List of primers used for mRNA expression analyses.

	Forward primer	Reverse primer
Actin	5′-GGCACCACACCTTCTACAATG-3′	5′-GTGGTGGTGAAGCTGTAGCC-3′
Arf	5′-GCCGCACCGGAATCCT-3′	5′-TTGAGCAGAAGAGCTGCTACGT-3′
Ccl2	5′-TCTCTCTTCCTCCACCACCA-3′	5′-TCATTGGGATCATCTTGCTG-3′
Csf1	5′-TGCTAGGGGTGGCTTTAGG-3′	5′-CAACAGCTTTGCTAAGTGCTCTA-3′
Csf2	5′-GGGCAATTTCACCAAACTCA-3′	5′-ATGAAATCCGCATAGGTGGT-3′
Cxcl1	5′-AGCCACACTCAAGAATGGTC-3′	5′-GTCAGAAGCCAGCGTTCAC-3′
Cxcl2	5′-CTCAAGGGCGGTCAAAAAGT-3′	5′-TTTTTCTTTCTCTTTGGTTCTTCC-3′
Cxcl10	5′-AAGTGCTGCCGTCATTTTCT-3′	5′-TATGGCCCTCATTCTCACTG-3′
Icam1	5′-CTGTTTGAGCTGAGCGAGAT-3′	5′-AGGGTGAGGTCCTTGCCTAC-3′
Il1a	5′-AAGTCTCCAGGGCAGAGAGG-3′	5′-CTGATTCAGAGAGAGATGGTCAA-3′
Il1b	5′-AAAAGCCTCGTGCTGTCG-3′	5′-AGGCCACAGGTATTTTGTCG-3′
Il1rn	5′-TTGTGCCAAGTCTGGAGATG-3′	5′-GTTGTGCAGAGGAACCATCC-3′
Il6	5′-GTTCTCTGGGAAATCGTGGA-3′	5′-GGTACTCCAGAAGACCAGAGGA-3′
Ink4a	5′-TACCCCGATTCAGGTGAT-3′	5′-TTGAGCAGAAGAGCTGCTACGT-3′
Mmp3	5′-CGGGGAGAAGTCCTGTTTTT-3′	5′-GGAAGAGATGGCCAAAATGA-3′
Oct4 (total)	5′-GTTGGAGAAGGTGGAACCAA-3′	5′-CCAAGGTGATCCTCTTCTGC-3′
Pai1	5′-CCAACATCTTGGATGCTGAA-3′	5′-GCCAGGGTTGCACTAAACAT-3′
Tgfb1	5′-TGCGCTTGCAGAGATTAAAA-3′	5′-CTGCCGTACAACTCCAGTGA-3′
Tnf	5′-GCCTCTTCTCATTCCTGCTT-3′	5′-CTCCTCCACTTGGTGGTTTG-3′

and quantification was performed in a completely automated manner using the AxioVision software package (Zeiss). For each staining, several slides were quantified per mouse (at least 3 mice per group).

SAβG staining of histological sections

For pancreas samples, SAβG staining was performed in tissue cryosections preserved in OCT freezing medium using the Senescence β-Galactosidase Staining Kit (Cell Signaling, #9860). Briefly, 12-μm tissue cryosections were fixed at room temperature for 5 min, with a solution containing 2% formaldehyde and 0.2% glutaraldehyde in PBS, washed three times with PBS, and incubated 48 h at 37°C with the staining solution containing X-gal in N-N-dimethylformamide (pH 6.0). Sections were counterstained with nuclear fast red. For stomach samples, whole-mount SAβG staining was performed. Tissue samples were fixed with the same fixative solution for 45 min and then washed and incubated for 24 h at 37°C with the staining solution. After incubation, tissues were dehydrated for 30 min with 50% ethanol and overnight with 70% ethanol, after which they were paraffin-embedded. Image analysis and quantification was performed in a completely automated manner as indicated above for the immunohistochemistry.

Statistical methods

Samples (cells or mice) were allocated to their experimental groups according to their predetermined type (cell type or mouse genotype) and therefore there was no randomization. Investigators were not blinded to the experimental groups (cell types or mouse genotypes). Quantitative PCR data were obtained from independent biological replicates (n values correspond to the biological replicates, that is number of mice or number of independent MEF preparations; technical replicates of the PCR were not considered in the n value). Statistical significance was assessed using Student's t-test (two-tailed, unpaired) with Welch's correction, Fisher's exact test (two-tailed), or one-way ANOVA with Bonferroni post-hoc test, as indicated in the figure legends.

REFERENCES AND NOTES

1. D. A. Robinton, G. Q. Daley, The promise of induced pluripotent stem cells in research and therapy. *Nature* **481**, 295–305 (2012). doi: 10.1038/nature10761; pmid: 22258608
2. K. Takahashi, S. Yamanaka, Induction of pluripotent stem cells from mouse embryonic and adult fibroblast cultures by defined factors. *Cell* **126**, 663–676 (2006). doi: 10.1016/j.cell.2006.07.024; pmid: 16904174
3. M. Abad *et al*., Reprogramming in vivo produces teratomas and iPS cells with totipotency features. *Nature* **502**, 340–345 (2013). doi: 10.1038/nature12586; pmid: 24025773
4. K. Ohnishi *et al*., Premature termination of reprogramming in vivo leads to cancer development through altered epigenetic regulation. *Cell* **156**, 663–677 (2014). doi: 10.1016/j.cell.2014.01.005; pmid: 24529372
5. Y. Zhao *et al*., Two supporting factors greatly improve the efficiency of human iPSC generation. *Cell Stem Cell* **3**, 475–479 (2008). doi: 10.1016/j.stem.2008.10.002; pmid: 18983962
6. A. Banito *et al*., Senescence impairs successful reprogramming to pluripotent stem cells. *Genes Dev.* **23**, 2134–2139 (2009). doi: 10.1101/gad.1811609; pmid: 19696146
7. H. Li *et al*., The *Ink4/Arf* locus is a barrier for iPS cell reprogramming. *Nature* **460**, 1136–1139 (2009). doi: 10.1038/nature08290; pmid: 19668188
8. R. M. Marión *et al*., A p53-mediated DNA damage response limits reprogramming to ensure iPS cell genomic integrity. *Nature* **460**, 1149–1153 (2009). doi: 10.1038/nature08287; pmid: 19668189
9. T. Kawamura *et al*., Linking the p53 tumour suppressor pathway to somatic cell reprogramming. *Nature* **460**, 1140–1144 (2009). doi: 10.1038/nature08311; pmid: 19668186
10. J. Utikal *et al*., Immortalization eliminates a roadblock during cellular reprogramming into iPS cells. *Nature* **460**, 1145–1148 (2009). doi: 10.1038/nature08285; pmid: 19668190
11. H. Hong *et al*., Suppression of induced pluripotent stem cell generation by the p53–p21 pathway. *Nature* **460**, 1132–1135 (2009). doi: 10.1038/nature08235; pmid: 19668191
12. A. Freund, A. V. Orjalo, P.-Y. Desprez, J. Campisi, Inflammatory networks during cellular senescence: Causes and consequences. *Trends Mol. Med.* **16**, 238–246 (2010). doi: 10.1016/j.molmed.2010.03.003; pmid: 20444648
13. R. Salama, M. Sadaie, M. Hoare, M. Narita, Cellular senescence and its effector programs. *Genes Dev.* **28**, 99–114 (2014). doi: 10.1101/gad.235184.113; pmid: 24449267
14. J.-P. Coppé *et al*., Senescence-associated secretory phenotypes reveal cell-nonautonomous functions of oncogenic RAS and the p53 tumor suppressor. *PLOS Biol.* **6**, 2853–2868 (2008). pmid: 19053174
15. T. Kuilman *et al*., Oncogene-induced senescence relayed by an interleukin-dependent inflammatory network. *Cell* **133**, 1019–1031 (2008). doi: 10.1016/j.cell.2008.03.039; pmid: 18555778
16. J. C. Acosta *et al*., Chemokine signaling via the CXCR2 receptor reinforces senescence. *Cell* **133**, 1006–1018 (2008). doi: 10.1016/j.cell.2008.03.038; pmid: 18555777
17. C. López-Otín, M. A. Blasco, L. Partridge, M. Serrano, G. Kroemer, The hallmarks of aging. *Cell* **153**, 1194–1217 (2013). doi: 10.1016/j.cell.2013.05.039; pmid: 23746838
18. D. Muñoz-Espin, M. Serrano, Cellular senescence: From physiology to pathology. *Nat. Rev. Mol. Cell Biol.* **15**, 482–496 (2014). doi: 10.1038/nrm3823; pmid: 24954210
19. J. Chang *et al*., Clearance of senescent cells by ABT263 rejuvenates aged hematopoietic stem cells in mice. *Nat. Med.* **22**, 78–83 (2016). doi: 10.1038/nm.4010; pmid: 26657143
20. Y. Zhu *et al*., Identification of a novel senolytic agent, navitoclax, targeting the Bcl-2 family of anti-apoptotic factors. *Aging Cell* **15**, 428–435 (2015). doi: 10.1111/acel.12445; pmid: 26711051
21. R. Yosef *et al*., Directed elimination of senescent cells by inhibition of BCL-W and BCL-XL. *Nat. Commun.* **7**, 11190 (2016). doi: 10.1038/ncomms11190; pmid: 27048913
22. M. A. Dickson, Molecular pathways: CDK4 inhibitors for cancer therapy. *Clin. Cancer Res.* **20**, 3379–3383 (2014). doi: 10.1158/1078-0432.CCR-13-1551; pmid: 24795392
23. Y. Chien *et al*., Control of the senescence-associated secretory phenotype by NF-κB promotes senescence and enhances chemosensitivity. *Genes Dev.* **25**, 2125–2136 (2011). doi: 10.1101/gad.17276711; pmid: 21979375
24. A. Freund, C. K. Patil, J. Campisi, p38MAPK is a novel DNA damage response-independent regulator of the senescence-associated secretory phenotype. *EMBO J.* **30**, 1536–1548 (2011). doi: 10.1038/emboj.2011.69; pmid: 21399611
25. A. V. Gasparian *et al*., Targeting transcription factor NFκB: Comparative analysis of proteasome and IKK inhibitors. *Cell Cycle* **8**, 1559–1566 (2009). doi: 10.4161/cc.8.10.8415; pmid: 19372735
26. J. C. Acosta *et al*., A complex secretory program orchestrated by the inflammasome controls paracrine senescence. *Nat. Cell Biol.* **15**, 978–990 (2013). doi: 10.1038/ncb2784; pmid: 23770676
27. J. J. Brady *et al*., Early role for IL-6 signalling during generation of induced pluripotent stem cells revealed by heterokaryon RNA-Seq. *Nat. Cell Biol.* **15**, 1244–1252 (2013). doi: 10.1038/ncb2835; pmid: 23995732
28. M. Narlik-Grassow, C. Blanco-Aparicio, A. Carnero, The PIM family of serine/threonine kinases in cancer. *Med. Res. Rev.* **34**, 136–159 (2014). doi: 10.1002/med.21284; pmid: 23576269
29. K. Kim, J. H. Kim, B. U. Youn, H. M. Jin, N. Kim, Pim-1 regulates RANKL-induced osteoclastogenesis via NF-κB activation and NFATc1 induction. *J. Immunol.* **185**, 7460–7466 (2010). doi: 10.4049/jimmunol.1000885; pmid: 21068407
30. K. Nihira *et al*., Pim-1 controls NF-κB signalling by stabilizing RelA/p65. *Cell Death Differ.* **17**, 689–698 (2010). doi: 10.1038/cdd.2009.174; pmid: 19911008
31. K. Aoshiba, T. Tsuji, A. Nagai, Bleomycin induces cellular senescence in alveolar epithelial cells. *Eur. Respir. J.* **22**, 436–443 (2003). doi: 10.1183/09031936.03.00011903; pmid: 14516132
32. K. Aoshiba *et al*., Senescence-associated secretory phenotype in a mouse model of bleomycin-induced lung injury. *Exp. Toxicol. Pathol.* **65**, 1053–1062 (2013). doi: 10.1016/j.etp.2013.04.001; pmid: 23688655
33. M. A. Blasco *et al*., Telomere shortening and tumor formation by mouse cells lacking telomerase RNA. *Cell* **91**, 25–34 (1997). doi: 10.1016/s0092-8674(01)80006-4; pmid: 9335332
34. I. García-Cao *et al*., Increased p53 activity does not accelerate telomere-driven ageing. *EMBO Rep.* **7**, 546–552 (2006). doi: 10.1038/sj.embor.7400667; pmid: 16582880
35. J. Krishnamurthy *et al*., *Ink4a/Arf* expression is a biomarker of aging. *J. Clin. Invest.* **114**, 1299–1307 (2004). doi: 10.1172/JC122475; pmid: 15520862
36. C. Soria-Valles, C. López-Otín, iPSCs: On the road to reprogramming aging. *Trends Mol. Med.* **22**, 713–724 (2016). doi: 10.1016/j.molmed.2016.05.010; pmid: 27286740
37. K. R. Jessen, R. Mirsky, P. Arthur-Farraj, The role of cell plasticity in tissue repair: Adaptive cellular reprogramming. *Dev. Cell* **34**, 613–620 (2015). doi: 10.1016/j.devcel.2015.09.005; pmid: 26418293
38. T. Jacks *et al*., Tumor spectrum analysis in *p53*-mutant mice. *Curr. Biol.* **4**, 1–7 (1994). doi: 10.1016/S0960-9822(00)00002-6; pmid: 7922305
39. M. Serrano *et al*., Role of the *INK4a* locus in tumor suppression and cell mortality. *Cell* **85**, 27–37 (1996). doi: 10.1016/S0092-8674(00)81079-X; pmid: 8620534
40. X. Fu, The immunogenicity of cells derived from induced pluripotent stem cells. *Cell. Mol. Immunol.* **11**, 14–16 (2014). doi: 10.1038/cmi.2013.60; pmid: 24336164
41. R. A. Dickins *et al*., Probing tumor phenotypes using stable and regulated synthetic microRNA precursors. *Nat. Genet.* **37**, 1289–1295 (2005). doi: 10.1038/ng1651; pmid: 16200064
42. C. Trapnell *et al*., Differential gene and transcript expression analysis of RNA-seq experiments with TopHat and Cufflinks. *Nat. Protoc.* **7**, 562–578 (2012). doi: 10.1038/nprot.2012.016; pmid: 22383036
43. B. Langmead, C. Trapnell, M. Pop, S. L. Salzberg, Ultrafast and memory-efficient alignment of short DNA sequences to the human genome. *Genome Biol.* **10**, R25 (2009). doi: 10.1186/gb-2009-10-3-r25; pmid: 19261174
44. H. Li *et al*., The Sequence Alignment/Map format and SAMtools. *Bioinformatics* **25**, 2078–2079 (2009). doi: 10.1093/bioinformatics/btp352; pmid: 19505943
45. A. Subramanian *et al*., Gene set enrichment analysis: A knowledge-based approach for interpreting genome-wide expression profiles. *Proc. Natl. Acad. Sci. U.S.A.* **102**, 15545–15550 (2005). doi: 10.1073/pnas.0506580102; pmid: 16199517

ACKNOWLEDGMENTS

We are grateful to R. Serrano, L. Martínez, O. Domínguez, P. González, M. Gómez, M. Udriste, Z. Vega, M. Lozano, and G. Hernández for technical support. L.M. was a recipient of an FPU contract from the Spanish Ministry of Education (MECD). N.A. was a recipient of an FPI contract from the Spanish Ministry of Economy (MINECO). D.C. and M.R. were recipients of a fellowship from La Caixa. P.J.F.-M. was funded by the Spanish Association Against Cancer (AECC). Work in the laboratory of M.S. is funded by the CNIO and by grants from the MECD cofunded by the European Regional Development Fund (SAF project), the European Research Council (ERC Advanced Grant), the Regional Government of Madrid cofunded by the European Social Fund (ReCaRe project), the European Union (RISK-IR project), the Botín Foundation and Banco Santander (Santander Universities Global Division), the Ramón Areces Foundation, and the AXA Foundation. Work in the laboratory of M.A.B. is funded by the CNIO, MINECO, ERC Advanced Grant, the European Union, the Botin Foundation, and Banco Santander, WRC, and the AXA Research Foundation. The funders had no role in study design, data collection and analysis, decision to publish, or preparation of the manuscript. M.S. is a paid adviser for UNITY Biotechnology Inc., a company developing senolytic medicines.

SUPPLEMENTARY MATERIALS

www.sciencemag.org/content/354/6315/aaf4445/suppl/DC1
Supplementary Text
Figs. S1 to S6
Reference (*46*)

9 February 2016; resubmitted 1 July 2016
Accepted 6 October 2016
10.1126/science.aaf4445

REPORTS

COLD ATOMS

An atom-by-atom assembler of defect-free arbitrary two-dimensional atomic arrays

Daniel Barredo,* Sylvain de Léséleuc,* Vincent Lienhard, Thierry Lahaye,† Antoine Browaeys

Large arrays of individually controlled atoms trapped in optical tweezers are a very promising platform for quantum engineering applications. However, deterministic loading of the traps is experimentally challenging. We demonstrate the preparation of fully loaded two-dimensional arrays of up to ~50 microtraps, each containing a single atom and arranged in arbitrary geometries. Starting from initially larger, half-filled matrices of randomly loaded traps, we obtain user-defined target arrays at unit filling. This is achieved with a real-time control system and a moving optical tweezers, which together enable a sequence of rapid atom moves depending on the initial distribution of the atoms in the arrays. These results open exciting prospects for quantum engineering with neutral atoms in tunable two-dimensional geometries.

The past decade has seen tremendous progress over the control of individual quantum objects (*1*, *2*). Many experimental platforms, including trapped ions (*3*) and superconducting qubits (*4*), are being actively explored. The current challenge is to extend these results to large assemblies of such objects while keeping the same degree of control, with a view toward applications in quantum information processing (*5*), quantum metrology (*6*), or quantum simulation (*7*). Neutral atoms offer some advantages over other systems for these tasks. Besides being well isolated from the environment and having tunable interactions, systems of cold atoms hold the promise of being scalable to hundreds of individually controlled qubits. Control of atomic positions at the single-particle level can be achieved with optical potentials. In a "top-down" approach using optical lattices and quantum gas microscopes, hundreds of traps can now be created and addressed individually (*8*). By making use of the superfluid–Mott insulator transition, single-atom filling fractions exceeding 90% are achieved (*9*), albeit at the expense of relatively long experimental duty cycles and constraints in the lattice geometries.

Single atoms can also be trapped in two-dimensional (2D) arrays of microscopic optical tweezers with single-site resolution using holographic methods (*10*–*12*). This bottom-up approach offers faster preparation and a higher degree of tunability of the underlying geometry. However, achieving unit filling of the arrays is hampered by the stochastic nature of the loading and has remained elusive. Although proof-of-principle demonstrations of quantum gates (*13*) and quantum simulations (*14*) using this latter platform have been reported (*15*), this nondeterministic loading poses a serious limitation for applications where large-scale ordered arrays are required. Several approaches have been considered to solve this problem, such as exploiting the Rydberg blockade mechanism (*16*) or using tailored light-assisted collisions (*17*). To date, despite these efforts, loading efficiencies of around 90% at best for a single atom in a single tweezers could be achieved (*18*, *19*), so the probability of fully loading large arrays would still be exponentially small.

A different approach toward this goal, pioneered in (*20*) for a few atoms and revisited recently in (*21*, *22*), consists of sorting disordered arrays of atoms by means of moving optical potentials (*23*). Here, we demonstrate the deterministic preparation of arrays as large as $N \sim 50$ individual atoms in arbitrary 2D geometries with filling fractions η up to 98%, which enables us to engineer defect-free arrays with a fast repetition rate. This is accomplished through the use of a fast programmable control system to perform sequential assembly of the atoms in the arrays. Starting from stochastically loaded half-filled arrays with ~$2N$ traps, we analyze in real time the initial atom distribution and use a fast-moving optical tweezers to rearrange the atoms into a user-defined target spatial configuration. We thus implement an atom-sorting device reminiscent of Maxwell's demon (*24*). [Only the entropy associated with the atomic positions in the arrays is removed; the (much higher) entropy associated with the motion of each atom in each trap remains unaffected.] We anticipate that this approach could be scaled up to a few hundreds of atoms, still maintaining filling fractions close to unity, as the size of the arrays we can prepare is at present mostly limited by the available laser power. These results may lead to an alternative procedure for initializing 2D arrays of single atoms for quantum simulation, using, for example, strong interactions between Rydberg states (*14*).

Our experimental setup (*25*, *26*) is shown schematically in Fig. 1A. We use a spatial light modulator (SLM) to create arbitrary 2D arrays of up to 100 traps, separated by distances $a > 3$ μm in the focal plane of a high–numerical aperture (NA = 0.5) aspheric lens. Each trap has a $1/e^2$ radius of ~1 μm and a depth of $U_0/k_B \approx 1$ mK (for a power of about 5 mW), yielding radial trapping frequencies around 100 kHz and longitudinal trapping frequencies around 20 kHz. In the single-atom regime, the traps are stochastically loaded from a magneto-optical trap with cold single ^{87}Rb atoms with a probability $p \sim 0.5$. We monitor the occupancy of the traps by observing the fluorescence of the atoms at 780 nm with a charge-coupled device (CCD) camera with a time resolution of 50 ms. For deterministic atom transport, we superimpose a second moving 850-nm laser beam on the trapping beam. This moving optical tweezers (with $1/e^2$ radius of ~1.3 μm) is controlled using a 2D acousto-optic deflector (AOD).

Figure 1B shows how we use the moving optical tweezers to extract an atom from a filled trap. We first set the horizontal and vertical AOD frequencies to position the beam at the source trap, and ramp up linearly the optical power diffracted by the AODs to reach a tweezers depth $U \sim 10U_0$ in a time τ (inset). The applied optical potential effectively captures the atom from the trap. We then steer the beam toward the target trap, at velocity v, by sweeping the vertical and horizontal AOD frequencies. Finally, we release the atom from the tweezers in the target trap. For $\tau \sim 0.3$ ms and $v \sim 10$ nm/μs, the probability of successful transfer of the atoms from the source to the target traps reaches 99.3% (*27*).

Our method of synthesizing fully loaded arrays of N atoms is sketched in Fig. 1C and works as follows: We use an array of ~$2N$ traps, which contains the target array as a subset, and load it from the magneto-optical trap. The loading of the array is stopped as soon as at least N traps are filled with single atoms, and a fluorescence image is acquired to record the initial position of the atoms. After analysis of the image, an algorithm (see below) computes in real time a list of individual atom moves that can rearrange the configuration into the desired 2D pattern. This list is then sent to microcontrollers via serial port communication. The microcontroller program converts this list into a series of voltage sweeps to control the radio-frequency drivers driving the AODs. Finally, after the rearrangement operation is completed (in about 50 ms for $N \sim 50$), a final image is acquired to reveal the new positions of the atoms in the array.

Laboratoire Charles Fabry, Institut d'Optique Graduate School, CNRS, Université Paris-Saclay, 91127 Palaiseau Cedex, France.
*These authors contributed equally to this work. †Corresponding author. Email: thierry.lahaye@institutoptique.fr

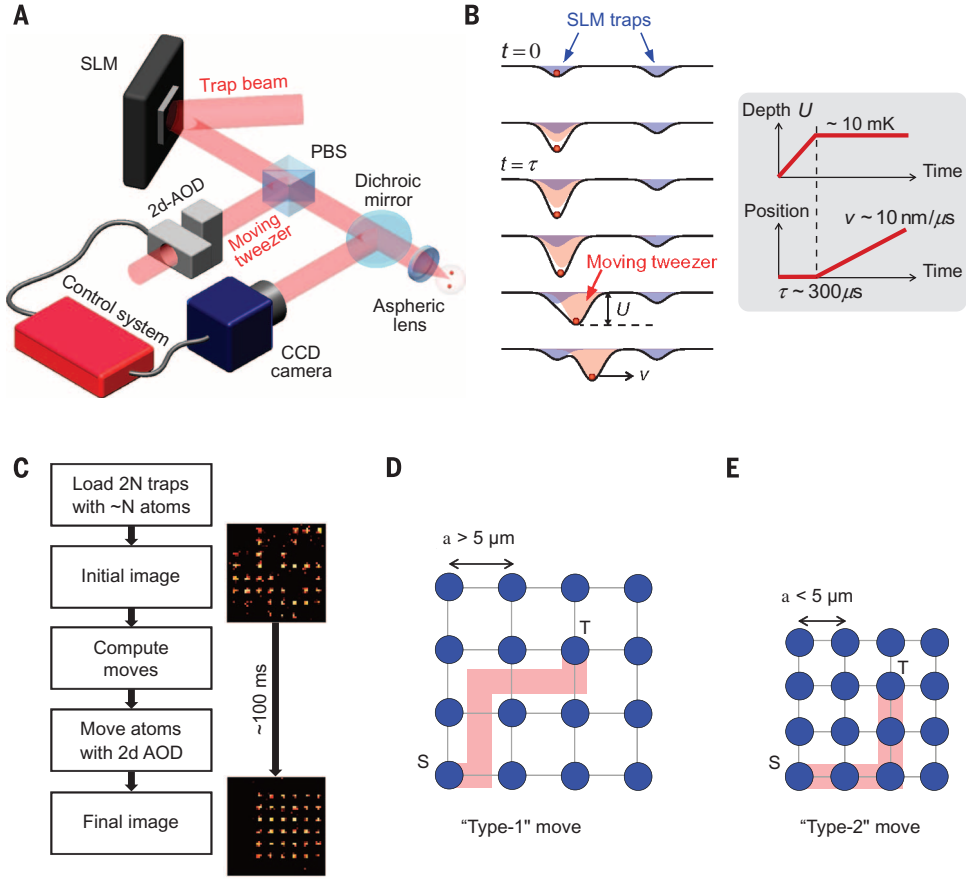

Fig. 1. Principle of the atom assembler. (**A**) Schematics of the experimental setup. Arbitrary 2D arrays of microtraps are created by using a SLM to imprint an appropriate phase onto the dipole trap beam, then focusing the beam with a high-NA aspheric lens. The moving beam is generated with a 2D AOD and superimposed on the trap beam with a polarizing beam-splitter (PBS). The CCD camera collects the fluorescence of the atoms in each trap. A control system comprising a computer, two microcontrollers, and two AOD drivers allows us to implement a series of rapid moves to reshuffle the atomic array. (**B**) Left: Extracting a single atom (red disk) from a fixed trap (blue Gaussian) with the moving optical tweezers (red Gaussian). Right: Time evolution of the moving tweezers' depth and position. (**C**) Block diagram of the control system. Depending on the initial configuration, where on average half of the traps are filled, the control system steers each atom toward its target final position. (**D** and **E**) Basic moves implemented in the atom-sorting algorithms. (D) If the nearest-neighbor distance in the array is large enough (typically, $a > 5$ μm), we move the tweezers directly from the source to the target, passing between adjacent atom rows ("type 1" moves). (E) Otherwise, the atoms are moved along the lattice links ("type 2" moves).

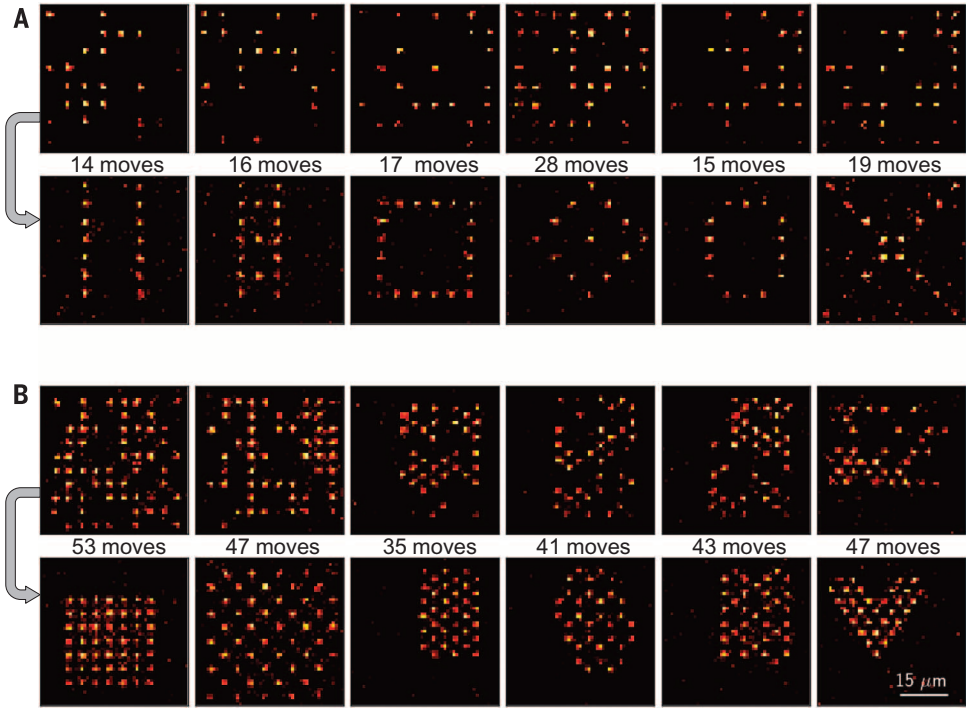

Fig. 2. Gallery of fully loaded arrays. Arbitrary, user-defined 2D arrays (bottom images) are obtained from the initial, random configurations (top images). All images are single shots. (**A**) Type 1 moves were used; (**B**) type 2 moves were used. The number of elementary moves needed to achieve the sorting are indicated.

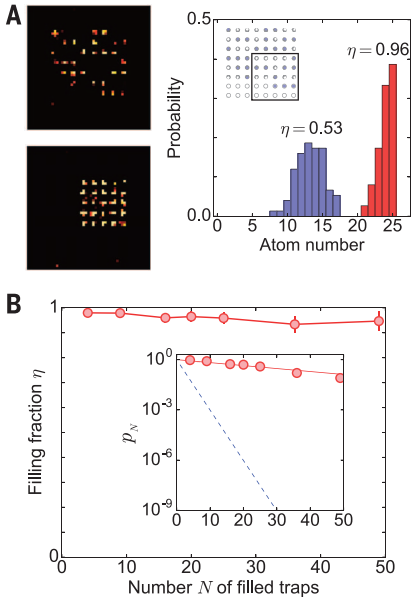

Fig. 3. Loading statistics of reordered arrays. (**A**) Left: Images of the initial and final configurations for a square array of 25 atoms. Right: Distribution of the number of atoms in the target 5 × 5 square array (black square in the inset) before sorting (blue) and after sorting (red) in 100 repetitions of the experiment. The sorted array has a filling fraction η = 96% (with a standard deviation of 4%), and defect-free arrays are obtained in ~40% of the cases. (**B**) Evolution of η as a function of the number of traps in the sorted array; data are means ± SE. Inset: Circles show the observed probability p_N of obtaining a defect-free array of N atoms; the dashed line shows the result $p_N = 2^{-N}$ corresponding to random loading.

To implement the atom-sorting shown schematically in Fig. 1C, we have used, depending on the nearest-neighbor distance a in the target arrays, two types of elementary moves to transfer an atom from a source trap to a target trap (Fig. 1, D and E). "Type 1" moves transfer an atom by moving it between other traps, which allows us to minimize the number of moves needed to assemble an array. However, type 1 moves were found to lead to atom loss in the traps close to the trajectory of the moving tweezers when $a < 5$ μm; thus, for such arrays, we used "type 2" moves, in which atoms are moved along the links of the arrays.

Choosing the best algorithm to calculate the atom moves would ideally require finding the optimal list that minimizes the number of moves and the total distance (thus minimizing the time it takes to reorder the array). In our arrays, trapped atoms have a vacuum-limited lifetime $\tau_{vac} \sim 10$ s, and the estimated lifetime of a configuration with N atoms is thus τ_{vac}/N. The total sequence should remain shorter than this to achieve high fidelities. However, finding the optimum set of paths is a difficult computational task, reminiscent of the traveling salesman problem. We have developed a heuristic path-finding algorithm, which first computes a list of all possible individual moves, and then orders it according to their length; we then select moves from source traps to target traps, starting from the shortest ones, until all target traps are filled. This results in ~N/2 moves (however, this does not necessarily minimize the total travel distance). We finally discard the unused extra atoms (if any) by moving them to positions far away from any trap. Additionally, for type 2 moves, we have to avoid moving the tweezers over filled traps (to prevent the tweezers from dragging other atoms along during its motion). We enforce this constraint in the following way: If the source atom S needs to be moved to the target trap T (we denote this move by $S \rightarrow T$) and an "obstacle" O is along the way, we replace the move $S \rightarrow T$ by the two moves $O \rightarrow T$ and $S \rightarrow O$. This increases slightly the number of needed moves, as sometimes some filled traps are "in the way," but the overhead is moderate (*27*).

For our largest arrays, the total arrangement process is typically performed within less than 50 ms after the initial image is acquired—a time scale still shorter than the lifetime of the initial configuration. Despite being quite simple and nonoptimal, our algorithm is efficient and versatile. However, finding better algorithms might be important for scaling up our approach to hundreds of atoms.

Figure 2 shows a gallery of 2D trap arrays with arbitrary, user-defined geometries relevant for quantum simulation (e.g., 1D chains, ladders, or lattices with square, triangular, honeycomb, or kagome structures). Neighboring traps are separated by distances $3 < a < 6$ μm, for which interactions in the MHz range can be achieved by exciting the atoms to Rydberg states (*14*). In (Fig. 2A), type 1 moves were used, whereas in (Fig. 2B), type 2 moves were used. For each array, we show a fluorescence image of single atoms obtained with the CCD camera at the beginning of the sequence. Because the probability for each trap to be filled is $p \sim 0.5$, the arrays are initially half-filled. In the accompanying lower image, we show the final fluorescence image after the sorting is completed. Analyzing 100 repetitions of the experiment for a 5×5 square target array (Fig. 3A), we achieve a filling fraction η > 96%, mainly limited by background gas collisions during the rearrangement (*27*). This corresponds to a probability of getting a defect-free array of about 40%. The filling fraction decreases only marginally when the number of atoms increases, showing the scalability of our approach (Fig. 3B). To achieve even higher filling fractions, one could iterate the procedure presented here by skipping the disposal of unused atoms, analyzing the "final" image, and filling in defects (if any) with remaining atoms.

Analysis of the technical limitations of the current implementation suggests that preparing hundreds of individual atoms in arrays of arbitrary geometries very close to unit filling is realistic with state-of-the-art technology (*27*). These results, possibly combined with Raman sideband cooling of atoms in optical microtraps (*28*, *29*), open promising paths to studying many-body physics in two dimensions and constitute an important resource for quantum information processing with cold neutral atoms. In the future, using the same technique, it should be possible to insert atoms one at a time into a microtrap (*30*), thus preparing small samples with an exact atom number for applications such as cold chemistry. A similar approach for one-dimensional systems is reported in (*31*).

REFERENCES AND NOTES

1. S. Haroche, *Rev. Mod. Phys.* **85**, 1083–1102 (2013).
2. D. J. Wineland, *Rev. Mod. Phys.* **85**, 1103–1114 (2013).
3. R. Islam *et al.*, *Science* **340**, 583–587 (2013).
4. R. Barends *et al.*, *Nature* **534**, 222–226 (2016).
5. M. A. Nielsen, I. L. Chuang, *Quantum Computation and Quantum Information* (Cambridge Univ. Press, 2000).
6. V. Giovannetti, S. Lloyd, L. Maccone, *Nat. Photonics* **5**, 222–229 (2011).
7. I. M. Georgescu, S. Ashhab, F. Nori, *Rev. Mod. Phys.* **86**, 153–185 (2014).
8. W. S. Bakr, J. I. Gillen, A. Peng, S. Fölling, M. Greiner, *Nature* **462**, 74–77 (2009).
9. J. Zeiher *et al.*, *Phys. Rev. X* **5**, 031015 (2015).
10. F. Nogrette *et al.*, *Phys. Rev. X* **4**, 021034 (2014).
11. M. Schlosser *et al.*, *New J. Phys.* **14**, 123034 (2012).
12. M. J. Piotrowicz *et al.*, *Phys. Rev. A* **88**, 013420 (2013).
13. L. Isenhower *et al.*, *Phys. Rev. Lett.* **104**, 010503 (2010).
14. H. Labuhn *et al.*, *Nature* **534**, 667–670 (2016).
15. A. Browaeys, D. Barredo, T. Lahaye, *J. Phys. B* **49**, 152001 (2016).
16. M. Ebert *et al.*, *Phys. Rev. Lett.* **112**, 043602 (2014).
17. T. Grünzweig, A. Hilliard, M. McGovern, M. F. Andersen, *Nat. Phys.* **6**, 951–954 (2010).
18. Y. H. Fung, M. F. Andersen, *New J. Phys.* **17**, 073011 (2015).
19. B. J. Lester, N. Luick, A. M. Kaufman, C. M. Reynolds, C. A. Regal, *Phys. Rev. Lett.* **115**, 073003 (2015).
20. Y. Miroshnychenko *et al.*, *Nature* **442**, 151 (2006).
21. W. Lee, H. Kim, J. Ahn, *Opt. Express* **24**, 9816–9825 (2016).
22. H. Kim *et al.*, *Nat. Commun.* **7**, 13317 (2016).
23. J. Beugnon *et al.*, *Nat. Phys.* **3**, 696–699 (2007).
24. D. S. Weiss *et al.*, *Phys. Rev. A* **70**, 040302(R) (2004).
25. L. Béguin, A. Vernier, R. Chicireanu, T. Lahaye, A. Browaeys, *Phys. Rev. Lett.* **110**, 263201 (2013).
26. H. Labuhn *et al.*, *Phys. Rev. A* **90**, 023415 (2014).
27. See supplementary materials on *Science* Online.
28. A. M. Kaufman, B. J. Lester, C. A. Regal, *Phys. Rev. X* **2**, 041014 (2012).
29. J. D. Thompson, T. G. Tiecke, A. S. Zibrov, V. Vuletić, M. D. Lukin, *Phys. Rev. Lett.* **110**, 133001 (2013).
30. Y. Miroshnychenko *et al.*, *Phys. Rev. Lett.* **97**, 243003 (2006).
31. M. Endres *et al.*, *Science* **354**, 1024–1027 (2016).

ACKNOWLEDGMENTS

We thank V. Josse for lending us AODs and H. Labuhn for contributions in the early stage of the experiment. Supported by European Union FET–Open Xtrack Project HAIRS and H2020 FET–PROACT Project RySQ, the "PALM" Labex (project QUANTICA), and the Région Île-de-France in the framework of DIM Nano-K.

SUPPLEMENTARY MATERIALS

www.sciencemag.org/content/354/6315/1021/suppl/DC1
Supplementary Text
Figs. S1 to S3
Movie S1

17 June 2016; accepted 7 October 2016
Published online 3 November 2016
10.1126/science.aah3778

COLD ATOMS

Atom-by-atom assembly of defect-free one-dimensional cold atom arrays

Manuel Endres,[1,2]*† Hannes Bernien,[1]* Alexander Keesling,[1]* Harry Levine,[1]* Eric R. Anschuetz,[1] Alexandre Krajenbrink,[1]‡ Crystal Senko,[1] Vladan Vuletic,[3] Markus Greiner,[1] Mikhail D. Lukin[1]

The realization of large-scale fully controllable quantum systems is an exciting frontier in modern physical science. We use atom-by-atom assembly to implement a platform for the deterministic preparation of regular one-dimensional arrays of individually controlled cold atoms. In our approach, a measurement and feedback procedure eliminates the entropy associated with probabilistic trap occupation and results in defect-free arrays of more than 50 atoms in less than 400 milliseconds. The technique is based on fast, real-time control of 100 optical tweezers, which we use to arrange atoms in desired geometric patterns and to maintain these configurations by replacing lost atoms with surplus atoms from a reservoir. This bottom-up approach may enable controlled engineering of scalable many-body systems for quantum information processing, quantum simulations, and precision measurements.

The detection and manipulation of individual quantum particles, such as atoms or photons, is now routinely performed in many quantum physics experiments (*1*, *2*); however, retaining the same control in large-scale systems remains an outstanding challenge. For example, major efforts are currently aimed at scaling up ion-trap and superconducting platforms, where high-fidelity quantum computing operations have been demonstrated in registers consisting of several qubits (*3*, *4*). In contrast, ultracold quantum gases composed of neutral atoms offer inherently large system sizes. However, arbitrary single-atom control is highly demanding, and its realization is further limited by the slow evaporative cooling process necessary to reach quantum degeneracy. Only in recent years has individual particle detection (*5*, *6*) and basic single-spin control (*7*) been demonstrated in low-entropy optical lattice systems.

Here, we demonstrate atom-by-atom assembly of large defect-free one-dimensional (1D) arrays of cold neutral atoms (*8*, *9*).

We use optical microtraps to directly extract individual atoms from a laser-cooled cloud (*10*–*12*) and employ recently demonstrated trapping techniques (*13*–*16*) and single-atom position control (*17*–*20*) to create desired atomic configurations. Central to our approach is the use of single-atom detection and real-time feedback (*17*, *20*) to eliminate the entropy associated with the probabilistic trap loading (*10*) [currently limited to 90% loading probability even with advanced techniques (*21*–*23*)]. Related to the fundamental concept of "Maxwell's demon" (*8*, *9*), this method allows us to rapidly create large defect-free arrays and, when supplemented with appropriate atom-atom interactions (*15*, *16*, *24*–*30*), provides a potential platform for scalable experiments with individually controlled neutral atoms.

The experimental protocol is illustrated in Fig. 1A. An array of 100 tightly focused optical tweezers is loaded from a laser-cooled cloud. The collisional blockade effect ensures that each individual tweezer is either empty or occupied by a single atom (*10*). A first high-resolution image yields single-atom-resolved information about the trap occupation, which we use to identify empty traps and to switch them off. The remaining occupied traps are rearranged into a regular, defect-free array, and we detect the final atom configuration with a second high-resolution image.

Our implementation relies on fast, real-time control of the tweezer positions (Fig. 1B), which we achieve by employing an acousto-optic deflector (AOD) that we drive with a multitone radio-frequency (RF) signal.

This generates an array of deflected beams, each controlled by its own RF tone (*15*, *16*). The resulting beam array is then focused into our vacuum chamber and forms an array of optical tweezers, each with a Gaussian waist of $\approx$ 900 nm, a wavelength of 809 nm, and a trap depth of $U/k_B \approx 0.9$ mK [Boltzmann constant (k_B)] that is homogeneous across the array within 2% (*31*).

The tweezer array is loaded from a laser-cooled cloud of Rubidium-87 atoms in a magneto-optical trap (MOT). After the loading procedure, we let the MOT cloud disperse and we detect the occupation of the tweezers with fluorescence imaging. Fast, single-shot, single-atom-resolved detection with 20-ms exposure is enabled by a sub-Doppler laser-cooling configuration that remains active during the remainder of the sequence (*31*) (see Fig. 2, A to C). Our fluorescence count statistics show that individual traps are either empty or occupied by a single atom (*10*, *31*), and we find probabilistically filled arrays with an average single-atom loading probability of $p \approx 0.6$ (see Figs. 2A and 3A).

The central part of our scheme involves the rearrangement procedure for assembling defect-free arrays (*31*) (see Fig. 1A). In the first step,

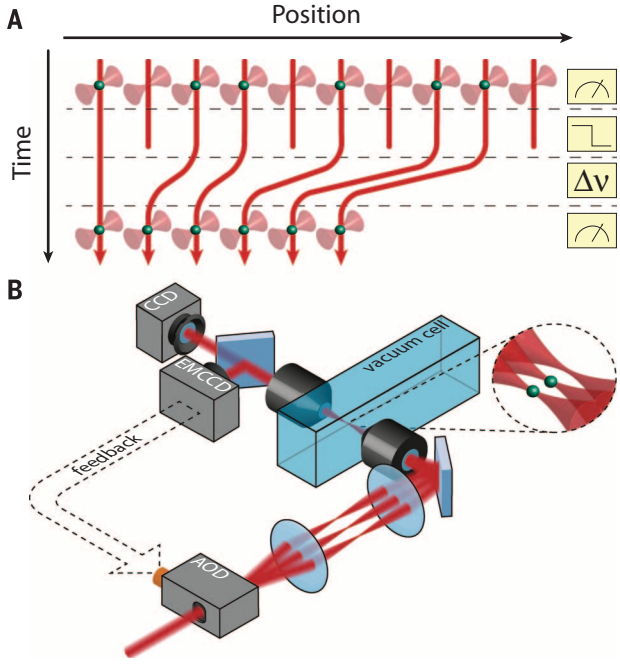

Fig. 1. Protocol for creating defect-free arrays. (**A**) A first image identifies optical microtraps loaded with a single atom, and empty traps are turned off. The loaded traps are moved to fill in the empty sites, and a second image verifies the success of the operation. (**B**) The trap array is produced by an acousto-optic deflector (AOD) and imaged with a 1:1 telescope onto a 0.5-NA microscope objective, which creates an array of tightly focused optical tweezers in a vacuum chamber. An identical microscope objective is aligned to image the same focal plane. A dichroic mirror allows us to view the trap light on a charge-coupled-device camera (CCD) while simultaneously detecting the atoms via fluorescence imaging on an electron-multiplied-CCD camera (EMCCD). The rearrangement protocol is realized through fast feedback onto the multitone radio-frequency (RF) field driving the AOD.

[1]Department of Physics, Harvard University, Cambridge, MA 02138, USA. [2]Division of Physics, Mathematics, and Astronomy, California Institute of Technology, Pasadena, CA 91125, USA. [3]Department of Physics and Research Laboratory of Electronics, Massachusetts Institute of Technology, Cambridge, MA 02139, USA.
*These authors contributed equally to this work. **†Corresponding author. Email: mendres@caltech.edu** ‡Present address: CNRS-Laboratoire de Physique Theorique de l'Ecole Normale Superieure, 24 Rue L'Homond, 75231 Paris Cedex, France.

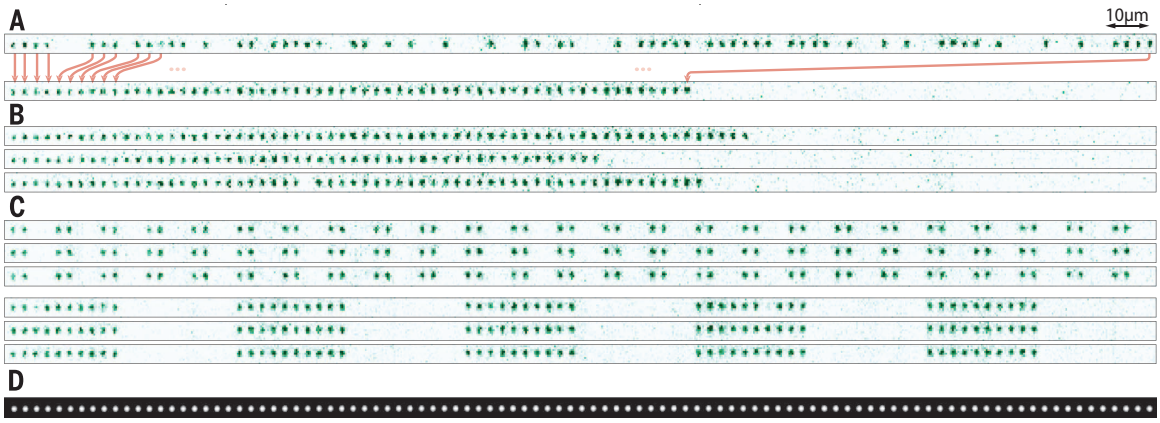

Fig. 2. Assembly of regular atom arrays. (**A**) Single-shot, single-atom-resolved fluorescence images recorded with the EMCCD before (top) and after (bottom) rearrangement. Defects are identified, and the loaded traps are rearranged according to the protocol in Fig. 1, indicated by arrows for a few selected atoms. (**B**) Two instances of successfully rearranged arrays (first two pictures), and one instance where a defect is visible after rearrangement (last picture). (**C**) The final arrangement of atoms is flexible, and we generate, e.g., clusters of 2 (top) or 10 (bottom) atoms. Nonperiodic arrangements and adjustable lattice spacings are also possible. (**D**) High-resolution CCD image of trap array. Our default configuration for loading atoms consists of an array of 100 tweezers with a spacing of 0.49 MHz between the RF tones, corresponding to a real-space distance of 2.6 μm between the focused beams (*31*).

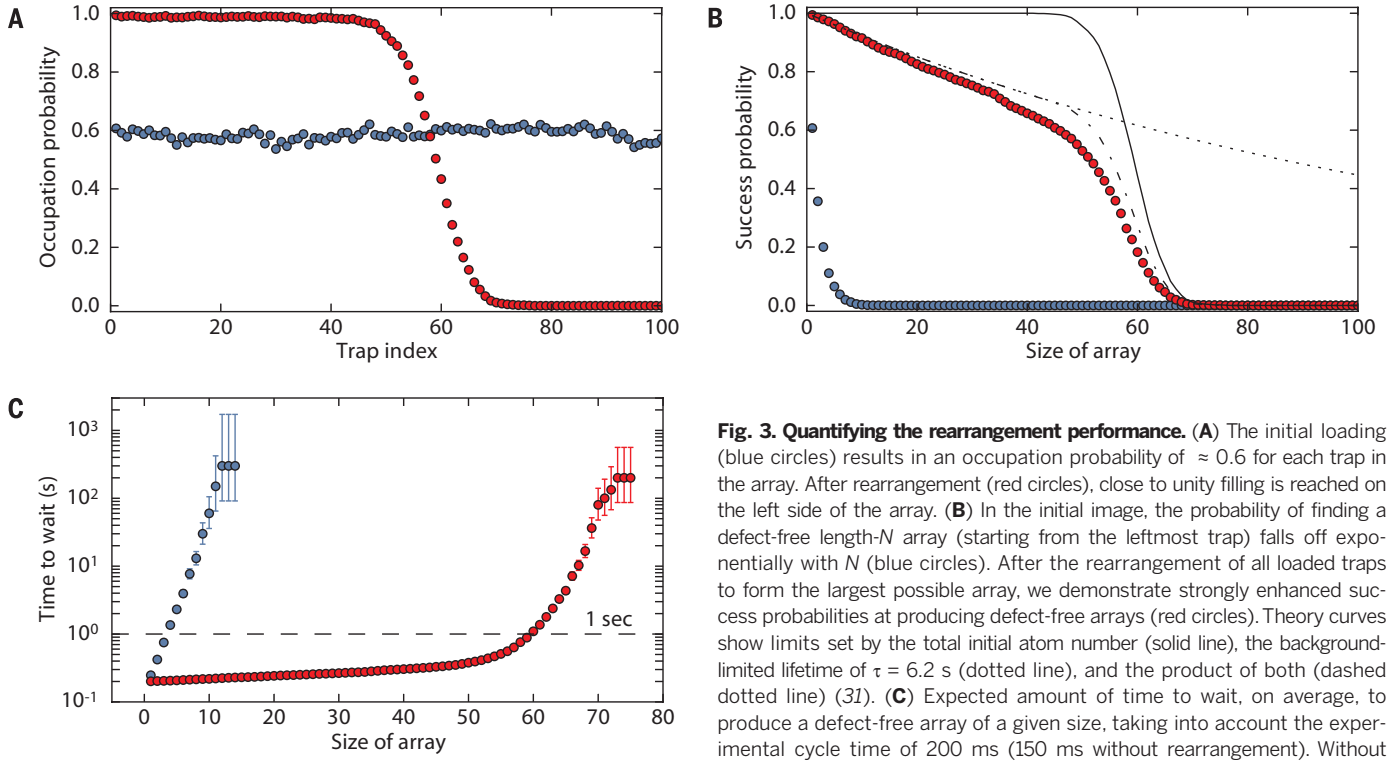

Fig. 3. Quantifying the rearrangement performance. (**A**) The initial loading (blue circles) results in an occupation probability of ≈ 0.6 for each trap in the array. After rearrangement (red circles), close to unity filling is reached on the left side of the array. (**B**) In the initial image, the probability of finding a defect-free length-*N* array (starting from the leftmost trap) falls off exponentially with *N* (blue circles). After the rearrangement of all loaded traps to form the largest possible array, we demonstrate strongly enhanced success probabilities at producing defect-free arrays (red circles). Theory curves show limits set by the total initial atom number (solid line), the background-limited lifetime of τ = 6.2 s (dotted line), and the product of both (dashed dotted line) (*31*). (**C**) Expected amount of time to wait, on average, to produce a defect-free array of a given size, taking into account the experimental cycle time of 200 ms (150 ms without rearrangement). Without rearrangement, the wait time grows exponentially (blue circles). Employing the rearrangement procedure, we can produce arrays of length 50 in less than 400 ms (red circles). Error bars denote 68% confidence intervals, which are smaller than the marker size in (A) and (B).

unoccupied traps are switched off by setting the corresponding RF amplitudes to zero. In a second step, all occupied tweezers are moved to the left until they stack up with the original spacing of 2.6 μm. This movement is generated by sweeping the RF tones to change the deflection angles of the AOD and lasts 3 ms (*31*). Finally, we detect the resulting atom configuration with a second high-resolution image. These steps implement a reduction of entropy via measurement and feedback. The effect is immediately visible in the images shown in Fig. 2, A and B. The initial filling of our array is probabilistic, whereas the rearranged configurations show highly ordered atom arrays. Our approach also allows us to construct flexible atomic patterns (Fig. 2C).

The rearrangement procedure creates defect-free arrays with high fidelity. This can be quantified by considering the improvement of single-atom occupation probabilities (Fig. 3A) and the success probabilities, p_N, for creating defect-free arrays of length N (Fig. 3B). The single-atom occupation probability in the left-most 40 traps increases from ≈ 0.6 before rearrangement to 0.988(3) after rearrangement, demonstrating our ability for high-fidelity single-atom preparation. Furthermore, the success probabilities for creating defect-

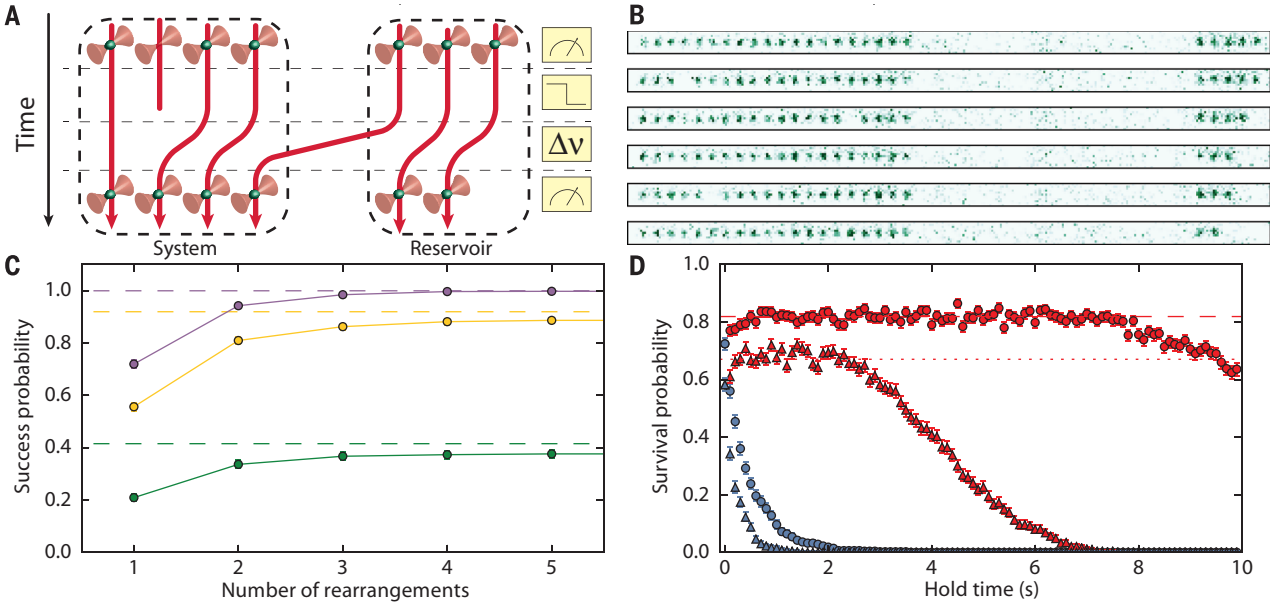

Fig. 4. Creating and maintaining regular arrays using an atomic reservoir. (**A**) For a given target array size, surplus atoms are kept in a reservoir and used for repetitive reloading of the array. (**B**) A 20-atom target array with a reservoir of atoms on the right. Defects occasionally develop in the target array and are replaced by atoms in the reservoir. The reservoir depletes as it is used to fill in defects. (**C**) By performing repeated rearrangements (once every 50 ms), the probability to successfully produce a defect-free array in any of these attempts increases and approaches the limit set by the number of initially loaded atoms (dashed lines). We show data for targeting 40 (purple), 50 (yellow), and 60 (green) atom arrays. Solid lines are guides to the eye. (**D**) Probing for defects and filling them once every 100 ms from the reservoir extends the lifetime of a defect-free array. Shown is the success probability of maintaining arrays of 20 (circles) and 40 (triangles) atoms with (red) and without (blue) replenishing atoms from the reservoir. With replenishing, the probability to maintain a defect-free array remains at a fixed plateau for as long as we have surplus atoms in the reservoir. The initial plateau value is set by the probability that no atoms in the array are lost in 100 ms (calculated value for 10-s single-atom lifetime shown as the dotted line). Error bars denote 68% confidence intervals, which are smaller than the marker size in (C).

free arrays show an exponential improvement. Before rearrangement, the probability of finding a defect-free array of length N is exponentially suppressed with $p_N = p^N$, where $p \approx 0.6$ (blue circles, Fig. 3B). After rearrangement, we find success probabilities as high as $p_{30} = 0.75(1)$ and $p_{50} = 0.53(1)$ (red circles, Fig. 3B).

The same exponential improvement is observed by considering the average wait time for producing defect-free arrays, given by T/p_N, where $T = 200$ ms is the cycling time of our experiment (see Fig. 3B). For example, we are able to generate defect-free arrays of 50 atoms with an average wait time of less than 400 ms (red circles, Fig. 3C).

The success probabilities can be further enhanced through multiple repetitions of the rearrangement protocol. Figure 4 illustrates the procedure in which we target an atomic array of fixed length and create a reservoir from surplus atoms in a separate zone. After the initial arrangement of atoms into the target and reservoir zones, we periodically take images to identify defects in the target array and pull atoms from the reservoir to fill in these defects. This enhances our initial success probabilities at producing defect-free arrays within one MOT-loading cycle to nearly the ideal limit (Fig. 4C).

Finally, a similar procedure can be used for correcting errors associated with atomic loss. This becomes a substantial limitation for large arrays because for a given lifetime of an individual atom in the trap τ, the corresponding lifetime of the N atom array scales as τ/N. To counter this loss, we repeatedly detect the array occupation after longer time intervals and replenish lost atoms from the reservoir. This procedure leads to exponentially enhanced lifetimes of our arrays (Fig. 4D).

These results demonstrate the ability to generate and control large, defect-free arrays at a fast repetition rate. The success probabilities are limited by two factors: the initial number of loaded atoms and losses during rearrangement. For example, the average total atom number in our array is 59 ± 5 (*31*), which results in the cutoff in the success probability in Fig. 3B starting from $N \approx 50$ (solid line). For shorter arrays, the fidelity is mostly limited by losses during rearrangement. These losses are dominated by our finite vacuum-limited lifetime, which varies from $\tau \approx 6$ s to $\tau \approx 12$ s (depending on the setting of our atomic dispenser source), and are only minimally increased by the movement of the atoms (*31*). The single-atom occupation probability is correspondingly reduced by a factor $\exp(-t_r/\tau)$, where $t_r = 50$ ms is the time for the whole rearrangement procedure (*31*). This results in the success probabilities of creating length-N arrays scaling as $\exp(-t_r N/\tau)$, which dominates the slope for $N = 50$ in Fig. 3B (dotted line). Currently, we reach vacuum-limited lifetimes only with sub-Doppler cooling applied throughout the sequence. However, the lifetime without cooling could be improved—for example, by using a different trapping laser and trapping wavelength (*31*).

The size of the final arrays can be considerably increased by implementing a number of realistic experimental improvements. For example, the initial loading probability could be enhanced to 0.9 (*21*–*23*) and the vacuum-limited lifetime could be improved to $\tau \approx 60$ s in an upgraded vacuum chamber. Increasing the number of traps in the current configuration is difficult because of the AOD bandwidth of ≈ 50 MHz and strong parametric heating introduced when the frequency spacing of neighboring traps approaches ≈ 450 kHz (*31*). However, implementing 2D arrays could provide a path toward realizing thousands of traps, ultimately limited by the availability of laser power and the field of view of high-resolution objectives. Such 2D configurations could be realized by either directly using a 2D-AOD or by creating a static 2D lattice of traps [using spatial light modulators (*14*) or optical lattices (*12*)] and sorting atoms with an independent AOD (*31*). With increased loading efficiencies (*21*–*23*), realistic estimates for the rearrangement time t_r in such 2D arrays indicate that the robust creation of defect-free arrays of hundreds of atoms is feasible (*31*). Finally, the repetitive interrogation techniques,

in combination with periodic reservoir reloading from a cold atom source (such as a MOT), could be used to maintain arrays indefinitely.

Atom-by-atom assembly of defect-free arrays forms a scalable platform with unique possibilities. It combines features that are typically associated with ion-trapping experiments, such as single-qubit addressability (*32*, *33*) and fast cycling times, with the flexible optical trapping of neutral atoms in a scalable fashion. Furthermore, in contrast to solid-state platforms, such atomic arrays are highly homogeneous (*31*) and mostly decoupled from their environment. The homogeneity of our array should also allow for cooling of the atomic motion via simultaneous sideband cooling in all tweezers at once (*34*, *35*).

These features provide an excellent starting point for multiqubit experiments, for studies of quantum many-body effects, and for exploring future applications. The required interactions between the atoms can be engineered using several approaches. Even without sideband cooling, exciting the atoms into high-lying Rydberg states would introduce strong dipole interactions that can be used for fast entangling gates (*24*, *25*, *27*). The parallelism afforded by our flexible atom rearrangement enables efficient diagnostics of such Rydberg-mediated entanglement. These interactions may also enable approaches to quantum simulations that involve both coherent coupling and engineered dissipation (*26*, *27*), as well as large-scale entangled quantum states for applications in precision measurements (*36*).

An alternative approach to engineering interactions involves the integration of atom arrays with nanophotonic platforms as demonstrated previously (*28*, *29*). These enable photon-mediated interactions that can be employed to couple the atoms within a local multiqubit register or for efficient communication between the registers using a modular quantum network architecture (*3*).

Finally, our platform could enable new bottom-up approaches to studying quantum many-body physics in Hubbard models (*15*, *16*, *30*), where atomic Mott insulators with fixed atom number and complex spin patterns could be directly assembled. This requires atom temperatures close to the ground state, coherent tunneling between the traps, and sizable on-site interactions. With side-band cooling, ground-state fractions in excess of 90% have already been demonstrated (*34*, *35*) and can likely be improved via additional optical trapping along the longitudinal tweezer axes, which would also increase on-site interaction strengths. Coherent tunneling of Rb atoms between similarly sized tweezers has been observed before by reducing the tweezer distance (*15*, *16*). The parametric heating, currently limiting the minimal distance between our traps, could be reduced by working with shallower traps, as needed for tunneling, and by employing fewer traps to increase the frequency separation between neighboring traps. Eventually, this approach could be applied to create ultracold quantum matter composed of exotic atomic species or complex molecules (*37*, *38*) that are difficult to cool evaporatively.

REFERENCES AND NOTES

1. S. Haroche, *Ann. Phys.* **525**, 753–776 (2013).
2. D. J. Wineland, *Rev. Mod. Phys.* **85**, 1103–1114 (2013).
3. C. Monroe, J. Kim, *Science* **339**, 1164–1169 (2013).
4. M. H. Devoret, R. J. Schoelkopf, *Science* **339**, 1169–1174 (2013).
5. W. S. Bakr *et al.*, *Science* **329**, 547–550 (2010).
6. J. F. Sherson *et al.*, *Nature* **467**, 68–72 (2010).
7. C. Weitenberg *et al.*, *Nature* **471**, 319–324 (2011).
8. D. S. Weiss *et al.*, *Phys. Rev. A* **70**, 040302 (2004).
9. J. Vala *et al.*, *Phys. Rev. A* **71**, 032324 (2005).
10. N. Schlosser, G. Reymond, I. Protsenko, P. Grangier, *Nature* **411**, 1024–1027 (2001).
11. M. Weber, J. Volz, K. Saucke, C. Kurtsiefer, H. Weinfurter, *Phys. Rev. A* **73**, 043406 (2006).
12. K. D. Nelson, X. Li, D. S. Weiss, *Nat. Phys.* **3**, 556–560 (2007).
13. M. J. Piotrowicz *et al.*, *Phys. Rev. A* **88**, 013420 (2013).
14. F. Nogrette *et al.*, *Phys. Rev. X* **4**, 021034 (2014).
15. A. M. Kaufman *et al.*, *Science* **345**, 306–309 (2014).
16. A. M. Kaufman *et al.*, *Nature* **527**, 208–211 (2015).
17. Y. Miroshnychenko *et al.*, *Nature* **442**, 151 (2006).
18. J. Beugnon *et al.*, *Nat. Phys.* **3**, 696–699 (2007).
19. M. Schlosser *et al.*, *New J. Phys.* **14**, 123034 (2012).
20. H. Kim, *et al., Nat. Commun.* **7**, 13317 (2016).
21. T. Grünzweig, A. Hilliard, M. McGovern, M. F. Andersen, *Nat. Phys.* **6**, 951–954 (2010).
22. B. J. Lester, N. Luick, A. M. Kaufman, C. M. Reynolds, C. A. Regal, *Phys. Rev. Lett.* **115**, 073003 (2015).
23. Y. H. Fung, M. F. Andersen, *New J. Phys.* **17**, 073011 (2015).
24. D. Jaksch *et al.*, *Phys. Rev. Lett.* **85**, 2208–2211 (2000).
25. M. Saffman, T. G. Walker, K. Mølmer, *Rev. Mod. Phys.* **82**, 2313–2363 (2010).
26. H. Weimer, M. Müller, I. Lesanovsky, P. Zoller, H. P. Büchler, *Nat. Phys.* **6**, 382–388 (2010).
27. A. Browaeys, D. Barredo, T. Lahaye, *J. Phys. B* **49**, 152001 (2016).
28. J. D. Thompson *et al.*, *Science* **340**, 1202–1205 (2013).
29. A. Goban *et al.*, *Nat. Commun.* **5**, 3808 (2014).
30. S. Murmann *et al.*, *Phys. Rev. Lett.* **115**, 215301 (2015).
31. See supplementary materials on *Science* Online.
32. T. Xia *et al.*, *Phys. Rev. Lett.* **114**, 100503 (2015).
33. Y. Wang, X. Zhang, T. A. Corcovilos, A. Kumar, D. S. Weiss, *Phys. Rev. Lett.* **115**, 043003 (2015).
34. A. M. Kaufman, B. J. Lester, C. A. Regal, *Phys. Rev. X* **2**, 041014 (2012).
35. J. D. Thompson, T. G. Tiecke, A. S. Zibrov, V. Vuletić, M. D. Lukin, *Phys. Rev. Lett.* **110**, 133001 (2013).
36. P. Kómár *et al.*, *Phys. Rev. Lett.* **117**, 060506 (2016).
37. J. F. Barry, D. J. McCarron, E. B. Norrgard, M. H. Steinecker, D. DeMille, *Nature* **512**, 286–289 (2014).
38. N. R. Hutzler, L. R. Liu, Y. Yu, K.-K. Ni, https://arxiv.org/abs/1605.09422 (2016).
39. D. Barredo, S. de Léséleuc, V. Lienhard, T. Lahaye, A. Browaeys, *Science* **354**, 1021–1023 (2016).

ACKNOWLEDGMENTS

We thank K.-K. Ni, N. Hutzler, A. Mazurenko, and A. Kaufman for insightful discussion. This work was supported by NSF, Center for Ultracold Atoms, National Security Science and Engineering Faculty Fellowship, and Harvard Quantum Optics Center. H.B. acknowledges support by a Rubicon Grant of the Netherlands Organization for Scientific Research (NWO). During the completion of this work, we became aware of a related approach (*39*).

SUPPLEMENTARY MATERIALS

www.sciencemag.org/content/354/6315/1024/suppl/DC1
Materials and Methods
Figs. S1 to S5
Movies S1 to S3
References (*40*, *41*)

17 June 2016; accepted 17 October 2016
Published online 3 November 2016
10.1126/science.aah3752

GEOPHYSICS

Mega-earthquakes rupture flat megathrusts

Quentin Bletery,[1]* Amanda M. Thomas,[1] Alan W. Rempel,[1] Leif Karlstrom,[1] Anthony Sladen,[2] Louis De Barros[2]

The 2004 Sumatra-Andaman and 2011 Tohoku-Oki earthquakes highlighted gaps in our understanding of mega-earthquake rupture processes and the factors controlling their global distribution: A fast convergence rate and young buoyant lithosphere are not required to produce mega-earthquakes. We calculated the curvature along the major subduction zones of the world, showing that mega-earthquakes preferentially rupture flat (low-curvature) interfaces. A simplified analytic model demonstrates that heterogeneity in shear strength increases with curvature. Shear strength on flat megathrusts is more homogeneous, and hence more likely to be exceeded simultaneously over large areas, than on highly curved faults.

Past mega-earthquakes, such as the magnitude (*M*) 9.6 Chile earthquake in 1960 and the *M* 9.3 Alaska earthquake in 1964, occurred in areas where the subducting lithosphere was relatively young (and buoyant) and the plate convergence rate was relatively high (*1*). These observations led some authors to hypothesize that maximum earthquake size is controlled by these two geological parameters (*2*, *3*). The development of space-based geodesy enabled refined measurements of plate motion that challenged the role of convergence rate (*4*–*6*). Additionally, the moment magnitude (M_w) 9.0 Tohoku-Oki earthquake (*7*) ruptured lithosphere that is over 120 million years old (*8*), ruling out lithospheric age as the dominant control. Weak correlations appear in recent data sets among a variety of parameters, including forearc structure (*9*, *10*); age, density, and buoyancy of the slab (*6*); upper plate motion (*11*); upper plate strain (*12*); long-term trench migration (*11*); trench sediment thickness (*12*); and width of the seismogenic

[1]Department of Earth Sciences, University of Oregon, 1272 University of Oregon, Eugene, OR 97403, USA. [2]Université Côte d'Azur, CNRS, OCA, IRD, Géoazur, 250 rue Albert Einstein, Sophia Antipolis, 06560 Valbonne, France.
*Corresponding author. Email: qbletery@uoregon.edu

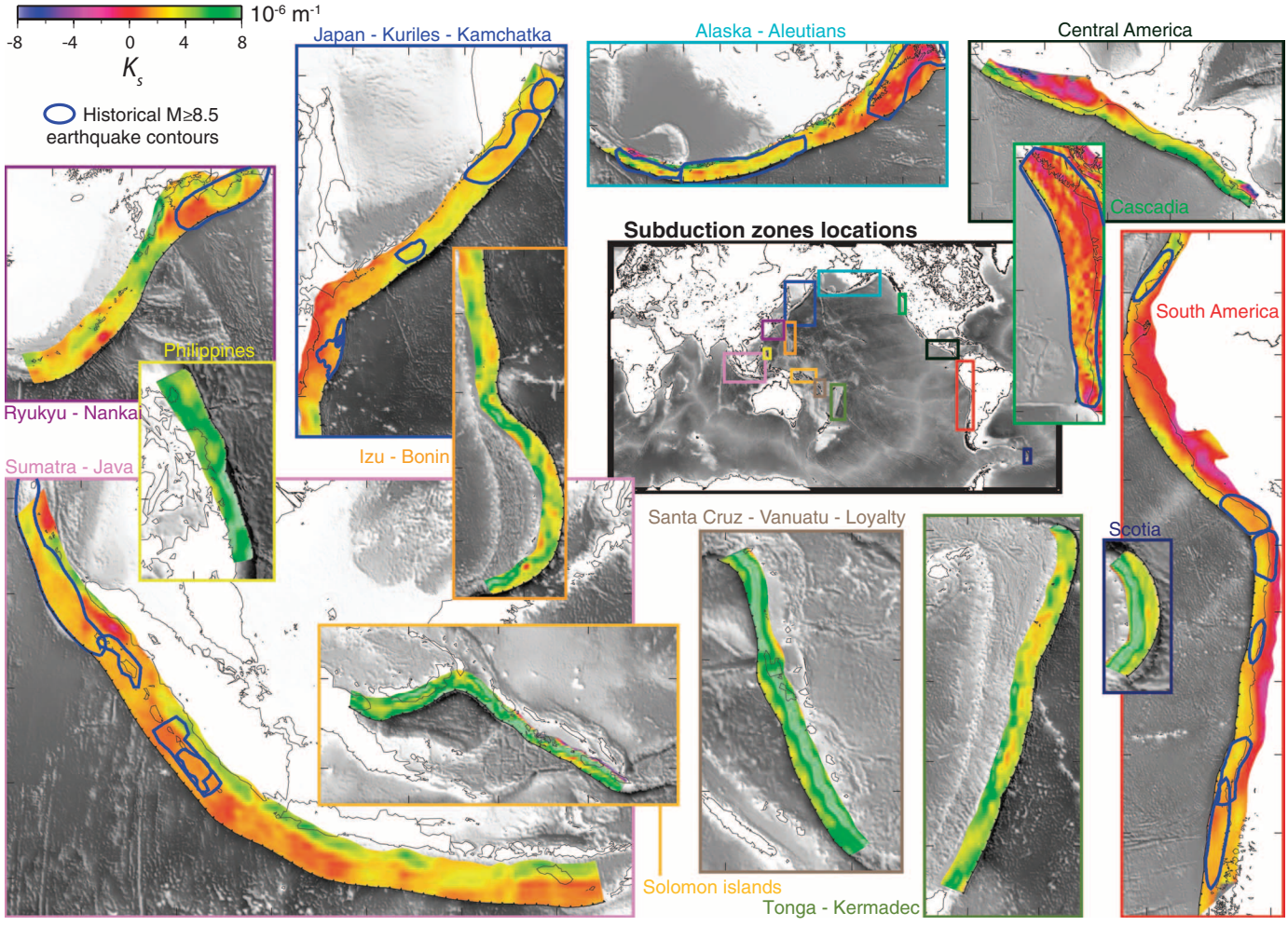

Fig. 1. Variations in megathrust curvature and distribution of historical mega-earthquakes. Along-dip curvature $K_s = d\theta/ds$ on the megathrust is shown for the 13 main subduction zones of the world, overlaid with the estimated slip contours of known historical mega-earthquakes ($M \geq 8.5$) (see table S1 for a list of events). Tick marks in each panel are spaced at 5° increments.

zone (*11*, *13*, *14*). However, aside from dip angle and seismogenic width [coefficient of correlation $r = 0.61$ (*14*)], none of these parameters correlate strongly ($|r| < 0.5$) with the maximum earthquake magnitude recorded in the different zones (*11*). Stronger correlations are found with fault properties such as thrust interface dip angle (*11*) and apparent friction derived from heat flow measurements (*15*).

Today, forecasts of potential large earthquakes focus mainly on imaging the slip deficit with respect to the relative plate motion, because such deficits are thought to result in stress loading that is ultimately released in earthquakes [e.g., (*16*)]. We followed a complementary approach by analyzing large-scale geometrical features of subduction faults and assessing their possible influence on the physical conditions favoring large earthquake ruptures. Seismic moment $M_0 \propto \Delta\sigma S^{3/2}$ (*17*) depends mainly on the surface area S over which an earthquake ruptures, because the stress drop $\Delta\sigma$ (the difference in stress before and after an earthquake) is roughly constant among earthquakes over a large range of magnitudes (*18*). Here we demonstrate that slab interface curvature exerts a leading-order control on the spatial extent of potential ruptures in subduction zones and hence on the magnitude of the largest earthquakes.

Data sets from active- and passive-source seismology have been combined to constrain the slab1.0 model for the geometry of the world's major subduction zones (*14*) [details and limitations of the slab1.0 model are discussed in the supplementary materials (*19*)]. We computed maps of the along-dip interface curvature $K_s = d\theta/ds$, hereafter referred to as curvature [where θ is the dip angle and s is the tangent to the interface pointing in the down-dip direction (*19*)], using the slab1.0 model (*14*, *20*) (Fig. 1). Because K_s is almost always positive (Fig. 1), we hereafter interchangeably refer to low-K_s fault regions as flat, low-curvature, or planar. Similarly, we computed the along-strike gradient of the dip angle $K_t = d\theta/dt$ (fig. S1). Comparison with a catalog of historical events (*19*) reveals a tendency for mega-earthquakes to occur on relatively flat (low-K_s) megathrusts (Fig. 1). The curvature is particularly small in the Japan-Kuriles-Kamchatka, Alaska-Aleutians, Sumatra-Java, South America, and Cascadia subduction zones, which are known to produce $M \geq 9.0$ earthquakes. Subduction zones with large curvatures, such as the Philippines, Solomon Islands, Izu-Bonin, Santa Cruz–Vanuatu-Loyalty, and Tonga-Kermadec zones, lack historic mega-earthquakes. At a smaller scale, we also observe that the down-dip limit of mega-earthquakes offshore of Sumatra—and to a lesser extent, in the Aleutians, Alaska, Nankai, and Kamchatka—coincides with an abrupt change in the slope, suggesting that the conditions required to generate large earthquakes are directly related to the local curvature along the megathrust interface.

To further explore the role of subduction geometry, we calculated the average dip angle $\overline{\theta}$ (Fig. 2A), the average curvature $\overline{K_s}$ (Fig. 2B), and the average along-strike gradient of dip angle $|\overline{K_t}|$ (fig. S2) from the trench to 60 km depth, and we compared these values with the magnitude of the largest megathrust earthquake M_{max} recorded in each subduction zone. We found that M_{max} anticorrelates ($r = -0.72$) with $\overline{\theta}$ (Fig. 2A) and anticorrelates even more strongly ($r = -0.80$) with $\overline{K_s}$ (Fig. 2B). The anticorrelation with $|\overline{K_t}|$ is weaker ($r = -0.64$) but still significant (fig.

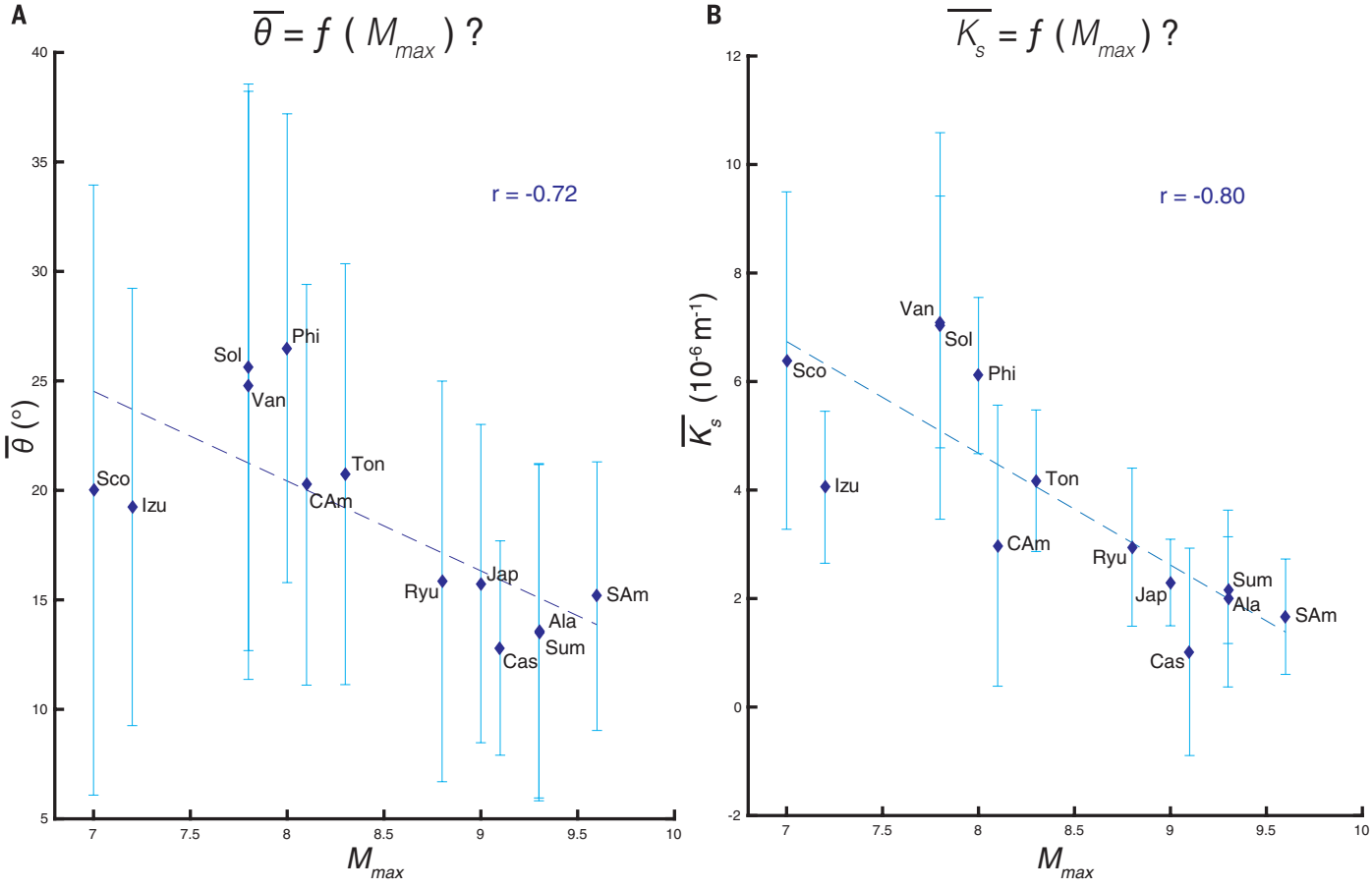

Fig. 2. Correlation of average dip angle and curvature with maximum earthquake magnitude. (**A**) Average dip angle $\overline{\theta}$ of the 13 main subduction zones of the world as a function of the maximum event magnitude M_{max} recorded on the megathrust (see table S2 for a list of events). The coefficient of correlation r is −0.72. (**B**) Same as (A), but for the average along-dip curvature $\overline{K_s}$ (r = −0.80). Light blue bars show the standard deviation for the distribution of $\overline{\theta}$ (A) and $\overline{K_s}$ (B) in each subduction zone. These bars should not be considered as error bars because we are reasoning with averages; they rather indicate how θ and K_s are distributed along the different subduction zones. Blue dashed lines are the linear regressions. Ala, Alaska-Aleutians; CAm, Central America; Cas, Cascadia; Izu, Izu-Bonin; Jap, Japan-Kuriles-Kamchatka; Phi, Philippines; Ryu, Ryukyu-Nankai; SAm, South America; Sco, Scotia arc; Sol, Solomon Islands; Sum, Sumatra-Java; Ton, Tonga-Kermadec; Van, Santa Cruz–Vanuatu-Loyalty.

S2). We suggest, on the basis of our observations, that planar slab interfaces are prone to hosting larger earthquakes. Multiple factors, including the subducting (*21*) or overriding (*22*) plate thickness and viscosity contrast (*23*), have been invoked as controls on subduction curvature; these studies (*21*–*23*) provide a useful introduction to this field of research.

The average curvature within mega-earthquake slip contours is consistent with the linear regression in Fig. 2B, with observed values always smaller than 3.76×10^{-6} m^{-1} (fig. S5B). Given the distribution of K_s across the different megathrusts of the world, the likelihood that all known mega-earthquakes occurred by chance on $K_s \leq 3.76 \times 10^{-6}$ m^{-1} areas is 0.8% (*19*), allowing us to affirm with >99% confidence that earthquake magnitude is related to megathrust curvature. The distribution of the average dip angle within mega-rupture contours is much broader (fig. S5A), confirming the stronger relationship of earthquake size with curvature than with dip angle (*19*). Nevertheless, known mega-earthquakes do not exhibit a strong tendency to rupture the lower-curvature portions of their host subduction zones (*19*). This suggests that over the long term, mega-earthquakes might rupture any portion of a low-curvature subduction thrust, such as those of the Cascadia, South America, Alaska-Aleutians, Sumatra-Java, Japan-Kuriles-Kamchatka, Ryukyu-Nankai, and Central America subduction zones. Large earthquakes are preferentially hosted by megathrusts with low dip angles in part as a consequence of larger down-dip seismogenic extents making ruptures possible over wider fault areas (*11*, *13*, *14*). However, the stronger relationship of earthquake size with curvature than with dip angle noted above (Fig. 2B) warrants a more thorough description of fault loading.

The present understanding of seismic ruptures can be framed in terms of the asperity model: Earthquakes are caused by the sudden failure of locked macroscopic asperities that accumulate stress during interseismic periods (*24*). In this context, the extent of an earthquake has a leading-order dependence on the size of the rupturing asperity and the neighboring region that is pushed to failure by coseismic stress change. Recent efforts aimed at characterizing the nature of asperities and their immediate surroundings have mostly focused on potential variations in friction along faults [e.g, (*25*–*28*)]. The capacity of a fault segment to accumulate stress is bounded by the Coulomb failure criterion

$$|\tau^c| = \mu(\sigma_n^c - p) \quad (1)$$

where τ^c is the critical shear stress required to initiate a rupture (hereafter referred to as shear strength), μ is the coefficient of friction, p is the pore pressure, σ_n^c is the normal stress when the rupture initiates, and cohesion is neglected. The Coulomb failure criterion is met when the accumulated shear stress reaches the frictional shear strength and an earthquake initiates. From Eq. 1, one can define an asperity as a fault area characterized by a particularly high friction coefficient μ. Alternatively, one can also explain the time-dependent behavior of asperities by appealing to variations in pore pressure p that accompany fluid migration [e.g., (*29*)]. We explore here a different hypothesis, which is that the locations of

asperities can be determined by analyzing variations in normal stress σ_n that are governed by large-scale geometrical characteristics of megathrust interfaces. Assuming constant friction μ and hydrostatic pore pressure $p = \rho_w g h$ (with ρ_w being the water density, g the acceleration of gravity, and h the local interface depth), we illustrate the effect of variations in normal stress σ_n on variations in shear strength [this method is reminiscent of the consideration of normal force in (*16*) but invokes different causative factors, i.e., curvature instead of plate tectonic forces].

We considered a simple two-dimensional (2D) fault model: a fault interface subjected to the pressure of the upper plate mass and an unknown horizontal tectonic stress. We also treated the convergence direction as aligned with the horizontal projection of the local along-dip direction (i.e., pure dip-slip convergence). This latter simplification is justified by the dominantly dip-slip mechanisms of most megathrust earthquakes [e.g., figures 14, 15, and 16 of (*30*)]. Even though subduction zones present, to varying degrees, oblique convergences, this obliquity is usually accommodated for the most part by large strike-slip faults in the back arc. One notable exception is the Solomon Islands subduction zone, which presents a very strong oblique convergence and hosts megathrust earthquakes that typically exhibit large strike-slip components. Our idealized description of the convergence direction allows us to treat the 3D problem with a 2D model (fig. S6). Within this framework, the shear strength—defined as the critical shear stress required to initiate slip at a given location—can be expressed as a function of the crustal density ρ, the friction μ, the depth h, the dip angle θ, and the angle ψ between the maximum principal component of stress and the horizontal

$$\tau^c = \frac{gh\mu(\rho-\rho_w)(\sin2\theta + \tan2\psi\cos2\theta)}{\sin2\theta-\mu(1-\cos2\theta) + \tan2\psi(\cos2\theta-\mu\sin2\theta)} \quad (2)$$

τ^c increases with θ ($\partial\tau^c/\partial\theta \geq 0$) (*19*) meaning that large dip angles imply greater shear strength. If the dominant control of earthquake magnitude were the amplitude of shear strength, we might expect a positive correlation between M_{max} and θ. The negative correlation that we observe (Fig. 2A) points to other factors.

Because the magnitude of an earthquake is primarily controlled by the area of rupture, homogeneous distributions of shear strength over large fault areas may favor the occurrence of mega-earthquakes. In this framework, the shear-strength gradient $d\tau^c/ds$ is a critical parameter. Treating μ, ρ, ρ_w, and g as constants, spatial variations of τ^c obtained by differentiation of Eq. 2 satisfy

$$\frac{d\tau^c}{ds} = g\mu(\rho-\rho_w)\left(A_\mu(\theta,\psi)\sin\theta + B_\mu(\theta,\psi)hK_s + C_\mu(\theta,\psi)h\frac{d\psi}{ds}\right) \quad (3)$$

where $\rho > \rho_w$ and the functions $A_\mu(\theta,\psi)$, $B_\mu(\theta,\psi)$, and $C_\mu(\theta,\psi)$ are positive for $\mu = 0.6$ and values of θ and ψ typically encountered in subduction zones (*19*). Therefore, $|d\tau^c/ds|$ increases with K_s [a similar argument can be made to show that $|d\tau^c/dt|$ increases, on average, with $|K_t|$ (*19*)]. Shear-strength heterogeneity increases with curvature: The flatter the megathrust interface (lower K_s), the more homogeneous the shear-strength distribution. Stress accumulation along faults is complex, and heterogeneities in driving stress can result from the effect of stress concentrations inherited from past events or changes in coupling associated with variations in the friction coefficient or pore fluid pressure. However, dynamic stress perturbations induced by earthquake propagation are more likely to overstep the resistance to failure over broad areas if shear strength is homogeneously distributed along a large fault surface. In contrast, barriers to earthquake propagation are more likely for heterogeneous shear-strength distributions, because the dynamic stress perturbations required to reach local values of shear strength will tend to be larger in some regions. The idea that geometrical heterogeneity may limit earthquake propagation has been previously invoked (*15*, *31*) and is consistent with the observation that many large earthquake ruptures terminate near subducting seamounts or other structural heterogeneities (*31*, *32*).

During an earthquake, fault slip will propagate as long as the dynamic stress perturbation induced by the earlier phase of the rupture, $\delta\tau$, is larger than the difference between shear strength and shear stress in the surrounding area, $\Delta\tau$. Hence, one way to generate mega-earthquakes is to initiate a large dynamic stress perturbation by the failure of a strongly locked asperity so that $\delta\tau > \Delta\tau$ over a large surrounding fault area. In this scenario, mega-earthquakes are characterized by the rupture of one or several asperities where shear strength is particularly high. Our finding that large earthquakes rupture flat megathrusts suggests that another way to generate mega-earthquakes is if $\Delta\tau$ is small in a large area surrounding rupture nucleation, and thus even relatively small dynamic stress perturbations $\delta\tau$ can continue to propagate rupture. The 2004 Sumatra-Andaman earthquake, a unilaterally propagating 1600-km-long rupture without evidence of a localized high stress drop (*33*), exemplifies this second scenario, because it is unlikely that the energy released during the early phases of rupture could have initiated slip on fault portions as far as 1600 km away if the entire ruptured area was not already close to failure. In this situation, mega-earthquakes are not characterized by the rupture of asperities in regions where strength is much greater than in the surrounding area but, on the contrary, by the absence of strong variations in strength. The limiting case of homogeneous null shear strength results in constant creep and the absence of earthquakes of any magnitude. Hence, although the amplitude of τ^c is an important parameter, the observation that mega-earthquakes preferentially occur on flat subduction zones (Fig. 2) seems to indicate that the homogeneity of the shear-strength distribution is among the most critical factors in enabling the generation of mega-earthquakes.

It has recently been proposed that any subduction zone may produce a $M \geq 9$ earthquake (*34*). Our results suggest that earthquake size is limited by curvature and, if our interpretation is correct, mega-earthquakes might be physically incapable of rupturing highly curved subduction zones with large shear-strength gradients, such as the Philippines, the Solomon Islands, Scotia arc, and Santa Cruz–Vanuatu-Loyalty; heterogeneous shear strength creates natural barriers that stop earthquake propagation. It is possible that heterogeneous shear stress could build to match a heterogeneous shear-strength distribution and allow rare large events, but such scenarios are expected to be less likely, and therefore more infrequent, than on megathrusts with more homogeneous shear strength. As indicated by Fig. 2B, some subduction zones, such as Izu-Bonin or Central America, may yet host earthquakes larger than previously recorded. Cascadia is noteworthy because the last mega-earthquake that it hosted is thought to have ruptured the entire subduction fault and therefore reached the maximum possible magnitude for this subduction zone (*35*). At a smaller scale, some areas, such as Peru, Java, or the large low-to-negative K_s fault region in Central America (Fig. 1), which includes the Guerrero gap but extends much farther, show favorable features for a possible very large rupture—implying in the Guerrero case the potential for an even larger earthquake than that inferred from the extent of the gap. Moreover, large flat portions of subduction faults may sometimes rupture as one mega-earthquake and sometimes as several smaller earthquakes. Such behavior is documented, for instance, in Nankai (*36*), where two nearby asperities sometimes break as two separate consecutive earthquakes (as in 1854 and 1944–1946) and sometimes as one larger earthquake (1707; blue contour in the Ryukyu-Nankai box). This suggests that high-curvature regions of generally flat subduction zones may act as barriers to rupture most of the time and still sometimes be overcome by coseismic stress changes. Planar fault areas may thus host moderate-sized earthquakes for a long time and still have the potential to generate mega-earthquakes in the future.

It is possible that frictional properties and geometry are related. Such mechanical relationships are well described in accretionary wedges (*37*) and are certainly expected, though more difficult to constrain, along the deeper portions of megathrusts. Slab curvature has also been proposed to promote higher permeability (*38*–*41*) and thus to have an impact on the pore fluid pressure as well. Nevertheless, we have shown that spatial variations in friction and pore fluid pressure are not required to explain the gross distribution of mega-earthquakes. The observation that mega-earthquakes preferentially rupture flat megathrusts (Figs. 1 and 2B) is consistent with the inference that shear strength tends to be more homogeneously distributed along such subduction interfaces (Eq. 3), facilitating synchronized

failure over large areas. This implies that the critical feature at play in the generation of mega-earthquakes is not the amplitude of shear strength but its spatial variations. Thus, the absence of asperities on large faults may counterintuitively be a source of higher hazard. Though our study focused on subduction earthquakes, flatness may favor large earthquakes on long strike-slip faults as well.

REFERENCES AND NOTES

1. H. Kanamori, *Philos. Trans. R. Soc. A* **364**, 1927–1945 (2006).
2. L. Ruff, H. Kanamori, *Phys. Earth Planet. Inter.* **23**, 240–252 (1980).
3. L. Ruff, H. Kanamori, *Tectonophysics* **99**, 99–117 (1983).
4. R. McCaffrey, *Geophys. Res. Lett.* **21**, 2327–2330 (1994).
5. S. Stein, E. A. Okal, *Bull. Seismol. Soc. Am.* **97**, S279–S295 (2007).
6. T. Nishikawa, S. Ide, *Nat. Geosci.* **7**, 904–908 (2014).
7. Q. Bletery *et al.*, *J. Geophys. Res. Solid Earth* **119**, 7636–7653 (2014).
8. R. D. Müller, M. Sdrolias, C. Gaina, W. R. Roest, *Geochem. Geophys. Geosyst.* **9**, Q04006 (2008).
9. T.-R. A. Song, M. Simons, *Science* **301**, 630–633 (2003).
10. R. E. Wells, R. J. Blakely, Y. Sugiyama, D. W. Scholl, P. A. Dinterman, *J. Geophys. Res. Solid Earth* **108**, 2507 (2003).
11. W. Schellart, N. Rawlinson, *Phys. Earth Planet. Inter.* **225**, 41–67 (2013).
12. A. Heuret, C. Conrad, F. Funiciello, S. Lallemand, L. Sandri, *Geophys. Res. Lett.* **39**, L05304 (2012).
13. J. F. Pacheco, L. R. Sykes, *Bull. Seismol. Soc. Am.* **82**, 1306 (1992).
14. G. P. Hayes, D. J. Wald, R. L. Johnson, *J. Geophys. Res. Solid Earth* **117**, B01302 (2012).
15. X. Gao, K. Wang, *Science* **345**, 1038–1041 (2014).
16. C. H. Scholz, J. Campos, *J. Geophys. Res. Solid Earth* **117**, B05310 (2012).
17. R. Madariaga, *J. Geophys. Res.* **84**, 2243 (1979).
18. H. Kanamori, D. L. Anderson, *J. Geophys. Res.* **80**, 1075–1078 (1975).
19. Materials and methods are available as supplementary materials on *Science* Online.
20. P. A. McCrory, J. L. Blair, F. Waldhauser, D. H. Oppenheimer, *J. Geophys. Res. Solid Earth* **117**, n/a (2012).
21. W. P. Schellart, J. Freeman, D. R. Stegman, L. Moresi, D. May, *Nature* **446**, 308–311 (2007).
22. A. F. Holt, B. A. Buffett, T. W. Becker, *Geophys. Res. Lett.* **42**, 3802–3810 (2015).
23. W. Schellart, *J. Geophys. Res. Solid Earth* **115**, B11406 (2010).
24. T. Lay, H. Kanamori, L. Ruff, *Earthq. Predict. Res.* **1**, 3 (1982).
25. S. T. Tse, J. R. Rice, *J. Geophys. Res.* **91**, 9452 (1986).
26. J. Dieterich, *J. Geophys. Res. Solid Earth* **99**, 2601–2618 (1994).
27. C. H. Scholz, *Nature* **391**, 37–42 (1998).
28. C. Marone, *Nature* **391**, 69–72 (1998).
29. Y. Guglielmi, F. Cappa, J.-P. Avouac, P. Henry, D. Elsworth, *Science* **348**, 1224–1226 (2015).
30. B. P. Allmann, P. M. Shearer, *J. Geophys. Res. Solid Earth* **114**, B01310 (2009).
31. K. Wang, S. L. Bilek, *Tectonophysics* **610**, 1–24 (2014).
32. K. Wang, S. L. Bilek, *Geology* **39**, 819–822 (2011).
33. Q. Bletery, A. Sladen, J. Jiang, M. Simons, *J. Geophys. Res. Solid Earth* **121**, 5116–5135 (2016).
34. R. McCaffrey, *Geology* **36**, 263 (2008).
35. K. Satake, K. Wang, B. F. Atwater, *J. Geophys. Res. Solid Earth* **108**, 2535 (2003).
36. T. Furumura, K. Imai, T. Maeda, *J. Geophys. Res. Solid Earth* **116**, B02308 (2011).
37. F. Dahlen, *Annu. Rev. Earth Planet. Sci.* **18**, 55–99 (1990).
38. R. J. Lisle, J. M. Robinson, *J. Struct. Geol.* **17**, 739–750 (1995).
39. C. R. Ranero, J. Phipps Morgan, K. McIntosh, C. Reichert, *Nature* **425**, 367–373 (2003).
40. M. Faccenda, T. V. Gerya, L. Burlini, *Nat. Geosci.* **2**, 790–793 (2009).
41. T. Nishikawa, S. Ide, *Geophys. Res. Lett.* **42**, 7081–7089 (2015).

ACKNOWLEDGMENTS

We thank R. Bürgmann for his valuable comments on the manuscript. The slab1.0 model is available online at earthquake.usgs.gov/data/slab/. The U.S. Geological Survey catalog of historical earthquakes ($M \geq 8.0$ since 1900) that we used in this study can be found at http://earthquake.usgs.gov/earthquakes/world/historical.php. For the subduction zones that have not experienced any $M \geq 8.0$ earthquakes since 1900, this catalog was complemented by the Global Centroid Moment Tensor catalog (www.globalcmt.org/). We used Generic Mapping Tools to compute the distributions of dip-angle gradients (gmt.soest.hawaii.edu/). This work was supported by NSF grant EAR-1520238, ANR project TO-EOS, and the French Ministry of Research and Education.

SUPPLEMENTARY MATERIALS

www.sciencemag.org/content/354/6315/1027/suppl/DC1
Materials and Methods
Figs. S1 to S8
Tables S1 to S2
References (*42*–*53*)

6 May 2016; accepted 19 October 2016
10.1126/science.aag0482

CATALYSIS

Direct and continuous strain control of catalysts with tunable battery electrode materials

Haotian Wang,[1] Shicheng Xu,[2] Charlie Tsai,[3,4] Yuzhang Li,[5] Chong Liu,[5] Jie Zhao,[5] Yayuan Liu,[5] Hongyuan Yuan,[6] Frank Abild-Pedersen,[4] Fritz B. Prinz,[2,5] Jens K. Nørskov,[3,4] Yi Cui[5,7]*

We report a method for using battery electrode materials to directly and continuously control the lattice strain of platinum (Pt) catalyst and thus tune its catalytic activity for the oxygen reduction reaction (ORR). Whereas the common approach of using metal overlayers introduces ligand effects in addition to strain, by electrochemically switching between the charging and discharging status of battery electrodes the change in volume can be precisely controlled to induce either compressive or tensile strain on supported catalysts. Lattice compression and tension induced by the lithium cobalt oxide substrate of ~5% were directly observed in individual Pt nanoparticles with aberration-corrected transmission electron microscopy. We observed 90% enhancement or 40% suppression in Pt ORR activity under compression or tension, respectively, which is consistent with theoretical predictions.

Highly efficient electrocatalysts for renewable energy conversion processes, such as in H_2 fuel cells and water-splitting electrocatalysis, is becoming increasingly important (*1*–*3*). One strategy for systematically improving the activities of known catalysts is to modify their electronic structure (*4*–*6*). Numerous examples have been demonstrated in H_2O–O_2–H_2 electrocatalysis, such as the changing of d band filling in perovskite oxides for oxygen evolution (*7*), transition-metal alloying for the oxygen reduction reaction (ORR) (*4*, *8*–*11*), and our recent studies of using lithium (Li)–ion intercalation and extraction in layered materials for water-splitting (*12*, *13*).

Lattice strain, either compressive or tensile, can alter the surface electronic structure by modifying the distances between surface atoms and in turn catalytic activity (*14*–*17*). For platinum (Pt), previous studies have suggested that the 5d-band center of Pt can be shifted by ~0.1 eV with only 1% lattice strain (*18*), which can appreciably strengthen or weaken bonding of reaction intermediates to the surface (*14*, *18*). Lattice-mismatch between metals can be generated by directly synthesizing core-shell structures (*19*–*23*) or by selectively removing atoms from an alloy (for example, stripping away Cu from a Pt-Cu alloy) (*8*, *14*, *24*–*26*). However, because of the larger lattice of Pt as compared with that of most metal cores, this method is typically restricted to compressive strain (*14*, *27*). Additionally, both electronic charge transfer between the different metal atoms (ligand effects) and changes in the surface stability—and thus surface area—are present, making it difficult to identify and control the effects of strain alone (*14*, *25*). Another strategy is to deposit catalysts onto flat substrates that undergo physical transformations as external forces are applied or the temperatures varied (*28*, *29*). Those flat and tunable substrates present great importance to fundamental analysis, but only a few of them have been successfully demonstrated effective in electrocatalysis (*28*). Thus, new methods that can flexibly and effectively control both tensile and compressive lattice strain in catalysts without introducing additional effects are needed.

[1]Department of Applied Physics, Stanford University, Stanford, CA 93205, USA. [2]Department of Mechanical Engineering, Stanford University, Stanford, CA 93205, USA. [3]SUNCAT Center for Interface Science and Catalysis, Department of Chemical Engineering, Stanford University, Stanford, CA 94305, USA. [4]SUNCAT Center for Interface Science and Catalysis, SLAC National Accelerator Laboratory, 2575 Sand Hill Road, Menlo Park, CA 94025, USA. [5]Department of Material Science and Engineering, Stanford University, Stanford, CA 94305, USA. [6]Department of Physics, Stanford University, Stanford, CA 94305, USA. [7]Stanford Institute for Materials and Energy Sciences, SLAC National Accelerator Laboratory, 2575 Sand Hill Road, Menlo Park, CA 94025, USA.
***Corresponding author. Email: yicui@stanford.edu**

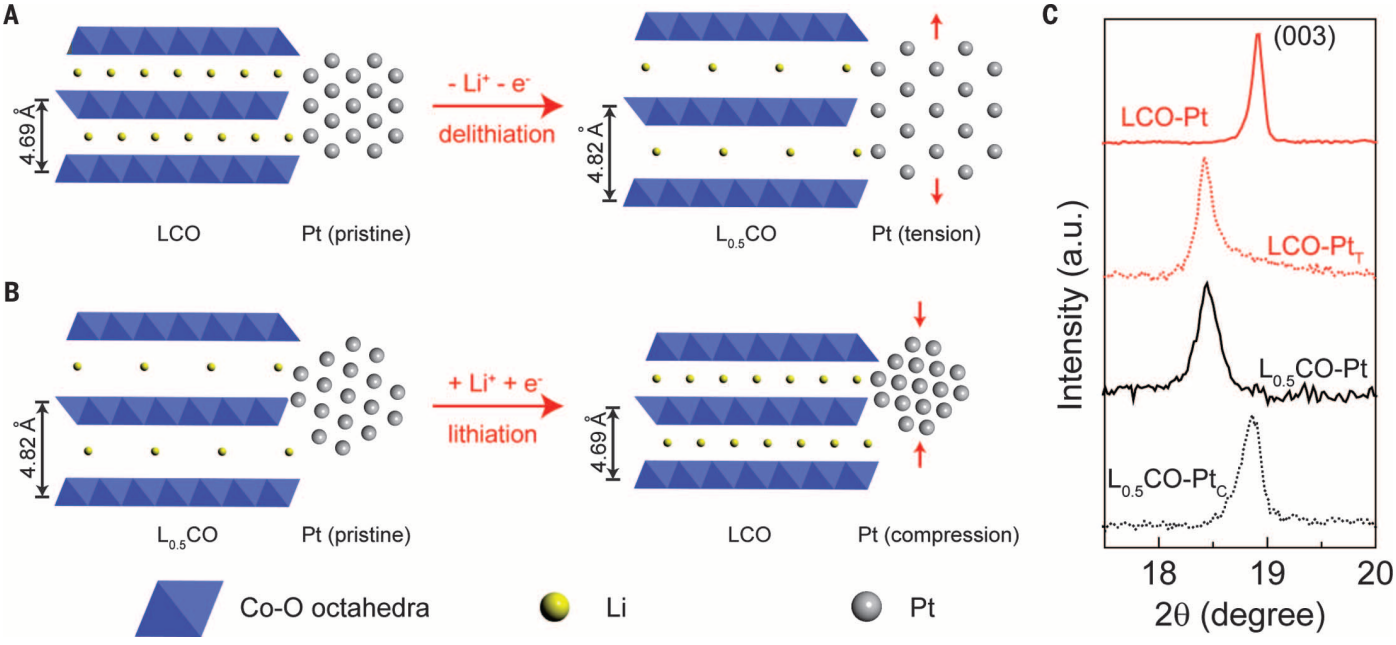

Fig. 1. Schematic of the lattice constant change of LCO substrates and how the lattice strains are induced to Pt NPs. (**A**) Pristine LCO shows a Co-O layer spacing of 4.69 Å. By electrochemically extracting half of the Li ions out, the layer spacing is increased to 4.82 Å. (**B**) LCO is first delithiated into $L_{0.5}CO$ with layers expanded and then coated with Pt NPs. By intercalating back those Li ions, the Co-O layer spacing is decreased so as to induce compression on Pt NPs. The orientation of Pt NP is set to be different from (A) as a suggestion of nonepitaxial ALD growth. (**C**) The XRD peak shifts of LCO (003) represent the tensile and compressive strain induced to Pt NPs coated on these substrates.

We report a way to tune catalyst strain by exploiting the widely tunable lattice constant of Li-ion battery electrode materials as the catalyst support. When Li ions are electrochemically intercalated into or extracted out of electrode materials such as graphite, transition-metal dichalcogenides, silicon (Si), or Li metal oxides, the volume and lattice spacing change from several percent to severalfold (*12*, *30*–*32*). For example, the Si electrode can expand up to four times its original size when fully lithiated to $Li_{4.4}Si$ (*30*), and $LiCoO_2$ (LCO) undergoes ~3% volume changes during charge and discharge (*31*, *33*). This smaller value is still sufficient to generate strain that can alter catalysis. Li ions are sandwiched by Co-O octahedra slabs in LCO (Fig. 1A) (*34*), and during charging, half of the Li^+ are extracted to form $Li_{0.5}CoO_2$ ($L_{0.5}CO$). The Co-O slabs with negative charge experience stronger electrostatic repulsions from each other, which increases the layer spacing (Fig. 1A) (*31*, *33*). When Li^+ intercalates back during discharge, the lattice returns to its original spacing (Fig. 1B).

We deposited small Pt nanoparticles (NPs; ~5 nm) onto the surface of LCO or $L_{0.5}CO$ particle supports (~500 nm). By controlling the charging or discharging states of the substrate, we directly observed ~5% compressive and tensile strain on Pt (111) facets using transmission electron aberration-corrected microscopy (TEAM) in individual particles. The ORR catalytic activities of Pt NPs in alkaline solution were tuned over a wide range, achieving nearly 90% improvement or more than 40% decrease in activity under compressive and tensile strain, respectively. These results agree well with predictions from density functional theory (DFT) calculations.

Our strategy for introducing and controlling strain is shown in the schematic in Fig. 1. We obtained the battery electrode material LCO using a cotton-assisted pyrolysis method (*35*). The sizes of LCO particles are ~500 nm in the scanning electron microscopy (SEM) images (fig. S1, A and B) (*35*). We then used 150 cycles of atomic layer deposition (ALD) to deposit ~5 nm Pt NPs onto the surface of LCO (LCO-Pt) (figs. S2A and S3). The reason for this small loading is that (i) strain decays from substrate to the top surface and (ii) the gaps between Pt NPs are important for Li-ion transport into and out of LCO.

To induce lattice tension on the Pt NPs, LCO-Pt was assembled in a battery cell for the electrochemical charging process, with half of the Li ions extracted ($LCO\text{-}Pt_T$) (fig. S4). The x-ray diffraction (XRD) peak corresponding to the LCO (003) facets shifted from 18.92° to 18.42° in Fig. 1C, corresponding to an increase in layer spacing from 4.69 to 4.82 Å (Fig. 1A) (*35*). This nearly 3% expansion in the substrate can induce strong uniaxial tension on Pt NPs (*28*). Expansion in other LCO facets was also observed during the delithiation process (fig. S5).

Compressive strain on Pt catalyst was achieved with a reverse process (Fig. 1B). LCO substrate was first electrochemically delithiated to be $L_{0.5}CO$ with layers opened up, and then followed by ALD growth of Pt NPs ($L_{0.5}CO$-Pt). No appreciable differences in the morphology were observed when transforming from LCO and LCO-Pt to $L_{0.5}CO$ and $L_{0.5}CO$-Pt, respectively (figs. S1, C and D, and S2B). By intercalating Li ions into $Li_{0.5}CO$-Pt, the distances in the molecular layer decreased back to that of LCO, creating compressive strain on Pt NPs ($L_{0.5}CO\text{-}Pt_C$). This change was also confirmed by the XRD peaks in Fig. 1C. Because of the shift in the lattice between LCO/$L_{0.5}CO$ in the *z* direction (4.69 versus 4.82 Å) and Pt (3.92 Å), we suspect that the ALD growth of Pt NPs on LCO and $L_{0.5}CO$ substrates was not epitaxial and thus did not introduce strain (*36*–*39*). TEAM characterization revealed different Pt orientations relative to the supports (fig. S6). With strong bonding between Pt and LCO/$L_{0.5}CO$, the expansion or compression of substrates would lead to lattice strains in the catalysts.

Because of the broadening of peaks for small Pt NPs as well as the wide distribution of strain in different Pt NPs, XRD is insufficient for accurately determining the amount of strain on different sites of substrates (fig. S7). Instead, we used high-resolution TEAM, as shown in Fig. 2 (*35*). For compressive strain, a comparison between the pristine $L_{0.5}CO$-Pt and the compressed $L_{0.5}CO\text{-}Pt_C$ is shown in Fig. 2, A to D, and similarly for tensile strain for $LCO\text{-}Pt_T$ in Fig. 2, E to H. We focus on Pt (111) as a representative facet for studying the lattice strain as well as catalytic activities. For a fair comparison, Pt NPs with the $[1\bar{1}0]$ direction in the zone axis were selected in all of the four samples, thus providing the lattice spacing for the (111), $(11\bar{1})$, and (002) facets in the TEAM images. In addition, the Co-O layers of LCO are parallel to the TEAM electron beam (fig. S8), which suggests the uniaxial strain direction applied on those Pt NPs. As indicated in Fig. 2,

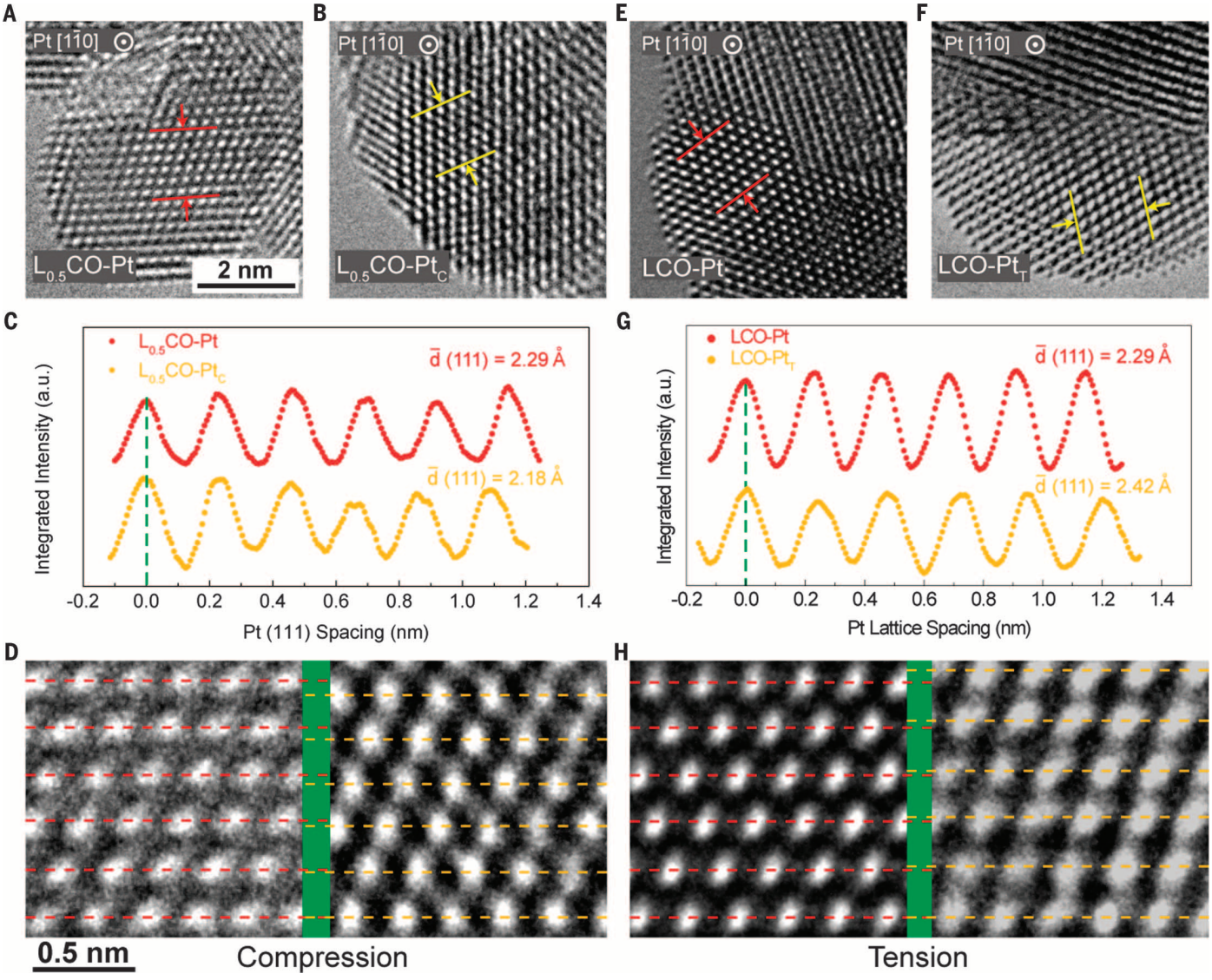

Fig. 2. High-resolution TEAM images of pristine and strained Pt NPs with (111) lattice compression and tension. Compression, (A) to (D); tension, (E) to (H). (**A** and **B**) TEAM images of $L_{0.5}$CO-Pt and $L_{0.5}$CO-Pt_C. The red and yellow bars denote the areas we analyzed for (111) spacing. (**C**) The integrated pixel intensities of pristine and compressed Pt along (111) spacing directions (which is perpendicular to the facets). The peaks and valleys represent the atoms and gaps, respectively. The spacing of Pt (111) facets is averaged over six atomic layers for high accuracy. The pristine (111) is measured to be 2.29 Å, whereas the constrained (111) shows only 2.18 Å. (**D**) The bottom layers of pristine and compressed Pt (111) lattice fringes are aligned for the direct evidence of lattice constraint. The top atomic layer of compressed Pt locates at a much lower position than the pristine one. (**E** and **F**) TEAM images of LCO-Pt and LCO-Pt_T. (**G**) More than 5% tensile strain is observed with an increased (111) spacing of 2.42 Å. (**H**) A direct evidence of tensile strain with the top atomic layer of LCO-Pt_T much higher than that of LCO-Pt. Another example of tensile strain is also shown and aligned in figs. S13 and S14. (A), (B), (E), and (F) share the same scale bar, and (D) and (H) share the same scale bar.

A, B, E, and F, we examined the central regions of the Pt NPs and obtained the averaged (111) facet spacing over six atomic layers, avoiding possible surface defects as well as blurry boundaries between Pt and the substrates.

Shown in Fig. 2C are the integrated pixel intensities for the pristine and compressed Pt (111) lattices as selected in Fig. 2, A and B, respectively (*35*). The averaged pristine Pt (111) spacing is 2.29 Å, which agrees well with calculations from previously reported Pt lattice constants (*35*). The intensity profile of constrained Pt suggests a much smaller lattice distance compared with that of the pristine Pt, with an averaged spacing of 2.18 Å, which represents ~5% compressive strain. This 5% lattice strain appears to be even greater than the lattice change of the LCO substrate (~3%), which can be explained by a possible inhomogeneity of the Li concentration near the LCO surface and within the bulk during the charging or discharging processes (*40*). The surfaces may have a greater change in Li concentration and thus lead to larger changes in the lattice. For example, the $L_{0.25}$CO lattice can expand ~6.3% from LCO, which doubles the expansion of $L_{0.5}$CO (*41*).

To have an intuitive understanding of how much the compressive lattice strain is, we aligned the (111) atomic layers on the bottom in Fig. 2D. After five layers of accumulation in spacing differences, the top layer of compressed Pt locates to a much lower position than that of the pristine Pt, offering direct evidence of the lattice compression. The successful observation of compressive strain in the Pt (111) facet led us to study whether there were any changes in the other two facets, (11$\bar{1}$) and (002), as well as the angles between them (figs. S9 and S10) (*42*). However, the spacing of these two facets in the compressed Pt NP is consistent with that of the unstrained catalyst, and we observed only slight distortions in the plane angles. This difference is caused by the direction of uniaxial strain applied by the LCO

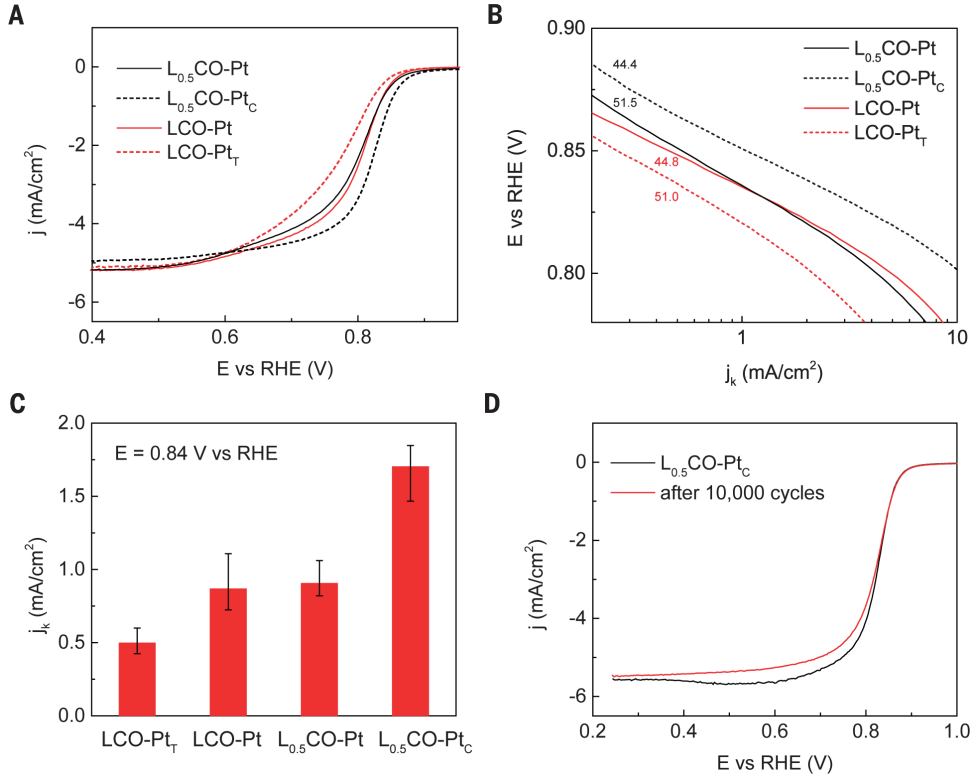

Fig. 3. Electrochemical characterizations of pristine and strained Pt NPs in O_2-saturated 0.1 M KOH for ORR electrocatalysis. (**A**) The ORR polarization curves $L_{0.5}$CO-Pt, $L_{0.5}$CO-Pt_C, LCO-Pt, and LCO-Pt_T under 1600 rotations per minute (rpm). The pristine Pt NPs on LCO and $L_{0.5}$CO substrates show negligible differences in ORR activity. Compressive strain shows an improved ORR activity, and tensile strain shows a decreased one. (**B**) The Tafel slopes of pristine and strained Pt NPs. j_K represents the kinetic current density. (**C**) The comparison of ORR activities under 0.84 V versus RHE. The error bars are based on at least three identical samples for each condition. (**D**) The ORR polarizations of compressive $L_{0.5}$CO-Pt_C before and after 10,000 CV cycles between 0.6 and 1.0 V versus RHE.

substrate being perpendicular to Pt (111) facets (fig. S8), resulting in outstanding lattice constraint in the (111) but not the (11$\bar{1}$) or (002) facets. However, because there are different Pt orientations on LCO/$L_{0.5}$CO substrates (fig. S6), the strain applied by the substrates is not always perpendicular to Pt (111) but also to other facets, which can induce strains in other facets.

Tensile strain was also revealed with TEAM (Fig. 2, E to H) by directly aligning the expanded Pt (111) planes with the pristine one in Fig. 2H, with the averaged spacing increased from 2.29 Å toward 2.42 Å (figs. S11 and S12). This roughly 5.7% expansion, together with the demonstrated compression, strongly suggests the efficacy of a LCO battery electrode in flexibly tuning lattice strain in both tensile and compressive directions over a full range of ~10%. The observed Pt (111) lattice strains in individual NPs can only represent a general trend (compression or tension) of the NP systems, as suggested in the Pt XRD peak shifts (fig. S7). We have included additional TEAM examples of Pt lattice strain (figs. S13 to S16) with different strain ranges. These Pt NPs have similar sizes with those in Fig. 2 but show different strain ranges, demonstrating that the particle size is not the only factor in determining the lattice strain. The strain condition in each Pt NP is strongly affected by its shape, crystallinity, location, and surface defects, as well as the contact facets of both the Pt particle and the LCO substrate. In addition, we also performed aberration-corrected scanning transmission electron microscope high-angle annular dark-field (STEM-HAADF) imaging on the tensile strain case in order to suppress the substrate effects on Pt NPs in TEM characterizations (figs. S17 to S19). Convergent beam electron diffraction (CBED) of pristine and tensile Pt NPs is also shown in figs. S20 to S22, further demonstrating the existence of lattice strain introduced by the support.

The relation between Pt lattice strain and its ORR catalytic activities was examined in a rotating-disc three-electrode system (*35*). Four samples were tested: $L_{0.5}$CO-Pt and $L_{0.5}$CO-Pt_C for studying compressive strain and LCO-Pt and LCO-Pt_T for tensile strain. The mass ratio of Pt in those catalysts was determined to be ~17% (table S1) (*35*). Several cycles of cyclic voltammetry (CV) were applied before testing their ORR activities (fig. S23). In the polarization curves in Fig. 3A, the compressed Pt compared with the pristine catalyst presents a positive shift in onset as well as half-wave potentials by ~20 mV. In contrast, tensile strain induced a negative effect on ORR activity, requiring a larger overpotential to drive the reaction. The catalytic activity shifts caused by strain are consistent with previous works (*14*, *25*, *27*, *28*). Background contributions from $L_{0.5}$CO and LCO substrates have been ruled out (fig. S24) (*28*). Because of the high density of free electrons in Pt metal, the charge transfer effects from the semiconducting support can be easily screened within one or two Pt atomic layers and will not affect the electronic properties of Pt surface sites for catalysis. We plotted the kinetic current densities of the pristine and strained samples versus potential and obtained their Tafel slopes in Fig. 3B, suggesting similar Tafel slopes ranging from 44.4 to 51.5 mV/decade within the measurement errors (fig. S25). The kinetic activities of pristine and strained Pt under 0.84 V potential are compared in Fig. 3C. The pristine Pt on both $L_{0.5}$CO and LCO substrates shows similar activities at around 0.9 mA/cm^2, which is elevated to 1.7 mA/cm^2 under the compressive strain, representing a nearly doubled enhancement, but expanding the lattice of Pt NPs caused the ORR activity to decrease to only 0.5 mA/cm^2. The pristine $L_{0.5}$CO-Pt sample shows nearly the same ORR activity after 10,000 CV cycles (fig. S24), suggesting the good stability of Pt NPs on the LCO/$L_{0.5}$CO support as well as the strong interaction between them. In addition, the effect of lattice strain can also sustain during this long-term stability test without noticeable degradation, except for a slightly smaller diffusion-limiting current (Fig. 3D), which indicates that the strain effect does not affect its ORR stability.

Comparisons can be made of the data in Fig. 3 with our present theoretical model of the ORR (*35*). The close-packed Pt surfaces are most active for ORR (*43*), so we focused on the Pt (111) facets. The effect of strain on the adsorption free energies ΔG_i of the reaction intermediates (i = O*, OH*, and OOH*), which are strongly related with the Pt 5d band (fig. S26), is illustrated in Fig. 4A. These adsorption energies are computed as $\Delta G_i = \Delta E_i + \Delta ZPE - T\Delta S$, where ΔE_i is the formation of an intermediate i relative to H_2O and H_2, accounting for solvent-induced stabilizations; ΔZPE is the difference in zero point energies; and ΔS is the change in entropy (*43*). All quantities in Fig. 4A were determined relative to the unstrained Pt (111), which is defined as zero. Negative ΔG represents stronger binding, and positive ones represent weaker binding. For uniaxial strain in the range of 5% (tensile) to –5% (compressive), the adsorption free energies for all reaction

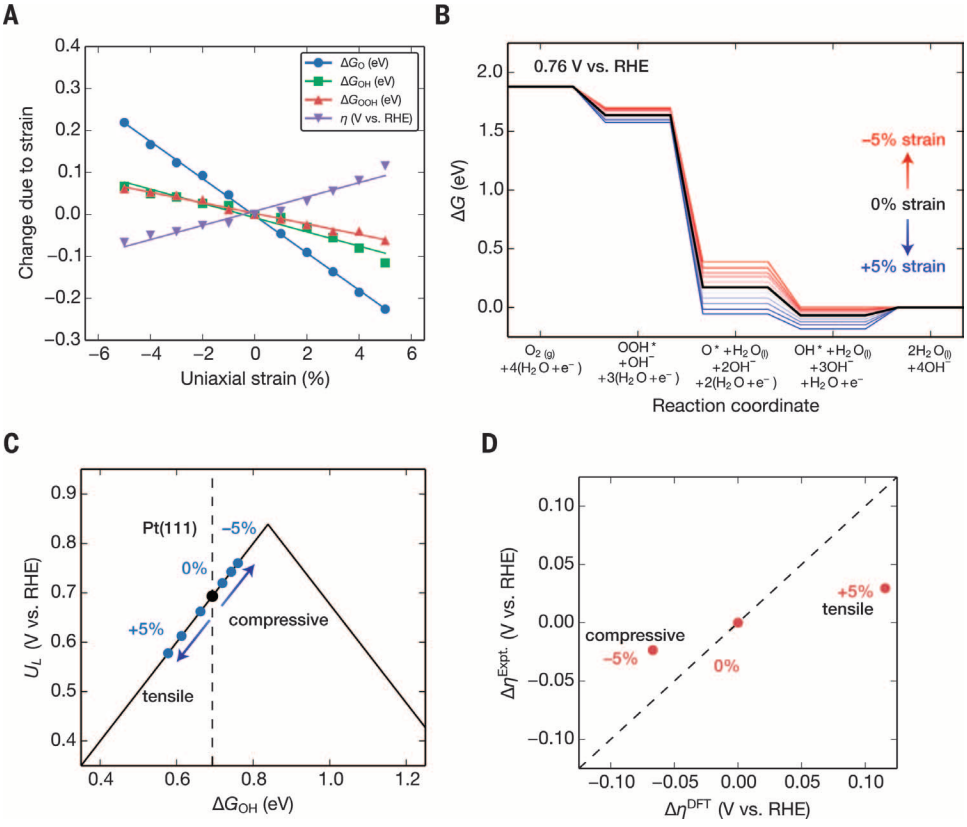

Fig. 4. Theoretical predictions for the effect of uniaxial strain on the Pt ORR activity. (**A**) The change in binding energies for O*, OH*, and OOH* intermediates as well as the change in the overpotential η as a function of uniaxial strain. The lines are linear fits to the data points. (**B**) The free-energy diagram for ORR at 0.76 V versus RHE, where all steps for the –5% strained Pt (111) are exergonic. The change in stabilities for each step caused by uniaxial strain is shown in red (compressive) and blue (tensile). (**C**) Illustration of the limiting potential "volcano" as a function of the change in ΔG_{OH}. The U_L improved with increasing compressive strain. The intermediate strains are ±2 and ±4%. (**D**) Comparisons between the change in experimental half-wave potential and the change in theoretical overpotential caused by strain. ±5% strain was chosen for the DFT values, corresponding to our TEM results in Fig. 2.

intermediates decrease (stronger binding) with tensile strain and increase (weaker binding) with compressive strain (*17*). Changes in ΔG_{OH} and ΔG_{OOH} are the same, whereas ΔG_O has a stronger dependence caused by its threefold coordination to the surface (*44*). The strain effects on these reaction intermediates have all been included in the free energy diagram in Fig. 4B, in which the free energy for each step was determined by adding a potential-dependence for ΔGi using the computational hydrogen electrode model (*45*).

Because tensile strain makes the binding of all intermediates stronger, and $OH^* + H^+ + e^- \rightarrow H_2O(l)$ is the limiting step for pristine Pt (*43*, *45*), the thermodynamic sink for this final step only becomes deeper with tensile strain. Compressive strain weakens OH* binding and leads to more facile desorption of the final product, $H_2O(l)$. The theoretical overpotential η [defined as the potential below the equilibrium potential of 1.23 V versus reversible hydrogen electrode (RHE) required to make all reaction steps exergonic] thus decreases with compressive strain (becomes more active) and increases with expansive strain (becomes less active). At the applied potential of 0.76 V versus RHE, all steps become exergonic for the maximum –5% strain. The applied potential required to make all steps in the pathway exergonic is known as the limiting potential U_L. A lower U_L thus indicates higher activity. The binding energies of all intermediates scale linearly with one another (*45*, *46*), which means that the energy for a single intermediate is sufficient for describing the entire pathway. Thus, U_L can be determined solely on the basis of the binding strength of one of the intermediates, such as ΔG_{OH}. The ORR activity based on U_L as a function of ΔG_{OH} (a descriptor for all reaction intermediates) is illustrated by the volcano relation in Fig. 4C, in which the theoretical maximum limiting potential U_L occurs at ΔG_{OH} 0.84 eV. On the left leg, the limiting step is final H_2O desorption with $U_L = \Delta G_{OH}$, whereas on the right leg, the limiting step is the initial OOH* adsorption. The peak arises from the aforementioned linear scaling between the binding strengths of OH* and OOH* (*45*, *46*), which prevents them from being modified independently. For the same reason, we could also use ΔG_O or ΔG_{OOH} as the descriptor for Fig. 4C, with no changes in trends of the volcano plot. Regardless, compressive strain of ~5% should lead to improved activity toward the ORR. Although the 5% strain is not representative of all Pt particles on different LCO surface sites in the experimental samples, the trends are expected to be in good agreement. The experimental half-wave potentials and theoretical limiting potentials for the strained and unstrained Pt catalysts are presented in Fig. 4D with qualitative agreement. The remaining discrepancies likely arise from the strain distribution, which is not expected to be uniform across all sites on the LCO/$L_{0.5}$CO substrates. Pt NPs that undergo less strain would still contribute to the total activity.

Given the wide variety of tunable battery electrode materials in existence, and the vast number of catalysts and reactions that can be improved with strain, we demonstrate a highly general approach for studying these effects in the design of next-generation catalytic materials. In addition to fundamental studies, practical applications can also be extended by including large-scale synthesis and strain-tuning methods such as solution-coating of Pt, aqueous solution electrochemical tuning, or chemical extraction/intercalation of Li ions. Other types of battery electrode materials—such as layered MoS_2, TiO_2, Bi_2Se_3, and black phosphorus—can also be used to greatly extend the scope of this strain-tuning method toward acidic electrocatalysis.

REFERENCES AND NOTES

1. M. S. Dresselhaus, I. L. Thomas, *Nature* **414**, 332–337 (2001).
2. M. G. Walter *et al.*, *Chem. Rev.* **110**, 6446–6473 (2010).
3. R. Bashyam, P. Zelenay, *Nature* **443**, 63–66 (2006).
4. J. Greeley *et al.*, *Nat. Chem.* **1**, 552–556 (2009).
5. Y. Bing, H. Liu, L. Zhang, D. Ghosh, J. Zhang, *Chem. Soc. Rev.* **39**, 2184–2202 (2010).
6. S. Mukerjee, S. Srinivasan, M. P. Soriaga, J. McBreen, *J. Electrochem. Soc.* **142**, 1409–1422 (1995).
7. J. Suntivich, K. J. May, H. A. Gasteiger, J. B. Goodenough, Y. Shao-Horn, *Science* **334**, 1383–1385 (2011).
8. C. Chen *et al.*, *Science* **343**, 1339–1343 (2014).
9. X. Huang *et al.*, *Science* **348**, 1230–1234 (2015).
10. V. R. Stamenkovic *et al.*, *Nat. Mater.* **6**, 241–247 (2007).
11. V. R. Stamenkovic, B. S. Mun, K. J. J. Mayrhofer, P. N. Ross, N. M. Markovic, *J. Am. Chem. Soc.* **128**, 8813–8819 (2006).
12. H. Wang *et al.*, *Proc. Natl. Acad. Sci. U.S.A.* **110**, 19701–19706 (2013).
13. Z. Lu *et al.*, *Nat. Commun.* **5**, 4345 (2014).
14. P. Strasser *et al.*, *Nat. Chem.* **2**, 454–460 (2010).
15. H. Li *et al.*, *Nat. Mater.* **15**, 48–53 (2016).
16. D. Voiry *et al.*, *Nat. Mater.* **12**, 850–855 (2013).
17. M. Mavrikakis, B. Hammer, J. K. Nørskov, *Phys. Rev. Lett.* **81**, 2819–2822 (1998).
18. B. Hammer, J. K. Nørskov, *Adv. Catal.* **45**, 71–129 (2000).
19. J. Zhang *et al.*, *J. Phys. Chem. B* **109**, 22701–22704 (2005).
20. D. Wang *et al.*, *Nat. Mater.* **12**, 81–87 (2013).
21. X. Wang *et al.*, *Nat. Commun.* **6**, 7594 (2015).
22. L. Zhang *et al.*, *Science* **349**, 412–416 (2015).
23. A. Jackson *et al.*, *ChemElectroChem* **1**, 67–71 (2014).

24. S. Koh, P. Strasser, *J. Am. Chem. Soc.* **129**, 12624–12625 (2007).
25. I. E. L. Stephens *et al.*, *J. Am. Chem. Soc.* **133**, 5485–5491 (2011).
26. L. Gan, R. Yu, J. Luo, Z. Cheng, J. Zhu, *J. Phys. Chem. Lett.* **3**, 934–938 (2012).
27. Q. Jia *et al.*, *ACS Nano* **9**, 387–400 (2015).
28. M. Du, L. Cui, Y. Cao, A. J. Bard, *J. Am. Chem. Soc.* **137**, 7397–7403 (2015).
29. L. Yang *et al.*, *Sci. Rep.* **4**, 5649 (2014).
30. C. K. Chan *et al.*, *Nat. Nanotechnol.* **3**, 31–35 (2008).
31. T. Ohzuku, A. Ueda, *J. Electrochem. Soc.* **141**, 2972–2977 (1994).
32. G. Csányi, P. B. Littlewood, A. H. Nevidomskyy, C. J. Pickard, B. D. Simons, *Nat. Phys.* **1**, 42–45 (2005).
33. S. Choi, A. Manthiram, *J. Electrochem. Soc.* **149**, A162–A166 (2002).
34. Y. Shao-Horn, L. Croguennec, C. Delmas, E. C. Nelson, M. A. O'Keefe, *Nat. Mater.* **2**, 464–467 (2003).
35. Materials and methods are available as supplementary materials on *Science* Online.
36. S. M. George, *Chem. Rev.* **110**, 111–131 (2010).
37. A. Asthagiri, D. S. Sholl, *J. Chem. Phys.* **116**, 9914–9925 (2002).
38. S. T. Christensen *et al.*, *Small* **5**, 750–757 (2009).
39. The nonepitaxial growth does not necessarily mean that the interaction between Pt and LCO/$L_{0.5}$CO is not strong enough to transfer lattice strain. The Pt atoms on the edge sites of LCO or $L_{0.5}$CO substrates can form strong bonding with dangling O or Co atoms.
40. K. Zhao, M. Pharr, J. J. Vlassak, Z. Suo, *J. Appl. Phys.* **108**, 073517 (2010).
41. F. Xiong *et al.*, *Int. J. Electrochem. Sci.* **7**, 9390–9400 (2012).
42. L. Wang *et al.*, *Nat. Commun.* **4**, 2413 (2013).
43. V. Viswanathan, H. A. Hansen, J. Rossmeisl, J. K. Nørskov, *ACS Catal.* **2**, 1654–1660 (2012).
44. L. Li, F. Abild-Pedersen, J. Greeley, J. K. Nørskov, *J. Phys. Chem. Lett.* **6**, 3797–3801 (2015).
45. J. K. Nørskov *et al.*, *J. Phys. Chem. B* **108**, 17886–17892 (2004).
46. V. Viswanathan, H. Hansen, *Top. Catal.* **57**, 215–221 (2014).

ACKNOWLEDGMENTS

We acknowledge support from the Global Climate Energy Project at Stanford University. H.W. acknowledges support from the Stanford Interdisciplinary Graduate Fellowship. S.X. and F.B.P. were supported by the Center on Nanostructuring for Efficient Energy Conversion (CNEEC) at Stanford University, an Energy Frontier Research Center funded by the U.S. Department of Energy (DOE), Office of Science, Basic Energy Sciences, under award DE-SC0001060. F.A.-P. and J.K.N acknowledge financial support from the DOE, Office of Basic Energy Sciences, to the SUNCAT Center for Interface Science and Catalysis. C.T. acknowledges support from the National Science Foundation Graduate Research Fellowship Program (GRFP) grant DGE-114747. Y.C. acknowledges support to initiate the catalysis research from the DOE, Basic Energy Sciences, Materials Sciences and Engineering Division, under contract DE-AC02-76SF00515. The authors acknowledge the help of aberration-corrected STEM-HAADF from P. Yang and Y. Yu at the National Center for Electron Microscopy at the Molecular Foundry. Work at the Molecular Foundry was supported by the DOE Office of Science, Office of Basic Energy Sciences, under contract DE-AC02-05CH11231. The authors also acknowledge helpful discussions with M. Logar. All of the data are available in the main paper and supplementary materials.

SUPPLEMENTARY MATERIALS

www.sciencemag.org/content/354/6315/1031/suppl/DC1
Materials and Methods
Figs. S1 to S30
Table S1
References (*47*–*58*)

13 December 2015; resubmitted 28 March 2016
Accepted 17 October 2016
10.1126/science.aaf7680

AUTOPHAGY

The ATG conjugation systems are important for degradation of the inner autophagosomal membrane

Kotaro Tsuboyama,[1]* Ikuko Koyama-Honda,[1]* Yuriko Sakamaki,[2] Masato Koike,[3] Hideaki Morishita,[1] Noboru Mizushima[1]†

In macroautophagy, cytoplasmic contents are sequestered into the double-membrane autophagosome, which fuses with the lysosome to become the autolysosome. It has been thought that the autophagy-related (ATG) conjugation systems are required for autophagosome formation. Here, we found that autophagosomal soluble *N*-ethylmaleimide–sensitive factor attachment protein receptor (SNARE) syntaxin 17–positive autophagosome-like structures could be generated even in the absence of the ATG conjugation systems, although at a reduced rate. These syntaxin 17–positive structures could further fuse with lysosomes, but degradation of the inner autophagosomal membrane was significantly delayed. Accordingly, autophagic activity in ATG conjugation–deficient cells was strongly suppressed. We suggest that the ATG conjugation systems, which are likely required for the closure (i.e., fission) of the autophagosomal edge, are not absolutely essential for autolysosome formation but are important for efficient degradation of the inner autophagosomal membrane.

Macroautophagy (hereafter, autophagy) is a highly inducible intracellular degradation system (*1*–*3*). First, a flat membrane sac, termed the isolation membrane or the phagophore, elongates, bends, and sequesters a part of the cytoplasm. Then, its edge is closed by membrane fission to form the double-membrane structure, the autophagosome (*4*). The autophagosome fuses with lysosomes and becomes the autolysosome. Lysosomal enzymes selectively degrade the inner autophagosomal membrane (IAM), but not the outer autophagosomal membrane (OAM), and then finally degrade the enclosed cytoplasmic contents.

To characterize autophagosome maturation in mammalian cells, we used the autophagosomal soluble *N*-ethylmaleimide–sensitive factor attachment protein receptor (SNARE) syntaxin 17 (STX17) as an autophagosome marker (*5*). Elongating isolation membranes were microtubule-associated protein light chain 3 (LC3) positive but STX17 negative (Fig. 1A, red arrows, and movie S1) (*5*). Later, STX17 was recruited to the whole circumference of ring-shaped structures (Fig. 1A, green arrows). The shape of elongating isolation membranes was elliptical but became almost completely spherical when STX17 was recruited (Fig. 1B). We hypothesize that fission between the OAM and IAM during the closure of the autophagosomal edge causes a morphological change into stable spherical bodies that occurs immediately before or after the recruitment of STX17.

After STX17 recruitment, several small LAMP1-positive lysosomes (or late endosomes) associated with the autophagosomes (Fig. 1C, 2 to 8 min, blue arrows). Then, the autophagosomal membrane became LAMP1-positive (Fig. 1C, 10 to 16 min, blue arrows). At almost the same time, these structures became positive for LysoTracker Red (LTR), a weak-base probe for acidic compartments. The LTR signals appeared also as ring-shaped structures on the STX17-positive structures (Fig. 1C, 4 to 10 min, red arrows), which suggests that the space between the OAM and IAM is acidified. Next, the ring-shaped LTR signal collapsed, and the lumen of the autolysosomes filled with LTR, which indicated the IAM degradation (Fig. 1C, 12 to 16 min). The STX17 signal gradually disappeared after the collapse of the LTR ring structure (Fig. 1C, 12 to 14 min). This STX17 dissociation was independent of luminal acidification because it was not affected by bafilomycin A_1 treatment (fig. S1). Thus, we detected four steps during autophagosome maturation: STX17 recruitment (step a), lysosomal fusion (step b), IAM degradation (step c), and STX17 release (step d) (Fig. 1C). The total lifetime of STX17 (steps a to d) and the durations (means ± SEM) between each step (a to b, b to c, and c to d) were 11.0 ± 0.6, 2.1 ± 0.3, 6.6 ± 0.6, and 2.2 ± 0.2 min, respectively (Fig. 1C).

Autophagosome formation requires the two ubiquitin-like systems: the ATG12 conjugation system and the ATG8 (LC3s and γ-aminobutyric acid receptor–associated proteins in mammals) conjugation system (*6*, *7*). Ubiquitin-like ATG12 and ATG8 are covalently conjugated to ATG5 and phosphatidylethanolamine (PE), which are catalyzed by the common E1-like protein ATG7 and the specific E2-like proteins ATG10 and ATG3, respectively. Conjugation of ATG8 or LC3 with

[1]Department of Biochemistry and Molecular Biology, Graduate School and Faculty of Medicine, The University of Tokyo, Tokyo 113-0033, Japan. [2]Research Center for Medical and Dental Sciences, Tokyo Medical and Dental University, Tokyo 113-8510, Japan. [3]Departments of Cell Biology and Neuroscience, Juntendo University Graduate School of Medicine, Bunkyo-Ku, Tokyo 113-8421, Japan.
*These authors contributed equally to this work.
†Corresponding author. Email: nmizu@m.u-tokyo.ac.jp

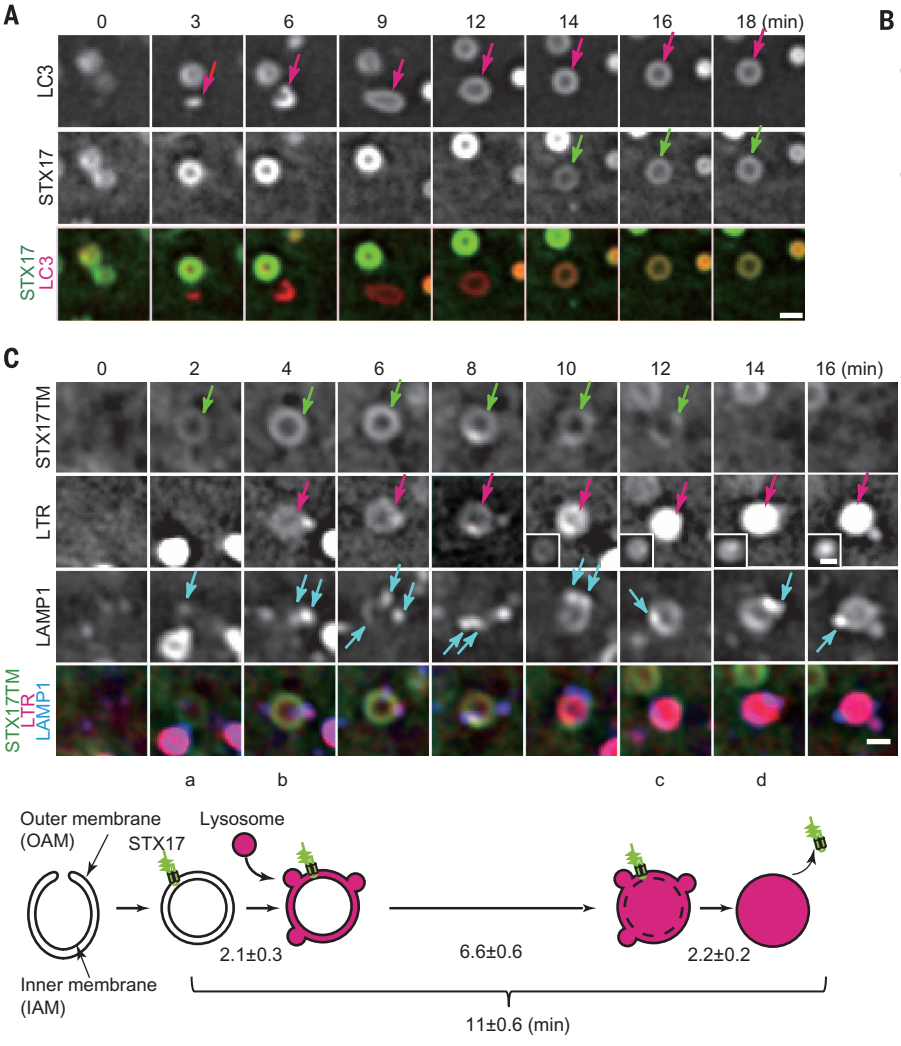

Fig. 1. The life of the autophagosome. (**A**) Selected frames from a time-lapse movie (movie S1) of starved wild-type (WT) mouse embryonic fibroblasts (MEFs) stably expressing Venus-LC3 and Turquoise2-STX17. A newly formed autophagosome is indicated by the red and green arrows, respectively. Scale bar, 1 μm. (**B**) The oblateness (O) of LC3-positive structures 1 min before and after appearance of STX17 signals (n = 20). (**C**) Time-lapse analysis of WT MEFs stably expressing CFP-STX17TM [consisting of only the C-terminal region, including the two transmembrane domains, which can translocate to autophagosomes normally (*5*)] and LAMP1-Venus cultured in starvation medium containing LysoTracker Red (LTR). A newly formed CFP-STX17TM–positive and LTR-positive autophagosome is indicated by the green and red arrows, respectively. Insets in the LTR panels show the same structures indicated by red arrows with weaker contrast adjustment to avoid saturating the signals. Associated LAMP1-Venus–positive structures are indicated by the blue arrows. Step a, STX17 is recruited to the OAM; step b, the intermembrane space of the autophagosome becomes acidified after fusion with lysosomes; step c, the IAM is degraded as represented by collapse of LTR ring-shaped structures; step d, disappearance of STX17. Scale bars, 1 μm. Duration between each step is shown in the scheme [n = 26, means ± SEM (min)].

PE depends on ATG12–ATG5 (*8*, *9*). ATG8 seems to be essential for an early stage of autophagosome formation in yeast (*10*, *11*). By contrast, accumulation of elongated isolation membranes and even double-membrane autophagosome-like structures, but not autolysosomes, has been observed in mouse embryonic stem cells lacking ATG5 (*9*); mouse embryonic fibroblasts (MEFs) lacking ATG5 (*12*) or ATG3 (*13*, *14*); and NIH-3T3 cells overexpressing a dominant-negative mutant of ATG4B (*15*). These findings led to the suggestion that the ATG conjugation systems are required for the closure step. However, the fate of these elongated isolation membranes is unknown, because the sole autophagosome marker LC3 and any other ATG proteins cannot localize to autophagosomes in these cells (*16*, *17*).

To overcome this limitation, we used STX17 as an autophagosome marker. Unexpectedly, a number of STX17-positive punctate or ring-shaped structures were observed under starvation conditions in ATG conjugation–deficient cells, such as ATG3 knockout (KO), ATG5 KO, and ATG7 KO MEFs (Fig. 2, A and B, and movie S2) and ATG3 KO HeLa cells (fig. S2A). These STX17-positive structures also accumulated even under growing (nonstarvation) conditions in ATG conjugation–deficient cells (Fig. 2, A and B, and fig. S2A). In ATG9A KO, FIP200 (also known as RB1CC1) KO, and ATG14 KO MEFs, STX17 did not form puncta, which is consistent with a known lack of isolation membranes in these cells (*12*). These STX17-positive rings did not represent mislocalization of STX17; immunoelectron microscopy showed the recruitment of STX17 on autophagosome-like structures in ATG3 KO MEFs (Fig. 2C, fig. S2D). Indeed, lactate dehydrogenase, a cytosolic enzyme, was sequestered in these structures (fig. S3). Furthermore, these STX17-positive structures in ATG3 KO cells were formed by the canonical pathway, because their formation was abolished by additional knockdown (fig. S2B) or knockout (fig. S2C) of FIP200 or ATG14 or treatment with wortmannin (Fig. 2, A and B).

These STX17-positive autophagosome-like structures in ATG3 KO cells were positive for SNAP29 (Fig. 2D) and became LTR positive (Fig. 2E). The STX17 structures were mostly colocalized with LAMP1 (Fig. 2F). The time between STX17 recruitment and acidification (i.e., between steps a and b in Fig. 1C) in ATG3 KO MEFs was only slightly longer than that in wild-type (WT) MEFs (Fig. 2E). Thus, the fusion between autophagosome-like structures and lysosomes occurs almost normally in ATG3 KO MEFs.

To reevaluate the autophagic activity in ATG KO cells, we generated ATG3 KO, ATG5 KO, ATG9A KO, and FIP200 KO HeLa cells by the CRISPR-Cas9 genome-editing method (fig. S4) and confirmed that autophagic flux was blocked in these cells by an LC3 conversion assay (*9*, *13*, *18*) (fig. S4), accumulation of p62 (also known as SQSTM1), and lysosomal long-lived protein degradation assay (Fig. 3A). Thus, both selective and nonselective autophagy are considerably suppressed in ATG conjugation–deficient cells.

The appearance rate of Venus-ATG5–positive structures was 1.27 ± 0.14 (n = 9) in WT and 1.03 ± 0.11/min per cell (n = 9) in ATG3 KO MEFs, suggesting that isolation membranes are generated at a normal rate in ATG3 KO cells. The lifetime of Venus-ATG5–positive structures in ATG3 KO MEFs appeared to be longer than that in WT MEFs, as previously reported (Fig. 3B) (*13*). The rate of the transition of Venus-ATG5–positive

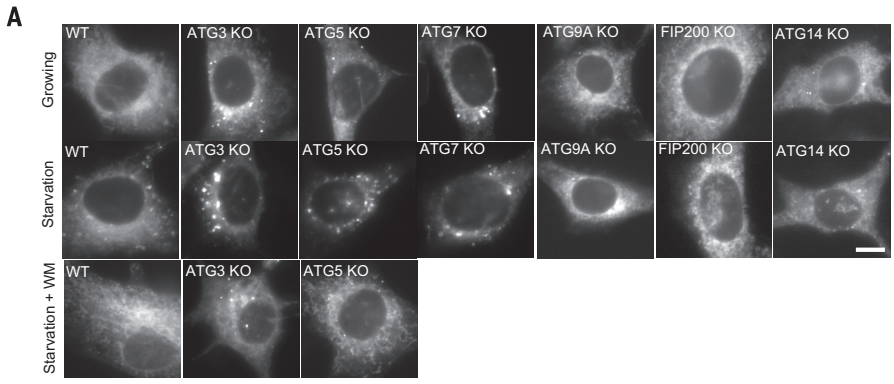

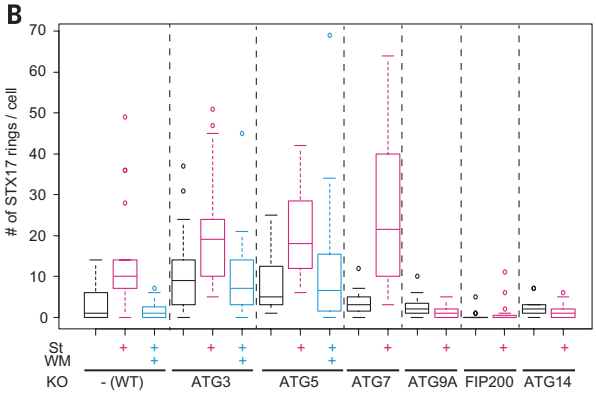

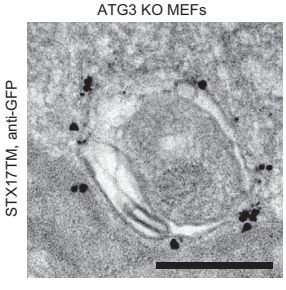

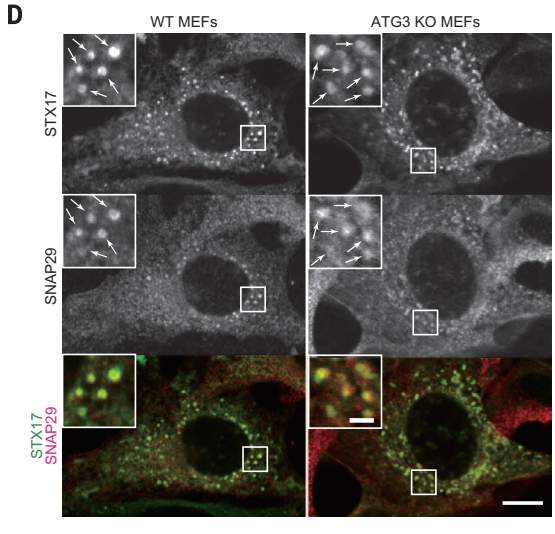

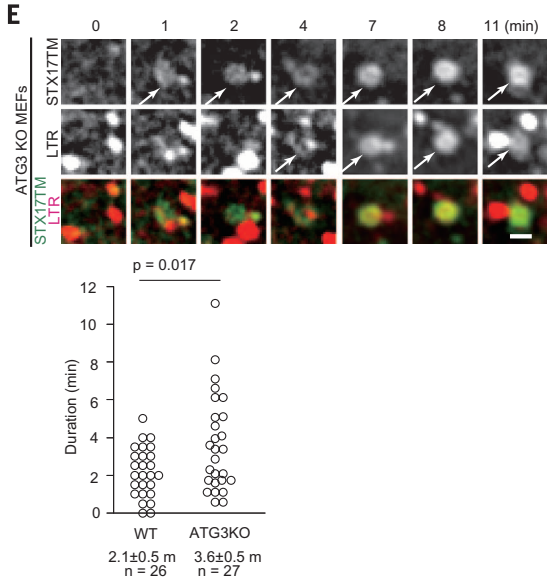

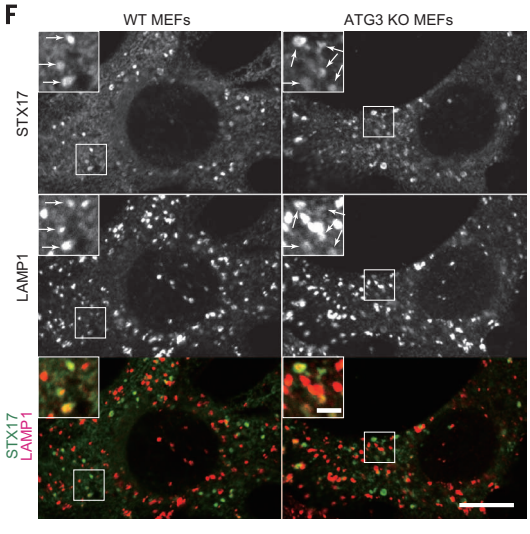

Fig. 2. Autophagosome-like structures can acquire STX17 and fuse with lysosomes in ATG conjugation–deficient cells. (**A**) MEFs (as labeled) stably expressing CFP-STX17TM were cultured in growing or starvation medium with or without 100 nM wortmannin (WM) for 1 hour. Scale bar, 10 μm. (**B**) Quantification of the number of CFP-STX17TM–positive structures per cell (n > 11 cells). The solid bars indicate median, the boxes indicate the interquartile range (25th to 75th percentile), the whiskers extend to 1.5 times the interquartile range, and outliers are plotted individually. (**C**) ATG3 KO MEFs stably expressing CFP-STX17TM were starved for 1 hour and subjected to immunoelectron microscopy using an antibody against green fluorescent protein (GFP) (anti-GFP). A double-membraned autophagosome-like structure containing cytoplasmic constituents is shown. A larger field is shown in fig. S2D. Scale bar, 200 nm. (**D** and **F**) WT and ATG3 KO MEFs stably expressing Turquoise2-STX17 and myc-SNAP29 (D) or Turquoise2-STX17 (F) were starved for 1 hour and subjected to immunofluorescence microscopy. Arrows indicate colocalization. Scale bars, 10 μm and inset, 2 μm. (**E**) Time-lapse analysis of starved ATG3 KO MEFs stably expressing CFP-STX17TM. A new CFP-STX17–positive LTR ring-shaped structure is indicated by the arrows. Duration from the appearance of the CFP-STX17TM–positive ring to that of the LTR signal in WT (n = 26) and ATG3 KO (n = 27) MEFs is shown [mean times ± SEM (min)]. Scale bar, 1 μm.

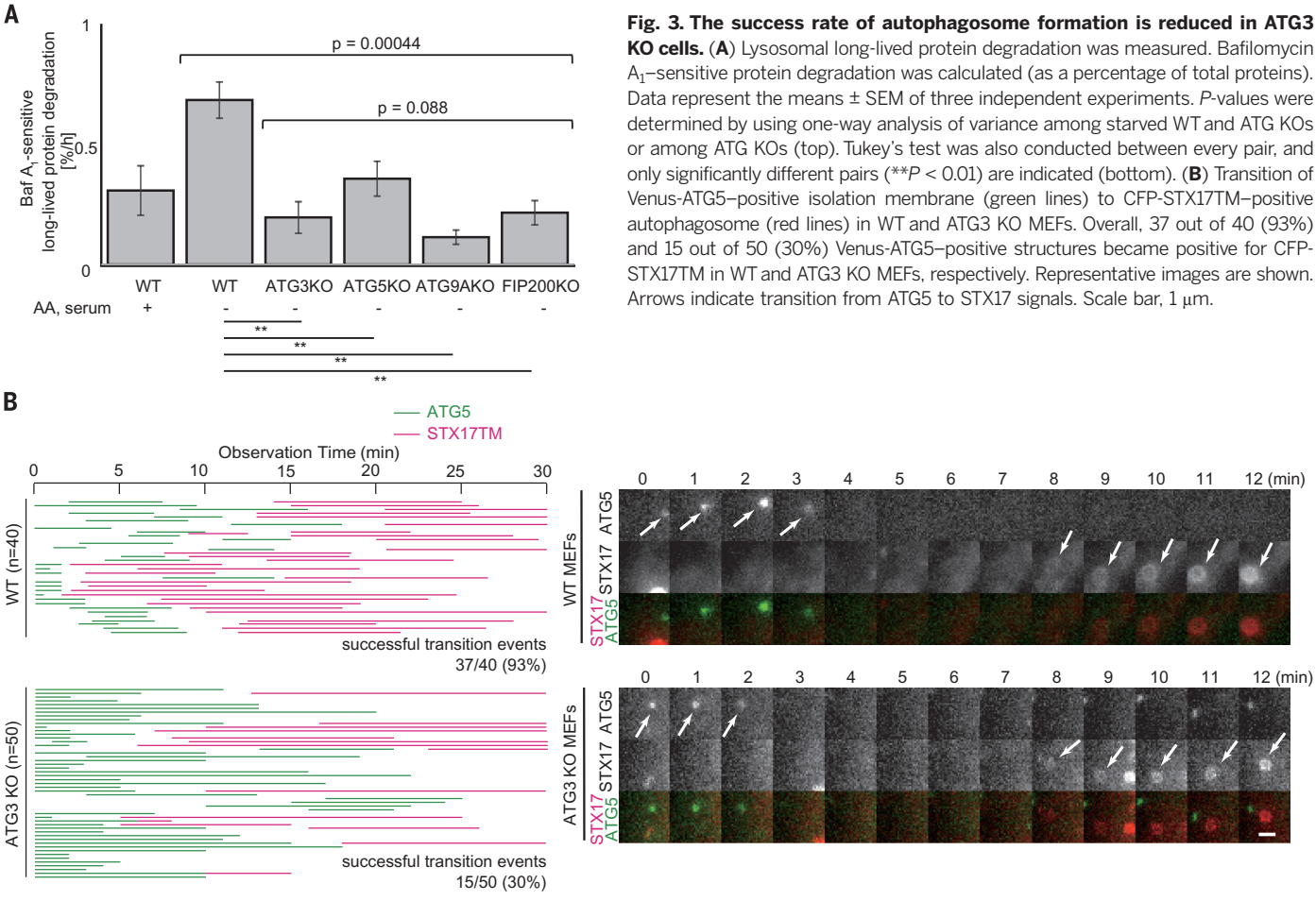

Fig. 3. The success rate of autophagosome formation is reduced in ATG3 KO cells. (**A**) Lysosomal long-lived protein degradation was measured. Bafilomycin A_1–sensitive protein degradation was calculated (as a percentage of total proteins). Data represent the means ± SEM of three independent experiments. *P*-values were determined by using one-way analysis of variance among starved WT and ATG KOs or among ATG KOs (top). Tukey's test was also conducted between every pair, and only significantly different pairs (**$P < 0.01$) are indicated (bottom). (**B**) Transition of Venus-ATG5–positive isolation membrane (green lines) to CFP-STX17TM–positive autophagosome (red lines) in WT and ATG3 KO MEFs. Overall, 37 out of 40 (93%) and 15 out of 50 (30%) Venus-ATG5–positive structures became positive for CFP-STX17TM in WT and ATG3 KO MEFs, respectively. Representative images are shown. Arrows indicate transition from ATG5 to STX17 signals. Scale bar, 1 μm.

structures to structures positive for cyan fluorescent protein (CFP)–labeled transmembrane domains of STX17 (STX17TM), which represents the success rate of autophagosome formation, was only 30% in ATG3 KO MEFs compared with 93% in WT MEFs (Fig. 3B). Thus, the ATG conjugation systems are indeed important for the late step of autophagosome formation.

Finally, we found that STX17-positive LTR ring-shaped structures were maintained for a much longer period (>30 min) in ATG3 KO, ATG5 KO, and ATG7 KO MEFs compared with WT and rescued ATG3 KO MEFs (Fig. 4, A and B). Thus, degradation of the IAM is significantly delayed in ATG conjugation–deficient cells. Indeed, by immunoelectron microscopy, intact IAMs could be detected in LAMP1-positive autophagosome-like structures in ATG3 KO MEFs (Fig. 4C, fig. S5). This was not due to a lysosomal defect, because degradation of epidermal growth factor receptor and activity of cathepsin B were normal in ATG3 KO cells (fig. S6). Thus, in ATG3 KO cells, the IAM becomes resistant to degradation by lysosomal enzymes.

Nonetheless, collapse of the IAM was occasionally observed after a certain time even in ATG3 KO MEFs (Fig. 4D, red arrows). Consistently, autolysosomes containing digested cytoplasmic materials were observed—but only rarely (fig. S7) (*13*). STX17 remained on the autophagosome-like structures as long as the IAM was maintained (although the intermembrane space was acidified) but immediately dissociated from the membrane after the collapse of the IAM (Fig. 4D, green arrows). Thus, dissociation of STX17 is triggered by IAM degradation rather than acidification. Accordingly, the lifetime of STX17-positive structures was longer in ATG3 KO MEFs than that in WT MEFs (Fig. 4E).

Many of the STX17-positive autophagosome-like structures in ATG3 KO MEFs were not spherical but elliptical compared with those in WT MEFs (Fig. 4F). If the fission between the OAM and IAM causes the spherical change (Fig. 1, A and B), the elliptical shape of the STX17 structures suggests that the final fission process is impaired in ATG3 KO MEFs. Indeed, in a few cases, the edges of the STX17-positive structures were not closed (Fig. 4G). In extreme cases, the edge became wide open, followed by disappearance of the STX17 signal. These data suggest that, even though STX17 is recruited, fission of the edge of the autophagosomes is likely not completed in ATG3 KO cells.

Our observation does not represent so-called "Atg5- or Atg7-independent alternative autophagy," which was proposed to initiate from the trans-Golgi, not from the endoplasmic reticulum (ER), and typically was induced by etoposide treatment (*19*). We observed, however, that ATG5- or STX17-positive punctate structures were generated in a canonical manner in close proximity to the ER throughout the cytoplasm, not exclusively in the Golgi region in ATG3 KO cells (movie S2 and S3, fig. S8, A and B).

Here, we showed that ATG3 is important for two critical steps: (i) efficient transition from the isolation membrane to the autophagosome and (ii) efficient degradation of the IAM (Fig. 4H). The former finding is consistent with the previously proposed hypothesis that the ATG conjugation systems are required for closure and/or fission of the edge (*11*). We hypothesize that ATG conjugation–dependent closure is important for the subsequent processes, including spherical morphological change and efficient IAM degradation, but not absolutely essential for STX17 recruitment and lysosomal fusion (Fig. 4H). The inward membrane fission could be a common mechanism for efficient degradation by vacuolar or lysosomal enzymes. For example, during formation of the multivesicular body and vacuolar or lysosomal microautophagy, invaginated membranes become sensitive to lysosomal or vacuolar degradation only after separation from the outer membranes, which are resistant to degradation (fig. S9).

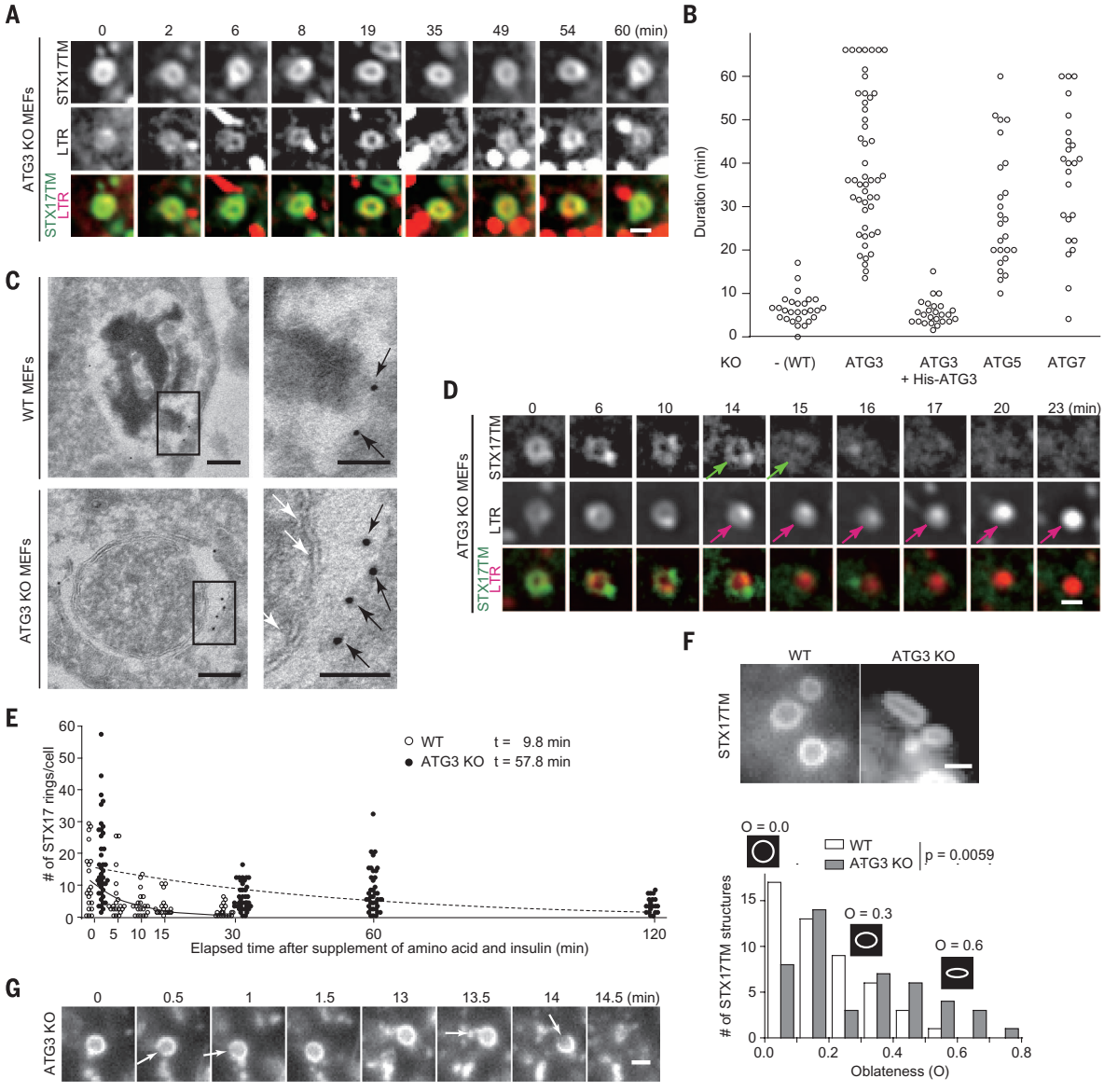

Fig. 4. Degradation of the IAM is defective in ATG3 KO cells. (**A**) Time-lapse analysis of starved ATG3 KO MEFs stably expressing CFP-STX17TM. A representative image of a LTR ring structure with prolonged lifetime (more than 60 min) is shown. Scale bar, 1 μm. (**B**) Duration of the CFP-STX17-positive LTR ring-shaped structures in WT, ATG3 KO, rescued ATG3 KO, ATG5 KO, and ATG7 KO MEFs (n > 23 structures). (**C**) WT and ATG3KO MEFs were starved for 1 hour and subjected to immunoelectron microscopy using ultrathin cryosections with anti-LAMP1 antibody (10-nm colloidal gold). Black arrows indicate the LAMP1 signal on the OAM, and white arrows indicate IAMs. Larger fields are shown in fig. S5. Scale bar, 200 nm and inset, 100 nm. (**D**) Disappearance of the CFP-STX17TM signal (green arrows) and collapse of the IAM (red arrows) in ATG3 KO MEFs. Scale bar, 1 μm. (**E**) WT and ATG3 KO MEFs expressing CFP-STX17TM were starved for 1 hour to accumulate autophagosomes, and then amino acid mixture and insulin were added (at time 0) to suppress new autophagosome formation. Cells were incubated and fixed at the indicated time points. The number of CFP-STX17TM–positive structures per cell is shown (n = 18 to 40 cells). The histogram was fitted with an exponential decay, and the decay constant indicates the lifetime (t) of CFP-STX17TM–positive structures. (**F**) Representative images of CFP-STX17TM–positive structures in WT and ATG3 KO MEFs. Scale bar, 1 μm. The oblateness of each structure in WT (n = 49) and ATG3 KO (n = 46) MEFs is shown in the histogram. P-value was determined using the Brunner-Munzel test (*26*). (**G**) Time-lapse images of starved ATG3 KO MEFs stably expressing CFP-STX17TM. The open edges of CFP-STX17TM structures are indicated by the arrows. Scale bar, 1 μm. (**H**) Models of autophagosome formation and maturation in WT and ATG3 KO MEFs.

It is not expected that autophagosome-like structures can mature into autolysosomes after degradation of the IAM in ATG conjugation–deficient cells, which suggests that autophagic activity remains at a very low level. It may explain the phenotypic difference among ATG KO mice: Embryonic lethality is observed in mice lacking upstream ATGs—such as FIP200, ATG9A, and ATG13 (*20*–*22*), whereas mice lacking ATG conjugation components, such as ATG3, ATG5, ATG7, ATG12, and ATG16L1, can survive the embryonic period (but die shortly after birth) (*13*, *18*, *23*–*25*). So far, the function of ATG proteins has been investigated only in the context of autophagosome formation, but our findings also revealed a function of ATGs with regard to the maturation steps.

REFERENCES AND NOTES

1. N. Mizushima, M. Komatsu, *Cell* **147**, 728–741 (2011).
2. C. A. Lamb, T. Yoshimori, S. A. Tooze, *Nat. Rev. Mol. Cell Biol.* **14**, 759–774 (2013).
3. A. Abada, Z. Elazar, *EMBO Rep.* **15**, 839–852 (2014).
4. R. L. Knorr, R. Lipowsky, R. Dimova, *Autophagy* **11**, 2134–2137 (2015).
5. E. Itakura, C. Kishi-Itakura, N. Mizushima, *Cell* **151**, 1256–1269 (2012).
6. N. Mizushima *et al.*, *Nature* **395**, 395–398 (1998).
7. Y. Ichimura *et al.*, *Nature* **408**, 488–492 (2000).
8. K. Suzuki *et al.*, *EMBO J.* **20**, 5971–5981 (2001).
9. N. Mizushima *et al.*, *J. Cell Biol.* **152**, 657–668 (2001).
10. T. Kirisako *et al.*, *J. Cell Biol.* **147**, 435–446 (1999).
11. T. Noda, N. Fujita, T. Yoshimori, *Cell Death Differ.* **16**, 984–990 (2009).
12. C. Kishi-Itakura, I. Koyama-Honda, E. Itakura, N. Mizushima, *J. Cell Sci.* **127**, 4089–4102 (2014).
13. Y. S. Sou *et al.*, *Mol. Biol. Cell* **19**, 4762–4775 (2008).
14. T. Uemura *et al.*, *Mol. Cell. Biol.* **34**, 1695–1706 (2014).
15. N. Fujita *et al.*, *Mol. Biol. Cell* **19**, 4651–4659 (2008).
16. Y. Kabeya *et al.*, *EMBO J.* **19**, 5720–5728 (2000).
17. N. Mizushima, T. Yoshimori, B. Levine, *Cell* **140**, 313–326 (2010).
18. A. Kuma *et al.*, *Nature* **432**, 1032–1036 (2004).
19. Y. Nishida *et al.*, *Nature* **461**, 654–658 (2009).
20. B. Gan *et al.*, *J. Cell Biol.* **175**, 121–133 (2006).
21. T. Kojima *et al.*, *Reprod. Biol.* **15**, 131–138 (2015).
22. T. Kaizuka, N. Mizushima, *Mol. Cell. Biol.* **36**, 585–595 (2016).
23. M. Komatsu *et al.*, *J. Cell Biol.* **169**, 425–434 (2005).
24. R. Malhotra, J. P. Warne, E. Salas, A. W. Xu, J. Debnath, *Autophagy* **11**, 145–154 (2015).
25. T. Saitoh *et al.*, *Nature* **456**, 264–268 (2008).
26. E. Brunner, U. Munzel, *Biom. J.* **42**, 17–25 (2000).

ACKNOWLEDGMENTS

We thank N. Tamura, S. Kawahara, and M. Yoshimura for help with establishment of ATG knockout and rescued cells; S. Yamaoka for the pMRXIP vector; Y. Tanaka for LAMP1 cDNA and anti-LAMP1 antibody; A. Miyawaki for Venus, superenhanced CFP, and mRFP cDNAs; M. Komatsu for ATG3 KO and ATG7 KO cells; J.-L. Guan for FIP200 KO MEFs; T. Saitoh and S. Akira for ATG9A KO and ATG14 KO MEFs; and T. Yasui for the pCG-VSV-G and pCG-gag-pol plasmids. This work was supported by Japan Society for the Promotion of Science KAKENHI Grant-in-Aid for Scientific Research on Innovative Areas 25111005 (to N.M.) and JP16H06280 (Resource and technical support platforms for promoting research "Advanced Bioimaging Support") (to M.K.). The data are provided in the main manuscript and supplement.

SUPPLEMENTARY MATERIALS

www.sciencemag.org/content/354/6315/1036/suppl/DC1
Materials and Methods
Figs S1 to S9
References (*27*–*37*)
Movies S1 to S3

3 March 2016; resubmitted 16 July 2016
Accepted 10 October 2016
Published online 20 October 2016
10.1126/science.aaf6136

BEHAVIORAL IMMUNOLOGY

Social status alters immune regulation and response to infection in macaques

Noah Snyder-Mackler,[1,2]* Joaquín Sanz,[3,4]* Jordan N. Kohn,[5] Jessica F. Brinkworth,[3,6] Shauna Morrow,[1] Amanda O. Shaver,[1]† Jean-Christophe Grenier,[4] Roger Pique-Regi,[7,8] Zachary P. Johnson,[5,9]‡ Mark E. Wilson,[5,10] Luis B. Barreiro,[4,11]§|| Jenny Tung[1,12,13,14]§||

Social status is one of the strongest predictors of human disease risk and mortality, and it also influences Darwinian fitness in social mammals more generally. To understand the biological basis of these effects, we combined genomics with a social status manipulation in female rhesus macaques to investigate how status alters immune function. We demonstrate causal but largely plastic social status effects on immune cell proportions, cell type–specific gene expression levels, and the gene expression response to immune challenge. Further, we identify specific transcription factor signaling pathways that explain these differences, including low-status–associated polarization of the Toll-like receptor 4 signaling pathway toward a proinflammatory response. Our findings provide insight into the direct biological effects of social inequality on immune function, thus improving our understanding of social gradients in health.

Many human societies exhibit social gradients in health (*1*). Socioeconomic status has been called the "fundamental cause" of health inequalities (*2*), and, in the United States, differences between the highest versus lowest socioeconomic stratum may affect adult life span by more than a decade (*3*). These patterns arise, in part, from differences in resource access and health risk behaviors. However, studies in hierarchically organized animal species suggest that they may also be more deeply embedded in our evolutionary history (*4*). In rhesus macaques and long-tailed macaques, social subordination has been linked to changes in cardiovascular health, hypothalamic-pituitary-adrenal axis function, inflammation, and gene expression in peripheral blood mononuclear cells (PBMCs) (*5*–*7*). Such findings suggest strong parallels between responses to social adversity in humans and other social primates, especially in their consequences for the regulation of the immune system (*8*, *9*).

We aimed to test how social status influences immune system function at multiple scales, using an experimental design that allowed us to infer its direct causal effects. We experimentally manipulated the dominance ranks of 45 adult female rhesus macaques, a species that naturally forms stable, linear social hierarchies. In captivity, female rank can be manipulated by sequential introduction of adult females into newly constructed social groups, such that earlier introduction predicts higher status (*10*) (measured here with continuous Elo ratings: a higher status corresponds to a higher value) (*11*). We constructed nine groups of five female macaques each (table S1). We maintained these groups for 1 year (phase one) (Fig. 1, A and B) and then rearranged group composition by performing sequential introduction of phase-one females from the same or adjacent ranks into new groups, which we again followed for 1 year (phase two).

Our study maximized within-individual changes in dominance rank (Pearson's correlation coefficient $r = 0.06$, $P = 0.68$ between phases) (fig. S1), thus avoiding the possibility of confounding rank effects on immune function with other study-subject characteristics. In both phases, the order of introduction predicted social status (phase one Pearson's $r = -0.57$, $P = 4.1 \times 10^{-5}$; phase two $r = -0.68$, $P = 3.3 \times 10^{-7}$) (Fig. 1C), and social status in turn influenced rates of received harassment (higher for low-status females) (Fig. 1D) and affiliative grooming behavior (higher for high-status females) (Fig. 1E).

[1]Department of Evolutionary Anthropology, Duke University, Durham, NC 27708, USA. [2]Duke Center for the Study of Aging and Human Development, Duke University, Durham, NC 27708, USA. [3]Department of Biochemistry, Faculty of Medicine, Université de Montréal, Montréal, Quebec H3T1J4, Canada. [4]Department of Genetics, Centre Hospitalier Universitaire Sainte-Justine Research Center, Montréal, Quebec H3T1C5, Canada. [5]Yerkes National Primate Research Center, Emory University, Atlanta, GA 30322, USA. [6]Department of Anthropology, University of Illinois at Urbana–Champaign, Urbana, IL 61801, USA. [7]Center for Molecular Medicine and Genetics, Wayne State University, Detroit, MI 48201, USA. [8]Department of Obstetrics and Gynecology, Wayne State University, Detroit, MI 48201, USA. [9]Department of Human Genetics, Emory University School of Medicine, Atlanta, GA 30322, USA. [10]Department of Psychiatry and Behavioral Sciences, Emory University School of Medicine, Atlanta, GA 30322, USA. [11]Department of Pediatrics, Faculty of Medicine, Université de Montréal, Montréal, Quebec H3T1J4, Canada. [12]Department of Biology, Duke University, Durham, NC 27708, USA. [13]Institute of Primate Research, National Museums of Kenya, Nairobi 00502, Kenya. [14]Duke Population Research Institute, Duke University, Durham, NC 27708, USA.
*These authors contributed equally to this work. †Present address: Department of Genetics, University of Georgia, Athens, GA 30602, USA. ‡Present address: Illumina, San Diego, CA 92122, USA. §These authors contributed equally to this work. **||Corresponding author. Email: jt5@duke.edu (J.T.); luis.barreiro@umontreal.ca (L.B.B.)**

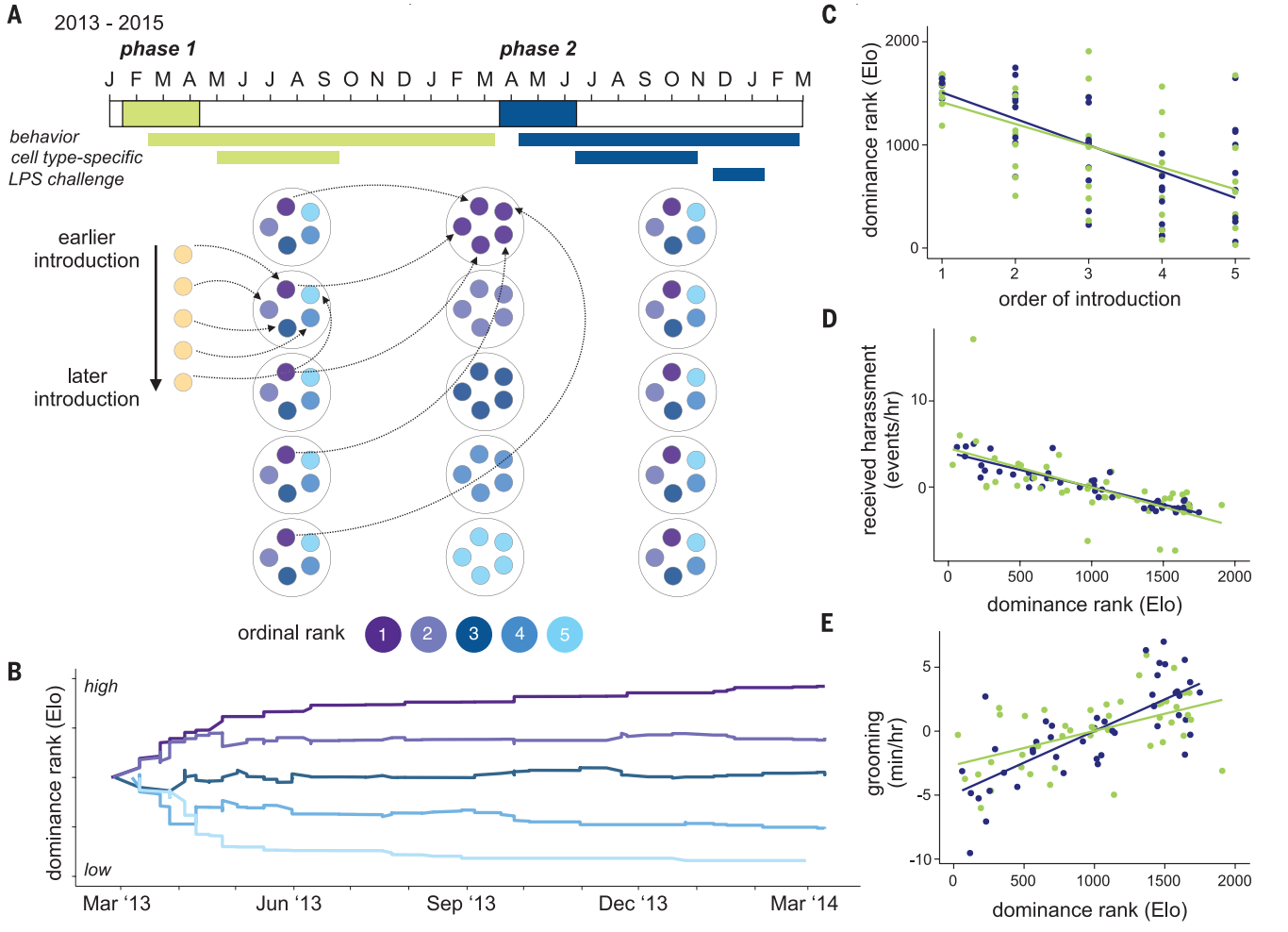

Fig. 1. Experimental paradigm. (**A**) Timeline for group formation in phase one (green: January 2013 to March 2014) and phase two (blue: March 2014 to March 2015), with timelines for behavioral data collection and sample collection shown below. The schematic below the timeline illustrates how groups were formed in phase one, rearranged at the study midpoint, and allowed to organize into new hierarchies during phase two. (**B**) Example of group formation: Each line represents a different female, introduced sequentially into a new social group. All females entered the group with the same Elo rating but rapidly established a stable hierarchy that persisted until the end of phase one. (**C**) Order of introduction into a newly formed social group predicted dominance rank (Elo rating) in phase one (green: Pearson's $r = -0.57$, $P = 4.1 \times 10^{-5}$) and phase two (blue: $r = -0.68$, $P = 3.3 \times 10^{-7}$). (**D**) Dominance rank predicted rates of received harassment in phase one (green: $r = -0.64$, $P = 2.0 \times 10^{-6}$) and phase two (blue: $r = -0.90$, $P = 1.8 \times 10^{-17}$). (**E**) Rates of grooming interactions in phase one (green: $r = 0.53$, $P = 2.1 \times 10^{-4}$) and phase two (blue: $r = 0.75$, $P = 4.0 \times 10^{-9}$). In (C) to (E), lines show the best-fit slope and intercept from a linear model. Rates of harassment and grooming in (D) and (E) are mean-centered to 0 for each social group.

These manipulations revealed both compositional and cell type–specific effects on the immune system. Across phases, high-ranking females had increased proportional representation of $CD3^+CD8^+$ cytotoxic T cells [linear mixed model $P = 9.9 \times 10^{-3}$, consistent with (*5*)] and double-positive $CD3^+CD8^+CD4^+$ T cells ($P = 6.9 \times 10^{-3}$) and trended toward decreased polymorphonuclear and increased natural killer (NK) cell representation ($P = 0.11$ for both) (fig. S2). To investigate intracellular changes in gene expression independently of variation in leukocyte composition, we used fluorescence-activated cell sorting to isolate the five major PBMC cell types: $CD3^+CD4^+$ helper T cells, $CD3^+CD8^+$ cytotoxic T cells, $CD3^-CD20^+$ B cells, $CD14^+$ monocytes, and $CD3^-CD16^+$ NK cells (fig. S3 and table S2). RNA-seq (RNA sequencing) profiling on the resulting samples ($n = 440$ female-phase-cell population combinations following quality control) (table S3) enabled us to separate the distinct cell types according to the relationships expected from hematopoietic cell differentiation (Fig. 2A).

Within cell types, we identified variable signatures of dominance rank on gene expression levels. NK cells were by far the most sensitive to social status [$n = 1676$ rank-responsive genes, false discovery rate (FDR) < 10%], followed by a secondary signal in helper T cells ($n = 284$ genes). In contrast, we identified weak effects of dominance rank in B cells and cytotoxic T cells ($n = 68$ and 15 genes, respectively) and no detectable effect of dominance rank in purified monocytes (Fig. 2A and table S4). Within the set of NK cell rank-responsive genes, Gene Ontology (GO) enrichment analysis revealed increased expression of lymphocyte proliferation [Fisher's exact test (FET) $P = 7.8 \times 10^{-3}$], innate immune response ($P = 9.9 \times 10^{-4}$), and cytokine response genes in low-ranking females ($P = 5.0 \times 10^{-4}$), consistent with a proinflammatory phenotype (fig. S4 and table S5). However, this relationship was generally plastic: Although female ranks were scrambled between study phases, the effects of rank were positively correlated and highly directionally concordant between phase one and phase two for rank-responsive genes (helper T cells: Pearson's $r = 0.41$, $P = 1.95 \times 10^{-34}$, 69.3% concordant; NK cells: $r = 0.49$, $P = 6.62 \times 10^{-71}$, 79.7% concordant) (Fig. 2B and fig. S5). Improvements in social status are thus rapidly reflected in gene expression patterns, even in relatively long-lived cell types such as T cells (*12*).

Our results suggest that most effects of social status are cell type–specific, in contrast to the high degree of sharing observed for genetic effects on gene expression levels [i.e., expression quantitative

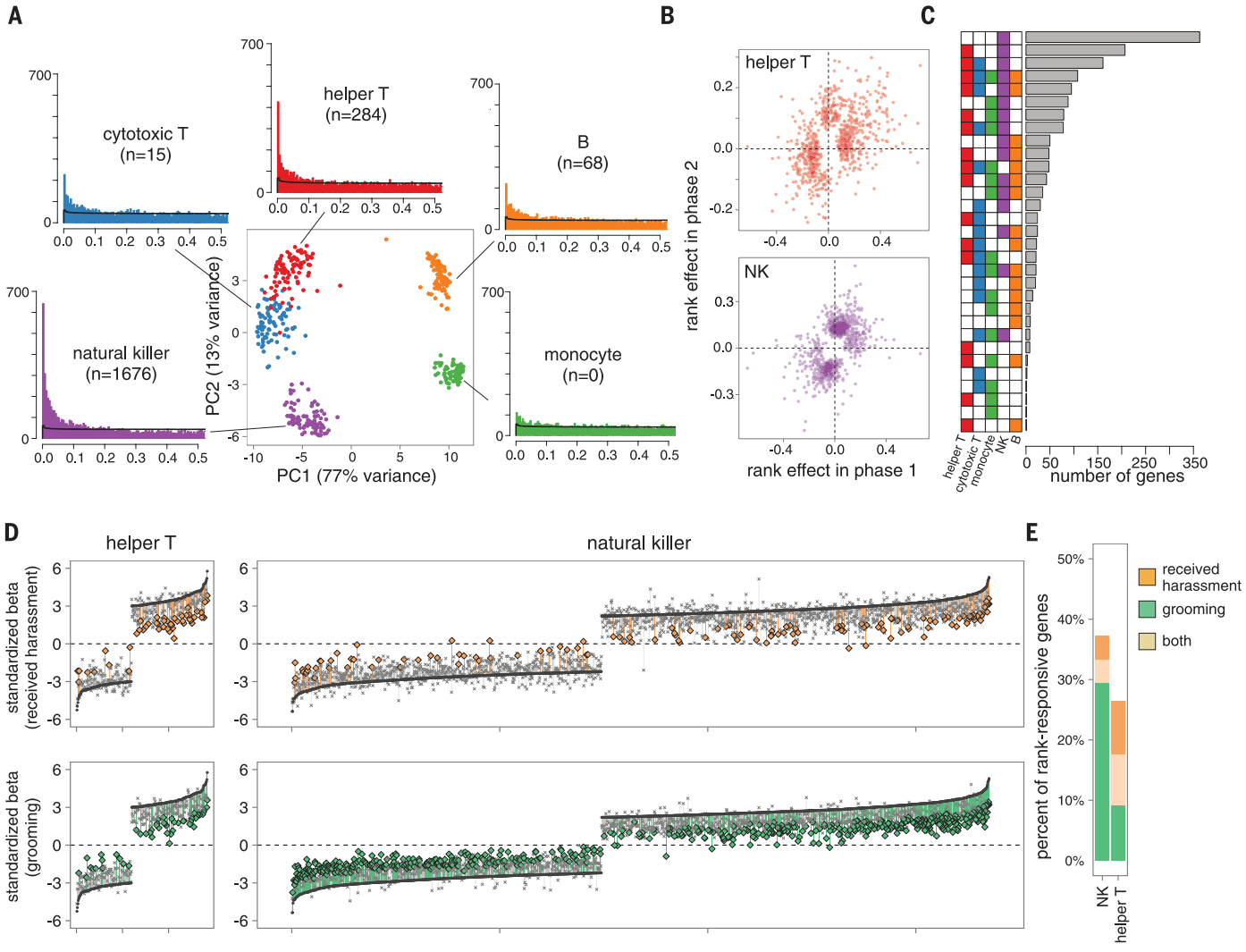

Fig. 2. Cell type–specific effects of dominance rank on gene expression. (**A**) PCA separates the five FACS-purified immune cell types we investigated (sampled from 45 distinct females in two phases of the study; see table S3). The number of rank-responsive genes in each cell type is shown in parentheses (FDR < 10%; black line shows permutation-based null expectations). (**B**) Rank effects on gene expression in phase one are positively correlated with rank effects on gene expression in phase two, indicating plasticity in these effects (see also fig. S5). (**C**) Meta-analysis across cell types identifies NK-specific effects as the most common pattern, followed by effects that are shared across NK and helper T cells. (**D**) Mediation analysis for received harassment (top) and grooming rates (bottom) for helper T cells (left) and NK cells (right). Genes are ordered by the effect size of rank on gene expression levels (dark gray crossmarks; gaps in effect sizes occur because only rank-responsive genes are shown), and "lollipops" connect the effect of dominance rank without including the mediator to the effect of dominance rank when the mediator is taken into account. Colored lines show significant mediating effects, based on 1000 bootstrap iterations. (**E**) Proportion of rank-responsive genes with significant mediation effects for received harassment (orange), grooming (green), or both (beige).

trait loci (*13*, *14*)]. However, analyzing each cell type in isolation tends to be anticonservative with respect to cell type specificity, because shared effects could be missed if a gene falls below the significance threshold in one cell type but slightly above it in another. We therefore performed a meta-analysis on genes that were detectably expressed in all five cell types and rank-responsive in at least one cell type (n = 1622 genes). Of the 32 possible combinations of rank effects (present or absent in each of the five cell types), we identified an NK-specific configuration as the most common (n = 363 genes), followed by shared effects across the two most-sensitive cell types, NK and helper T cells (n = 207 genes) (Fig. 2C). Thus, substantial cell type heterogeneity in rank-responsive genes is supported even when using a conservative, meta-analytic approach.

We next investigated the behavioral mechanisms that give rise to social status effects on gene expression, focusing on NK and helper T cells where the observed effects were strongest. Mediation analysis revealed that rates of received harassment—a measure of the agonistic, competitive element of social status inequality—contributed to these effects for 17.3% (helper T) and 7.8% (NK) of rank-responsive genes, respectively. However, in rhesus macaques, dominance rank also influences affiliative social interactions (*15*). Grooming rates mediated rank effects on gene expression levels for 17.6% of genes in helper T cells, comparable to the results for agonistic interactions. In contrast, grooming behavior was more important than harassment for rank-responsive NK genes (n = 560 genes, 33.4% of all rank-responsive genes; χ^2 test $P = 1.33 \times 10^{-74}$) (Fig. 2, D and E). A lack of positive social interactions may therefore be equally or more important than social subordination per se in shaping social status effects on gene expression, consistent with the known effects of social integration on health and mortality in both humans and other primates (*16*–*18*).

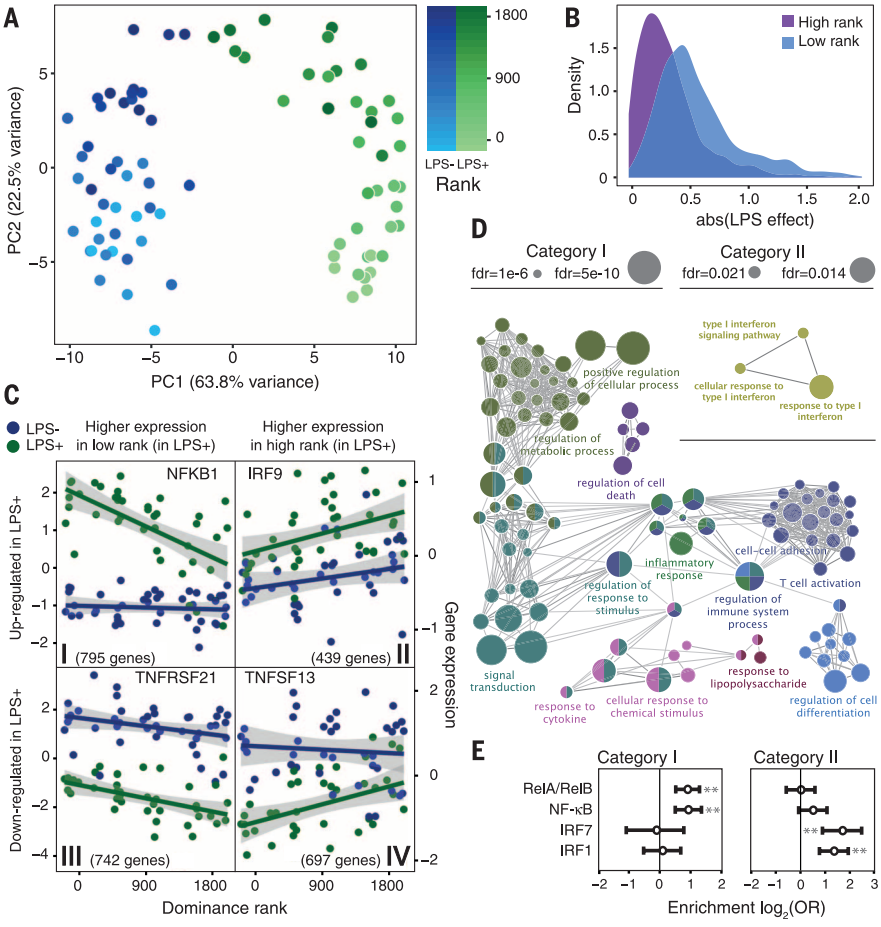

Fig. 3. Social status influences the immune response to LPS stimulation. (**A**) PCA decomposition of the control (LPS−) and LPS–stimulated (LPS+) gene expression data. PC1 separates samples by condition; PC2 separates by rank. (**B**) Across all LPS-responsive genes, the effect of LPS stimulation is larger in low-ranking females than in high-ranking females (data for lowest- versus highest-ranking females are shown). abs(LPS effect): absolute value of the LPS effect on gene expression levels. (**C**) The four categories of genes affected by LPS in a rank-dependent manner. (**D**) Selected GO term enrichment for category I and II genes (see table S7 for the complete set). (**E**) Open chromatin regions near category I genes are enriched for predicted NF-κB binding sites, whereas open chromatin regions near category II genes are enriched for interferon regulatory factor binding sites. Error bars denote the 95% confidence interval of the odds ratio (OR); asterisks indicate statistical significance at $P < 0.0001$.

The patterns we observed are most likely to contribute to social gradients in health if they affect the ability to respond to external threats, such as pathogen exposure. Thus, we next tested for social status–dependent effects on the response to lipopolysaccharide (LPS), a component of Gram-negative bacteria that invokes a strong inflammatory response [an aspect of immune function thought to be influenced by social environmental conditions (*4*, *5*, *9*)]. We collected two blood samples from each female in phase two: (i) a control sample incubated for 4 hours in media and (ii) an experimental sample incubated in parallel in media plus 1 μg/ml LPS. We then used RNA-seq to profile gene expression levels for the white blood cell fraction from each sample (n = 40 LPS and 43 control samples retained after quality control) (table S3).

Principal components analysis (PCA) of the gene expression data reveals robust signals of both condition (control versus LPS) and social status (Fig. 3A). In both conditions, control and LPS-stimulated samples separate on PC1 (Student's $t = 24.72$, $P = 4.4 \times 10^{-34}$), and females separate according to dominance rank on PC2 (Pearson's $r = 0.83$, $P = 3.5 \times 10^{-22}$). Immune stimulation also exacerbates the effects of rank. Although social status effects were globally correlated across conditions (Pearson's $r = 0.50$, $P < 10^{-300}$), we identified twice as many rank-responsive genes in the LPS condition than in the control condition (3494 versus 1799 genes, FDR < 1%) (fig. S6 and table S6). This observation may be partially explained by status-related variation in glucocorticoid (GC) physiology (*19*). Sensitivity to dexamethasone challenge significantly mediated social status effects on gene expression for 42 rank-responsive genes in the control condition and 155 genes in the LPS condition, including key regulators of the inflammatory response such as *TRAF3* and *MAP2K1*. Further, these GC mediation effects were significantly larger in the LPS condition than in the control condition, consistent with the known immunomodulatory effects of GC signaling (Mann-Whitney test $P = 1.5 \times 10^{-4}$) (fig. S7). These results suggest that social status directly affects the immune response in addition to gene expression at the baseline. We identified 1834 genes (FDR < 1%) for which the intensity of the response to LPS varied depending on dominance rank (table S6), with a stronger overall response in low-ranking females (Mann-Whitney test $P = 2.0 \times 10^{-145}$) (Fig. 3B).

We next stratified the data set on the basis of the direction of the response to LPS and the direction of the dominance rank effect after LPS stimulation (Fig. 3C). Among the four resulting gene sets, only two exhibited biologically coherent enrichment for specific pathways. Among LPS–up-regulated genes more highly expressed in low-status females after stimulation (category I genes, n = 795 genes), we found enrichment for GO terms associated with the response to bacterial infection (Fig. 3D and table S7), including the inflammatory response (FET $P = 8.4 \times 10^{-10}$) and cytokine production (FET $P = 4.2 \times 10^{-6}$). Notably, category I contains several master regulators of the innate immune response, including components of the nuclear factor κB (NF-κB) transcription factor complex (*NFKBID*, *NFKBIZ*, and *NFKB1*) (Fig. 3C) and the transcription factors *STAT3* and *STAT5A*, which are involved in the response to proinflammatory cytokines and growth factor signaling (*20*, *21*). In contrast, LPS–up-regulated genes more highly expressed in high-status females after stimulation (category II genes, n = 439 genes) were enriched specifically for GO terms associated with type I interferon signaling (Fig. 3D).

To further investigate signaling pathways associated with categories I and II, we generated ATAC-seq (Assay for Transposase-Accessible Chromatin with high-throughput sequencing) data for PBMCs sampled from three female macaques to identify open chromatin regions. Overlapping open chromatin regions with category II gene locations revealed enrichment for predicted interferon regulatory factor binding sites within 5 kb of the transcription start site (IRF1, FET $P = 7.43 \times 10^{-6}$; IRF7, $P = 3.67 \times 10^{-5}$) (Fig. 3E and table S8). In contrast, the same analysis for category I genes revealed enrichment for NF-κB binding sites (RELA/RELB, $P = 5.30 \times 10^{-6}$; NF-κB, $P = 1.88 \times 10^{-5}$) (Fig. 3E) but no enrichment for IRF signaling. Notably, binding sites for inflammation-related transcription factors, including NF-κB, were also enriched among social status–responsive genes in NK cells (fig. S8 and table S8).

The immune response to LPS is primarily mediated by monocytes and polymorphonuclear cells (fig. S9) and, specifically, signaling from Toll-like receptor 4 (TLR4), the receptor for LPS. LPS binding to TLR4 triggers two alternative

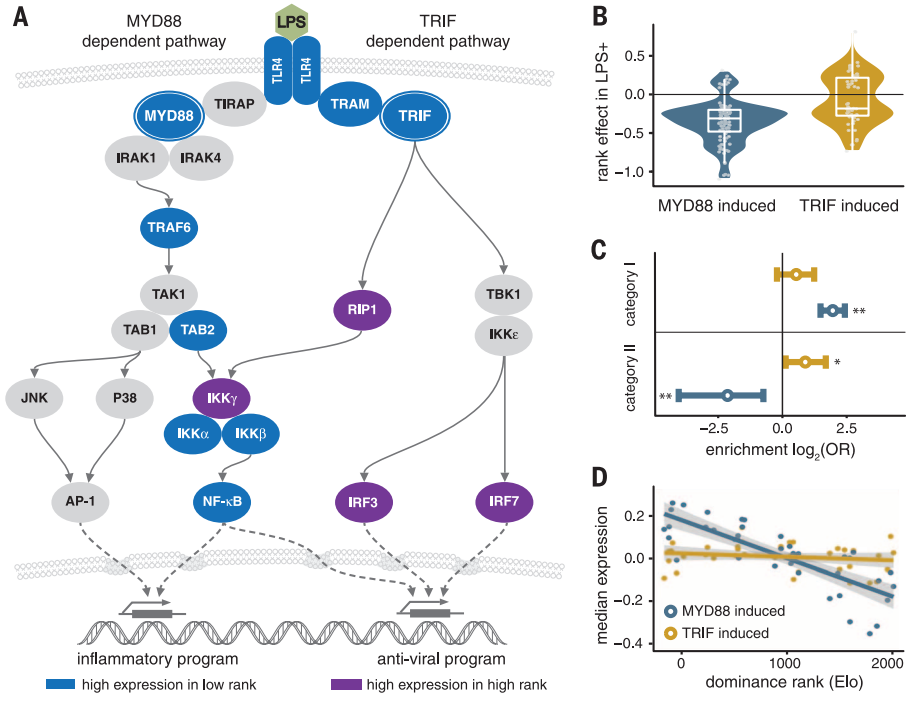

Fig. 4. Dominance rank polarizes TLR4 responses to LPS stimulation. (**A**) Key players in the MyD88-dependent and TRIF-dependent response to LPS-induced TLR4 signaling. Rank-responsive genes in these pathways are shown in blue (category I genes) and purple (category II genes). (**B**) Rank-responsive genes that are up-regulated upon stimulation via the MyD88 pathway ("MyD88-induced") are almost universally (89.3%) more highly expressed in low-status females in the LPS+ condition, whereas TRIF-induced, rank-responsive genes are split (Mann-Whitney test for the difference between MyD88-induced and TRIF-induced genes: $P = 8.31 \times 10^{-7}$). (**C**) MyD88-induced genes are overrepresented among category I genes [FET $\log_2(OR) = 1.95$, $P = 1.6 \times 10^{-15}$] but significantly underrepresented in category II [$\log_2(OR) = -2.14$, $P = 4.1 \times 10^{-4}$]. TRIF-induced genes are significantly overrepresented in category II [$\log_2(OR) = 0.89$, $P = 0.04$]. (**D**) Median gene expression levels across all MyD88- and TRIF-induced genes for each female, by female dominance rank.

signaling pathways: a MyD88-dependent pro-inflammatory pathway, mediated at the transcriptional level by NF-κB, and a TRIF-dependent antiviral pathway, mediated at the transcriptional level by IRF3 and IRF7 (*22*). The GO and transcription factor binding site enrichment analyses for category I and category II genes suggest that low- and high-status females use different pathways in response to immune challenges. Specifically, low-status females show enhanced activation of the MyD88-dependent pathway, whereas high-status individuals are shifted toward the TRIF-dependent antiviral response (Fig. 4A). Rank-responsive genes induced by LPS via the MyD88-dependent pathway [on the basis of comparisons between wild-type and knockout mice (*23*)] are almost exclusively category I genes, whereas TRIF-dependent genes are slightly enriched and MyD88-dependent genes are significantly underrepresented in category II (Fig. 4, B and C). As a result, median gene expression levels across all rank-responsive MyD88-dependent genes are predicted by dominance rank (Pearson's $r = -0.80$, $P = 4.6 \times 10^{-10}$) (Fig. 4D), supporting status-related differences in the TLR4-mediated immune response.

Together, our findings show that social subordination alone is sufficient to alter immune function even in the absence of variation in resource access, health care, or health risk behaviors. As macaques are close evolutionary relatives of humans, these results likely point to mechanisms that also underlie social status effects in humans, where experimental studies are not possible (*24*). Our results also demonstrate that social status influences the immune system at multiple scales, ranging from coarse leukocyte compositional patterns, to changes in cell type–specific gene expression patterns, to altered usage of specific signaling pathways in response to an immune challenge that models bacterial infection. In particular, we provide genome-wide experimental evidence for the idea that social hierarchies polarize the immune response toward a pro-inflammatory, antibacterial phenotype in low-status individuals and an antiviral phenotype in high-status individuals (*8*). This distinction raises questions about the disease conditions and potential selection pressures associated with variation in social status, including whether status predicts investment in more- or less-costly forms of immune defense (*25*). Our findings also lay the groundwork for further investigation of social status effects on other aspects of immune function, such as viral defense and adaptive immunity.

REFERENCES AND NOTES

1. M. Marmot, *Lancet* **365**, 1099–1104 (2005).
2. B. G. Link, J. Phelan, *J. Health Soc. Behav.* **35**, 80–94 (1995).
3. R. Chetty *et al.*, *JAMA* **315**, 1750–1766 (2016).
4. R. M. Sapolsky, *Science* **308**, 648–652 (2005).
5. J. Tung *et al.*, *Proc. Natl. Acad. Sci. U.S.A.* **109**, 6490–6495 (2012).
6. V. Michopoulos, K. M. Reding, M. E. Wilson, D. Toufexis, *Horm. Behav.* **62**, 389–399 (2012).
7. C. A. Shively, T. B. Clarkson, J. R. Kaplan, *Atherosclerosis* **77**, 69–76 (1989).
8. S. W. Cole, *PLOS Genet.* **10**, e1004601 (2014).
9. M. R. Irwin, S. W. Cole, *Nat. Rev. Immunol.* **11**, 625–632 (2011).
10. H. Jarrell *et al.*, *Physiol. Behav.* **93**, 807–819 (2008).
11. C. Neumann *et al.*, *Anim. Behav.* **82**, 911–921 (2011).
12. J. Sprent, *Curr. Opin. Immunol.* **5**, 433–438 (1993).
13. T. Flutre, X. Wen, J. Pritchard, M. Stephens, *PLOS Genet.* **9**, e1003486 (2013).
14. K. G. Ardlie *et al.*, *Science* **348**, 648–660 (2015).
15. N. Snyder-Mackler *et al.*, *Anim. Behav.* **111**, 307–317 (2016).
16. E. A. Archie, J. Tung, M. Clark, J. Altmann, S. C. Alberts, *Proc. Biol. Sci.* **281**, 20141261 (2014).
17. J. B. Silk *et al.*, *Curr. Biol.* **20**, 1359–1361 (2010).
18. J. Holt-Lunstad, T. B. Smith, J. B. Layton, *PLOS Med.* **7**, e1000316 (2010).
19. J. N. Kohn *et al.*, *Psychoneuroendocrinology* **74**, 179–188 (2016).
20. T. Lawrence, *Cold Spring Harb. Perspect. Biol.* **1**, a001651 (2009).
21. J. J. O'Shea, P. J. Murray, *Immunity* **28**, 477–487 (2008).
22. S. Akira, K. Takeda, *Nat. Rev. Immunol.* **4**, 499–511 (2004).
23. S. A. Ramsey *et al.*, *PLOS Comput. Biol.* **4**, e1000021 (2008).
24. M. G. Marmot, R. Sapolsky, in *Sociality, Hierarchy, Health: Comparative Biodemography*, M. Weinstein, M. A. Lane, Eds. (National Academies Press, 2014), pp. 365–388.
25. R. Hamilton, M. Siva-Jothy, M. Boots, *Proc. Biol. Sci.* **275**, 937–945 (2008).

ACKNOWLEDGMENTS

We thank J. Whitley, A. Tripp, N. Brutto, and J. Johnson for maintaining the study subjects and collecting behavioral data; I. Cummings for assistance with flow cytometry; M. Gutierrez for help with figures; and S. Cole, A. J. Lea, A. Graham, and members of the Tung and Barreiro labs for helpful comments and discussion. This work was supported by NIH grants R01-GM102562, P51-OD011132, and T32-AG000139; NSF grant SMA-1306134; the Canada Research Chairs Program 950-228993; and NSERC RGPIN/435917-2013. J. S. was supported by the Fonds de recherche du Québec–Nature et technologies and the Fonds de recherche du Québec–Santé. We thank Calcul Québec and Compute Canada for providing access to the supercomputer Briaree from the University of Montreal. RNA-seq and ATAC-seq data have been deposited in Gene Expression Omnibus (accession number GSE83307). Code and data are available at github.com/nsmackler/status_genome_2016.

SUPPLEMENTARY MATERIALS

www.sciencemag.org/content/354/6315/1041/suppl/DC1
Materials and Methods
Supplementary Text
Figs. S1 to S13
Tables S1 to S8
References (*26*–*54*)

16 June 2016; accepted 17 October 2016
10.1126/science.aah3580

MEMORY RESEARCH

Retrieval practice protects memory against acute stress

Amy M. Smith,* Victoria A. Floerke, Ayanna K. Thomas

More than a decade of research has supported a robust consensus: Acute stress impairs memory retrieval. We aimed to determine whether a highly effective learning technique could strengthen memory against the negative effects of stress. To bolster memory, we used retrieval practice, or the act of taking practice tests. Participants first learned stimuli by either restudying or engaging in retrieval practice. Twenty-four hours later, we induced stress in half of the participants and assessed subsequent memory performance. Participants who learned by restudying demonstrated the typical stress-related memory impairment, whereas those who learned by retrieval practice were immune to the deleterious effects of stress. These results suggest that the effects of stress on memory retrieval may be contingent on the strength of the memory representations themselves.

The effects of experimentally induced stress on memory have been studied for more than a decade (*1*–*7*). The results support a robust consensus that stress impairs memory retrieval (*8*). These studies used a common method whereby participants learn words or images and return 24 hours later for a memory test. Before testing, psychosocial stress is induced. Critically, the memory test is administered ~25 min after stress introduction [for exceptions, see (*5, 6*)], when the stress hormone cortisol reaches peak poststress levels in the blood. Researchers have primarily examined memory after this delay because cortisol has been shown to affect brain regions that are implicated in memory retrieval (*9*).

Previous research on this topic has not been expressly concerned with the quality of encoding during initial learning. Before encoding, participants were typically instructed to "memorize" stimuli. However, the processes that take place at encoding influence memory representation and accessibility (*10*). Without guidance as to how to approach learning material, participants may choose ineffective encoding strategies, resulting in unstable memory representations. Many participants in these studies likely chose to learn by rereading, given that this method is often reported as the most popular study strategy (*11*). Rereading is a poor learning strategy, insofar as it creates relatively weak memory representations (*12*). Thus, it is unclear whether all memories are subject to the detrimental effects of stress, or whether only weakly encoded representations are vulnerable.

In our experiment, we addressed this by strengthening memory at encoding through the use of retrieval practice, the act of taking practice tests. Among a host of options for study techniques, we chose retrieval practice for two reasons. First, retrieval practice has consistently yielded long-term memory retention that is equal to or better than restudying (*13*–*15*) and a plethora of other learning strategies such as mental imagery (*12*), concept mapping (*16*), and the keyword mnemonic (*17*). Thus, we chose to use retrieval practice as an encoding technique because it had the most potential to create memories that were resilient to stress. Second, retrieval practice is an easily implemented learning strategy (*12*). We reasoned that if retrieval practice was successful at creating stress-resistant memories, our findings could be readily applied in real-world scenarios (e.g., test anxiety).

A second limitation of previous research on stress and memory concerns the timing of the final memory test. Researchers typically assessed memory 25 min after stress induction and found detrimental effects. However, contesting the consensus that stress generally impairs retrieval, recent research showed that participants who were tested immediately after stress induction exhibited memory performance that was better than or comparable to a no-stress control group (*5*, *6*). Thus, a secondary aim of our study was to investigate the potentially facilitative effects of the immediate stress response in the context of a retrieval practice encoding manipulation.

In our experiment, 120 participants studied either 30 concrete nouns or 30 images of nouns, one item at a time. Half of the items in each list were of negative valence and half were of neutral valence. Whether words or images were studied first was counterbalanced. Sixty participants then engaged in study practice (SP), in which they restudied the 30 items. The other 60 participants engaged in retrieval practice (RP), in which they recalled as many items as they could remember. RP participants were not given feedback on the free recall test or on any subsequent tests. This procedure (item presentation followed by restudy or free recall) was then repeated for the 30 items of the other type. Afterward, SP participants restudied all 60 stimuli, whereas RP participants attempted to recall the words and images in any order. After a short distractor task, SP participants again restudied all 60 items, and RP participants attempted to recall all items.

Twenty-four hours later, 30 SP and 30 RP participants underwent stress induction, and 30 SP and 30 RP participants completed a time-matched nonstressful task. Our encoding and stress manipulations were fully crossed, so there were four between-subject groups: nonstressed SP, stressed SP, nonstressed RP, and stressed RP. During stress induction, participants gave extemporaneous speeches and solved math problems in front of two judges and three peers (*18*).

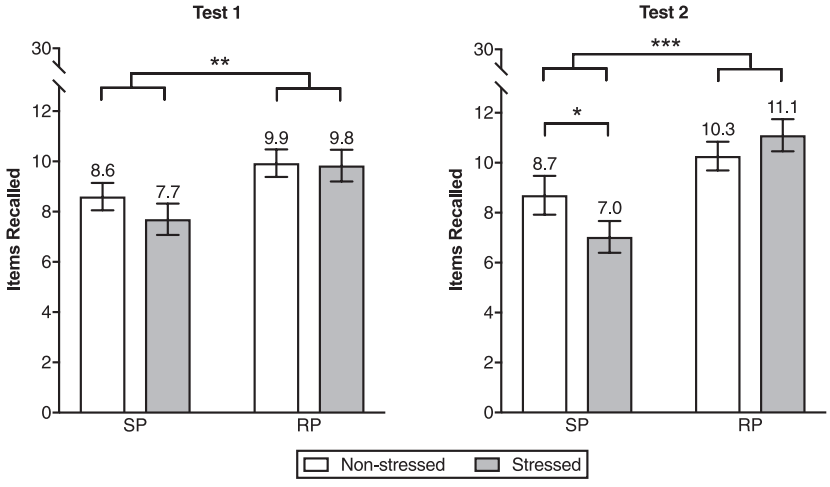

Fig. 1. Average number of items accurately recalled on tests 1 and 2. Test 1 was administered immediately after the onset of stress. Test 2 followed after a 25 min delay. Retrieval practice (RP) refers to the learning technique in which participants study stimuli and take three subsequent recall tests. Study practice (SP) refers to the learning technique in which participants study stimuli four times. Tests occurred on the day after learning. Error bars represent standard errors of the mean. *$P < 0.05$; **$P < 0.01$; ***$P < 0.001$.

Tufts University, 490 Boston Avenue, Medford, MA 02155, USA.
*Corresponding author. Email: amy.smith@tufts.edu

Measures of physiological arousal confirmed the effectiveness of the stress induction procedure (*19*). Five minutes into the stress induction or control task, participants completed test 1, in which they recalled either the words or images that were studied the previous day. Test 1 was given to examine memory during the immediate stress response. Twenty minutes later, participants completed test 2, in which they recalled the items that were not assessed on test 1. Test 2 was given to examine memory during the delayed stress response.

The results of our experiment are characterized by three key findings. First, on test 2, stressed SP participants recalled fewer items than nonstressed SP participants [Cohen's *d* effect size (*d*) = 0.44; 95% confidence interval (CI) = (0.03, 3.37)], whereas this difference was not evident for RP participants. As shown in Fig. 1, stress resulted in the memory impairment that researchers have repeatedly observed, but only for participants who encoded stimuli through SP. Not only did stressed RP participants outperform nonstressed SP participants [*d* = 0.61; 95% CI = (0.36, 4.37)], they demonstrated recall performance that was similar to nonstressed RP participants, as though stress had not been present.

Second, consistent with one of two recent studies that examined memory performance during both the immediate and delayed stress response (*6*), we found no difference in memory performance for stressed versus nonstressed participants on test 1. Stress neither impaired nor enhanced memory performance 5 min after the onset of stress (Fig. 1). Table 1 provides a more detailed report of test 1 and test 2 performances.

Third, we replicated the robust testing effect (*13*, *20*). Participants who encoded through RP recalled significantly more stimuli than those who encoded through SP on test 1 [partial η^2 effect size (η_p^2) = 0.06; 95% CI = (0.45, 2.77)] and test 2 [η_p^2 = 0.13; 95% CI = (1.38, 3.98)]. SP and RP participants respectively recalled, on average, 8.2 and 9.9 items on test 1 and 7.9 and 10.7 items on test 2.

Our results call into question the growing consensus that stress generally impairs memory retrieval. We did not find this effect when stress acted on strong memory representations or when memory was assessed immediately after the onset of stress. Regarding the former, we showed that using a highly effective learning strategy to strengthen memory at encoding inoculated memory against the deleterious effects of the delayed stress response.

A combination of physiological evidence and cognitive theory helps to explain this finding. The delayed stress response is thought to impair retrieval through a physiological mechanism: Cortisol binds to glucocorticoid receptors in the hippocampus, impeding retrieval-related processing in this region (*8*, *9*). Cognitive theories suggest that retrieval practice is a highly effective learning strategy because it creates multiple routes by which information can be accessed (*14*). When attempting to recall an item from memory, evidence suggests that associated (*21*–*24*) and/or contextual (*14*) information accompanies that attempt. More retrieval attempts thus create more distinct routes by which the same item can be accessed. Supporting this, a neuroimaging study found that, relative to study practice, retrieval practice increased hippocampal connectivity with other brain regions (*25*). In the case of our study, retrieval practice may have created multiple, contextually distinct retrieval pathways by which to access information. Although cortisol may have disrupted access to information by certain pathways, the robustness of the memory representation created by retrieval practice may have facilitated access to that information by alternate, undisrupted routes.

The ability for retrieval practice to strengthen memory against stress also has implications for real-world scenarios. For example, strong memory representations may reduce the retrieval failures that are common for students who experience test-related anxiety. Scenarios in which test anxiety impairs memory may thus be reconceptualized as scenarios that can be avoided when information is well encoded and accessible via many retrieval pathways.

Our finding that memory was unaffected when tested immediately after stress can likely be attributed to the biphasic nature of the physiological stress response. Immediately after the onset of stress, the body responds with two major hormonal changes: (i) the rapid and short-lived secretion of epinephrine and norepinephrine and (ii) the gradual and longer-lasting secretion of cortisol (*26*). The former response may facilitate neural processing (*27*), whereas the latter response impedes processing in memory-related brain regions (*9*). Thus, memory may be unchanged or even bolstered immediately after stress.

Several previous studies were unanimous in showing that memory, when measured after a poststress delay, was impaired by stress. Our results contest this robust finding. Whereas we did find memory retrieval impairment during the delayed stress response when information was encoded by restudying, that impairment was absent when information was encoded by retrieval practice. Thus, we argue that stress may not impair memory retrieval when stronger memory representations are created during encoding. Future research should be geared toward determining the cognitive mechanism by which retrieval practice protects memory against stress. The results of this line of research have the potential to fundamentally transform the way that researchers have viewed the relationship between stress and memory.

Table 1. Average number of items recalled on test 1 and test 2 as a function of valence and item type. Tests occurred on the day after learning. Standard errors of the mean are given in parentheses.

	Negative	Neutral	Negative	Neutral
Test 1	**Words**		**Images**	
Nonstressed SP	4.4 (0.48)	2.9 (0.36)	5.0 (0.52)	4.9 (0.57)
Stressed SP	3.5 (0.54)	2.7 (0.36)	5.3 (0.69)	3.8 (0.45)
Nonstressed RP	4.5 (0.49)	4.1 (0.43)	6.2 (0.47)	5.4 (0.68)
Stressed RP	4.6 (0.58)	4.1 (0.36)	6.3 (0.79)	4.9 (0.29)
Test 2				
Nonstressed SP	5.3 (0.61)	3.9 (0.74)	4.5 (0.68)	3.8 (0.50)
Stressed SP	3.7 (0.61)	3.0 (0.61)	4.8 (0.47)	2.6 (0.36)
Nonstressed RP	5.1 (0.43)	4.2 (0.49)	5.6 (0.45)	5.4 (0.46)
Stressed RP	5.6 (0.37)	5.2 (0.69)	6.1 (0.50)	5.3 (0.60)

REFERENCES AND NOTES

1. T. W. Buchanan, D. Tranel, R. Adolphs, *Learn. Mem.* **13**, 382–387 (2006).
2. T. W. Buchanan, D. Tranel, *Neurobiol. Learn. Mem.* **89**, 134–141 (2008).
3. V. Hidalgo *et al*., *Behav. Brain Res.* **292**, 393–402 (2015).
4. S. Kuhlmann, M. Piel, O. T. Wolf, *J. Neurosci.* **25**, 2977–2982 (2005).
5. P. Schönfeld, K. Ackermann, L. Schwabe, *Psychoneuroendocrinology* **39**, 249–256 (2014).
6. L. Schwabe, O. T. Wolf, *Cogn. Affect. Behav. Neurosci.* **14**, 1041–1048 (2014).
7. T. Smeets, H. Otgaar, I. Candel, O. T. Wolf, *Psychoneuroendocrinology* **33**, 1378–1386 (2008).
8. L. Schwabe, M. Joëls, B. Roozendaal, O. T. Wolf, M. S. Oitzl, *Neurosci. Biobehav. Rev.* **36**, 1740–1749 (2012).
9. E. R. de Kloet, M. S. Oitzl, M. Joëls, *Trends Neurosci.* **22**, 422–426 (1999).
10. E. L. Bjork, R. A. Bjork, in *Psychology and the Real World: Essays Illustrating Fundamental Contributions to Society*, M. A. Gernsbacher *et al*., Eds. (Worth Publishers, 2011), pp. 56–64.
11. J. D. Karpicke, A. C. Butler, H. L. Roediger 3rd, *Memory* **17**, 471–479 (2009).
12. J. Dunlosky, K. A. Rawson, E. J. Marsh, M. J. Nathan, D. T. Willingham, *Psychol. Sci. Public Interest* **14**, 4–58 (2013).
13. H. L. Roediger 3rd, J. D. Karpicke, *Perspect. Psychol. Sci.* **1**, 181–210 (2006).
14. J. D. Karpicke, M. Lehman, W. R. Aue, in *The Psychology of Learning and Motivation*, B. H. Ross, Ed. (Elsevier Academic Press, 2014), pp. 237–284.
15. H. L. Roediger, J. D. Karpicke, *Psychol. Sci.* **17**, 249–255 (2006).
16. J. D. Karpicke, J. R. Blunt, *Science* **331**, 772–775 (2011).
17. C. O. Fritz, P. E. Morris, M. Acton, A. R. Voelkel, R. Etkind, *Appl. Cogn. Psychol.* **21**, 499–526 (2007).

18. B. von Dawans, C. Kirschbaum, M. Heinrichs, *Psychoneuroendocrinology* **36**, 514–522 (2011).
19. Materials and methods are available as supplementary materials on *Science* Online.
20. C. A. Rowland, *Psychol. Bull.* **140**, 1432–1463 (2014).
21. S. K. Carpenter, *J. Exp. Psychol. Learn. Mem. Cogn.* **35**, 1563–1569 (2009).
22. S. K. Carpenter, *J. Exp. Psychol. Learn. Mem. Cogn.* **37**, 1547–1552 (2011).
23. S. K. Carpenter, E. L. DeLosh, *Mem. Cognit.* **34**, 268–276 (2006).
24. M. A. Pyc, K. A. Rawson, *Science* **330**, 335 (2010).
25. E. A. Wing, E. J. Marsh, R. Cabeza, *Neuropsychologia* **51**, 2360–2370 (2013).
26. G. S. Everly, J. M. Lating, *A Clinical Guide to the Treatment of the Human Stress Response* (Springer Science+Business Media, ed. 3, 2013).
27. E. J. Hermans *et al.*, *Science* **334**, 1151–1153 (2011).

ACKNOWLEDGMENTS

A full description of the materials, methods, and statistical analyses described in this manuscript is available in the supplementary materials. The data described in this paper are available from the first author upon request. This research was funded by the U.S. Army Natick Soldier Research, Development and Engineering Center.

SUPPLEMENTARY MATERIALS

www.sciencemag.org/content/354/6315/1046/suppl/DC1
Materials and Methods
Supplementary Text
Tables S1 to S3
References (*28*–*33*)

6 July 2016; accepted 24 October 2016
10.1126/science.aah5067

BIOCATALYSIS

Directed evolution of cytochrome c for carbon–silicon bond formation: Bringing silicon to life

S. B. Jennifer Kan, Russell D. Lewis, Kai Chen, Frances H. Arnold*

Enzymes that catalyze carbon–silicon bond formation are unknown in nature, despite the natural abundance of both elements. Such enzymes would expand the catalytic repertoire of biology, enabling living systems to access chemical space previously only open to synthetic chemistry. We have discovered that heme proteins catalyze the formation of organosilicon compounds under physiological conditions via carbene insertion into silicon–hydrogen bonds. The reaction proceeds both in vitro and in vivo, accommodating a broad range of substrates with high chemo- and enantioselectivity. Using directed evolution, we enhanced the catalytic function of cytochrome c from *Rhodothermus marinus* to achieve more than 15-fold higher turnover than state-of-the-art synthetic catalysts. This carbon–silicon bond-forming biocatalyst offers an environmentally friendly and highly efficient route to producing enantiopure organosilicon molecules.

Silicon constitutes almost 30% of the mass of Earth's crust, yet no life form is known to have the ability to forge carbon–silicon bonds (*1*). Despite the absence of organosilicon compounds in the biological world, synthetic chemistry has enabled us to appreciate the distinctive and desirable properties that have led to their broad applications in chemistry and material science (*2*, *3*). As a biocompatible carbon isostere, silicon can also be used to optimize and repurpose the pharmaceutical properties of bioactive molecules (*4*, *5*).

The natural supply of silicon may be abundant, but sustainable methods for synthesizing organosilicon compounds are not (*6*–*8*). Carbon–silicon bond-forming methods that introduce silicon motifs to organic molecules enantioselectively rely on multistep synthetic campaigns to prepare and optimize chiral reagents or catalysts; precious metals are also sometimes needed to achieve the desired activity (*9*–*19*). Synthetic methodologies such as carbene insertion into silanes can be rendered enantioselective using chiral transition metal complexes based on rhodium (*11*, *12*), iridium (*13*), and copper (*14*, *15*). These catalysts can provide optically pure products, but not without limitations: They require halogenated solvents and sometimes low temperatures to function optimally and have limited turnovers (<100) (*16*).

Because of their ability to accelerate chemical transformations with exquisite specificity and selectivity, enzymes are increasingly sought-after complements to, or even replacements for, chemical synthesis methods (*17*, *18*). Biocatalysts that are fully genetically encoded and assembled inside of cells are readily tunable with molecular biology techniques. They can be produced at low cost from renewable resources in microbial systems and perform catalysis under mild conditions. Although nature does not use enzymes to form carbon–silicon bonds, the protein machineries of living systems are often "promiscuous"—that is, capable of catalyzing reactions distinct from their biological functions. Evolution, natural or in the laboratory, can use these promiscuous functions to generate catalytic novelty (*19*–*21*). For example, heme proteins can catalyze a variety of non-natural carbene-transfer reactions in aqueous media, including N–H and S–H insertions, which can be greatly enhanced and made exquisitely selective by directed evolution (*22*–*24*).

We hypothesized that heme proteins might also catalyze carbene insertion into silicon–hydrogen bonds. Because iron is not known to catalyze this transformation (*25*), we first examined whether free heme could function as a catalyst in aqueous media. Initial experiments showed that the reaction between phenyldimethylsilane and ethyl 2-diazopropanoate (Me-EDA) in neutral buffer (M9-N minimal medium, pH 7.4) at room temperature gave racemic organosilicon product ***3*** at very low levels, a total turnover number (TTN) of 4 (Fig. 1A). No product formation was observed in the absence of heme, and the organosilicon product was stable under the reaction conditions.

We next investigated whether heme proteins could catalyze the same carbon–silicon bond-forming reaction. Screening a panel of cytochrome P450 and myoglobin variants, we observed product formation with more turnovers compared to the hemin and hemin with bovine serum albumin (BSA) controls, but with negligible enantioinduction (table S4). Cytochrome c from *Rhodothermus marinus* (*Rma* cyt c), a Gram-negative, thermohalophilic bacterium from submarine hot springs in Iceland (*26*), catalyzed the reaction with 97% enantiomeric excess (ee), indicating that the reaction took place in an environment where the protein exerted excellent stereocontrol. Bacterial cytochromes c are well-studied, functionally conserved electron-transfer proteins that are not known to have any catalytic function in living systems (*27*). Other bacterial and eukaryotic cytochrome c proteins also catalyzed the reaction, but with lower selectivities. We thus chose *Rma* cyt c as the platform for evolving a carbon–silicon bond-forming enzyme.

The crystal structure of wild-type *Rma* cyt c [Protein Data Bank (PDB) ID: 3CP5; (*26*)] reveals that the heme prosthetic group resides in a hydrophobic pocket, with the iron axially coordinated to a proximal His (H49) and a distal Met (M100), the latter of which is located on a loop (Fig. 1, B and C). The distal Met, common in cytochrome c proteins, is coordinatively labile (*28*, *29*). We hypothesized that M100 must be displaced upon iron-carbenoid formation, and that mutation of this amino acid could facilitate formation of this adventitious "active site" and yield an improved carbon–silicon bond-forming biocatalyst. Therefore, a variant library made by site-saturation mutagenesis of M100 was cloned and recombinantly expressed in *Escherichia coli*. After protein expression, the bacterial cells were heat-treated (75°C for 10 min) before screening in the presence of phenyldimethylsilane (10 mM),

Division of Chemistry and Chemical Engineering, California Institute of Technology, Pasadena, CA 91125, USA.
***Corresponding author. Email: frances@cheme.caltech.edu**

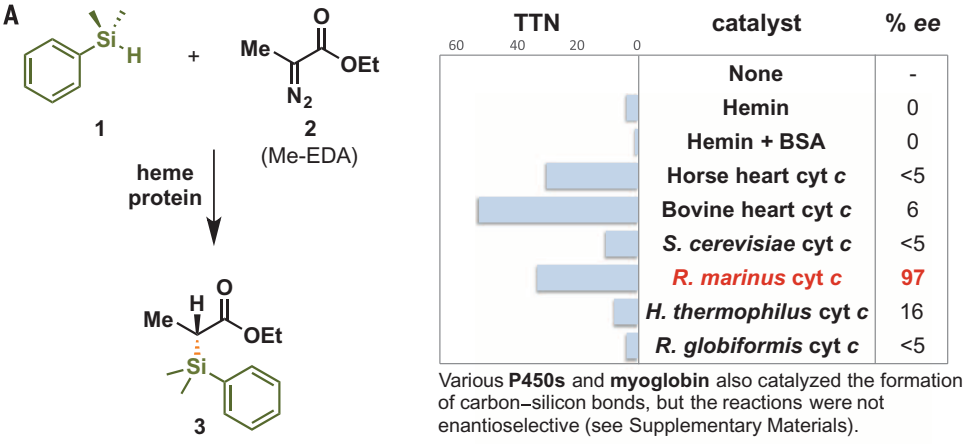

Various **P450s** and **myoglobin** also catalyzed the formation of carbon–silicon bonds, but the reactions were not enantioselective (see Supplementary Materials).

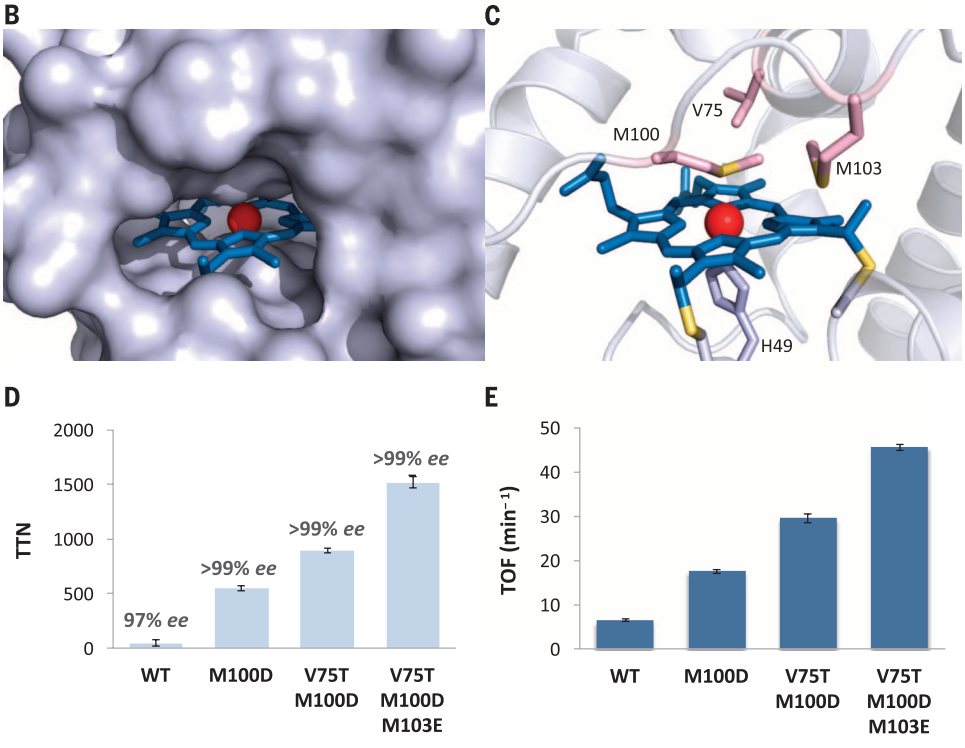

Fig. 1. Heme protein–catalyzed carbon–silicon bond formation. (**A**) Carbon–silicon bond formation catalyzed by heme and purified heme proteins. (**B**) Surface representation of the heme-binding pocket of wild-type *Rma* cyt c (PDB ID: 3CP5). (**C**) "Active site" structure of wild-type *Rma* cyt c showing a covalently bound heme cofactor ligated by axial ligands H49 and M100. Amino acid residues M100, V75, and M103 residing close to the heme iron were subjected to site-saturation mutagenesis. (**D**) Directed evolution of *Rma* cyt c for carbon–silicon bond formation [reaction shown in (A)]. Experiments were performed using lysates of *E. coli* expressing *Rma* cyt c variant (OD_{600} = 15; heat-treated at 75°C for 10 min), 10 mM silane, 10 mM diazo ester, 10 mM $Na_2S_2O_4$, 5 vol % MeCN, M9-N buffer (pH 7.4) at room temperature under anaerobic conditions for 1.5 hours. Reactions were done in triplicate. (**E**) Carbon–silicon bond forming rates over four generations of *Rma* cyt c. Single-letter abbreviations for the amino acid residues are as follows: D, Asp; E, Glu; M, Met; T, Thr; and V, Val.

Me-EDA (10 mM), and sodium dithionite ($Na_2S_2O_4$ 10 mM) as a reducing agent, at room temperature under anaerobic conditions. The M100D mutation stood out as highly activating: This first-generation mutant provided chiral organosilicon **3** as a single enantiomer in 550 TTN, a 12-fold improvement over the wild-type protein (Fig. 1D).

Amino acid residues V75 and M103 reside close (within 7Å) to the iron heme center in wild-type *Rma* cyt c. Sequential site-saturation mutagenesis at these positions in the M100D mutant led to the discovery of triple-mutant V75T M100D M103E, which catalyzed carbon–silicon bond formation in >1500 turnovers and >99% ee. This level of activity is more than 15 times the total turnovers reported for the best synthetic catalysts for this class of reaction (*16*). As standalone mutations, both V75T and M103E are activating for wild-type *Rma* cyt c, and the beneficial effects increase with each combination (table S5). Comparison of the initial reaction rates established that each round of evolution enhanced the rate: Relative to the wild-type protein, the evolved triple mutant catalyzes the reaction more than seven times faster, with turnover frequency (TOF) of 46 min^{-1} (Fig. 1E).

Assaying the new enzyme against a panel of silicon and diazo reagents, we found that the mutations were broadly activating for enantioselective carbon–silicon bond formation. The reaction substrate scope was surveyed with the use of heat-treated lysates of *E. coli*–expressing *Rma* cyt c V75T M100D M103E under saturating conditions for both silane and diazo ester to determine TTN. Whereas many natural enzymes excel at catalyzing reactions on only their native substrates and little else (especially primary metabolic enzymes), the triple mutant catalyzed the formation of 20 silicon-containing products, most of which were obtained cleanly as single enantiomers, demonstrating the broad substrate scope of this reaction with just a single variant of the enzyme (Fig. 2). The reaction accepts both electron-rich and electron-deficient silicon reagents, accommodating a variety of functional groups including ethers, aryl halides, alkyl halides, esters, and amides (**5** to **10**). Silicon reagents based on naphthalenes or heteroarenes (**11** to **13**), as well as vinyldialkyl- and trialkylsilanes, could also serve as silicon donors (**14**, **15**, **18**). In addition, diazo compounds other than Me-EDA could be used for carbon–silicon bond formation (**16**, **17**) (*16*).

The evolved *Rma* cyt c exhibits high specificity for carbon–silicon bond formation. Even in the presence of functional groups that could compete in carbene-transfer reactions, enzymatic carbon–silicon bond formation proceeded with excellent chemoselectivity. For example, styrenyl olefins, electron-rich double bonds, and terminal

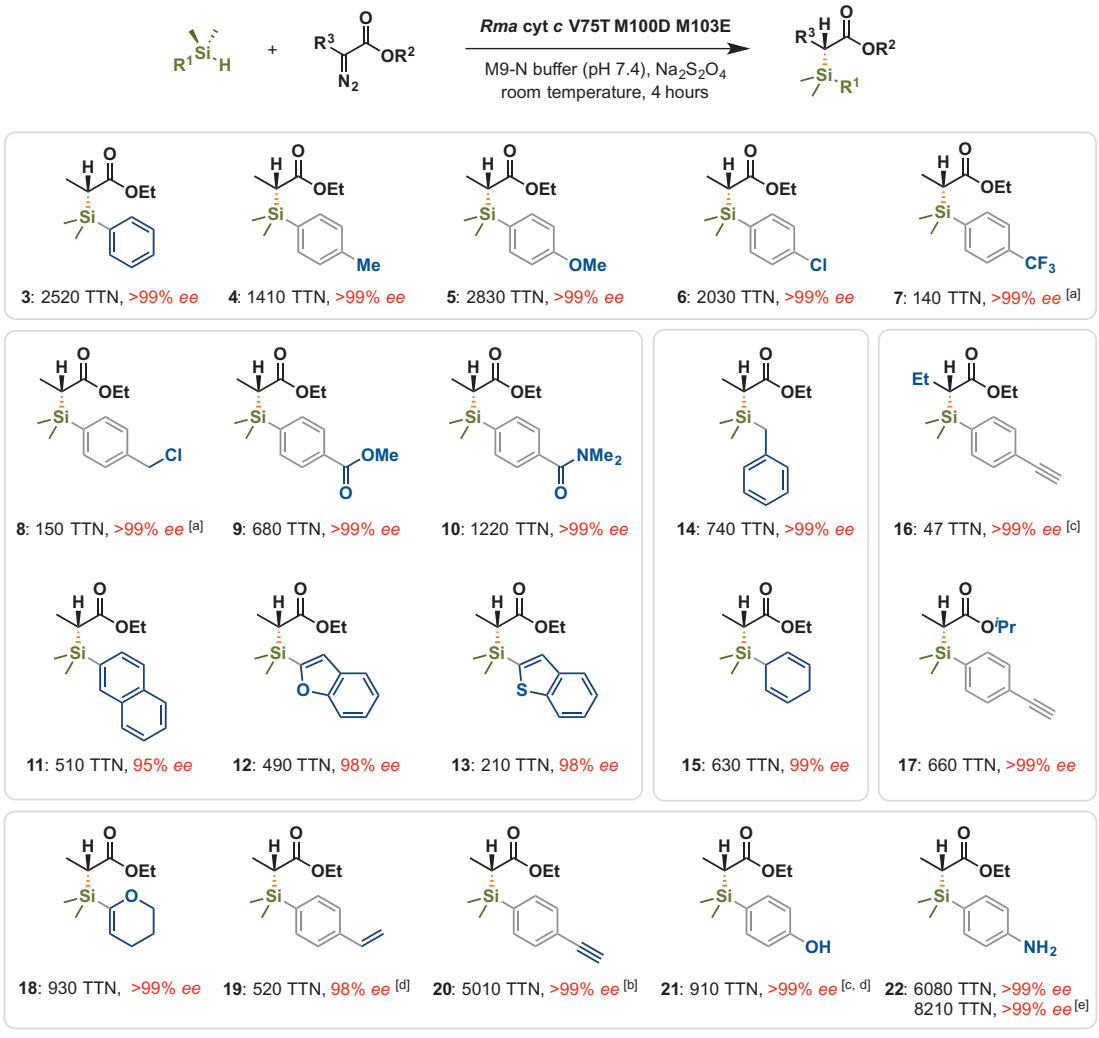

Fig. 2. Scope of *Rma* cyt c V75T M100D M103E-catalyzed carbon–silicon bond formation. Standard reaction conditions: lysate of *E. coli* expressing *Rma* cyt c V75T M100D M103E (OD_{600} = 1.5; heat-treated at 75°C for 10 min), 20 mM silane, 10 mM diazo ester, 10 mM $Na_2S_2O_4$, 5 vol % MeCN, M9-N buffer (pH 7.4) at room temperature under anaerobic conditions. Reactions performed in triplicate. [a] OD_{600} = 5 lysate. [b] OD_{600} = 0.5 lysate. [c] OD_{600} = 15 lysate. [d] 10 mM silane. [e] OD_{600} = 0.15 lysate.

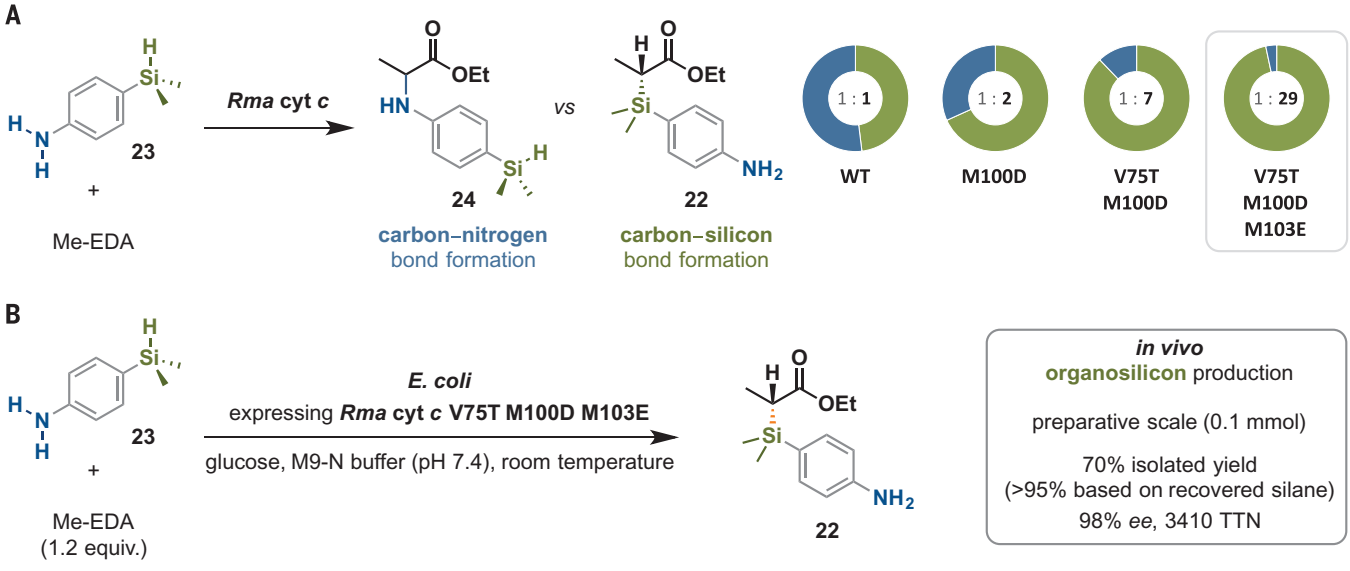

Fig. 3. Chemoselectivity and in vivo activity of evolved *Rma* cyt c. (**A**) Chemoselectivity for carbene Si–H insertion over N–H insertion increased markedly during directed evolution of *Rma* cyt c. Standard reaction conditions as described in Fig. 2. Reactions were performed in duplicate using heat-treated lysates of *E. coli* expressing *Rma* cyt c with protein concentration normalized across variants. Product distribution was quantified after 2 hours of reaction time (before complete conversion, no double insertion product was observed under these conditions). (**B**) In vivo synthesis of organosilicon compound **22**.

alkynes that are prime reaction handles for synthetic derivatization are preserved under the reaction conditions, with no competing cyclopropanation or cyclopropenation activity observed. As a result, organosilicon products **12** and **13** and **18** to **20** were afforded with 210 to 5010 turnovers and excellent stereoselectivities (98 to >99% ee). Preferential carbon–silicon bond formation could also be achieved with substrates bearing free alcohols and primary amines, yielding silicon-containing phenol **21** (910 TTN, >99% ee) and aniline **22** (8210 TTN, >99% ee). This capability removes the need for functional-group protection and/or manipulation, offering a streamlined alternative to transition-metal catalysis for incorporating silicon into small molecules. Indeed, when the same reactants were subjected to rhodium catalysis [1 mol % $Rh_2(OAc)_4$], O–H and N–H insertions were the predominant reaction pathways, and copper catalysis [10 mol % $Cu(OTf)_2$] gave complex mixtures of products (table S7). Tolerance of these highly versatile functionalities in enzymatic carbon–silicon bond-forming reactions provides opportunities for their downstream processing through metabolic engineering, bioorthogonal chemistry, and other synthetic endeavors.

We next asked whether all *Rma* cyt c variants would catalyze carbon–silicon bond formation selectively over insertion of the carbene into an N–H bond in the same substrate. We re-examined the evolutionary lineage and tested all four generations of *Rma* cyt c (wild-type, M100D, V75T M100D, and V75T M100D M103E) with Me-EDA and 4-(dimethylsilyl)aniline (**23**), a reagent that could serve as both nitrogen and silicon donor, to probe the proteins' bond-forming preferences. The wild-type cytochrome c exhibited a slight preference for forming amination product **24** over organosilicon product **22**. Even though silane **23** was not used for screening, and the *Rma* cyt c, therefore, did not undergo direct selection for chemoselectivity, each round of evolution effected a distinct shift from amination to carbon–silicon bond-forming activity (Fig. 3A). This evolutionary path that focused solely on increasing desired product formation culminated in a catalyst that channeled most of the reactants (97%) through carbon–silicon bond formation (>30-fold improved with respect to the wild type), presumably by improving the orientation and binding of the silicon donor.

Some fungi, bacteria, and algae have demonstrated promiscuous capacities to derivatize organosilicon molecules when these substances were made available to them (*1*). The possibility of ultimately establishing silicon-based biosynthetic pathways led us to investigate whether the evolved *Rma* cyt c could produce organosilicon products in vivo. *E. coli* whole cells [optical density at 600 nm (OD_{600}) = 15] expressing *Rma* cyt c V75T M100D M103E in glucose-supplemented M9-N buffer were given silane **23** (0.1 mmol) and Me-EDA (0.12 mmol) as neat reagents. The enzyme in this whole-cell system catalyzed carbon–silicon bond formation with 3410 turnovers, yielding organosilicon product **22** in 70% isolated yield (>95% yield based on recovered silane **23**) and 98% ee (Fig. 3B). These in vitro and in vivo examples of carbon–silicon bond formation using an enzyme and Earth-abundant iron affirm the notion that nature's protein repertoire is highly evolvable and poised for adaptation: With only a few mutations, existing proteins can be repurposed to efficiently forge chemical bonds not found in biology and grant access to areas of chemical space that living systems have not explored.

REFERENCES AND NOTES

1. M. B. Frampton, P. M. Zelisko, *Silicon* **1**, 147–163 (2009).
2. Z. Rappoport, Y. Apeloig, Eds., *The Chemistry of Organic Silicon Compounds* (Wiley, 2003), vol. 3.
3. S. A. Ponomarenko, S. Kirchmeyer, *Adv. Polym. Sci.* **235**, 33–110 (2011).
4. G. A. Showell, J. S. Mills, *Drug Discov. Today* **8**, 551–556 (2003).
5. A. K. Franz, S. O. Wilson, *J. Med. Chem.* **56**, 388–405 (2013).
6. P. T. Anastas, J. Warner, *Green Chemistry: Theory and Practice* (Oxford Univ. Press, New York, 1998).
7. A. M. Tondreau *et al.*, *Science* **335**, 567–570 (2012).
8. A. A. Toutov *et al.*, *Nature* **518**, 80–84 (2015).
9. B. Marciniec, Ed., *Hydrosilylation: A Comprehensive Review on Recent Advances* (Springer, Netherlands, 2009).
10. T. Lee, J. F. Hartwig, *Angew. Chem. Int. Ed.* **55**, 8723–8727 (2016) and references therein.
11. R. Sambasivan, Z. T. Ball, *J. Am. Chem. Soc.* **132**, 9289–9291 (2010).
12. D. Chen, D.-X. Zhu, M.-H. Xu, *J. Am. Chem. Soc.* **138**, 1498–1501 (2016).
13. Y. Yasutomi, H. Suematsu, T. Katsuki, *J. Am. Chem. Soc.* **132**, 4510–4511 (2010).
14. Y.-Z. Zhang, S.-F. Zhu, L.-X. Wang, Q.-L. Zhou, *Angew. Chem. Int. Ed.* **47**, 8496–8498 (2008).
15. S. Hyde *et al.*, *Angew. Chem. Int. Ed.* **55**, 3785–3789 (2016).
16. See supplementary materials for details.
17. U. T. Bornscheuer *et al.*, *Nature* **485**, 185–194 (2012).
18. J. L. Tucker, M. M. Faul, *Nature* **534**, 27–29 (2016).
19. P. J. O'Brien, D. Herschlag, *Chem. Biol.* **6**, R91–R105 (1999).
20. S. D. Copley, *Curr. Opin. Chem. Biol.* **7**, 265–272 (2003).
21. O. Khersonsky, D. S. Tawfik, *Annu. Rev. Biochem.* **79**, 471–505 (2010).
22. P. S. Coelho, E. M. Brustad, A. Kannan, F. H. Arnold, *Science* **339**, 307–310 (2013).
23. Z. J. Wang, N. E. Peck, H. Renata, F. H. Arnold, *Chem. Sci.* **5**, 598–601 (2014).
24. V. Tyagi, R. B. Bonn, R. Fasan, *Chem. Sci.* **6**, 2488–2494 (2015).
25. Only stoichiometric iron carbenoid insertion into Si–H bonds has been reported (*30*).
26. M. Stelter *et al.*, *Biochemistry* **47**, 11953–11963 (2008).
27. J. G. Kleingardner, K. L. Bren, *Acc. Chem. Res.* **48**, 1845–1852 (2015).
28. B. D. Levin, K. A. Walsh, K. K. Sullivan, K. L. Bren, S. J. Elliott, *Inorg. Chem.* **54**, 38–46 (2015).
29. S. Zaidi, M. I. Hassan, A. Islam, F. Ahmad, *Cell. Mol. Life Sci.* **71**, 229–255 (2014).
30. E. Scharrer, M. Brookhart, *J. Organomet. Chem.* **497**, 61–71 (1995).

ACKNOWLEDGMENTS

This work was supported in part by the National Science Foundation, Office of Chemical, Bioengineering, Environmental and Transport Systems SusChEM Initiative (grant CBET-1403077); the Caltech Innovation Initiative (CI2) Program; and the Jacobs Institute for Molecular Medicine at Caltech. Any opinions, findings, and conclusions or recommendations expressed in this material are those of the author(s) and do not necessarily reflect the views of the funding organizations. R.D.L. is supported by a NIH–National Research Service Award training grant (5 T32 GM07616). We thank A. Buller, S. Dodani, S. Hammer, and C. Prier for helpful discussions and comments on the manuscript and N. Peck for screening P450 variants. We are grateful to S. Virgil and the Caltech Center for Catalysis and Chemical Synthesis and to N. Torian and the Caltech Mass Spectrometry Laboratory for generous analytical support; the Beckman Institute Laser Resource Center (BILRC) at Caltech for use of their CD spectrometer; B. Stoltz for use of the polarimeter; and H. Gray for providing the pEC86 plasmid. A provisional patent application has been filed through the California Institute of Technology based on the results presented here. All data necessary to support this paper's conclusions are available in the supplementary materials.

SUPPLEMENTARY MATERIALS

www.sciencemag.org/content/354/6315/1048/suppl/DC1
Materials and Methods
Figs. S1 to S6
Tables S1 to S7
References (*31*–*67*)

22 July 2016; accepted 11 October 2016
10.1126/science.aah6219

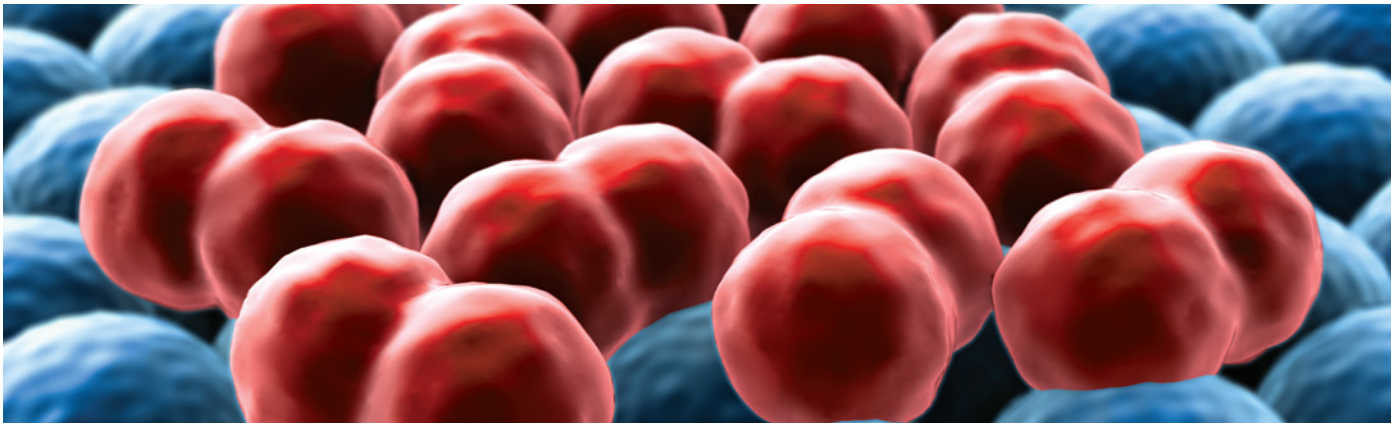

Cell biology shapes up

Cell biologists no longer rely only on pictures from microscopes—pixels and pulses from cell sorters and other devices now enhance their research. By borrowing tools and techniques from computer scientists and engineers, they have upgraded their approach to studying cell morphology.
By Alan Dove

The shape we're in

Since its inception, cell biology has been a fundamentally visual science. Fibroblasts are elongated; neurons are dendritic. Mitotic cells have spindles; apoptotic cells have blebs. The field's clinical cousins—pathology and hematology—also rely heavily on cell shape. Pathologists classify tumors by how far their cells deviate from their normal forms, while hematologists identify and count different leukocytes by sight.

This visual approach has driven decades of crucial discoveries and decorated countless labs with stunning wall art, but it's also revealed the limits of traditional techniques. To push the field further, cell biologists have begun borrowing machine-learning and data-mining tools from computer science, while engineers are designing imaging and microscopy systems that enable entirely novel analyses.

At the same time, biologists are gaining a better appreciation of the importance of cell morphology. Although researchers have long known that genetic and epigenetic mechanisms can alter cells' shapes, recent work has shown that the reverse is also true. Now, a combination of innovative 3D culture systems, automated image analysis, and sophisticated microscopic shape mapping is driving a rush of groundbreaking discoveries.

Faces in the crowd

For immunologists and hematologists, cell morphology research has enjoyed decades of steady progress. Since the development of the earliest clinical hematology analyzers, automated cell counting based on cellular shapes has been a staple technique of medical and basic research laboratories. Fluorescence-activated cell sorters added the ability to separate cells into containers based on which molecular markers they carry.

More recently, engineers have added complete imaging capability and artificial intelligence to some of these machines, yielding systems that can simultaneously photograph and classify thousands of cells per hour. "They aim not just to quantify markers … you're actually able to localize [markers], look at them, and make deductions from the cell shape or the nuclear shape overall," says Shaf Yousaf, head of technology and business development at **MilliporeSigma** in Billerica, Massachusetts. He adds that "they can do all the things classical flow cytometers do, as well as look at images of individual cells."

The MilliporeSigma systems produce immense quantities of data, which is both a blessing and a curse. Because no human could reasonably sift through thousands of cell images to distinguish relevant morphological differences, the machines rely heavily on image analysis software. Depending on which device they buy, researchers can photograph cells at anywhere from 20x to 60x magnification, and use the included software to sort them by purely visual characteristics such as shape and size, fluorescent markers, or both.

Automated image analysis enables studies that would be difficult or impossible with traditional microscopy. One MilliporeSigma system user is developing label-free assays to distinguish blood cancers. "When you look at the varying types of cell morphologies that correspond to different leukemias, you can statistically look at enough cells using this system to be able to classify different kinds of leukemias," says Yousaf. The ability to track markers inside and outside a cell simultaneously, and to map them atop images showing the cell's shape, is also helping researchers study the metabolic effects of signaling molecules, such as G-protein-coupled receptors.

MilliporeSigma sells a range of options with its imaging flow cytometers, but whether an individual laboratory is buying a low-end unit or a core facility is installing a more complex one, researchers should expect to spend some time learning how to use these instruments. The

Upcoming Features
Genomics—January 13 ■ *Digital Lab Management—February 3* ■ *Bioengineering—March 24*

Featured Participants

Definiens
www.definiens.com

GE Healthcare Life Sciences
www.gelifesciences.com

Genentech
www.gene.com

Lawrence Berkeley National Laboratory
www.lbl.gov

MilliporeSigma
www.emdgroup.com/emd/products/life_science/life_science.html

Molecular Devices
www.moleculardevices.com

Park Systems
www.parkafm.com

bulk of the training focuses on experimental design and data analysis. Typically, scientists use a set of manually validated cell images to "train" the software's learning algorithms on the desired morphological traits. They then run samples through the system, see whether the machine is identifying the correct shapes, and retrain the algorithm as necessary.

Enter the matrix

While blood cells live in a convenient, easily studied liquid, most other cell types have been harder to analyze in the laboratory. That's why cell biologists were justifiably fascinated when 2D cell culture first became available. Growing immortalized cells on petri dishes provided unprecedented control over experiments, but at a cost. "Of course we learned quite a bit from that technique, but at the same time they were also using completely [artificial conditions]," recalls Mina Bissell, a distinguished scientist in the Biological Systems and Engineering Division at **Lawrence Berkeley National Laboratory** in Berkeley, California.

During her postdoctoral work, Bissell noticed that removing mammary cells from a mouse and putting them into a culture dish caused them to lose not only their normal in vivo shapes, but also their ability to secrete milk. "I said 'Hey, why don't we put these things in something that looks like a basement membrane?'" says Bissell. That idea led eventually to a 3D culture system, in which isolated mammary cells retained their shapes and also their milk-secreting ability. Since then, Bissell and a growing number of colleagues have embraced the idea that for solid tissues, cell context and shape are at least as influential as genes.

"Signaling pathways and gene expression profiles are very different in cells that grow in 2D and 3D cultures," says Oksana Sirenko, a research scientist at **Molecular Devices** in Sunnyvale, California. Besides displaying more natural signaling patterns, 3D cultures allow researchers to mix cell types in ways that mimic their interactions in living tissue, providing more accurate models of normal physiology and pathogenesis. As a result, 3D cell culture systems have become a staple of cell biology. "3D culture is trying to bridge a gap between in vivo biology and in vitro cell biology," says Sirenko.

In a typical 3D culture system, cells cling to each other, forming spheroids that float in liquid culture media or expand into a soft matrix. Investigators can watch the cells change shape as these spheroids grow and respond to stimuli. For example, researchers can grow spheroids that mimic early-stage tumors, then treat them with candidate chemotherapies and watch for the spheroids to stop growing or start shrinking. Tracking such changes manually, however, is slow and subjective.

"[The] challenge is how to get reliable information and do it in a more high-throughput and more reproducible manner—so here comes technology," says Sirenko. Companies making high-content cell imaging equipment such as confocal microscopes and plate readers are now adding software tools to process images of 3D cell cultures. In a typical algorithm, the software first scans each image for spheroid-like structures, then defines the boundaries of likely cells within the spheroids. Researchers can query the data to score how many live and dead cells the spheroids contain in each plate or well. They can also track standard molecular markers for mitochondria, nuclei, and other subcellular structures. "You can not only evaluate changes such as cells dying, for example, but you can also see more subtle phenotypic changes between different [conditions]," adds Sirenko.

Molecular Devices integrates this type of software into high-throughput screening platforms, so scientists can quickly scan thousands of spheroids growing in varied culture conditions. The system can yield dose-response curves for candidate drugs, screen the phenotypes of large numbers of gene mutations, or execute complex custom protocols for completely new experiments. Despite the heavy automation, though, Sirenko emphasizes that researchers retain the ability to evaluate the cells manually: "I can check any number or I can check an entire plate and see whether it [matches] my visual assessment." Other companies offer similar tools on their own high-content screening platforms, such as **GE Healthcare Life Sciences'** IN Cell Analyzer system.

Pharmaceutical companies are one obvious market for high-throughput cell morphology equipment, but competition and rapidly increasing computing power have now driven prices down to levels many academic users can afford. Sirenko estimates that basic research laboratories now comprise about half the users of these systems.

You know it when you see it

The ability to automate morphology assays on 3D cell cultures is a powerful tool, but some scientists are now pushing the technology even further, with algorithms that can classify structures in living animals and clinical specimens. Those analyses have long relied on qualitative changes in cell shape to track physiological shifts. For example, neurobiologists can track the activation of microglia, the brain's native immune cells, based on their shapes. "It was well known for decades that activated microglia retract these very branched filopodia, and they become round," explains Cleo Kozlowski, a scientist at **Genentech** in South San Francisco, California. cont.>

However, that assay doesn't pinpoint the moment of activation or provide a straightforward way to quantify the connections between microglial activation and gene expression patterns. Kozlowski tackled that problem computationally; using the popular MATLAB programming environment, she and her colleagues developed an algorithm that classifies the shapes of microglia in confocal microscopy images with 90% accuracy. The technique works in sectioned brain tissue, and also in the brains of live mice with transparent windows implanted into their skulls. By quantifying the cells' shapes, the algorithm allows researchers to determine precisely how far along the activation pathway they are. Overlaying that information onto data from gene-expression profiling characterizes the microglia with unprecedented precision. Since publishing the technique in 2012, Kozlowski says she has provided the code to numerous researchers on request.

More recently, Kozlowski has focused on diagnosing colitis. "Colitis is generally assessed by a pathologist, so they have to sit down, look at various areas under a microscope, [and] score how bad the inflammation and the morphological changes of the crypts are in the intestines," says Kozlowski, adding, "I just wanted to speed up that process."

Pathologists typically use hematoxylin and eosin (H&E) staining to highlight the intestinal structure. Unfortunately, this type of staining is hard for computers to interpret. "It doesn't stain a specific molecule of interest—it gives you a kind of overview of the tissue structure, so it's really about morphology and shape," says Kozlowski. She compares fluorescence microscopy to searching an image of the night sky for stars, whereas using H&E is more like picking out cities on Google Maps, a much harder computational problem.

To make the analysis work, Kozlowski and her colleagues built their algorithm inside a powerful, proprietary image-processing framework from **Definiens** in Munich, Germany. The result was a system that can distinguish healthy intestine from colitis quickly and accurately, but at a price only very well-funded corporate researchers can afford—the Definiens license is prohibitively expensive for most laboratories.

The major challenge for automated pathology assays, though, may be cultural. "That will be the biggest hurdle, really convincing a lot of people who don't really think that this kind of thing can be done by machines to say, 'Oh, yes it can,'" explains Kozlowski.

Look and feel

Besides devising unique ways to analyze conventional cell images, researchers are also using new microscopy techniques to better define cell shapes. In atomic force microscopy (AFM), a silicon probe scans across a surface and builds a 3D image of the cells it encounters, much like someone reading a relief map with their fingers. AFM is especially useful for identifying changes in the cytoskeleton and studying relatively hard surfaces such as bone.

"AFM didn't catch the details of microvilli and other structures on the cell surface. If we adopt [SICM], we can actually open a new chapter in cell biology."
—Sang-Joon Cho

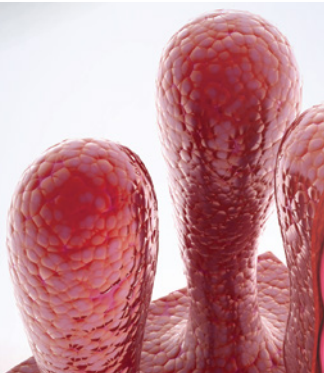

For soft cells, though, AFM yields fuzzier images. "Looking at live cell membranes is almost impossible, because the cell membrane is not a simple structure; there are a lot of glycoproteins as well as the extracellular matrix," explains Sang-Joon Cho, chief scientist and director of R&D at **Park Systems** in Suwon, Korea. The silicon probe tends to squash the membranes of soft cells while measuring them, deforming many of the structures that cell biologists are most interested in seeing.

To address this problem, Cho and his colleagues turned to scanning ion-conductance microscopy (SICM). Instead of a solid silicon probe, SICM squirts a stream of saline solution through a thin capillary tube. Measuring changes in a voltage bias applied to the saline reveals how close the capillary tube is to the cell, allowing researchers to scan subtle structures on the cell surface without disrupting them.

For Cho, the results were revelatory. Comparing images of embryonic stem cells made with AFM and SICM, he found that the SICM images revealed things that had been invisible under AFM. "AFM didn't catch the details of microvilli and other structures on the cell surface," says Cho, adding that "if we adopt this technology, we can actually open a new chapter in cell biology."

Park's SICM systems also have AFM and optical microscopes built in, so scientists can view cells with all three techniques and compare or superimpose the resulting images. The systems can also enhance other techniques, such as patch clamp measurements applied in electrophysiology. Investigators can use SICM to pick a specific point on the cell membrane, then attach the patch clamp there to measure the membrane's electrical potential. They can also deliver precise doses of drugs, nucleic acids, or proteins to targeted points on the cell.

Both AFM and SICM require specialized training, but most biologists find the latter instrument easier to learn. "When I train people, they take several months to get certain images from soft biological samples using atomic force microscopy, but with SICM they can get them in a week," says Cho.

Regardless of the approach they take, experts in cell morphology agree that the field is poised for a major leap. "The two keys for me moving forward are machine learning and better optics," says Kozlowski, adding, "it's a very exciting time in image analysis."

Alan Dove is a science writer and editor based in Massachusetts.

DOI: 10.1126/science.opms.p1600110

Single-Cell Analysis

The ICELL8 Single-Cell System can isolate thousands of single cells and process specific cells for analysis, including NGS. It also includes an imaging station and CellSelect software, which images each nanowell and provides automatic selection of single cells for downstream processing. ICELL8 can isolate up to 1,800 single cells, ranging from 5 µm–100 µm in size on a single chip, including cells from solid tumors, brain cells, pulmonary airway cells, and multiple cell lines. The SmartChip platform can be used for profiling and validating molecular biomarkers, and can perform massively parallel singleplex PCR for one-step target enrichment as well as library preparation for clinical NGS. The Apollo 324 library preparation system can be used to process DNA and RNA from clinical samples to NGS-ready libraries. These technologies offer a powerful set of tools for biological analysis at the molecular and single-cell level in the life sciences, pharmaceutical, and clinical laboratory industries.

WaferGen Biosystems
For info: 877-923-3746
www.wafergen.com

Manual Colony Counter

The aCOLade 2 manual colony counter with automatic count recording is an ideal choice for budget-conscious microbiology laboratories. It consists of an illuminated receiver plate and a large LED display. The pressure of marking a colony with a felt-tip pen registers a cumulative count on the digital display with confirmation by an audible tone (that can be turned on or off). A built-in averaging facility calculates the average count over multiple plates. Counting results, as well as useful statistics such as standard deviation, can be sent to the accessory printer or to a computer via the supplied USB cable. Substage illumination by low-energy bright LEDs allows glare-free optimum viewing. A switchable black background is provided to enhance viewing of translucent and difficult-to-see colonies. Two Wolfhuegel graticules and dish-centering adapters facilitate use with 50 mm–90 mm dishes. A choice of magnifiers and a printer are available as optional accessories.

Synbiosis
For info: +44-(0)-1223-727125
www.synbiosis.com/acolade

Live-Cell Metabolic Assay Platform

The Agilent Seahorse XFp Analyzer measures metabolic functions of live cells with same-day results. From routine analysis to cutting-edge research, it enables researchers to rapidly assess both mitochondrial respiration and glycolysis in live cells, generate metabolic phenotypes of precious samples (as few as 15,000 cells per condition), and conduct functional metabolic assays without the need for special bioenergetics expertise. Seahorse XF test kits and reagents simplify cellular bioenergetics by providing precalibrated, pretested reagents for metabolic phenotyping, mitochondrial respiration, glycolysis, and fatty-acid oxidation in cells. Because Seahorse XF measurements are nondestructive, the metabolic rate of the same cell population can be measured repeatedly while up to four different drugs are injected sequentially into each well. Total assay time is typically 60 minutes to 90 minutes. To maintain normal cell physiology, a temperature control system maintains the cellular environment at 37°C (or another preset temperature).

Agilent Technologies
For info: 877-424-4536
www.agilent.com

Microplate Stacker

The patented BioStack 4 Microplate Stacker from BioTek Instruments features unique automatic microplate delidding and relidding technology, which is especially useful in cell-based assay workflows. The BioStack 4 facilitates increased throughput and greater productivity in processes involving lidded and unlidded 96-, 384-, and 1,536-well microplates, as well as select 6- to 48-well microplates. Its design incorporates a two-position carrier for ultrafast transfer times, and its small overall footprint allows operation in biosafety cabinets. A rotational gripper enhances versatility in portrait or landscape orientation, while the unique lid-gripping method minimizes exposure of the microplate's contents during transfer. Finally, interchangeable plate storage stacks are available for the throughput needs of up to 30 lidded or 50 unlidded microplates, with automated restacking. Many of BioTek's imagers, readers, washers, and dispensers may be integrated with the BioStack 4, which is directly controlled via the respective instrument's integrated software.

BioTek Instruments
For info: 888-451-5171
www.biotek.com

Fluorescence Cell Analyzer

The Countstar Fluorescence Cell Analyzer can do all that a traditional flow cytometer does but faster, easier, and at much lower cost. A compact, benchtop unit featuring an integral processor and display screen, the Countstar has a number of advantages over conventional systems. First, it is very easy to operate due to its high level of automation, which makes training very simple—so researchers can quickly start to create results. Second, it is always ready to use—there are no set times or preparation periods needed. Third, it is significantly less expensive to purchase and run than any of the traditional flow cytometry systems. A standard system could take up to 165 minutes to process 15 samples, while the Countstar can do the same job in 50 minutes.

Eikonix
For info: +44-(0)-1223-515440
www.eikonix.com

Electronically submit your new product description or product literature information! Go to www.sciencemag.org/products/newproducts.dtl for more information.

Newly offered instrumentation, apparatus, and laboratory materials of interest to researchers in all disciplines in academic, industrial, and governmental organizations are featured in this space. Emphasis is given to purpose, chief characteristics, and availability of products and materials. Endorsement by *Science* or AAAS of any products or materials mentioned is not implied. Additional information may be obtained from the manufacturer or supplier.


Genomics has
met its match
MEET METABOLON, GENOMICS' PERFECT COMPLEMENT
Explore the relationship between genotype and phenotype with Metabolon's revolutionary solutions.
Our team of experts takes metabolomics to the next level with a unique approach to bioinformatics.
We turn data into actionable insight so you can unlock the full potential of the genome.
See why genomics and metabolomics are better together at **metabolon.com/ebook**
METABOLON®
Where **knowing** comes to **life**™

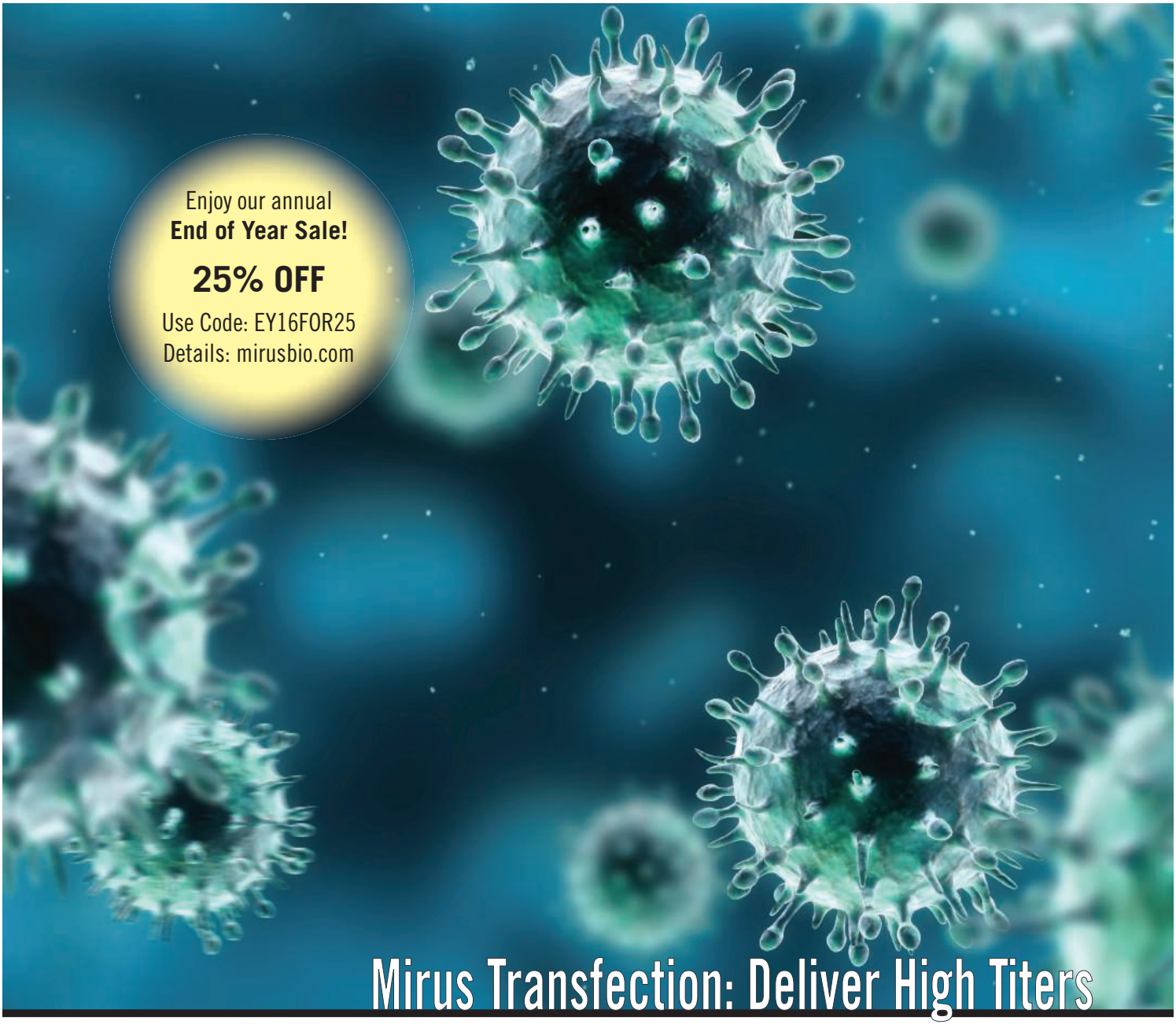

Harness the Power of Lentivirus

NEW! *Trans*IT®-Lenti Transfection Reagent is designed to enhance delivery of packaging and transfer vectors to adherent 293T cell types to increase lentivirus production within your existing workflow.

Benefits of the reagent include:

- **High Titers** – Provide up to eight-fold higher functional titers
- **Simple Protocol** – No media change required; single harvest
- **Animal Origin Free** – Regulatory friendly

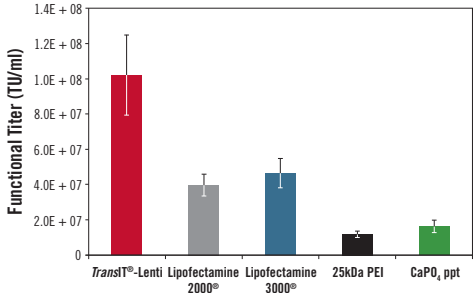

*Trans*IT®-Lenti Transfection Reagent outperforms leading reagents.

Visit www.mirusbio.com/transit-lenti to request a FREE sample of *Trans*IT®- Lenti Transfection Reagent.

Delivery by Mirus

www.mirusbio.com

Hope for clinical collaborations at SciLifeLab

SciLifeLab, Science for Life Laboratory, is a Swedish research center within molecular biosciences with focus on health and environment. To further strengthen the research environment at the center SciLifeLab regularly recruits young, talented research leaders to become SciLifeLab fellows.

Each fellow is recruited by one of the center host universities and receives funding from them. One of the newest fellows is Vicent Pelechano, recruited by Karolinska Institutet/SciLifeLab from EMBL, Heidelberg, Germany in 2016.

High throughput biology approaches

Vicent Pelechano's research focuses on understanding how apparently identical cells respond differently to the same stimulus. He and his colleauges use state of the art genomic technologies to study the regulatory mechanism leading to the appearance of divergent gene expression programs in clonal populations of cells.

Photo: Susanna Appel

Vicent Pelechano

"The fellows positions at SciLifeLab are very attractive for high throughput biology approaches, which is what I like to do," Vicent Pelechano said.

The group also combines experimental and computational work to develop novel genome-wide techniques to study eukaryotic transcription in budding yeast and mammalian cell lines.

"I am especially interested in drug-tolerant cancer persister cells that, although genetically sensitive to a drug, do not respond to it," Vicent Pelechano said. "At SciLifeLab we have the right environment to start clinical collaborations and we are moving to that direction."

Expertize from multiple fields available

"It is amazing that we have people from so many universities and so many different backgrounds here at SciLifeLab, that opens up many possibilities for collaborations. If I need to use any specific method, I basically knock on the door to my colleague and we have it there, from chrystallography to protein analysis. People are actively helping me to establish myself here and that is something that you don't find in many places."

"Stockholm is also a really nice city to live in. It is a small capital but still big enough and there are parks just everywhere. I feel very welcome here."

"Thanks to the fellows program I have some time to attract more funding. Hopefully I will stay here in Sweden for many years."

SciLifeLab – a national resource

SciLifeLab is a Swedish research center within molecular biosciences with focus on health and environment. It is also a national center with the mission to develop, use and provide advanced technologies. The center infrastructure encompasses a multitude of biomolecular technologies and bioinformatics services. National funding makes SciLifeLab's services and expertize available to researchers in all of Sweden.

The center is a joint effort by four Swedish universities (Karolinska Institutet, KTH Royal Institute of Technology, Stockholm University and Uppsala University). Founded in 2010, the center today encompasses more than 1 200 researchers mainly located in and around the two center nodes in Stockholm and Uppsala.

SciLifeLab

www.scilifelab.se

Frontiers in Research Excellence and Discovery

Physicist Carlos Meriles, City College of New York, is the first recipient of the Frontiers in Research Excellence and Discovery (FRED) Award from Research Corporation for Science Advancement. His work focuses on manipulating and storing information in nitrogen point defects within diamond crystals at room temperature.

The FRED Award, $250,000, supports early stages of exceptional, high-risk/high-reward research that may potentially transform a field of scientific inquiry. It is presented to highly creative Cottrell Scholars whose ideas and potential solutions, though not readily funded by conventional grant programs, address major current challenges in the recipients' areas of research expertise.

By developing unique perspectives for solving key challenges, FRED awardees create new approaches that accelerate basic science research for the benefit of society.

Since 1994 the Cottrell Scholar program has developed outstanding teacher-scholars recognized by their scientific communities for the quality and innovation of their research programs and their academic leadership skills.

2016 Frontiers in Research Excellence and Discovery Awardee

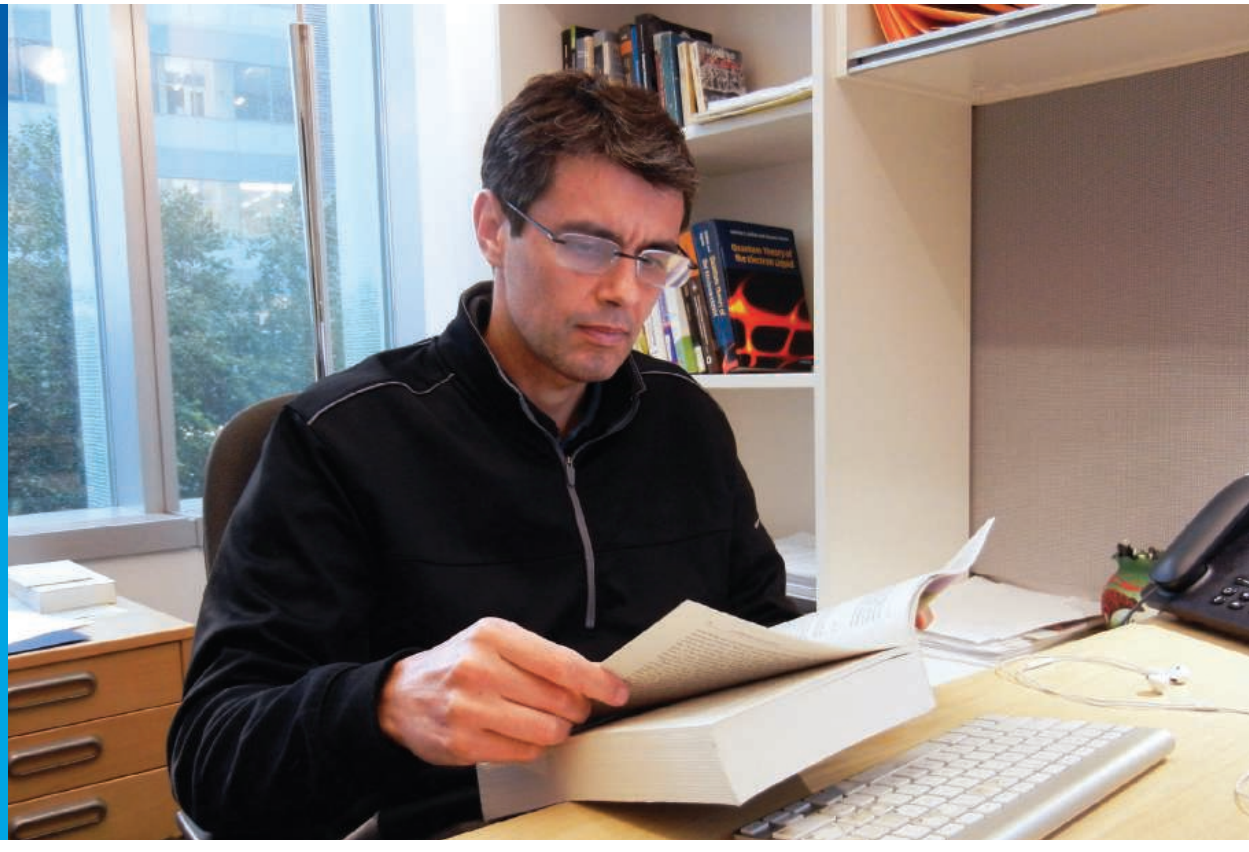

CARLOS MERILES
Professor of Physics
City College of New York

To view a brief video on Meriles' work, visit www.rescorp.org

RESEARCH CORPORATION *for* SCIENCE ADVANCEMENT

A foundation dedicated to science since 1912.

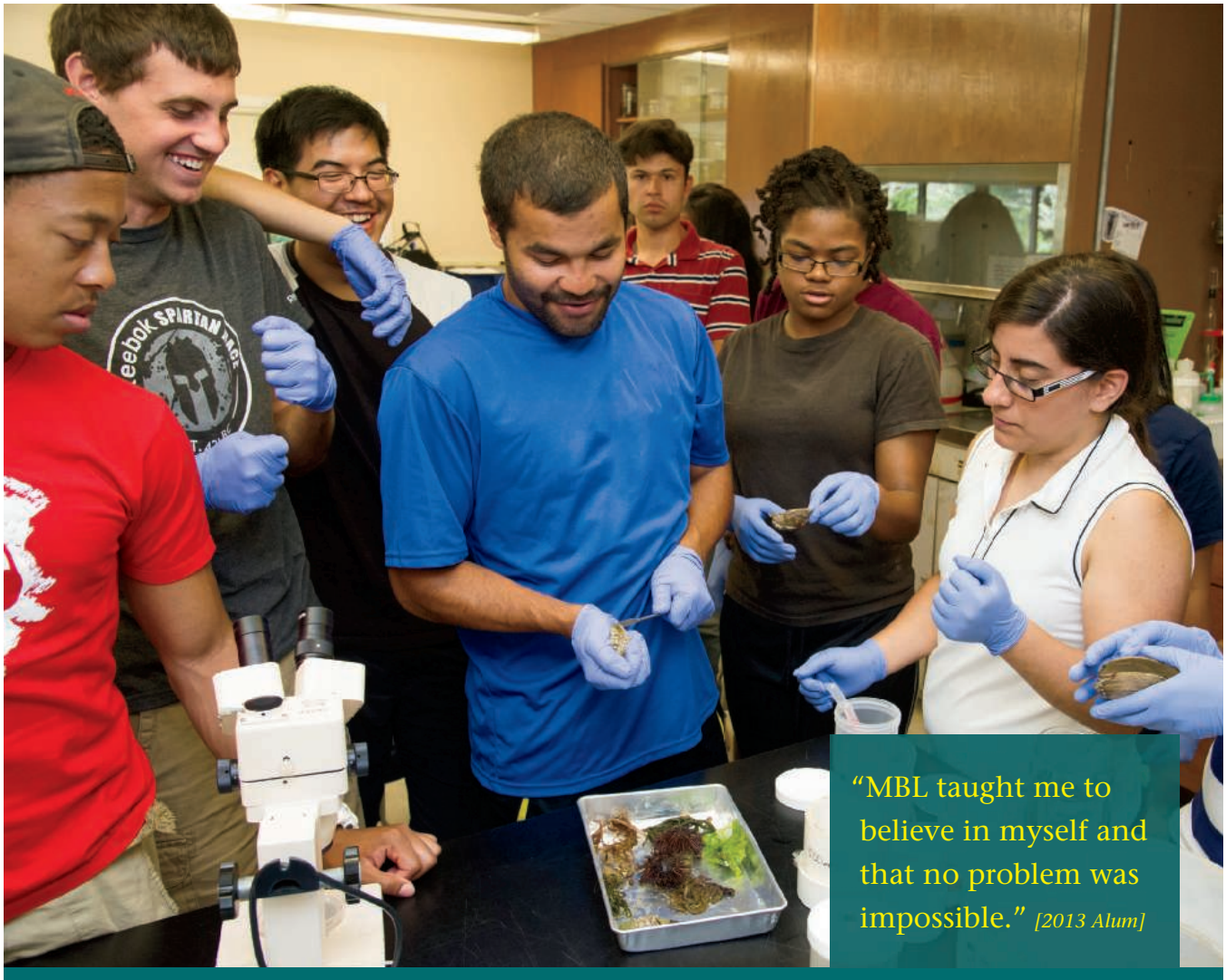

2017 Advanced Research Training Courses

on Cape Cod in Woods Hole, MA

Investigate contemporary research problems and learn cutting-edge approaches from an internationally renowned faculty.

Each year, MBL courses attract a diverse population of over 500 of the best and brightest students in the world, from more than 300 institutions and over 30 countries. Applicants must be in training for, or possess, a PhD or equivalent degree.

Discovery Courses are 6-8 week full immersion courses for those who seek advanced, hands-on training in pioneering research fields.

Special Topics Courses are 1-4 week long courses that provide intense training in specialized research areas.

Taking an MBL course is *transformative.*

Substantial financial assistance is available.

Marine Biological Laboratory | THE UNIVERSITY OF CHICAGO **mbl.edu/courses**

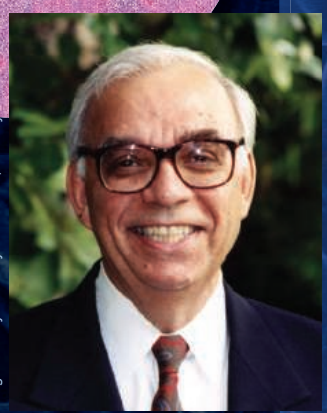

Image courtesy University of California, Berkeley

Nicholas R. Cozzarelli,
former PNAS Editor-in-Chief.

Call for 2016 Cozzarelli Prize Nominations

The PNAS Editorial Board is now accepting nominations through January 6, 2017 for the 2016 Cozzarelli Prize. This award recognizes scientific excellence and will be given to six papers published in PNAS during 2016.

Nominations should be sent to pnas@nas.edu and should include a citation and brief explanation of the merits of the work. The award recipients will be recognized during the PNAS Editorial Board Meeting and the NAS Annual Meeting Awards Ceremony on April 30, 2017 in Washington, DC.

PNAS
www.pnas.org

For a list of previous winners and podcasts with the authors, visit www.pnas.org/site/misc/cozzarelliprize.xhtml.

CELL SIGNALING TECHNOLOGY

Deciphering Cancer

Antibodies to evaluate key signaling networks in growth and differentiation.

Download pathways at www.cellsignal.com/cancerpathways

16PADDBI00072ENG

Cell Signaling TECHNOLOGY®

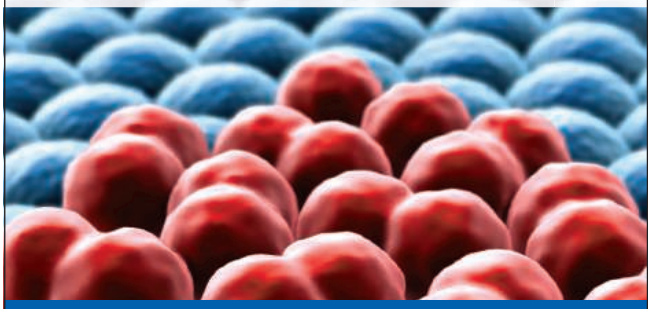

Cell biology shapes up

Cell biologists no longer rely only on pictures from microscopes—pixels and pulses from cell sorters and other devices now enhance their research. By borrowing tools and techniques from computer scientists and engineers, they have upgraded their approach to studying cell morphology.

See the full story on page 1052.

Upcoming Features

Genomics—January 13
Digital Lab Management—February 3
Bioengineering—March 24

Produced by the *Science*/AAAS Custom Publishing Office

AAAS 2017 ANNUAL MEETING

FEBRUARY 16-20 • BOSTON

SERVING SOCIETY THROUGH

SCIENCE POLICY

Browse the Online Program and Register Now

The 2017 program focuses on how to inform policies with the best available scientific evidence.

aaas.org/meetings

AAAS, publisher of *Science*, thanks the sponsors and supporters of the 2017 Annual Meeting

European Commission

RESEARCH COUNCILS UK

SUBARU

HELMHOLTZ ASSOCIATION

THE KAVLI FOUNDATION

for its generous support of the Science Journalism Awards

NANYANG TECHNOLOGICAL UNIVERSITY

SNOLAB

Bristol-Myers Squibb

As of October 31, 2016

THE SCREENING ADVANTAGE

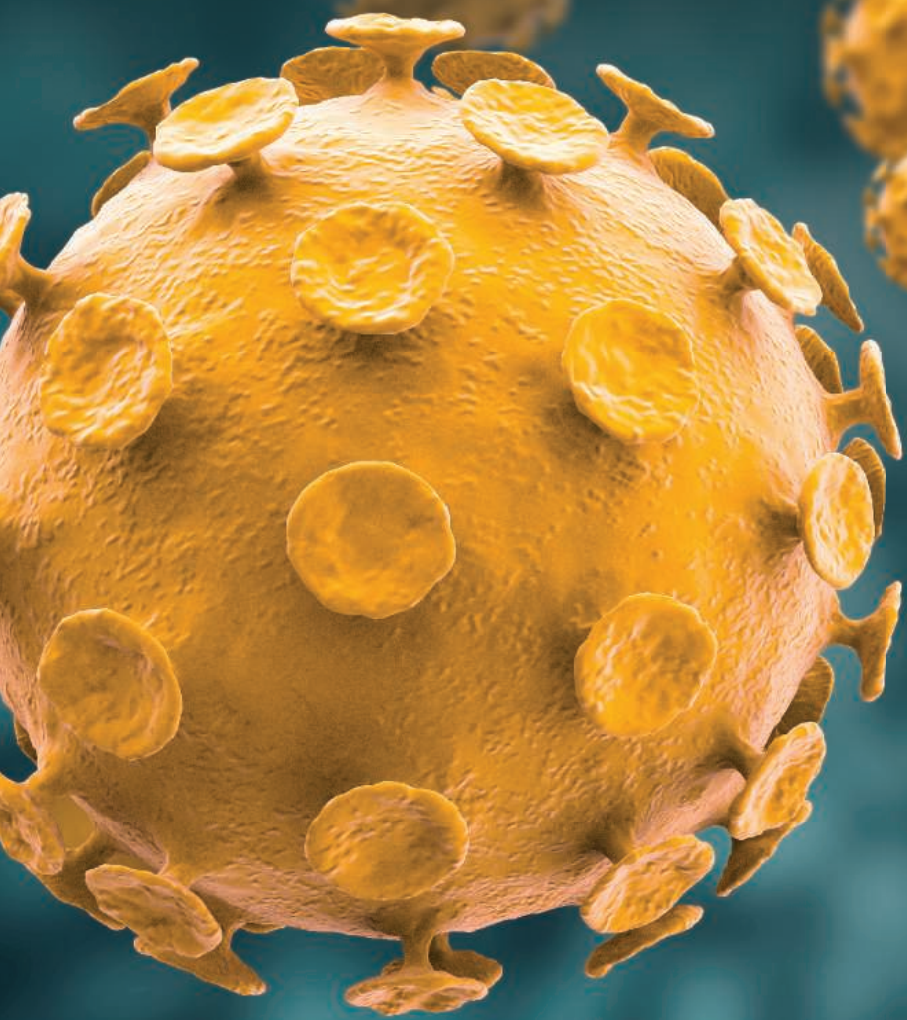

Whether you are reducing gene expression using shRNA or completely knocking out gene expression with CRISPR, we have the right library for your needs.

Available formats:

- Arrayed
- Pooled

Learn more at:
sigma-aldrich.com/screening

sh10014

SIGMA-ALDRICH®

NEW ENGLAND BioLabs® Inc.

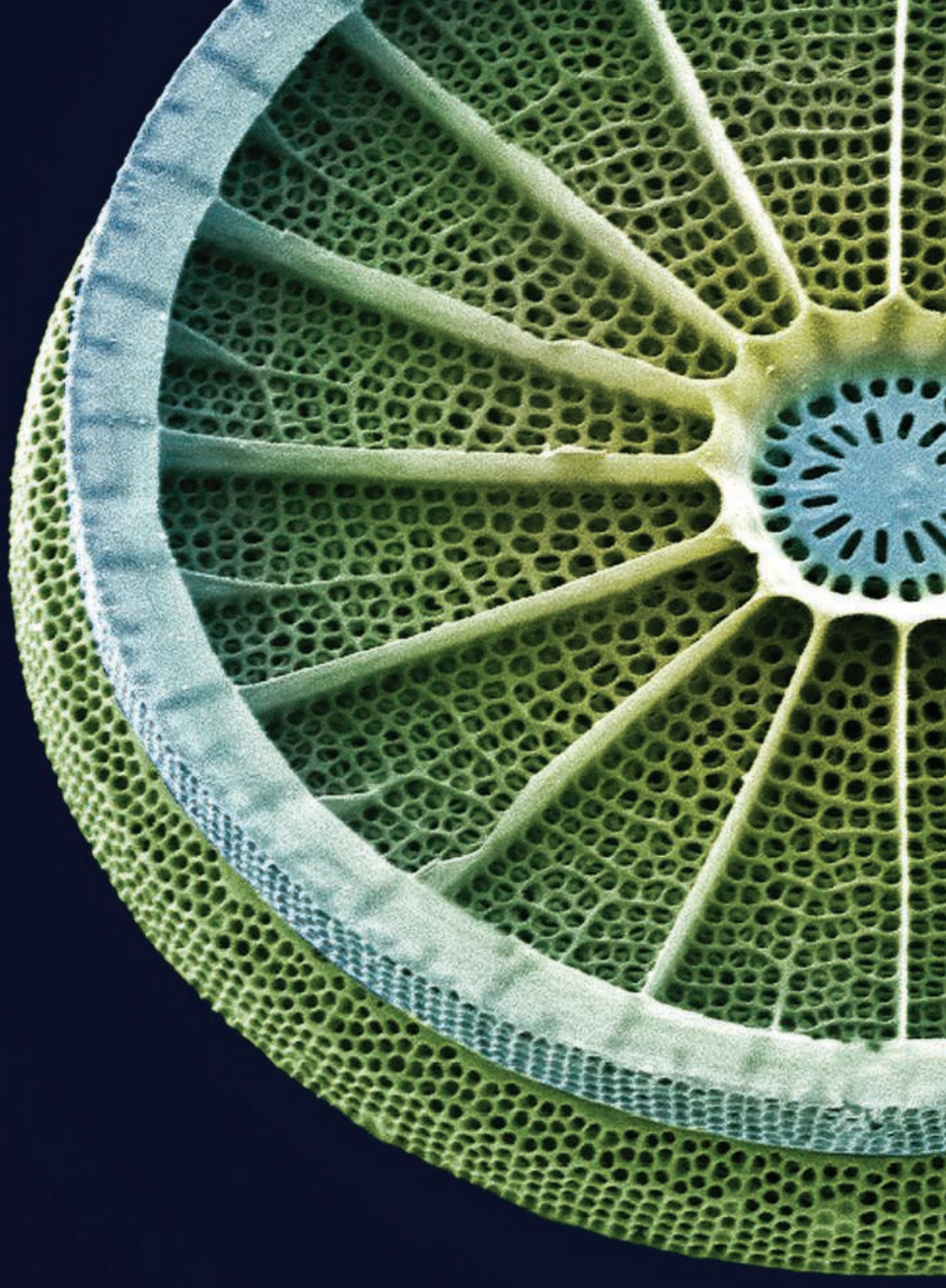

Target with precision.

Introducing the NEBNext Direct™ Cancer HotSpot Panel

Using a unique approach, the NEBNext Direct Cancer HotSpot Panel enriches for 190 common cancer targets from 50 genes prior to next generation sequencing. Combining a novel method for hybridization-based target enrichment with library preparation, the NEBNext Direct technology reduces processing time and minimizes sample loss. Ideal for automation, NEBNext Direct enables highly-specific deep sequencing of genomic regions of interest for the discovery and identification of low frequency variants from challenging sample types.

Visit **NEBNextDirect.com** to learn more and to inquire about sampling this product.

TARGETS INCLUDE REGIONS FROM THE FOLLOWING CANCER-RELATED GENES, INCLUDING >18,000 COSMIC FEATURES:

ABL1	EGFR	GNAQ	KRAS	PTPN11
AKT1	ERBB2	GNAS	MET	RB1
ALK	ERBB4	HNF1A	MLH1	RET
APC	EZH2	HRAS	MPL	SMAD4
ATM	FBXW7	IDH1	NOTCH1	SMARCB1
BRAF	FGFR1	IDH2	NPM1	SMO
CDH1	FGFR2	JAK2	NRAS	SRC
CDKN2A	FGFR3	JAK3	PDGFRA	STK11
CSF1R	FLT3	KDR	PIK3CA	TP53
CTNNB1	GNA11	KIT	PTEN	VHL

For research use only; not intended for diagnostic use.

There's only one Science

Science Careers Advertising

For full advertising details, go to ScienceCareers.org and click For Employers, or call one of our representatives.

Tracy Holmes
Worldwide Associate Director
Science Careers
Phone: +44 (0) 1223 326525

THE AMERICAS

E-mail: advertise@sciencecareers.org
Fax: +1 (202) 289 6742

Tina Burks
Phone: +1 (202) 326 6577

Nancy Toema
Phone: +1 (202) 326 6578

Online Job Posting Questions
Phone: +1 (202) 312 6375

EUROPE / INDIA / AUSTRALIA / NEW ZEALAND / REST OF WORLD

E-mail: ads@science-int.co.uk
Fax: +44 (0) 1223 326532

Sarah Lelarge
Phone: +44 (0) 1223 326527

Kelly Grace
Phone: +44 (0) 1223 326528

Online Job Posting Questions
Phone: +44 (0) 1223 326528

JAPAN

Katsuyoshi Fukamizu (Tokyo)
E-mail: kfukamizu@aaas.org
Phone: +81 3 3219 5777

Hiroyuki Mashiki (Kyoto)
E-mail: hmashiki@aaas.org
Phone: +81 75 823 1109

CHINA / KOREA / SINGAPORE / TAIWAN / THAILAND

Danny Zhao
E-mail: dzhao@aaas.org
Phone: +86 131 4114 0012

ScienceCareers
FROM THE JOURNAL SCIENCE AAAS

ScienceCareers.org

myIDP: A career plan customized for you, by you.

For your career in science, there's only one Science

my IDP ScienceCareers

Recommended by leading professional societies and the NIH

Features in myIDP include:

- Exercises to help you examine your skills, interests, and values.
- A list of 20 scientific career paths with a prediction of which ones best fit your skills and interests.
- A tool for setting strategic goals for the coming year, with optional reminders to keep you on track.
- Articles and resources to guide you through the process.
- Options to save materials online and print them for further review and discussion.
- Ability to select which portion of your IDP you wish to share with advisors, mentors, or others.
- A certificate of completion for users that finish myIDP.

Visit the website and start planning today!
myIDP.sciencecareers.org

ScienceCareers In partnership with:

advancing the life sciences 1912-2012 FASEB Federation of American Societies for Experimental Biology

Medical College of Wisconsin

UCSF University of California San Francisco

Burroughs Wellcome Fund

The University of Georgia

ASSISTANT PROFESSOR IN CELL BIOLOGY – TENURE TRACK

The Department of Cellular Biology at the University of Georgia invites applications for a tenure track Assistant Professor position. The candidate is expected to have an outstanding research program addressing important questions in cell biology as well as a commitment to excellence in teaching. Successful applicants will be expected to develop an extramurally-funded research program, and to teach cell biology at undergraduate and graduate levels. A Ph.D. degree in Cellular Biology or a related field is required and postdoctoral research of two or more years is expected. A competitive package of start-up funds and salary will be offered. This search is part of the University of Georgia signature research initiative, "Inquiring and Innovating to Improve Human Heath".

For full consideration, applications should be submitted by **December 31, 2016**. To apply, submit a CV, a statement of teaching philosophy (1 page), a concise statement of proposed research (2 pages) and the names of 3 referees at **http://facultyjobs.uga.edu/postings/1453**. Teaching in the Department of Cell Biology is guided by the NSF-AAAS "Vision and Change" core concepts. Questions about the search can be sent to: cbsearch@uga.edu. Evaluation of applications will continue until the position is filled.

The Franklin College of Arts and Sciences and the University of Georgia is committed to increasing the diversity of its faculty and students, and sustaining a work and learning environment that is inclusive. Women, minorities, and people with disabilities are encouraged to apply. Georgia is well known for its quality of life both outdoor and urban (www.exploregeorgia.org). UGA (www.uga.edu) is a land grant/sea grant institution located 75 miles northeast of Atlanta. The University of Georgia is an Equal Opportunity/Affirmative Action Employer. All qualified applicants will receive consideration for employment without regard to race, color, religion, sex, national origin, disability, gender identity, sexual orientation or protected veteran status.

WAYNE STATE UNIVERSITY

Tenure/Tenure Track Faculty Position in Biological Sciences

The Department of Biological Sciences at Wayne State University invites applications for a tenure-track opening for a **Neuroscientist and/or Cell Biologist**. Rank will be dependent upon qualifications. We are particularly interested in candidates who use innovative state-of-the-art approaches to complement our existing research areas. WSU has a growing neuroscience community and the department's research strengths include aging, developmental & cancer biology, metabolism, lipids & membranes, cell signaling and genomics. Successful applicants must have a doctorate, postdoctoral experience and an outstanding record of research achievement commensurate with rank. Successful applicants are expected to establish and maintain vigorous, externally funded research programs and participate in graduate and undergraduate education.

Wayne State University is a comprehensive nationally ranked urban research institution that offers state-of-the-art research facilities and highly competitive start-up packages. WSU is located in midtown Detroit, a vibrant and international neighborhood close to cultural, educational and sport attractions. The Detroit metropolitan area offers an excellent standard of living and easy proximity to Michigan's lakes, forests and recreational sites.

Please apply at **https://jobs.wayne.edu** (posting #042322) by **December 20, 2016** for full consideration. In addition to an online application that includes cover letter and curriculum vitae, applicants must submit a 2-page research statement and provide three letters of reference to: **Faculty Search Committee, Department of Biological Sciences, Wayne State University, Detroit, MI 48202** or to Dr. David Njus, Chair at (**ad5348@wayne.edu**). Applications will be considered only when all materials have been received.

Wayne State University is an Affirmative Action/Equal Opportunity Employer. Women and members of minority groups are especially encouraged to apply.

novo nordisk fonden

FUNDING OPPORTUNITIES

ENABLING TODAY'S SCIENTIFIC LEADERS

Novo Nordisk Foundation Laureate Research Grants

Call for applications – biomedicine & biotechnology

For outstanding established scientists to come to Denmark to strengthen their leading research programs

Applicants have directed their own independent groups for 7 or more years in total

GRANT FUNDING

- Individual grants up to **DKK 40 million** over 7 years
- Grant holders can apply for continued funding, up to DKK 35 million over 7 additional years

APPLICATIONS

December 7, 2016 - January 24, 2017

SUPPORTING TOMORROW'S LEADING SCIENTISTS

Novo Nordisk Foundation Young Investigator Awards

Call for applications – biomedicine & biotechnology

For outstanding younger scientists to come to Denmark to expand their leading research programs

Applicants have directed their own independent groups for less than 7 years in total

GRANT FUNDING

- Individual grants up to **DKK 20 million** over 7 years
- Award holders can apply for further funding from other Novo Nordisk Foundation programs

APPLICATIONS

December 7, 2016 - January 24, 2017

CONNECTING FRONTIER SCIENTISTS

Copenhagen Bioscience Conferences

World-leading researchers and young talents discuss the latest scientific results and hottest topics within biomedicine and biotechnology.

- Top-level debate and knowledge sharing in a unique setting
- Speakers and participants of all career levels selected for their scientific accomplishments and motivation
- Registration fee and accommodation covered by the Novo Nordisk Foundation

APPLY FOR

- **Data-driven Biotechnology.** May 7-11, 2017
  Application deadline: February 2017
- **Metabolism in Action.** October 1-5, 2017
  Application deadline: June 2017

EDUCATING THE NEXT GENERATION OF SCIENTISTS

Copenhagen Bioscience PhD Programme

Exceptional students can apply now to this fully funded international PhD programme. The 4-year programme starts with a pre-doctoral year followed by 3 years of PhD education in world-class biomedicine or biotechnology labs in the Novo Nordisk Foundation Research Centre Cluster.

The Novo Nordisk Foundation will fund up to **16 students** to be enrolled in September 2017.

- Funding available for exceptional graduates from any country
- Selection based on academic achievements, research experience, references and interviews
- Interviews in Copenhagen, Denmark: March 19-22, 2017

APPLICATIONS NOW OPEN

Deadline: **December 15, 2016**

FURTHER INFORMATION

To learn more about these opportunities and the Novo Nordisk Foundation, please visit www.novonordiskfoundation.com

POSITIONS OPEN

HARVARD UNIVERSITY

Professor of Psychology

The Department of Psychology seeks to appoint a tenured professor whose interdisciplinary research and teaching explores multifaceted factors that guide and affect human mind and behavior. The successful appointee will be expected to strengthen links between the Department of Psychology and the broader scholarly community. The search is open to individuals trained in neighboring fields. The appointment is expected to begin on July 1, 2018. The professor will teach and advise at the undergraduate and graduate levels.

Candidates are required to have a doctorate. Demonstrated excellence in teaching and research is desired. Candidates should also evince intellectual leadership and impact on the field and potential for significant contributions to the Department, University, and wider scholarly community.

Candidates should submit a cover letter, curriculum vitae, research and teaching statements to:

http://academicpositions.harvard.edu/postings/6093

Questions regarding this position can be addressed to **randy_buckner@harvard.edu**. Applications will be considered starting on **December 1, 2016**.

We are an Equal Opportunity Employer and all qualified applicants will receive consideration for employment without regard to race, color, religion, sex, sexual orientation, gender identity, national origin, disability status, protected veteran status, or any other characteristic protected by law.

PRIZES

DEPRESSION CENTER
UNIVERSITY OF MICHIGAN HEALTH SYSTEM

Frances and Kenneth Eisenberg Research Prize

The University of Michigan Comprehensive Depression Center is accepting nominations for the Frances and Kenneth Eisenberg Research Prize. This prestigious award is given annually to a world-renowned scientist and honors breakthrough research accomplishments that advance knowledge in the understanding of mechanisms and personalized treatments for depressions, bipolar illnesses, or related disorders.

Prize: $50,000: The Prize is a $50,000 award, unrestricted, to be used at the recipient's sole discretion for the support of research operations and/or equipment. Disbursement of the Prize to the recipient shall take place at a scientific presentation given by the Prize winner.

Eligibility:

- Nominee must hold an M.D., Ph.D., or equivalent international degrees.
- Research shall be in depression, bipolar illness and related disorders, broadly defined.
- International scientists are eligible.
- University of Michigan scientists are not eligible.
- Self-nomination is permitted.
- Nominee must be able to devote two days as Visiting Professor with a special lecture at the University of Michigan.
- If selected for the Prize, recipients must agree to join the Eisenberg Research Prize review panel to select subsequent recipients of the Prize.

Deadline: January 16, 2017

Nomination Guidelines: For a nomination to be considered, the following items must be submitted:

- A brief electronic nomination must summarize the applicant's contributions, emphasize strategies for linking basic neuroscience advances to clinical investigative strategies, potential for translational breakthroughs, describe their potential contributions to improving treatment outcomes, the impact they have made in the field, and indicate future research directions.
- Biosketch and/or curriculum vita of the nominee.

Submissions shall be made through the following website: **http://www.depressioncenter.org/award/**. Incomplete nominations will not be presented to the nomination committee. If you have any questions, please email **kimweber@med.umich.edu**.

JOB FOCUS: CELL BIOLOGY

Assistant, Associate or Full Professor of Cancer Biology

Perelman School of Medicine
University of Pennsylvania

The Department of Cancer Biology at the **Perelman School of Medicine** at the **University of Pennsylvania** seeks candidates for an Assistant, Associate, and/or Full Professor position in the tenure track.

The successful applicant will have experience in the field of cancer biology, including but not limited to cancer cell biology, cancer cell metabolism, cancer genetics and epigenetics, cancer immunology, tumor microenvironment, stem cells, and metastasis. Responsibilities include maintenance of an externally funded independent research program, as well as teaching and mentoring of students.

Applicants must have an Ph.D. and/or M.D. degree and have demonstrated excellent qualifications in education and research.

We seek candidates who embrace and reflect diversity in the broadest sense.
The University of Pennsylvania is an EOE.
Minorities/Women/Individuals with disabilities/Protected Veterans are encouraged to apply.

To apply:

http://www.med.upenn.edu/apps/faculty_ad/index.php/g304/d4441

Achieving Leadership in China's Medical Research through a Convergence of Topnotch Talents

Developments in Chinese medical research

Zhimin Li

Director of Center for Science and Technology Development
Ministry of Education, People's Republic of China

As the basis for human understanding of and interactions with the natural world, the natural sciences are the consequence of humankind's unremitting exploration of the physical world. In contrast, medical science is aimed at curing diseases and mitigating pain, and has evolved synchronously with human civilization. From a foundation set more than 400 years ago, medical science has gradually taken shape through 300 years of systematic classification, and is now closely integrated with modern science and technology. As the life sciences now accelerate their pace, it is now possible to study life using similar approaches to those that were previously purely the domain of the natural sciences.

In the struggle against disease, medical scientists are continuing to accumulate a large base of knowledge, by both experimental and empirical observation. However, it is possible this approach to research may be on the wrong track, since the emotional and conscious components of life are often overlooked. Through the lens of the natural sciences, the human body is a perfect and exquisitely coordinated machine, where, for instance, the respiratory function of the lung is closely integrated with the circulatory function of the heart. The body acts as a dynamic chemical factory and a high performance computer, housed in a structure comprising materials and mechanisms that fit together precisely to optimally perform complex functions such as digestion, decomposition and absorption of food. Medical science strives to identify and deconstruct these functions and their mechanisms, and to solve mysteries such as how the human body can subsist for decades or even a century on just grains.

Although the main objective of medical science has been to cure disease, disease prevention may be just as powerful an approach, particularly when the organs and phenomenon of the body are considered not in isolation, but rather in the context of other abnormalities and changes that occur during disease progression. Just as modern science addresses microscale phenomena, such as molecular biology, along with the macroscale, the human itself should be studies as an entire entity that interacts with nature as well as its social environment.

Propelled by progress in the natural sciences, medical science has greatly advanced in modern times. Medical technology has made unprecedented progress by combining the methods and theories of molecular with systematic medicine. However, this approach is limited in that it only considers health and diseases from the biological prospective. For the optimal development of medical and health services, a comprehensive view of human health and disease that takes into account diverse perspectives and systematic hinking will be necessary.From the Chinese perspective, medical science comprises two distinct systems: micro-based medical science introduced from the West, and macro-based Traditional Chinese Medicine (TCM).

These systems were born from different academic traditions, created different medical paradigms, and gave rise to different theoretical systems. They continue to develop on divergent paths. On one hand, Western medicine is based on the application of medical science to practice, and is mainly used to cure diseases and promote health. TCM, on the other hand, is also effective for preventing disease and preserving health, but involves a systematic approach based on repeating experiments that take into account the human in its entirety. TCM and Western medicine originated from disparate religions, social environments, and philosophical and scientific thought, resulting in vast differences in both their theory and methods. Differences also lie in their respective approaches deciphering the relationship between human health and the environment as well as mechanisms of pathology. Nonetheless, both TCM and Western medicine aim to cure disease and save the patient. Consider the famous Chinese serenade Er Quan Ying Yue (“the brilliant moonlight in water of two springs”). It is equally musical when played with a violin or a Chinese Ehru: both are musical instruments.

The principles of respect and nonmaleficence are both basic to scientific research, and medical science in particular, and research that violates either of these two principles are unacceptable according to ethical codes. Medical research must respect basic human rights like dignity, will and privacy, and not cause irreversible damage to individuals, society, environment or future generations.

However, progress is bringing along with it a multitude of ethical dilemmas. Cloning technology, for instance, may positively impact the quality of human life, but it presents revolutionary concepts that challenge mankind’s basic codes of ethics. From 1997, when Dolly the sheep was cloned by British scientists, to generated by British scientists, to 2007, when human-mouse chimeric embryos were produced in a US laboratory, cloning research continues to challenge the limits of human ethics, raising fears that these activities will eventually be directed toward human reproduction. Such developments would raise profound ethical questions relating to the welfare and status of individuals produced by cloning technologies. Life extension through biotechnology presents other ethical dilemmas, such as how future generations and the definition of human life itself would be impacted. It is critical that medical research conforms to relevant ethical principles and regulations, to avoid disastrous repercussions to human health and wellbeing.

A shortage of talents

In 2015, Chinese pharmacologist Tu Youyou, Japanese biochemist Satoshi Omura and Irish parasitologist William C. Campbell won the Nobel Prize in Physiology and Medicine. As the first for Chinese medicine, it gave further encouragement to the flourishing area of Traditional Chinese Medicine. However, given the much larger number of Nobel Prizes in Medicine that Japan has won, China is contemplating the possible causes for such a disparity, and is taking action by investing more heavily in medical and scientific research. Likely it will take decades for these changes to translate into another Nobel Prize, due to the need for scientific findings to be replicated and validated.

Modern scientific research requires multidisciplinary cross collaboration entailing resource sharing and teamwork to undertake complex large-scale projects involving massive data analysis. Cancer research now involves a combination of biotechnology, computational mathematics, bioinformatics, computer science, immunology and clinical medicine to determine how environmental, lifestyle, and genetic interact to cause tumors. Hence, medical talents from diverse areas will be needed.

We warmly welcome top medical talents who can bring to China the teaching and implementation of international methods. Through such improvements in training of physician scientists and leading talents in medicine, we can achieve the goal of bringing China to the leading edge of international medicine.

Further information can also be located at **www.edu.cn/jjyx**

Jianguang Xu
President of Shanghai University of Traditional Chinese Medicine

Double Tops Program will facilitate Chinese universities to become world-class universities. The key to success is gathering first-class talents. Against the background of "Healthy China 2030", Shanghai University of Traditional Chinese Medicine will seize opportunity, continue to inherit and give full play to the strength of TCM. We warmly welcome talents from around the world to Shanghai, China and join us in the great mission of building a world-renowned university of Chinese Medicine.

Baofeng Yang
President of Harbin Medical University

Academic disciplines are the cornerstone for the development of a university and talents are the driving force for its development. Baofeng Yang, an academician of the Chinese Academy of Engineering, claims that Harbin Medical University will reinforce the connotative development of academics, scholars and students. Aimed towards the initiative of first-class universities and disciplines of the world, HMU strives to become first-class in China and well-known in the world.

Yunxia Cao
President of Anhui Medical University

Top-ranking teaching staff is the key to high-level university. Against the background of the state's vigorously advocating Double Top Program, Anhui Medical University aims to be a high-level medical university, setting up the development concept that talent is the core competency. Adhering to the strategy of strengthening university through talents and actively creating favorable atmosphere for talent development, Anhui Medical University has built up a stage for talent introduction, cultivation, and accumulation to promote the comprehensive strength of talent team continuously. Hence we warmly welcome talents from home and abroad to join us and favorable conditions have been created for you to make the most of your intelligence. Let us make concerted efforts for the Dream of Anhui Medical University.

Jun-Li Cao

Dean of the School of Anesthesiology, Xuzhou Medical University

The past 35 years have witnessed the development of the Anesthesiology Department in Xuzhou Medical University, forming a complete disciplinary system with the integration of medical care, education and research. The educational system of Anesthesiology with Chinese characteristics, honored as the cradle for professional talents cultivation in China, has been playing an exemplary and guiding role in the field concerned. Jiangsu Province Key Laboratory of Anesthesiology has well established technological platforms for Anesthesiology and Neuroscience. We sincerely welcome advanced talents from around the world to engage in the development of the School of Anesthesiology.

Zhongren Sun

President of Heilongjiang University of Chinese Medicine

Traditional Chinese medicine (TCM) is a treasure of ancient Chinese science, as well as a key to the treasure house of Chinese civilization. Heilongjiang University of Chinese Medicine is committed to improving the ability of TCM to prevent and treat major diseases, attaching equal importance to inheritance and innovation, promoting the modernization of TCM, and constructing a first-class university of TCM with distinctive characteristics.

Deliang Wen

President of China Medical University

University education involves creating a learning environment that is both comfortable to students and conductive to developing their interests, providing scholars with an academic environment which is free and encourages creativity, nurturing excellent talents for society and yielding achievements or ideology that brings about social developing and progress.

Yuhui Qin

President of Hunan University of Chinese Medicine

Chinese medicine has a unique historical position and great scientific value, and has made an important contribution to the Chinese nations thriving and prosperous. Chinese medicine is facing unprecedented opportunities for the development. The internationalization and modernization of Chinese medicine need to cultivate a large number of talents who have international vision, familiar with modern scientific methods and proficient in Chinese medicine.

Huixian Cui

President of Hebei Medical University

Hebei Medical University has been enjoying a glorious history of more than 120 years. It is authorized to be co-constructed with a jointly effort from China's National Health and Family Planning Commission, Ministry of Education, as well as Hebei Provincial People's Government. Hebei Medical University is striving to build itself into an innovative high-level medical university. We expect a bright future with global talents and fully committed endeavor.

Qiu Li

President of Children's Hospital of Chongqing Medical University

The Children's Hospital of Chongqing Medical University is one of top children's medical institutions in China. It has the only Demonstrative Bases of International Technology Cooperation on Children Important Developmental Disorders and National Standardized Residents Training Demonstrative Base and the most key national programs for clinical specialty construction. Guided by the "Double Tops" and embracing "Health China 2030", CHCMU dedicates to the mission of "All for the Children". Gathering talents from all over the world, it aims to be an international level of children's medical center and to be model for the scientific research of children's health.

Weimin Li

President of West China School of Medicine/West China Hospital, Sichuan University

Established in 1892, West China Hospital (WCH) of Sichuan University is one of top medical institutions in China, well recognized for its quality medical services, research and education. As one of the most important medical research and innovation incubators in China, WCH equips itself with over 40 open labs and platforms at national and provincial levels, notably a National Translational Medical Center and a National Geriatric Clinical Research Center. We therefore welcome talents all over the world from the related fields, including bio-therapy for major diseases, precision medicine, neuroscience and biomedical big data.

Cheeloo College of Medicine (CCOM), Shandong University Recruits Global Outstanding Talents

Shandong University was founded in 1901, under the direct jurisdiction of the Ministry of Education, is a key comprehensive university with a long history, a variety of disciplines, strong academic strength, and distinctive characteristics, which has great influence both at home and abroad. Shandong University is a member university of Project 211 and Project 985, two national key construction projects to support the development of high-quality universities. Shandong University is one of the initiative universities of modern Chinese higher education.

The history of medicine discipline of Shandong University can be traced back to 1864 when Tengchow Wen Hui Kuan was built. It has experienced various historical stages of Shantung Union Medical, Medical School of Cheeloo University, Shandong Medical College, Shandong Medical University and now, Cheeloo College of Medicine(CCOM), Shandong University, which has the honor of "Northern Union, Southern XiangYa, Eastern Cheeloo, Western West China"(They are the four most brilliant medical colleges). Today, it plays indispensable role in medical technology and education field in China. For accelerating the Construction of World-Class University and Discipline, Shandong University and CCOM have established the eminent scholar systems to provide positions for high-level talents in the world. We sincerely welcome talents at home and abroad to join us!

I.Positions:

Honorary Professor, Chair Professor, Distinguished Professor, SDU Distinguished Young Scholars, Cheeloo Young Scholars, Part-time Chair Professor, Part-time Distinguished Professor, Young Teachers and Foreign Teachers.

II.Available Disciplines:

Basic Medicine and Biology, Clinical Medicine, Oral Medicine, Nursing, Psychology, Public Health, Clinical Medicine, Medicinal Chemistry, Pharmaceutics, Pharmacology, Developmental Biology, Epidemiology.

III.Treatment:

Please refer to *http://www.qlyxrc.sdu.edu.cn/showarticle.php?articleid=2108* for details.

IV.Contacts:

Human Resources of Cheeloo College of Medicine (CCOM)
Xiugui Qin, Naiting Zhang
Phones: +86-531-88380106, +86-531-88381085
E-mail: *yxbzzh@sdu.edu.cn*
Address: No.44, Culture West Road, Jinan City, Shandong Province
Zip code: 250012

安徽醫科大學

High-end Talents Recruitment
Anhui Medical University

Anhui Medical University, whose predecessor is Dongnan Medical University established in Shanghai, in May, 1926, is now co-invested by People's Government of Anhui Province, the Ministry of Education and the National Health and Family Planning commission of PRC.

The university is located in Hefei, Anhui Province, characterized by its beautiful campus and convenient transportation. There are 22 directly affiliated teaching institutions, 5 directly affiliated hospitals, 28 disciplines authorized to offer Doctorate Degree, 15 national key disciplines (key clinical specialties) and 28 key laboratories at provincial and national level.
For details, please refer to :
http://www.ahmu.edu.cn/s/1/t/3/p/1/c/13/list.htm .

Now the university plans to recruit high-level talents from the whole world, and the qualifications are as follows:
1. With membership of "China's Thousand Talents Program" and "China's Ten Thousand Talents Program";
2. Doctoral degree holders and associate professors or above, or academic leaders with assistant professorship or above in a university abroad, under the age of 45;
3. Outstanding doctoral degree holders and post doctors who have already completed their scientific research work, under the age of 40.

Salary negotiable.

Contact person:
Wenbing Yao Xiaohui Huang
Email: **rsc@ahmu.edu.cn**
Tel: +86-551-65161028/65172106
Address: Personnel Department of Anhui Medical University, No. 81, Meishan Road, Hefei 230032, Anhui Province, China.
For more ways to contact us, please refer to : **http://rsc.ahmu.edu.cn/**.

徐州醫科大学 XUZHOU MEDICAL UNIVERSITY 江苏省麻醉学重点实验室 Jiangsu Province Key Laboratory of Anesthesiology

Tenure-Track position at the Assistant/Associate/Full Professor level in Anesthesiology and Neuroscience

Jiangsu Province Key Laboratory of Anesthesiology (**State Key Laboratory Cultivation Base for Anesthesiology**) at Xuzhou Medical University (**http://www.xzmc.edu.cn**) invites applications from scientists for a tenure-track position at the rank of Assistant/Associate/Full Professor level in Anesthesiology or related field. Applicants must have a Ph.D. and/or M.D. degree, postdoctoral training. We are particularly interested in candidates who is with research training in the field of anesthesiology and neuroscience and can use cutting edge approaches involving electrophysiological, genetic, cellular, molecular, or behavioral techniques to address key problems related to Anesthesiology, especial in 1) Pain, 2) Post operative cognitive dysfunction (POCD) and 3) Mechanisms of anesthetics and its neuronal toxic. The successful candidate is expected to develop and/or maintain an independent program of research with external funding.

The University and Department provide a very supportive research environment with excellent resources conducive to developing a successful research program. Laboratory space is also exceptional, with Jiangsu Province Key Laboratory of Anesthesiology located in a two-year old 45000 sq. foot, state-of-the-art animal research building.

Please submit a letter of application, cv, a research statement, sample publications, and provide three letters of reference to: **rsc@xzhmu.edu.cn** and **caojl0310@aliyun.com**. Questions about the position should be directed to Professor Jun-Li Cao, Director, Jiangsu Province Key Laboratory of Anesthesiology, at **caojl0310@aliyun.com** or to Yuan-Dong Li, Human Resources, at **rsc@xzhmu.edu.cn**.


上海交通大學
SHANGHAI JIAO TONG UNIVERSITY

Faculty Positions in the School of Pharmacy Shanghai Jiao Tong University

Established in 1896, Shanghai Jiao Tong University (SJTU) is a top research University in China. The School of Pharmacy was established in 2000, had been fully accredited to offer bachelor, master and doctoral degrees in pharmaceutical sciences, and went into strategical partnership with China Institute of Pharmaceutical Industry (CIPI) to form a Center for Pharmaceutical Innovation. For more information about the School, please visit http://pharm.sjtu.edu.cn.

We are recruiting exceptional candidates for full-time faculties/Principal Investigators with offering dual appointments which affiliate with SJTU and CIPI. The candidates should demonstrate strong track record in basic research with industrial application potential. The applicant should obtain Ph.D in pharmaceutical sciences or biological or chemistry and the research areas include therapeutic targets and drug discovery, pharmacology, medicinal chemistry, chemical biology, pharmacognosy, pharmaceutical analysis, biopharmaceutical sciences, pharmaceutical technology, drug delivery, and other related fields. Candidates from both academic organization and pharmaceutical industry are encouraged to apply.

Applicants for "Distinguished Professor", who will be qualified for "National 1000-talent Plan", "Shanghai 1000-talent Plan" and "Eastern Scholar" etc, should have been working as an associate professor or higher at a major university or research institution with excellent publication record.

Junior applicants must have a PhD with strong research background, and will be welcomed to apply for "1000-talents Plan, Young Scholars", Special Research Scientists plan at SJTU and other entry-level faculty positions.

SJTU/CIPI will offer competitive compensation with sufficient starting package, relocation benefit, and assist funding application through local and central government. Applicants should email curriculum vitae, a brief description of research interests, a proposal for future work and three references to the Search Committee at pharmfaculty@sjtu.edu.cn.

FUDAN UNIVERSITY 1905

復旦大學

Faculty Positions Available in Institutes of Biomedical Sciences, Fudan University

The Institutes of Biomedical Sciences (IBS) at Fudan University, established in 2005, pursues cutting-edge biomedical research from an interdisciplinary and inter-institutional perspective. Under the consistent and strong supports from Fudan University and various China government funding agencies, Fudan IBS has now developed into a vibrant research institution consisting of Epigenetics Research Center, Systems Biology of Medicine Research Center, Molecular Cell Biology Research Center, with the intension to initiate innovative research fields that are centered in China and emphasizing translational medicine.

Principle Investigators

Applicants should have a strong research profile to establish and conduct innovative research in the areas of Stem Cell Technology, Bioinformatics and Big-data Analysis, Immunity and Immunotherapy, Epigenetics, Molecular Cell Biology, Biomedical Nanotechnology, Proteomics, Electron Microscopy 3D Reconstruction, Structure Biology, Small Active Molecule for Drug Screening, Translational Medicine for Cancer, Cardiovascular Diseases and Birth Defect.

As an eligible candidate for professorship, you should have:

- PhD degree and more than 3 years working experience abroad.
- High-profiled publications as corresponding author.
- ≤ 40-years old is preferred

Treatment

The university will provide munificent salary, internationally competitive start-up support, laboratory construction and organizing the research team.

For more information, please check : **http://www.ibsfudan.org**

Contact person:
Ms. Mengxue Zhang
Email: **zhangmx@fudan.edu.cn**
Tel: +86-21-51237550

Children's Hospital of Chongqing Medical University Calls For Global Talents

Hospital Profile

The Children's Hospital of Chongqing Medical University (CHCMU) was established in 1956 when the whole department of pediatrics of the Shanghai First Medicine College transferred to Chongqing. It is a comprehensive pediatric hospital that integrates medical services, teaching and research. The hospital ranks the top three among all pediatric hospitals in China in terms of its medical service and S & T influence. It is one of the first pediatric hospitals approved by the central government to establish the master and doctoral degree programs and postdoctoral research station, one of the first hospitals that have the national key pediatric specialty, key laboratory of the Ministry of Education (MOE), the national-level pilot base for international Science and Technology (S & T) cooperation, national-level teaching team and the institution appointed by the China Food and Drug Administration (CFDA) for medicine clinical test; with complete specialties and the most key national programs for clinical specialty construction. The hospital is located in Chongqing, a beautiful mountainous city with the greatest GDP growth among key central cities in China, and as the largest pediatric hospital in China, covering an area of 50 acres in total of its main campus and Lijia campus, the hospital has 43 clinical and auxiliary departments, and provides health services across China with the outpatients of 2.5 million and nearly 70,000 inpatients every year.

It plays a leading role in China in the aspects of children liver transplantation, primary immunodeficiency disease allogeneic bone marrow transplantation, solid tumor treatment with High-intensity Focused Ultrasound (HIFU) and the clinical molecular diagnosis.

Pediatric Research Institute

Founded in 1991, the pediatric research institute has 7500㎡ research rooms, standard SPF class animal center, with more than 20 million dollars instruments and equipments.

With the institute support, the hospital becomes the only Demonstrative Bases of International Technology Cooperation on Children Important Developmental Disorders and National Standardized Residents Training Demonstrative Base and National Clinical Test -GCP center and the key laboratories of the MOE.

During the past 5 years, the hospital has been at the leading rank in the pediatric circle due to the major, key and surface programs in the China-Canada cooperation financially supported by the National Natural Science Foundation of China and given with 23 awards including one special scientific research program in the healthcare industry, Grade II award by the MOE for S & T progress, the first grade S & T progress award by Chongqing municipal government and Soong Ching Ling Award for Pediatric Medicine Achievements as well as the Chinese Medical Award, etc. Institute has the journal of the *Journal of Pediatric Pharmacy*.

Key laboratory appointedby MOE for pediatric development diseases

The key laboratory appointed by MOE for pediatric development diseases was backed with the national key discipline of pediatrics, successfully determines four research directions of the nervous and spiritual development and recognition diseases, child immune development and infection, born defects and tissue engineering as well as tumor pathogenesis and individualized treatment by embrace the "Double Tops" and focusing on the main thread of "Development and Diseases", and adheres to performing researches on application basis and transformation of applied research. Equipped with three platforms of core facility, research team and transformation medical science, the Lab is now one of the key bases for high-level talent training in pediatric research in China.

International Exchange

By insisting on the open-up and cooperation, the hospital has established a long-term cooperative relations with academic institutes in more than 20 countries and regions such as Cincinnati Children's Hospital, University of British Columbia, University of Oxford and University of Chicago etc., and worked together with excellent talents at home and abroad who devote themselves to children health. "ALL for the children", this is our common goal.

WHAT WE OFFER

- Incentive high salary
- Competitive settling-in allowance
- Sufficient research start-up fund
- Provide research assistants
- Help to apply national talent plan

Contact Information

Address: Personnel Division, 5F, Building 7#, 136, Zhongshan Er Road, Yuzhong District, Chongqing, 400014
Contact: Xiaoxia Yu Huili Han
Tel: +86 02363632294 02363622754
E-mail: ***etyyrsc@163.com*** ***etyykyc@163.com***
Website: ***http://www.chcmu.com***

This Job Advertisement is Long-term Effective

EXPLORE

Interested in the human cell?
Open this poster to learn about the most detailed mapping of the human cell ever done. The Human Protein Atlas project is presenting a high-resolution map of the human cell. The proteins have been localized with high precision to cellular organelles, structures and sub-structures, with high-resolution images freely available for you to explore.

The antibodies used are Triple A Polyclonals provided by Atlas Antibodies.

MADE IN SWEDEN

ATLAS ANTIBODIES
Totally human

HOW TO TARGET VALIDATE YOUR ANTIBODY

MAKE SURE IT WORKS IN YOUR APPLICATION!

THE GUIDELINES

Due to the need for properly validated antibodies, the International Working Group on Antibody Validation (IWGAV) has made an effort to standardize best practices, resulting in a publication proposing "Conceptual Pillars for Validation of Antibodies." The pillars presented here are directed to both users and producers of antibodies.

ANTIBODYPEDIA

The Antibodypedia database lists antibodies provided by academia and commercial companies. Antibodypedia ranks antibodies based on the amount and quality of the knowledge associated with them, putting the antibody with the most information available on top of the search list, and assisting you in selecting the most appropriate antibody for your experiment.

GENETIC STRATEGIES

Genetic strategies can be used to generate genetically modified samples where the target protein is knocked out or knocked down. This method provides a direct link between the gene and the target protein. The antibody is considered validated for its target when the signal from the original sample is significantly downregulated in the genetically modified sample.

ORTHOGONAL STRATEGIES

Orthogonal strategies compare an antibody-based method with an antibody-independent method, for example targeted proteomics approaches using labeled internal standards. Identifying and measuring your target protein in a set of samples with a method not involving antibodies should give comparable results to the antibody-based method.

INDEPENDENT ANTIBODIES

Independent antibody strategies use two or more antibodies recognizing different epitopes (binding sites) on the target protein. This method minimizes the likelihood of off-target binding to the same unrelated protein. Antibody validation is achieved when the unique antibodies give comparable results when using the same detection method.

TAGGED PROTEINS

Tagging proteins on the genetic level with an affinity tag or a fluorescent protein can be used to validate the antibody for the target protein. Tagged proteins should preferably be expressed at endogenous levels. The expression pattern of the tag should overlap with the expression pattern created when using the antibody for protein detection.

IMMUNO-CAPTURE MS

Immunocapture is a method that uses an antibody to isolate a protein from a solution. When coupling this technique with mass spectrometry (MS), the proteins captured by the antibody can be identified. The peptides for the target protein should be on the top of the generated peptide list in order for the antibody to be considered specific.

FIVE CONCEPTUAL PILLARS FOR ANTIBODY VALIDATION. Antibodies are powerful tools used in many different applications to detect proteins. The power of the antibody lies in its ability to recognize a specific target. It is crucial to properly validate the antibody for binding to its intended target, to test the antibody in the intended application, and to understand the context where it will be used. The five pillars for antibody validation are summarized below.

	PILLAR				
Application	Genetic Strategies	Orthogonal Strategies	Independent Antibodies	Tagged Proteins	Immunocapture Mass Spectrometry
Western blotting (WB)	◆	◆	◆	◆	
Immunohistochemistry (IHC)	◆	◆	◆	◆	
Immunocytochemistry (ICC)	◆	◆	◆	◆	
Flow sorting (FS)	◆	◆	◆	◆	
Sandwich assays (SA)	◆	◆	◆		
Immunoprecipitation (IP)	◆		◆		◆
Reverse phase protein arrays (RPPA)	◆	◆	◆		

This table summarizes for which applications the five conceptual pillars are recommended. The ◆ represents support for the pillar in the application. Ref.: M. Uhlen *et al.*, A proposal for validation of antibodies. *Nat. Methods* **13**, 823–827 (2016).

Percentage utilization of antibodies in listed applications according to data in Antibodypedia. Western blotting (WB) is the most commonly used application, followed by immunohistochemistry (IHC), immunocytochemistry (ICC), and flow sorting (FS).

antibodypedia

www.antibodypedia.com

REVEALING THE CELL'S SECRETS

Our DNA might provide the blueprint for how to build our bodies, but it is the proteins that really do the heavy lifting. While there are around 20,000 genes encoded in our DNA, the total number of proteins is estimated to be many times more—possibly as many as a million*. This is because a single gene might produce multiple variants of a particular protein through, for example, alternative splicing of the messenger RNA. Posttranslational modification of the nascent protein, such as phosphorylation and glycosylation, may also significantly or subtly change its function, yielding many possible functional protein variants.

Understanding how a particular DNA sequence gives rise to a particular protein provides us with some insight into that protein, but a deeper investigation of how the protein is made, where it is located, and how much of it is present in different cell types is required to enable a true understanding of its function. As mentioned above, changes to the protein soon after its translation can impact its final function, as well as its final location. Conversely, its location may also affect its function. Intensive study has therefore gone into finding out as much as possible about the lifecycle of proteins.

The study of the entire complement of human proteins is known as proteomics. Researchers in this field seek to identify and characterize each and every protein in a specific location—be it the whole body or a specific tissue. A previous *Science* poster† looked predominantly at the tissue proteome, highlighting how tissues have unique patterns of protein expression and how this pattern might be disrupted by dysfunction and disease.

The poster that you are now viewing aims to delve down an additional layer into the *cellular* proteome, taking a journey into the subcellular compartments within a single cell to discover what secrets each organellar proteome might hold. Characterizing the distribution of individual proteins at a subcellular level provides important clues to the pathways and processes in which these proteins are involved. Fourteen compartments are covered, including mitochondria, the cytosol, and the nucleoplasm. The description for each compartment hyperlinks the reader back to the free Protein Atlas resource, where a rich trove of data resides, open for exploration by anyone—from serious researchers to those who may just have an interest in cell biology.

Alongside this information, the poster includes a helpful timeline that highlights important milestones in the history of microscopy, from the first compound microscope in the late 1500s to more recent developments in superresolution imaging. Paralleling that timeline is another outlining the important discoveries in cell biology. All of these advances made it possible for us to be where we are today—finally beginning to unravel the complexity of the proteome and gaining a clearer understanding of how our DNA renders our proteins, and how those proteins are organized, interact, and ultimately define who and what we are as human beings.

Sean Sanders, Ph.D.
Editor, Custom Publishing,
Science

*proteomics.cancer.gov/whatisproteomics
†poster.sciencemag.org/humanproteome

Writers: Mikaela Wiking, M.Sc.; Tove Alm, Ph.D.; Mathias Uhlen, Ph.D.; Emma Lundberg, Ph.D.
Illustrator/Designer: Luca Marziani ■ Editor: Sean Sanders, Ph.D.

Roger Goncalves, Sales Manager
Custom Publishing
Europe, Middle East, and India
rgoncalves@science-int.co.uk
+41-43-243-1358

Sponsored by
THE HUMAN PROTEIN ATLAS
Knut och Alice Wallenbergs Stiftelse
Science AAAS
Produced by the *Science*/AAAS Custom Publishing Office

THE HUMAN CELL

Cells are the machinery of life. Much of the bustling activity in the human cell results from proteins performing specific tasks in designated compartments, the organelles. This poster describes the results and ongoing creation of an image-based atlas of the subcellular distribution of the human proteome. Explore it further at **www.proteinatlas.org**.

THE HUMAN PROTEIN ATLAS

The Human Protein Atlas presents the translated human genome captured in millions of images collected using high-resolution microscopy. The Cell Atlas, Tissue Atlas, and Cancer Atlas provide a comprehensive overview of gene expression–together with the spatial distribution of corresponding proteins–across organs, tissues, and cell lines at subcellular resolution.

ORGANELLE PROTEOME

The cellular function of proteins is dictated by their location and interactions with other proteins or substrates. Revealing the human proteome's spatial distribution is thus essential to understanding cell biology. By visualizing the nonsecreted human proteome using high-resolution confocal microscopy, the molecular composition of organelles and substructures has been determined.

MULTILOCALIZING PROTEOME

Over one-third of human proteins are found in multiple organelles. The presence of a single protein at several locations may reflect its dynamic distribution, and suggests multiple roles in cell physiology. Understanding the multilocalizing proteome is key for discovering novel pathways underpinning cellular dynamics and developing a holistic view of the human cell.

CELL CYCLE-DEPENDENT PROTEOME

The cell cycle describes the process by which cells grow and divide. This dynamic and tightly regulated process drives changes in abundance and spatial redistribution of many proteins. Cell cycle dysregulation can lead to diseases such as cancer. Knowledge about the cell cycle proteome is therefore essential for understanding health, aging, and disease.

CELL LINE TRANSCRIPTOME

Expression of protein-coding genes has been analyzed in a large set of human cell lines of different cellular origins. One-third of all genes are differentially expressed, indicating cell type-specific functions related to the origin of the cell line. The majority of genes are expressed in all cells and drive rudimentary processes such as metabolism or proliferation.

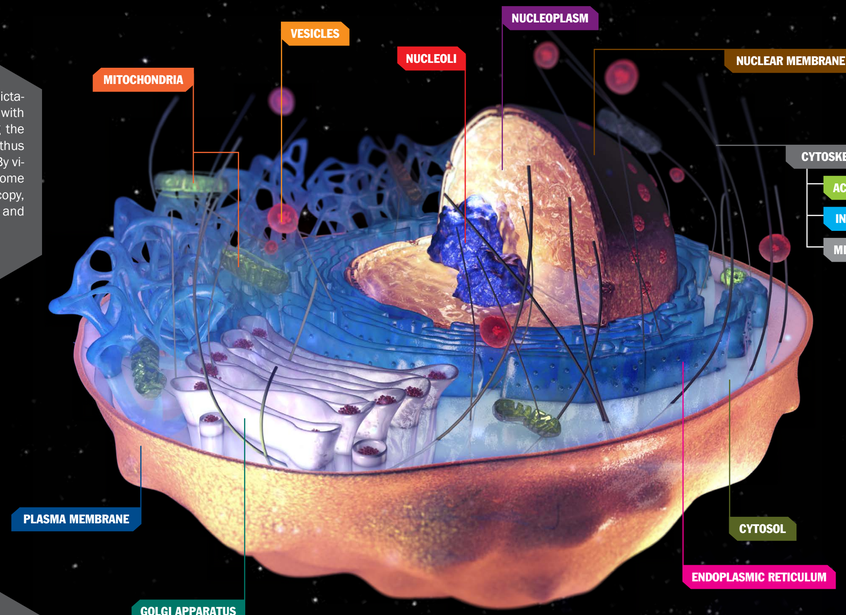

NUCLEOPLASM

The nucleoplasm is enclosed by the nuclear membrane and embeds the nucleoli to form the nucleus. It surrounds the chromatin and nuclear substructures, the nuclear bodies. The nucleoplasm is the site of DNA replication and transcription, tightly regulated processes controlling cellular growth and division.

NUCLEOLI

The nucleoli are nonmembrane-bound structures in the nucleus. They are the sites of ribosome synthesis, processing, and assembly. These are complex processes controlled in nucleolar substructures such as the fibrillar center. Nucleoli also comprise proteins involved in cell cycle regulation and cell stress responses.

NUCLEAR MEMBRANE

The nuclear membrane physically isolates the DNA in the nucleus from the cytoplasm. The inner membrane is the anchoring site of nuclear chromatin, while the outer membrane is continuous with the endoplasmic reticulum. Nuclear pores are scattered throughout the membrane, regulating large molecule transport in and out of the nucleus.

ACTIN FILAMENTS

The actin filaments are polarized filaments that are part of the cytoskeleton and provide structure to the cell. They interact directly with focal adhesions and membrane-bound proteins, allowing the cell to respond to extracellular stimuli and control cellular motility. This dynamic remodeling ability also makes them essential for cellular division.

INTERMEDIATE FILAMENTS

The intermediate filaments are part of the cytoskeleton and provide physical support and stabilization to the cell, enabling it to withstand mechanical stress and tension. They also participate in chromatin organization by anchoring the DNA to the nuclear lamina, which lines the inner part of the nuclear membrane.

MICROTUBULES

The microtubules are the stiffest of the cytoskeleton components and are essential for maintaining the internal architecture and polarity of the cell. They are involved in spindle formation during mitosis, and also form a network facilitating intracellular transport. Cell motility requires rapid rearrangement of microtubules.

MITOCHONDRIA

Each mitochondrion is enclosed by double membranes, the inner one folding into cristae. They are responsible for production of cellular energy, and are also involved in signaling, cell death, and cellular differentiation. They are the only organelle with their own genome, which codes for rRNA, tRNA, and proteins involved in energy metabolism.

CYTOSOL

The cytosol is the semifluid substance within the cell that, together with all nonnuclear organelles, forms the cytoplasm. It is composed mainly of proteins, ions, and amino acids. Several cellular processes, including protein synthesis, interorganelle transport, and many metabolic reactions occur in the cytosol.

CENTROSOME

The centrosome is a small and distinct organelle responsible for organizing microtubules in the cell. It consists of two centrioles, which are surrounded by a matrix of proteins named the "pericentriolar material." The centrosome is a key regulator of cell division and also important for cell shape, polarity, and mobility.

ENDOPLASMIC RETICULUM

The endoplasmic reticulum (ER) is a membranous network consisting of sheets and tubules that span the cytoplasm. The rough ER is covered with ribosomes that translate most of the transmembrane and secreted proteins. The smooth ER lacks ribosomes, but contains the machinery for synthesis of lipids and other biomolecules.

GOLGI APPARATUS

The Golgi apparatus consists of stacks of interconnected membranous disks, cisternae, in a ribbon-like structure close to the nucleus. It plays a central role in the secretory pathway, since it is involved in the modification and sorting of proteins that are transported to other organelles in the cell, as well as to the extracellular space.

VESICLES

The small membrane-bound organelles, known collectively as vesicles, include endosomes, lysosomes, peroxisomes, lipid droplets, and transport vesicles including secretory granules. The diversity of vesicles is reflected in their plethora of functions, such as specialized metabolic reactions, transport, secretion, and degradation of biomolecules.

PLASMA MEMBRANE

The plasma membrane physically separates the cell's interior from the surrounding environment. It is the site of cell–cell interactions and communications, and anchors the cell to neighboring cells or the extracellular matrix. Transmembrane proteins in the cell membrane are important for signal transduction and transportation of molecules.

SECRETED

Secreted proteins can often be identified by the presence of a signal peptide. This localization signal results in active transport out of the cell, predominantly via the secretory pathway. They play a crucial role for inter- and intracellular communication and include antibodies, peptide hormones, coagulation factors, growth factors, and other signaling molecules.

HIGHLIGHTS OF CELL BIOLOGY AND MICROSCOPY

- **1595-1610** The first compound microscopes made
- **1665** Robert Hooke coins the term "cell"
- **1673** Antonie van Leeuwenhoek manufactures single lens microscope
- **1833** Robert Brown describes the cell nucleus
- **1838-39** Matthias Schleiden and Theodor Schwann formulate "cell theory"
- **1852** George Stokes describes wavelength change between fluorescent absorption and emission (Stokes shift)
- **1873** Ernst Abbe describes resolution limit for light microscopes
- **1890** Richard Altmann describes bioblasts (later mitochondria) in muscle of beetle, *D. marginalis*
- **1891** Paul Ehrlich describes antibodies (Nobel Prize 1908)
- **1898** Camillo Golgi describes internal reticular apparatus later known as the Golgi apparatus (Nobel Prize 1906)
- **1933** Ernst Ruska develops first electron microscope (Nobel Prize 1986)
- **1935** Frits Zernike develops phase contrast microscopy (Nobel Prize 1953)
- **1941** Albert Coons is first to use antibodies coupled to fluorescent molecules
- **1945** Keith Porter, Albert Claude, and Ernest Fullam describe organization of cell using TEM (A. Claude Nobel Prize 1974)
- **1955-56** Christian de Duve describes lysosome and peroxisome vesicles; George Palade describes ribosomes on endoplasmic reticulum (Nobel Prize 1974)
- **1957** Marvin Minsky patents principles of confocal microscopy
- **1962** Osamu Shimomura describes GFP isolated from jellyfish, *A. victoria* (Nobel Prize 2008)
- **1975** Günter Blobel elucidates role of signal peptide for subcellular localization of proteins (Nobel Prize 1999); Georges Köhler and César Milstein develop first monoclonal antibodies (Nobel Prize 1984)
- **1985** Nils Åslund publishes first 3D stack from confocal laser scanning microscope
- **1989** William Moerner detects single fluorophore (Nobel Prize 2014)
- **1994** Stefan Hell develops STED microscopy (Nobel Prize 2014)
- **1995-96** Martin Chalfie develops GFP as gene expression marker; Roger Tsien creates multicolored mutants of GFP (Nobel Prize 2008)
- **2001** First draft of the human genome completed (Human Genome Project and Celera Genomics)
- **2006** Eric Betzig develops PALM (Nobel Prize 2014)
- **2015** Tissue-based human proteome published (Human Protein Atlas)

CELL BIOLOGY HIGHLIGHTS

MICROSCOPY HIGHLIGHTS

GFP = Green fluorescent protein
TEM = Transmission electron microscopy
STED = Stimulated emission depletion microscopy
PALM = Photoactivated localization microscopy

Sponsored by THE HUMAN PROTEIN ATLAS

Knut och Alice Wallenbergs Stiftelse

Science AAAS

Produced by the *Science*/AAAS Custom Publishing Office

To explore the human proteome in more depth, visit:
www.proteinatlas.org

Online version of this poster:
posters.sciencemag.org/humancell

Scan this QR code to learn more about the human cell.

By **Amanda Zellmer**

Family-friendly science

A little more than a decade ago, as an aspiring scientist working toward my Ph.D., I spent an unfortunate number of hours debating with myself and discussing with my peers whether it was possible to have kids and be a successful scientist. As the media and, often, scientists themselves portrayed it, success in science meant spending all hours in the lab, neglecting family and skipping holiday dinners to attend to petri dishes. Despite my passion for nature, the prospect of those trade-offs made me question whether I was committed enough. This self-doubt only deepened when, near the completion of my graduate work, my announcement that I was pregnant prompted a warning to not let it affect my work.

At first I tried to follow that admonition. I defended my thesis with spit up on my blouse while my 8-month-old daughter waited in the hallway with a babysitter. I lugged her to field sites, carrying her on my back while wading into ponds to collect data on frog populations.

But over time, this approach wore me out. I was both disappointed in myself for not being productive enough in my research and frustrated that I wasn't spending enough time enjoying my family. I lost my confidence and started looking for excuses to leave science. I watched jobs and fellowships go by because I doubted my qualifications. After 2 years as a postdoc living off a salary that couldn't cover day care costs, I took a year off to re-evaluate my plans and goals.

"Being a scientist was actually very conducive to raising kids."

In those long days at home, I gradually realized how much I had let the stereotype of the scientist who sacrifices family life define me. There I was, Mama Ph.D., desperately trying to keep myself busy with projects around the house while my intellectual skills—writing, data analysis, critical thinking—went to waste. I decided I'd rather be a scientist whose kids affect her work than not be a scientist at all.

I jumped back into the workforce as an adjunct professor teaching biology. I found a scientist-mom mentor who fought for me, making sure I wouldn't get taken advantage of as an adjunct or as a woman. Her support also helped inspire me to get back into research by starting a new postdoc, and for the first time to feel confident in my work.

Over the next 3 years, I juggled teaching, research, and being a mom (among other things). I was surprised to find that being a scientist was actually very conducive to raising kids. I took advantage of the flexible hours of an academic scientist to spend time with my family, and I was also lucky to have on-site child care facilities and an endless supply of babysitters living across the street from my house. At the same time, being a parent improved my science. I learned to plan more efficient experiments and to think more carefully about which questions were really worth pursuing. My daughter became my favorite field assistant, helping me scour the woods for salamanders to study.

But it wasn't until a colleague asked me whether I would be applying for a recently announced tenure-track position that I realized how much scientific and professional progress I had made in those years juggling research and motherhood. With her encouragement I applied, and glowingly showed off my 8-month pregnancy bump during an on-campus interview for my current job as an assistant professor.

My life now is a true merging of research and family. It happens in small moments, such as when a sick day turns into an impromptu "let's see what we can find under the microscope" day. Other times my double life results in epic adventures, for example when I co-led an undergraduate course in the Costa Rican rainforest while pregnant with my second child, with my daughter and scientist-husband by my side. I now know how misguided those thoughts and "advice" in grad school were. In letting my kids affect my research, I learned not only that it is possible to balance being a scientist with having children, but also that doing so benefits both our children and our science. ■

Amanda Zellmer is an assistant professor at Occidental College in Los Angeles, California. Send your career story to SciCareerEditor@aaas.org.

ILLUSTRATION: ROBERT NEUBECKER